Biogeochemical Cycles in Globalization and Sustainable Development

Vladimir F. Krapivin
Costas A. Varotsos

Springer

PRAXIS

Biogeochemical Cycles in Globalization and Sustainable Development

Vladimir F. Krapivin and Costas A. Varotsos

Biogeochemical Cycles in Globalization and Sustainable Development

Springer

Published in association with
Praxis Publishing
Chichester, UK

PRAXIS

Professor Dr. Vladimir F. Krapivin
Institute of Radioengineering
and Electronics
Russian Academy of Sciences
Moscow
Russia

Associate Professor Costas A. Varotsos
University of Athens
Department of Applied Physics
Laboratory of Upper Air
Athens
Greece

SPRINGER–PRAXIS BOOKS IN ENVIRONMENTAL SCIENCES
SUBJECT *ADVISORY EDITOR*: John Mason B.Sc., M.Sc., Ph.D.

ISBN 978-3-540-75439-8 Springer Berlin Heidelberg New York

Springer is part of Springer-Science + Business Media (springer.com)

Library of Congress Control Number: 2007941937

Cover design: Jim Wilkie
Project management: Originator Publishing Services Ltd, Gt Yarmouth, Norfolk, UK

Printed on acid-free paper

Contents

Preface

In recent decades globalization has become widespread and civilization's activities have aggravated and brought about many problems in the interaction between nature and society. To find answers to these problems, we clearly need to develop new concepts and approaches to the interpretation of global environmental change, which would enable us to select the top-priority directions for future scientific studies and to reliably assess the state of the nature–society system. Undoubtedly, predicting the global ecodynamics trend is one of these priorities. The growing interest in globalization and sustainable development as a result of contradictory estimates of the anthropogenic contribution to climate change necessitates the need for systematization of knowledge about change in the observed nature–society system and the causes of this change. Despite the many projects and programs dedicated to studying past and present ecodynamics trends, the problem of reliable prediction of future ecodynamics change is far from being solved. Emissions to the atmosphere of greenhouse gases, mainly carbon dioxide, are considered one of the main causes of expected climate warming, resulting in a poor prognosis for humankind. At the same time, many experts in the field suggest that anthropogenic emissions of aerosols could cancel out the greenhouse-warming effect. The problem lies in combining these factors while keeping the numerous strategies adopted for human society development in mind. Therefore, we attempt in this book to construct a formalized tool to assess the level of the greenhouse effect due to anthropogenic sources of carbon dioxide as well as the effect of other gas components.

In an attempt to understand the factors that determine the feedbacks from the global nature–society system of the cycles of carbon and other chemicals, we construct a hierarchy of model units to parameterize all the known physical and biogeochemical processes that are responsible for the transport of various substances. We substantiate these units by means of partial models which estimate the balance between relationships at the boundaries of different media. The correlations between biogeochemical cycles and the many activities of human society are the basic objectives of this book.

The book consists of seven chapters. Chapter 1 discusses the interactive processes between present-day globalization of humankind's environmental strategy and biogeochemical cycles. It further considers the greenhouse effect and relevant contradictory results obtained from various climate studies. Globalization of many human activities is also considered in the context of wealth and human health as indicators of sustainable development. Chapter 2 considers the role of biogeochemical cycles in global ecodynamics. Chapter 3 gives a new view on the global biogeochemical carbon cycle by looking at the spatial structure of carbon sources and sinks. For example, a new mechanism for carbon dioxide loss in the geosphere is introduced. The global carbon cycle is parameterized through its correlation with biosphere resources and climate change. The subject of Chapter 4 is the combined parameterization of global biogeochemical cycles of the basic greenhouse gases and other chemicals that control bioproductivity and environment quality. Chapter 5 focuses on the observational data of the biogeochemical processes and gives algorithms for data processing. Chapter 6 describes the results of multi-dimensional analysis of the interaction between global ecodynamics and the Arctic Basin's environment. Chapter 7 presents the retrospective and present-day development of the nature–society system by looking at the existing distribution of energy resources and analyzing current trends in world energy.

The book further develops methods, algorithms, and principles that may help toward solving problems regarding globalization and sustainable development. To this end, simulation experiments have shown that

- existing climate models are simply not good enough at assessing the consequences of given anthropogenic scenarios being realized;
- the level of uncertainty in climate forecasts can be reduced by giving broader consideration in global models to interactive bonds in the nature–society system and to the little known mechanism of biotic regulation of the environment, as well as general improvement of the global monitoring system;
- the use of hydrocarbon energy sources in the 21st century will not lead to catastrophic climate change as long as there is little further change to natural land cover and the World Ocean is protected from pollution.

In addition to analyzing present trends in the way civilization is developing and assessing global ecodynamics, the book considers global biogeochemical cycles, one of the main indicators of sustainable development. Assessment of the role biogeochemical cycles play in global ecodynamics is based on the GIMS technology developed earlier by the authors.

The problems facing civilization and its development are so broad and multifaceted that the aspects considered here are but a small part of the wider field of scientific and methodical studies of the processes involved in the interation between nature and society. The proposed adaptive evolutionary scheme of combining monitoring data with the results of simulation modeling may turn out to be a mechanism to facilitate the transition to sustainable development.

The book is aimed at specialists dealing with the development of information technologies to protect the natural world. Global modeling, climate change, the problems inherent in relationships between society and nature, and geopolicy are all studied in depth.

Figures

Tables

Abbreviations and acronyms

a.s.l.	above sea level
AAOE	Airborne Antarctic Ozone Experiment
AAPCHO	Association of Asian Pacific Community Health Organization
AAPI	Asian Americans and Pacific Islanders
AARS	Asian Association on Remote Sensing
AATSR	Advanced Along-Track Scanning Radiometer
ABL	Atmospheric Boundary Layer
ACC	Anthropogenic Climate Change
ACE	Aerosol Characterization Experiment
ACIA	Arctic Climate Impact Assessment
ACRS	Asian Conference on Remote Sensing
ACSYS	Arctic Climate SYStem Study
ADCP	Acoustic Doppler Current Profiler
ADEOS	ADvanced Earth Observing Satellite
AFB	Air Force Base
AGCM	Atmospheric Global Climate Model
AGU	American Geophysical Union
AH	Arctic Haze
AHLCB	Atmosphere–Hydrosphere–Lithosphere–Cryosphere–Biosphere
AIBS	American Institute of Biological Sciences
AIDS	Acquired Immune Deficiency Syndrome
AIRS	Atmospheric InfraRed Sounder
AMAP	Arctic Monitoring and Assessment Program
AMIP	Atmospheric Model Intercomparison Project
AMSR-E	Advanced Microwave Scanning Radiometer for EOS
AMSU	Advanced Microwave Sounding Unit

AO	Arctic Oscillation
AOD	Aerosol Optical Depth
AOT	Aerosol Optical Thickness
APDA	Arctic Precipitation Data Archive
APEC	Asia–Pacific Economic Cooperation
APM	Air Pollution transport Model
ARCSS	ARCtic System Science
ARCUS	Arctic Research Consortium of the U.S.
ARDB	Arctic Run-off Data Base
ARF	Aerosol Radiative Forcing
ARISTI	All-Russian Institute for Scientific and Technical Information
ARM	Atmosphere Radiation Measurement
ASAR	Advanced Synthetic Aperture Radar
ASHOE	Airborne Southern Hemisphere Ozone Experiment
ASTER	Advanced Spaceborne Thermal Emission and reflection Radiometer
ASTTP	Advanced Sensor Technology Transfer Program
ATEX	Atlantic Trade wind EXperiment
ATLAS	Arctic Transitions in the Land–Atmosphere System
ATSR	Along-Track Scanning Radiometer
AVHRR	Advanced Very High Resolution Radiometer
AVIM	Atmosphere–Vegetation Interaction Model
AVNIR	Advanced Visible and Near-Infrared Radiometer
AYRS	Angara–Yenisey River System
AYRSSM	Angara–Yenisey River System Simulation Model
BATS	Bermuda Atlantic Time-series Study
BC	Black Carbon
BGC	BioGeochemical Cycle
BIBEX	BIomass Burning EXperiment
BOD	Biochemical (biological) Oxygen Demand
BP	British Petroleum
BSS	Biosphere–Society System
BTU	British Thermal Unit
BVOC	Biogenic VOC
CAAA	Clean Air Act Amendments
CABM	Coupled Atmosphere–Biosphere Model
CAGL	Central AeroGeophysical Laboratory
CALIPSO	Cloud-Aerosol Lidar and Infrared Pathfinder Satellite Observation
CART	Cloud And Radiation Testbed
CASA	Carnegie–Ames–Stanford Approach
CASES	Canadian Arctic Shelf Ecosystem Study
CC	Cloud/Column
CC-Vex	CALIPSO-CloudSat Validation experiment

CCGG	Carbon Cycle Greenhouse Gas
CCM1-Oz	NCAR Community Climate Model
CCN	Cloud Concentration Nucleus
CCSM	Community Climate System Model
CCSP	U.S. Climate Change Science Program
CCSS	Carbon–Climate–Society System
CDC	Centers for Disease Control
CDNC	Cloud Droplet Number Concentration
CEOP	Coordinated Enhanced Observing Period
CEPEX	Central Equatorial Pacific EXperiment
CER	Certified Emission Reduction
CERES	Clouds and the Earth's Radiant Energy System
CETT	Centro Español Teófilo Tabernera
CGCM	Certified Graphic Communications Manager
CGSDI	Consultative Group on Sustainable Development Indicators
CIESIN	Center for International Earth Science Information Network
CliC	Climate and Cryosphere (CliC) project
CLIVAR	CLImate VARiability and predictability
CLRTAP	Convention on Long-Range Transboundary Air Pollution
CM	Climate Model
CO	Carbon monoxide
COADS	Comprehensive Ocean–Atmosphere Data Set
COLA	Center of the Ocean–Land–Atmosphere system study
COP	Conference of the Parties
CORP	Chinese Ozone Research Program
CPI	Consumer Price Index
CPL	Cloud Physics Lidar
CPR	Continuous Plankton Recorder program
CRC	Chemical Rubber Company
CRF	Cloud Radiative Forcing
CRP	Conservation Reserve Program
CRS	Cloud Radar System
CSD	Commission on Sustainable Development
CSIRO	Commonwealth Scientific and Industrial Research Organization
DA	Dust Aerosol
DEAD	Dust Entrainment And Deposition
DEBITS	DEposition of Biochemically Important Trace Species
DFA	Detrended Fluctuation Analysis
DJSGI	Dow Jones Sustainability Group Index
DMUU	Decision-Making Under Uncertainty
DNA	DeoxyriboNucleic Acid
DO	Dansgaard–Oeschger
DOC	Dissolved Organic Carbon

DOE	Department Of Energy
DOM	Dead Organic Matter
DORIS	Doppler Orbitography and Radiopositioning Integrated by Satellite system
DTR	Diurnal Temperature Range
DUP	Data Used Program
DVI	Difference Vegetation Index
ECHAM	European Center/HAMburg
ECMWF	European Center for Medium-range Weather Forecast
ECOHAB	ECOlogy of Harmful Algal Blooms
EDGAR	Emission Database for Global Atmospheric Research
EEA	European Environment Agency
EES	European Economic Society
EEZ	Exclusive Economic Zone
EFMN	European Foresight Monitoring Network
EIA	Energy Information Administration
EME	Europe and Middle East
ENSO	El Niño–Southern Oscillation
ENVISAT	ENVIronmental SATellite
EOLSS	Encyclopedia Of Life Support Systems
EOS	Earth Observing System
EOSAT	Earth Observation SATellite
EPA	Environmental Protection Agency
ERB	Earth Radiation Balance
ERBS	Earth Radiation Budget Satellite
EROS	Earth Resources Observation System
ERS	European Remote sensing Satellite
ESA	European Space Agency
ESI	Environmental Sustainability Index
ESSP	Earth System Science Partnership
EU	European Union
EVI	Enhanced Vegetation Index
EXPRESSO	EXPeriment for REgional Sources and Sinks of Oxidants
FAO	Food and Agriculture Organization
FBI	Family Biotic Index
FCCC	Framework Climate Change Convention
FGGE	First GARP Global Experiment
GAME	GEWEX Asian Monsoon Experiment
GARP	Global Atmospheric Research Program
GASG	Gas Analysis and Sensing Group
GBS	Geosphere–Biosphere System
GC	Gas Chromatograph
GCC	Global Carbon Cycle
GCM	General Circulation Model; Global Climate Model
GCMA	General Circulation Model of the Atmosphere

GCOS	Global Climate Observing System
GCP	Global Carbon Project
GCTE-SEN	Global Change and Terrestrial Ecosystems-Soil Erosion Network
GDP	Gross Domestic Product
GEF	Global Ecological Fund
GEM-E3	General Equilibrium Model for Energy–Economics–Environment
GEMS	Global Environmental Monitoring System
GENEMIS	GENeration and evaluation of EMISsion data
GENESIS	Global ENvironmental and Earth Science Information System
GEO	Group on Earth Observations
GEOS-CHEM	Goddard Earth Observing System/CHEMistry
GEOSS	Global Earth Observation System of Systems
GEWEX	Global Energy and Water cycle EXperiment
GFDL	Geophysical Fluid Dynamics Laboratory
GHG	GreenHouse Gas
GIMMI	Geographical Information and Mathematical Model Inter-operability
GISP2	Greenland Ice Sheet Project 2
GISS	Goddard Institute for Space Studies
GLOBEC	GLOBal ocean ECosystems dynamics program
GMNSS	Global Model of the Nature–Society System
GMS	Geostationary Meteorological Satellite
GNP	Gross National Product
GOCART	GOddard Chemistry Aerosol Radiation and Transport
GOES	Geostationary Operational Environmental Satellite
GOFS	Global Ocean Flux Study
GOME	Global Ozone Monitoring Experiment
GOME-CHEM	Global Ozone Monitoring Experiment-CHEMistry
GOMOS	Global Ozone Monitoring by Occultation of Stars
GOOS	Global Ocean Observing System
GOCR	Global Ocean Carbon Research program
GPM	Global Precipitation Measurement
GPS	Global Positioning System
GRACE	Gravity Recovery And Climate Experiment
GSA	Geological Society of America
GSM	Global Simulation Model
GST	Global Surface Temperature
GTOS	Global Terrestrial Observing System
GWP	Global Warming Potential
HARC	Human dimensions of the ARCtic system
HB	Hydrological Block
HC	HydroCarbon

HDI	Human Development Index
HIRHAM-4	HIgh-Resolution High Atmosphere Model
HIV	Human Immunodeficiency Virus
HLZ	Holdridge Life Zone
HOE	Health Organizations in Eurasia
HOT	Hawaii Ocean Time series
HSB	Humidity Sounder for Brazil
HSRL	High-Spectral-Resolution Lidar
IA	Integrated Assessment
IABP	International Arctic Buoy Program
IAHS	International Association of Hydrological Sciences
IAMAS	International Association of Meteorology and Atmospheric Sciences
IAPP	International Arctic Polynya Program
IASC	International Arctic Science Committee
IASI	Infrared Atmospheric Sounder Interferometer
IBP	International Biological Program
ICAR	International Conference on Aeolian Research
ICARTT	International Consortium for Atmospheric Research on Transport and Transformation
ICD	Interface for Control of the Database
ICE	Indice Biotico Esteso
ICESat	Ice, Cloud, and land Elevation Satellite
ICI	Interface for Control of Identifiers
ICV	Interface for Control of Visualization
IDAF	Initiative DEBITS in AFrica
IEA	International Energy Agency
IEEE	Institute of Electrical and Electronics Engineers
IEO	International Energy Outlook
IFA	International Franchise Association
IGAC	International Global Atmospheric Chemistry
IGBP	International Geosphere–Biosphere Program
IGBP PAGES	International Geosphere–Biosphere Program Pilot Analysis of Global Ecosystems
IGCC	Integrated Gasification Combined Cycles
IGES	Institute for Global Environmental Strategies
IGOS	Integrated Global Observing Strategy
IHDP/GEC	International Human Dimensions Program/Global Environmental Change
IHDP	International Human Dimensions Program
IHP	International Hydrology Program
IIASA	International Institute for Applied System Analysis
IISD	International Institute for Sustainable Development
IM	Illumination Model
IMF	International Monetary Fund

INDOEX	INDian Oceanic EXperiment
INI	International Nitrogen Initiative
INTEX-NA	INTercontinental Chemical Transport EXperiment-North America
IOC	Intergovernmental Oceanographic Commission of UNESCO
IPCC	Intergovernmental Panel on Climate Change
IR	InfraRed
IREE	Institute of Radio Engineering and Electronics
ISAC	International Study of Arctic Change
ISCCP	International Satellite Cloud Climatology Project
ISEW	Index of Sustainable Economic Welfare
ISF	Influence of Stochastic Forcing
ISO	International Organization for Standardization
ISPM	Independent Summary for Policy-Makers
ISY	International Sea Year
ITCT	Intercontinental Transport and Chemical Transformation
ITCZ	Inter-Tropical Convergence Zone
ITEX	International Tundra EXperiment
ITOP	International Transport of Ozone and Precursors
IUCN	International Union for the Conservation of Nature and natural resources
IWMI	International Water Management Institute
JAXA	Japan Aerospace eXploration Agency
JERS	Japanese Earth Resources Satellite
JGOFS	Joint Global Ocean Flux Study
JRC	European Union's Joint Research Center
KAFEC	Kansk-Achinsk's Fossil-Energy Complex
KBG	Kara Bogaz Gol
KP	Kyoto Protocol
LACE 98	Lindenberg Aerosol Characterization Experiment 1998
LAI	Leaf Area Index
LAII	Land–Atmosphere–Ice Interaction
lidar	light detection and ranging
LIS	Lightning Imaging Sensor
LRTP	Long-Range Transport Potential
LSAT	Land Surface Air Temperature
LSM	Land Surface Model
LTER	Long-Term Ecological Research
LW	Long Wave
LWC	Liquid Water Content
LWD	LongWave Deficit
MABL	Marine Atmospheric Boundary Layer
MAPS	Measurement of Air Pollution from Satellites
MAPSS	Mapped Atmosphere–Plant–Soil System
MAS	MODIS Airborne Simulator

MBB	Marine Biota Block
MBRAI	Monterey Bay Aquarium Research Institute
MBWB	Model of Biospheric Water Balance
MEA	Millennium Ecosystem Assessment
MEAP	Millennium Ecosystem Assessment Program
MEF	Model for Energy Flow
MERIS	MEdium Resolution Imaging Spectrometer instrument
MET	METeorology
METOP	METeorological Operational Polar mission
METSAT	METeorological SATellite
MFB	Model of the Functioning of Biota
MGC	Minor Gas Constituent
MGNC	Model of Global Nitrogen Cycle
MGOC	Model of Global Oxygen Cycle
MIPAS	Michelson Interferometer for Passive Atmospheric Sounding
MIRAS	Microwave Imaging Radiometer using Aperture Synthesis
MISR	Multi-angle Imaging SpectroRadiometer
MISRC	Management Information Systems Research Center
MIT	Massachusetts Institute of Technology
MLS	Microwave Limb Sounder
MM5	Mesoscale Model 5
MMF	Multiple Multiplicative Factor
MMT	Model for heavy Metal Transport through foodchains
MOBY	Marine Optical BuoY
MODIS	MODerate resolution Imaging Spectroradiometer
MOPITT	Measurements Of Pollution In The Troposphere
MOS	Marine Observation Satellite
MOS/IRS	Modular Optoelectronic Scanner/Indian Remote Sensing
MOSS	Monterey Ocean Observing System
MOT	Model for the process of Oil hydrocarbon Transport
MOZART	Model for OZone And Related chemical Tracers
MPI	Max-Planck-Institute
MPR	Model for the Process of Radionuclide transport
MPT	Model for Pollution Transport
MRF	Model of River Flow
MSD	Macromolecular Structure Database
MSOM	Method of Self-Organizing Models
MSSA	Multi-channel Singular Spectrum Analysis
MTI	Multispectral Thermal Imager
MWD	Model for the Water Dynamics of the Arctic Basin
MWR	MicroWave Radiometer
MWS	Model of Water Salinity
MWT	Model for calculating Water Temperature
NACP	North American Carbon Program
NADP	National Atmospheric Deposition Program

NAFTA	North American Free Trade Agreement
NAM	Northern Annual Mode
NAO	North Atlantic Oscillation
NAPAP	National Acidic Precipitation Assessment Program
NARCM	Northern Aerosol Regional Climate Model
NASA	National Aeronautics and Space Administration
NASA-CASA	NASA Carnegie–Ames–Stanford Approach
NASDA	NAtional Space Development Agency of Japan
NAT	Nocturnal Air Temperature
NBP	Net Biome Productivity
NCAR	National Center for Atmospheric Research
NCDC	National Climatic Data Center
NCEP	National Center for Environmental Prediction
NDVI	Normalized Difference Vegetation Index
NEAR	North East Asia Region
NEE	Net Ecosystem Exchange
NEON	National Ecological Observatory Network
NEP	Net Ecosystem Production
NEW	North East Water polynya
NH	North Hemisphere
NLCD	National Land Cover Data
NM	Nutrient Model
NMHC	Non-Methane HydroCarbon
NOAA	National Oceanic and Atmospheric Administration
NOW	NOrth Water polynya
NPOESS	National Polar-orbiting Operational Environmental Satellite System
NPP	Net Primary Production
NPS	Nuclear Power Station
NSS	Nature–Society System
OACES	Ocean Atmosphere Carbon Exchange Program
OAII	Ocean–Atmosphere–Ice Interaction
OASIS	Observational Activities for the Study of the Indian Ocean climate System
OCO	Orbiting Carbon Observatory
OCTS	Ocean Color Temperature Scanner
ODS	Ozone Destroying Substance
OECD	Organisation for Economic Co-operation and Development
OFP	Oceanic Flux Program
OM	Organic Matter
ONR	Office of Naval Research
OOPC	Ocean Observations Panel for Climate
OOS	Ocean Observing System
OPEC	Organization of Petroleum Exporting Countries
OSPAR	OSlo/PARis convention

p_a	Partial pressure in the atmosphere
PACE	Permafrost And Climate in Europe
PAGES	Pilot Analysis of Global EcoSystems
PAHO	Pan American Health Organization
PALE	Paleoclimates of Arctic Lakes and Estuaries
PAR	Photosynthetic Active Radiation
PARCS	Paleoenvironmental ARCtic Science
PBL	Planetary Boundary Layer
PCM	Parallel Climate Model
PDV	Pacific Decadal Variability
PhA	Phytogenic Aerosol
PIK	Potsdam-Institut für Klimafolgenforschung
PIRA	Petroleum Industry Research Associates
PIRATA	PIlot Research moored Array in the Tropical Atlantic
POC	Permanganate Oxidizable Carbon
POLDER	POLarization and Directionality of the Earth's Reflectances
	Princeton Ocean Model
POP	Persistent Organic Pollutant
PPP	Purchasing Power Parity
PR	Precipitation Radar
PSM	Pollution Simulation Model
RA	Radar Altimeter
RADAM	RADar na AMazônia
RAISE	Russian–American Initiative on Shelf-land Environments
RAL	Rutherford Appleton Laboratory
RAMS	Regional Atmospheric Modeling System
RANS	Russian Academy of Natural Sciences
RCTM	Regional Chemical Transport Model
RegCM2	Regional Climate Model-2
RF	Radiative Forcing
RGGI	Regional Greenhouse Gas Initiative
RH	Radiative Humidity
RIDGE	Ridge Interdisciplinary Global Experiment
rms	root-mean-square
RPI	Retail Price Index
RS	Remote Sensing
RTDI	Research and Technological Development and Innovation
SA	Sulfate Aerosol
SAFARI	Southern Africa Fire–Atmosphere Research Initiative
SAGE	SOLAS Air–sea Gas Exchange
SAM	Southern Annual Mode
SAMUM	SAharan Mineral dUst experiMent
SAR	Synthetic Aperture Radar
SAS	Surface Active Substance
SAT	Surface Air Temperature

SAVI	Soil-Adjusted Vegetation Index
SB	Service control Block
SBI	Shelf–Basin Interactions project
SC	Sun Constant
SCALDS	Social Cost of Alternative Land Development Scenarios
SCE	Snow Cover Extent
SCIAMACHY	SCanning Imaging Absorption SpectroMeter for Atmospheric CartograpHY
SCOPE	Scientific Committee on Problems of the Environment
SDS	Scott Data System
SEARCH	Study of Environmental ARctic CHange
SeaWiFS	Sea Wide-Field-of-view Sensor
SEDAAR	Strategic Environmental Distributed Active Archive Resource
SEVERI	Spinning Enhanced VisiblE and infra Red Imager
SGM	Spatial Global Model
SGP	Southern Great Plains
SH	Southern Hemisphere
SHADE	SaHAran Dust Experiment
SHEBA	Surface HEat Budget of the Arctic Ocean project
SHF	Super High Frequency
SIAM	Society for Industrial and Applied Mathematics
SiB2	Simple Biosphere model-2
SIM-CYCLE	SIMulation model of carbon CYCle in Land Ecosystems
SIMS	Synthesis, Integration, and Modeling Study
SLIP	St. Lawrence Island Polynya
SMOS	Soil Moisture and Ocean Salinity
SO	Southern Oscillation
SOLAS	Safety Of Life At Sea
SOOP	Ship-of-Opportunity Program
SP	Special Publications
SPARC	Stratospheric Processes And their Role in Climate
SPIE	International Society for Optical Engineering
SPM	Summary for Policy-Makers
SRB	Surface Radiation Budget
SRES	Special Report on Emissions Scenarios
SS	Simulator of Scenarios
SSCRO	Simulation System to Control the Regional Ozonosphere
SSM/I	Special Sensor Microwave/Imager
SSMAE	Spatial Simulation Model of the Arctic Ecosystem
SST	Sea Surface Temperature
STEP	Solar–Terrestrial Energy Program
STIB	Stratosphere Troposphere Interactions and the Biosphere
STOCHEM	A global 3-D Lagrangian chemistry transport model
STT	Scientific and Technical Translation

SW	ShortWave
TAO	Tropical Atmosphere Ocean Project
TAR	Third Assessment Report
TBI	Trent Biotic Index
TD	Technical Document
TEM	Terrestrial Ecosystem Model
TEMIS	Tropospheric Emission Monitoring Internet Service
TEPA	Taiwan Environment Protection Administration
THC	ThermoHaline Circulation
TIR	Third IPCC Report
TIROS-N	Television InfraRed Observational Satellite-Next
TMI	TRMM Microwave Imager
TO	Tropospheric Ozone
TOA	Top Of Atmosphere
TOGA	Tropical Oceans and Global Atmosphere experiment
TOMS	Total Ozone Mapping Spectrometer
TOPEX	TOPography EXperiment
TOVS	TIROS Operational Vertical Sounder
TR	Technical Report
TRACE-P	TRansport And Chemical Evolution over the Pacific
TREND	Technology REsearch aNd Development
TRITON T	TRIangle Trans-Ocean buoy Network
TRMM	Tropical Rainfall Measuring Mission
TSAVI	Transformed SAVI
TSP	Total Soluble Protein
UAE	United Arab Emirates
UARS	Upper Atmospheric Research Satellite
UCAR	University Corporation for Atmospheric Research
UCSF	University of California, San Francisco
UDS	Uniform Data Systems
UHF	Ultra High Frequency
U.N.	United Nations
UNCED	U.N. Conference on Environment and Development
UNDP	U.N. Development Program
UNDP/GEF	U.N. Development Program/Global Ecological Fund
UNEP	U.N. Environment Program
UNESCO	U.N. Educational, Scientific and Cultural Organization
UNFCCC	U.N. Framework Convention on Climate Change
UQL	Upper Quasi-homogeneous Layer
USGCRP	U.S. Global Change Research Program
UV	UltraViolet
VHRR	Very High Resolution Radiometer
VI	Vegetation Index
VIRS	Visible InfRared Scanner
VOC	Volatile Organic Compound

WB	World Bank
WBCSD	World Business Council for Sustainable Development
WCRP	World Climate Research Program
WEO	World Energy Outlook
WG-I	Working Group I (IPCC)
WHO	World Health Organization
WI	Wuppertal Institute
WMI	Weather Modification Inc.
WMO	World Meteorological Organization
WOCE	World Ocean Circulation Experiment
WS	Wind Scatterometer
WSSD	World Summit on Sustainable Development
WTF	Wet Tropical Forest
WWW	World Weather Watch
XRF	X-Ray-Fluorescent spectrometer

About the authors

Vladimir F. Krapivin was educated at the Moscow State University as a mathematician. He received his Ph.D. in geophysics from the Moscow Institute of Oceanology in 1973. He became Professor of Radiophysics in 1987 and Head of the Applied Mathematics Department at the Moscow Institute of Radioengineering and Electronics in 1972. He was appointed Grand Professor in 2003 at the World University for Development of Science, Education, and Society. He is a full member of the Russian Academy of Natural Sciences and Balkan Academy of Sciences, New Culture, and Sustainable Development. He has specialized in investigating global environmental change by the application of modeling technology and has published 20 books in the fields of ecoinformatics, game theory, and global modeling.

Costas A. Varotsos received his B.Sc. in Physics at Athens University in 1980, and a Ph.D. in Atmospheric Physics in 1984. He was appointed Assistant Professor in 1989 at the Laboratory of Meteorology of the Physics Department of the Athens University, where he also set up the Laboratory of the Middle and Upper Atmosphere. In 1999 he became Associate Professor of the Department of Applied Physics at Athens University. He is Editor of the *International Journal of Remote Sensing* and Advisor to the *Environmental Science & Pollution Research* journal. He has published more than 300 papers and 20 books in the fields of atmospheric physics, atmospheric chemistry, and global change.

1

Globalization and biogeochemical cycles

1.1 GLOBAL CHANGES OF BIOGEOCHEMICAL CYCLES

1.1.1 Key aspects of global biogeochemical cycles

Interactions between the abiotic factors of the environment and the living organisms of the biosphere are accompanied by a continuous matter cycle in nature. Different species of living organisms assimilate substances needed for their growth and life support emitting to the environment products of metabolism and other complex mineral and organic compounds of chemical elements in the form of non-assimilated food or dead biomasses. As a result of biospheric evolution, a stable chain of global biogeochemical cycles has been formed whose violation in the second half of the 20th century has made humankind face many principal problems such as an unpredicted climate change due to the greenhouse effect, a decrease of biodiversity, progressing desertification, and many others. Indeed, questions about what's the matter with the Earth's climate and what are the consequences of ozone layer depletion remain unanswered despite huge economic expenditures on their study. It is now clear that these and other nature protection questions cannot be answered without developing an effective global monitoring system based on the Global Model of the Nature–Society System (GMNSS), one of the basic units of which is the unit simulating the biogeochemical cycles of basic chemical elements of the biosphere (Zhu and Anderson, 2002; Kondratyev *et al.*, 2002b). It is this approach, by implementing ideas put forward in the Kyoto Protocol (KP), that will make it possible to assess the anthropogenic fluxes of pollutants and to estimate permissible emissions of carbon, chlorine, sulfur, fluorine, methane, and other chemical elements to the environment as well as to regulate the problems of the GHG emissions market (Pan, 2005; Kalb, Pamsters, and Siebers, 2004).

Fundamental connections between the characteristics of the biological state of the environment, such as biodiversity in ecosystems, the state and dynamics of food

chains, and interactions of the biosystem with the cycle of biogenic elements, have been poorly studied, both in land and in water ecosystems. Among the numerous questions resulting from studies of the global biogeochemical processes the following are of key importance:

(1) What physical, biological, chemical, and social processes are basic to regulation of the cycles of carbon, nitrogen, sulfur, water, and other elements both in space and in time?
   - What mathematical relations are determinants in the parameterization of biological processes in the computer models of biogeochemical cycles?
   - What are the dependences between biodiversity, stricture of ecological chains, and biogeochemical cycles in land and water ecosystems?
   - What processes are determinants in the transport of biogenic salts and pollutants in space, in general, and between various ecosystems, in particular?
   - What are mechanisms that relate one biogeochemical cycle to another, and do the general principles of parameterization of these relations exist or do they depend on the type of chemical elements and ecosystems under consideration?

(2) What are the forms and ways of anthropogenic interference with global biogeochemical cycles?
   - How do humans influence biogeochemical cycles and change the rates and spatial distributions of chemical elements that form the inputs and outputs of numerical models, and what are the consequences of this interference?
   - How does a change in land use strategy affect the re-distribution of chemical elements in space and in time?
   - What anthropogenic pollutants are involved in the biogeochemical influence on ecosystems, and how to predict them?

(3) What mechanisms control the ability of ecosystems to rapidly restore themselves and what are the indicators that reflect this ability of ecosystems?
   - How does the introduction of new species to ecosystems and the appearance of new, unstudied diseases affect the development of biogeochemical cycles in land and water ecosystems?
   - What feedbacks between ecosystems and climate are critical, and how are these feedbacks parameterized in computer models?
   - Can the data on the past biogeochemical cycles be used for their prediction in the future?
   - What basic parameters and characteristics of ecosystems affect their ability to restore themselves after anthropogenic forcings?

The global CO_2 biogeochemical cycle is in the center of attention of scientists. Specialists from many countries are trying to answer the following questions:

(i) What concentrations of CO_2 can be expected in future with present or predicted rates of organic fuel burning?

(ii) What climate changes can result from increased concentrations of CO_2?
(iii) What are the consequences of climate change for the biosphere?
(iv) What can humankind do to either reduce the negative consequences of climate change or prevent them?

Clearly, according to rough model estimates, the industrial world should now search for new sources of energy that would decrease the rates of organic fuel burning and, hence, reduce external forcings on natural biogeochemical cycles. The atmosphere is one of the important reservoirs involved in formation of these cycles. Overall, it is the chemistry and physics of atmospheric processes that suffer changes, without a study of which reliable assessment of the state of the atmosphere and the dynamics and photochemical processes in it is impossible (Brasseur, 2005).

During the last decade the words ''greenhouse effect'' could be seen in numerous publications on the problems of global climate change on Earth (Ichikawa, 2004). This term implies all the descriptions of the effects appearing in the climate system that are connected with the number of natural and anthropogenic processes. On the whole, the notion of the greenhouse effect refers to an explanation of changes in the atmospheric thermal regime, as a result of the impact of some gases on the process of solar radiation absorption. Many gases are characterized by high stability and long residence in the atmosphere (Table 1.1). Carbon dioxide is one of them. As for the role of CO_2, more than a century ago Arrhenius (1896) was the first to draw the conclusion that its emission in fuel burning can lead to climate warming. In subsequent decades this sagacious conclusion turned out to be an accurate though gloomy forecast. After all, in the global historical long-range perspective, CO_2 content in the atmosphere had been changing stably with variations of about 20 ppm, for at least 11,000 years before the industrial epoch. In this long-term context the anthropogenic increase of atmospheric CO_2 by $\sim$100 ppm for the last 200 years is a dramatic change in the global carbon cycle. This increase is connected with emissions

Table 1.1. Characteristics of the most important greenhouse gases.

Greenhouse gas	*Lifetime in the atmosphere* (yr)	*Anthropogenic emission* (MtC) (%)	*Average concentration* (*n*)	*Distribution in the atmosphere* (%)	*Increase in speed* (%)	*Percent of total*
CO_2	3–5	1,585.7 (84)	362 ppmv	76	0.5	99.438
NO_x	100–150	97.5 (5)	308 ppbv	6	0.25	0.471
CH_4	11	175.8 (9)	1,815 ppbv	13	1.0	0.084
Fluorocarbons (HCFC, HFC, PFC)	75–111	31.4 (2)	0.34–0.54 ppbv	5	7	0.007

ppmv = parts per million by volume, ppbv = parts per billion by volume.

to the atmosphere of ~400 petagrams of C (PgC)[1] during this period mainly due to deforestation and fossil fuel burning.

Numerous long-term observations in various latitudinal belts show a high level of correlation between temperature and CO_2 content. The atmosphere–ocean interaction contributes most to this dependence. Though the atmosphere and the ocean are in equilibrium with respect to CO_2 exchange, this equilibrium is still regularly violated. The most serious causes of this violation are

(1) SST variations;
(2) changes in ocean volume; and
(3) changes in the regime of the vertical circulation of the ocean.

In general, the efficiency of these causes can be characterized by the following ratio of the forcing on CO_2 concentrations in the atmosphere. The first cause contributes about 65% to the change of CO_2 partial pressure in the atmosphere (p_a). The remaining 35% are contributed by the second and third causes. Quantitatively, this relationship is characterized by a 6% increase of atmospheric CO_2 partial pressure per 1°C increase of the temperature of the ocean's upper layer. Also, a 1% decrease of the ocean volume raises p_a by 3%. On the whole, as Perry (2001) notes, understanding the role of the atmosphere–ocean system in global changes requires a study of its dynamics with consideration of various kinds of information over a long historical period. Of course, it is reasonable here to use the respective models and data from the paleocenographic record. This is only possible by coordinating various programs on the study of the atmosphere–ocean system.

An assessment of the greenhouse effect requires a complex consideration of the interaction of all processes of energy transformation on Earth. However, in the diversity of processes (from astronomical to biological) that affect the climate system on various time scales, there exists a hierarchy in their significance. But this hierarchy cannot be constant, since the role of some processes can vary widely in their significance for climatic variations. Consideration of one factor in isolation simplifies the analysis of its impact on climate. In fact, the impact of the greenhouse effect is determined by surface temperature T_L exceeding effective temperature T_e. The Earth's surface temperature T_L is a function of surface emissivity κ. The effective temperature T_e is a function of emissivity α of the atmosphere–land–ocean system. In general, the parameters κ and α depend on many factors, in particular on the CO_2 concentration in the atmosphere. There are a lot of both simple and complicated numerical models where attempts have been made to parameterize these dependences. Unfortunately, there is not a single model that can meet the requirements of adequacy and reliably describe the prehistory of the climatic trends on Earth. Nevertheless, we can state that the greenhouse effect depends non-linearly on the difference $T_L - T_e$ (i.e., on atmospheric turbidity), especially in the long-wave region. The more CO_2 in the atmosphere, the stronger the atmospheric turbidity. The strongest effect of CO_2 on atmospheric turbidity is in the long-wave region

[1] A petagram is equal to 10^{15} grams.

12 μm–18 μm. This effect is weaker in the wavelength intervals 7 μm–8 μm, 9 μm–10 μm, 2.0 μm, 2.7 μm, and 4.3 μm. It is clear that with the increasing partial pressure of CO_2 in the atmosphere the role of various bands of CO_2 will grow, and this means that, with intensified CO_2 absorption bands, the upward long-wave radiation flux will decrease. At the same time, the downward long-wave radiation flux on the Earth surface will increase. From the available estimates, a reduction of the upward and increase of the downward fluxes are estimated at $2.5\,W\,m^{-3}$ and $1.3\,W\,m^{-2}$, respectively.

Thus, to estimate the level of the greenhouse effect due to CO_2 and other GHGs (Table 1.2), it is necessary to know how to predict their concentration in the atmosphere, with all feedbacks in their global biogeochemical cycle taken into account (Watson *et al.*, 2000). This problem touches on several spheres of science: biogeochemistry, geochemistry, soil science, ecology, agrichemistry, geology,

Table 1.2. Greenhouse gases and global warming potentials (GWPs).

Gas	*100-year GWP*	ΔGWP (%)
Carbon dioxide (CO_2)	1	55
Methane (CH_4)	21	17
Nitrous oxide (N_2O)	310	5
HFC-23 (CHF_3)	11,700	0.96
HFC-125 (C_2HF_5)	2,800	0.75
HFC-134a (CH_2FCF_3)	1,300	0.34
HFC-143a (CF_3CH_3)	3,800	0.75
HFC-152a (CH_3CHF_2)	140	0.28
HFC-227ea (C_3HF_7)	2,900	0.69
HFC-236fa ($C_3H_2F_6$)	6,300	0.75
HFC-43-10mee ($C_5H_2F_{10}$)	1,300	0.75
Perfluoromethane (CF_4)	6,500	1.15
Perfluoroethane (C_2F_6)	9,200	0.75
Perfluorobutane (C_4F_{10})	7,000	0.87
Perfluorohexane (C_6F_{14})	7,400	0.75
Sulfur hexafluoride (SF_6)	23,900	0.30

oceanology, physiology, and radiochemistry. The present methods of global ecoinformatics enable the knowledge accumulated in these fields to be combined.

Of course, the global cycle of chemical elements should be studied not only to be able to assess the climatic consequences of anthropogenic activity but also to understand the consequences on environmental dynamics from the viewpoint of the quality and possibility of life. Since the cycles of the chemical elements in nature are closely connected with living substance activity, we can single out the geological, biogenic, and biological cycles of this rotation. The biogenic cycle includes sub-cycles, such as biogeochemical, biogeocenotic, and geochemical. Tables 1.3 through 1.9 give some estimates and parameters of these cycles.

1.1.2 Biogeochemical cycles in land ecosystems

Land ecosystems play an important role in the dynamics of biogeochemical cycles on Earth. Anthropogenic changes in vegetation cover affects biogeochemical cycles and, thereby, other processes, climate included. The most well-known and important biogeochemical cycles include the cycles of carbon, nitrogen, oxygen, phosphorus, and water. Biogeochemical cycles always involve equilibrium states: a balance in the cycling of the element between land surface compartments. Chemical elements participate in the processes of photosynthesis and respiration of plants, as well as their dying off, these processes form spatial transport of chemical elements between compartments and elements of land ecosystems. The most characteristic features of the biogeochemical cycles of individual chemical elements are as follows:

- The nitrogen cycle is a complicated biogeochemical cycle because it involves living parts and non-living parts including water, land, and air. Nitrogen is a very important element in that it is part of both proteins, present in the composition of the amino acids that make up proteins, and nucleic acids such as DNA and RNA, present in nitrogenous bases. The largest reservoir of nitrogen is the atmosphere, in which about 78% of nitrogen is contained as nitrogen gas (N_2). Nitrogen gas is "fixed" in a process called nitrogen fixation. Nitrogen fixation combines nitrogen with oxygen to create nitrates (NO_3).
- The oxygen cycle is the biogeochemical cycle that describes the movement of oxygen within and between its three main reservoirs: the atmosphere, the biosphere, and the lithosphere. The main driving factor of the oxygen cycle is photosynthesis, which is responsible for the modern Earth's atmosphere and life.
- The carbon cycle is the biogeochemical cycle by which carbon is exchanged between the biosphere, geosphere, hydrosphere, and atmosphere of the Earth. The cycle is usually thought of as four major reservoirs of carbon interconnected by pathways of exchange. The reservoirs are the atmosphere, the terrestrial biosphere (which usually includes freshwater systems and non-living organic material, such as soil carbon), the oceans, and sediments.
- The phosphorus cycle is the biogeochemical cycle that describes the movement of phosphorus through the lithosphere, hydrosphere, and biosphere. Unlike many other biogeochemicals, the atmosphere does not play a significant role in the

Table 1.3. Average dry air composition.

Gas	*Molecular weight*	*Average concentration (%)*	
		By volume	*By weight*
Nitrogen, N_2	28.016	78.084	75.53
Oxygen, O_2	32.000	20.946	23.14
Carbon dioxide, CO_2	44.010	0.0325	0.046
Carbon oxide, CO		$(0.8–5) \times 10^{-5}$	
Nitrogen protoxide, N_2O	44.01	$(2–5) \times 10^{-5}$	$7.6(10^{-5}$
Nitric oxide, NO		10^{-6}–10^{-4}	
Nitrogen dioxide, NO_2		10^{-6}–10^{-4}	
Sulphur dioxide, SO_2		7×10^{-7}–10^{-4}	
Ozone, O_3	48.000	$(0–5) \times 10^{-6}$–5×10^{-5}	$(0\text{-}1) \times 10^{-5}$–$10^{-4}$
Ammonia, NH_3		$\leq 10^{-4}$	
Formaldehyde, HCHO		$\leq 10^{-5}$	
Xenon, Xe	131.3	(8.7-9.0) × 10-6	$(3.6\text{-}3.7) \times 10^{-5}$
Hydrogen, H_2	2.016	5×10^{-5}	3×10^{-6}
Krypton, Kr	83.8	$(1.14–1.2) \times 10^{-4}$	$(2.9–3.3) \times 10^{-4}$
Methane, CH_4	16.04	$(1.2–2.0) \times 10^{-4}$	$(7.75–9) \times 10^{-5}$
Helium, He	4.003	$(5.24–5.3) \times 10^{-4}$	$(7.2–7.4) \times 10^{-5}$
Neon, Ne	20.183	1.818×10^{-3}	1.25×10^{-3}
Argon, ^{40}Ar	39.944	0.934	1.27
Water vapor, H_2O		≤ 4	
Radon, Rn	222.0	$(0.06–0.45) \times 10^{-16}$	6×10^{-18}

movements of phosphorus, because phosphorus and phosphorus-based compounds are usually solids at the typical ranges of temperature and pressure found on Earth.

- The essential steps of the sulfur cycle are
  (1) Mineralization of organic sulfur to the inorganic form, hydrogen sulfide (H_2S).
  (2) Oxidation of sulfide and elemental sulfur (S) and related compounds to sulfate (SO_4^{2-}).

Table 1.4. Evaluation of some parameters of the global cycle of chemical elements.

Parameter	*Parameter estimation*
Coefficient of molecular diffusion in the air at temperature $T_a = 0°C$ and pressure 1 atm.:	
Hydrogen	0.634
Water vapors	0.250
Oxygen	0.178
Carbon dioxide	0.139
Absolute gas constant, cal $mol^{-1}\,K^{-1}$	1.9872
Atmospheric mass (t):	
Total atmosphere	$(5.2–5.51) \times 10^{15}$
Troposphere (up to 11 km)	4×10^{15}
Quantity of moles in the atmosphere	1.8×10^{20}
Organic mass in photosynthesis (billion tons per year)	100
Land vegetation (%)	66
Plankton and algae (%)	34
Balance of photosynthesis (billion tons per year)	
Water consumption	130
Oxygen emission	155
Number of active volcanoes:	
Lava	527
Mud	220
Number of molecules in the atmosphere per square km	2.1×10^{35}
World metal consumption (billion tons per year)	
Iron	38
Aluminum, copper, zinc, lead	2
Other	0.3

(3) Reduction of sulfate to sulfide.
(4) Microbial immobilization of sulfur compounds and subsequent incorporation in the organic form of sulfur.

- The water cycle is the continuous circulation of water within the Earth's hydrosphere. As water moves through the cycle, it changes state between liquid, solid, and gas phases.
- Hydrogen is one of the constituents of water. It recycles as in other biogeochemical cycles. It is actively involved with the other cycles like the carbon cycle, nitrogen cycle, and sulfur cycle.

A detailed description of the biogeochemical cycles of carbon, nitrogen, phosphorus, sulfur, and water in land ecosystems has been given in a work of

Table 1.5. Character and origin of basic substances polluting the atmosphere.

Pollutant character	*Pollutant origin*
	Gases
Carbon dioxide	Natural and industrial potential carbon sources exist: volcanic activity, living organism respiration, fossil fuel combustion, cement production, changes in land use. Natural CO_2 fluxes into and out of the atmosphere exceed the human contribution by more than an order of magnitude. The rise in atmospheric CO_2 concentration closely parallels the emission history from fossil fuels and land use changes.
Carbon monoxide	Carbon monoxide is an odorless, colorless, and toxic gas. Sources of carbon monoxide: volcanic activity, internal combustion engines, unvented kerosene and gas space heaters, generators and other gasoline-powered equipment, tobacco smoke.
Hydrocarbons	Hydrocarbons are the simplest organic compounds that consist of only C and H atoms. Main sources of hydrocarbons are plants, bacteria, and internal combustion engines. Almost all usable supplies of hydrocarbons are obtained from combustion of coal, petroleum, and natural gas.
Organic compounds	An organic compound is any member of a large class of chemical compounds whose molecules contain carbon: carbonates, carbon oxides, and cyanides. Most organic compounds today are artificially produced: chemical industry, waste combustion, and different fuels.
Sulfuric gas and other sulfur derivatives	Sulfuric gas is the chemical compound with the formula SO_2. This important gas is the main byproduct of combustion of sulfur compounds and is of significant environmental concern. SO_2 is produced by volcanoes, sea breezes, fossil fuel combustion, bacteria, and in various industrial processes.
Nitrogen derivatives	Bacteria, anaerobic micro-organisms, and burning.
Radioactive substances	The principal sources of radionuclides released into the environment include nuclear weapon testing; fallout from accidents such as the Chernobyl accident in 1986 or from foundering of nuclear submarines; from the dumping of nuclear waste into the deep ocean and from discharges from nuclear power plants and nuclear reprocessing plants.

(*continued*)

Table 1.5 (*cont.*)

Pollutant character	*Pollutant origin*
	Particles
Heavy metals, mineral aggregates	Volcanic activity, meteorites, wind erosion, mist spray, industry, internal combustion engines.
Organic substances (natural and manufactured)	Forest fires, chemical industry, various fuels, waste burning, agriculture (pesticides).
Radioactive aerosols	Aerosols containing radionuclides are called radioactive aerosols. They have natural and artificial origin. Artificial radioactive aerosols are formed during nuclear explosions, in accelerator tunnels during operation, and during heating operation of activated metals.

Table 1.6. Classification of atmospheric pollutants. From Jacobson (2002a,b), Straub (1989).

Basic class	*Subclasses*	*Typical elements*	*Commentaries*
Inorganic gases	Oxides of nitrogen Oxides of sulfur Other inorganics	Nitrogen dioxide, nitric oxide Sulfuric acid, sulfur dioxide Carbon monoxide, chlorine, ozone, hydrogen sulfide, hydrogen fluoride, ammonia	One of the principal pollutants is sulfur dioxide, which is a corrosive acid gas that combines with water vapor in the atmosphere to produce acid rain.
Organic gases	Hydrocarbons Aldehydes, ketones Other organics	Benzene, butadiene, butene, ethylene, isooctane, methane Acetone, formaldehyde Acids, alcohols, chlorinated hydrocarbons, peroxyacyl nitrates, polynuclear aromatics	There are two main groups of hydrocarbons of concern: volatile organic compounds (VOCs) and polycyclic aromatic hydrocarbons (PAHs).
Aerosols	Solid particulate matter Liquid particulates	Dust, smoke Fumes, oil mists, polymeric reaction products.	Airborne particulate matter varies widely in its physical and chemical composition, source and particle size.

Table 1.7. Assessment of the annual volume of particles with radius less than 20 μm emitted to the atmosphere. From Jacobson (2002a, b).

Particle type	*Particle flow* (10^6 t yr^{-1})
Natural particles, soil and rock particles	100–500
Particles from forest fires and combustion of timber industry waste	3–150
Marine droplets	300
Volcanic dust	25–150
Particles generated in gas production	
Sulfates from H_2S	130–200
Ammonium salts from HN_3	80–270
Nitrates from NO_x	60–430
Hydrocarbons from vegetable aggregates	75–200
Particles as a result of manufacturing	10–90

Table 1.8. Sources of atmospheric pollution.

Pollution source	*Pollutant*
Natural	
Volcanoes, fumaroles, solfataras	Gases, volcanic dust, mercury vapors
Natural surges of natural gas and oil	Hydrocarbons
Mercury deposits	Mercury vapors
Sulfide deposits	Sulfuric gas
Radioactive ore deposits	Radon
Wind blowing from surface of seas and oceans	Chlorides, oil, sulfids
Underground coal fires	CO_2, CO, SO_2, hydrocarbons
Natural forest and steppe fires	Smoke
Plant transpiration	Water vapors, aromatic and other flying materials
Anthropogenic	
Incineration of hard and fluid organic material	CO_2, CO, SO_2, lead, hydrocarbons, mercury vapors, cadmium, nitric oxides
Metallurgy of black, colored, and rare metals	Dust, SO_2, mercury vapors, metals
Atomic industry	Radioactive materials
Nuclear blasts	Radioactive isotopes
Cement industry	Dust
Building blasts	Dust
Forest and steppe fires arising due to humans	Smoke
Oil and gas extraction	Hydrocarbons
Motor transport	CO, smog, nitric oxides

Table 1.9. Characteristics of some atmospheric components depending on their lifetime.

Component	*Length of time of life in the atmosphere*
Carbon dioxide	3–5 years
Carbon monoxide	0.1–3 years
Water vapor	9–10 days
Sulfur dioxide	3 days
Ozone	10 days
Hydrogen chloride	3–5 days
Nitric oxide	5 days
Nitrogen dioxide	5 days
Nitrogen protoxide	100–120 years
Ammonia	2–5 days
Methane	3 years
Freons	50–70 years

Kondratyev *et al*. (2003b). The main reservoirs of these elements are biomass and soil, between which matter exchange takes place through the respiration of plants, their photosynthesis, and dying off. Modeling of this exchange requires knowledge of the spatial structure of vegetation cover and its classification.

- Population density
- Potential natural vegetation
- Cropland extent from 1700 to present
- Grazing land extent
- Built-up land extent
- Major crops extent
- Land suitability for cultivation.

Of course, an accurate assessment of the fluxes of chemical elements in the atmosphere–vegetation–soil system is only possible with a detailed inventory of land covers. For instance, Fang *et al*. (2001) have undertaken such an inventory for seven time periods over the territory of China, including both planted and natural forests. It was shown that a maximum rate ($0.035\,\mathrm{PgC\,yr^{-1}}$) of carbon assimilation from the atmosphere was observed between 1989 and 1993. Under this, different types of forest had various time periods for a maximum rate of carbon assimilation. This confirms

the fact that for accurate and reliable calculation of carbon fluxes in the atmosphere–vegetation–soil system we need to understand the characteristics of vegetation covers of different types distributed in space and time. And since there is no such concentrated data, all available estimates of CO_2 sinks on land cannot be considered reliable. This is confirmed by data of the structural analysis of forest ecosystem biodiversity in South-East Asia, the Far East, and Japan held by the Institute for Global Environmental Strategies (IGES), in which estimates of the rates of forest degradation are given (Inoue and Isozaki, 2003). As Austin *et al.* (2004) have shown, the sporadic nature of water availability in arid and deserted territories is the cause of great shifts in the C/N ratio and, hence, considerable heterogeneities in the biogeochemical cycles of these territories.

From the estimates of Stoll-Kleemann and O'Riordan (2004), about 70% of the land surface are anthropogenically affected causing changes in biodiversity thousands of times faster than would take place naturally. Global biodiversity cannot be maintained without changing the strategy of human behaviour in the sphere of environmental protection. Therefore, we should expect a crisis in biodiversity, unless international cooperation toward its protection becomes effective.

1.1.3 The regular dependence of water ecosystems on biogeochemical cycles

The global scales of variability of the biogeochemical cycles of many elements raises the problem of how to control the state of water ecosystems not only taking local sources of pollution into account, but also, and to a greater extent, distant transports of chemical matter and biological pollution. The input of various substances into water ecosystems leads to a degradation of fish populations and a change in sanitary conditions for the population in adjacent regions. The ways undesired substances get into water ecosystems are diverse, including river and shore runs-off as basic highways of pollutant propagation. Therefore, the protection of water ecosystems under the present-day conditions of globalization requires technologies and systems to control additional fluxes of nitrogen and phosphorus which minimize oxygen balance violation and preserve the natural trends of living element biomass. As Fourie *et al.* (2004) noted, it is especially important for water ecosystems in many regions of Africa, where the atmosphere is the sole external source of additional biogenic elements.

Inland water ecosystems are divided into freshwater and saltwater ecosystems. The simplest scheme of life organization in these ecosystems consists in interactions of living elements with abiotic components (penetration of light, water currents, dissolved nutrient concentrations, and suspended solids). The producers supply O_2 to the aquatic systems through photosynthesis. This O_2 is then used by the producers, consumers, and decomposers through aerobic respiration. CO_2 enters an aquatic system from the atmosphere and through the aerobic respiration by producers, consumers, and decomposers and is removed by photosynthesizing producers. The concentration of oxygen in water depends on the amount of pollutant entering the ecosystem. These pollutants, depending on their type, can affect aquatic organisms directly, and through the process of eutrophication indirectly. As a result, the input of

pollutants to the water ecosystem leads to a change of its role in the gas exchange with the atmosphere.

There are no fewer than 1,500 substances recognized as pollutants in freshwater ecosystems. Among them are the following:

- *Acids and alkalis*. Most freshwater lakes, streams, and ponds have a natural pH in the range of 6 to 8. Acid deposition has many harmful ecological effects when the pH of most aquatic systems falls below 6 and especially below 5.
- *Anions*. The most toxic form of cyanide is free cyanide, which includes the cyanide anion itself and hydrogen cyanide, HCN, either in a gaseous or aqueous state. One teaspoon of a 2% cyanide solution can kill a person.
- *Detergents*. There are two kinds of detergents with different characteristics: phosphate detergents and surfactant detergents. Detergents that contain phosphates are highly caustic, and surfactant detergents are very toxic.
- *Gases*. Some gases that can harm aquatic freshwater life include chlorine, ammonia, and methane.
- *Heat*. Respiration and growth rates may be changed and these may alter the feeding rates of organisms. The reproduction period may be brought forward and development may be speeded up. Parasites and diseases may also be affected. An increase of temperature also means a decrease in oxygen solubility.
- *Heavy metals*. The most common heavy-metal pollutants are arsenic, cadmium, chromium, copper, nickel, lead, and mercury. Some metals, such as manganese, iron, copper, and zinc, are essential micronutrients. Each type of heavy metal in its own way affects water ecosystem biochemistry and can accumulate in bottom deposits and in the biomass of living elements.
- *Nutrients*. Too many nutrients stimulate the rapid growth of plants and algae, clogging waterways and sometimes creating blooms of toxic blue-green algae. This process is called eutrophication.
- *Organic pollution*. Organic pollution occurs when large quantities of organic compounds, which act as substrates for micro-organisms, are released into watercourses. Organic pollutants consist of proteins, carbohydrates, fats, and nucleic acids in a multiplicity of combinations. Organic pollution affects the organisms living in a stream by lowering the oxygen available in the water.
- *Pathogens*. A pathogen is an organism that produces a disease.

The process of eutrophication is the most widespread phenomenon in the life of water ecosystems. Too much nitrogen and phosphorus leads to a rapid growth of phytoplankton or algae biomass, and as a result, the content of oxygen in the water decreases sharply, and the mortality of living organisms grows substantially. Gas exchange with the atmosphere is violated. From available estimates, the share of eutrophicated lakes in different continents constitutes Asia (54%), Europe (53%), North America (48%), South America (41%), and Africa (28%). In the present-day world, it is difficult to differentiate the anthropogenic process of eutrophication from the natural one because of globalized biogeochemical cycles and difficult control of the fluxes of chemical elements through the atmosphere and river run-off.

1.2 INTERACTION BETWEEN GLOBALIZATION PROCESSES AND BIOGEOCHEMICAL CYCLES

1.2.1 The interplay between nature and society

Globalization processes are so versatile and complicated that their study, parameterization, and prediction require a trans-disciplinary approach. Van der Leeuw and Aschan-Leygonie (2000) have stated that in both physical and life sciences (and especially in social sciences) it is impossible to avoid a trans-disciplinary approach to environment problems. Here the theory of complex systems saves the day because it makes it possible to understand and interpret the differences between "cultural" and "natural" processes, as well as to some extent to explain the difference between the notions of "resilience" and "sustainability". The resilience of socio-natural systems in many situations depends on the capacity of the human communities involved to process all the information necessary to deal effectively with the complex dynamics of the system as a whole. Rosenberg (2001) develops an erudite and lively critique of the contemporary globalization theory, which most experts connect with the notion of sustainability. His arguments are that fashionable preoccupations with spatiality have generated deep intellectual confusions that stand in the way of a clear understanding of the modern world. It is shown how these confusions ultimately condemn globalization theorists to a peculiar and quixotic stance. In general, the advocates of globalization believe that all global and regional problems can be solved automatically through free trade. An unusual examination of Chomsky's libertine views on global economic hegemony has been given by Fox (2001). The notion of "free trade" as a universal means to solve the economic problems of Third World countries is a direct deception and leads to their further enslavement by big companies. Even in the case of former U.S.S.R. countries and Russia, as a large and rich-in-natural-resources country, this "solution" has turned out to be counterproductive (Nechaev, 1997; Kondratyev, 2005; Malinetskii, 2007).

The program put forward by the international organization "Nature and Society Forum" is dedicated to the study of the nature–society interaction. The main goal of this program is to promote the health and well-being of human beings and the environment through

(1) a deeper understanding by the community of the processes of life, the place occupied by humans in nature, as well as the health and environmental issues facing us today;
(2) encouraging informed discussions and debates on the practical meaning of this understanding, for individuals, families, organizations, and for society as a whole; and
(3) communicating the outcome of the Forum's activities as widely as possible through publications and the Internet.

These and similar general postulates direct, to some extent, public opinion toward regulating human–environment relationships with the view of getting a reasonable

and well-balanced result. Unfortunately, it is impossible with this approach to divide the world population into groups of influence. Such a division into countries and groups of countries with the same level of economic development cannot be considered optimal. A mechanism for calculation of the level of survivability of one group suggested by Kondratyev *et al.* (2004a) enables us to develop a global model of influence and to find a solution with it. This approach will be discussed in detail in Section 6.6.2.

The problem of nature–society interaction in the context of global change in the environment and climate has been discussed in detail at the All-World Conference on Climate Change in Moscow (Izrael *et al.*, 2004) and at the APEC Summit-2007 (September 2007, Sydney, Australia). The "Sydney Declaration on Climate Change" was signed on September 8th, 2007 by 21 APEC leaders. It indicates the wish of signatories to work toward non-binding "inspirational" goals on energy efficiency per unit of GDP. In this connection, Australian Prime Minister John Howard said that 21 leaders agreed on three very important and quite specific things: "Firstly, the need for a long-term inspirational, global emissions reduction goal ... Secondly, the need for all nations, no matter what their stage of development, to contribute, according to their own capacities and their own circumstances, to reducing greenhouse gases. Thirdly, we have agreed on specific APEC goals on energy intensity and forestry and we've also agreed on the important role of clean coal technologies."

In particular, Bolin (2004), while emphasizing the anthropogenic character of the observed climate change, still recognizes the uncertainties in assessments of sensitivity of the climate system to human impacts. This uncertainty leads to the fact that neither models nor expert estimates can determine in detail the possible characteristics of climate changes or how rapidly and where they will take place, and to what extent they will affect the well-being of population. Here a limited knowledge of biogeochemical cycles and the role played in them by the human factor contributes most to this uncertainty. The impact of the growing concentration of CO_2 and aerosols in the atmosphere on greenhouse warming is directly proportional, and this takes place both naturally and due to anthropogenic factors.

The greenhouse effect estimated by the equivalent concentration of CO_2 and aerosol in the atmosphere constitutes $2.7\,W\,m^{-2}$ and $-1.3\,W\,m^{-2}$, respectively. But here we should point out the functional difference between these impacts consisting in that whereas the life time of aerosols in the atmosphere is a week to a month, GHGs can reside in the atmosphere from decades to centuries. It is in this difference that the inertial uncertainty of climate changes lies.

1.2.2 Sustainable development and environmental disasters

Climate changes manifest themselves both on global and regional scales. Natural catastrophes are one manifestation of these changes. Their intensity and number increased year on year. A serious increase in the number of great natural catastrophes was observed between 1960 and 2005. The frequency of these events more than doubled during this period. Subsequent years were characterized by various

anomalous phenomena which confirm the instability and poor predictability of the occurrence of natural anomalies unfavorable for population. To confirm this, it is enough to mention some events that took place in 2007.

- The formation of subtropical storm Andrea on May 9, 2007 marked an earlier beginning of the Atlantic hurricane season. This was the second occasion in five years that a storm formed before the official season start date.
- Hurricane Dean (August 13–23, 2007) reaching speeds of 270 km hr^{-1} wreaked havoc in the Caribbean and Mexico.
- Heatwaves affected vast territories of Europe. For instance, the air temperature in Greece, Romania, Hungary, and Bulgaria reached 46°C in the shade, which led to numerous forest fires. The ones in Greece reached were pronounced a national disaster.
- Unprecedented (at least for the last 60 years) floods covered central and southern territories of England, destroying a million houses and leaving tens of thousands of people without electricity and drinking water.

As has been repeatedly mentioned, the interactive components of the present-day climate system include a wide spectrum of natural and natural–anthropogenic subsystems and processes, without a complex study of which it is impossible to reliably single out the prevailing trends in climate change. Here are some of the most important (Kondratyev *et al.*, 2006b; Levinson and Waple, 2004):

- Global water cycle. Impact of cloud feedbacks.
- Global carbon cycle. Water–carbon cycle interaction.
- Land use and land surface changes.
- Present-day trends in GHG content in the atmosphere and mechanisms to control them.
- Interactions between the climate and productivity of land ecosystems. Land ecosystem dynamics.
- Impact of climate regime shifts on marine ecosystems.
- Control of natural resources to neutralize the negative consequences of human activities.
- Socio-economic aspects of ecodynamics and climate, and their analysis to optimize land use strategy.
- Interactions between processes in the geosphere and biosphere, and their dependence on space.

1.2.3 Greenhouse gases and climate

Infrared (IR) active gases, like water vapor (H_2O), carbon dioxide (CO_2), ozone (O_3), methane (CH_4), nitrous oxide (N_2O), chlorofluorocarbons CFC-11 (CCl_3F) and CFC-12 (CCl_2F_2) naturally and anthropogenically present in the Earth's atmosphere, absorb thermal IR radiation emitted by the Earth's surface and atmosphere. This phenomenon is known as the "atmospheric greenhouse effect", and the IR active

gases responsible for the effect are referred to as "greenhouse gases". The rapid increase in concentrations of GHGs since the industrial period began has given rise to concern over the potential resultant climate changes. The total combination of climatic effects is explained by the series of natural and anthropogenic processes connected mainly with the biogeochemical cycle of CO_2. However, as has been mentioned in publications (Kondratyev and Varotsos, 1995; Kondratyev, 1999b; Kondratyev and Demirchian, 2000; Kelley, 1987), many scientists and even politicians draw conclusions on the problem of the "greenhouse" role of CO_2 based on one-sided estimates without consideration of many important feedbacks and especially without consideration of the role of other GHGs. As follows from numerous studies, this role is rather substantial.

- Although there is approximately 220 times more CO_2 than methane in the Earth's atmosphere (Keppler *et al.*, 2006), each kilogram of CH_4 averaged over 100 years, warms the Earth 23 times more strongly than the same mass of CO_2.
- Water vapor is the most important absorber (its share in the greenhouse effect constitutes 36%–66%), and together with clouds it makes up 66%–85%. CO_2 alone contributes 9%–26%, while O_3 and other minor GHG absorbers contribute 7% and 8%, respectively.

As Monin and Shishkov (1990) noted, the difficulty is assessing the change in greenhouse effect with a change in the content of any gas in the atmosphere consists in that the atmosphere–ocean–land system involves numerous positive and negative feedbacks. Leaving out of account any of them can lead to rather distorted and erroneous conclusions and estimates. So, for instance, with increasing CO_2 content and, hence, temperature, evaporation should intensify and, respectively, water vapor content should increase, which, in its turn, absorbs additional energy and leads to a new temperature increase. Moreover, when the temperature rises, CO_2 solubility in the ocean worsens. But at the same time, the albedo changes, and the regime of aerosol removal from the atmosphere changes too. A 70% decrease (increase) of the planetary albedo depending on clouds leads to an increase (decrease) of the assimilated amount of solar energy, which leads to a warming (cooling) of climate. Estimates of the present-day greenhouse effect vary round the value $\Delta T = 33.2\,\mathrm{K}$, which is mainly formed due to water vapor (20.6 K, 62%), CO_2 (2.4 K, 7.2%), nitrous oxide (1.4 K, 4.2%), and CH_4 (0.8 K, 2.4%).

1.2.4 Aerosols and climate

Aerosol particles in the atmosphere play a significant role in climate change. They influence climate in two main ways, referred to as direct forcing and indirect forcing. Many scientific groups study the aerosol effects on climate-forming processes by developing various techniques to compute the flow of solar radiation through an atmosphere containing aerosols, clouds, and gases. Various conceptual aspects of the climate problem are also discussed in numerous documents of international organizations. In particular, the main conclusion of the summary of the IPCC 2001 report

(IPCC, 2001) which claims that an increasing body of observations gives a collective picture of a warming world and most of the observed warming over the last 50 years is likely to have been due to human activities.

It is to be regretted that the former Chairman of IPCC Working Group I (WG-I) Professor J. Houghton in a recent article (Houghton, 2003) in the British newspaper *The Guardian*, compared the threat of anthropogenic climate changes with weapons of mass destruction and admonished the U.S.A. for their refusal to support the concept of dangerous, anthropogenic global warming and thus the Kyoto Protocol. No matter how paradoxical it may seem, such claims are in fact being made against the background of an increasing understanding of the imperfections of current global climate models and their still inadequate verification. This makes predictions on the basis of numerical modeling no more than conditional scenarios (Jaworowski, 1999; Kondratyev, 1992, 1998b, 1999a, b, 2004a; Kondratyev and Galindo, 1997; Soon *et al.*, 2003). As for the U.S.A., we should welcome the huge efforts of this country to support climate studies, manifested through both special attention to improvement of observational systems and to developments in the field of climate problems, in general (Mahoney, 2003). The U.S. spends $2 billion a year on climate research. In 2004, the U.S.A. spent $4.5 billion on these problems.

The statement of the Intergovernmental Group G-8 published on July 2, 2003 (WSSD, 2003) has justly emphasized that in the years to come efforts will be concentrated on three directions.

- Strengthen international co-operation on global observation.
- Accelerate the research, development, and diffusion of energy technologies.
- Agriculture and biodiversity.

The Earth's climate system has indeed changed markedly since the industrial revolution, with some changes being of anthropogenic origin. The consequences of climate change do present a serious challenge to the policy-makers responsible for environmental policy, and this alone makes the acquisition of objective information on climate change, of its impact and possible responses, most urgent. With this aim in mind, the World Meteorological Organization (WMO) and the U.N. Environmental Program in 1988 set up the Intergovernmental Panel on Climate Change (IPCC) and divided it into three working groups (WGs) with spheres of responsibility for the

(1) scientific aspects of climate and its change (WG-I);
(2) effects on and adaptation to climate (WG-II);
(3) analysis of possibilities to limit (mitigate) climate changes (WG-III).

The IPCC has so far prepared five detailed reports (Houghton, Jenkins, and Ephraums, 1990; Watson, Zinyowera, and Moss, 1996; IPCC, 2001, 2005, 2007) as well as several special reports and technical papers. Griggs and Noguer (2002) have briefly reviewed the first volume of the *Third IPCC Report* (TIR) prepared by WG-I for the period June 1998–January 2001 with the participation of 122 leading authors and 515 experts. Four hundred and twenty experts reviewed the first volume and 23

experts edited it. Several hundred reviewers and representatives of many governments made additional remarks. With the participation of delegates from 99 countries and 50 scientists recommended by the leading authors, the final discussion of TIR was held in Shanghai on January 17–20, 2001. A "Summary for decision-makers" was approved after a detailed discussion by 59 specialists.

Analysis of the observational data as contained in TIR led to the conclusion that global climate change is taking place. The IPCC Reports (IPCC, 2001, 2007) give a detailed review of the observational data of the spatiotemporal variability of the concentrations of various GHGs and aerosol in the atmosphere. The adequacy of numerical models was discussed from the viewpoint of the climate-forming factors and the usefulness of models to predict climate change in the future. The main conclusion about anthropogenic impacts on climate was that "there is new and stronger evidence that most of the warming observed during the last 50 years has been determined by human activity." According to all prognostic estimates considered in TIR, both SAT increase and sea level rise should take place during the 21st century.

When characterizing the IPCC data for the empirical diagnostics of climate, Folland *et al.* (2002) drew attention to the uncertainty of the definitions of some basic concepts. According to IPCC terminology, climate changes are statistically substantial variations of an average state or its variability, whose stability is preserved for long time periods (decades and longer). Climate changes can be natural in origin (connected both with internal processes and external impacts) and/or may be determined by anthropogenic factors, such as changes in atmospheric composition or land use. This definition differs from that suggested in the Framework Climate Change Convention (FCCC) where climate changes are only of anthropogenic origin in contrast to natural climate change. In accordance with the IPCC terminology, climatic variability means variations of the average state and other statistical characteristics (MSD, repeatability of extreme events, etc.) of climate on every temporal and spatial scale, beyond individual weather phenomena. Hence climate variability can be both of natural (due to internal processes and external forcings) and anthropogenic origin, and possess both internal and external variability. As Folland *et al.* (2002) noted, seven key questions are most important for the diagnostics of observed changes and climate variability.

(1) How significant is climate warming?
(2) Is the currently observed warming significant?
(3) How rapidly had the climate changed in the distant past?
(4) Have precipitation and atmospheric water content changed?
(5) Do changes in the general circulation of the atmosphere and ocean take place?
(6) Have climate variability and climate extremes changed?
(7) Are observed trends internally coordinated?

In order to answer the above questions, the reliability of observational data is fundamental. Without such observational data adequate empirical diagnostics of climate remains impossible. Yet the information concerning numerous meteoro-

logical parameters, so very important for documentation, detection, and attribution of climate change, remains inadequate for the drawing of reliable conclusions. This is especially true for the global trends of those parameters (e.g., precipitation), which are characterized by great regional variability.

Folland *et al.* (2002) answered some of the questions above. A comparison of the secular change of global average annual sea surface temperature (SST), land surface air temperature (LSAT), and nocturnal air temperature (NAT) over the ocean for the period 1861–2000 on the whole revealed some similarity, though the warming in the 1980s from LSAT data turned out to be stronger, and the NAT data showed a moderate cooling at the end of the 19th century not demonstrated by SST data. The global temperature trend can be interpreted cautiously as equivalent linear warming over 140 years constituting 0.61°C at a 95% confidence level with an uncertainty range of ±0.16°C. Later on, in 1901 a warming by 0.57°C took place with an uncertainty range of ±0.17°C. These estimates suggest that beginning with the end of the 19th century, an average global warming by 0.6°C took place with the interval of estimates corresponding to a 95% confidence level equal to 0.4°C–0.8°C.

The spatial structure of the temperature field in the 20th century was characterized by a comparatively uniform warming in the tropics and by a considerable variability in extratropical latitudes. The warming between 1910 and 1945 was initially concentrated in the northern Atlantic and adjacent regions. The Northern Hemisphere was characterized by cooling between 1946 and 1975, while in the Southern Hemisphere some warming was observed during this period. The temperature rise observed during the last decades (1970–2000) turns out, on the whole, to have been globally synchronous and clearly manifested across Northern Hemisphere continents in winter and spring. In some Southern Hemisphere regions and in the Atlantic, however, a small all-year-round cooling was observed. A temperature decrease in the northern Atlantic between 1960 and 1985 was later followed by an opposite trend. On the whole, climate warming over the period of measurements was more uniform in the Southern Hemisphere than in the Northern Hemisphere. In many continental regions between 1950 and 1993, the temperature increased more rapidly at night than during daytime (this does not refer however to coastal regions). The rate of temperature increase varied from 0.1°C to 0.2°C/10 years.

According to the data of aerological observations, the air temperature in the lower and middle troposphere increased after 1958 at a rate of 0.1°C/10 years, but in the upper troposphere (after 1960) it remained more or less constant. Combined analysis of aerological and satellite information has shown that in the period 1979–2000 the temperature trend in the lower troposphere was weak, whereas near the land surface it turned out to be statistically significant and reached 0.16 ± 0.06°C/10 years. The statistically substantial trend of the difference between the Earth's surface and the lower troposphere constituted 0.13 ± 0.06°C/10 years, which differs from the data for the period 1958–1978, when the average global temperature in the lower troposphere increased more rapidly (by 0.03°C/10 years) than near the surface. The considerable differences between the temperature trends in the lower troposphere and near the surface are most likely to be real. So far, these differences cannot be convincingly explained. Climate warming in the Northern Hemisphere observed in

the 20th century was according to Folland *et al.* (2002) the most substantial over the last 1,000 years.

Special attention has been paid in the IPCC Reports (IPCC, 2001, 2007) to the possibility for predicting future climatic changes. The chaotic character of atmospheric dynamics limits long-term weather forecasts to one or two weeks and prevents the prediction of detailed climate change (e.g., it is impossible to predict precipitation in the U.K. for the winter of 2050). However, it is possible to consider climate projections; that is, to develop scenarios of probable climate changes due to the continuing growth of GHG concentrations in the atmosphere. Such scenarios, if credible, may be useful for decision-makers in the field of ecological policy. The basic method to make such scenarios tangible involves the use of numerical climate models that simulate interactive processes in the atmosphere–ocean–land surface–cryosphere–biosphere climatic system. As Collins and Senior (2002) noted, because there are so many such models, the serious difficulty arises as to which is the best one to choose. As this problem of choice is insoluble, there remains the possibility of comparing the climate scenarios obtained by using various models.

According to the IPCC recommendations, four levels of projection reliability are considered.

(1) From reliable to very probable (in this case there is agreement between the results for most models)
(2) Very probable (an agreement on new projections obtained with the latest models)
(3) Probable (new projections with an agreement for a small number of models)
(4) Restrictedly probable (model results are not certain but changes are physically possible).

A principal difficulty in giving substance to the projections is the impossibility of determining agreed predictions on how GHG concentrations will evolve in future, which makes it necessary to take into account all the various scenarios. The huge thermal inertia of the World Ocean dictates the possibility of delayed climatic impacts of GHG concentrations, which has already increased.

Calculations of annual average global SAT using the energy–balance climate model with various scenarios of temporal variations of CO_2 concentrations have led to SAT intervals in 2020, 2050, and 2100 to be 0.3°C–0.9°C, 0.7°C–2.6°C, and 1.4°C–5.8°C, respectively. Due to the thermal inertia of the ocean, delayed warming should manifest itself within 0.1°C–0.2°C/10 years (such a delay can take place over several decades).

The following conclusions can be attributed to the category of projections with the highest reliability (Collins and Senior, 2002):

(1) surface air warming should be accompanied by tropospheric warming and stratospheric cooling (the latter is due to a decrease of the upward long-wave radiation flux from the troposphere);

(2) faster warming on land compared with oceanic regions (as a result of the great thermal inertia of the ocean), and faster warming in high-mountain regions (due to albedo feedbacks);
(3) aerosol-induced atmospheric cooling restrains a SAT increase (new estimates suggest a weaker manifestation of the aerosol impact);
(4) presence of warming minima in the North Atlantic and in the circumpolar regions of the oceans in the Southern Hemisphere due to oceanic mixing;
(5) decrease of the snow and sea ice cover extent in the Northern Hemisphere;
(6) increase of the average global content of water vapor in the atmosphere, enhancement of precipitation and evaporation, as well as intensification of the global water cycle;
(7) intensification (on average) of precipitation in tropical and high latitudes, but its attenuation in sub-tropical latitudes;
(8) increase of precipitation intensity (more substantial than expected as a result of precipitation enhancement, on average);
(9) summertime decrease of soil moisture in the middle regions of the continents due to intensified evaporation;
(10) intensification of the El Niño regime in the tropical Pacific with a stronger warming in eastern regions than in western ones, which is accompanied by an eastward shift of precipitation zones;
(11) intensification of the interannual variability of the summer monsoon in the Northern Hemisphere;
(12) more frequent appearance of high-temperature extremes but infrequent occurrence of temperature minima (with an increasing amplitude of the diurnal temperature course in many regions and with a greater enhancement of nocturnal temperature minima compared with daytime maxima);
(13) higher reliability of conclusions about temperature changes compared with those about precipitation;
(14) attenuation of thermohaline circulation (THC), which causes a decrease in warming in the North Atlantic (the effect of THC dynamics cannot however compensate for the warming in West Europe due to the growing concentration of GHGs); and
(15) most intensive penetration of warming into the ocean depth in high latitudes where vertical mixing is most intensive.

As for estimates characterized by a lower level of reliability, the conclusion (at Level 4) about the lack of an agreed view on the changing frequency of storms in middle latitudes, is of special interest here, as is a similar lack of agreement about the changing frequency of occurrence of tropical cyclones under global warming. An important future task is to improve climate models aimed at reaching eventually a level of reliability that would enable the prediction of climatic changes.

Allen (2002) discussed the basic conclusions contained in the ''Summary for policy-makers'' (SPM) of the Third IPCC Report and especially of its main conclusion that ''There is new and stronger evidence that most of the warming observed

during the last 50 years should be attributed to human activity.'' This conclusion supplements the statement according to which ''... as follows from the present climate models, it is very unlikely that the warming taking place during the last 100 years was determined only by the internal variability'' (''very unlikely'' means that there is less than one chance in ten for an opposite statement to be well-founded).

McKitrick (2007) writes:

> ''The following concluding statement is not in the Fourth Assessment Report, but was agreed on by the ISPM writers based on their review of the current evidence. The Earth's climate is an extremely complex system and we must not understate the difficulties involved in analyzing it. Despite the many data limitations and uncertainties, knowledge of the climate system continues to advance based on improved and expanding data sets and improved understanding of meteorological and oceanographic mechanisms.
>
> The climate in most places has undergone minor changes over the past 200 years, and the land-based surface temperature record of the past 100 years exhibits warming trends in many places. Measurement problems, including uneven sampling, missing data and local land-use changes, make interpretation of these trends difficult. Other, more stable data sets, such as satellite, radiosonde and ocean temperatures yield smaller warming trends. The actual climate change in many locations has been relatively small and within the range of known natural variability. There is no compelling evidence that dangerous or unprecedented changes are underway.
>
> The available data over the past century can be interpreted within the framework of a variety of hypotheses as to cause and mechanisms for the measured changes. The hypothesis that greenhouse gas emissions have produced or are capable of producing a significant warming of the Earth's climate since the start of the industrial era is credible, and merits continued attention. However, the hypothesis cannot be proven by formal theoretical arguments, and the available data allow the hypothesis to be credibly disputed.
>
> Arguments for the hypothesis rely on computer simulations, which can never be decisive as supporting evidence. The computer models in use are not, by necessity, direct calculations of all basic physics but rely upon empirical approximations for many of the smaller scale processes of the oceans and atmosphere. They are tuned to produce a credible simulation of current global climate statistics, but this does not guarantee reliability in future climate regimes. And there are enough degrees of freedom in tunable models that simulations cannot serve as supporting evidence for any one tuning scheme, such as that associated with a strong effect from greenhouse gases.
>
> There is no evidence provided by the IPCC in its Fourth Assessment Report that the uncertainty can be formally resolved from first principles, statistical hypothesis testing or modeling exercises. Consequently, there will remain an unavoidable element of uncertainty as to the extent that humans are contributing to future climate change, and indeed whether or not such change is a good or bad thing.''

Clearly, the reality of such a statement depends on adequate modeling of the observed climatic variability. Analysis of the results of the relevant calculations using six different models has shown that three of six models reproduce climate variability on time scales from 10 to 50 years which agrees with observational data.

Another conclusion in SPM (Third Assessment Report) is that "reconstruction of data on climate for the last 1000 years shows that the present warming is unusual and it is unlikely that it can be of only natural origin" ("unlikely" means that there is less than one chance in three for an opposite conclusion).

This conclusion is supplemented with the following: "Numerical modeling of the response to only natural disturbing forces ... does not explain the warming that took place in the second half of the 20th century." This view is based on analysis of the results from the numerical modeling of changes in the average global SAT during the last 50 years. It follows from this that a consideration of natural forcings (solar activity, volcanic eruptions) has demonstrated a climatic cooling (mainly due to large-scale eruptions in 1982 and 1991) which has allowed the conclusion that the impact of only natural climatic factors is unlikely. However, there is only one chance in three that it was so: such a conclusion is based on indirect information concerning natural forcings in the past.

The results of numerical modeling cannot explain the pre-1940 climate warming by only taking anthropogenic factors into account, but are quite adequate when both natural and anthropogenic impacts are considered (GHGs and sulfate aerosol). As was mentioned in the SPM of the TAR, "these results ... do not exclude possibilities of contributions of other forcings." It is possible therefore that good agreement between the calculated and observed secular trends of SAT may in part be determined by the forcings that were not taken into consideration. Another important illustration of the inadequacy of the numerical modeling results is their difference from observations concerning temperature changes near the Earth's surface and in the free troposphere. If, as according to models, the tropospheric temperature increases more rapidly than near the surface, then the analysis of observational data between 1979 and 2000 reveals that the temperature increase in the free troposphere is slower and probably is absent.

When assessing the content of the IPCC 2001 Report, Griggs and Noguer (2002) argued that this report

(1) contains a most complete description of the current ideas about the known and unknown aspects of the climate system and the associated factors;
(2) is based on the knowledge of an international group of experts;
(3) is prepared based on open and professional reviewing; and
(4) is based on scientific publications.

Sadly, none of these statements can be convincingly substantiated. The IPCC 2001 Report has therefore been strongly criticized in the scientific literature (Babu *et al.*, 2004; Borisenkov, 2003; McKitrick, 2002; Soon *et al.*, 2003; Victor, 2001), the most important items of which we shall now discuss. The problems of global warming were discussed earlier (Loginov and Mikutski, 2000; Kondratyev and Demirchian,

2000; Boehmer-Christiansen, 2000; Adamenko and Kondratyev, 1999). In principle, the positions of the anthropogenic global-warming supporters and "climate skeptics" have not changed since the IPCC (2007) publication.

1.2.4.1 Empirical diagnostics of the global climate

The main cause of contradictions in studies of the present climate and its changes is the inadequacy of available observational databases. They remain incomplete and of poor quality. In this connection, Mohr and Bridge (2003) carried out a thorough analysis of how the global observing system has evolved. As is well known, climate is characterized by many parameters, such as

- air temperature and humidity near the Earth surface and in the free atmosphere;
- precipitation (liquid or solid);
- amount of cloud cover and the height of its lower and upper boundaries, and the microphysical and optical properties of clouds;
- radiation budget and its components, and the microphysical and optical parameters of atmospheric aerosols;
- atmospheric chemical composition, and more.

However, the empirical analysis of climatic data is usually limited by the results of SAT observations, with data series available for no more than 100–150 years. Even these data series are heterogeneous, especially with regard to the global database, which is the main source of information for proving evidence for the global-warming idea. Also, it should be borne in mind that the globally averaged secular trend of SAT values is based, to a large extent, on the use of imperfect observed data of SST.

The most important (and controversial) conclusion by Jacobson (2002a, b) concerning the anthropogenic nature of present-day climate change is based on analysis of the SAT and SST combined data (i.e., on the secular trend of mean average annual global surface temperature, GST). In this connection, two questions arise:

- first, about the information content of the notion of GST (this problem was formulated by Essex and McKitrick (2002); and
- second, about the reliability of GST values determined, in particular, by fragmentary data for the Southern Hemisphere, as well as the still unresolved problem of urban "heat islands" (Loginov and Mikutski, 2000).

Studies on the reliability of the SAT observations are continuing from the perspective of observational techniques. For more than 100 years SAT was measured using glass thermometers, but now arrangements to protect the thermometers from direct solar radiation and wind have been repeatedly changed. This dictates a necessity for filtering out SAT data to provide homogeneous data series. In the period from April to August 2000 at the Nebraska State University station ($40^{\circ}83'$N; $96^{\circ}67'$W), Hubbard and Lin (2002) carried out comparative SAT observations over smooth

grass cover using various means of protecting thermometers. At the same time, direct solar radiation and wind speed were measured. Analysis of the observations has shown that differences from observed data can reach several tenths of a degree. Therefore, a technique was proposed to increase the homogeneity of observation series which substantially increases the homogeneity of the series. However, it does not permit the exclusion of the effect of calibration errors and drift of the temperature sensor's sensitivity.

For diagnostics of the observational data, emphasis should be put on the analysis of climate variability in which consideration not of averages—but moments—of higher orders is important. Unfortunately, there have been no attempts to use this approach. The same approach refers to estimates of the internal correlation of observation series. McKitrick (2002), having analyzed the secular trend of SAT, showed that with the filtered-out contribution to temperature variations during the last several decades at the expense of internal correlations (i.e., determined by the climatic system's inertia), it turns out that temperature has practically not changed. There is a paradox: the increase in the global average SAT during the last 20–30 years is the principal basis for the conclusion concerning human contribution to present-day climate changes.

1.2.4.2 Air temperature diagnostics

From satellite observations (beginning in 1979), the trend of global average temperature for the lower troposphere (0 km–8 km) was $+0.07^{\circ}$C per 10 years (Christy and Spencer, 2003). According to the data from aerological sensings there was an increase in global average temperature of the lower troposphere by about 0.03°C per 10 years, which is much below the SAT increase ($\sim 0.15^{\circ}$C per 10 years) (Waple and Lawrimore, 2003). This difference in warming manifests itself mainly in the oceanic regions in the tropics and sub-tropics, and it is not clear why this is so (Christy and Spencer, 2003). The results of numerical climate modeling show that global warming should be stronger in the free troposphere than near the surface.

The difference in temperature trends near the surface and in the troposphere has caused heated discussion in the scientific literature (Christy and Spencer, 2003; Waple and Lawrimore, 2003). Since the reliability of satellite remote-sensing data raises no doubts, and their spatial representativeness (on global scales) is more reliable than that of the data of surface measurements, this difference should be interpreted as necessitating further analysis of SAT and SST data adequacy.

Data on changes in the height of the tropopause have recently attracted rapt attention (Hoskins, 2003; Randel *et al*., 2003; Santer *et al*., 2003; Varotsos, 2004). As Santer *et al*. (2003) noted, since 1979 the height of the tropopause increased by several hundred meters, agreeing with the results of numerical climate modeling and in line with growing GHG concentrations, whose contribution prevails again in "enigmatic" agreement with observed and calculated data.

Studies of the dynamics of the tropical tropopause layer are of great interest for quantitative estimates of climate change and an understanding of the mechanisms

behind troposphere–stratosphere interactions. These circumstances have stimulated recent serious attention to studies of the climatic structure and variability of the tropical tropopause as well as oof the mechanisms responsible for the formation of this structure. Serious attention has also been paid to analysis of data on the content of water vapor in the stratosphere and the mechanisms for the formation of thin cirrus clouds in the tropics. Randel *et al.* (2003) undertook studies of the structure and variability of the temperature field in the upper troposphere and lower stratosphere of the tropics (at altitudes about 10 km–30 km) from the data of radio-occultation observations for the period from April 1995 to February 1997 using the Global Positioning System (GPS). Comparison with a large number (several hundreds) of synchronous aerological sensings has shown that retrieval of the vertical temperature profiles from GPS/MET data provides reliable enough information.

Analysis of the obtained results suggested that the spatial structure and variability of the tropopause altitude determined by a "cool point" (minimum temperature) of the vertical temperature profile are governed mainly by fluctuations like Kelvin waves. A strong correlation was observed between temperature from GPS/MET data and outgoing long-wave radiation, which can serve as an indirect indicator of penetrating convection in the tropics. This correlation confirms the temperature fluctuation revealed from GPS/MET data and opens up possibilities for quantitative assessments of the response of the large-scale temperature field in the tropics to time-varying conditions of convection revealing coherent wavelike variations at altitudes between 12 km and 18 km.

1.2.4.3 Snow and ice cover

In the Northern Hemisphere, sea ice and snow cover reach their minimum and maximum extents in September and February, respectively. This variation determines the significance of global snow and ice cover for climate change. Recent trends in snow and ice conditions assessed by global monitoring systems show that variations in snow and ice cover reflect a number of the effects cause by a shift in climate, including changes in both air temperature and precipitation patterns. Seasonal variations in snow cover are the main source of run-off in the dry season in many mountain regions determining both the water supply and possible natural disasters (floods, avalanches, and landslides).

Numerical modeling using global climate models has shown (by considering the growing concentration of GHGs and aerosols) that climate warming should increase in the Arctic because of the feedback determined by the melting of the sea ice and snow cover causing a decrease in surface albedo. On the other hand, from the observed data, SAT has increased during the last decades over most of the Arctic. One of the regions where warming has taken place is northern Alaska (especially in winter and in spring). In this connection, Stone *et al.* (2002) have analyzed the data on climatic changes in the North of Alaska to reveal their impact on the annual trend in snow cover extent (SCE) and the impact of SCE changes on the surface radiation budget (SRB) and SAT.

1.2.4.4 Sea surface level and ocean upper-layer heat content

Numerous satellite-derived data provide useful information on the thermal structure of the upper ocean. Sea surface variations are given by measurements from TOPEX/POSEIDON. Sea surface temperature is derived from NOAA/AVHRR. In this context, Arruda *et al.* (2005) presented a semi-dynamic model that combines sea surface height anomalies, infrared satellite-derived SST, and hydrographic data to generate maps of the upper-ocean heat content anomaly, which are suitable for climate variability studies. McPhaden and Hayes (1991) examined the surface layer heat balance using wind, current, and temperature data from equatorial moorings along 165°E focused primarily on daily to monthly time scale variations during the 1986–1987 El Niño/Southern Oscillation (ENSO) event. They inferred that evaporative cooling related to wind speed variations accounts for a significant fraction of the observed SST and upper-ocean heat content variability. This evaporative heat flux converges non-linearly in the surface layer, giving rise to larger temperature variations in the upper 10 m than below. Other processes, such as wind-forced vertical advection and entrainment, and lateral advection, were negligible or of secondary importance relative to evaporative cooling. A large fraction of the SST and surface layer heat content variance could not be directly related to wind fluctuations; this unexplained variance is probably related to short-wave radiative fluxes at the air–sea interface.

Cai and Whetton (2002) drew attention to the fact that ocean dynamics can considerably affect future global-scale precipitation. Developments in these difficult problems are based on the use of both observed data and the results of numerical modeling, and have led to quite different conclusions. The climatic warming of the last decades was characterized by the spatial structure similar to that of the ENSO event. But since there are no data on such a structure for the whole century, the observed structure of warming is assumed to be a manifestation of the multi-decadal natural variability of climate, not the result of greenhouse forcing.

Moritz *et al.* (2002) revealed the substantial inadequacy of climate models when applied to Arctic conditions. In most cases the calculated AO (Arctic oscillation) trends turned out to be weaker than those observed. Calculated climate warming is greater in the fall over the Arctic Ocean, while observed warming is at a maximum in winter and over the continents in spring.

1.2.4.5 Other climatic parameters

Data on GST are important for climate diagnostics. As Majorovicz *et al.* (2002) have noted, analysis of the GST data obtained in different regions of Canada by measuring the ground temperature in boreholes revealed considerable spatial differentiation both in the GST increase observed in the 20th century, and in the onset of warming. For instance, from measurements in 21 boreholes covering the last 1,000 years, warming was detected (within 1°C–3°C) during the last 200 years. Warming was preceded by a long cooling trend in the region 80°W–96°W, 46°N–50°N, which continued until the beginning of the 19th century. According to data for ten boreholes in central Canada, the temperature reached a minimum in ~1820 with

subsequent warming by about 1.5°C. In western Canada, during the last 100 years warming reached 2°C.

Analysis was made by Majorovicz *et al.* (2002) of more adequate information on GST from the data of measurements in 141 boreholes at a depth of several hundred meters. The holes were drilled in 1970–1990. The results obtained revealed intensive warming that started in the 18th–19th centuries, which followed a long period of cooling (especially during the Little Ice Age) continuing during the rest of the millennium. The time of the onset of the present warming differed between regions. Analysis of the spatial distribution of GST changes in Canada revealed a substantial delay in the onset of the present warming in the east-to-west direction, with a higher level of GST increase in the 20th century in western Canada. This conclusion is confirmed by the data of SAT observations. It should be noted that the GST increase in eastern Canada had begun about 100 years before the industrial era.

The characteristics of atmospheric general circulation are important components of climate diagnostics. As Wallace and Thompson (2002) pointed out, the west to east zonal wind component averaged over the 55°N latitudinal belt can be a representative indicator of the primary mode of surface air pressure anomalies: the Northern Annual Mode (NAM) (Krahmann and Visbeck, 2003). Both the NAM and a similar index SAM for the Southern Hemisphere are typical signatures of the symbiotic relationships between the meridional profiles of the west to east transport in the respective hemisphere and wave disturbances superimposed on this transport. Their index determined (using a respective normalization) that a coefficient for the first term of NAM expansion in empirical orthogonal functions can serve as the quantitative characteristic of the modes. The presence of a positive NAM (or SAM) index denoted the existence of a relatively strong west to east transport.

In recent years it has been recognized that dynamic factors contribute much to observed temperature trends. For instance, in 1995 a marked similarity was observed between the spatial distributions of the SAT field and NAM fluctuations for the last 30 years, with a clear increase in the NAM index. The increasing trend of the index was accompanied by mild winters, changes in the spatial distribution of precipitation in Europe, and ozone layer depletion in the latitudinal belt >40°N. Similar data are available for the Southern Hemisphere. The main conclusion is that along with the ENSO event, both NAM and SAM are the leading factors in global atmospheric variability. In this connection, attention should be focused on the problem of the 30-year trend of NAM toward its increase, the more so that after 1995 the index lowered. It is still not clear whether this trend is a part of long-term oscillations.

The observational data show that during the 20th century an increase of precipitation constituted 0.5%–1% per 10 years over most land surfaces in the middle and high latitudes of the Northern Hemisphere, but a decrease (by about 0.3% per 10 years) took place over most of the land surface in sub-tropical latitudes, which has recently weakened, however. As for the World Ocean, the lack of adequate observational data has not permitted identification of any reliable trends of precipitation. In recent decades, intensive and extreme precipitation in the middle and high latitudes of the Northern Hemisphere has probably become more frequent. Since the mid-1970s the ENSO events have been frequent, stable, and intensive. Such ENSO dynamics

was reflected in specific regional variations of precipitation and SAT in most of the zones of the tropics and sub-tropics, Data on the intensity and frequency of occurrence of tropical and extra-tropical cyclones as well as local storms still remain fragmentary and inadequate and do not permit conclusions on any trends to be drawn.

Changes in the biosphere are also important indicators of climate. One is the bleaching of corals. It is important to recognize that enhanced atmospheric forcings on coral reefs lead not to their disappearance but to their transformation into more resistant species (Hughes *et al.*, 2003). Changes in seawater properties are another indicator (Broecker, 2003).

1.2.4.6 Concentrations of greenhouse gases and anthropogenic aerosol in the atmosphere

The transport, diffusion, and chemical transformation of pollutants in the atmosphere over many regions of the world are the main factors that regulate the greenhouse gas role in climate change. In this context, Otero *et al.* (2004) analyzed the physical and optical properties of biomass-burning aerosols in a continental dry region of South America and Argentina to understand the atmospheric radiative processes in the region. It is known that biomass burning generates small particles, water vapor, and gases like CO, CO_2, nitrogen oxide, and VOCs. These emissions are not evaluated on a global scale at sufficiently high precision to provide useful additional information for climate models.

As for the properties of atmospheric aerosol and its climatic impact, respective current information were reviewed in detail in Anderson *et al.* (2003), Kondratyev (1999a, 2003), Melnikova and Vasilyev (2004), Vasilyev and Melnikova (2002), Varotsos *et al.* (2001, 2005). In this connection, it is pointed out again that the supposed anthropogenic nature of the present global climate warming was explained by warming caused by the growth in GHG concentrations (primarily CO_2 and CH_4) as well as cooling due to anthropogenic aerosols. However, if the estimates of "greenhouse" warming can be considered reliable enough, then the respective calculations of radiative forcing (RF) due to aerosol are very uncertain. Of no less importance is the fact that while the global distribution of "greenhouse" RF is comparatively uniform, in the case of "aerosol" RF it is characterized by a strong spatiotemporal variability (including changes in the sign of radiative forcing).

1.2.4.7 Paleoclimatic information

Paleoclimatic information is an important source of data for comparative analysis of the present and past climates. Analysis of the data of paleoclimatic observations reveals large-scale abrupt climate changes in the past when the climate system had exceeded certain threshold levels. Though some mechanisms for such changes have been identified and the existing methods of numerical climate modeling are being gradually improved, the existing models still do not permit reliable reconstruction of past climatic changes. As a result of the emphasis on the climatic implications of the growth of GHG concentrations in the atmosphere, less effort has been made to study

possible sudden climate changes that may be of natural origin, though possibly intensified by anthropogenic forcings.

Since such changes lie beyond the problems addressed in the UNFCCC, Alley *et al*. (2002) undertook a conceptual evaluation of the problem of large-scale abrupt climate changes. Though the available long-term stabilizing feedbacks have determined the existence on Earth of a stable global climate for about 4 billion years, with characteristic time scales from one year to one million years, feedbacks prevailing in the climate system favored an enhancement of forcings on climate. So, for instance, changes in global average SAT within 5°C–6°C during the glaciation cycles apparently resulted from very weak forcings due to variations of the orbital parameters.

Still more surprising is that for several decades and in the absence of external forcings, regional changes have taken place reaching 30%–50% of those that had taken place in the epochs of glaciations. Data from the period of instrumental observations have revealed abrupt climatic changes, quite often accompanied by serious socio-economic consequences. For instance, the warming in many northern regions in the 20th century took place in two rapid "steps", leading to the supposition that in this case there was a superposition of the anthropogenic trend on inter-annual natural variability. Special attention was paid to the role of the ENSO event. The latter also refers to a sharp change in the climate system in the Pacific region in 1976–1977.

Considerable abrupt changes in regional climate in the Paleocene were detected from paleoclimatic reconstructions. They had been manifested as changes in the frequency of occurrence of hurricanes, floods, and especially droughts. Regional SAT changes reaching 8°C–16°C had happened over periods of 10 years and shorter. Dansgaard–Oeschger (DO) oscillations can serve as an example of large-scale sudden changes (Dansgaard *et al*., 1993).

The climatic system involves numerous factors that intensify climatic changes with minimum forcings. The withering or death of plants, for example, may cause a decrease in evapotranspiration and hence lead to precipitation attenuation, which may further increase drought conditions. In cold-climate regions snow cover formation is accompanied by a strong increase in albedo, which favors further cooling (the so-called "albedo effect"). Substantial climatic feedbacks are associated with the dynamics of thermohaline circulation.

While the factors of enhancement of either changes to or the stability of climate are comparatively well known, understanding is very much weaker of the factors involved in the spatial distribution of anomalies over large regions, including the globe. In this connection, further studies of the various modes of the general circulation of the atmosphere and the ocean (ENSO, DO oscillations, etc.) are important, as they are necessary for the respective improvement of general circulation models. Most important here are the potential effects of abrupt climatic changes on ecology and economy as current estimates are generally based on the assumption of slow and gradual change.

Abrupt climate changes are especially substantial in transitions from one climatic state to another. Therefore, if anthropogenic forcings of climate do favor the drifting

of the climate system toward a threshold level, the possibility of raising the probability of abrupt climate changes also increases. Of great importance is not only the amount—but also the rate—of anthropogenic forcings on the climate system. So, for instance, faster climate warming should favor stronger attenuation of the thermohaline circulation as this may accelerate the shift to the threshold of climatic changes (it is important that under these conditions the dynamics of thermohaline circulation becomes less predictable). To gain adequate solutions in the field of ecological policy, a deeper understanding of the whole spectrum of possible sudden climate changes is extremely important. Difficulties in the identification and quantitative estimation of all possible causes of sudden climate change and low predictability near threshold levels testify to the fact that the problem of abrupt climate changes will always be aggravated by more serious uncertainties than the problem of slow change. Under these conditions the development of ways to provide the stability and high adaptability of economics and ecosystems is of great importance.

1.2.4.8 Radiative forcing

Estimates of RF changes contained in the IPCC 2007 Report, which characterize an enhancement of the atmospheric greenhouse effect and are determined by the growth of concentrations of MGCs well mixed in the atmosphere, gave the total value $3.44\,W\,m^{-2}$, with the following contributions of various MGCs: CO_2 ($1.49\,W\,m^{-2}$ to $1.83\,W\,m^{-2}$), CH_4 ($0.43\,W\,m^{-2}$ to $0.53\,W\,m^{-2}$), halocarbon compounds ($0.31\,W\,m^{-2}$ to $0.37\,W\,m^{-2}$), N_2O ($0.14\,W\,m^{-2}$ to $0.18\,W\,m^{-2}$). The ozone depletion observed during the last two decades could lead to a negative RF constituting $0.15\,W\,m^{-2}$, which can be reduced to zero in this century if successful measures to protect the ozone layer are taken. The growth in tropospheric ozone content beginning from 1750 (by about one-third) could produce a positive RF of about $0.33\,W\,m^{-2}$.

From the time of the IPCC 1996 Report, RF estimates have substantially changed, being determined not only by the purely scattering sulfate aerosol considered above, but also by other types of aerosol, especially carbon (soot) characterized by considerable absorption of solar radiation as well as organic, sea salt, and mineral aerosol. The strong spatiotemporal variability of the aerosol content in the atmosphere and its properties seriously complicates an assessment of the climatic impact of aerosol (Kondratyev, 1999a; Melnikova and Vasilyev, 2004). New results from a number of climate models have radically changed the understanding of the role of various factors in RF formation. According to Kondratyev and Demirchian (2000), there is an approximate mutual compensation of climate warming due to the growth of CO_2 concentration and cooling caused by anthropogenic sulfate aerosol. Under these conditions, anthropogenic emissions of methane (mainly due to rice fields) and carbon (absorbing) aerosol should play a more important role.

Estimates of RF obtained with due regard to GHGs and aerosol are of importance in giving substance to conclusions concerning the contribution of anthropogenic factors to climate formation. The correctness of these conclusions is restricted, however, by three factors. One is that the interactivity of these factors

seriously limits (if not excludes) the possibility of adequate estimates of contributions of individual factors. The second, no less important, factor consists in that the above-calculated estimates refer to average global values and therefore are the results of smoothing the RF values characterized by strong spatiotemporal variability. Finally, the most complicated problem is the impossibility of reliably assessing aerosol RF because of its direct and indirect components. According to estimates by Podgorny and Ramanathan (2001), the value of direct RF at the surface level can increase to $50\,W\,m^{-2}$, and Chou *et al.* (2002) obtained values exceeding $-100\,W\,m^{-2}$ during forest fires in Indonesia. Vogelmann *et al.* (2003) estimated the RF due to radiative heat exchange from which it follows that during daytime near the surface the RF value is usually equal to several $W\,m^{-2}$. From the data of Pavolonis and Key (2003), the total RF at the surface level in the Antarctic varies within $0.4\,W\,m^{-2}$–$50\,W\,m^{-2}$. Yabe *et al.* (2003) obtained the average value $85.4\,W\,m^{-2}$, and Lindsey and Simmon (2003) found RF in the U.S.A. to be $7\,W\,m^{-2}$–$8\,W\,m^{-2}$.

Weaver (2003) analyzed the possible role of changes in cloud RF (CRF) at the atmospheric top level, especially in extra-tropical latitudes, as a climate-forming factor whose role consists in regulating poleward meridional heat transport. The cloud dynamics in extra-tropical latitudes and related changes in CRF depend on formation in the atmosphere of vortices responsible for the evolution of storm tracks. It is vortices determining the formation of storm tracks that contribute most to meridional heat transport.

It was shown by Weaver (2003) that the average annual radiative cooling of clouds in high latitudes has the same order of magnitude as the convergence of vortices-induced meridional heat flux, but of an opposite sign. Since there is a close correlation between CRF and storm track dynamics, we can suppose two ways for the impact of storm tracks dynamics on poleward heat transport:

(1) Directly via vortices-induced heat transport in the atmosphere.
(2) Indirectly via CRF changes. The efficiency of heat transport by vortices is reduced by radiative cloud cooling. Changes in efficiency can be a substantial climate-forming factor. Various levels of efficiency can determine the possibility of the existence of different climatic conditions.

In the context of the problem of CRF formation due to long-wave radiation, Wang *et al.* (2003) considered specific features of the spatial distribution of cloud cover during the unusually intensive El Niño event in 1997–1998 from the data of observations from the SAGE-II satellite. Data on the cloud cover frequency of occurrence in this period and CRF are unique information for the verification and specification of schemes of interaction parameterization in the cloud–radiation–climate system used in models of atmospheric general circulation. Based on using the occultation technique of remote sensing (RS), the SAGE-II data provide vertical resolution above 1 km and a quasi-global survey (70°N–70°S). Analysis of the results under discussion revealed

(1) the occurrence of upper-level opaque clouds exceeding the normal level in the eastern sector of the tropical Pacific and an opposite situation in the "warm

basin'' of the Pacific; existing anomalies of an opaque cloudiness located at altitudes above 3 km can be explained by the impact of the spatial structure of anomalies of SST fields and precipitation observed in the tropics;
(2) the same laws are characteristic of cloudiness near the tropical tropopause recorded at the detection threshold;
(3) the zonal mean distribution is characterized by a decrease in the amount of opaque clouds in low latitudes (except the SH tropics at altitudes below 10 km) and an enhancement of clouds in high latitudes as well as by an increase (decrease) in cloud amount (at the detection threshold) in the SH tropics (in the upper troposphere of the NH sub-tropics); and
(4) the geographical distribution of calculated CRF anomalies which agrees well with the data of satellite observations of the Earth radiation budget. New estimates of direct and indirect RF have been obtained by Giorgi *et al.* (2003).

Markowicz *et al.* (2003) undertook a study to estimate the aerosol RF due to long-wave radiation (radiative heat exchange). They studied aerosol radiative forcing at infrared (IR) wavelengths using data from the Aerosol Characterization Experiment, ACE-Asia (which took place on the National Oceanic and Atmospheric Administration research vessel *Ronald H. Brown*). The mean IR aerosol optical thickness at 10 m was 0.08 and the single-scattering albedo surface forcing reached $10\,W\,m^{-2}$ during this cruise, which is a significant contribution compared with the total direct aerosol forcing. The surface IR aerosol radiative forcing was between 10% and 25% of the short-wave aerosol forcing. Over the Sea of Japan, the average IR aerosol radiative forcing was $4.6\,W\,m^{-2}$ at the surface, and $1.5\,W\,m^{-2}$ at the TOA. IR forcing efficiency at the TOA was a strong function of aerosol temperature (which is coupled to vertical structure) and changes between $10\,W\,m^{-2}$ and $18\,W\,m^{-2}$ (per IR optical depth unit), while surface IR forcing efficiency varied between $37\,W\,m^{-2}$ and $55\,W\,m^{-2}$ (per IR optical depth unit).

From these and other data it follows that accuracy in the estimate of radiation balance as a function of space coordinates depends on cloud distribution, their state, and atmospheric pollution, as well as on the chosen size of pixels for spatial averaging. In this connection, Henderson and Chýlek (2005) used image data from the Multispectral Thermal Imager to evaluate the effect of spatial resolution on aerosol optical depth retrieval from satellite imagery. It was shown that aerosol optical depth (AOD) depends weakly on pixel size in the range $40 \times 80\,m^2$ to $2{,}040 \times 4{,}080\,m^2$ in the absence of clouds and changes monotonically with the growing size of pixels in clouds.

The versatile and ambiguous role of aerosols in climate changes and their influence on human beings is demonstrated in the work of Otero *et al.* (2004), where the temporal variability of aerosol optical properties was investigated during intense biomass burning at the Córdoba-CETT site (continental dry region in South America and Argentina). Due to the high frequency of occurrences of biomass burning in the dry season, it was important to characterize aerosol optical properties to understand the atmospheric radiative processes in the region. Such a study is important in general not only for evaluation and prediction of climate changes but also for total control of

environmental quality; for example, particles with diameters $<2.5\,\mu m$ can cause respiratory desease.

Rossow (2003) justly warned that attempts to isolate and describe a greater number of climatic feedbacks and to quantitatively estimate them using methods proposed earlier have become confusing and disorienting, since application of a simple linear theory consisting of many sub-systems is completely unacceptable.

Changes in extra-atmospheric solar radiation are a climate-forming factor that should be taken into account. The contribution of these changes to RF starting from 1750 could have reached ~20% compared with the contribution of CO_2, which is mainly determined by an enhancement of extra-atmospheric insolation in the second half of the 20th century (it is important to consider the 11-year cycle of insolation). However, possible mechanisms of enhancement of the climatic impact of solar activity are still far from being understood (Haigh, 2001; Kondratyev, 1998b).

Shamir and Veizer (2003) found, for instance, a high correlation between the intensity of galactic cosmic rays and temperature for the last 500 million years. On this basis, it was concluded that 75% of temperature variability in that period had been determined by the contribution of this factor (this problem was also considered earlier by Kondratyev, 1998b).

1.2.4.9 Some aspects of climatic data reliability

Conclusions about observed and, even more so, potential future climatic changes are very uncertain, both with respect to the data of diagnostics of present climate dynamics and to the results of numerical modeling. According to IPCC (2001), developments in the following seven fields should receive top priority:

- stop any further degradation of the network of conventional meteorological observations;
- continue studies in the field of global climate diagnostics in order to obtain a long-term series of observational data with a higher spatiotemporal resolution;
- seek a more adequate understanding of the interaction between the ocean–climate system components (including its deep layers) and the atmosphere;
- more realistically understand the laws of long-term variability of climate;
- broaden the application of an ensemble approach to climate modeling in the context of assessments of probabilities; and
- develop a totality (''hierarchy'') of global and regional models with emphasis on the numerical modeling of regional impacts and extreme changes.

It should be added that in order to understand the physical laws governing present and future climates, studies of paleoclimate are also important, especially of sudden short-term changes. The intensive development of space-borne remote sensing has not provided adequate global information about the diagnostics of the climate system because the way the existing system of space-borne and conventional observation works remains far from optimal.

The reliability of ARF estimates depends on many factors, one being the reliability of information about aerosol optical thickness (AOT).

As Chýlek *et al.* (2003) noted, the maximum permissible error in outgoing radiation flux determination from satellite data $\Delta F = 0.5\,\mathrm{W\,m^{-2}}$ determines the necessity to retrieve the atmospheric optical thickness, τ, with an error not more than $\Delta\tau = 0.015$ on land and 0.010 over the oceans. However, this level of error has still not been achieved. Using AVHRR data, the MSD of τ values varies within 0.06–0.15, whereas in the case of MODIS data over land, $\Delta\tau = 0.05$–0.2τ, which corresponds to the interval of $\Delta\tau$ values from 0.07 to 0.21, with τ varying from 0.1 to 0.8. The use of the extra-nadir data of multi-spectral thermal video-radiometer MTI for intermediate angles of scattering provides the level of error $\Delta\tau = 0.03$.

According to numerical modeling results, the main obstacle to an increase in τ retrieval accuracy is the unreliability of data on the scattering function (determined by the absence of reliable information about aerosol size distribution, shape, and the optical properties of particles). Such uncertainties have a greater effect on the reliability of τ retrieval at large scattering angles (as a rule, close to nadir) than in the case of extra-nadir angles (this corresponds to moderate values of the scattering angle). From the experience of τ retrieval from MTI data, it was shown by Chýlek *et al.* (2003) that to provide the needed accuracy of τ retrieval from the data of satellite observations, we should use a single or dual direction of viewing at extra-nadir scattering angles in the interval 50°–100°.

Myhre *et al.* (2004, 2005) performed comparisons of retrieval algorithms for AOT over the ocean using the data of satellite observations for 8 months (November 1996–June 1997) made with the AVHRR, OCTS, POLDER, and TOMS instrumentation. Comparisons revealed the presence of considerable differences (by a factor of 2 and more) between retrieved AOT values. Most substantial were differences in the Southern Hemisphere, and the cause of this was apparently insufficient reliability of cloud impact filtering.

According to the IPCC Report published in 1996, an indirect (connected with the effect of aerosol on the optical properties of clouds) globally averaged impact of aerosol on climate, characterized by the values of indirect RF, varies from $0\,\mathrm{W\,m^{-2}}$ to $-1.5\,\mathrm{W\,m^{-2}}$. Six years later (in IPCC 2001), the range of uncertainties was broadened to $0\,\mathrm{W\,m^{-2}}$–$4.8\,\mathrm{W\,m^{-2}}$, and in IPCC 2007 it was evaluated as $-1.2\,\mathrm{W\,m^{-2}}$ to $-0.4\,\mathrm{W\,m^{-2}}$.

As Brenguier (2003) noted, a contributing factor to the uncertainty is drizzle in clouds that form in the atmospheric boundary layer (ABL). In particular, this circumstance illustrates the importance of the adequate retrieval of cloud cover dynamics in the ABL. Another problem is connected with consideration (parameterization) of small-scale processes in the ABL and their non-linearity. For instance, aerosols acting as cloud concentration nuclei (CCN) can be determined from upward motions at the cloud bottom which should be reproduced at a spatial resolution (in the horizontal) of the order of 100 m. The present parameterization schemes still do not meet these requirements.

The necessity to take into account the interaction between various processes determining cloud cover dynamics and its effect on microphysical and optical

properties of clouds are fraught with serious difficulties. In this connection, emphasis was first given to the aerosol-induced growth of cloud droplet number density resulting in respective changes in cloud albedo and indirect radiative forcing. This was called the first indirect impact of clouds on climate. But, then it was necessary to also take into account the second indirect impact manifesting itself through a change in precipitation formation intensity. The retrieval of this impact needs a description of the interaction between the microphysical characteristics of clouds and ABL dynamics. Also, analysis was made of the significance of the ''semi-direct'' effect due to short-wave radiation absorption by aerosol, which reduces cloud cover development (Johnson *et al.*, 2004).

An important problem is to provide an interactive consideration of the three types of aerosol impact on the ABL, clouds, and the indirect RF mentioned above. Solution of this problem was one of the main objectives of the second field observational experiment (ACE-2) on studies into aerosol characteristics in 1997 in the Canary Islands. Part of the program of this experiment (called ''CloudColumn'') was especially dedicated to a study of the indirect impact of anthropogenic aerosol on climate. In 1999, the European Commission supported further studies in this direction within the PACE project on the development of parameterization schemes for the impact of aerosol on climate.

As Mitra (2004) pointed out, the Indian oceanic experiment (INDOEX) was the first complex problem-oriented observational international program aimed mainly at studies of the aerosol-induced radiative and climatic forcing of regional and global climate that take respective feedbacks into account. The preliminary stage of the accomplishment of INDOEX began in 1996–1997, and the basic part of complex observations was accomplished in 1998–1999 with the participation of specialists from different countries (India, U.S.A., Western Europe, Mauritius, and the Maldives). The obtained results were based on the use of surface, ship, aircraft, and satellite observational means.

The observational program included getting information about the content and properties of atmospheric aerosol and most substantial optically active MGCs (O_3, CO, NO_x, SO_2, etc.), but concentrated on aerosol studies to retrieve data on direct and indirect aerosol RF (ARF). The most interesting (and in many respects unexpected) results were connected with detection of a thick aerosol layer in the troposphere (an important feature of aerosol chemical composition consisted in the presence of a considerable black carbon component) and distinct manifestations of the long-range transport of both aerosol and MGCs.

The available information about aerosol, though complex, has opened up possibilities to analyze its impact on climate, human health, and agriculture, and available information about MGCs the prospects for development in the ''Chemical weather'' problem. An important component of the INDOEX program was observations on board the Indian ship *Sagar Kanya* in January–March 1999 (before the American ship *Ronald H. Brown*) which plied the east to west voyage along the 20°S parallel in regions of clear atmosphere south of the Inter-Tropical Convergence Zone (ITCZ), as well as in the Red Sea (along 15°N, toward India). Comparison of the ARF data in regions of unpolluted atmosphere and in the presence of a thick aerosol layer showed

that in the second case the ARF was 6–10 times greater reaching $-35\,W\,m^{-2}$ (the coastal zone) and $-18.6\,W\,m^{-2}$ (the dust-loaded atmosphere over the ocean).

From data of surface observations caried out at a rural location in the Great Plains, Oklahoma within the atmospheric radiation measurements (ARM) program, Feingold (2003) and Feingold *et al.* (2003) tested the hypothesis of the indirect impact of atmospheric aerosol on climate proposed by Twomey (1974). According to this hypothesis, aerosol particles (entering clouds and functioning as CCN) favor an increase in fine droplet number density and thereby cause an increase in cloud albedo, which causes climate cooling (an important aspect of the hypothesis is that cloud water content is assumed to be constant).

Solution to the problem of understanding the aerosol–cloud interaction is seriously complicated by the many feedbacks that appear in interacting microphysical, dynamic, and chemical processes. With the equivalent water content of clouds assumed to be constant, an analysis was made (Feingold *et al.*, 2003) of the response of non-precipitating liquid water clouds to changes in aerosol content. This response was characterized as the relative change in effective radius of cloud droplets with the relative change in aerosol-induced extinction. The effective radius of droplets was retrieved from radiation and microwave-sensing data (the spatiotemporal resolution of the observational results constituted, respectively, -100 m and 20 s). Raman lidar data served to retrieve aerosol-induced extinction in the sub-cloud layer (Philbrick, 2002). An analysis of observational results demonstrated that aerosol contained in marine air masses or in air masses from the north affects clouds more strongly than aerosol coming with air masses from the northwest. There is a sufficiently high correlation (0.67) between the response of cloudiness to aerosol and the intensity of turbulent mixing in clouds.

The interaction processes in the aerosol–cloud–radiation system that determine the indirect impact of aerosol on climate remain poorly studied, though they are an important factor in RF formation (the respective estimates vary between $0\,W\,m^{-2}$ and $-4.8\,W\,m^{-2}$). The contribution to indirect climatic impact by aerosol due to lower-level stratus clouds is important since

- their albedo is more sensitive to changes in the microphysical characteristics of clouds than those of upper-level high-albedo clouds (this is the first indirect impact of aerosol on clouds and climate); and
- the moderate geometrical thickness of clouds is often sufficient for droplets to reach the size of precipitating droplets, and therefore even a small increase in cloud droplet number density, N, can prevent precipitation, which affects the water content and albedo of clouds (this is the second indirect impact of aerosol on climate).

To analyze the formation and variability of the indirect climatic impact of aerosol within the second field experiment on studies of aerosol (ACE-2) and the PACE program to substantiate parameterization of this impact, Menon *et al.* (2003) undertook a comparison of six 1-D numerical models of the processes in the aerosol–cloud–radiation system that determine the climatic impact of aerosol under

conditions of clear and polluted ABL. They divided this into three stages. The first was aimed at analysis of the adequacy of numerical modeling of how aerosol acts as condensation nuclei, radiation transfer, and precipitation formation at high vertical resolution, as was the case of *in situ* observations at the time of the ACE-2 experiment. At the second stage, similar tests of the adequacy were made but this time at a rougher vertical resolution. The objective of the third stage was numerical modeling for a 24–48-hour period to assess the possibilities of forecasting clouds in the ABL taking into consideration the large-scale fields of meteorological parameters. To forecast cloud droplet number density, N, several parameterization schemes were used.

The results obtained by Menon *et al.* (2003) revealed substantial differences in the use of physically substantiated prognostic schemes of how aerosol acts taking into account vertical velocity and empirical schemes based on diagnostic data on the vertical velocity at cloud bottom level. Prognostic schemes are characterized by the stronger variability of results compared with diagnostic ones because of differences in scheme of the interaction between the processes of aerosol activation and precipitation of drizzle when calculating N.

When initializing 1-D models at a high vertical resolution taking into account the observed vertical profiles of cloud water content, a comparison was made of the results of numerical modeling with observational data which revealed a satisfactory agreement, which deteriorates, however, if we confine ourselves to consideration at a low vertical resolution. Predicted precipitation turned out to be strongly underestimated, but this difference reduces if we take into account the sub-grid variability of the water content. It follows from calculations for the 24–48-hour period that, as a rule, estimates of cloud morphology turn out to be inadequate. Eventually, numerical modeling leads to considerable errors in assessing the optical properties of clouds. The forecasting of cloud morphology becomes more reliable with the use of parameterization schemes of the process of formation of cloud thickness as well as with consideration of the external large-scale RF of the processes of cloud formation.

Accomplishment of the complex observational experiment LACE-98 made it possible to obtain extensive information about atmospheric aerosol (aircraft measurements of the size distribution and number density of fine aerosols, coefficients of aerosol absorption, backscattering and depolarization, chemical composition of aerosol, as well as surface observations of the spectral optical thickness of the atmosphere, coefficients of extinction and backscattering). Fiebig *et al.* (2002) compared the observational data on optical parameters obtained from the results of numerical modeling for total H_2SO_4 aerosol near the tropopause as well as for the ammonium sulfate/soot mixture in the remainder of the air column (Osborne *et al.*, 2004).

This comparison provided closure (according to calculation results and observational data) with an error not exceeding 25% in the case of aerosol optical thickness (with due regard to aerosol formed in biomass burning in North America and long-range transport with soot having a 35% share). Assuming a spherical shape of particles (with an average non-sphericity ratio of 1:3), the calculated depolarization of such aerosols agrees with the data of lidar sensings, whereas a comparison of

calculated and observed values of the backscattering coefficient showed that soot aerosol should be a component with non-absorbing particles. Using the two-stream approximation of the theory of radiation transfer, the ARF at the level of the tropopause in a cloud-free atmosphere was estimated at $-5.8\,\mathrm{W\,m^{-2}}$ for AOT = 0.09 (at $\lambda = 710\,\mathrm{nm}$) and solar zenith angle 56°. The value of ARF due to aerosol formed in biomass burning is equally sensitive to the state of particle mixture (external or internal) and to surface albedo.

In an attempt to understand the indirect climatic impact of atmospheric aerosol through aerosol-induced changes of microphysical and optical characteristics of clouds, Peng and Lohmann (2003) discussed the results of field studies into the impact of anthropogenic aerosol on cloud droplet size distribution carried out in Canada. Comparison of the calculated values of cloud albedo with observations showed that the best agreement is observed when the calculated values are corrected by taking into account the parameters of scaling β (which depends on the relative MSD of the sizes of droplets), and ε (which characterizes the average radius of droplets and radius of MSD). Here $\beta = (1 + 2\varepsilon^2)^{2/3}/(1 + \varepsilon^2)^{1/3}$. There is a positive correlation between the parameter and droplet number density. This linear correlation was used in numerical climate modeling by the ECHAM-4 AGCM model (Kemball-Cook *et al.*, 2002; Roeckner *et al.*, 1996). Calculations have shown that the globally averaged value of aerosol-induced indirect RF at the TOA decreased by $0.2\,\mathrm{W\,m^{-2}}$ after correction, with the β parameter taken into account.

The indirect climatic impact of aerosol at the ABL is determined by numerous interactions between aerosol and the dynamics of the microphysical and optical properties of clouds. The input to the atmosphere of anthropogenic aerosol particles functioning as CCN favors an increase in cloud droplet number density. As mentioned above, the related increase in the optical thickness and albedo of clouds, with their constant water content, was called the "first indirect effect", which characterizes the climatic impact of aerosol.

On the other hand, also important is the change in cloud droplet size distribution, which affects its dynamics (mainly via the process of precipitation formation leading to changes of cloud lifetimes and their spatial extent, on which cloud albedo depends). Such a microphysical feedback affecting the cloud cover dynamics was called the "second indirect effect", which determines the climatic impact of aerosol. Although cloud albedo increase is comparatively small, being connected with manifestations of indirect effects, it can be substantial on global scales as a factor of attenuation of warming due to the atmospheric greenhouse effect. Therefore, studies of the indirect climatic impact of aerosol and its satellite monitoring are extremely urgent.

Brenguier *et al.* (2003) discussed the ACE-2 CC project, one of the five projects accomplished within the ACE-2 program of the second field experiment on studies of aerosol characteristics with the aim of understanding the indirect climatic impact of aerosol for marine stratocumulus clouds and to substantiate the strategy of "closed" aerosol–cloud–radiation experiments. Observations within the CC project were made in June–July 1997 in the Canary Islands using instruments onboard three flying laboratories and installed at a surface network.

Brenguier *et al.* (2003) discussed the results of eight series of aircraft measurements of the microphysical characteristics of marine stratocumulus clouds in a broad range of observation conditions (different physico-chemical properties of aerosol, number density values in the interval $50\,cm^{-3}$–$25\,cm^{-3}$, etc.). The unique complex of synchronous observations of the microphysical and radiative characteristics of cloud cover obtained can be used to assess the indirect impact of aerosol on clouds and climate based on analysis of the ratio between the cloud optical thickness and effective radius of cloud droplets. Correlation between these values is usually negative, but in a heavily polluted atmosphere it can be positive. From the observational data obtained during ACE-2, the polluted systems of clouds turned out to be somewhat drier and therefore thinner, resulting in the positive correlation between the indirect impact of aerosol on climate and the effective radius of droplets.

The product of incomplete burning of various fuels (mainly fossil fuel and biomass burning) is called "black carbon" (BC), made up of soot and smoke aerosol that absorbs short-wave radiation. Estimates of direct RF due to BC and organic matter (OM) have led to values in the interval from $+0.16\,W\,m^{-2}$ to $+0.42\,W\,m^{-2}$, and total absorbed radiation within $0.56\,W\,m^{-2}$–$2\,W\,m^{-2}$ (the parameter BC + OM is the soot component that appears as a result of fossil fuel burning). About 10% (by mass) BC constitutes aerosol formed in biomass burning, for which RF values were obtained from $-0.16\,W\,m^{-2}$ to $-0.74\,W\,m^{-2}$, whereas the radiation absorbed by aerosol varies within $0.75\,W\,m^{-2}$ to $2\,W\,m^{-2}$.

Components of the products of biomass and fossil fuel burning responsible for radiation scattering (along with water-soluble organic and inorganic components emitted to the atmosphere as part of smoke and soot compounds) can also function as CCN. This means that emissions of BC and OM participate in the formation of indirect RF due to the impact of CCN on the formation of clouds and their properties. It follows from available estimates that such a contribution can exceed 80% with respect to total indirect RF. The BC impact can also manifest itself by local warming of the atmosphere and a decrease in cloud amount and their water content, which leads to an albedo decrease.

In connection with the earlier estimates of related "semi-direct" RF, it was concluded there exists a possibility of additional climate warming. In connection with this, Penner *et al.* (2003) evaluated the effect of soot and smoke aerosols on climate using a global climate model (GCM) that took into account the effect of BC in cloud droplets on cloud albedo. Table 1.10 shows the annual average values of the total content of various types of aerosol used in this model. The numerical modeling of direct, semi-direct, and indirect RF, with due regard to RF as a result of both short-wave and long-wave radiation, has led to the conclusion that the effect of the latter determines a decrease or even a change in sign of semi-direct RF—but no enhancement in warming.

Total RF substantially depends on the altitude of aerosol emissions since emissions at high altitudes enhance negative long-wave RF. Moreover, emissions of absorbing aerosols at higher altitudes can enhance clouds at lower altitudes, where, as a rule, a temperature decrease takes place. According to estimates of the direct global average short-wave RF at the top of the atmosphere (TOA), it constitutes

Table 1.10. Annual average values of the total content ($mg\,m^{-2}$) in the atmosphere of different types of aerosol in the Northern and Southern Hemispheres and over the globe.

Type of aerosol	*NH*	*SH*	*Globe*
Anthropogenic sulfates, SO_4^{2-}	0.87	0.22	1.09
Natural sulfates, SO_4^{2-}	0.45	0.42	0.86
OC due to fossil fuels	0.39	0.03	0.41
BC due to fossil fuels	0.08	0.01	0.09
OC due to biomass burning	1.28	1.24	2.52
BC due to biomass burning	0.13	0.13	0.26
OC emissions at surface level	0.49	0.52	1.02
BC emissions at surface level	0.05	0.06	0.11
Natural OC	0.13	0.10	0.23
Dust (radius <1 μm)	11.11	3.57	14.68
Sea salt aerosol (radius <1 μm)	1.82	2.85	4.68

OC = organic carbon, BC = black carbon, NH = Northern Hemisphere, SH = Southern Hemisphere.

$0.17\,W\,m^{-2}$. The concept of "quasi-RF" makes it possible to partially take into account the impact of climatic feedbacks, resulting in RF values of $0.28 \pm 0.32\,W\,m^{-2}$.

If, according to the earlier results, radiation absorption by aerosol leads to a decrease in cloud amount and cancels out aerosol-induced cooling, it follows from numerical modeling results (based on the concept of quasi-RF) that the total RF (determined both by short-wave and long-wave radiation) turns out to be less (more negative) than before. Thus, the impact of smoke and soot aerosol manifests itself as a cooling taking into account the changes in cloudiness and temperature that occur in the process of RF formation.

Calculations of short-wave RF considering all the anthropogenic aerosol in the region, where the content of BC exceeds $2\,mg\,m^{-2}$, gave values of $-3.0\,W\,m^{-2}$ and $-3.1\,W\,m^{-2}$ for aerosol emissions due to biomass burning near the surface and in the middle troposphere, respectively. If soot aerosol emissions take place near the surface then they determine, on average, a tropospheric warming at all levels and a decrease in cloud amount near the surface where emissions take place. The total "quasi-RF" with due regard to both short-wave and long-wave radiation in the case of soot aerosol is close to zero.

Recent estimates testify to the very strong impact of the phase state of atmospheric ammonium sulfate aerosol (with radiative humidity ~80%) on the level of

aerosol-induced RF. Also, of great interest is the impact of the aerosol phase state on the course of heterogeneous chemical reactions. Although the processes of deliquescence (water assimilation) and efflorescence (water loss) of pure ammonium sulfate have been well studied, the problem consists in the complexity of the chemical composition of aerosol particles including up to 50% and more (by mass) of organic compounds.

Analysis of aerosol samples obtained at several locations in Western Europe has shown that about 60% of the content of organic carbon in tropospheric aerosol is the share of water-soluble organic compounds. According to observational data, at a rural location in Austria, mono- and dicarboxylic acids constitute about 11% (with respect to the total content of organic carbon in cloud water). While insoluble organic compounds hamper the assimilation of water by aerosol, soluble organic matter, as a rule, favors water assimilation.

In view of insufficient information about the role of the phase transformations of aerosol, Brooks *et al*. (2003) carried out laboratory measurements in a running-water vat using an IR Fourier spectrometer to distinguish between particles' phase states as well as to study the processes of deliquescence and efflorescence in the case of ammonium sulfate, maleic acid, as well as the internally mixed aerosol particles of the maleic acid/ammonium sulfate mixture. The results obtained indicate that in the case of aerosol particles of maleic acid, the assimilation of water by them begins at a low radiative humidity (RH) of about 20% and continues until a maximum RH level (89%) is reached, at which the assimilation of water is still possible. For particles of mixed composition (maleic acid/ammonium sulfate), the assimilation of water begins at a lower RH than for particles consisting of one of the components. Studies into efflorescence have led to the conclusion that the crystallization of maleic acid particles takes place at $RH < 30\%$. On the whole, the results obtained reflect the fact that the presence in aerosol of water-soluble organic matter mixed internally with ammonium sulfate, broadens the range of conditions under which the aerosol is in a liquid state.

Zender *et al*. (2003) developed a numerical model which makes it possible to precalculate the number density and size distribution of atmospheric dust aerosol, which is to be used as a component of numerical models of climate and chemical processes in the atmosphere. The discussed DEAD model was used to simulate the global distribution of dust aerosol (DA) taking into account the processes of transformation of aerosol properties determined by involvement, dry and wet deposition, and chemical reactions with the participation of dust aerosol. Calculations have been made on the assumption that the soil texture is globally homogeneous and contains a sufficient amount of components which favor the process of saltation. Soil erodibility is parameterized using a new physically substantiated geomorphic index, which is proportional to the river catchment's area located upstream from the region of each DA source. The processes of dry deposition are described with due regard to sedimentation and turbulent mixing. The processes of nucleation and size-dependent washing out of DA particles in stratus and convective clouds are taken into account.

Comparison of the numerical modeling results with surface and satellite observational data revealed, on the whole, satisfactory agreement. With the contribution of anthropogenic aerosol neglected, the DEAD model adequately simulates, for

instance, the annual change of migration of the trans-Atlantic dust plume formed due to dust storms in Africa as well as a maximum of DA outflow from the Asian continent to the region of the Pacific Ocean. According to the results of numerical modeling, the global characteristics of DA and its variability in 1990 (particles with the diameter $D < 10$ μm were considered) are as follows: $1{,}490 \pm 160\,\mathrm{Tg\,yr^{-1}}$ (total DA emissions); $17 \pm 2\,\mathrm{Tg\,yr^{-1}}$ (the amplitude of the interannual variability of emissions); 0.030 ± 0.004 (optical thickness at the wavelength $\lambda = 0.63$ μm). The following data characterize the contribution of various continents ($\mathrm{Tg\,yr^{-1}}$)[2]: 980 (Africa), 415 (Asia), 37 (Australia), 35 (South America), 8 (North America). All these estimates are substantially less than the values obtained earlier. The discussed results are characterized by underestimated transport and deposition of DA from Eastern Asia and Australia to some regions of the Pacific Ocean, which is partially determined by the underestimated contribution of the long-range transport of particles >3 μm. The results under discussion reflect the existence of hot spots (positive anomalies of DA emissions) in regions where easily saltating alluvial deposits accumulate.

Strong anthropogenic emissions of great amounts of MGCs and aerosols in large cities attract rapt attention to this problem in the context of possible impacts both on the environment and humans (in particular, on RF formation). One of the relevant examples is Mexico City located at an altitude of 2,240 m a.s.l., and its air basin (~18°N–20°N, 98°W–100°W) surrounded with mountains which serve as a barrier to atmospheric circulation. The processes of urban heat island formation are hindered in Mexico City by the complicated relief. In the morning, when cold air masses "flow down" from the mountains to the urban territory, a situation of air stagnation occurs and, respectively, pollutant concentration. After sunrise, a warming of the southwestern slopes of mountains favors the input of wet air masses from the Gulf of Mexico. The high altitude of Mexico City causes a reduction in oxygen concentration and promotes an increase in surface ozone concentration.

Based on the use of the NARCM regional model of climate and formation of the field of concentration and size distribution of aerosol, Munoz-Alpizar *et al.* (2003) calculated the transport, diffusion, and deposition of sulfate aerosol using an approximate model of the processes of sulfur oxidation that does not take the chemical processes in urban air into account. However, the 3-D evolution of microphysical and optical characteristics of aerosol was discussed in detail. The results of numerical modeling were compared with observational data near the surface and in the free troposphere carried out on March 2, 4, and 14, 1997. Analysis of the time series of observations at the airport in Mexico City revealed low values of visibility in the morning due to the small thickness of the ABL, and the subsequent improvement of visibility as ABL thickness increased. Estimates of visibility revealed its strong dependence on wind direction and aerosol size distribution. Calculations have shown that increased detail in size distribution presentation promotes a more reliable simulation of the coagulation processes and a more realistic size distribution characterized by the presence of the accumulation mode of aerosol with the size of particles ~0.3 μm. In this case, the results of visibility calculations become more reliable, too.

[2] 1 teragram equals 10^{12} grams.

In connection with the important role of sulfate aerosol (SA) in the formation of the direct and indirect impact of anthropogenic SA on RF, which affects climate, great attention has been recently paid to ARF numerical modeling. The calculated values of the global average direct and indirect ARF change, respectively, from $-0.2\,W\,m^{-2}$ to $-0.8\,W\,m^{-2}$ and from $0\,W\,m^{-2}$ to $-1.5\,W\,m^{-2}$ (i.e., they are comparable with positive RF due to the growth in GHG concentration). The wide range of uncertainties in calculated ARF is mainly determined by approximate results of numerical modeling of the global spatiotemporal variability of the aerosol content in the atmosphere as well as by difficulties in getting adequate consideration of the aerosol–cloud interaction.

Gong and Barrie (2003) undertook a numerical modeling of the impact of aerosol on climate with the use of an aerosol module developed in Canada, describing the global variability of sea salt and sulfate (both natural and anthropogenic) aerosol (considering its size distribution) and the latest (third-generation) model of global climate. The size distribution of both types of aerosol is parameterized by dividing the spectrum of particles size into 12 intervals. The aerosol is assumed to be internally mixed. A comparison of calculated spatiotemporal variability of aerosol concentration with that observed revealed satisfactory agreement. This refers, in particular, to the marine ABL (MABL). It has been shown by Gong and Barrie (2003) that sea salt aerosol particles favor suppression of the process of nucleation, an increase in surface area for condensation, and a change in the properties of clouds in the MABL, which determines a re-distribution of mass concentration and number density of sulfate aerosol. The results of separate numerical modeling of the dynamics of sea salt and sulfate aerosol suggested the conclusion that the presence of sea salt aerosol almost doubles the diameter of sulfate aerosol particles in the MABL at a high concentration of sea salt aerosol but causes a decrease (on global scales) of the mass of sulfate aerosol in the surface layer of the MABL within 5%–75% (depending on the distribution of sea salt aerosol particles).

Most substantial impacts of this kind take place in mid-latitudes of the Northern and Southern Hemispheres, and minimum impacts near the equator. The anthropogenic pollution of the atmosphere in the regions of the Pacific and Atlantic Oceans in the Northern Hemisphere results in decreasing concentrations of sulfate aerosol within 10%–30% due to sea salt aerosol. The greatest decrease (down to 50%–75%) takes place in the SH Roaring Forties in the spring and in the fall. The average global estimates of the impact of sea salt aerosol on decreasing mass and number of sulfate particles are, respectively, 9.13% and 0.76%.

The impact of sea salt aerosol determines the decrease in droplet number concentration in marine clouds (CDNC) by 20%–60%, with a maximum decrease in the NH Roaring Forties (40%–70%) and NH mid-latitudes (20%–40%), characterized by the high concentration of sea salt aerosol. Some increase in CDNC due to sea salt aerosol was also observed in the equatorial band. The impact of changes in aerosol content and cloud cover on global climate will be estimated in future.

The first indirect climatic effect of aerosol (the Twomey effect) is based on the assumption that with a constant equivalent liquid water content (LWC) of clouds an increase in atmospheric aerosol number density (and, hence, concentration of CCN)

should lead to an increase of cloud droplet concentration and cloud albedo (Twomey, 1974). In this connection, Feingold (2003) carried out a numerical modeling to analyze the possibilities of using the extinction coefficient, α, retrieved from the data of surface remote sensing, for the sub-cloud atmosphere as an indirect indicator of the impact of aerosol on the size distribution of cloud droplets. An adiabatic model of cloud droplets limited by consideration of a thin layer of non-precipitating strato-cumulus clouds (it is in this case that the supposition with respect to adiabatic nature can be considered acceptable) makes it possible to reproduce the hygroscopic growth of CCN and to take into account water vapor condensation on droplets (neglecting the growth of droplets due to coalescence). The model considered was used to calculate cloud droplet size distribution at a given size distribution of ammonium sulfate aerosol when the masses move upward at a velocity of $20\,\mathrm{cm\,s^{-1}}$–$300\,\mathrm{cm\,s^{-1}}$. The one-modal size distribution of aerosol, N, is approximated by the log-normal size distribution of particles at $20\,\mathrm{cm^{-3}} \leq N_a \leq 3{,}000\,\mathrm{cm^{-3}}$, median radius of particles $0.03\,\mu\mathrm{m} \leq r_g \leq 0.1\,\mu\mathrm{m}$, and distribution width $1.3 \leq \sigma \leq 2.2$. Different values of the mass share of ammonium sulfate and cloud water content are prescribed.

Estimates of the sensitivity of the effective radius of droplets, r_e, to various input parameters showe that r_e changes especially strongly depending on LWC (the impact of variations in this parameter was earlier neglected when estimating the indirect effect of aerosol on clouds and climate). The relative role of other parameters changes depending on observation conditions, but the importance of N_a remains unchanged. The impact of vertical motions manifests itself most at a high concentration of aerosol. Analysis of all the results obtained has led to the conclusion that the use of the extinction coefficient as an indirect indicator of the impact of aerosol on cloud droplet size distribution can lead to underestimation of the importance of the first indirect impact. The levels of possible systematic errors of the extinction coefficient remain uncertain in view of their dependence on the varying characteristics of aerosol (e.g., the aerosol number density, N_a, cannot be retrieved from the data of remote sensing), vertical motions, and LWC.

Fortmann (2004) discussed in detail the microphysical and optical characteristics of atmospheric aerosol which determine the formation of aerosol radiative forcing (ARF) (i.e., the climatic impact of aerosol in the Arctic). In particular, the following problems were considered:

(1) the physical and optical parameters of tropospheric aerosol and its specific impact on climate and on the formation of the Arctic haze;
(2) the general problems of measurements and numerical modeling of aerosol properties;
(3) a regional climate model HIRHAM-4 with parametrization of the aerosol dynamics for the Arctic (latitudes $>65°$N);
(4) a 1-D model of radiation transfer and consideration of the impact of aerosol and clouds on radiation transfer;
(5) the use of the HIRHAM-4 climate model to assess the climatic impact of the Arctic haze (AH); and
(6) an assessment of ARF from observational data.

Analysis of the numerical modeling results showed that consideration of AH determines an additional positive ARF within $1\,W\,m^{-2}$–$8\,W\,m^{-2}$ at the atmospheric top level over the snow ice surface of the Arctic Ocean, but over the open water of the Atlantic and Pacific Oceans the ARF values become negative, constituting about $2\,W\,m^{-2}$. The impact of AH on ARF at surface level manifests itself as an additional negative ARF reaching a maximum ($-7.5\,W\,m^{-2}$) over the open water of the ocean. An averaging of the shortwave ARF over the whole region of the Arctic gave a value of about $-2.4\,W\,m^{-2}$. Thus, the total ARF at the surface level is $-1.7\,W\,m^{-2}$.

The estimates of aerosol-induced changes in SAT obtained using the climate model showed that these changes vary from -1 K (over the East Siberian Sea and Canada Archipelago) to $+1$ K (in the region of Spitzbergen, Barents Sea, Kara Sea, and Taimyr Peninsula). There is the possibility of considerable interannual variations of monthly mean SAT reaching 2 K. It was shown that both direct and indirect (through affecting clouds) impacts of aerosol on climate are equally important. Use of observational data of aerosol characteristics near Spitzbergen (within the ASTER program on studies of tropospheric aerosol and radiation) demonstrated a strong regional variability for the impact of aerosol on SAT,from a cooling of -2 K in the Baffin Gulf and in the Laptev Sea to a warming of about 3 K in the Beaufort Sea.

Feczkó *et al.* (2002) estimated the radiative forcing due to aerosol and GHGs for Hungary of the early 1980s. The obtained results revealed considerable changes in RF due to ammonium sulfate and CO_2 for the last two decades. While the contribution to climate warming of the greenhouse effect as a result of increasing CO_2 concentration increased by 60%, the anthropogenic contribution to climate cooling due to sulfate aerosol decreased by 45% (i.e., the impact of both these atmospheric components on climate manifested themselves as a warming).

Various kinds of vegetation emit to the atmosphere a great amount of non-methane hydrocarbons (NMHCs). The total level of emissions in the vegetation growth period of such NMHCs as isoprene (C_5H_8), monoterpenes ($C_{10}H_{16}$), sesquiterpenes ($C_{15}H_{28}$), and oxygen-containing compounds ($C_nH_{2n-2}O$) constitutes $825\,TgC\,yr^{-1}$–$1{,}150\,TgC\,yr^{-1}$, exceeding the level of respective anthropogenic emissions (about $100\,TgC\,yr^{-1}$).

As Barr *et al.* (2003) pointed out, the importance of such emissions is determined mainly by their impact on the three processes taking place in the atmosphere. The first consists in that such NMHCs as isoprene form in the course of carboxylization in plants and contribute much thereby to the formation of biospheric carbon cycle. The second process is connected with NMHCs exhibiting high chemical activity with respect to such main oxidants as hydroxyl radicals (OH), ozone (O_3), and nitrate radicals (NO_3). Reactions with the participation of such components result in the formation of radicals of alkylperoxides (RO_2), which favor efficient transformation of nitrogen monoxide (NO) into nitrogen dioxide (NO_2), which favors an increase of ozone concentration in the ABL. Finally, NMHC oxidation leads to the formation of such carbonyl compounds as formaldehyde (HCHO), which stimulates the processes of O_3 formation. Finally, the oxidation of monoterpenes and sesquiterpenes results in the intensive formation of fine carbon aerosol with a particle diameter of $<0.4\,\mu m$

(the share of such aerosol production reaches 10%–30%), substantially affecting various processes in the ABL.

Barr *et al.* (2003) performed an analysis of the impact of phytogenic aerosol (PhA) which is defined as forming mainly due to monoterpene oxidation (primarily, α- and β-pinenes), on the radiative regime of the ABL over the forest in the eastern part of Canada. In the forest ecosystem the level of emissions to the atmosphere of biogenic hydrocarbons is moderate, with the concentration of α- and β-pinenes constituting about 1.6 ppb. NMHC oxidation resulted in the formation of PhA at a number density of particles of about $5 \cdot 10^8\ \mathrm{cm}^{-3}$. For a given concentration and size distribution of aerosol, its impact on the short-wave radiation transfer in the ABL was assessed.

Under clear sky conditions in July and with aerosol number density within $(2–5) \cdot 10^3\ \mathrm{cm}^{-3}$, the diurnal mean attenuation of global radiation constituted $0.04\ \mathrm{W\,m}^{-2}$ with the contribution of scattered radiation equal to $0.01\ \mathrm{W\,m}^{-2}$. A maximum level of global radiation attenuation due to PhA reached $0.2\ \mathrm{W\,m}^{-2}$. It follows from the obtained results that the PhA-induced reduction of the input of shortwave radiation can markedly compensate (on a regional scale) for the contribution of warming due to an enhanced atmospheric greenhouse effect. The PhA is also important as a factor of the impact on the optical properties of clouds functioning as CCN.

The global contribution of vegetation cover to emissions of volatile organic compounds (VOCs) to the atmosphere constitutes about 90%. Biogenic VOC emissions (BVOC) include isoprenes (C_5H_8), monoterpenes ($C_{10}H_{16}$), and other chemically active carbon compounds. The total content of carbon in global emissions of BVOC can exceed $1\ \mathrm{Pg\,yr}^{-1}$. Many BVOCs react with surface ozone and other oxidants in the atmosphere, substantially affecting chemical processes in the atmosphere on local, regional, and global scales. The presence of BVOCs determines, for instance, an increase of the lifetime of methane in the troposphere by about 15%. Due to BVOC transformation, $13\ \mathrm{Tg\,yr}^{-1}$–$24\ \mathrm{Tg\,yr}^{-1}$ of secondary organic aerosol are formed in the global atmosphere, which is comparable with the level of carbon aerosol formation due to fossil fuel and biomass burning. As Levis *et al.* (2003) noted, biogenic aerosol seriously affects the formation of radiation budget and CCN. This means that BVOC emissions strongly affect the global climate formation through their effect on chemical processes, atmospheric aerosol concentration, and the global carbon cycle. Therefore, the IPCC has recommended VOC emissions be taken into account in scenarios for emissions used in numerical climate modeling. According to respective estimates, the level of anthropogenic VOC emissions in 1999 averaged about $140\ \mathrm{TgC\,yr}^{-1}$, and estimates for 2100 give possible limits from $<100\ \mathrm{TgC\,yr}^{-1}$ to $>550\ \mathrm{TgC\,yr}^{-1}$. BVOC emissions depend on the type of vegetation and on environmental conditions (air temperature, solar radiation, water supply of plants, O_3 and CO_2 concentrations).

Levis *et al.* (2003) described an algorithm based on the data of field and laboratory measurements that enables calculation of BVOC emissions being used as a component of the interactive climate model CCSM (Version 2.0) for the atmosphere–ocean–land–sea ice cover system developed by National Center for

Atmospheric Research (NCAR) (U.S.A.) scientists. This development is a first step toward constructing a global climate model that takes into account the dynamics of biogeochemical cycles. To analyze the functioning of the CCSM model, two numerical experiments were carried out that took into account

(1) only land surface processes with a prescribed state of the atmosphere and satellite data on vegetation cover; and
(2) completely interactive processes in the climate system (including the pre-calculated dynamics of vegetation cover).

Calculation results have shown that in both cases an enhancement of BVOC emissions takes place in warm and forested regions (compared with other regions), agreeing with observed data. With the prescribed distribution of vegetation cover, global emissions of isoprene on land constitute $507\,\mathrm{TgC\,yr^{-1}}$, which closely corresponds to the results of interactive numerical modeling. When using an interactive model, BVOC emissions depend on climate change and vegetation cover, which vary from year to year. The interannual variability of calculated anthropogenic emissions can exceed 10% with respect to annual anthropogenic emissions corresponding to IPCC scenarios. This necessitates a consideration of BVOC emissions in the interactive global climate model.

The validity of this conclusion is confirmed by results of studies of RF due to organic aerosol obtained by Maria *et al.* (2004). A consideration of carbonaceous components in dust aerosol and aerosol products of combustion detected in Africa, Asia, and North America, showed that the rate of chemical reactions with participation of MGCs is three times lower than the characteristic values usually used in numerical climate modeling. Slower rates of transformation of volatile or hydrophobic organic compounds into condensed and hygroscopic ones results in an increasing amount of carbonaceous particles taken into account in climate models up to 70%. As a result, the climatic RF due to secondary organic aerosol increases to $-0.8\,\mathrm{W\,m^{-2}}$ (cooling due to scattering) and $+0.3\,\mathrm{W\,m^{-2}}$ (warming due to absorption). As a result, an absolute RF difference constitutes $1.1\,\mathrm{W\,m^{-2}}$ (i.e., it reaches one-half of the "greenhouse" RF, $2.2\,\mathrm{W\,m^{-2}}$).

1.2.5 Climate change, forests, and agriculture

Forest and agricultural ecosystems are the environmental components most sensitive to climate change. Forests determine many characteristics of GHG biogeochemical cycles, and agricultural systems form human–environment relationships vital for food production. An important indicator of the level of food demand is the size of population whose increase, by FAO (2006) estimates, will require a 5% increase in food production by the year 2015, compared with the present-day level. The problems arising are thoroughly studied in many international programs on the environment and climate. U.S. national programs pay special attention to them. In particular, analysis of the consequences of using various scenarios of possible global climate changes has led to the conclusion that in some scenarios of the impact on forestry and

agriculture in the U.S.A. they will be economically favorable. Partly this is connected with the growth in forest productivity (with a CO_2 concentration increase) and with the capability of forests to adapt themselves to climate changes. Of particular concern is the state of forests in the Amazon, with their greatest biodiversity in the world and, at the same time, the highest rate of deforestation due to the expansion of cities and farms (Barbieri and Carr, 2005).

During the last 100 years, about half the Earth's surface has been transformed (i.e., affected anthropogenically), and this means that ~50% of net primary production (NPP) has changed and, hence, practically all trophic levels of the land have changed their energy. Milesi *et al.* (2005), using satellite observations of NPP at 0.5° resolution and data on the global distribution of population, temperature, water, and clouds, analyzed the global NPP trends and found that more than half the world population live in regions where $NPP = 490\ gC\ m^{-2}\ yr^{-1}$. Before 1998, about 56% of the population lived in regions where the availability of water determined the NPP level. On average, 40% of NPP on the vegetation-covered surface correlates with climate variations due to ENSO, which affects almost 2.8 billion people.

Yue *et al.* (2005) studied the impact of climate changes on the land ecosystems of China. They give data on temperature and precipitation obtained since 1960 at 735 meteorological stations in China, and using the HLZ (Holdridge Life Zone) model, they show that the spatial distribution of these characteristics has strongly changed during the last several decades. In particular, in a snow-covered region and a subtropical arid steppe average values of these characteristics have rapidly decreased and they may disappear in 159 and 96 years, respectively, if these territories shrink at the present-day rate. The alpine dry tundra and cool moderate undergrowth have continuously expanded their areas during the last 40 years, on average, at a rate of 13.1% and 3.4% per decade, respectively. A warm moderate steppe, a subtropical moist forest, and cool moderate moist forest have shifted their boundaries during this period by 1,781.45 km, 1,208.14 km, and 977.43 km, respectively.

As for agriculture, according to prognostic estimates for the period to 2060, the positive impact of global warming on U.S. agriculture will be less economically favorable than follows from the estimates obtained earlier. Guerschman and Paruelo (2005) analyzed a relationship between the agricultural use of land and CO_2 assimilation on the American continent, using satellite measurements of NDVI for the period 1989–1998 and showed that CO_2 sinks in land ecosystems are functions of their state, and their changes can reach considerable magnitudes as a result of human activity. Lamptey *et al.* (2005), using the MM5 model, studied climatic sensitivity to changes in land covers in agriculture and in cities, with the northeastern part of the U.S.A. territory as an example. It was established that urbanization leads to a SAT increase of more than 1 K with a 0.04 K decrease in daily oscillations. The transformation of forested territories into agricultural lands leads to a SAT rise of more than 0.5 K in winter and 1 K in summer.

Hays *et al.* (2005) showed that stubble burning can cause a global change in atmospheric air. A study of the physical and chemical characteristics of substances emitted when burning the straw of rice and wheat has shown that the atmosphere receives particles 100 nm–1,000 nm in diameter, with the level of CO_2 content and the

CO/CO_2 ratio being important indicators of this process. The input of solid particles to the atmosphere for wheat and rice is estimated at $4.7 \pm 0.04\,g\,kg^{-1}$ and $13 \pm 0.3\,g\,kg^{-1}$ of dry biomass fluxes, respectively. For wheat straw, its burning delivers to the atmosphere K (31% weight/weight) and Cl (36% weight/weight), and for rice straw the emitted substances are mostly carbonaceous (84% weight/weight). Spectrometric analysis has shown that gases constitute 18% of emitted matter in straw burning. A study carried out by Otero *et al.* (2004) showed that biomass burning in South America in a dry season are of global-scale importance, since they lead to a considerable change in the optical characteristics of the atmosphere over vast territories as well as they change the elements of the hydrological regime due to water vapor condensation on smoke particles.

Unfortunately, due to the global and poorly studied character of correlation between climate change and vegetation cover behavior (forest ecosystems, in particular), at present there are no reliable estimates of the climate change consequences for their productivity. The problems arising here are just beginning to be studied. This especially refers to the boreal forests that cover ~15% of the land area (75% of them are in Eurasia, mainly in Russia). It is in these forests that the intensive gas and heat exchange with the atmosphere takes place.

1.2.6 Observational data for global change

Numerous national and global environmental programs and observational systems exist to provide data about the environment. One is the U.S. Global Change Research Program (USGCRP), a general objective of which is to provide space-based global observations which together with other observations and studies can generate new scientific information to help understand the Earth system. Global climatological information is supplied by the World Meteorological Organization (WMO), an intergovernmental organization with a membership of 188 Member States and Territories. Annual WMO reports survey a wide series of environmental problems. The most important questions answered in these reports are as follows:

- Is climate warming taking place?
- Is water cycle intensity changing?
- Are the atmospheric and ocean general circulations changing?
- Are extreme climate changes (storms, droughts, floods) intensifying?
- Is a reliable estimation of the anthropogenic contribution to climate change possible?

There exist many observational and theoretical studies that are trying to answer these questions. For example, Moron *et al.* (1998) undertook a detailed analysis of all available data on the spatiotemporal variability of SST worldwide and for individual regions, using Multi-channel Singular Spectrum Analysis (MSSA). The main goal of the analysis was to reveal the laws of variability and inter-basin relationships between

SST fields on time scales from interannual to interdecadal. The length of the observations series was enough for a reliable analysis of SST variability on time scales of 2–15 years, though it is more difficult to guarantee the statistical reliability of results for much longer periods.

In view of the great interest in SST variability in the Atlantic Ocean, emphasis was concentrated on this region. The irregular long-term SST trend turned out to be the strongest climate signal. Application of the MSSA method to data processing for the 20th century revealed well-known regularities: a gradual increase in SST in both hemispheres in the 1910s–1940s, with a subsequent increase in the Southern Hemisphere; cooling of the NH ocean in the 1960s to the end of the 1940s, whereas in the Southern Hemisphere the SST first was stable and then it increased, which determined a change in sign of the SST inter-hemispherical contrast in the early 1970s; finally, a SST increase in both hemispheres in the 1980s with a slight decrease in this trend in recent years. The results under discussion represent a stage of developments aimed at comparing the results of numerical modeling with the use of 2-D and 3-D models of the atmosphere–ocean system and the data of observations.

Analysis of the data on temperature measured in boreholes made an important contribution ito ideas about SAT changes in the past. For instance, Bodri and Čermák (1999) noted that if the amplitude of long-term SAT variations during transitions from glaciations to interglacial periods had reached 10 K–15 K in the Holocene (the last 10,000–14,000 years), changes of several °K would have taken place on time scales from decades to centuries. In this connection, analysis has been made of the data on the vertical profiles of temperature measured at different depths in boreholes, and maps have been drawn of SAT changes over the Czech Republic, which took place between 1100 BC to 1300 BC (small climatic optimum), between 1400 and 1500, and between 1600 and 1700 (main phases of the Little Ice Age).

Huang *et al.* (2000) discussed the results of processing measured temperature at different depths in 616 boreholes, 453 in the Northern Hemisphere and 163 in the Southern Hemisphere, from which global mean temperature for five centuries was retrieved. Data for 479 boreholes revealed a 1.0 K global warming during the last five centuries. It was only during the 20th century, which turned out to be the warmest, that the increase in continental surface temperature reached 0.5 K (about 80% of climate warming fell on the 19th and 20th centuries). The warming that took place over these five centuries was stronger in the Northern Hemisphere (1.1 K) than in the Southern Hemisphere (0.8 K). On the whole, the results agree with conclusions drawn from tree rings, though the latter revealed a somewhat weaker secular trend of SAT, which can be explained by particular features of the dendroclimatic method.

Analysis of the paleoinformation on SAT obtained from the data on oxygen isotopes in Greenland ice kerns from the Quaternary showed that long-term temperature changes are superimposed by much faster changes on time scales from a millennium down to 10 years (Bowen, 2000). Analysis of Antarctic ice kerns revealed similar changes. In particular, in the Holocene substantial temperature changes took place in both polar regions. Information about CO_2 dynamics during the last ice age can be evaluated based on studies of lake deposits in northern latitudes (Rundgren *et al.*, 2005).

Data on the planktonic foraminifer *Neogloboquadrina pachyderma* from the northeastern region of the Atlantic Ocean (west of Ireland) enabled retrieval of SST and the tracing of Heinrich events associated with iceberg kicks.

Information on the content of carbon dioxide and methane in air bubbles contained in ice kerns reflects the important role of these minor gas constituents (MGCs) in climate formation, but it is still unclear what took place first: change in temperature or in MGC content. For instance, it was recently shown that during four interglacial periods, changes in temperature in the Antarctic took place about 4,000 years before the changes in CO_2 concentration.

New results from numerical modeling of El Niño dynamics determined by variations in orbital parameters reproduced quite satisfactorily the Milankovitch Frequencies for the last 150,000 years, as well as variations on time scales of a millennium. However, most surprising were climate variations with a period of 1,450 years detected from different data for different global regions. These changes were regularly repeated (in particular, in Greenland) for the last 110,000 years, including the last glaciation and the Holocene (at times of glaciation the amplitudes of these changes were increasing).

These results reflect the radical reorganization of the climate system that took place during comparatively short periods. The Holocene seemed (compared with these changes) a period of a comparatively stable climate. There is no doubt that without climatic feedbacks the growth in GHG concentration in the atmosphere should cause climate warming. However, the actual situation is much more complicated, and to understand it, it is necessary to reliably detect and estimate the role of feedbacks. Otherwise, it is impossible to reliably predict future climate change. Since peat bogs are one of the most important sources of such information, they should be protected.

Having analyzed the data of SST satellite observations since 1982, Strong *et al.* (2000) noted a warming over a large part of the tropics and in mid-latitudes of the Northern Hemisphere (with the global mean trend of $+0.005^{\circ}\mathrm{C\,yr^{-1}}$). Data on SAT in the Southern Hemisphere are less representative and reflect the existence of an opposite cooling trend (the problem of SST data variability needs a thorough study).

According to the data obtained by Levitus *et al.* (2000) for the 50-year period (1948–1998), the World Ocean has become substantially warmer. The upper 300 m layer has warmed most (by 0.31°C, on average), whereas the temperature of the 3 km layer rose by 0.06°C. This increase in ocean upper-layer temperature preceded a SAT increase that began in the 1970s.

Satellite data on sea ice cover extent are important as an indicator of global climate dynamics. Gloersen *et al.* (1999) detected a statistically substantial shrinking of the global area of sea ice constituting $(-0.01 \pm 0.003) \cdot 10^6\,\mathrm{km^2}$ per 10 years. Researchers from NASA, the National Snow and Ice Data Center, and others using satellite data detected a significant loss of Arctic sea ice in recent years. On September 21, 2005, the sea ice extent dropped to 7.03 million $\mathrm{km^2}$, the lowest extent yet recorded in the satellite record. Incorporating the 2005 minimum with a projection for ice growth in the last few days of September 2007 brings the estimated decline in

Arctic sea ice to 8.5% per decade. Different explanations have been proposed for Arctic sea ice decline, including the strong positive mode of the Arctic Oscillation (AO). This oscillation is an alternating pattern of atmospheric pressure at polar latitudes and mid-latitudes. Data collected by several countries bordering the Arctic allow the construction of maps of the lateral sea ice extent since the beginning of the 20th century (Walsh and Chapman, 2001).

SHF remote-sensing data are special. Their analysis has not revealed any marked changes in the average temperature of the lower troposphere in recent decades. This is confirmed by the results of aerological sensings. From the data of Woodcock (1999a, b), the global mean SAT in October 1999 was 0.2°C below the average value for the period 1979–1999.

Santer *et al.* (2000) discussed the causes of differences between trends of SAT and lower tropospheric temperature. Having analyzed the SAT data for 1925–1944 and 1978–1999, Delworth and Knutson (2000) came to the conclusion that the main cause of SAT change was a combined impact of anthropogenically induced RF and unusually substantial multi-decadal internal variability of the climate system.

Satellite data on changes in the balance of Greenland glacier mass are an important indicator of climate dynamics. The results of laser altimetry for northern Greenland for 1994–1999 show that at altitudes above 2 km the ice sheet was, on the whole, in balance with local changes of different signs. A decrease in glacier thickness prevailed at low altitudes exceeding $1\,\mathrm{m\,yr^{-1}}$, which was enough to raise the World Ocean level by $0.13\,\mathrm{mm\,yr^{-1}}$ (this is equivalent to ~7% of the observed rise in ocean level). Satellite observations indicate that Greenland's glaciers have been dumping ice into the Atlantic Ocean at a rate that doubled between 2001 and 2006.

Observational data on water cycle parameters still remain fragmentary. An exception are such publications as Russo *et al.* (2000), which analyzed a change in the diurnal sum of precipitation at Genuine University Observatory for 1833–1985 and detected a decrease in the number of days with precipitation over the whole period of observations and a considerable growth of precipitation rate since 1950. During the last 50 years the number of days with intensive precipitation has substantially grown. Yu *et al.* (1999) analyzed both observed and calculated data. The radiation balance of the atmosphere was found from data of satellite observations of outgoing short- and long-wave radiation fluxes, as well as radiation fluxes at the surface level retrieved from satellite data. The values of turbulent heat flux at the surface level were taken from observations within the framework of the COADS program, and horizontal heat transport was calculated using the respective meteorological information. To minimize random errors, spatiotemporal averaging was carried out: zone-averaged atmospheric heat balance components were considered for the latitudinal belt 50°N–50°S, as well as values for this latitudinal belt.

Analysis of these data showed that the heat balance cannot be closed: an additional input of $\sim 20\,\mathrm{W\,m^{-2}}$ to the atmosphere is needed. Attempts to use different versions of input data bases were unable to remove this imbalance. Since water vapor balance could be closed using the same data, it seems that this imbalance is caused by inadequate estimates of the atmospheric radiation balance as a result of underestimation of calculated values of solar radiation absorbed by the atmosphere.

Having analyzed the adequacy and reliability of available observational data on climate, Folland *et al.* (2000) came to the conclusion that the existing volume and quality of data do not permit the questions enumerated above to be adequately answered. In this connection, the degradation of the systems of routine meteorological observations during the last decade is alarming. These observations are important for calibration of satellite remote-sensing results. Therefore, for some regions of Africa and vast regions of the World Ocean it is difficult even to retrieve the average values of climatic parameters.

Discussing the observed temporal regularities of global climate change and its causes, Wallace (1998) noted a first-priority necessity to consider the following problems:

(1) Periodic climate changes due to variations in extra-atmospheric solar radiation.
(2) Quasi-periodic variability of climate (its most vivid manifestations are quasi-biennial oscillations in the equatorial stratosphere).
(3) El Niño/Southern Oscillation (in view of a wide range of frequencies this event cannot be considered quasi-periodic).
(4) Interdecadal climatic variations which to a great extent are determined by internal intra-seasonal and intra-annual variability of the climate system).
(5) Climatic variability on time scales from interdecadal to secular.
(6) Analysis of the statistical significance of assessments of unprecedented events and "shifts of regimes" in light of the non-stationary character of the time series of many climatic parameters.
(7) Detection of phase ratios between climate changes on time scales from interannual to interdecadal.

The fact that most climate variability can be described by separately considering its dependences on time and space coordinates is important. In view of the baffling complexity of the climate system with its numerous degrees of freedom and feedbacks, the highly ordered structures and modes of climate evolution should be considered the exception—rather than the rule. "Rough" conceptualization schemes that do not attempt to simulate in excess detail the structure and evolution of climatic anomalies should be more stable. Really important climatic "signals" in solving the problems of detection and prediction of global climate changes need to be seen with the naked eye. A much more complicated problem than it is usually presumed to be is an evaluation of the statistical significance of any quantitative characteristics of climate change, especially unprecedented events and "shifts of regime" from data on short time series (because, as a rule, such series are unstable).

Apparently, a future direction for studies into climatic instability and related catastrophic events, like Hurricane Katrina (13 years after the most powerful in the history of Miami: Hurricane Andrew) in late August 2005 did huge economic damage, completely flooding New Orleans and destroying many buildings, is a search for connections between temperature variations at different scales in different basins

of the World Ocean. For instance, Chang *et al.* (2000) and Yamagata *et al.* (2004) showed that between SST variability in the Indian and Pacific Oceans there exists a sufficiently persistent correlation, which is especially manifested in the monsoon season in the basin of the Indian Ocean. The ENSO event that promotes the propagation of the subtropical anticyclone over the Western Pacific plays a marked role in stirring up the feedback mechanisms. Studies of the correlations that appear here are being successfully carried out using the interactive CGCM developed at the Center of the Ocean–Land–Atmosphere system study (COLA).

There are two key regions in the Pacific Ocean that play an important role in variations of upper-layer temperature: the western and central basins of the northern Pacific. The changes taking place here affect the climatic situation in many regions of Asia and in more distant regions. Therefore, it is important to study the complicated climatic composition in the Pacific region to reveal latent dependences between stimulators of future global climate change.

In studies of climate-forming processes, permafrost occupies a special place. Osterkamp (2005) gives the results of experimental measurements since 1977 in Alaska to determine the impact of climate on permafrost. It was established that during the period of observations the atmosphere and permafrost surface temperatures were gradually rising, with different spatial distributions in seasons, with maximum gradients in October–May and minimum ones from June to September. In the early 1980s, the permafrost temperature increased and then decreased as a result of a slight cooling of the atmosphere and growth of the snow cover. The Arctic sites once again started warming from 1986, and the inner continental regions from 1988. The general level of permafrost warming by 2003 reached 3°C–4°C on the Arctic coastline of Alaska, 1°C–2°C in northern and southern foothills, and 0.3°C–1°C south of the Yukon river. The rate of permafrost melting in different years varied within $4\,\mathrm{cm\,yr^{-1}}$–$10\,\mathrm{cm\,yr^{-1}}$.

1.2.7 Globalization and human-induced factors of climate change

Considering the prospects for developments within the CLIVAR program to study climatic variability, Bolin (1999) emphasized that the IPCC was very cautious in its evaluation in order not to go beyond the conclusions known from the scientific literature, on which such evaluations were based. The key fact is that it is necessary to distinguish between what can be considered reliable and what remains uncertain. As far as the prediction of climate in the future is concerned, there are still a lot of uncertainties. This approach gave the scientific community the confidence to make concrete decisions and should be preserved in the future.

Bolin (1999) emphasized that though IPCC 1995 contains a statement that global climate changes in the 20th century were partly determined by human activity, this conclusion was formulated rather cautiously. In this context, evaluation of the probable contribution of random climatic variations independent of human influence is critical. Results of recent studies have substantially elucidated this problem, showing that random variations in global mean SAT on time scales from decades

to centuries for the last 600 years were within $\pm 0.2^{\circ}C$ or less. (This conclusion, as mentioned above, disagrees with observational data, from which it follows that SAT had changed in the past within much wider limits.) In this connection (as Bolin, 1999 believes), with regard to evaluation of the contribution of anthropogenic warming during the last 50–75 years, the skeptics should be asked: How can we explain the much stronger global warming observed during recent decades?

In the addresses of official representatives of several countries at conferences in Kyoto and Buenos Aires as well as in the mass media, weather and climate anomalies, such as tropical hurricanes and unusual El Niños, were ascribed to global warming. Such opinions require, however, thorough scientific verification, though the possibility of more frequent anomalous phenomena under global warming conditions cannot be excluded. Therefore, the development of methods of climate prediction on a regional scale becomes urgent, and especially for the period 2008–2012.

In Bolin's (1999) opinion, to assess the socio-economic consequences of implementing the measures for GHG emission reduction recommended by the Kyoto Protocol, of great importance is the development of integral models representing a combination of the models of climate, carbon cycle, energy development, and socio-economic development, which will require much time and effort.

In this connection, a difficult problem is how to validate such models to analyze their reliability. The absence of adequate validation means that the results of numerical modeling using integral models can be considered only as possible scenarios—but not forecasts.

Characterizing climatic forcings, Hansen *et al.* (1998, 1999) noted that they have not been determined with sufficient accuracy for reliable climate predictions. There is sufficiently reliable information about the atmospheric content of GHGs that determine a positive RF, but serious difficulties are connected with assessment of the impacts determined by such factors as atmospheric aerosols, clouds, changes in land use, which result in a negative RF that partly cancels out the "greenhouse" warming of climate. One of the consequences of this compensation is the possibly more important role of changes in extra-atmospheric insolation (i.e., the Sun Constant, SC) as a climate-forming factor, than it was supposed earlier based on numerical modeling that only took GHG contribution into account (calculations of "greenhouse" RF due to the growth of CO_2 concentration since the beginning of the industrial revolution gave about $1.5\,W\,m^{-2}$).

In connection with this, Hansen *et al.* (1998, 1999) obtained new estimates for global mean RF. Table 1.11 shows the results of analytical approximations (with an $\sim$10% error) of various components of "greenhouse" RF (the recent detection of CF_5CF_3 as an important GHG testifies to the fact that the problem of substantiation of GHG priority cannot be considered solved). The total RF value is $2.3 \pm 0.25\,W\,m^{-2}$. It is interesting that in the period 1950–1970 RF grew from $0.01\,W\,m^{-2}$ to $0.04\,W\,m^{-2}\,yr^{-1}$, and during the subsequent 20 years it decreased down to $0.3\,W\,m^{-2}\,yr^{-1}$ in connection with a slowdown in the growth of CO_2 (despite the continuing growth of CO_2 emissions) for reasons unknown. A contribution was also made by a slowdown in the increase of CH_4 concentration, again for reasons unknown.

Table 1.11. Greenhouse radiative forcing F since the industrial revolution.

Gas	*Radiative forcing*
CO_2	$F = f(c) - f(c_0)$ where $f(c) = 5.04\,\lg(c + 0.0005c^2)$, c is CO_2 concentration (ppm)
CH_4	$0.04(m^{1/2} - m_0^{1/2}) - [g(m, n_0) - g(m_0, n_0)]$; $g(m, n) = 0.5\,\lg[1 + 0.00002(mn)^{0.75}]$ where m is CH_4 concentration (ppb)
N_2O	$0.04(n^{1/2} - n_0^{1/2}) - [g(m_0, n) - g(m_0, n_0)]$ where n is N_2O concentration (ppb)
CFC-11	$0.25(x - x_0)$ where x is CFC-11 concentration (ppb)
CFC-12	$0.30(y - y_0)$ where y is CFC-12 concentration (ppb)

Calculations of RF due to the growth in tropospheric ozone concentration gave a value of $0.4 \pm 0.15\,W\,m^{-2}$. A decrease in total content of ozone in the stratosphere could lead to RF equal to $-0.2 \pm 0.1\,W\,m^{-2}$. Though these changes in sign mutually cancel each other out to a great extent, this does not imply that they are insignificant, since variations of the ozone content in the troposphere and stratosphere affect substantially—but differently—the formation of the temperature vertical profile.

As for RF due to aerosol, it is still determined unreliably in view of the absence of adequate information about real atmospheric aerosols. Numerical modeling that takes anthropogenic sulfate and organic and soil aerosols into account for given global distributions of aerosol optical depth made it possible to evaluate the global distributions of RF and equilibrium surface temperature and then to obtain respective global mean changes in RF (ΔF) and surface temperature (ΔT_s) for purely scattering aerosols (single-scattering albedo $\omega = 1$) and more realistic aerosol (Table 1.12).

Table 1.12. Global mean RF for three types of anthropogenic aerosol.

Type of aerosol	$\varpi = 1$		*More realistic* ϖ	
	ΔF (W/m^2)	ΔT_s (°C)	ΔF (W/m^2)	ΔT (°C)
Sulfate	−0.28	−0.19	−0.20	−0.11
Organic	−0.41	−0.25	−0.22	−0.08
Dust	−0.53	−0.28	−0.12	−0.09
Total	*−1.22*	*−0.72*	*−0.54*	*−0.28*

$\varpi = k_a(k_a + k_s)^{-1}$ is the single-scattering albedo, k_a is the absorption coefficient, k_s is the scattering coefficient.

Hansen *et al.* (1998) noted that the most reliable estimate of total RF due to aerosol constitutes $-0.4 \pm 0.3\,W\,m^{-2}$ instead of the earlier estimate 0.54, though in any case such an estimate is still very uncertain due to unreliable input data on aerosol properties.

The anthropogenic changes to RF due to clouds are probably much more substantial than those due to aerosols, but even more uncertain. Such changes (including the impact of aircraft contrails) are mainly the result of an indirect impact of anthropogenic aerosols which cause variations in the particle size distribution and optical properties of clouds. Rough estimates give "cloud" RF from $-1\,W\,m^{-2}$ to $-15\,W\,m^{-2}$, but this can change by an order of magnitude (depending on prescribed input parameters). Conditionally, a value of $-1^{+0.5}_{-1}\,W\,m^{-2}$ can be accepted. Apparently, some increase in the cloud amount observed in the 20th century can be ascribed to an indirect impact of aerosols. Specification of such estimates means carrying out complex observational programs in different parts of the world.

The contribution of land use changes to RF variations is connected with deforestation, desertification, and biomass burning, affecting the albedo and roughness of the surface, as well as evapotranspiration (Chuang *et al.* 2006). It is also important to remember that a bare surface albedo changes more strongly with a settled snow cover than with a vegetation-covered surface. Approximate estimates of the Earth radiation balance due to land use evolution gave $-0.2 \pm 0.2\,W\,m^{-2}$.

Nature-induced RF for the last century due to SC changes (including an indirect impact on the ozone layer) can be assumed to be $0.4 \pm 0.2\,W\,m^{-2}$. Since total RF constitutes only about $1\,W\,m^{-2}$, the contribution of variations in extra-atmospheric insolation could play a substantial role.

Volcanic eruptions cause changes in RF from $0.2\,W\,m^{-2}$ to $-0.5\,W\,m^{-2}$ (these values, however, are very conditional). To analyze the possible anthropogenic impacts on global climate, estimates of the sensitivity of the climate system to external forcings are very important. Hansen *et al.* (1998) assumed that a change in global mean SAT with a doubled CO_2 concentration should constitute $3 \pm 1^{\circ}C$. The unreliable character of RF estimates makes it worthwhile to use different scenarios of RF changes. Developments in this field can be exemplified by the work of Tett *et al.* (1999).

Crowley (2000) estimated the contributions of various factors to climate formation (SAT changes) for the last 1,000 years using an energy–balance model of climate. According to the results obtained

(1) changes in global mean SAT during the last millennium can be explained as a result of the combined impact of known RFs (in the pre-industrial epoch 41%–64% of SAT changes took place due to extra-atmospheric insolation and volcanic activity);
(2) the global warming observed in the 20th century was mainly anthropogenic ("greenhouse") in nature, much exceeding the internally induced variability of the climate system.

Unfortunately, the arguments put forward by Crowley (2000) are unconvincing

even from the viewpoint of explaining the secular change in global mean SAT. For instance, the causes of climate cooling in the late 19th–early 20th century were not explained. Of course, the model considered cannot reproduce changes in regional climate. The role of northern Atlantic oscillations in climate formation was not revealed. On the whole, there is little doubt that the capabilities of approximate energy–balance models are confined to substantiating only very conditional scenarios of climate—but they cannot describe the dynamics of the real climate system. This conclusion also applies to results obtained using much more complicated global interactive models of climate (Knutson *et al*., 1999).

Emphasizing that low-resolution ($\sim 3^\circ$–6° latitude) climate models cannot reliably reconstruct (and, what is more, predict) climate change on a regional scale, Mearns *et al*. (1999) showed that these problems can be solved with two approaches.

(1) Statistical (with observational data taken into account) scaling (reducing to a higher spatial resolution) of numerical modeling results obtained using low-resolution models.
(2) Supplementing these models with a higher resolution "nest" of regional models.

In this connection, Mearns *et al*. (1999) undertook a comparison of the scenarios of anthropogenic climate change (with a CO_2 doubling) calculated using the stand-alone RegCM2 model developed at the National Center for Atmospheric Research (NCAR) and a semi-empirical method of scaling (SDS). In both cases large-scale numerical modeling was carried out using the GCM model developed at the Australian Commonwealth Scientific and Industrial Organization (CSIRO).

The results obtained show that the RegCM2 model reveals stronger spatial variability in the fields of temperature and precipitation than the SDS model. However, the SDS model shows a much greater amplitude in temperature annual change than the RegCM2 model or the GCM. The diurnal change in temperature turned out to be weaker with the SDS and the GCM than the RegCM2 model, and the amplitude of the diurnal change in precipitation varied between that corresponding to the SDS and RegCM2. RegCM2 calculations reproduced both an increase and decrease in precipitation probability with a doubled CO_2 concentration, whereas with the SDS only precipitation intensified.

One of the reasons for these differences could be the fact that the semi-empirical model SDS was based on data only from the 700 gPa surface level, whereas the two other models took into account the vertical structure of the atmosphere. However, this comparison does not allow us to draw a conclusion about which of the obtained results "correctly" reflect the effect of forcing. To answer this question and to determine the reasons for the above-mentioned differences, numerical modeling needs to be further improved.

An important illustration of the high level of uncertainty of theoretical estimates about the causes of climate change is the recent re-evaluation of the role of "Milankovitch mechanisms" as the main factor in climatic paleodynamics. The Milankovitch mechanism links climatic change with changes in the orientation of the Earth in its orbit around the Sun. According to Milankovitch theory (Crowley

and Kim, 1994), changes in paleoclimate are determined by re-distribution of the extra-atmospheric insolation both in latitude and in annual change as a result of variations in the Earth's orbital parameters (especially referring to glacial–interglacial cycles in the Quaternary), which include

(1) Inclination of the rotation axis with respect to the orbital plane (fluctuating within 22°–24.5°, with the present-day value 23.4°; the average periodicity of variation constitutes 41,000 years and mainly affects high-latitude insolation).
(2) Equinox precession affecting the time of onset of equinoxes and solstices, which is displayed mainly on low-latitude insolations (precession is characterized by a dual periodicity of 19,000 and 23,000 years).
(3) Eccentricity of the Earth's orbit, which varies from almost circular to strongly elliptical with a periodicity of about 95,800 years (these changes modulate precession).

Milankovitch (Rubincam, 2004) supposed, in particular, that the low level of insolation in summer high latitudes caused glaciation and ice sheet formation. The accompanying increase in surface albedo brought about a positive feedback, enhancing the effect of insolation decrease. The low level of insolation in summer took place at a minimum angle of orbital inclination, high eccentricity, and the NH summer apogee. According to Milankovitch's calculations, such a configuration took place 185,000, 115,000, and 70,000 years ago.

Though the Milankovitch conception has recently obtained further (but not general) recognition, its individual aspects have been subject to critical analysis. There are two reasons for this.

(1) Many new geological data have appeared after analyses of the kerns of sea bottom rocks and ice.
(2) Considerable progress has been achieved in the numerical modeling of climate.

Analysis of both these information sources has shown that an adequate explanation of paleoclimate changes is only possible after taking into account not only variations in the orbital parameters but also other climate-forming factors (in particular, variations in GHG content in the atmosphere, including CO_2, the most important one). In this connection, Palutikof *et al.* (1999) analyzed new geological data on paleoclimate changes with a high temporal resolution in the context of present-day ideas about global climate dynamics. Data from the analysis of ice kerns and pollen obtained in 1990 led to the following two important general conclusions:

(1) Some of the observed data do not confirm the description of cycles of glaciation by the Milankovitch mechanism (this refers, in particular, to the data on $\delta^{18}O$ in a vein of calcite at Devil's Hole in Nevada, which testify to the antiphase nature of cycles of glaciation).
(2) It follows from other data that this mechanism can explain only slow quasi-

periodic variations, but not transient variability (on scales from decades to millennia) which had occurred much more frequently than was supposed earlier.

Climate researchers Palutikof and Holt (2004) say that droughts appear to be linked to the formation of blocking zones of intense high pressure over the Atlantic Ocean that divert rain-bearing wind depressions away from the Mediterranean. This blocking may be related to the cycles of El Niño, the periodic reversal of winds and waves in the tropical Pacific Ocean. Due to the effects of toxic gases, it is assumed that year-round average temperature in southern Europe will reach 18°C by the year 2030 and rainfall will diminish by 19% to 20%.

This variability in global mean temperature could reach several degrees during several decades. A sudden large-scale climate cooling occurred in the Emsian interglacial (~122,000 years ago), when climatic conditions were very close to those of today. Typical examples of transient climatic variability are Heinrich events (Heinrich, 1988) and Dansgaard–Oeschger phenomena (Dansgaard *et al.*, 1993). Such events can repeat in the future.

Many uncertainties also remain about the impact of present changes in extra-atmospheric insolation on climate. Soon *et al.* (2000) detected, for instance, the super-sensitivity of the climate system to changes in UV insolation whose impact is enhanced by the feedback due to the statistical stability of clouds, influence of tropical cirrus clouds, and stratospheric ozone (the ozone–climate problem needs special analysis) (Kondratyev and Varotsos, 2000).

Interactive consideration of the dynamics of the biosphere as a climatic system component is particularly interesting. The importance of this problem can be exemplified by estimates of the climatic impact of the clearing of tropical forests in the Amazon basin obtained by Bunyard (1999). The Amazon River basin, consisting mainly of wet tropical forest (WTF), performs several important and still inadequately considered functions, including the input of energy from tropical to higher latitudes, which is under threat in view of the high rate of WTF destruction.

According to present-day estimates, up to 17 million ha of tropical forests are being destroyed every year, 6 million ha of which are in the Amazon basin. By the end of 1988, an area of 21 million ha was deforested, and 10 years later this area reached 27.5 million ha, which exceeds the size of the U.K.

The felling of WTF has an important impact on the global carbon cycle, since there is a danger of transforming WTF zones from sinks to sources of carbon for the atmosphere. The ecological aspects of WTF felling are also important in view of the ecological uniqueness of the tropical forests in Central and South America. According to available estimates, deforestation only in the Amazon River basin (over an area of ~360 million ha) will bring about an annual sink of carbon up to 0.56 billion tons, and globally the level of this source could reach $4 \cdot 10^9$ tC yr^{-1}. In 1998 forest fires resulted in tropical deforestation over an area of ~9 million ha, and from this source alone the atmosphere may well have received 1–2 billion tC.

Potter *et al.* (2005) analyzed the fluxes of carbon over the vegetation cover for a 17-year period (1982–1998) from ground and satellite measurements and, using the NASA-CASA model based on MODIS/AVHRR measurements and the radiation

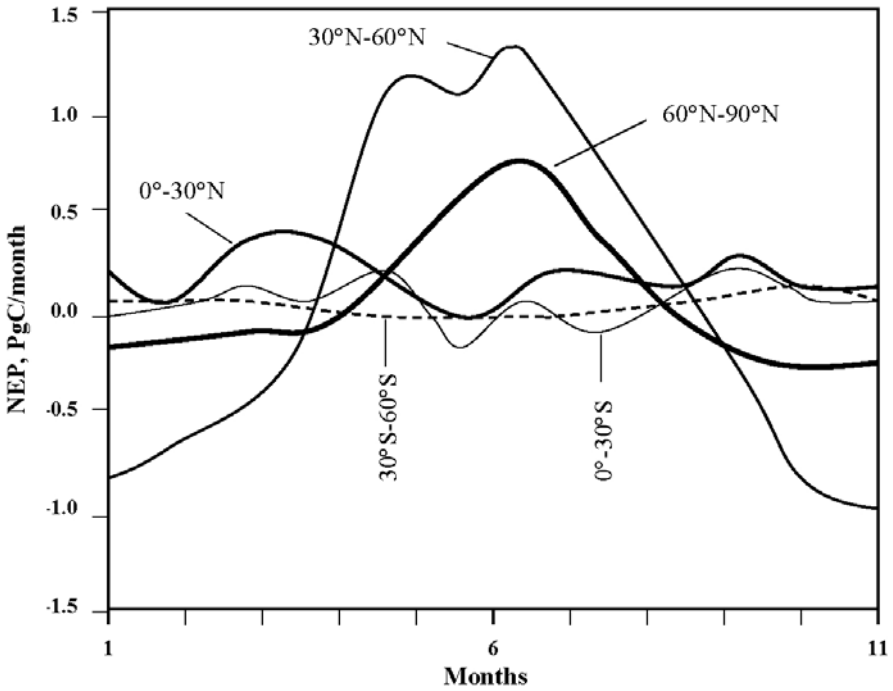

Figure 1.1. Zonal and temporal dynamics of NEP for land ecosystems. From Potter *et al.* (2003).

transfer algorithm, showed that the surface sink of CO_2 for Eurasia since 1988 constituted $0.3\,\mathrm{PgC\,yr^{-1}}$–$0.6\,\mathrm{PgC\,yr^{-1}}$, with a strong interannual variability in NEP. On the whole, for the year 2001, NEP was estimated at $+3.6\,\mathrm{PgC\,yr^{-1}}$ (Potter *et al.*, 2003). West Europe, the Balkan mountains, Scandinavia, northern and western Russia, eastern Siberia, Mongolia, western China, and central India were characterized by peculiar variability. This variability correlated with anomalous changes in precipitation and solar radiation over given territories. The general pattern of NEP distribution by latitudinal belts and months is shown in Figure 1.1. It can be seen that the latitudinal belt 30°N–30°S is characterized by oscillations in ecosystem pure primary production from $-0.5\,\mathrm{PgC\,mo^{-1}}$ to $+0.5\,\mathrm{PgC\,mo^{-1}}$. Total pure primary production increased from $45\,\mathrm{PgC\,yr^{-1}}$–$51\,\mathrm{PgC\,yr^{-1}}$ for the period 1982–1998 to $52.6\,\mathrm{PgC\,yr^{-1}}$ in 2001 (Potter *et al.*, 2003).

Over virgin tropical forests, about 75% of incoming solar radiation is spent on evapotranspiration. Therefore, WTF deforestation will result in radical changes in energy exchange and global atmospheric circulation. Still more substantial will be changes in local climate, especially from the viewpoint of the rain rate which could decrease by as much as 65%. Another problem is that we still do not know the threshold level for WTF destruction. This level determines an ecosystem's ability to self-support. If, for instance, this level is 20%, then the threshold has already been exceeded.

Bengtsson (1999) emphasized that since non-linear processes have the greatest effect on climate system variability, it is impossible to establish any simple connection between external forcings (e.g., the growth in GHG content or extra-atmospheric insolation variability) and the response of the climate system to these forcings. By taking the unpredictability of some factors of climate into account, the difficulty of distinguishing between anthropogenic and natural climatic variability becomes clear, and it is further hindered by the fact that both internal and forced modes of climatic variability are determined by the same mechanisms and feedbacks.

Despite considerable progress being recently made in numerical modeling of the climate system, it refers mainly to the atmosphere, which is demonstrated by the good agreement of the results of numerical modeling of atmospheric circulation with observational data. The results of "ensemble" numerical experiments indicate that the 3-D atmospheric circulation in the tropics is determined mainly by the impact of boundary conditions, whereas at high latitudes the impact of atmospheric dynamics prevails. A reconstruction of the water cycle in the atmosphere turned out to be realistic, too.

Considerable progress in modeling the interactive atmosphere–ocean system has made it possible to successfully predict seasonal and interannual variability and, in particular, El Niño events. The sufficiently adequate consideration of land surface processes ensured a substantial increase in hydrological prediction reliability (river run-off included).

In this context, Bengtsson (1999) discussed three directions taken in progressing numerical modeling of the climate. Successful accomplishment of the TOGA program promoted operational predictions of seasonal and interannual variability with prescribed SST changes in the tropics taken into account, which determined the critical significance of reliable SST data.

The second direction is connected with numerical modeling of climate change on a scale of decades and longer (in particular, with an explanation of the secular change in global annual mean SAT). Apparently, in the case of long-term climatic variability the influence of stochastic forcing (ISF) can be considered a zero hypothesis.

Consideration of the impact of low-frequency fluctuations of climate on Caspian Sea level showed that the long-term variability of the level is connected mainly with SST anomalies in the eastern part of the tropical Pacific Ocean. It turns out that positive SST anomalies correlate with the growing rain rate in the Volga River watershed basin and *vice versa*. The main reason for variations in Caspian Sea level is the long-term dynamics of El Niño events, which should be considered as chaotic.

An important part of the problem under consideration is the study of anthropogenic climate variability. Calculations showed that a doubling of CO_2 concentration should result in a decrease in outgoing long-wave radiation of $3.1\,W\,m^{-2}$ at the tropopause, and an increase of $1.3\,W\,m^{-2}$ in downward stratospheric long-wave radiation flux. Thus, the total radiative ISF at the top of the troposphere will be $4.4\,W\,m^{-2}$. Calculations of the resulting SAT change using climate models revealed a warming within 2.1°C–4.8°C as well as an increase in global mean rain rate within 1%–10%.

According to Bengtsson (1999), the secular trend in global mean SAT was characterized before 1980 by the prevailing contribution of natural variability with subsequent enhancement of the anthropogenic contribution. An important problem facing subsequent developments is an improvement in numerical modeling (mainly from the viewpoint of a more adequate consideration of various feedback mechanisms) in order to provide sufficiently reliable predictions on regional and local scales. An urgent problem facing global modeling consists in interactive consideration of biogeochemical cycles.

One of the most important aspects of numerical climate modeling is an evaluation of anthropogenic climate-forming factors. In this connection, Allen *et al.* (1999) discussed the possibilities of recognition, estimation, and prediction of the contribution of anthropogenic global climate changes characterized by SAT using the available data of observations and numerical modeling. The latter was carried out with consideration given to the internal variability of the climate system, the greenhouse effect (and related climate warming), and sulfate aerosol (climate cooling effect).

Application of four global 3-D models of the interactive atmosphere–ocean system gave values for global mean SAT increase over the period 2036–2046 (compared with the pre-industrial level) within 1.1 K–2.3 K. Calculations of climate system sensitivity to CO_2 concentration doubling gave values within 2.5 K–3.5 K. According to the HadCM2-G5 climate model developed at the Hadley Centre (U.K.), the global mean "greenhouse" warming in the period 1996–2046 should constitute 1.35 K, and with sulfate cooling equal to 0.35 the resulting warming will reach 1 K.

With the anthropogenic increase of SAT in the 20th century assumed to be (0.25-0.5) K/100 years, calculations made by a simple climate model give the level of uncertainty about a balanced SAT predicted by 2040 constituting (1–2) K. However, such estimates can be sufficiently reliable only by adequately considering the characteristic time for ocean adaptation. The necessity to take into account possible sudden non-linear climate changes, which seriously confines advance prediction, is a critically important aspect of prognostic estimates.

The most promising prospect for estimation and prediction of anthropogenic SAT changes has to do with an analysis of the spatiotemporal variability of SAT fields, which takes into account the impacts of the greenhouse effect and aerosols. Realization of this approach is seriously complicated, however, by the impossibility of reliably assigning the aerosol forcing on the SAT field. Another serious problem is the necessity to take into account the impact on climate of changes in the content of stratospheric and tropospheric ozone.

1.2.8 Contradiction between observational data and modeling results

The problem of anthropogenic climate warming is now the center of attention of not only specialists—but also of the general public. As we better understand this problem, so the sensation of inconsistency in the results obtained in this field increases, especially for the last decade. In this connection, Mahlman (1998) carried out an overview of such results to analyze the fundamental scientific aspects of the problem

under discussion, with emphasis on the role of numerical modeling and analysis of observational data in understanding present climate change. The works of Weber (1992) and Lau and Waliser (2005) were dedicated to this subject.

The main difficulty in understanding the causes of climate change is connected with the impossibility of considering climatic feedbacks sufficiently reliably. Primarily, this refers to cloud–radiation feedback, direct and indirect (by the effect on radiation properties of clouds) impacts of atmospheric aerosols on climate, and the impact of the atmosphere–ocean interaction on climate formation.

The often ignored peculiarity of the way in which greenhouse climate warming manifests itself consists in its great time constant determined by the inert nature of the climate system (the thermal ''memory'' of deep layers of the ocean lasts for centuries and even thousands of years). Schlesinger *et al.* (2000), for instance, found from observational data for the period 1858–1992 global oscillations of SAT with a period of about 65–70 years. It is important to take into account the principal differences between the numerical modeling (and prediction) of weather and climate. In the case of climate, it is important to ''tune'' and adjust in view of the difficulty of adequate consideration of the complicated totality of interactive processes and spatiotemporal scales. In this context, the use of paleoclimatic data plays a substantial role, though they cannot serve as analogs to possible climate change in the future.

Another serious concern relates to the adequacy of global observing systems, and especially the degradation of ground observations manifested in some cases. Mahlman (1998) emphasized that the contradictory character of the problem of anthropogenic climate change consists in the absence of reliable quantitative estimates of relationships between the contributions of natural and anthropogenic factors of change. It is this fact that creates serious difficulties for practical realization of Kyoto Protocol recommendations.

Such conclusions, discussed earlier in detail, are gaining growing recognition, as illustrated by the recent overview of Grassl (2000). In this context, the widespread use of the term ''climate change'' (implying it is caused only by anthropogenic factors) is rather bewildering. Also illegitimate is substitution of the term ''global warming'' for the notion of ''climate change'' (in its true meaning), since both observational data and numerical modeling results testify to the high spatial heterogeneity of present-day climate change.

This terminological misunderstanding is not accidental, however. In fact, it is aimed at disinformation for the sake of establishing a false conception of anthropogenic (greenhouse) global warming, which was convincingly explained by Boehmer-Christiansen (2000) who analyzed the political motivation behind this conception.

In August 1997, Secretary of the U.S. Geological Survey Bruce Babbitt, in his address to about 3,000 participants at the *Annual Meeting of the Ecological Society of America*, said that they should fulfill their civic duty; they should convince the skeptical American people that global warming is real and dangerous. In this connection, Morris (1997) carried out an overview of the available scientific information to analyze the grounds for this statement, since many specialists do not support the apocalyptic predictions of anthropogenic global warming. Emphasis in the overview

was placed on the problem of distinguishing between natural and anthropogenic climatic changes. In addition to the evidence that global warming is not so far an anthropogenically caused phenomenon, Kaiser (2000) gave values of the process of land dehydration in the south of the U.S.A. since 1930, and showed that these processes observed for the last 50 years took place during the last 2,000 years. In the mid-1970s, forecasts of global cooling due to sulfate aerosol predicted, for instance, that this impact would confine any increase in global mean temperature due to enhanced atmospheric greenhouse effect to a value of $<2^{\circ}C$ even with an eight-fold increase in CO_2 concentration. The cooling trend that appeared in the 1980s made the problem of climate warming the center of attention. At the height of the sultry summer of 1988, Congressman John R. Hansen declared at the U.S. Congress a 99% probability of anthropogenic climate warming and its destructive consequences for ecosystems in the future as well as the presence of consensus on this problem among specialists, though many meteorologists and climatologists did not share these opinions: respective developments did not allow reliable cause-and-effect relationships to be established between anthropogenic emissions of GHGs and observed climate change.

The political motivation behind support of the global "greenhouse" warming conception brought about a huge increase in governmental financing of such developments in the U.S.A. for the period 1990–1995 from £600 million to $1.8 billion.

In the context of estimating the contribution of various factors to global climate formation, Morris (1997) indicated the importance of combined consideration of the contributions of the greenhouse effect and solar activity, which over the period of measurements constituted $0.31^{\circ}C$ and $0.41^{\circ}C$, respectively. According to these estimates, a doubling of CO_2 concentration will lead to global warming within $(1.26–1.33)^{\circ}C$. With such changes in climate there are no grounds to expect often-predicted catastrophic consequences, such as a rise in World Ocean level and an increase of epidemiological diseases. There is little doubt, however, that we should expect an increase in crop yield. On the whole, the consequences of climate warming should be positive. Even though reliable forecasts of the ecological consequences of GHG emissions are impossible, it is clear that their reduction will be harmful for the economy. Therefore, the main conclusion is that we should not try to prevent still unreliably predicted climate changes, but adapt oneself to them. However, the grounds for such a conclusion were disputed in numerous publications (Hansen *et al.*, 1998; Houghton, 2001; Hulme *et al.*, 1999; Wigley, 1999).

In view of the complexity of the climate problem, in scientific publications on this subject the emphasis is usually placed on the serious uncertainty of existing estimates, which, on the one hand, favors continuation of studies, but, on the other hand, is fraught with important consequences in the context of ecological policy. As Boehmer-Christiansen (1997) noted, the "ecological" bureaucracy and experts as well as well-organized representatives of the fuel and energy industry are strongly interested in proof of the existence of anthropogenic warming and want to get the needed support of science. These three groups, which share common interests, support non-governmental ecological organizations and thoroughly strengthened them after the *Rio de Janeiro Conference*.

The main targets of "green" pressure are governmental departments which, in view of the wide range of their responsibilities, either do not want to or cannot accomplish the required measures, such as ecological taxes, subsidizing renewable energy sources, nuclear energy, public transport, energy efficiency, etc. The World Bank (WB) and Global Ecological Fund (GEF), which support numerous and costly developments (pure technologies, etc.) controlled by a great number of the specially employed experts and specialists in the sphere of finance, are also lobbied.

It is no mere chance that the IPCC was contemplated in 1985, planned in 1987, and started functioning in 1988. Governments of different countries support the plans for GHG emission reduction not for ecological—but for other reasons: intensification of national nuclear energy (Germany), an increase in the export potential for power energy produced by nuclear power stations (NPSs) and gas stations (France, Norway), an increase in financial support, etc. Naturally, those countries where power energy depends on coal are the most skeptical about "greenhouse" warming.

Having analyzed the role of different international organizations and programs in the problem of global climate changes, Boehmer-Christiansen (1997) emphasized that climate-related policy cannot be understood without a deeper analysis of the role of science and scientific understanding of the coalition of non-ecological interests (both commercial and bureaucratic), which are the driving forces behind the development of events on an international scale. It still remains unclear where the coalition will take us.

Constructive prospects to solution of this problem are connected with the development and application of complex models to evaluate possible changes in climate and socio-economic development. Parson and Fisher-Vanden (1997, 1999) and Dessler and Parson (2005) prepared a detailed overview of the methods and results of numerical modeling of global climate changes with the dynamics of socio-economic processes taken into account, in which basic aspects of so-called integrated assessments (IAs) were discussed. The main goal of such developments is substantiation of recommendations for decision-makers in the sphere of ecological policy.

Four concrete goals include the following:

(1) assessment of possible response to climate change;
(2) analysis of the structure of scientific principles of modeling and characteristics of the uncertainties of the results obtained;
(3) comparative assessments of possible risks;
(4) analysis of scientific progress achieved.

During the last few decades, two approaches have dominated in the development of IA models: (1) the use of values obtained by inter-disciplinary groups of experts; (2) formal numerical modeling. The first of these approaches is characteristic of IPCC efforts and developments within the framework of the Montreal Protocol, whereas the second approach is practiced by individual specialists. The use of IA in the analysis of possible impacts of climate changes on the development of energy and economy in the context of the problem of CO_2 emissions to the atmosphere has attracted special attention.

A general evaluation of the obtained results consists in that IA models cannot be used to substantiate highly specialized measures, because they are not sufficiently detailed. Application of such models, however, is of great importance for the assessment of possible uncertainties and, hence, the expediency of making decisions. In this connection, it is essential that most substantial uncertainties in the system on the whole or in recommendations for the needed ecological policy can turn out to be not the uncertainties that are most important for understanding the environmental changes or are widely variable.

When considering data for concrete models uncertainties can be ranged by their significance, but this ranging depends on the specific character of the models. Though the use of IA models has made it possible to substantiate some interconnections between socio-economic development dynamics and environmental variability, the obtained results should be considered only as preliminary. So far, the use of IA models has only slightly contributed to the assessment of comparative risks and helped to answer the fundamental question to what degree and in what respects are possible climate changes most substantial.

In view of these circumstances, so far results from the use of IA models to substantiate an adequate ecological policy have been rather limited, and this refers even to purely didactic assessments on the basis of simple models. The main problems of IA model improvement include insufficient understanding of probable impacts and possibilities of adaptation; poorly substantiated or totally absent description of social and behavioral processes in developing countries; an extremely limited idea of unlikely, non-radical climate changes. Despite these and other unsolved problems, the urgent need of further efforts in developing IA models raises few doubts.

In recent years, neuron models have been successfully used; they are more stable than traditional climate models. For instance, Pasini *et al.* (2006) considered an application of the neural network for climate modeling. The study was carried out into the temperature trend on regional and global scales for the last 140 years. It showed that the model based on the neural network reproduces with high accuracy the non-linear effects observed in temperature variations over the northern Atlantic.

Finally, again, we emphasize that the global observing system must be improved. The urgency of this problem can be illustrated by the results of the work of Demirchian *et al.* (2002) which demonstrates a complicated spatiotemporal variability of SAT in high latitudes of the Northern Hemisphere as well as the unsubstantiated stereotype of the conception of "greenhouse" warming, according to which under Arctic conditions the impact of the growing concentration of GHGs in the atmosphere should be especially strong.

1.3 LONG-RANGE TRANSPORT OF AEROSOLS AND TRACE GASES

Numerous observations of the content of chemical compounds in the atmosphere over different territories showed that there is undoubted evidence for their movements over large distances. Among the key moments of such studies the following results should be mentioned (Matthies and Scheringer, 2001; Kravtsov, 2002):

- ozone from North America prevails in the ozone distribution over the northern Atlantic in summer;
- emissions of chemical elements in Asia affect chemical processes over the northwestern basins of the Pacific;
- sulfur oxidized over the western Pacific comes from sources located in Asia;
- there is a stable mechanism for the transport of pollutants from North America to northern Atlantic basins;
- transport of pollutants between continents is controlled by meteorological fronts and by the impact of moving air masses;
- balance of ozone in the troposphere over the northern Atlantic depends on NO_x and VOC content in the atmosphere over North America;
- formation of the ozone layer in the free troposphere over the northern Atlantic depends strongly on NO_x emissions by aircraft;
- in the Northern Hemisphere, there is an intercontinental transport of CO due to forest fires and biomass burning;
- a summer-positive and winter-negative correlation between CO and O_3 concentrations is found over the northern Atlantic;
- long-range transport of dust particles from Asia and Africa to other territories was recorded in some international experiments;
- there is much evidence of the accumulation of chemical elements in organisms, soils, and water basins that originate from distant regions; and
- exploitation of oil deposits in Siberia ensures an input to tundra and taiga of a wide spectrum of heavy metals and organic compounds.

Observations of the long-range transport of atmospheric pollutants, organized within the framework of some international programs such as IGAC, facilitated the discovery of a number of effects, among which the following should be mentioned:

- the summertime ozone flux to the northern Atlantic from anthropogenic sources in North America totals (1.0–1.6) g mole da^{-1} and is detected at distances 1,500 km–3,000 km; and
- the amount of NO_x delivered to the lower troposphere of the northern Atlantic in the summer period promotes an increase in ozone content by 1 ppbv da^{-1}–4 ppbv da^{-1}.

Thus, the long-range transport of substances and gases is one of the important factors of the spatiotemporal variability of aerosol and gas concentration in the atmosphere. Though most aerosols remain in the planetary boundary layer (PBL), some desert dust and biomass-burning smoke can be lifted to the free troposphere and transported over great distances, even between continents. For instance, the long-range transport of pollutants to the western coast of North America from Asia was confirmed by numerous analyses of the content of chemical compounds in deposits, snow, fish, and birds. Pesticides, nitrates, sulfates, heavy metals, polychlorobiphenyl, among others were found to have been transported across the Pacific Ocean. In particular, such distant transport was confirmed in April 1998 during a

powerful dust storm in the west of China, with resulting dust clouds recorded by satellite survey. A detailed study of the intercontinental transport and transformation of aerosols and gases was carried out in the summer of 2004 in the INTEX-NA experiment within the international program ICARTT where measurements from satellites Aqua, Terra, and Envisat were used together with observations from NASA's DC-8 and J-31 aircraft. Emphasis was placed on assessment of the quality of the regional atmosphere, effects of intercontinental transport of chemical compounds, and calculations of atmospheric radiation balance.

Ginoux *et al.* (2002), from observations at Barbados and Miami, showed that there is a dependence of interannual and seasonal oscillations of atmospheric aerosol concentration over the northern Atlantic on climate conditions in North Africa. A comparison of these observations for the period 1981–1995 along with the results of modeling the processes of aerosol transport using the GOCART model, suggested the conclusion that the input of dust from North Africa and its deposition over the Mediterranean is determined by the North Atlantic Oscillation (NAO). The main results of Ginoux *et al.* (2002) suggest that the interannual variability of dust over the Atlantic is a combination of variable dust emission and transport, both forced by the NAO.

In addition to these processes of long-range transport of atmospheric pollutants, there is the problem of evaluating the role of high concentrations of MGC aerosol particles recorded in the atmosphere of the Amazon River region and central Brazil during the dry season, which is connected with intensive biomass burning and natural forest fires. Freitas *et al.* (2005) estimated, for these reasons, the atmosphere of South America receives annually up to 30 Tg of aerosol particles, most of which reside in the atmosphere for about a week, with an additional input to the atmosphere of CO, VOC, NO, NO_2, and other gases. From the available data, even in the optical range the space-derived images record smoke clouds covering an area of 4 million km^2–5 million km^2. Such a smoke load can change the global radiation balance and strongly affect the biospheric water cycle. The consequences of smoke-loading of large territories can be assessed only with the help of global models such as GOCART, MOZART, or RAMS (Chin *et al.*, 2002). As studies showed (Freitas *et al.*, 2005), what is important in these assessments is the classification of the types of smoke sources connected with processes such as controlled biomass burning or natural forest fires. As a result of biomass burning the atmosphere receives, on average, $1{,}700\,gCO_2\,kg^{-1}$ and $60\,gCO\,kg^{-1}$, and as a result of natural forest fires these fluxes constitute $1{,}524\,gCO_2\,kg^{-1}$–$1{,}670\,gCO_2\,kg^{-1}$ and $70\,gCO_2\,kg^{-1}$–$140\,gCO\,kg^{-1}$, respectively. The burning of dry vegetation on meadows or in savannahs gives $65 \pm 20\,gCO\,kg^{-1}$.

Investigations carried out within the framework of the ITCT project under the IGAC program were aimed at studying the tropospheric chemistry and the atmospheric transport of ozone, small dust particles, and GHGs and their components. The main goal of these investigations was to understand how one continent can affect the air quality over another continent, and what chemical transformations take place during the intercontinental transport of atmospheric pollutants (Singh and Jacob, 2000). In carrying out these studies, an important problem is the choice of method for

evaluation of air quality. In this connection, Riccio *et al.* (2006) noted that to minimize the effect of unavoidable uncertainty in modeling air quality, the Bayesian approach is a good option as it makes it possible to carry out, with a high degree of accuracy, a spatiotemporal interpolation of experimental data.

During the long-range transport from a source region to a distant territory, the microphysical, optical, and radiative properties of aerosols get modified. Information about the impacts of transformation of aerosols and the processes of mixing during long-range transport is very important for

- quantitative estimates of RF due to aerosols;
- assessment of heterogeneous processes; and
- determination of synoptically and climatologically important characteristics such as optical thickness.

As part of some international and national projects, many measurements of atmospheric optical thickness were carried out. By using passive satellite sensors, estimates can be averaged vertically over a surface pixel. Therefore, to get a deeper understanding of the optical thickness of atmospheric layers, aircraft measurements are made which give the vertical distributions both of tropospheric aerosols and other characteristics of the atmosphere. Among successful airborne experiments we should highlight the ITOP, SHADE, and SAMUM experiments. These experiments made it possible to study the transformation of aerosols during the distant transport of smoke and desert dust.

As part of ITOP, measurements were carried out onboard the flying laboratory Falcon-20 which was able to monitor aerosol concentration and gas traces north of Paris in July–August 2004. Synchronous measurements were made with ground-based aerosol lidar which made it possible to assess the vertical structure of the atmosphere. During these measurements aerosols were detected from Canada and Alaska having crossed the North Atlantic, where at this time there was biomass burning. The Falcon-20's equipment enabled us to

- record particles from 4 nm to 100 μm in size;
- record particle size variability;
- determine the optical properties of non-spherical particles; and
- accumulate particles with a diameter <4 μm for further chemical analysis.

Atmospheric aerosols affect the Earth's radiation balance directly through interaction with solar and terrestrial radiation and indirectly through cloud condensation and ice particles in the atmosphere. Since polar regions are characterized by a sufficiently pure atmosphere, even an insignificant increase in aerosol concentration due to distant transport can strongly disturb the radiation fluxes in these regions. Studies within ACE-1 showed that even distant regions of the Arctic are not protected against the global scattering of Asian dust (Stone, 1998). Detection of chemical compounds in the Arctic atmosphere which could have been emitted from Asia or

any other region, where the sources of the pollutants detected in the atmosphere are unknown, is another global problem.

A further problem related to the distant transport of aerosols is evaluation of the consequences of possible ingress into the environment of heterogeneous micro-organisms capable of causing undesirable and uncontrolled changes in ecosystems. In any event, transported micro-drops of water or particles along with solid substances can contain micro-organisms (which penetrate them or reside on their surface) from cultivated soils, sources of industrial activity, forest fires, and dust storms in deserts, or storm processes on the ocean surface. Winds carry billions of tons of dust across the globe, and this amount grows simultaneously with developing desertification, more frequent occurrence of droughts, and large-scale change in hydrological structures.

Water drops in the atmosphere can contain dissolved ions and organic compounds, and solid dust can condense these drops on its surface. There are a lot of data on the climatic impact of aerosols (Kondratyev *et al.*, 2006a), but their role in the impact on biological processes due to the long-range transport of micro-organisms was studied inadequately. In connection with this, there are some unanswered questions.

- Can micro-organisms transported through the atmosphere as outlined above affect ecosystem evolution?
- How can micro-organisms survive under extreme conditions (e.g., radiation, temperature, snow, and ice in high latitudes) in other territories?
- Are there conditions under which pathogenic infections could remain in dust clouds for a long time and as a consequence be a threat to human health or biological communities?
- Is there enough information and data to be concerned about the impact of long-range atmospheric transport on possible environmental changes in regions far from civilization?
- What uncertainties limit the possibility to reliably assess the significance of long-range atmospheric transport, and what is its real contribution to current environmental changes in distant regions?

From a biological perspective, it is important to study the type and amplitude of chemical compounds which can propagate through the atmosphere at long distances. Several questions come to mind here too.

- How many chemical compounds of biogenic type can reach the atmosphere without being transported in it?
- Can these compounds be detected in the atmosphere, rain, or snowfall?
- Which of these chemical compounds are able to cause trophic effects after distant transport?
- Can chemical compounds of biogenic type transported at long distances cause changes in water ecosystems and over territories that have a low level of biogenic provision (e.g., high mountains)?

- What types of micro-organisms can be transported to distant regions through the atmosphere and what immunity against them do ecosystems located there have?

The transport of small-grain aerosol dust from the Mongolian Gobi desert to North America is normal in spring. Dust contains silicon, iron, aluminum, and calcium, and the sizes of particles are distributed between 2 μm and 4 μm. It is difficult to differentiate this dust from volcanic ash and aviation ejections. The creation of instruments to recognize these types of dust particles is important in connection with the dangerous long-range transport of micro-organisms. Asian dust transported for thousands of kilometers can be dangerous to human health elsewhere. Therefore, knowledge of the character and origin of dust residing in the atmosphere is of principal importance for human health protection. Hence, Beyer and Matthies (2001) studied the long-range transport potential (LRTP) of the exchange of chemical compounds between different natural domains.

To assess the global transport of CO and CH_4 in the lower troposphere, NASA launched in 1998 the Terra (EOS AM-1)/MOPITT satellite at an orbit of 705 km, it had a spatial resolution of 22×22 km and could scan a band 600 km wide. From processing the data obtained, Choi and Chang (2006) found that high concentrations of CO along the eastern coast of the Japan Sea were caused by the distant transport of CO from regions of biomass burning in Siberia and from industrial regions in China. The levels of CO over eastern China exceed 35 ppb due to biomass burning in Myanmar and Indo-China. The difference in CO concentrations over the eastern coast of the Japan Sea between periods of forest fires (217 ± 18 ppb) and their absence (186 ± 15 ppb) averaged 31 ppb. Also, the obtained estimates confirmed that the average rate of CH_4 concentration increase in the atmosphere is close to 1% per year, but a unique conclusion about the sources of this increase cannot be drawn. Inomata *et al.* (2006) made attempts to overcome the uncertainties in the biogeochemical cycle of chemical compounds in the region of the Japan Sea. In 1995 and 1996, measurements were made of the concentration of sulfur dioxide, ozone, sulfur, and volatile sulfurous compounds over the coast of the Japan Sea at altitudes between 0.5 km and 5.5 km. These measurements showed that concentrations of particles and short-lived sulfurous gases (CS_2, H_2S, SO_2) strongly differ in seasons due to a change in the direction of air mass movements and meteorological conditions. For instance, the mineral dust particles detected on April 23, 1996 were of desert origin and were driven by westerly winds from the Asian continent. On the other hand, the measurements on December 28, 1995 revealed low concentrations of particles and short-lived sulfurous gases.

Lin *et al.* (2005) assessed the impact of the long-range transport of pollutants on air quality over Taiwan from observational data made using the monitoring network TERA in 2000 and 2001 during winter monsoons. It was shown that distant transport adds 30 μg of pollutants to each cubic meter of atmospheric air. The partial pressures of CO and SO_2 increase by 230 ppb and 0.5 ppb, respectively. Air masses coming from Asian contain $71 \pm 34\ \mu g\,m^{-3}$ of dust. On the whole, the impact of distant transport shows up better in coastal zones than in inland cities.

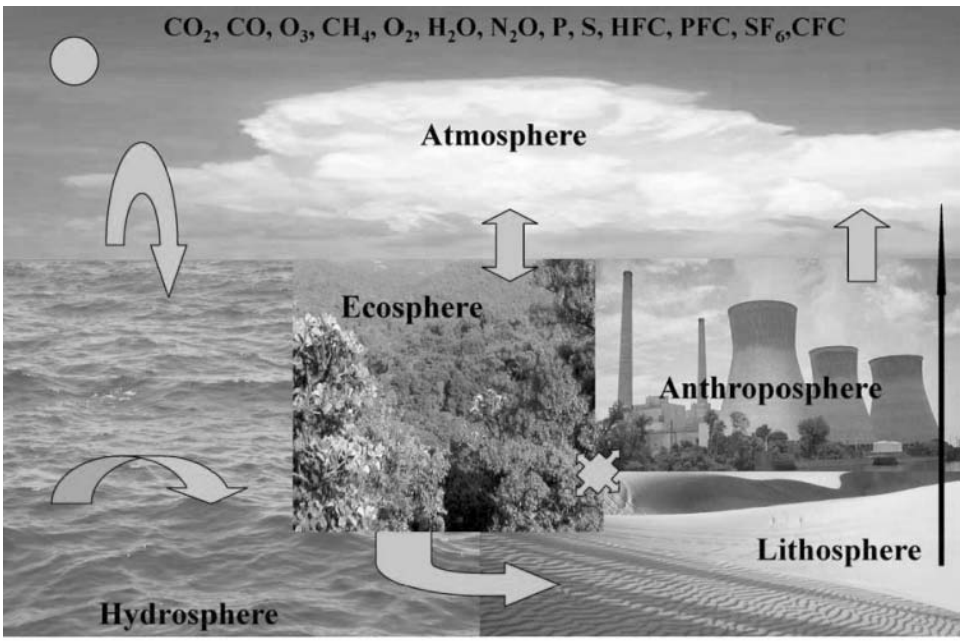

Figure 1.2. The structure of global environments, sources, and sinks of chemical contaminants that take part in biogeochemical cycles.

These and similar observations indicate that, to remove the uncertainties in assessing biogeochemical processes, a global model is needed of the biogeochemical cycle of chemical compounds which can combine the available knowledge and suggest regimes that need to be observed (Kondratyev *et al.*, 2005). Moreover, this model would need to parameterize the interaction of biogeochemical cycles and their impact on the climate system through the dynamics of GHG concentrations in the atmosphere (Schulze, 2000). The biogeochemical cycles of chemical elements cannot be considered separately from other manifestations of global ecodynamics, especially from those processes taking place in ecological and social spheres. The energy fluxes in these spheres, governed by nature and humans, affect directly the power of local and regional fluxes of gases and aerosols which due to the atmosphere and hydrosphere reach a global scale (Dearden and Mitchel, 2005). Therefore, the structure of the global domain shown in Figure 1.2 should be considered in the GMNSS along with both the spatial and temporal heterogeneities inherent in physical, chemical, biological, socio-economic, and even political processes.

The demonstration of human activity through impacts on natural biogeochemical cycles is shown in Figure 1.3, which explains the processes of anthropogenic interference in the nitrogen cycle. As follows from Figure 1.3, anthropogenic interfernce into the natural cycle of nitrogen can lead to a supersaturation of ecosystems with nitrates and to their further salination and eutrophication. This human interference in the nitrogen cycle stimulates a decrease in the C/N proportion in land ecosystems (Matson *et al.*, 2002; Cordova *et al.*, 2004).

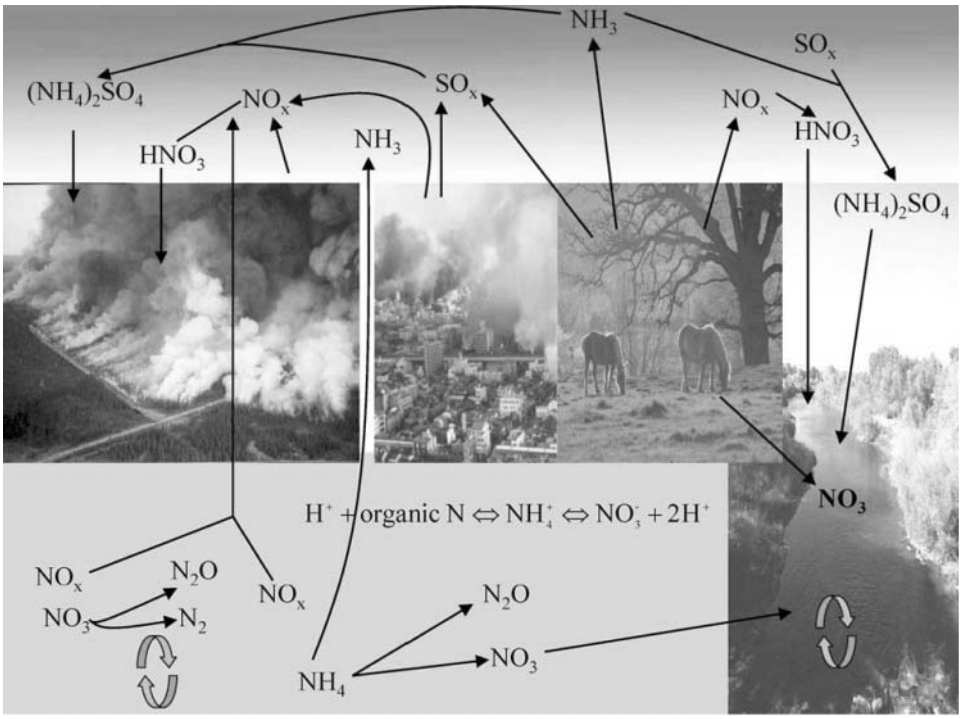

Figure 1.3. Schematic illustration of the structure of the nitrogen cycle in various environments. From Matson *et al.* (2002), Krapivin and Varotsos (2007).

1.4 GLOBAL DYNAMICS AND BIOGEOCHEMICAL CYCLES

The processes of globalization and their present trends pose a lot of problems connected with the search for a strategy to control the waste products of different economy sectors. Of special concern are regions where NSS development is unstable. In particular, the uncertainties in the further development of oil and gas import from the reservoirs of the Middle East and North Africa in connection with the broadening participation of China and India have led to uncertain predictions for future anthropogenic CO_2 fluxes. Keeping the trend of economy development in these regions at current levels, CO_2 emissions can increase by 52% by the year 2030 compared with the present level (WEO, 2002, 2004, 2005). In the Middle East and North Africa the need for energy is regulated by the needs of the growing population and economic development. The need for primary energy in this region by 2030 can more than double. At the same time, oil extraction can increase by 2030 by ~75% and that of gas can triple. The share of the region in total oil output will grow from 35% today to 44% in 2030. All this will be possible by investments in the energy infrastructure by the countries of the Middle East and North Africa of up to $50 billion every year (Cozzi, 2003).

A special IPCC report (IPCC, 2003) summarizing the results of a multi-year analysis of environmental changes, gives some estimates and draws some conclusions about the trends and causes of these changes.

- Global energy consumption and related input of CO_2 to the atmosphere in the 21st century continues to increase. Fossil fuels produce 86% of the world's energy and are a source of 75% of the anthropogenic input of CO_2 to the atmosphere. On the whole, in 2002 the world economy consumed 341 exajoules (EJ),[3] including 149 EJ of oil, 91 EJ of natural gas, and 1.1 EJ of coal.
- Global consumption of primary energy was growing, on average, by 1.4% annually during the period 1990–1995 and by 1.6% during 1995–2001. The rates of energy consumption were distributed through the economy sectors as follows: 0.3%–0.9% industry; 2.1%–2.2% transport; 2.1%–2.7% building, and −0.8 to −2.4% agriculture.
- About 38% and 17.3% of electric power are generated due to coal and natural gas burning, respectively; oil burning provides 9% of electric power; and nuclear power stations produce about 16.8%; 17.5% and 1.6% of electrical energy are generated at hydroelectric power stations and other renewable sources. Due to electrical energy production in 2001 the atmosphere received 2,250 MtC. In 2020, coal is expected to occupy 36% of the energy niche.
- The average global CO_2 emission increased by 1% in the period 1990–1995 and by 1.4% in 1995–2001, with the contributions of individual economy sectors constituting 1.7%–2.0% transport, 2.0%–2.3% building, and −1.0% to −2.8% agriculture.
- The average global rate of CO_2 emission in the periods 1990–1995 and 1995–2001 constituted 1% and 1.4%, respectively, which is below the rate of growth of energy consumption. Electrical energy generation produces most CO_2 emissions. The rate of growth of anthropogenic CO_2 fluxes by economy sector constituted 1.7%–2.0% industry, 2.0%–2.3% building, and −1.0% to −2.8% agriculture.
- From the estimates of numerous experts, a stabilization of CO_2 at the level 550 ppm by 2100 can be reached by reducing its emission by 7%–70% by this time. This uncertainty is connected with a difference in the estimates of CO_2 sinks and sources, both natural and anthropogenic.
- Total CO_2 emission due to fossil fuel burning in 2001 was estimated at 24 Gt CO_2 (6.6 GtC) per year with 47% of this emission made by industrial countries, 13% by countries with a transition economy, and 25% by the developing countries of the Pacific sector of Asia. The contribution of individual sources constituted: car production 263 MtC yr^{-1}, factories and building 1,173 MtC yr^{-1}, road transport 1,150 MtC yr^{-1}, and housing 520 MtC yr^{-1}.
- Among GHGs contributing to a change in the ERB the share of CO_2 is 20% and that of nitrogen oxides is 6%.

Tables 1.13 and 1.14 characterize the distribution of CO_2 emissions by economy sector and regions. It can be seen that the general volume of CO_2 emissions

[3] 1 exajoule equals 10^{18} joules.

Table 1.13. The distribution of CO_2 emissions due to energy production by economic sector and region (MtC) in 2002–2006. From IEA (2002, 2005a–c, 2007a, b).

Region	*Indicator of economic sector*								
	PEHP	VP	OES	MAC	T	CPS	R	OS	Σ
Countries with a transitional economy	325.7	113.9	31.1	151.9	92.3	16.9	91.1	37.2	860.1
The west sector of the OECD	307.7	37.1	62.9	203.3	292.4	49.8	139.1	27.3	1,119.6
U.S.A.	637.3	37.9	76.4	184.8	481.0	63.6	104.5	11.9	1,597.4
Pacific sector of the OECD	141.9	23.9	17.9	83.5	95.3	26.7	21.9	9.9	421.0
Central regions of South-East Asia	264.3	29.4	39.7	153.7	127.4	14.9	52.7	11.9	694.0
Asian countries with planned economics	368.0	10.7	37.9	269.3	67.2	20.8	61.5	34.4	869.8
Middle East	77.1	1.8	32.4	52.7	46.9	4.5	24.8	30.7	270.9
Africa	75.9	4.3	11.0	37.6	39.2	1.4	12.2	9.5	191.1
Latin America	61.1	10.1	36.7	76.3	108.2	4.9	22.1	11.3	330.7
Total	*2,259.0*	*269.1*	*346.0*	*1,213.1*	*1,349.9*	*203.5*	*529.9*	*184.1*	*6,354.6*

PEHP = production of electric power and heat for the population, VP = vehicle production, OES = other energy sources, MAC = manufactures and construction, T = transport, CPS = commerce and population service, R = residence, OS = other sectors, Σ = total energy.

constituting 24,409 Mt CO_2 in 2002 is expected to reach 33,284 Mt CO_2 in 2015, and by 2025 it will be 38,790 Mt CO_2, exceeding the 1990 level by 81%. Despite the fact that the Kyoto Protocol (after its ratification by Russia) came into force for more than 55 countries from February 16, 2005, its recommendation to reduce CO_2 emissions did not help to obtain a real forecast of the energy development for the next decades. Nevertheless, with all signatory powers supposed to follow KP

Table 1.14. List of basic stationary CO_2 sources emitting annually more than 0.1 $MtCO_2$. From WEO (2002).

Source	*Volumetric concentration of CO_2 in emitted gas* (%)	*Volume of CO_2 emitted* (MtC)	*Share of all emissions of CO_2* (%)	*Average value of CO_2 emission per source* (MtC/source)
Coal	12–15	2181.4	59.69	1.08
Natural gas	3–10	205.5–207.4	5.65	0.21–0.28
Petroleum	3–8	89.1–178.7	2.43–4.89	0.15–0.35
Other fossils	—	16.7	0.45	0.21
Hydrogen	—	0.8	0.02	0.35
Cement industry	3–20	218.0–254.6	5.97–6.97	0.22–0.34

recommendations, the rate of growth of CO_2 emissions due to fossil fuel combustion over the period 2002–2025 will average 2%. The information given in Table 1.15, where all economy sectors and most characteristic regions are compared by their development index, can help to forecast future energy development. Along with the growth in population size and GDP (Gross Domestic Product) increase, the impact of GDP efficiency reduction on the increase of the Human Development Index (HDI) should be taken into account. In any event, an ideal model of globalization should foresee the equalization of HDI over all countries due to a re-distribution of excess resources. However, such a model is far from reality, and therefore available predictions of the growth of CO_2 emissions differ strongly in their estimates of rates and volumes. Table 1.16 emphasizes the apparent heterogeneity of distribution of resources and, hence, the role of individual regions in improving the environment.

Rates of change in anthropogenic carbon flux intensity will vary in future according to technological progress, economic policy, and a change in priorities for power production in line with sustaining environmental quality. Bearing this prospect in mind, the expected increase in the efficiency of scientific–technical progress should continuously reduce the flux of anthropogenic CO_2 to the atmosphere, and this means that a high level of HDI in countries with a transitional and developing economy can be reached without sudden human-induced climate change. As can be seen in Table 1.16, a special place in this process is occupied by the U.S.A. which did not join the KP, but proposed a Regional Greenhouse Gas Initiative (RGGI) of their own, according to which GHG emission reduction has to be in the interests of the U.S.A. This initiative supposes the development of methods to control GHG emissions by means of quota exchange between states.

An important aspect of globalization is the impossibility under present NSS conditions to reliably assess the development of individual processes without

Table 1.15. Distribution of CO_2 emissions by economic sector and region with a prognosis to 2025. From IEA (2005b).

Region/ Country	*CO_2 emissions in 2002 from energy production* ($MtC \cdot yr^{-1}$)				*Prognosis of total volume for CO_2 emission* ($MtC \cdot yr^{-1}$)		
	Due to oil combustion	*Due to gas combustion*	*Due to coal combustion*	*Total emission*	*2010*	*2025*	σ
USA	671.3	328.7	565.6	1565.6	1853.3	2339.1	1.7
Canada	74.9	43.7	42.1	160.7	191.3	236.6	1.7
Mexico	69.9	22.7	6.3	98.9	120.8	173.5	2.5
West Europe	522.1	221.9	225.4	969.4	1055.2	1134.4	0.7
Japan	179.5	40.2	102.5	322.2	337.7	360.4	0.5
Australia/ New Zealand	38.0	16.9	67.5	122.4	145.4	181.1	1.7
Russia	97.3	212.0	106.6	415.9	500.0	629.5	1.8
Other CIS	61.5	101.4	76.8	239.7	298.9	397.3	2.2
East Europe	52.5	37.2	108.5	198.2	237.2	305.7	1.9
China	182.8	19.4	705.5	907.7	1583.6	2524.0	4.5
India	76.2	13.1	190.7	280.0	389.1	603.6	3.4
South Korea	65.8	13.1	44.0	122.9	157.4	231.1	2.8
Other Asia	205.2	73.0	106.3	384.5	535.0	845.6	3.5
Middle East	219.7	124.9	27.3	371.9	504.4	730.6	3.0
Africa	103.0	38.0	92.3	233.3	317.8	464.8	3.0
Brazil	75.1	7.1	11.2	93.4	125.4	207.1	3.5
Other Central and South America	119.4	48.4	8.7	176.5	248.6	350.8	3.0
Developed economies	1556.0	674.0	1009.3	3239.3	3703.6	4425.4	1.4
Transitional economies	211.2	350.5	291.8	853.5	1036.3	1332.2	2.0
Developing economies	1047.5	336.6	1186.3	2570.4	3861.2	5957.9	3.7
Total world	*2814.8*	*1361.2*	*2487.7*	*6663.7*	*8601.1*	*11715.6*	*2.5*

σ = average annual percent of CO_2 emission change for the period 2002–2025.

Table 1.16. Characteristics of regions and countries by the relationship between CO_2 emission and gross domestic product (GDP). From IEA (2005a).

Region/country	*Ratio between CO_2 emission* (tons) *and GDP* (mln. $U.S., 2000)					*Average annual rate of change* (%)	
	History			*Forecast*		1990–2002	2002–2025
	1970	1990	2002	2010	2025		
U.S.A.	1,117	701	571	501	393	−2.1	−1.6
Canada	1,046	691	612	562	481	−1.7	−1.0
Mexico	351	452	377	340	255	0.2	−1.7
West Europe	695	471	377	333	264	−1.9	−1/5
Japan	627	348	359	310	259	−1.7	−1.4
Australia/New Zealand	1,094	702	721	667	544	−1.3	−1.2
Russia	837	820	850	635	445	0.0	−2.8
Other CIS	1,211	1,843	1,346	926	602	0.3	−3.4
East Europe	1,454	1,198	679	549	372	−2.3	−2.6
Asia	890	637	470	434	300	−2.0	−1.9
China	2,560	1,252	605	570	375	−4.4	−2.1
India	286	346	324	272	185	0.4	−2.4
South Korea	791	698	680	555	454	−0.5	−1.7
Middle East	506	894	951	833	621	2.0	−1.8
Africa	522	609	595	549	431	0.4	−1.4
Central and South America	481	408	414	407	314	−0.5	−1.2
Total world	*853*	*649*	*517*	*461*	*344*	*−1.6*	*−1.8*

analyzing all correlations that exist in the present world. Hence, many subject-oriented international programs can only make sense as a means of accumulating data and knowledge—not as a means to study the global environment. There is a special dependence between power engineering and biogeochemical cycles.

Power engineering in the near future will continue to be closely linked to the use of natural gas, oil, and coal, the processing of which in industry and other economy sectors will unavoidably lead to emissions to the atmosphere, in addition to carbon

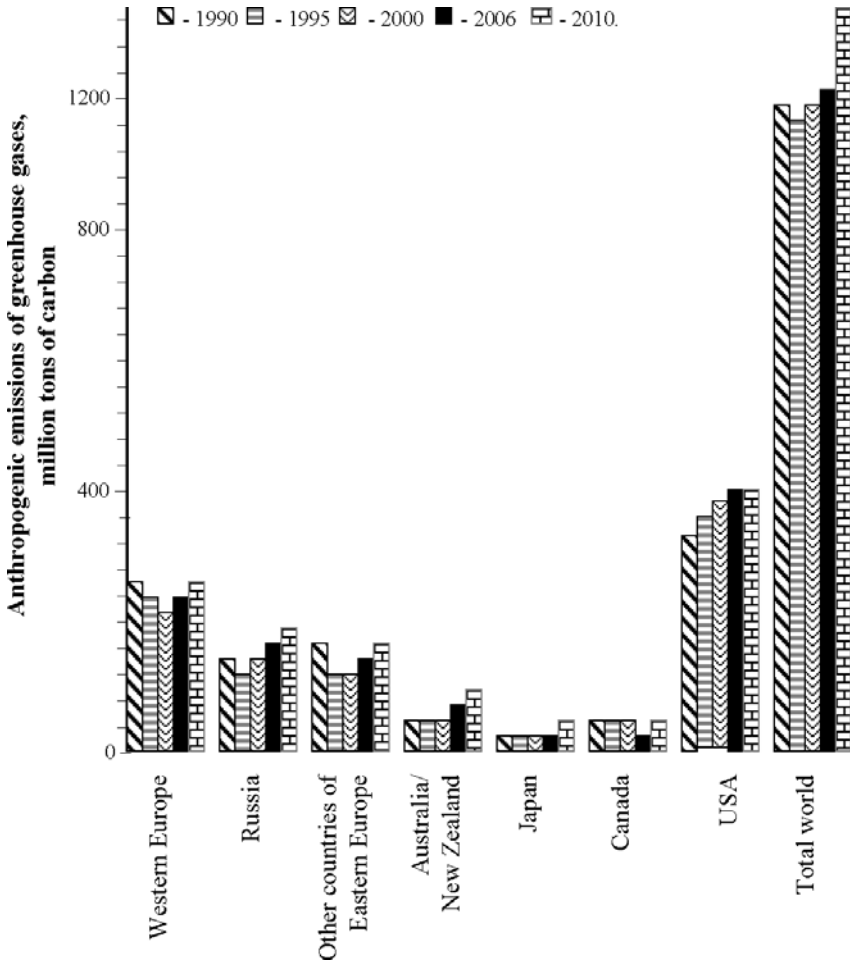

Figure 1.4. Regional distribution of non-CO_2 greenhouse gas emissions from developed countries projected to 2010. From EPA (2001, 2005, 2006).

dioxide, of many other gases with a higher potential for atmospheric warming (Figure 1.4). Prediction of how power engineering will develop and the related input to the atmosphere of GHGs depends on reliably parameterizing the socio-economic sector in the GMNSS. According to EIA (2005a–c), the globe can be divided into several clusters that differ in their economic development (Figure 1.5).

- Countries with a developed market economy are home to 15% of the world population. These are North America, Western Europe, Japan, Australia, and New Zealand.
- Countries with a transitional economy are home to 6% of the world population. They include Eastern Europe and the former U.S.S.R. countries.

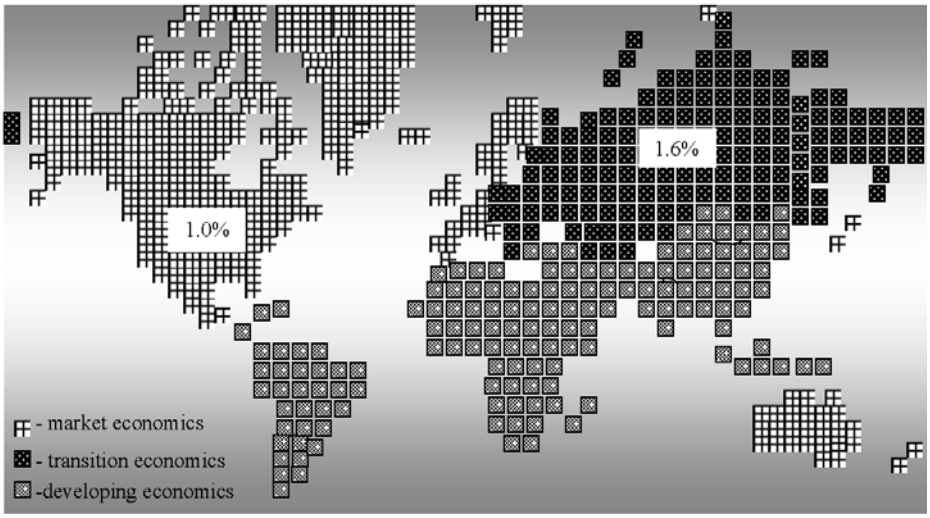

Figure 1.5. Schematic structure of world economies. From EIA (2005), WEO (2002, 2004, 2005). Percent annual growth in the need for energy resources is shown in the respective regions.

- Countries with a developing economy are home to 78% of the world population:
  (1) Asia (53%);
  (2) Africa (14%);
  (3) the Middle East (4%); and
  (4) South America (7%).

On the other hand, countries can be divided into groups organized by other principles.

- Countries that have ratified, agreed, joined, or approved the KP on GHG emission reduction.
- Countries of the European Economic Union (EU).
- G8 countries.
- The three member states of the North American Free Trade Agreement (NAFTA).
- The 30 countries that participate in the Organization for Economic Co-operation and Development (OECD).
- The 11 oil-exporting countries that make up the Organization of Petroleum Exporting Countries (OPEC).
- The eight countries of the developing Pacific basin.
- The seven countries of the Persian Gulf.

Clearly, in each of these clusters there are agreed strategies about energy development, but there are contradictions, too. The optimal version of such a global structure can be found with the model of (V, W)-exchange described in the work

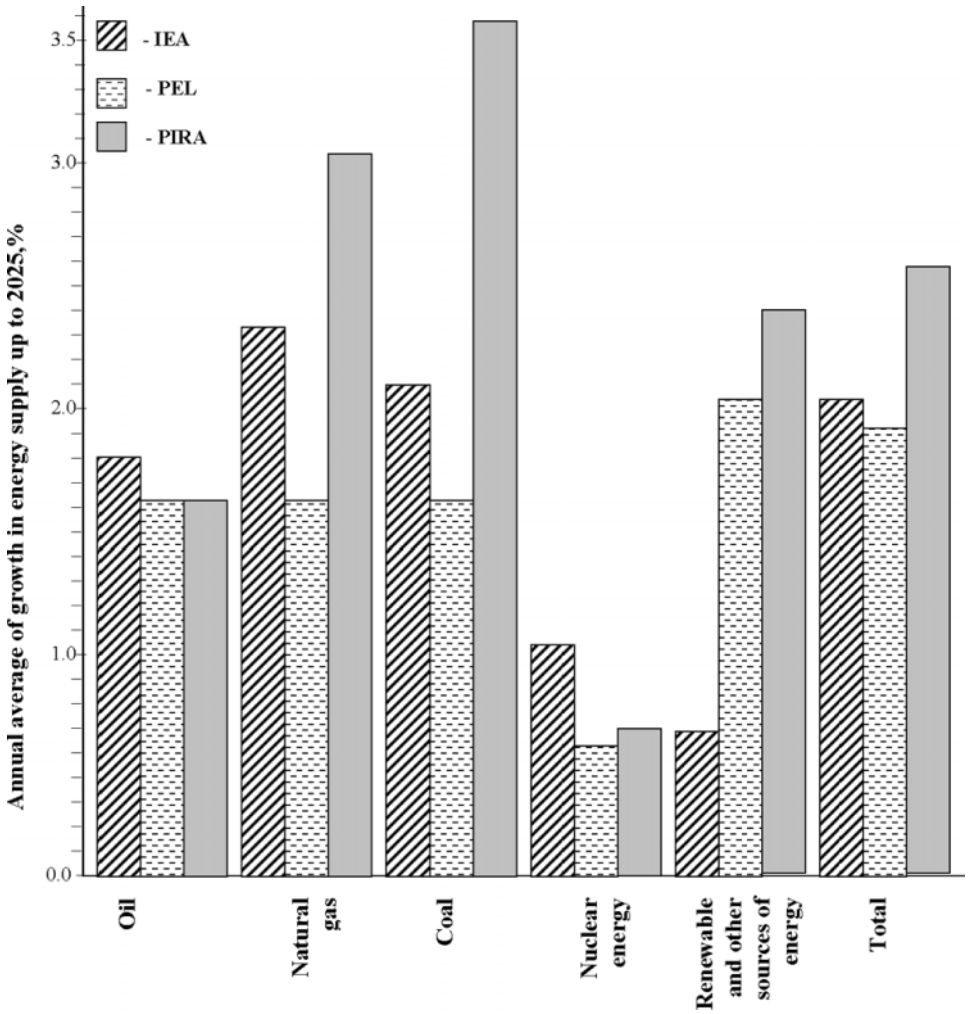

Figure 1.6. Forecasts of rates of average annual increase in energy supply made by the IEA, PEL, and PIRA. From IEA (2005a–c).

of Kondratyev *et al.* (2006b). The methods of predicting how power engineering will develop up to 2025 worked out in EIA (2005a–c) made it possible to obtain weighted estimates of the growth rate for the need of energy sources, the realization of which will lead in the late 21st century to a 550 ppm level of CO_2 concentration in the atmosphere (Figure 1.6). To some extent, this will be connected with a re-distribution of priorities between economy sectors. It is expected that the role of transport loading of the environment will substantially grow. If in 1990 the share of transport constituted about 20% of the consumed energy, by 2095 it will be 40%. But at the same time, the progress in industry will lead to a reduction in energy consumed from 38%

in 1990 to 17% in 2095. It is expected that the role of such economy sectors as energy production and building will not change substantially. The predictions shown in Figure 1.6 carried out by different scientific groups characterize the great uncertainty in the initial data used as the basis for the GMNSS biogeochemical unit. Hence, in modeling global biogeochemical cycles and assessing their role in the environment, the development of a global model of economic development deserves special attention.

1.5 GLOBALIZATION, WEALTH, AND HUMAN HEALTH

With the development of global infrastructures in trade, industry, agriculture, science, politics, and other spheres of human activity in the early 21st century the problem has appeared of not only NSS sustainable development but also, and to a greater extent, a search for balanced relationships between the environmental state, resources accumulated by individual countries, and human health (Kalb *et al*., 2004). The last 50 years witnessed an important and rapid transition of humankind from isolated social, political, and economic relationships to large-scale political and growing connections between ever distant regions. This has already led to appreciable changes in biodiversity, the structure of land and water ecosystems, and changes in the global biogeochemical cycles of important biospheric elements, such as water, nitrogen, carbon, and sulfur. The course of the biogeochemical cycles of these elements directly affects the conditions for life practically everywhere on the globe as well as human health (McMichael *et al*., 1999). Water plays a special role. The per capita daily need for water exceeds 1.4 litres. At present, only 0.65% of the freshwater on the planet is readily available (rivers, lakes, groundwater, soil moisture) (Table 1.17). Its biogeochemical cycle is a natural mechanism which guarantees the sustainability of water supplies, making it a renewable source. The heterogeneity of the spatial distribution of water supplies determines the maximum size of population over a given territory.

Unfortunately, there is practically no scientifically grounded conception of NSS development that foresees balanced development of all its vitally important indicators. For the first time, a note appeared in the IPCC Second Assessment Report (Fankhauser and Tol, 1997) that warned, ''the sustained health of human populations requires the continued integrity of Earth's natural systems.'' This statement should prompt studies of the relationships between the health of population at large and that of an individual, the dependence of which is not apparent. As Kalb *et al*. (2004) and Goodhand (1999) noted, globalization has brought forth a lot of purely intellectual problems, the solution of which will need to take a multitude of notions into account, such as livelihood, identity, governance, transnationalism, and knowledge. The present is characterized by a lot of continued conflicts whose effect on global ecodynamics has not as yet been evaluated.

The first time the problem of sustainable development was formulated constructively was in the works of Gorshkov (1990), Gorshkov *et al*. (2000), and Kondratyev *et al*. (2004b). The theory of biotic regulation is the basis for this constructive

Table 1.17. Water distribution in the biosphere.

Component	*Quantitative characteristics*			*Share of total volume of water* (%)
	Occupied square (10^6 km^2)	*Volume* (10^6 km^3)	*Level* (m)	
World amount of water	509	1454.193	2856.96	100
Water amount in oceans and seas	361.3	1370.323	3792.76	93.96
Land water	149	47.9871	322.06	3.3
Freshwater	148.8	28.2403	189.79	1.94
Saltwater	509	23.7468	46.65	1.63
Atmospheric water	509	0.0129	0.025	0.001
Water vapor in the atmosphere	509	0.011481	0.023	0.0008
Water droplets in the atmosphere	509	0.001129	0.0025	0.00009
Ice crystals in the atmosphere	509	0.000129	0.0005	0.000009
Water in the ice of Arctic countries and glaciers	16.2275	24.0641	1482.92	1.65
Ground ices of perennial frozen earth	21	0.3	14.29	0.021
Liquid water in the upper part of the terrestrial cortex	149	23.62593	158.56	1.62
Reservoirs	0.4	0.005	12.5	0.0003
Lakes	2.1	0.1764	84	0.12
Groundwater	134.8	23.4	174	1.61
Renevable groundwater	134.8	0.01332	0.1	0.0009
Soil moisture	82	0.0165	0.2	1.13
Marsh water	2.682	0.01147	4.28	0.0008
Rivers	148.8	0.00212	0.01	0.00001
Biological water	148.8	0.00112	0.008	0.00008

formulation, since it creates a bond between the key elements of the NSS. This theory states that the structural units of living space are cells of the mechanism that regulates and sustains the environment and thereby determines the ecological stability of humankind. As globalization widens this stability increasingly depends on decisions made by humans. The division of human society into those living in developing and developed countries uniquely determines the living standards of each individual. Though the notion of globalization is rather vague, nevertheless it implies an enhancement of the economical and political influence of international corporations on the life of the population at large. This influence results in the intensification and broadening of global economic integration, when the flows of finances, goods, technologies, population, and service are independent of frontiers. Inevitably, an economic elite dominates the scene and political conservatism originates with their desire to create a new world order irrespective of the health and standard of living of the population of many countries. In connection with this, Galeano (1997) noted that the wealth of many developed countries is a result of exploiting colonies and their natural and human resources, thereby growing richer and at the same time raising the poverty level in poor countries. The rhetoric on globalization and its advantages remains a shield for these processes.

Present-day globalization has the following special features:

- the growing scale and rate of transnational movement of goods, services, and finances limit the possibilities for many countries to participate freely in international trade;
- there is a certain asymmetry between the levels of legal protection in trade relations (where many international agreements and regulations are in force; for instance, within the WMO), and between social and environmental relationships (where the authority of governments over international organizations is limited);
- the GDP of some transnational corporations exceeds the GDP of many countries, which enables the former to dictate price policies and govern the global labor market practically independently of the governments of these countries;
- enhancement of the impact of market liberalization processes with participation of WB and IMF forces many countries to participate in global economic integration without any prospect of improving the living standards of the population;
- social, economic, environmental, and health issues are becoming "inherently global", rather than purely national or domestic. The environmental impacts of human activities are planetary in scale and scope; disease pandemics and economic stagnation partly underpin state collapse and regional conflict.

Despite the apparent negative aspects of globalization, it does accelerate the propagation of knowledge and technologies, medicine included. Of course, it brings with it national health services, education, and, in particular, protection for the health of women and children. In poor countries, globalization can reduce poverty and human health can reach an acceptable level. On the other hand, the critics of globalization advocate that it can be a means of propagating infectious diseases and creates

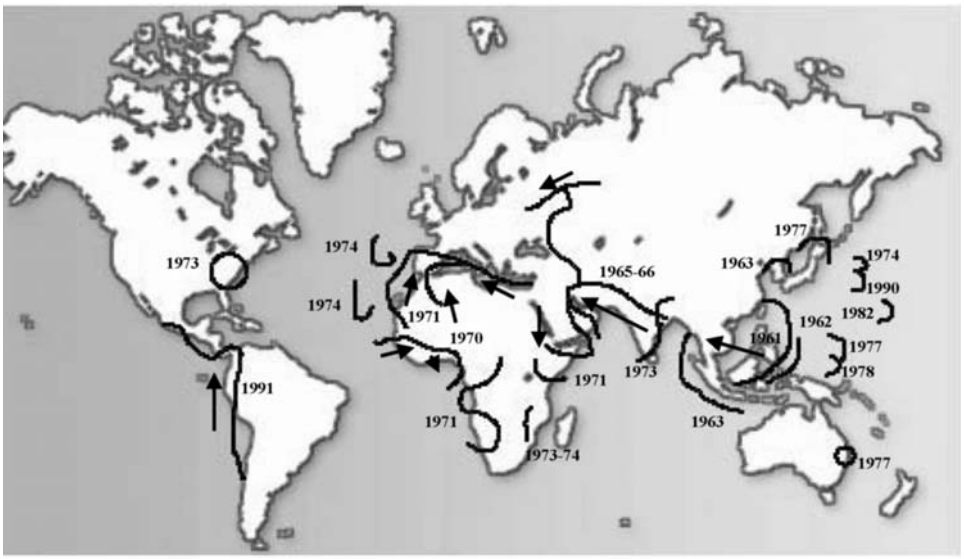

Figure 1.7. Global spread of cholera, 1961–1991. From Lee *et al.* (2002).

conditions under which Western living values are imposed, which runs counter to traditional local culture. It is not clear whether such integration in the global economy will always and under all conditions lead to economic growth and poverty reduction. China, Korea, Thailand, Malaysia, Indonesia, and Vietnam exemplify a reserved attitude to globalization with national values preserved. Countries that cannot protect themselves in such a way include those of Africa and South America, are strongly influenced by the WB and IMF, and where domestic economic activity is suppressed, with deteriorating balances of payments and, as a result, with growing poverty and deterioration of health.

Figure 1.7 and Table 1.18 characterize the propagation of one of the most dangerous diseases, cholera. It can be seen that there is a distinct correlation between the propagation of cholera and provision to the population of pure water and food. In general, the long-range transport of aerosols whose intensity depends on the state of land ecosystems, strongly promotes the propagation of dangerous diseases. Agents of dangerous diseases that can directly get into the lungs can hitch a lift on dust particles at long distances. From the estimates of Griffin *et al.* (2001), in this way 10 species of bacteria, 5 species of fungi, and 5 viruses are known to travel long distances and, as a result, anthrax, tuberculosis, diphtheria, bacterial meningitis, smallpox, etc. can propagate. The dust sources themselves are usually characterized by an increased susceptibility to asthma. Along with the direct impact on human health, the long-range transport of aerosols can affect health through food prepared from crops grown in ecosystems subject to fallout of pesticides and other pathogens. For instance, the fungal spores from the Cameroon in Africa are known to cross the Atlantic and reach the Dominican Republic in the Caribbean in 9 days. Sugar cane

Table 1.18. Cholera cases and fatalities. From Lee (2001), WHO (2000, 2006).

Year	*Number of cases*	*Number of deaths*	*Number of countries affected*
1991	596,419	15,286	54
1992	461,469	8,064	59
1993	376,767	6,779	62
1994	381,767	10,628	71
1995	210,049	5,034	78
1996	143,349	6,689	71
1997	147,425	6,274	65
1998	293,121	10,586	74
1999	254,310	9,175	71
2000	137,071	4,908	56
2001	184,311	2,728	58
2002	142,311	4,564	52
2003	111,575	1,894	45
2004	101,383	2,345	56
2005	131,943	2,272	52

rust (*Puccinia melanocephala*) is a classical example of ecosystem contamination in South America due to the transport of diseases from Africa.

Noji (2001) argued that, in addition to the current indirect human impacts on the process of propagation of dangerous diseases, there is a risk of direct human interference in this process. The notion of bioterrorism is one negative manifestation of globalization. A human being can deliberately cause an epidemic of a dangerous disease and panic among the population of a vast region, destroying its social infrastructure and leading inevitably to man victims. Thus, the spectrum of dangerous risks for the population of individual regions is growing and is not constrained by the direct economic mechanisms that regulate the living standards of the population.

Of particular danger for countries under the influence of the WB and IMF is the external funding of the import of cheep goods (a form of dumping). For instance, in Zambia, the opening up of the domestic market to textile import led to the collapse of the domestic textile sector with the closure of the majority of textile factories and the ensuing unemployment, closure of schools, reduced finance for the health service and

agriculture. In contrast, such countries as Cuba, Costa Rica, China have not completely opened their frontiers for import and, as a result, despite low indicators of per capita GDP, are characterized by a high level of human health. This testifies to the fact that the impact of globalization on the common wealth and health of a nation can manifest itself both through their improvement and aggravation, depending on a combination of many external and internal factors. It is clear that the uncontrolled liberalization of many branches of industry and agriculture can be a stimulus in aggravating national standards of living. Protectionist policies, including subsidies, may well preserve rural life and livelihood (arguments frequently advanced by the EU and Japan, see Labonte, 2001; Labonte and Sanger, 2006a, b). This benefits the health and quality of life of rural people. But such policies can also support ecologically unsustainable forms of production and increase oligopolistic corporate control over global food production. Thus, the question arises "Who gains and who loses?" This question can be answered by solving another problem which consists in evaluating the impact of globalization on health in the context of political, social, and economic traditions of the country as well as in its dependence on the level of economic development, natural resource supply, and general state of the society.

Lee *et al.* (2002) analyzed the discussions on the merits and shortcomings of globalization in the context of the health of population at large, noting that depending on ideological motives the opinions of experts are diametrically opposed. Their conclusions range between support for globalization and its complete denunciation. In this connection, two questions arise:

(1) What are the mechanisms and consequences of globalization that can lead to an improvement in human health globally as a whole and in each region individually?
(2) How can humankind control the consequences of globalization, and mold them to improve living standards?

Answers to these questions can be found in Kondratyev *et al.* (2003a, 2004a), where a constructive procedure was developed to evaluate the consequences of realizing the development scenarios based on simulation experiments using the GMNSS. The GMNSS parameterizes the fundamental links between population health, the environment, and economic development. Without a clean and prosperous Earth it is impossible to create the conditions necessary for life. Realization of this dream in the present world faces a lot of contradictions between the desire to raise living standards and preserve the environment. The GMNSS provides a coordinated method of resolving these contradictions as a result of simulation experiments that take into account data on global and regional geoinformation monitoring. Among the many programs delivering information for such experiments we can highlight SPARC under which data on stratospheric processes are obtained. These data are important for ERB specification.

The problem of health constantly appears as an unavoidable consequence of globalization, when the developing processes of urbanization, local violence, and regional conflicts (Anderson *et al.*, 2006) enhance the risks of morbidity and

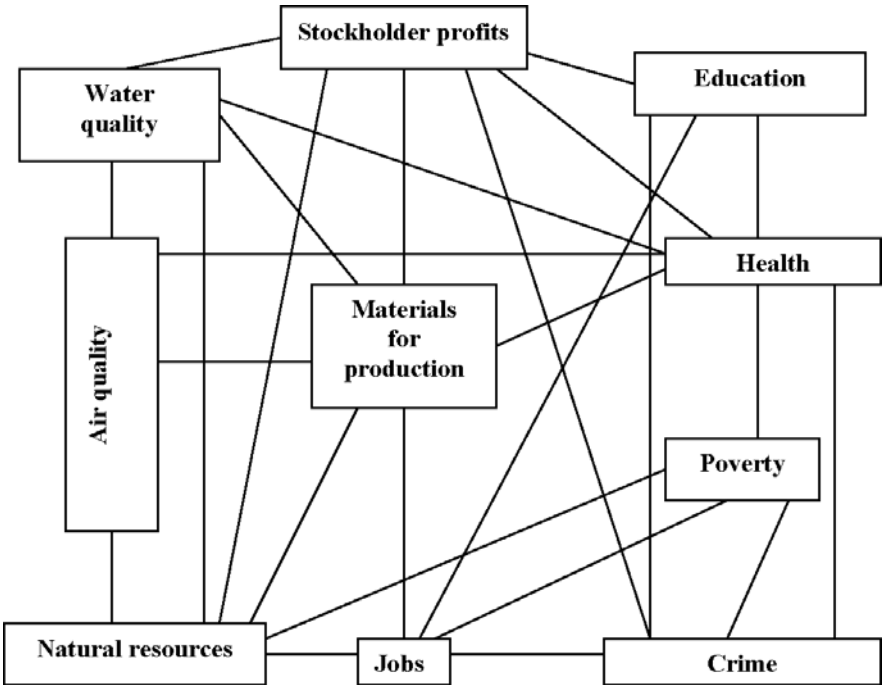

Figure 1.8. Interactions between the environment, the economy, and society.

mortality. This trend has led to the development of emergency medicine as a global discipline. In principle, the environmental state is the determining factor of the public health of countries at all levels of socio-economic development. Therefore, the problem of looking for information indicators to allow integral evaluation of the state of public health grows in importance. Many national and international organizations are trying to resolve these problem.

- *United States Environmental Protection Agency*. Protecting human health is an integral part of the EPA's mission. The EPA conducts numerous research programs throughout the world that study the effects of pollution on the human body. Research efforts include studies on how pollution affects children and people with asthma and other illnesses and how water contaminants may affect swimmers and beachgoers. Monitoring environmental quality also plays an important role in protecting human health. The EPA works with state and local agencies, as well as volunteer and other citizens groups, to monitor air and water quality and to reduce human exposure to contaminants in the air, land, and water.
- *Environmental Protection Agency Ireland*. The EPA's Viewpoint papers examine a variety of environmental topics, highlighting key environmental issues, the role of the EPA, government departments, local authorities, and other state agencies,

as well as listing recommendations for future action including agriculture and the environment, air quality, anaerobic digestion, bathing water quality, brownfield site redevelopment, climate change, drinking water quality, forestry and the environment, renewable energy, waste management, and waste prevention and minimization.

- *Environment Protection Authority, Victoria, Australia.* EPA Victoria's purpose is to protect, care for, and improve the environment. The basic question is how can people help protect the environment? Different approaches are considered as the means to solve this question, including
  (1) the use of environmentally friendly transport;
  (2) recycling, which is good news for the environment as it helps conserve natural resources and reduces pollution and littering;
  (3) composting and reduction of waste;
  (4) careful disposal of litter;
  (5) energy saving, which reduces air pollution and greenhouse gases.
- *World Health Organization.* WHO projects, initiatives, activities, and information products include numerous topics. Every year the World Health Report takes a new and expert look at global health, focusing on a specific theme, while assessing the current global situation. Using the latest data gathered and validated by WHO, each report paints a picture of the changing world of health and shows how, if recent lessons are understood and heeded, unprecedented health gains can be achieved.
- *The Pan American Health Organization.* PAHO topics include child health, epidemiology, food and nutrition, gender and health, health promotion, injuries and violence, lifestyles, maternal health, non-communicable diseases, etc.
- *Health Organizations in Eurasia.* The HOE controls many medical associations, institutes, and centers in the countries of the former Soviet Union and Asia, and organizes conferences and publications.
- *Association of Asian Pacific Community Health Organization.* AAPCHO's announcements include
  (1) a new UDS Fact Sheet giving patient demographic trends at AAPCHO member centers;
  (2) a statement in response to the CDC report on hepatitis;
  (3) in collaboration with the UCSF an updated AAPI HIV/AIDS Fact Sheet.

The words "health" and "wealth" are used by many socially oriented organizations both to introduce basic ideas about social justice in the world and to find the fundamental criteria for NSS development. To a great extent, these two notions are used to discover the strategy of an individual's behavior (Andrews, 2004) and to a lesser extent, at the social level. Clearly, the state of public health depends directly on the state of the economy. In developed countries, 5%–10% of GDP is spent on medical services and other measures to maintain public health—an impossibility for many developing countries. Therefore, a globalization priority should be the equalizing of economic potentials for use in sectors directly related to public health maintenance. And this equalization should be realized at the level of the UN.

2

The role of biogeochemical cycles in global ecodynamics

2.1 SUSTAINABILITY INDICATORS

Assessment of the state of a complicated system like the NSS requires several indicators to characterize its state by whatever criteria are chosen (e.g., at U.N. level). Essentially, it is a question of introducing some rule or norm to estimate any deviation of the NSS from its prescribed state. Formalization of this process is reduced to the choice of some functional $R(x_1, \ldots, x_n)$ where $\{x_i\}$ is the vector of the state of the NSS. The functional R determines the estimation rule of any deviation of the NSS from its optimal state. The problem consists in choosing the kind of R. The problem consists in determining this space and choosing the kind of R.

There are traditional indicators in some spheres of knowledge (Table 2.1) that are used to measure the state of some section of the NSS (e.g., in economy, sociology, and environmental protection, Munzi *et al.*, 2007). GDP-type indicators, through the financial state of the country, reflect the state of human health and environmental quality. The Index of Sustainable Economic Welfare (ISEW) broadens GDP functions, providing an assessment of economic progress. In economics, the consumer price index (CPI) or retail price index (RPI) is a statistical time series measure of the weighted average of prices of a specified set of goods and services purchased by consumers. The Environmental Sustainability Index (ESI) reflects the ability of society to protect the environment. The *2005 Environmental Sustainability Index* report (ESI, 2005) suggests 21 indicators of environmental sustainability, divided into 5 categories. To some extent, the proposed approach makes it possible to rate all countries and determine the shortcomings of their development strategies. The main difficulty in the formalized quantitative estimate of ESI is the choice of scale of such an estimate for each ESI constituent. Nevertheless, practically all countries have a

Table 2.1. 2005 Environmental Sustainability Index building blocks, indicators, and variables. From ESI (2005).

Components	*Indicators*	*Variables*
Environ-mental systems	Air quality Biodiversity Land Water quality Water quantity	Urban population weighted NO_2 concentration. Urban population weighted SO_2 concentration. Urban population weighted TSP concentration. Indoor air pollution from solid fuel use. Percentage of country's territory in threatened ecoregions. Threatened bird species as percentage of known breeding bird species in each country. Threatened mammal species as percentage of known mammal species in each country. Threatened amphibian species as percentage of known amphibian species in each country. National Biodiversity Index. Percentage of total land area (including inland waters) having very low anthropogenic impact. Percentage of total land area (including inland waters) having very high anthropogenic impact. Dissolved oxygen concentration. Electrical conductivity. Phosphorus concentration. Suspended solids. Freshwater availability per capita. Internal groundwater availability per capita.
Reducing environmental stress	Reducing ecosystem stress Reducing population pressure Reducing waste and consumption pressures Reducing water stress Natural resource management	Coal consumption per populated land area. Anthropogenic NO_x emissions per populated land area. Anthropogenic SO_2 emissions per populated land area. Anthropogenic VOC emissions per populated land area. Vehicles in use per populated land area. Annual average forest cover change rate from 1990 to 2000. Acidification exceedance from anthropogenic sulfur deposition. Percentage change in projected population 2004–2050. Total Fertility Rate. Ecological Footprint per capita. Waste recycling rates. Generation of hazardous waste. Industrial organic water pollutant (BOD) emissions per available freshwater. Fertilizer consumption per hectare of arable land. Pesticide consumption per hectare of arable land. Percentage of country under severe water stress. Productivity overfishing. Percentage of total forest area that is certified for sustainable management. World Economic Forum Survey on subsidies. Salinized area due to irrigation as percentage of total arable land. Agricultural subsidies.
Reducing human vulnerability	Environmental health Basic human sustenance	Death rate from intestinal infectious diseases. Child death rate from respiratory diseases. Children under five mortality rate per 1,000 live births. Percentage of undernourished in total population. Percentage of population with access to improved drinking water source.

Components	*Indicators*	*Variables*
	Reducing environment-related natural disaster vulnerability	Average number of deaths per million inhabitants from floods, tropical cyclones, and droughts. Environmental Hazard Exposure Index.
Social and institutional capacity	Environmental governance Eco-efficiency Private sector responsiveness Science and technology	Ratio of gasoline price to world average. Corruption measure. Government effectiveness. Percentage of total land area under protected status. World Economic Forum Survey on environmental governance. Rule of law. Local Agenda 21 initiatives per million people. Civil and Political Liberties. Percentage of variables missing from the CGSDI "Rio to Joburg Dashboard". IUCN member organizations per million population. Knowledge creation in environmental science, technology, and policy. Democracy measure. Energy efficiency. Hydropower and renewable energy production as a percentage of total energy consumption. Dow Jones Sustainability Group Index (DJSGI). Average Innovest EcoValue rating of firms headquartered in a country. Number of ISO 14001 certified companies per billion dollars GDP (PPP). World Economic Forum Survey on private sector. Environmental innovation. Participation in the Responsible Care Program of the Chemical Manufacturers' Association. Innovation Index. Digital Access Index. Female primary education completion rate. Gross tertiary enrollment rate. Number of researchers per million inhabitants.
Global stewardship	Participation in international collaborative efforts Greenhouse gas emissions Reducing transboundary environmental pressures	Number of memberships in environmental intergovernmental organizations. Contribution to international and bilateral funding of environmental projects and development aid. Participation in international environmental agreements. Carbon emissions per million $U.S. GDP. Carbon emissions per capita. SO_2 exports. Import of polluting goods and raw materials as percentage of total imports of goods and services.

service that estimates a huge amount of parameters as part of ESI:

- population growth rate;
- Gross National Product (GNP) growth rate;
- Human Development Index (HDI);
- energy consumption index;
- carbon and GHG emissions;
- production of hazardous wastes;
- annual rate of deforestation;
- protected areas;
- soil erosion;
- water use.

In each case, to choose the development strategy or to determine the optimal structure of the system to be studied, the problem of optimization is solved by

$$R(x_1^0, \ldots, x_n^0) = \min_{\{u_i\}} R(x_1(u_1, \ldots, u_m), \ldots, x_n(u_1, \ldots, u_m)),$$

where $\{x_i^0\}$ is the stable state of the system, and $\{u_i\}$ are the governing parameters.

Indicators of sustainability differ from traditional indicators of the environment state by their complex structure. Traditional indicators measure, for instance, the quality of water resources, the state of education, provision of population with food, etc. Sustainability indicators reflect more complicated connections between NSS components. Figure 1.8 shows the relationship between just three NSS segments. It can be seen that the three different segments are closely interrelated. At the same time, optimization of the criterion R can be followed by superposition of additional limitations inherent to a given nation, region, or group of population whose living standards differ strongly from the standards established, for instance, by the United Nations.

The problem of sustainable development of the NSS, initiated at the Rio de Janeiro 1992 Summit, is being discussed and supervised by the U.N. Commission on Sustainable Development (CSD). Its main mandate is to monitor the progress that has been made on the path toward a sustainable future. The CSD in its third session in 1995 adopted a five-year Work Program on Indicators of Sustainable Development. The elements of the Work Program on Indicators of Sustainable Development are as follows:

- enhancement of information exchange among interested actors;
- development of meteorological bulletins for governments;
- training and capacity building at regional and national levels;
- monitoring the experience of a few selected countries;
- evaluation of the indicators and their adjustment, if necessary;
- identification and assessment of linkages among the economic, social, institutional, and environmental aspects of sustainable development;
- development of highly aggregated indicators;

- further development of the conceptual framework for ISD enlisting the services of experts in economics, social sciences, physical sciences, as well as policy-makers, including non-governmental organizations and taking on board the views of local people.

Such a highly aggregated indicator was proposed by Kondratyev *et al.* (2004a). The NSS can be presented as a combination of nature (N) and human society (H), which constitutes a single planetary system. Therefore, separating them to derive global and regional models has to be done conditionally. The systems N and H have hierarchical structures $|N|$ and $|H|$, goals $\underline{N}$ and $\underline{H}$, and modes of behavior $\overline{N}$ and $\overline{H}$, respectively. From the mathematical point of view, any interaction between systems N and H can be considered a random process $\eta(t)$ with an unknown law of distribution, representing the level of intensity of the relationships between these systems or estimating the state of one of them. The goals and modes of behavior of systems are functions of the index η. The η index can vary in such a way that the modes of behavior of the systems can be antagonistic, indifferent, and cooperative.

The main goal of system H is to achieve a high standard of living with guaranteed prolonged survival. The goal of system N can be determined in terms of survival. System N behaves according to the objective laws of co-evolution. In this sense the selection of H and N is conditional and can be interpreted as a division of the many natural processes into controlled and uncontrolled. Without dwelling on the philosophy of this division, let us consider systems H and N to be open and symmetrical in their description. System H includes technologies, science, economic potential, industrial and agricultural production, sociological structure, size of population, etc. The H–N interaction causes changes in η, the level of which affects the structure of vectors $\underline{H}$ and $\overline{H}$. Of course, there exists a threshold of η_{max} beyond which humankind ceases to exist—but nature survives. The asymmetric nature of systems H and N causes changes in the goal and strategy of system H.

At present, the interaction between these systems $\eta \to \eta_{max}$ is occurring at a rapid pace, and therefore individual components of vector $\underline{H}$ can be attributed to the class of cooperative behavior. Since the present socio-economic structure of the world is presented by all the states in the world, we shall consider a country as a functional element of system H. The $\eta(t)$ function reflects the result of the interaction of countries both with each other and with nature. Let us describe the sum of the results of their interaction by the matrix $B = \|b_{ij}\|$, each element of which has a meaning of its own:

$$b_{ij} = \begin{cases} +1 & \text{for cooperative behavior;} \\ -1 & \text{for antagonistic relationships;} \\ 0 & \text{for indifferent situations.} \end{cases}$$

A country H_i has m_i possible ways to reach the goal $\underline{H}_i$; in other words, it uses a series of strategies $\{\overline{H}_i^1, \ldots, \overline{H}_i^{m_i}\}$. The weight of each strategy $\overline{H}_i^j$ is prescribed by the value $p_{ij}\left(\sum_{j=1}^{m_i} p_{ij} = 1\right)$. The resulting value of the η parameter is a function of the indicated

characteristics, and each time moment of the situation is described by a game-theoretic model (Krapivin, 1978).

An objective estimate of the dynamics of the natural medium $N = (N_1, N_2)$ is possible with some assumptions using models of the biosphere N_1 and climate N_2. The accumulated experience of numerous scientists in deriving such models has resulted in construction of point, regional, box, combined, and spatial models. This experience enables synthesizing a new type of global model, covering the key bonds between the hierarchical levels of natural and anthropogenic processes.

In general, the condition of systems H and N can be described by vectors $x_H(t) = \{x_H^1, \ldots, x_H^n\}$ and $x_N(t) = \{x_N^1, \ldots, x_N^m\}$, respectively. The combined trajectory of these systems in $n+m$-dimensional space is described by the function $\eta(t) = F(x_H, x_N)$ which is determined by solutions of the global model equations. The form of F is determined by knowledge of the laws of co-evolution, and therefore there is a possibility of investigations in different spheres of science. The available estimates of F (Krapivin, 1996) reveal a correlation between the notions *survivability* and *sustainability*. According to Ashby (1956), the dynamic system is "alive" within the time interval (t_a, t_b), if its determining phase coordinates are within "admissible limits" $x_{H,min}^i \le x_H^i \le x_{H,max}^i; x_{N,min}^j \le x_N^j \le x_{N,max}^j$. And since systems H and N have a biological basis and limited resources, one of the indicated boundary conditions turns out to be unnecessary (i.e., for the components of vector $x = \{x_H, x_N\} = \{x_1, \ldots, x_{n+m}\}$ the condition $x_{min} \le \eta = \sum_{i=1}^{n+m} x_i$ should be satisfied). This simple scheme requires that the total energy in the system be preserved and its elements be diverse.

Of course, the notion of "system survivability" is more capacious and informative. By "system ecology" many authors mean the stability and integrity of the system; in short, the system's ability to resist external forcings. In other words, survivability is measured by the tendency of the system to suppress large oscillations of its structure and elements, returning the system to its former equilibrium state. Thus, system survivability should be understood as its ability to actively resist the impact of external factors and preserve its characteristics indefinitely.

The biosphere Ω, as a complicated unique system, functions according to the laws of co-evolution of its sub-systems, human society H and nature N being the basic ones. The impact of human activity on nature, being comparatively small scale, can only (apparently) be assessed newly developed technology. Clearly, for this purpose a system approach is needed to formalize the ecological, technological, economic, and geopolitical interactions between sub-systems H and N. In general, system H has at its disposal technologies, science, economic structure, size of population, etc. System N has a set of mutually dependent processes; for example, climatic, biogeocenotic, biogeochemical, geophysical, etc. processes.

From the viewpoint of the theory of systems, H and N are open systems. Their division is a conditional procedure aimed at selecting controlled and non-controlled components of the environment. Without going into the philosophical and

methodical aspects of this procedure, we assume that both systems are symmetrical from the viewpoint of their simulation (i.e., we assume that each system has a goal, structure, and behavior of its own). Then, the H–N interaction can be described by the process of (V, W)-exchange consisting in that each of the systems, to reach its goal, spends resources V and, in exchange, obtains a new resource of an amount W. Each system is aimed at optimizing the (V, W)-exchange with another system (i.e., to maximize W and minimize V). Now, let us write the equations for (V, W)-exchange:

$$\left.\begin{aligned} W_H(H^*, N^*) &= \max_{\{H_s,|H|\}} \min_{\{N_s,|N|\}} W(H, N) = \min_{\{N_s,|N|\}} \max_{\{H_s,|H|\}} W(H, N) \\ W_H(H^*, N^*) &= \min_{\{H_s,|H|\}} \max_{\{N_s,|N|\}} W(H, N) = \max_{\{N_s,|N|\}} \min_{\{H_s,|H|\}} W(H, N) \end{aligned}\right\}, \tag{2.1}$$

where H^* and N^* are the optimal systems. Here, in contrast to traditional game theory models, there exists a power spectrum of the H–N interaction covering the final intervals of changes in the pay-offs W_H and W_N that depend on the aggressiveness of each. A concrete definition of the pay-off function requires a certain systematization of the mechanisms of the human and natural co-evolution. One of the widely used models of the balanced development of the world community and nature subjected to criterion (2.1) consists in identifying system H as all large cities with adjacent industrial and recreation zones. There are many ways of considering and formally describing such structures. In particular, there exist a well-known method of logic information modeling of the processes of rational nature use and a simulation method of controlling ecological–economic systems. According to these methods, to solve a concrete problem it is necessary to conceptualize the information base of the model and to select most of the general relationships between the elements of the interacting systems. This procedure is completed by enumerating all the functional elements of the systems and determining the capacity loads on their elements. The whole procedure ends with a synthesis of the simulation model, which, within assumed assumptions, becomes an instrument of investigation. In the case considered we assume that the structure of system H includes population G, pollutants Z, and natural resources M (i.e., $|H| = \{G, Z, M\}$). Similarly, the structure of system N consists of such elements as the climate parameter: temperature T, environmental quality Q, areas of forests σ_L, and agricultural lands σ_X (i.e., $|N| = \{T, Q, \sigma_L, \sigma_X\}$). The behavioral strategy of system H is formed from the distribution of investments to the retrieval of resources U_{MG}, struggle with pollution U_Z, and agricultural investments U_{BG} (i.e., $H_S = \{U_{MG}, U_{ZG}, U_{BG}\}$). The behavioral strategy of system N is identified with the rate of investments ageing T_V, population mortality μ_G, agricultural productivity H_X, the cost of resource retrieval G_{MG}, and the time constant of biospheric self-cleaning of pollutants T_B; that is

$$N_S = \{T_V, \mu_G, H_X, G_{MG}, T_B\}.$$

Equations (2.1) are the basic equations for the survival model. In general, this model is formulated in terms of the theory of the evolutionary technology of modeling. If all possible states of the biosphere with acceptable conditions for human life constitute the multitude $\Gamma = \{\Gamma_i\}$, then as a result of the effect of C_k on the biosphere,

two outcomes are possible: $C_k(\Gamma_i) \to \Gamma_i \in \Gamma$ and $C_k(\Gamma_i) \to \Gamma_i \notin \Gamma$. When the sequence of biospheric states $\{C_k(\Gamma_i)\} \in \Gamma$, then we can speak about persistent co-evolution of the system $H \cup N$. No doubt, there is a problem of adequacy between real processes and their simplified presentation as a model. Nevertheless, despite the philosophical doubt about the expediency of mathematical modeling for future assessment of the kinetics of biospheric parameters, the model approach has proved to be profitable. Use of the biospheric model instead of the biosphere itself is convenient: first, because there is more information about the model than about the biosphere; second, because the model is easier to handle; and, third, because direct experiments with the biosphere are dangerous. All these aspects are the subject of studies for global ecoinformatics aimed at achieving sufficient similarity between the observed behavior of the system $H \cup N$ and the model. This is possible with the constant renewal of data bases and broadening of knowledge in accordance with the technology underlying information formation on the multitude of biospheric parameters suggested by Krapivin and Kondratyev (2002).

2.2 IMPACTS OF POPULATION GROWTH AND DEVELOPMENT ON BIOGEOCHEMICAL CYCLES

Humans have always used the environment as a source of resources. However, for a lengthy period of time their activity did not markedly affect the biosphere. Only in the late 19th century did changes in the biosphere induced by human activity drop on human civilization like a ton of bricks. Trying to improve living standards and profit margins, humans continue to step up the rate of material production without little regard for the consequences (Tables 2.2–2.6). With such an approach, most of the resources taken from nature return to nature as waste, often poisonous or unfit for utilization. This threatens the existence of both the biosphere and humankind (Moiseev, 1990; Schwarzenbach, 2002).

The global processes of formation and movement of a living substance in the biosphere are connected with cycles of huge masses of matter and energy. In contrast to purely geological processes, biogeochemical cycles with the participation of living substances are characterized by much higher intensity, rate, and amount of matter involved in the cycle. With the appearance and development of humankind, the process of evolution has markedly changed. At earlier stages of civilization, the cutting down and burning of forests for agriculture, cattle grazing, craft, hunting wild animals, and wars had devastated whole regions, led to destruction of vegetation communities and extermination of some animal species. With civilization development, especially intensive after the industrial revolution in the late Middle Ages, humankind had become much more powerful, capable of exploiting huge masses of matter (both organic, living and mineral, inert) to satisfy their growing needs. The growth of population size and the extensive development of agriculture, industry, building, and transport led to deforestation in Europe and North America. Large-scale grazing led to the loss of forests and grass cover, as well as soil layer destruction. Dozens of species of animals in Europe, America, and Africa were exterminated. The

Table 2.2. Regional distribution of energy production in 2006. From BP (2007).

Region	*Oil* (1,000 bbl daily)	*Coal* (Mt oil equivalent)	*Natural gas* (billion m^3)	*Nuclear energy* (Mt oil equivalent)	*Primary energy* (Mt oil equivalent)	*Hydro-electricity* (Mt oil equivalent)
North America	13,700	632.8	754.4	212.3	2,803.0	152.0
South and Central America	6,881	51.4	144.5	4.9	528.6	147.9
Europe and Eurasia	17,563	445.7	1,072.9	287.8	3,027.2	184.6
Middle East	25,589	0.6	335.9	0	554.2	4.9
Africa	9,990	147.8	180.5	2.4	324.1	20.2
Asia Pacific	7,941	1,801.5	377.1	128.2	3,691.5	178.6
European Union 25	2,306	171.7	190.0	219.5	1,722.8	71.4
OECD	19,398	1,026.2	1,078.5	537.0	5,553.7	299.2
Former Soviet Union	12,299	236.7	1,007.5	58.4	4,278.7	56.4

building and exploitation of industrial enterprises, extraction of economic minerals led to serious violations of natural landscapes, and the contamination of soil, water, and air with different wastes.

The dynamics of the growth of population size on Earth is characterized by a certain stability which causes misgivings that the growing power of the present

Table 2.3. Current indicators of the state of the global consumer society.

Region/Country	*Population* (%)	*Resources* (%)	*Consumption of resources* (%)
U.S.A.	5	6	40
OPEC	15	10	40
Russia	3	25	5
Third world	77	59	15

Table 2.4. List of regions and countries in which primary energy consumption exceeds 0.5% of total energy generated in the world at the beginning of 21 century. From BP (2005).

Region/country	*Energy consumption* (Mt oil equivalent)							Δ_1	Δ_2
	2000	*2001*	*2002*	*2003*	*2004*	*2005*	*2006*	(%)	(%)
North America	*2,737.5*	*2,682.3*	*2,723.0*	*2,741.7*	*2,798.6*	*2,815.7*	*2,803.0*	*−0.5*	*25.8*
U.S.A.	2,311.9	2,257.1	2,291.0	2,298.5	2,343.5	2,350.4	2,326.4	−1.0	21.4
Canada	289.8	289.9	296.7	302.3	311.4	317.1	322.3	1.7	3.0
Mexico	135.8	135.3	135.3	140.4	143.8	148.2	154.2	4.0	1.4
South and Central America	*456.2*	*457.0*	*454.4*	*461.0*	*485.1*	*507.9*	*528.6*	*4.1*	*4.9*
Venezuela	61.9	65.2	66.1	58.5	65.2	69.0	70.4	2.0	0.6
Argentina	58.9	57.7	54.3	58.7	62.2	66.7	71.0	6.6	0.7
Brazil	182.8	179.5	183.9	186.1	193.5	199.2	206.5	3.7	1.9
Other South and Central America	152.6	154.6	150.1	157.7	164.2	173.0	180.7	4.5	1.7
Europe and Eurasia	*2,829.2*	*2,856.0*	*2,858.4*	*2,905.4*	*2,956.0*	*2,981.7*	*3,027.2*	*1.5*	*27.8*
Belgium/Luxemburg	66.4	64.0	64.9	68.6	71.1	72.2	73.9	2.4	0.7
France	254.9	258.4	256.7	259.8	263.4	262.9	262.6	−0.1	2.4
Germany	330.5	336.2	330.1	332.1	330.7	325.2	328.5	1.0	3.0
Italia	176.4	177.2	175.9	181.2	184.2	184.3	182.2	−1.1	1.7
Kazakhstan	41.0	42.3	44.1	47.9	51.2	56.6	60.3	6.5	0.6
Netherlands	86.4	88.3	89.0	90.4	93.1	94.7	92.3	−2.6	0.8
Russia	636.0	637.5	646.6	656.6	666.1	672.5	704.9	4.8	6.5
Spain	129.2	133.0	134.7	141.2	145.5	146.5	145.8	-0.5	1.3
Sweden	48.6	52.1	48.5	46.2	48.4	50.8	47.3	−6.9	0.4
Turkey	76.6	71.5	75.1	79.9	85.3	89.2	94.7	6.1	0.9
Ukraine	136.7	135.9	134.1	134.2	139.9	139.7	137.8	−1.4	1.3
U.K.	223.5	227.0	221.7	225.1	227.0	228.6	226.6	−0.9	2.1
Uzbekistan	51.4	54.8	56.2	52.4	49.5	49.1	48.5	−1.0	0.4
Other Europe/ Eurasia	571.6	577.8	645.7	659.4	671.7	681.6	695.7	2.1	5.7
Middle East	*402.9*	*420.1*	*445.1*	*464.0*	*501.0*	*532.9*	*554.2*	*4.0*	*5.1*
Iran	122.0	128.6	142.2	149.7	162.4	172.7	178.8	3.5	1.6
Saudi Arabia	116.4	120.2	123.7	131.7	142.8	151.4	158.9	5.0	1.5
U.A.E.	41.1	43.7	48.6	50.4	53.5	55.4	57.2	3.3	0.5
Other Middle East	123.4	127.6	130.6	132.2	142.3	153.4	159.3	3.8	1.5
Africa	*275.8*	*279.5*	*286.2*	*298.5*	*313.5*	*315.8*	*324.1*	*2.6*	*3.0*
Egypt	47.5	49.4	49.5	51.9	54.2	56.8	58.8	3.5	0.5
South Africa	108.4	107.0	110.9	117.3	123.6	118.7	120.2	1.3	1.1
Other Africa	93.1	95.2	96.8	99.1	104.4	107.6	111.5	3.6	1.4
Asia Pacific	*2,607.0*	*2,673.6*	*2,775.1*	*2,983.5*	*3,269.2*	*3,470.1*	*3,641.5*	*4.9*	*33.5*
Australia	111.2	113.4	116.7	116.6	119.0	119.6	120.8	1.1	1.1
China	966.7	1,000.0	1,057.8	1,228.7	1,423.5	1,566.7	1,697.8	8.4	15.6
India	320.4	324.2	338.7	348.2	380.1	401.6	423.2	5.4	3.9
Indonesia	95.2	101.4	104.4	103.9	110.6	114.7	114.3	−0.3	1.1
Japan	514.8	513.0	510.2	510.9	519.8	522.5	520.3	−0.4	4.8
Malaysia	45.8	47.8	51.3	56.3	60.4	65.1	67.0	3.0	0.6

Region/country	*Energy consumption* (Mt oil equivalent)							Δ_1	Δ_2
	2000	*2001*	*2002*	*2003*	*2004*	*2005*	*2006*	(%)	(%)
Pakistan	41.9	42.9	43.8	45.8	50.0	55.4	58.0	4.7	0.5
South Korea	191.1	195.9	205.0	211.8	217.3	224.9	225.8	0.4	2.1
Taiwan	95.3	95.1	98.1	104.0	107.7	110.5	113.6	2.7	1.0
Thailand	61.2	63.3	68.8	74.7	80.6	83.5	86.1	3.1	0.8
Other Asia Pacific	163.4	176.6	180.3	182.6	200.2	205.6	214.6	4.2	2.0
25 EU countries	1,654.9	1,681.9	1,666.8	1,697.5	1,719.1	1,719.6	1,722.8	0.2	15.8
OECD countries	5,359.6	5,327.7	5,366.4	5,421.9	5,522.9	5,559.9	5,553.7	−0.1	51.1
World	*9,308.7*	*9,368.6*	*9,458.9*	*9,856.5*	*10,323.4*	*10,624.0*	*10,878.5*	*2.4*	*100.0*

Table 2.5. Trends in the impact on natural resources and the environment. From Starke (2004).

Indicators	*Trends*
Fossil fuels and the atmosphere	In 2002, the global level of the use of coal, oil, and natural gas was 4.7 times higher than in 1950. The level of CO_2 concentration in the atmosphere in 2002 was by 18% higher than in 1960, and, apparently, by 31% higher than before the industrial revolution (1750).
Degradation of ecosystems	During the last decades, more than a half of the Earth's wetlands (from coastal marshes to intra-continental lowlands exposed to floods) has been lost due to various measures taken by humans, about half of virgin forests have been liquidated, 30% of the remaining forests have degraded. In 1999, the scale of the use of wood as a fuel and in industry had more than doubled as against 1950.
Sea level	In the 20th century the World Ocean level rose by 10 cm–20 cm (at an average rate of increase 1 mm/yr–2 mm/year due to melting of continental glaciers and thermal extension of water masses (under conditions of climate warming).
Soils/Land surface	About 10%–20% of agricultural lands have degraded in many respects (loss of fertility), which has brought a decrease (during the last 50 years) in yield by 18% on cultivated lands and by 4% on pastures.
Fishery	In 1999, the catch increased 4.8 times as against 1950. Creation of the modern fishing fleet has led to 90% of tunny-fish, cod, marlin, sword-fish, shark, halibut, flounder, cramp-fish being caught.
Water	Over-exploitation of groundwater has led to a decrease in the level of groundwater in many agricultural regions of Asia, North Africa, the Middle East, and the U.S.A. The impact of sewage, fertilizers, pesticides, oil product remains, heavy metals, stable phosphor-organic compounds and radioactive substances has led to a substantial decrease of groundwater quality.

Table 2.6. Energy consumption and living standards in different countries. From Prescott-Allen (2001).

Country	*WI*	*Per capita energy consumption (rank)*	*Share with respect to energy consumption in Sweden* (%)
Sweden	1	10	100
Finland	2	6	112
Norway	3	8	104
Austria	5	26	61
Japan	24	19	70
U.S.A.	27	4	140
Russia	65	17	71
Kuwait	119	3	162
U.A.E.	173	2	190

civilization could create such loads on the biosphere that it will lead to its complete reorganization (Moiseev *et al.*, 1985). In reality, the global population increases at a rate of ~80 million people annually. This growth leads to a number of crises, among which the following should be mentioned.

(1) Environmental threats

- Expansion of the sphere of human activity inevitably leads to habitat reduction caused by the global-scale extermination of plants and animals.
- Loss of biodiversity leads to ecosystem instability, especially with respect to climate changes and penetration in them of foreign elements (Leveque and Mounolou, 2003).
- Mass migration of population to cities in developing countries leads to over-exploitation of water resources and, as a result, to environmental conditions unfavorable for human health.
- Deforestation leads to breaking the global carbon cycle, which causes climate change.
- GHG emissions, increased rate of energy use, and consumption of non-renewable resources intensify the negative processes in the environment (Stevens and Verne, 2004; Manwell *et al.*, 2002).

(2) Poverty.

The growth of population size in developing countries is accompanied by a reduction in the means of subsistence. Only ~20% of the global population has adequate living conditions. The other 80% live under conditions of deficit. This imbalance will probably worsen, bearing in mind that in future 90% of the population increment will be observed in less developed countries. Poverty and poor living conditions will not help international nature protection organizations to provide sustainable development and reduction of negative impacts on biogeochemical cycles.

(3) Scarcity of food and freshwater

During the final years of the 20th century and especially in the early 21st century, productive agricultural systems have led to marked economic progress in many countries. But, at the same time, problems have appeared connected with the changing quality of soils in vast regions. This change is connected with the use of fertilizers, which substantially change the role of soil in the biogeochemical cycles of important elements such as nitrogen, carbon, and phosphorus. But, in connection with the lack of provisions, this process of soil quality transformation will grow in scale. In reality, the global market of grain and equivalent foodstuffs provides only 200 million tons annually. At the same time, approximate estimates of the annual need of foodstuff import for China and India reach 240 million tons and 30 million tons, respectively. Clearly, the question of weighted development of agriculture needs to be the subject of a special study. As Smil (1997) and Williams (2005) justly noted, only a model approach and reasonable policy will allow optimal solution of this problem. In this connection, Norton (2003) provides a clear, systematic review of important classes of policy issues in developing countries and discussed the emerging international consensus on viable approaches to those issues providing guidance for policy-makers and policy-analysts along with both real-world examples and conceptual frameworks.

The growth of population size and trends in civilization development bring with them many problems of global ecodynamics, especially the impact of society on climatic trends. The broader issues of the ecological, economic, and human effects of climate change were considered by Hardy (2003). The following aspects of the climate change problem were explained:

(i) The causes and effects of climate change from a natural and human environment perspective.
(ii) Mitigation options and policies that could reduce the impacts of climate change, and global impacts with case studies taken from North America, Europe, Australia, and elsewhere.

Climate change, population growth, improvement of technologies for natural resource utilization, change in the social structure of population, globalization, and an increase in living standards are all interactive components of the NSS. Therefore, consideration of each component leaving out of account its interaction with other

components does not give objective estimates and strategies of nature use. In many experts' opinions, the main cause of all the global problems of ecodynamics rests with the growth of population size. To some extent this is true, considering the emerging trends in the environmental pollution and expenditure of natural resources.

Among the biogeochemical cycles subject to powerful anthropogenic impact, the water cycle is arguably the most important. Under present conditions, along with growing water use in industry and agriculture, the need of humans for domestic water supplies grows, too. The per capita volume of consumed water per day for these purposes depends on region and living standard and ranges from 3 L to 700 L. For instance, in Moscow the per capita water consumption is 650 L, which is one of the highest indicators in the world. Canada consumes 1,600 m^3 of water per capita per year. America uses about 10^9 m^3 of water per day. In most countries, the spheres of freshwater consumption include domestic, public supply, industrial, irrigation, thermoelectric, mining, livestock, and aquaculture. In future, these spheres will broaden, which will inevitably lead to increased volumes of waste water. From the most optimistic predictions, the dynamics of the use of water resources will constitute 22% of the growth compared with 1995, reaching the indicator of water use of 4,772 $km^3\,yr^{-1}$ (Rosengrant *et al.*, 2002). On the environmental side, high consumption places stress on rivers, lakes, and groundwater aquifers and may require the construction of dams and hence flooding with serious ecological impacts.

It follows from analysis of water use during the last 50 years that the annual increase of irretrievable water consumption (i.e., when the water used is lost to nature for ever) constitutes 4%–5%. Future calculations show that at this rate of consumption, and considering the increase in population size and in the volume of production, by 2100 humankind may drain all supplies of freshwater (Cech, 2004; Pentius, 2003).

The present freshwater deficit is observed not only in the territories naturally short of water resources, but also in many regions where until recently water has been plentiful. At present, the need of freshwater is not satisfied for 20% of the urban population and 75% of the rural population of the planet.

The violation of the basic natural cycles of water by channeling it for anthropogenic needs can lead to degradation of vegetation cover, shifts of vegetation zones, and poorer crop harvests.

2.3 ANTHROPOGENIC SCENARIOS AND SUSTAINABLE DEVELOPMENT

The concept of sustainable development was defined in the U.N. Report by Brundtland (1987) as development that meets the needs of the present without compromising the ability of future generations to meet their own needs. In this context, Moody-Stuart (2006) writes:

> "Given the proportion of people in the world who are not adequately fed, not educated, have no modern medicine, and no means of adequate livelihood, we are plainly not meeting the needs of the present generation. I do not take an

> apocalyptic view of the environment, but in relation to climate change, we are potentially compromising the ability of future generation to meet their needs. If the needs of the developing part of the world are to be met, large amounts of additional energy will be needed. And yet we know that the fossil fuels on which our own economics are built are having an adverse impact on the global climate.''

Unfortunately, despite this widespread opinion on sustainable development no constructive mechanism for balanced development of the NSS has been proposed. The main problem is that people find it difficult to formulate a weighted criterion for further development. In other words, people are reluctant to place limits on their desires and needs by adjusting them to natural processes.

In this connection Moiseev (1988) wrote that the planet is entering a new stage in its history, when only a collective Mind, a collective Will, and joint purposeful efforts will make it possible to avoid disasters and open up prospects for the further development of civilization. In reality, *Homo sapiens* has entered a new era in its existence, when natural and anthropogenic processes have become comparable in power, when the vulnerability of development has become apparent, and when impacts on nature can cause irreversible processes. Essentially, people now face the prospect of having to choose from a restricted number of alternatives for further development of scientific–technical progress and how it fits with global ecodynamics. Vernadsky (1944, 1977) testified to the fact that humankind was approaching a threshold stage of evolution when the biosphere get transformed into the noosphere. And here, under the influence of numerous factors a moment of bifurcation might occur that is difficult to foresee, but after which a new but irreversible process begins. Knowledge of the mechanisms involved in the ramification of evolutionary processes helps us to foresee the consequences of realization of certain social development scenarios. Only on this basis will it be possible to form scenarios that could be realized.

Moiseev (1988) writes:

> ''And now, when at the stage of the noosphere, which is a stage of the revolutionary reorganization of the whole process of the planetary development, the determining factor of evolution is human activity, we should realize that Mind becomes a participant of the evolutionary process, exactly the participant which with all its power follows the common laws. And under such conditions, considering all limits, barriers inherent to Nature, we have the right to speak about the directed development of the biosphere.''

It is a question of limits established by natural laws, such as the law of conservation of mass, energy, etc. As Moiseev (1988) says, limits form like banks along the evolutionay canals, beyond which nature cannot go. Transition from one canal to another is only possible in places where they intersect, which can be determined using global modeling technology (Degermendzhy and Bartsev, 2003; Kondratyev *et al.*, 2005). Moiseev (1979) wrote:

> "Very important and interesting processes occur in present life caused by intensive development of science and engineering, owing to which the life structure of people and their world view change during 2–3 decades instead of centuries needed before."

This important remark is key to constructively comprehending the problems facing today's global society; most people are beginning to understand their role in environmental change. We witness fiery discussions of the causes of these changes and their correlations with the problems of life on Earth. The fact becomes increasingly apparent that continuing to experiment with the natural environment is dangerous and has unpredictable consequences, and that the only alternative to these experiments is to substitute them by modeling using accumulated knowledge.

As experience shows, development of a means to monitor global change with the present development of science on global processes is impossible using any of the models currently available to simulate the functioning of the nature–society system. No doubt, methods developed to model evolutionary technology raise hopes of creating a global model which, based on accumulated knowledge, will make it possible to obtain reliable enough long-term predictions of global change and to substantiate thereby conditions for the sustainable development of the environment. Obviously, success in this direction depends on the complex use of modeling technologies and environmental observations. So far, global models lack units to parameterize some processes in the nature–society system to formulate realistic scenarios. The construction of the latter is the result of expert knowledge and to a degree the imagination of an investigator. This problem was discussed in detail in Alcano *et al*. (2001), Gyalistras (2002), and in a special IPCC report (IPCC, 2001). To some extent, the Kyoto Protocol can serve as a scenario. Some countries of the EEC, who signed this protocol, agreed to reduce GHG emissions between 2008 and 2012 by 12.5%, and it is assumed that CO_2 emissions will decrease by 2010 by 20% compared with the year 1990. In each country diverse scenarios of this type bring with them a high level of global uncertainty, the solution of which is impossible without certain generalizations. Therefore, we shall now dwell for a while on some generalizing scenarios.

2.3.1 Fishery scenario

The use of World Ocean products in the 20th century was characterized by an increase in the trade of fish and other animals at higher trophic levels with trade intensity doubling every 10–15 years. The maximum catch in 1970 reached a level of 61 Mt. The annual per capita consumption of sea products varied within 7.2 kg to 11.8 kg. Numerous forecasts of the possible per capita use of World Ocean products give about 12 kg/yr. Therefore, let us assume a hypothetical dependence of the intensive fishing of nekton in each ith region:

$$\lambda_{Gti} = \begin{cases} \lambda_{G0i} - (\lambda_{G0i} - \lambda_{G\infty i})(t - t_0)/(t_{\lambda Gi} - t_0), & t_0 \le t \le t_{\lambda Gi}, \\ \lambda_{G\infty i}, & t > t_{\lambda Gi}, \end{cases} \tag{2.2}$$

where λ_{G0i} is fishing intensity at a moment t_0 (e.g., in 1970 $\lambda_{G0i} \approx 0.0286$; in 1999 $\lambda_{G0i} \approx 0.0312$); and $\lambda_{G\infty i}$ is the maximum possible trade intensity reached at moment $t_{\lambda Gi} \geq t_0$. The λ_{Gti} coefficient characterizes the fishing trade in the ith region and is considered in the demographic unit of the global model.

The contribution of fishing to the diet of *Homo sapiens* is determined by the ratio of the volume of products taken from the World Ocean to agricultural products. Numerous estimates of this contribution and prediction for the future differ widely, which is explained by the difficulties in calculating marine ecosystem productivity. In this connection we agree with Garcia and Grainger (2005) who state:

> ''Longer-term climate change will affect the ocean environment and its capacity to sustain fishery stocks and is likely to exacerbate the stresses on marine fish stocks, from fishing and other marine or land-based activities. The extent to which it will affect fisheries, in the different regions and species, is however not yet clear. Productivity might increase or decrease significantly. Ecosystem boundaries may be displaced and species composition may change remarkably (e.g., Blanchard and Boucher, 2002). In polluted areas, oxygen depletion will be aggravated, particularly if flooding facilitates the flow of pollutants to the sea. Fisheries infrastructures may have to be displaced, at high cost. Fisheries lacking mobility (e.g., small-scale fisheries) might suffer the most. Freshwater flows will be modified. New diseases may be introduced. Assuming such changes will occur more slowly than the already experienced natural variations, there should be little additional impact on supply/demand and prices. However, the existence of flexible management systems and access agreements between neighbouring countries would facilitate the adaptation to change (Everett *et al.*, 1995). More practically, the eventual impact cannot yet be accounted for but must be regarded as a major source of 'surprise'.''

By the year 2020, the price of fish is expected to increase by 6%–15%. This will be caused by achieving (probably exceeding) the maximum acceptable and calculated rates of withdrawal of marine products, allowing for variability of the productive potential of marine ecosystems. On the whole, whereas in the 20th century there was an increase of the volume of fish caught, in the 21st century a stabilization of the global fish catch is beginning to show at the level $(75–85) \cdot 10^6\,\mathrm{t\,yr^{-1}}$ (Pauly *et al.*, 2005; Gelchu and Pauly, 2007). Of course, to calculate an acceptable load on marine ecosystems, it is necessary to use Formula (2.2) to carry out simulation experiments with a global model of GMNSS type.

2.3.2 Scenario of the distribution of soil–plant formation areas

The intensity of food production on land depends on the area covered with crops and on their productivity. Clearly, within a global model, when considering details of all the processes and elements, it is impossible to predict every conceivable direction for agricultural development. Therefore, all the processes involved in increasing productivity have been generalized to reflect general trends. Let us introduce for agricultural

formation the identifier k and consider that in any region some of the territory can be occupied by cultivated land:

$$\sigma_{ki} = \begin{cases} \sigma_{k0i} + (\sigma_{k^*i} - \sigma_{k0i})(t - t_0)/(t_{ki} - t_0), & t_0 \le t \le t_{ki}; \\ \sigma_{k^*i}, & t > t_{ki}; \end{cases}$$
$$H_{ki} = \begin{cases} 1 + (H_{k^*i} - 1)(t - t_0)/(t_{ki} - t_0), & t_0 \le t \le t_{ki}; \\ H_{k^*i}, & t > t_{ki}; \end{cases} \tag{2.3}$$

where $\sigma_{ki} \le \sigma_i$ is the area of land cultivated in the ith region with area σ_i; H_{ki} is the indicator of changes in agricultural productivity R_{ki} for latitude φ and longitude λ with respect to the time moment $t_0(H_{kiS} = R_{ki}(\varphi, \lambda, t)/R_{ki}(\varphi, \lambda, t_0))$; and t_{ki} is the season in the ith region when cultivated land is constant.

In much the same way as Scenario (2.3), it is necessary to write similar relationships for all known types of plant formations and, using a global model, to evaluate the consequences of substitution of one type of vegetation cover for another (see Section 3.6.2 for details). But, of course, most important for studies is the process of substitution of forests for agricultural lands. At the present time, of the 148,000,000 km^2 (57 million mi^2) of land approximately 31,000,000 km^2 (12 million mi^2) are arable, and they expand at a rate of 100,000 km^2 (38,610 mi^2) per year. A major element of arable land loss is deforestation which continues to the present day, primarily in tropical countries through commercial over-exploitation of tropical forest.

2.3.3 Investment scenario

Let us suppose that in the ith region the area σ_{ki} under crops from moment t_0 changes following a linear law from σ_{k0i} to σ_{k^*i} in the time interval to t_{ki}. The time for reaching the level σ_{k^*i} depends on the amount of investment (coefficient q_{Vi}) in agriculture with the inverse proportion coefficient t_{k^*i} and on other factors affecting the time constant $t_{ki} : t_{ki} = t_0 + t_{ki} + t_{k^*i}/(q_{Vi}V_i)$. Possible changes in agricultural productivity H_{ki} are also approximated by a linear law where the value H_{k^*i} shows how many times productivity in the ith region can change from t_0 to t_{ki}. The reserves for increasing H_{ki} are rather large. Even highly productive plants such as sugarcane, during photosynthesis, consume annually only about 2% of the solar energy reaching the Earth surface, crops 1%, and other plants even less. Plant physiology and agro-technology have broad possibilities for multiple increase of agricultural productivity and, hence, the food available for *Homo sapiens*. Assume that to reach the level H_{k^*i}, the population of the ith region has the time $t_{ki} - t_0$:

$$t_{ki} = t_0 + \bar{t}_{ki} + t^*_{ki}(q_{Vi}V_i),$$

where the constituent $\bar{t}_{ki}$ is independent of agricultural investments; t^*_{ki} characterizes the efficiency of these investments; and V_i is the size of funds for the ith region.

According to the food spectrum for *Homo sapiens* a certain role is played here by forest ecosystems, the general trend in changes of their areas being characterized by a

negative derivative. On a global scale, forest resources are constantly depleting, so that on the border of the 20th and 21st centuries the total area of forests constitutes $\sigma_L = 4{,}184$ Mha, with a 31% density (about 28.3% of land area).

Two principal processes are observed in forestry: deforestation and afforestation. Let us describe the totality of these processes using the scenario of forest area change:

$$\sigma_{Li} = \begin{cases} \sigma_{L0i} + (\sigma_{L^*i} - \sigma_{L0i})(t - t_0)/(t_{Li} - t_0), & t_0 \le t \le t_{Li}; \\ \sigma_{L^*i}, & t > t_{Li} \end{cases}$$

This dependence foresees that the area under forests in the ith region up to moment t_{Li} varies linearly from σ_{L0i} to σ_{L^*i} and then remains constant. The values of the input parameters constitute the freedom of choice in simulation experiments.

To complete the formulation of the global scenario describing the level of food provision for *Homo sapiens*, consider the law of changing stock-breeding productivity. Suppose that with the constant constituent k_{FSi}, it increases in proportion with agricultural investments q_{Vi} with the coefficient k_{F^*i} and has the varying-in-time constituent with an exponential law of change:

$$k_{Fi} = k_{F3i} + k_{F^*i} q_{Vi} + (k_{F1i} - k_{F3i})[1 - \exp\{-k_{F2i}(t - t_0)\}].$$

The direction of human activity is determined by the intensity of pollution, time the pollution lasted (waste utilization), cost of environmental cleaning, amount of investment in the renewal of resources and in the prevention of environmental pollution, investment in industry and agriculture, rate of natural resource expenditure, and search for new sources, etc. The hypothetical trends of these processes should be set in order to realize the predictions using the global model.

Let the intensity of pollution vary between k_{Z0i} at time moment t_0 and k_{Z1i} at moment t_{Z^*i}. Similarly vary the time of waste utilization T_{Zi} and the cost of cleaning pollution G_{ZVi}, respectively, between the values $T_{Z0i} = T_{Zi}(t_0)$, $T_{Z1i} = T_{Zi}(t_{Zi})$, and $G_{2ZVi} = G_{ZVi}(t_0)$, $G_{1ZVi} = G_{ZVi}(t_{ZVi})$. Since the estimates of these indicators can vary for many reasons and at different times, the simplest scenario for the experiment will be the following functional presentations:

$$k_{Zi} = \begin{cases} k_{Z0i} - (k_{Z1i} - k_{Z0i})(t - t_0)/(t_{Z^*i} - t_0), & t_0 \le t \le t_{Z^*i}; \\ k_{Z1i}, & t > t_{Z^*i}; \end{cases}$$

$$T_{Zi} = \begin{cases} T_{Z0i} - (T_{Z1i} - T_{Z0i})(t - t_0)/(t_{Zi} - t_0), & t_0 \le t \le t_{Zi}; \\ T_{Z1i}, & t > t_{Zi}; \end{cases}$$

$$G_{ZVi} = \begin{cases} G_{2ZVi} - (G_{2ZVi} - G_{1ZVi})(t - t_0)/(t_{ZGi} - t_0), & t_0 \le t \le t_{ZGi}; \\ G_{1ZVi}, & t > t_{ZGi}. \end{cases}$$

Since it is difficult to specify the spheres of human activity, the spectrum of investments is confined here to the functions U_{ZG}, q_v, and U_{MG}. The strategy of

investment distribution for each region is determined by two-step functions of time:

$$U_{MGi} = \begin{cases} U_{MG1i}, & t_0 \le t \le t_{MGi}; \\ U_{MG2i}, & t > t_{GMi}; \end{cases}$$

$$U_{ZGi} = \begin{cases} U_{ZG1i}, & t_0 \le t \le t_{ZVi}; \\ U_{ZG2i}, & t > t_{ZVi}, \end{cases}$$

where t_{MGi} and t_{ZVi} are the moments of economic policy change in the ith region in the field of investments in the renewal of natural resources and prevention of pollution, respectively. Here the term "renewal of resources" denotes processes favoring an increase of M. In particular, this is a change of mineral resources for others, with their significance recalculated for the levels of significance of the previous ones.

Agricultural investment is one of the most important components of investment. To get high productivity from cultivated crops, it is necessary to completely satisfy their needs for water and minerals. This means that high yields require great amounts of energy. The same is true of protein food production, where the efficiency of transformation of vegetable food energy into the energy of meat and fat synthesized in animals is about 10% or, in other words, 10 calories of energy are spent on the production of 1 Calorie of protein. This energy production requires some share of the investment and consumption of the fossil fuel products of photosynthesis. Hence, in this case investment and energy expenditure are mutually dependent. The global model unit that describes agricultural investment is constructed by setting the dependences of agricultural productivity on energy expenditures. The investment parameter of the control U_{BGi} is described by the two-step function:

$$U_{BGi} = \begin{cases} U_{BG1i}, & t_0 \le t \le t_{BGi}; \\ U_{BG2i}, & t > t_{BGi}, \end{cases}$$

where t_{BGi} is the moment of change of the investment policy in agriculture in the ith region. The T_{Bi} parameter characterizing the time of assimilation of agricultural investments in the ith region can also change at moment t_{Bi}:

$$T_{Bi} = \begin{cases} T_{B1i}, & t_0 \le t \le t_{Bi}; \\ T_{B2i}, & t > t_{Bi}, \end{cases}$$

At present the need of humankind for energy is 90% satisfied due to the burning of fossil fuels (coal, oil, gas) and only 10% satisfied by hydro- and electric power stations. In future these relationships should change drastically as a result of new technologies of energy production and, in particular, increasing the efficiency of solar energy. The processes of accumulation and transformation of solar energy, and improving the technology of using World Ocean energy (waves, tides, ebbs, currents, etc.), will all play an important role. There will come a time when the human race will use new energy sources. Of course, this moment will be different for various regions. In the global model this is reflected by substitution of the initial value of the component M_i for a new M_{0GMi} value. The t_{GMi} parameter is the function of the multiplier m_{Gi} determined by the ratio of natural resource supplies to their annual expenditure

at a given moment. This can be regulated in each region by different means by taking the many aspects of human activity into account. Without dwelling on the details, take the following scenario of a possible change of multiplier m_{Gi}:

$$m_{Gi}(t) = \begin{cases} m_{G0i} - (m_{G0i} - m_{G\infty i})(t - t_0)/(t_{Mi} - t_0), & t_0 \le t \le t_{Mi}; \\ m_{G\infty i}, & t > t_{Mi}. \end{cases}$$

Within the time interval $[t_0, t_{MGi}]$ in each region the cost G_{MGi} of natural resource renewal can vary linearly from the value G_{MG0i} to the value G_{MG1i}:

$$G_{MGi}(t) = \begin{cases} G_{MG0i} - (G_{MG0i} - G_{MG1i})(t - t_0)/(t_{MGi} - t_0), & t_0 \le t \le t_{MGi}; \\ G_{MG1i}, & t > t_{MGi}. \end{cases}$$

The basic capital V_i $(i = 1, \ldots, m)$ invested in the development of industry, science, agriculture, construction, and other spheres of human activity eventually runs out and its efficiency decreases. To parameterize the processes that take place, let us introduce the term "aging time" T_{VG} (~40 years). Assessment of this parameter is a characteristic of each region. As before, assume that T_{VG} varies linearly from the value T_{VG0i} to the value T_{VG1i} within the time interval $t \in [t_0, t_{Vi}]$ and then remains constant:

$$T_{VGi}(t) = \begin{cases} T_{VG0i} - (T_{VG0i} - T_{VG1i})(t - t_0)/(t_{Vi} - t_0), & t_0 \le t \le t_{Vi}; \\ T_{VG1i}, & t > t_{Vi}. \end{cases}$$

2.3.4 Development scenarios

Moiseev (1990) called the 20th century "the age of warning", an "age of radical changes" in normal ideas about the environment. Indeed, the beginning of the 21st century has brought an actual problem of an alternative choice of the strategy of further NSS development. Moiseev (1990) wrote:

> "Our world society is at the parting of the ways. Of a multitude of ways open to us one should choose only one way! And without a new understanding, without a new comprehension of the whole process of development, its laws and trends we won't be able to make a needed choice."

This verdict is confirmed by practically all experts, who differ only in that their alternatives of global ecodynamics are sometimes controversial. Some problems naturally crop up here regarding the rational organization of society and creation of a technology that makes compromises between collective decisions about the interaction with nature.

Scenarios of human development are the basic subject of discussions at both global international and regional national levels (Yakovets, 1997; Troyan and Dementiev, 2005). Constructing global scenarios is based on the theory of sustainable development, the elements of which are rather difficult to create, and it is

accompanied by fiery discussions between experts (Kondratyev, 2000b, 2004b; Moiseev, 1993, 2001). The main components of development scenarios are economic and social in character with the first prevailing. In different regions their ratio depends on the prevailing source of economic development. In rich countries social components prevail. Developing countries, when working out development scenarios, have to consider a broader spectrum of alternatives including poverty reduction, higher education, increased agricultural productivity, development of industry, provision of a stable demography, etc. Both developed and developing countries run into many contradictory trends connected, for instance, with the direct dependence of people's living standards of people on areas of cultivated lands, with the resultant loss of natural habitats when developing tourism and agriculture. Overcoming these contradictions requires solution of many problems in planning the use of land and water resources, and development of urban infrastructure and the road network.

An important obstacle in working out an agreed future scenario for human development is the many contradictions between governments, ethnic groups, religions, and moral codes, overcoming which in the near future will require much effort by politicians, economists, sociologists, and religious figures to find a compromise not only between people but also with nature. Only by understanding the fundamental laws of nature, in accordance with which every living being and nature as a whole exist, will people be able to take their place in the environment and find the best way to make it possible to preserve life on Earth.

Many experts, despite the many pessimistic development scenarios, presume that humankind will find the way to sustainable development.

Among the most promising developments documented in numerous publications are the following (Renner, 2002):

- the continued rapid expansion of wind and solar-generated electricity;
- the steady decline in the amount of oil spilled accidentally;
- the outgoing reduction in production of ozone-destroying chemicals;
- the decreasing metal intensity of the world economy;
- the growing reliance on transboundary parks as tools for biodiversity conservation and peace and confidence-building;
- the expansion of commercial forest areas that have been certified as well managed; and
- reductions in the number of active armed conflicts.

2.3.5 Climate scenarios

A contradictory direction in global ecodynamics is the prediction of climate change depending on the strategy adopted for NSS development. Existing climate models do not give a direct result, and so various scenarios have been suggested based on analysis of the trends of climate change in the past and predictions of GHG concentrations (SRES, 2000). One such attempt is the IPCC report (IPCC, 2007) prepared by experts from more than 100 countries. Like previous similar reports (IPCC, 2001, 2005), the basic changes affecting the absorption, scattering, and

emission of radiation in the atmosphere and on the Earth surface are changes in atmospheric GHG and aerosol concentrations, solar radiation, and surface properties. These changes lead to changes in the radiation balance resulting in either warming or cooling. It was emphasized that the analysis of ice cores reveals a considerable increase in the present atmospheric concentration of the main greenhouse gas, carbon dioxide, for the last 650,000 years. In 2005, CO_2 concentration reached 370 ppm (against 280 ppm in the pre-industrial period), with its increase between 1995 and 2005 constituting 19 ppm per year. Present global concentrations of CH_4 and nitrous oxide have also exceeded the pre-industrial values for many tens of thousands of years. An increase in concentration of all three basic GHGs from the mid-18th century is mainly the result of human activity: carbon fuel burning and development of agriculture (carbon dioxide) as well as changes in land use (methane and nitrous oxide).

The IPCC report (IPCC, 2007) contains three basic gradations of anthropogenic causes of future climate change: ''rigid'', ''moderate'', and ''mild'' scenarios of anthropogenic emissions of GHGs and aerosols. As a result, the following conclusions have been drawn:

- In the period 2008–2030 global warming will take place at a rate of $\sim$0.2°C per decade. According to model calculations, even with fixed concentrations at the level of the year 2000, warming would go on at the expense of GHGs accumulated in the atmosphere at a rate of 0.1°C per decade.
- Preservation of GHG emissions at the present level, to say nothing of increasing emissions, will cause with a high probability further warming and numerous accompanying changes in the global climate system during the 21st century, which will exceed changes observed in the 20th century. With respect to the last 20 years of the 20th century, depending on scenario, by the end of the 21st century global warming will constitute from 1.8°C (a ''very mild'' scenario of anthropogenic impact B1 with probable limits from 1.1°C to 2.9°C) to 4.6°C (a ''very rigid'' scenario A1EI with probable limits from 2.4°C to 6.4°C), and sea level rise will average 0.19 m–0.58 m.
- A decrease in CO_2 assimilation by the ocean and land due to climate warming for Scenario A2 will lead to an additional increase in global warming by 1°C by the year 2100.
- Climate extremes will intensify (heat waves, heavy showers, etc.); the intensity of tropical cyclones (typhoons) will increase due to further SST rise at low latitudes; meridional circulation in the North Atlantic will decrease, on average, by 25%; extra-tropical cyclones will shift toward the poles.
- World Ocean ice cover is expected to decrease. According to some scenarios, by the end of the 21st century, the ice in the Arctic Ocean may well completely melt in late summer.

The diversity of climatic scenarios depends on the many versions of NSS development that take all manner of human activity into account. Table 2.7 lists the basic elements of such scenarios.

Table 2.7. Basic plotlines of scenarios of climate change in the 21st century. From IPCC (2001, 2007).

Scenario category	*Characteristic*
A1	A very rapid economic growth with indicators reaching maximum values in the mid-21st century with subsequent decrease and rapid introduction of new and more efficient technologies. The fundamental themes are gradual approach of different regions, reinforcement of the potential and energization of cultural and social relations with a considerable decrease of regional differences in per capita income. A1 is divided into three groups giving a description of alternative versions of the technological change in the energy system. Three A1 groups differ in their central technological element. A considerable share of the kinds of fossil fuel (A1F1), non-fossil sources of energy (A1T), or an equilibrium between all sources (A1B) (where the equilibrium is determined as slight dependence on one concrete source of energy, proceeding from the fact that similar rates of an increase in efficiency are used with respect to all technologies of energy supply and final use).
A2	A very heterogeneous world: self-provision and preservation of local originality. Indicators of birth rate in different regions approach each other very slowly, and as a result, the population size is constantly growing. Economic development has mainly a regional purpose, and per capita economic growth and technological changes are more fragmentary and slow compared with other plotlines.
B1	The plotline and scenario family B1 contain a description of the world moving in one direction with the same population size, which reaches a maximum in the mid-21st century and then decreases as in plotline A1; however, with rapid changes in the economic structures of service and information economy, with decreasing material intensity, and introduction of pure and resource-saving technologies. The emphasis is placed on global solution of the problem of economic, social, and ecological stability including greater justice but without additionary initiatives connected with climate.
B2	The plotline and scenario family B2 contain a description of the world in which the emphasis is placed on local solutions to the problem of economic, social, and ecological stability. It is a world with constantly increasing global population size at rates below A2, intermediate levels of economic development, and not so rapid and more diverse technological changes compared with plotlines A1 and B1. Though this scenario is also aimed at protection of the environment and social justice, the emphasis here is placed on local and regional levels.

2.4 BALANCE BETWEEN ECONOMIC GROWTH AND SOCIAL DEVELOPMENT

As repeatedly mentioned by many experts, reaching a stable balance between the economic and social processes in any country and in the world as a whole is a complicated problem, the solution of which will call for a complex approach to study the dynamics of the NSS. The authors of the collection of papers edited by Spoor (2004) tried to find a solution to this problem. Analyzing the internal mechanisms of the interaction between present global processes such as globalization, poverty, and conflict, the authors posed and tried to answer the following questions:

(1) Is "development" *passé*?
(2) Is it merely a byproduct or a "trickle down" effect of economic growth, spurred by globalization?
(3) Will poverty simply diminish with increased global markets?

These and other questions inevitably come before governments when they are determining how their countries should develop, at least for the foreseeable future. In this connection, Spoor (2004) considered various aspects and mechanisms to solve the problems caused by globalization, emphasizing three themes:

(i) globalization, inequality, and poverty;
(ii) governance, civil society, and poverty; and
(iii) resource degradation, institutions, and conflict.

One of the basic principles of economic growth is social capital. According to Vanin (2002), social capital is "the norms and social relations embedded in the social structure of a group that enable people to coordinate actions to achieve desired goals." Essentially, this is a hierarchy of socio-economic relationships, between different groups of people. The stability of these relationships depends on many factors, including social norms, the social structure, the level of development of civil obligations, social homogeneity, social justice, etc. Formalization of these relationships is reduced to construction of a game-theoretic model like that developed in Kondratyev *et al.* (2002b).

Economic growth and social development cannot be considered separately from the general global problem of the survival of humankind. In other words, it is necessary to consider the problem of co-evolution of two systems: *human society* (H) and *nature* (N). The systems H and N are determined by their structures (number of elements and relations among them) and behavior (responses to impacts). The internal behavior of such a system is aimed at maintaining its uninterrupted functioning. The external behavior of the system is aimed at achieving a certain outside goal. The temporal stability of a complex system is a necessary property without which all its other properties become meaningless. It is connected with the structural stability

of the material composition and energy balance of the complex system as well as with the regularity of its responses to the same external stimuli.

A breach in stability of a system may result from internal causes (the aging of its elements) or external causes associated with the unfavorable influence of the environment (an ill-intentioned enemy, in particular). The survivability of biological systems is determined by environmental conditions where human interference with nature is an important factor. In connection with this and the prospects of constructing artificial biological systems, optimization problems also arise; an increase of productivity of a biological system being the main criterion of optimality.

At the global scale the problem of survivability of the interacting systems is complicated by the hierarchy of interaction levels. For a complete explanation of H and N systems their openness has to be taken into account. Let us consider the interaction of two open complex systems H and N, defined by their goals H_G and N_G, structures H_S and N_S, and behavior H_B and N_B, respectively. It is suggested that the functioning of such systems should be described by the equations of (V, W)-exchange. Namely, the interaction of an open system with the environment (or other system) is represented as a process whereby the system exchanges a certain quantity V of resources spent in exchange for a certain quantity W of resources consumed. The aim of the system is the most advantageous (V, W)-exchange (i.e., it tries to get maximum W in exchange for minimum V). The V is a complex function of the structure and behavior of both systems:

$$V = V(W, H_S, N_S, H_G, N_G) = V(W, H, N). \tag{2.4}$$

As a result of their interaction, systems H and N get the following (V, W)-exchanges:

$$\begin{aligned} V_{H,max} &= V_{H,max}(W_H, H^*, N^*) = \max_{\{H_B,H_S\}} \min_{\{N_B,N_S\}} V_H(W_H, H, N) \\ V_{N,max} &= V_{N,max}(W_N, H^*, N^*) = \max_{\{N_B,N_S\}} \min_{\{H_B,H_S\}} V_N(W_N, H, N), \end{aligned} \tag{2.5}$$

where H^* and N^* are the optimal systems H and N, respectively.

From (2.4) and (2.5) we can see that the value of (V, W)-exchange depends on the goal of the system and may vary within certain limits: $V_{1,min} \le V_H \le V_{1,max}$, $V_{2,min} \le V_N \le V_{2,max}$, where $V_{i,min}$ $(i = 1.2)$ corresponds to the case when both systems are most aggressive, and $V_{i,max}$ $(i = 1, 2)$ to the case when they are most cautious. In a word, there is some *spectrum* of the interactions between H and N. For a formal description of these interactions we shall divide all the elements of both systems into three classes: the working, protective (defensive) and active elements, the latter designed to act on the environment. For short, we shall refer to the working elements of systems H and N as a and b-elements, to the protective elements as R_a and R_b-elements, and to the active elements as C_a and C_b-elements, respectively.

Let us assume that, before any interaction, the systems H and N have certain limited energy resources (i.e., vital "substrates") V_a and V_b, in which

$V_a = \{V_{aj}, j = 1, \ldots, m_a\}$, $V_b = \{V_{bi}, i = 1, \ldots, m_b\}$. These substrates generate working elements in such a way that substrate V_{aj} (V_{bi}) can generate H_j (N_i) $a(b)$-elements of the $j(i)$th type of values a_j (b_i).

The protective and active elements of each system are generated by the working elements. First, the protective $E^a_{Rm}(E^b_{Rm})$ and active $E^a_{Cm}(E^b_{Cm})$ substrates are created which, in their turn, generate R and C-elements of the mth type. These processes are described by the following dependences:

$$E^a_{Rm} = E^a_{Rm}(V_a, H_1, \ldots, H_{m_a}) = \sum_{j=1}^{m_a} w^a_{mj} f^a_{jR}(V_{aj}, H_j),$$

$$E^b_{Rm} = E^b_{Rm}(V_b, N_1, \ldots, N_{m_b}) = \sum_{j=1}^{m_b} w^b_{mj} f^b_{jR}(V_{bj}, N_j),$$

$$E^a_{Cm} = E^a_{Cm}(V_a, H_1, \ldots, H_{m_a}) = \sum_{j=1}^{m_a} w'^a_{mj} f^a_{jC}(V_{aj}, H_j),$$

$$E^b_{Cm} = E^b_{Cm}(V_b, N_1, \ldots, N_{m_b}) = \sum_{j=1}^{m_b} w^b_{mj} f^b_{jC}(V_{bj}, N_j),$$

where $w^{a(b)}_{mj}$, $w'^{a(b)}_{mj}$, and $f^{a(b)}$ are given present weights and functions, respectively.

We shall assume that, as a result of such hierarchical synthesis, the elements in systems H and N have at the beginning of the interaction ($t = 0$):

(1) m_j and n_j working elements of jth type with values a_j and b_j, respectively, where

$$\sum_{j=1}^{m_a} a_j H_j = M_a(0), \qquad \sum_{j=1}^{m_b} b_j N_j = M_b(0); \tag{2.6}$$

(2) r_a and r_b types of protective elements, the mth type having α_m and β_m elements, and:

$$\sum_{m=1}^{r_a} \alpha_m = M_{R_a}(0), \qquad \sum_{m=1}^{r_b} \beta_m = M_{R_b}(0); \tag{2.7}$$

(3) s_a and s_b types of active elements, the mth type having ν^a_m and ν^b_m elements and:

$$\sum_{m=1}^{s_a} \nu^a_m = D_a(0), \qquad \sum_{m=1}^{s_b} \nu^b_m = D_b(0), \tag{2.8}$$

respectively.

In the discrete case, the change of the average number of system elements that have survived until moment t_{i+1} will be described by the following relations:

$$H_s(t_{i+1}) = \max\{0, H_s(t_i) - \sigma^n_{hs}(t_i)p^n_{hs}(t_i)\}, \qquad s = 1, \ldots, m_h; \tag{2.9}$$

$$\alpha_j(t_{i+1}) = \max\{0, \alpha_j(t_i) - \sigma^n_{Rj}(t_i)p^n_{Rj}(t_i)\}, \qquad j = 1, \ldots, r_h; \tag{2.10}$$

$$\nu^h_m(t_{i+1}) = \max\{0, \nu^h_m(t_i) - \sigma^n_{Cm}(t_i)p^n_{Cm}(t_i)\}, \quad m = 1, \ldots, s_h; \tag{2.11}$$

$$N_l(t_{i+1}) = \max\{0, N_l(t_i) - \sigma^h_{nl}(t_i)p^h_{nl}(t_i)\}, \qquad l = 1, \ldots, m_n; \tag{2.12}$$

$$\beta_s(t_{i+1}) = \max\{0, \beta_s(t_i) - \sigma^h_{Rs}(t_i)p^h_{Rs}(t_i)\}, \qquad s = 1, \ldots, r_n; \tag{2.13}$$

$$\nu^n_m(t_{i+1}) = \max\{0, \nu^n_m(t_i) - \sigma^h_{Cm}(t_i)p^h_{Cm}(t_i)\}, \quad m = 1, \ldots, s_h, \tag{2.14}$$

where the $\sigma^{a(b)}_{\omega i}(t)$ values characterize the external behavior of both these systems:

$$\overline{H}^{(i)}_e = \{\|\sigma^a_{bl}\|, \|\sigma^a_{Rs}\|\}, \qquad \overline{N}^{(i)}_e = \{\|\sigma^b_{as}\|, \|\sigma^b_{Rj}\|\};$$

and $p^{a(b)}_{\omega i}(t)$ are the respective probabilities of death of the elements as a result of their interaction. The following limiting conditions should be taken into account here:

$$\sum_{i=0}^{T}\left\{\sigma^b_{Cs}(t_i)p^b_{Cs}(t_i) + \sum_{j=1}^{m_b}\sigma^a_{bj}(t_i) + \sum_{j=1}^{r_b}\sigma^a_{Rj}(t_i) + \sum_{j=1}^{s_b}\sigma^a_{Cj}(t_i)\right\} = \nu^h_l(0), \tag{2.15}$$

$$\sum_{i=0}^{T}\left\{\sigma^a_{Cs}(t_i)p^a_{Cs}(t_i) + \sum_{j=1}^{m_a}\sigma^b_{aj}(t_i) + \sum_{j=1}^{r_a}\sigma^b_{Rj}(t_i) + \sum_{j=1}^{s_a}\sigma^b_{Cj}(t_i)\right\} = \nu^n_l(0). \tag{2.16}$$

The stochastic solution of Equations (2.4)–(2.16) is very difficult. There are many real situations when the realization of an H^* or N^* system is impossible. Some tasks and algorithms were described by Krapivin and Klimov (1995, 1997).

2.5 SOCIAL RESPONSIBILITY AND ECONOMIC POTENTIAL

Under the influence of climate change, the differences between poor and rich countries will deepen, especially in the provision of elementary living conditions. Unfortunately, all available data on the dynamics of these differences confirm this trend. In many global regions temperature increase will inevitably lead to a decrease in soil fertility and water deficit. On the whole, we should expect that developing countries, as a result of predicted climate change, will experience difficulty in the provision of the necessary systems for life, which even the most socially irresponsible governments would not dare to resist. Pachauri (2004) outlined the pessimistic prospect for developing countries as a result of climate change and the lack of economic possibilities to reduce their vulnerability both in the sphere of foodstuffs and protection of their people from natural disasters. This disproportion between

developed and developing nations is also confirmed by the fact that during the last 50 years most damage in northern developed countries was fully insured and yet, compared with the southern developing countries, there was a minimum of people who suffered as a result of weather phenomena.

A basic notion of social responsibility is *corporative social responsibility*.

- It is the achievement of commercial progress that values ethical principles and respects people, communities, and the environment.
- It is understood as the promotion of practices by responsible businesses that are useful both for business itself and society and promote social, economic, and ecologically sustainable development through maximizing the positive impacts of business on society and minimizing the negative ones.
- It consists in obliging businesses to contribute to sustainable development, labor relations with workers, their families, the local community, and society as a whole, in order to improve the quality of life.
- It is the voluntary contribution of business to the development of society in the social, economic, and ecological spheres that are connected directly with the basic activity of the company and exceed the minimum determined by law.

Social responsibility under the present conditions of globalization reflects the whole complex of relations within the framework of a market economy. The most important component of social responsibility is the essence of business and its contribution to economy. But, business cannot exist isolated from society. It depends on a multitude of factors, important among which are human, organizational, and financial resources. Eventually, recognition of the economic potential of a country as a main element of the NSS will be the norm.

The economic potential of a country is determined by its available resources, which, used efficiently, make it possible to produce the maximum gross domestic product (GDP). The components of the economic potential of a country include the following:

- Nature resource potential, which characterizes the natural resources of the country either currently used in the economic cycle or yet to be mastered with available technologies and socio-economic relations.
- The production potential formed by material resources and manpower. These are the means of production (buildings, constructions, and equipment), technologies, laborers, engineers, and technicians.
- Labor potential or labor resources of the country, the volume and quality of which are determined by the size of the active able-bodied population, as well as their educational and professional level.
- The scientific and technical potential of the country in the field of scientific research and design, which includes achievements in fundamental and applied sciences, discoveries, and inventions, new technologies, as well as highly-qualified scientific, technical, and design personnel. The scientific and technical potential of a country can be considered the main lever of present economy development.

- Export potential, determined by the ability of the national economy to produce goods competitively on the world market and to export them in sufficient volumes at world prices.

Among the constituents that make up the social responsibility of the country are such important elements as the responsibility of the government, business, and citizens themselves for social well-being, determined by the growth of prosperity, level of education, and health of the nation. This means that, along with the economic potential, we should consider human capital. Realization of the social policy and development of the labor market in this context should be considered not as help for the poor and weakly protected layers of the population—but as actions to make up and increase the quality of human capital. Capital invested in the development of the social infrastructure should be considered as investment to the development of human resources of the country. Therefore, we should assess the efficiency of and grounds for this investment in the same way as any other investment is assessed. Government, business, and citizens are responsible for the realization of social policy. Therefore, when the social responsibility of business is questioned, it is important to understand that both the government and employees are responsible to business and businessmen. A socially responsible business also requires a socially responsible society and country.

2.6 BIOGEOCHEMICAL CYCLES AND QUALITY OF LIFE

Biogeochemical cycles, or the matter and energy exchange between various components of the biosphere, are cyclic in character and determined by the vital activity of organisms. In contrast to micro-organisms, birds, and animals, people try, whether realizing it or intuitively, to direct all processes taking place in nature toward improving conditions for their own lives. Here problems appear which are at the center of attention of practically all sciences.

The idea of biogeochemical cyclic recurrence was founded in the works of Vernadsky (1944) and further developed in biosphere science and biochemistry (Dunn, 2007; Schlesinger, 2005). The structure of the natural-science pattern of the world in recent decades drastically changed as a result of studies by Kondratyev (1986, 2004a, b) and Moiseev (1979, 1988, 1990). In these works emphasis was placed on the principal significance of the connections between living and inert substances as a fundamental basis for understanding the dynamics of biogeochemical cycles. Vernadsky (1977) wrote:

> "Between inert and living substances there exist, however, a constant bond which can be expressed as a continuous biogenic flow of atoms from a living substance to inert substance of the biosphere, and back. This biogenic flow of atoms is caused by a living substance. It is expressed through ceaseless respiration, nutrition, reproduction, etc."

It should be added that the main feature of biogeochemical cycles is that some of the time they are open. Substances often leave the biospheric cycle for a given duration and can return and close the cycle after a much longer time period.

Biospheric cycles are known to last from dozens and hundreds to several thousands of years, and the geological cycle lasts for millions of years. During the history of the biosphere (3.5–3.8 billion years), as a result of the openness (95%–98%) of biogeochemical cycles, the oxygen and nitrogen in the atmosphere was formed as were the deposits of coals, oil shale, limestone, phosphorites, bauxites, and other minerals in the Earth's crust.

Solar energy and the activity of living substances are the driving force of biogeochemical cycles. The energy accumulated in the process of photosynthesis is globally re-distributed depending on the trend of biogeochemical cycles, which are now governed by anthropogenic processes. As a result, regions of the biosphere appear with characteristic features of biogeochemical cycles expressed either as a shortage or an excess of certain chemical elements. John F. Kennedy, President of the U.S.A., in his address to Congress on February 23, 1961 said that society entirely depends on water, land, forests, and minerals, and the health, security, economy, and well-being of people depend on how society uses these resources. Indeed, resources that accumulate due to solar heat and light are governed by biogeochemical processes, and therefore their renewal and availability for use depend on natural and anthropogenic factors, the role and ratio of which in different regions are different. In contrast to mineral resources whose renewal interval is millions of years, resources of solar origin can be renewed in time intervals that are rapid enough for the maintenance of life of humans and animals. However, a problem consists in coordinating the rhythms of renewal and consumption of these resources. The growing demand for food, for instance, requires increased harvests, and hence, increased volumes of mineral resources are needed. The observed dynamics of food consumption is characterized by values: 2,552 kcal per capita per day in 1979/1981, 2,803 kcal per capita per day in 1997/1999, and *2,928 kcal per capita per day in 2006/2007*. Continuation of this trend in future will require food production of 2,940 kcal per capita per day. A number of questions arise, for instance:

(1) What is the possible maximum level of food production?
(2) What are the limits to increasing agricultural productivity?
(3) What is the limit to the land resources that can be used?

An obvious hindrance to development of a civilized attitude toward nature is a shortage of any resource (e.g., water and food). As industry, agriculture, and urbanization develop, interference with hydrological cycles grows due to the re-distribution of water flows. For instance, 8% of rains in the U.S.A., giving up to $0.42 \cdot 10^{15}$ L of water, are taken for industry, irrigation, and urban water supply. Some water returns after a delay to the natural cycle, but most water in land reclamation systems is spent on evaporation and transpiration and, hence, enters a different cycle. Dam construction and the creation of water reservoirs also violate the hydrological cycle by introducing once again the effect of delay. All these problems

become more complicated when the contamination of water systems is also taken into account. Polluted water cannot be used repeatedly, which means that it is not usually discharged into the same, initial reservoir. In this connection, Skinner (1979) justly noted that people are mistaken when they regard any natural resource, renewable or non-renewable, as if it can be used separately from all other resources. This means that all biogeochemical cycles should be studied as a complex (i.e., within a single system that analyzes natural and anthropogenic processes together).

The formation of the biomass of cultivated plants and humus in the soil layer has to do with the biogeochemical cyclicity of carbon, oxygen, hydrogen, natrium, phosphorus, sulfur, calcium, magnesium, potassium, nitrogen, and other biogenic elements. Farmers, when harvesting, violate the biogeochemical cycle over their farmland. To replace chemical elements removed during the harvest, it is necessary to introduce fertilizers to the soil. At this stage of the interaction between nature and humans there needs to be a means of optimizing the biogeochemical cycle. Violations of the biogeochemical cycles of nitrogen, phosphorus, and heavy metals (lead, zinc, cadmium, mercury, etc.) can lead to catastrophic consequences for human health. Therefore, renewal and maintenance of a balanced cyclicity of the most important biogenic elements, both over a given territory and in the biosphere as a whole, is a first-priority problem facing biosphere scientists.

The need to improve the quality of life in practically all global regions in the 20th and early 21st centuries has forced humankind to deliberately increase the rate of agricultural production of nitrogen-rich fertilizers. It is this cycle of nitrogen that determines to a great extent the purpose of many social and demographic processes. At the same time, the processes involved in soil mechanics and plant cultivation strongly affect the nitrogen cycle in nature. Considering the U.N.-predicted increase in global population size up to 9 billion by the year 2050, the problem of nitrogen cycle control is becoming urgent, especially if on a global scale an international mechanism for balanced application of fertilizers is not found. The productivity of the global agricultural system is growing annually by 1.4%–2.3%, struggling to keep up with the rate of growth in population size. Therefore, current studies of biogeochemical cycles with the remit of raising the level of living standards should prioritize the search for this balance (Figure 2.1). In this connection, Williams (2005) believes that progress can be achieved as long as a complex approach is used—but not when individual biogeochemical cycles are considered in isolation. It is the complex approach that will make it possible to reveal the anomalous responses of biogeochemical cycles to anthropogenic interferences and to calculate vitally important biospheric parameters. The cycles of phosphorus and carbon are closely related to the cycle of nitrogen as $C:N:P = 106:16:1$, due to evolution of the geosphere– biosphere system (GBS). As Zavarzin (2003) noted, in the GBS, along with determining direct bonds from the geosphere to biota, transforming feedbacks play an important role. In this evolution, micro-organisms are of principal importance. Apparently, they act as a buffer for the GBS, which governs the conditions that regulate biogeochemical cycles. At the same time, the biota itself directly governs biogeochemical cycles by assimilating biogenic salts from soils, respiration, and evapotranspiration. So, CO_2 assimilation according to the reaction

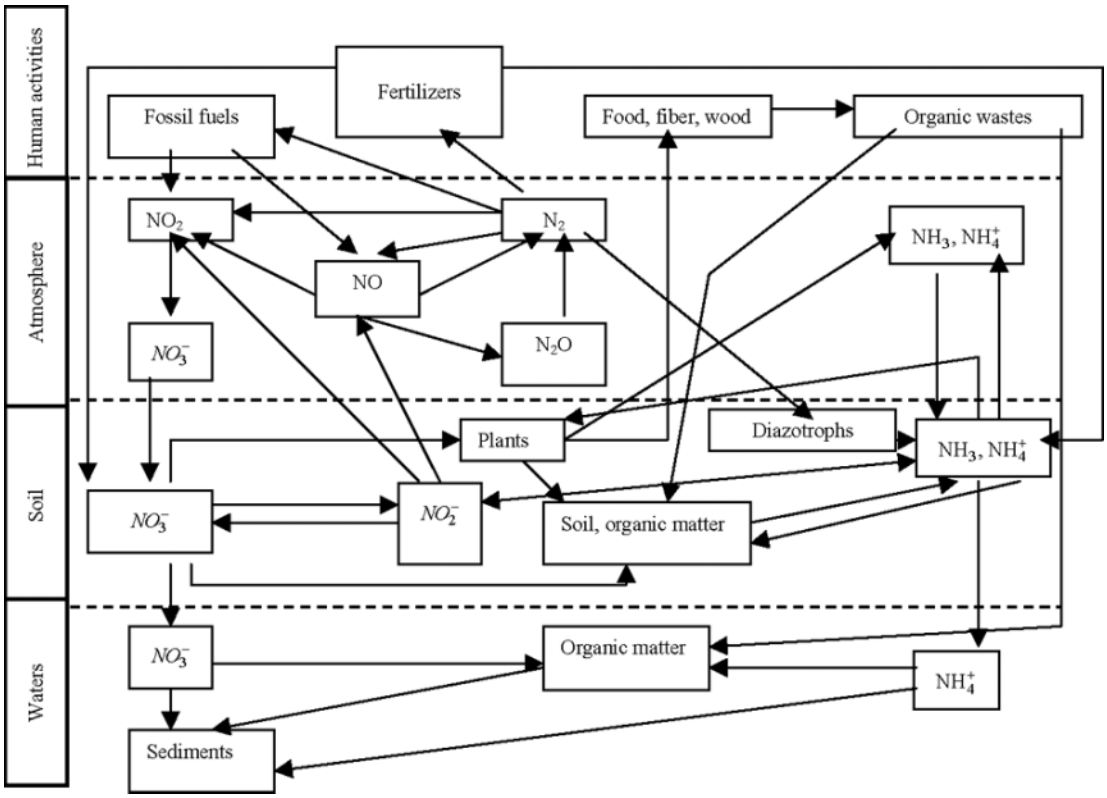

Figure 2.1. Conceptual scheme showing how the nature–society system functions.

$CO_2 + H_2O = [CH_2O] + O_2$ follows in molar ratio the rule $CO_2 : C_{org} : O_2 = 1:1:1$. The rate of atmospheric CO_2 sink under present biospheic conditions is 145 kgC per 1kg of chlorophyll. This level of sink is eventually the parameter that regulates the quality of life.

Let us return to the biogeochemical cycle of nitrogen and consider the role of the use of manure in agriculture. From the available estimates of experts, the introduction of 200 kg of manure per year per hectare to cultivated soil, with sufficient moisture content and moderate climate, can feed 15 people, on average. So, in China, 1 ha feeds 5–6 people, and in Japan this indicator is higher because of seafood. In a given region, this ratio greatly depends on the type and the characteristics of the soil. Unfortunately, no global model can achieve the level of soil parameterization that takes account of the available data, at least on the average parameters of a typical soil and its structure (Williams, 2004).

- The basic constituents of a typical soil include 5% organic matter, 25% water, and 25% air.

- Soil horizons differ in structure, density, composition, porosity, acidity, and color.
- There are three main soil horizons.
  (1) *A-horizon* (surface soil). This includes the mulch layer and plow layer. Living organisms are most abundant in this horizon, consisting of plant roots, bacteria, fungi, and small animals.
  (2) *B-horizon* (subsoil). This layer is an intermediate soil layer characterized by properties of both the A and C-horizons.
  (3) *C-horizon* (parent material). Soil parent materials are those from which the soil was formed.

As Austin *et al.* (2004) demonstrated, the episodic nature of water availability in arid and semiarid ecosystems substantially affects the cycles of carbon and biogenic elements in these territories. Pulsed water supplies directly govern soil processes by means of dry/moist soil cycles. The inevitable responses of micro-flora to this cyclicity can cause a shift in the C/N ratio, which changes the mineralization processes. By violating biogeochemical cycles, especially those of water and other GHGs, people affect the processes of biotic regulation of the environment, preparing the irreversible transition of climate to one that is unfit for life. This was illustrated by the work of Karibaeva *et al.* (2004) where three phase states of the climate are described.

(1) Complete glaciation of the planet at a temperature preserved at $-100°C$.
(2) Complete evaporation of the oceans at a temperature preserved at $+400°C$.
(3) Equilibrium between various processes in the environment preserving a globally averaged temperature $\sim+15°C$, which provides conditions suitable for life at many latitudes.

As noted in Kondratyev *et al.* (2005) and Krapivin and Varotsos (2007), people's quality of life is directly connected with biogeochemical cycles through such processes of consumption of food, energy, and other conditions and goods. Most of the global population (>1.7 billion people) fall in the "class of consumers", with about half of this population living in developing countries. Starke (2002) pointed out that more than 1.2 billion people live on less than U.S.$1 a day. It is this indicator that points up one of the main causes of instability in many countries: poverty, which creates ideal conditions for the propagation of various diseases.

In recent decades, the scale of consumption in developed countries is often termed a "revolution in consumption" and has been constantly growing. In 2000, total per capita consumption of goods and services reached U.S.$20 trillion, exceeding the level of 1960 by $4.8 trillion (in U.S.$ of 1995), with huge differences characterizing the situation in different countries. Sixty percent of per capita consumption falls on 16% of the global population living in the U.S.A. and western Europe, whereas the share of consumption for one-third of the global population in South Asia and sub-Saharan Africa constitutes only 3.2%. Such an "unhealthy level of consumption" results in increased impacts on the environment and natural resources. Table 2.5 summarizes this.

In addition to the Human Development Index (HDI) used to characterize living standards, the Wellbeing Index (WI) was proposed to list the top 180 countries regarding human well-being (health, standard of education, material security, and civil rights) and the environment. According to WI data, Sweden tops the table, and the United Arab Emirates closes the list, though the level of energy consumption in this country is almost double that of Sweden (Table 2.6). Austria occupies a very modest place according to energy consumption, but is characterized by a high level of well-being.

2.7 BIOLOGICAL, CHEMICAL, AND PHYSICAL INDICATORS OF THE QUALITY OF BIOGEOCHEMICAL CYCLES

Biogeochemical cycles are the complex processes of matter and energy transformation in the environment. Their analysis and study require the development of complex models, the use of which to assess the state of the biological cycle needs creation of simplified indicators that reflect individual aspects of its development or describe integral trends in changes of its characteristic (Cuffney *et al.*, 2000; Corstanje and Reddy, 2004; Leonova, 2004). In other words, the main function of an indicator is to reflect by means of a single parameter the behavior of the biological cycle, reveal its critical states, or outline the boundaries of possible negative consequences of anthropogenic interference with this cycle. The goal of the indicator is to give a reliable answer to the main question: What will happen to the biogeochemical cycle on realization of a given scenario of NSS development? Therefore, indicators are an important means to project and assess the strategies of human impacts on the environment enabling us, based on a simple indicator of its state, to make a decision about the expedience of realization of any anthropogenic scenario. It is especially important when assessing the role of the environment in the formation of life conditions for a population in a given region.

Smeets and Weterings (1999) introduced four types of indicators.

- Descriptive indicators. They answer the question concerning changes in a certain set of environmental characteristics and their impact on the biogeochemical cycle.
- Performance indicators. They measure deviations of the biogeochemical cycle from its prescribed state as a result of the impact of realization of a given scenario.
- Efficiency indicators. This type of indicator reflects the level of efficiency of an anthropogenic impact on the environment that can be seen by changes in biogeochemical cycles.
- Total welfare indicators. They point to the biogeochemical cycle's stability.

An important constituent of biogeochemical cycles is the water medium, by the state of which we can assess the level of change in the biogeochemical cycle of a certain element. The most widespread indicator of the quality of this constituent of

the biogeochemical cycle is the level of water eutrophication: as a rule this includes the five-day biological oxygen demand (BOD_5), fecal indicator, bacteria, and viruses.

BOD_5 represents the amount of oxygen consumed by bacteria and other microorganisms as they decompose organic matter under aerobic conditions at a specified temperature. But, there exist more complicated indicators, including that of the degree of heterogeneity or diversity of the ecosystem (e.g., the Shannon–Weaver Index, the formula of which is $H' = -p_i \log p_i$, where p_i is the fraction of individuals of species i). Clearly, the relationship $J = H'/H'_{max}$ characterizes an ecosystem's homogeneity, and when $J \to 0$ this level rises. Here H'_{max} is the value of H' computed with the same number of species, but equal p_i values.

Another indicator of the state of the ecosystem is the Simpson Index, $N_2 = [N(N-1)]/[n(n-1)]]$, where N is the total number of individuals of every species and n is the number of individuals of one species. In this case the equitability of abundance can then be derived by $V = N_2/N_{2max}$, where N_{2max} is N_2 calculated for the same number of species and individuals, but equal abundances for each. Species abundances are more evenly distributed as V approaches 1.0 (Cox, 1985).

Apart from the Shannon–Weaver and Simpson indicators, other indicators such as Eveness, Margalef, the Family Biotic Index (FBI), Trent Biotic Index (TBI), and Indice Biotico Esteso (IBE) are widely used. While the Shannon–Weaver, Simpson, Eveness, and Margalef are ecological indices created to measure diversity in ecological communities, the FBI is a synthetic index used in the field assessment of organic pollution. It can vary from 0 to 10, detecting seven classes of organic contamination. The IBE is based on two evaluation parameters: taxonomic richness and the presence of pollution-sensitive taxa (Fenoglio *et al.*, 2002). It is used to assess the "health" of river ecosystems. The TBI determines the pollution level of water merely by the presence/absence of certain invertebrates.

An unbroken biogeochemical cycle is widely manifested in different media by indicators of the stable dynamics of the content of chemical elements, or stable ecodynamics. In other words, correlation between the biogeochemical cycle and the ecological situation serves as a direct indicator of the state of the biogeochemical cycle. This is demonstrated by comparing biogeochemical cycles in background and anthropogenically violated media. For instance, by comparing the chemical composition of soils close to roadsides and territories far from anthropogenic sources of pollution, an abrupt increase in heavy metal content is observed, which leads to a change in the chemical composition of soils. The role of land vegetation manifests itself by altering the temporal characteristics of biogeochemical cycles. An important indicator of the state of the biogeochemical cycle in the atmosphere–plant–soil system is the response of the soil solution to the migratory activity of pollutants and specific features of vegetation cover, whose biosorption ability serves, to a certain extent, as a stabilizing factor. Of course, one of the most powerful ecological factors for biogeochemical cycle regulation here is soil moisture, which has a versatile influence on soil biota and leads to re-organization of soil microbial coenosis.

Vegetation plays the principal role in the biogeochemical cycles of many elements, regulating their spatial heterogeneity. In order to clarify this role, various vegetation indices are introduced which describe variations in the activity of vegeta-

tion in time and space and thereby reflect this variability in biogeochemical cycles, too. Among the well-known vegetation indices the MODIS Vegetation Index (VI), Leaf Area Index (LAI), Soil-Adjusted Vegetation Index (SAVI), Transformed SAVI (TSAVI), Enhanced Vegetation Index (EVI), Difference Vegetation Index (DVI), and Normalized Difference Vegetation Index (NDVI) stand out. All these indices measure vegetation cover brightness in the near-IR and visible red bands. We have, in particular:

$$\mathrm{VI} = X_{nir}/X_{red}, \qquad \mathrm{NDVI} = (X_{nir} - X_{red})/(X_{nir} + X_{red}),$$
$$\mathrm{SAVI} = (X_{nir} - X_{red})/(X_{nir} + X_{red} + L)/(1 + L),$$

where L is the correction factor; X_{nir} and X_{red} are the radiances for the NIR and red visible wavelengths, respectively. There are other formulas to calculate these indices. For instance, $\mathrm{LAI} = m_v/\beta$, where m_v is the water content of vegetation and β is the proportionality coefficient.

2.8 THE ROLE OF LIVING PROCESSES IN BIOGEOCHEMICAL CYCLES

People, in the process of their daily lives, change the environment in an attempt to improve their standards of living. As an NSS element, they follow certain laws and conditions, and therefore individual strategies of behavior depend to a great extent on public strategy and, of course, cannot be optimal. The integral impact of population on the environment is a function of numerous factors that mainly depend on population density. Anthropogenic impacts on ecosystems change the character of the interaction between its biotic and abiotic parts, and hence, fragments of the global biogeochemical cycle. The scale of this change is much greater in densely populated territories. More than 60% of the world population live within 100 km of the sea coast, and therefore the oceans are under growing anthropogenic influence despite many measures to reduce this by many countries. Marine biodiversity has reduced: from 1900 up to the present the predatory fish supply along the eastern coast of the U.S.A. and the western coast of Europe has decreased from more than $10\,\mathrm{t\,km^{-2}}$ to $3.75\,\mathrm{t\,km^{-2}}$ and continues to decrease. For the Atlantic region, during this period the supply of predatory fish decreased, on average, from $2.9\,\mathrm{t\,km^{-2}}$ to $1.0\,\mathrm{t\,km^{-2}}$ (Pauly and Maclean, 2003).

An alarming and pessimistic situation is currently occurring in Europe where ecological resources have been largely exhausted, and, hence, foreign resources are used. In some European countries hardly any virgin biosystems are left, except in Norway, Finland, Sweden to some extent, and, of course, European Russia. In the territory of Russia ($17 \times 10^6\,\mathrm{km^2}$) there are $9 \times 10^6\,\mathrm{km^2}$ of virgin territory and, hence, functioning ecological systems. A considerable part of this territory is covered by tundra that is biologically low in producton. Russian wooded tundra, taiga, and sphagnum (peat) bogs are ecosystems without which it is impossible to imagine the

normally functioning of biota over the globe. Russia, for instance, is the world's top assimilator (due to its vast forests and marshes) of CO_2, about 40%. It should be stated perhaps that there is nothing in the world more precious for the people of the world and their future than the continued preservation and functioning of the natural ecological system in Russia. In Russia, the ecological situation is aggravated by prolonged general crises due to the absence of national ecological programs and the economic shocks that have taken place (Makarov, 2000; Mironov, 2005)

- The level of industrial production in Russia in 1996 constituted 47% of the level in 1980.
- In 2000 the percentage of the population living below the poverty level was between 25 and 40.
- Life expectancy in 2007 averaged 65 years.
- Costs of measures to ensure ecological safety in 2007 constituted 0.1% of GDP.
- Costs of measure for the protection of nature in 2007 constituted 2% of GDP.

Therefore, it is rather difficult to undertake a global-scale assessment of the state of biogeochemical cycles (e.g., of GHGs) without reliable data for Russia. Russia is one of the main exporters of raw materials to the world market. Unfortunately, during the post-Soviet period Russia was unable to deal effectively with the many formidable environmental challenges.

Besides people, the globe is a habitat for the myriad organisms that form a hierarchy of groups and sub-groups in accordance with the similarities and differences in their structure and behavior. This difference and diversity of species is an important basis for understanding the role of living processes in biogeochemical cycles. After all, every species is connected directly or indirectly with a multitude of others in an ecosystem. Predator/victim interactions provide the cyclicity of biogeochemical cycles. But interactions between living organisms depend substantially on many other factors such as radiance level, temperature, precipitation, topography, biogenic elements, etc. Their life dynamics are regulated by the character of the use of the habitat's life resources, including food, space, light, heat, water, air, and shelter. One should emphasize here the difference between the role of humans and other living organisms in the control of biogeochemical cycles. In contrast to purposeful and mainly deliberate human activity, other living organisms interact with their environment following the laws of natural evolution. Unfortunately, current knowledge and available data bases are not up to the job of evaluating the ratio of the roles of humans and other living organisms (plants included) in regulating biogeochemical cycles.

Living organisms live in harmony with the environment through reactions from the exchange of matter and energy, whose content and rate are determined by different biophysical, biochemical, and geochemical parameters. It should be mentioned here that, for instance, the chemical composition of plants in the historical past was highly stable. In the pre-industrial epoch, processes of accumulation of chemical elements took place both in plants and in living organisms. Plants and

Table 2.8. Parameters of the heavy metal cycle in the birch forest of Kuznetsk Alatau. From Shugalei *et al.* (2005).

Indicator of the biogeochemical cycle	*Heavy metal*				
	Barium	*Manganese*	*Copper*	*Nickel*	*Zinc*
Storage in forest ecosystems ($kg \cdot ha^{-1}$)	871–1,485	520–688	21–26	12–66	56–91
Accumulation in NPP (dry weight) ($g \cdot ha^{-1}\ yr^{-1}$)	32–40	4.8–6.1	56–77	7–10	195–238
Recovery speed for return to the soil after leaf-fall ($g \cdot ha^{-1}\ yr^{-1}$)	25–32	3.8–5.1	14–27.7	4.3–8	156–199.9

living organisms had enough time to assimilate the chemical elements reaching their biomass, and therefore they were accumulated. For instance, the accumulation of heavy metals in the litter of vegetation cover is determined not only by the biological cycle but also by different intensity of abscission taken up by soil invertebrates and micro-organisms. For instance, fallen birch leaves and grass take 2.5–3 years to transform, and it takes decades to transform the trunk and branches. Such a difference in time of decomposition of litter components is a powerful regulator of the biogeochemical cycle of many elements assimilated by plants. Table 2.8 contains some estimates of heavy metal cyclicity parameters.

3

Numerical modeling of global carbon change

3.1 OVERVIEW OF THE GLOBAL CARBON CYCLE

3.1.1 Status and perspectives of carbon cycle science

In recent decades the problem of the global carbon cycle (GCC) has attracted special attention in connection with the many, often speculative, explanations of the role of CO_2 in future climate change (Kondratyev, 2000a, 2002, 2004a). Unfortunately, so far, there is no objective evaluation of this role. Recent works (Kondratyev, 2004b; Kondratyev and Krapivin, 2003a, b; Kondratyev *et al.*, 2002a, b, 2003a–c, 2004a, b; Fasham, 2003) contained reviews of the first results of creating a formalized technology to assess the CO_2-induced greenhouse effect, with the role of land and ocean ecosystems taken into account. An interactive connection was shown between the GCC in the form of CO_2 and climate change. Formalization of this connection is based on synthesizing global models of how the NSS functions with the spatial distribution of NSS elements taken into account, which makes it possible to reduce it to an interrelated scheme of the cause-and-effect relationships of carbon fluxes between their various reservoirs in the atmosphere, land biosphere, ocean, and geosphere (Figures 3.1–3.5).

To understand the laws of the GCC, it is necessary to have reliable information about the main sources and sinks of carbon and their inter-regional fluxes. Powerful sources of CO_2 ($>0.1\,Mt\,CO_2$) number 7,500. Their geographic distribution can be described in four clusters:

(1) North America (middle, east, and eastern coast of the U.S.A.);
(2) northwestern Europe;
(3) South-East Asia (eastern coast); and
(4) south Asia (Indian sub-continent).

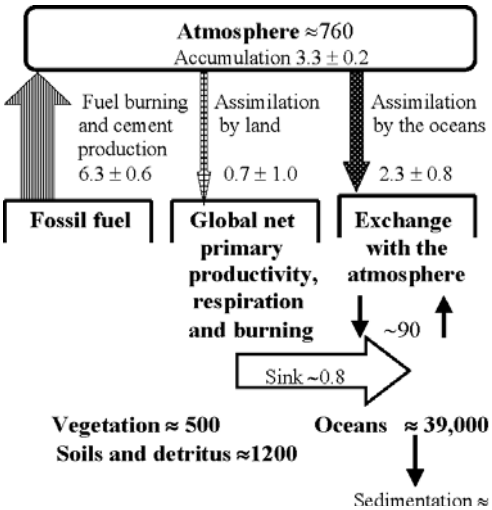

Figure 3.1. Global carbon cycle after Bolin and Sukumar (2000). Carbon supplies are given in GtC, and its fluxes in GtC/yr.

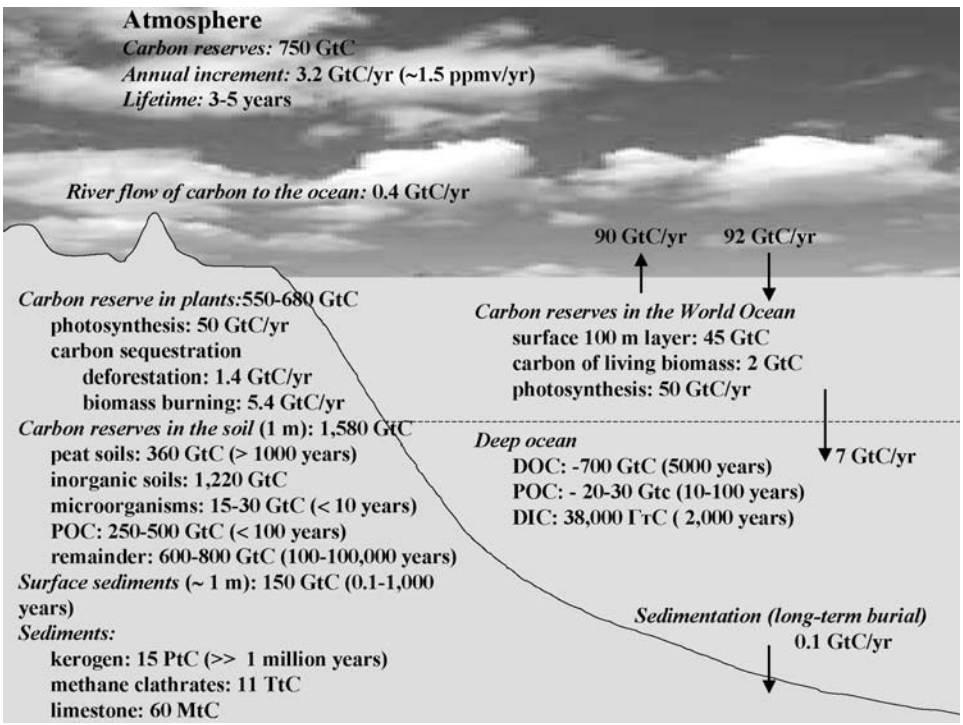

Figure 3.2. Global carbon reservoirs, fluxes, and turnover times.

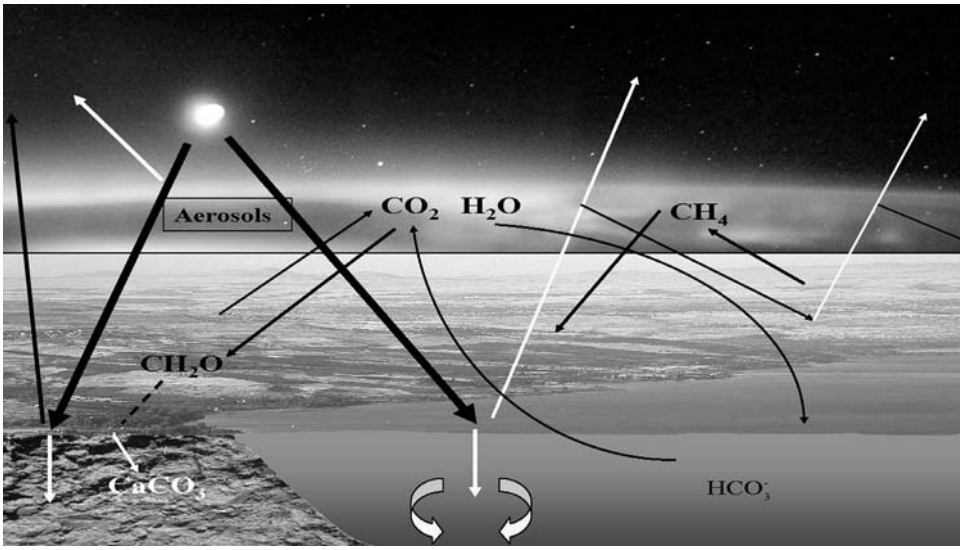

Figure 3.3. Conceptual scheme for the Earth's climate system.

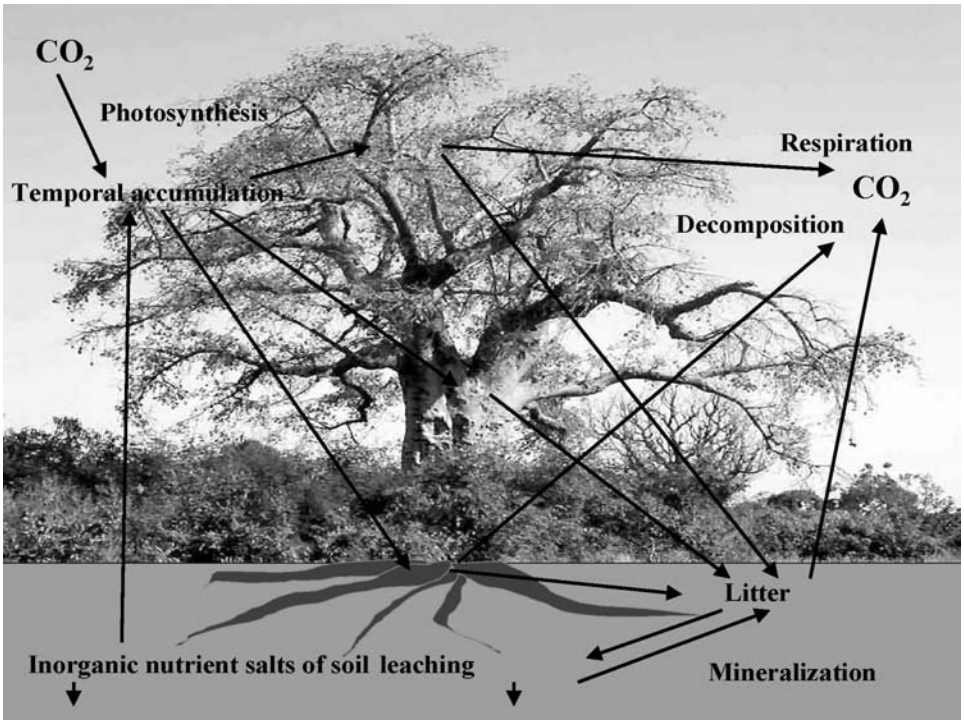

Figure 3.4. Carbon fluxes in the atmosphere–plant–soil system.

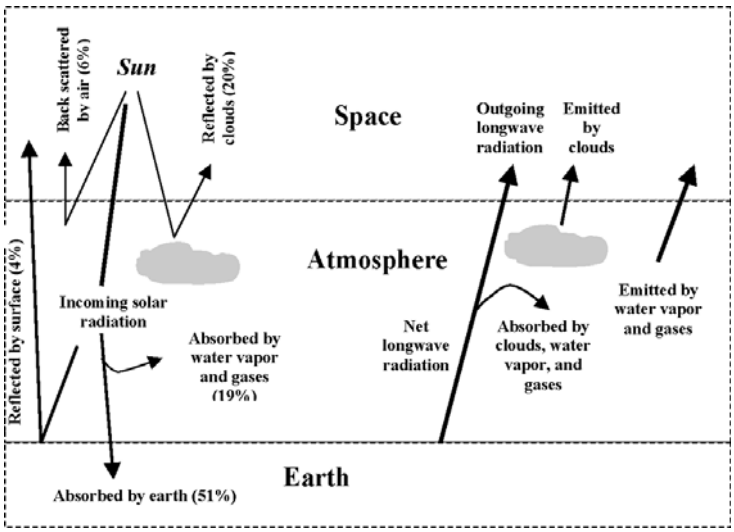

Figure 3.5. Radiation balance of the Earth.

The fourth cluster is characterized by the maximum rate of development; by 2050 a sudden increase in the number of CO_2 sources over this territory should be expected, and at the same time, their number in Europe should decrease. Of course, there is a certain dependence here between the geographical distribution of CO_2 sources and the geological supplies of fossil fuels.

In this connection, Baker *et al.* (2006) studied monthly CO_2 fluxes for the period 1988–2003 for its regional emissions in 22 countries based on measurements at 78 locations using 13 different models of the atmospheric transport, which reflect the role of winds and other environmental parameters. An objective formalization of biospheric sources and sinks of CO_2 as functions of environmental parameters as well as consideration of the real role of anthropogenic processes have become possible due to the global network created to measure surface CO_2 concentration and recent developments by many authors in constructing models that describe to different degrees the spatial distribution of carbon fluxes and their interaction with NSS components (Kondratyev *et al.*, 2004a). For instance, land sinks are determined by three basic factors (Kondratyev and Isidorov, 2001):

- functional dependence of ecosystem sensitivity to CO_2 concentration in the atmosphere and temperature;
- time shifts in the interactive atmosphere–ocean system; and
- the slow carbon cycle in the biospheric reservoir.

The assimilation of CO_2 by land ecosystems is determined by the difference between carbon assimilation due to photosynthesis and loss of carbon due to respiration. However, the subsequent climatic impact shows itself only in several decades in

view of the great thermal inertia of the ocean. The carbon cycle on land is also heterogeneous in its temporal characteristics. Carbon supplies in the land biosphere exist in two forms: about one-third in the form of biomass (mainly forests) and two-thirds as soil carbon. Both these forms include sub-reservoirs with different time constants of the cycle, which determines the variability in carbon sink on land. So, for instance, an increase in atmospheric CO_2 concentration intensifies the growth of forest and thereby increases the land sink of carbon, but because of the long lifetime of forest (100–200 years), accumulated carbon will returning to the atmosphere with a great time lag which is governed by many factors. Therefore, special attention must be paid to the study of the role of forests in the GCC (Medlyn *et al.*, 2005). Also of importance are studies of the carbon cycle in cultivated lands. For instance, from estimates of Verma *et al.* (2005), the sink of atmospheric CO_2 on an irrigated maize field can constitute from $381\,gC\,m^{-2}\,yr^{-1}$ to 517 and on a soybean field from $18\,gC\,m^{-2}\,yr^{-1}$ to $48\,gC\,m^{-2}\,yr^{-1}$.

The CO_2 flux at the atmosphere–vegetation cover boundary is determined in many respects by the soil processes involved in organic matter transformation. To better understand the biotic and abiotic mechanisms that control CO_2 emission from the soil, Jassal *et al.* (2005) compared measured CO_2 fluxes in a forest with their distribution profile in the soil of a 54-year-old coniferous forest on the eastern coast of Vancouver. It was established that CO_2 concentration grows at all depths of the soil layer with rising temperature and humidity. This is explained by soil diffusion reduction and changes in soil ecosystem functioning. It was noted that more than 75% of CO_2 emitted from the soil was generated at a depth of 20 cm, and almost total CO_2 flux forms from the 0 cm–50 cm layer.

Though it is usually supposed that the growth in atmospheric CO_2 concentration is anthropogenic and connected with the increasing scale of economic activity (mainly, energy production and consumption), it was shown that since 1980 natural factors have contributed more than the increasing level of fuel burning. Recent studies showed that the possible changes in ecosystem physiology connected, in particular, with the effect of fertilization (intensification of photosynthesis under conditions of increased CO_2 concentration) strongly affect carbon fluxes.

The Intergovernmental Panel on Climate Change (IPCC) agreement was signed by 189 countries, and it establishes a general agreement to stabilize GHG concentration to limit the anthropogenic impact on climate, though concrete levels have not been specified, and the KP levels of CO_2 are being disputed by many countries as scientifically ungrounded. A reduction in CO_2 emissions to the atmosphere includes:

- reduction of energy consumption (e.g., due to the growing efficiency in the development of industrial enterprises that consume less power;
- transition to new kinds of fuel or fuels with a lesser content of carbon (e.g., natural gas instead of coal);
- growing share of renewable sources of energy and nuclear energy;
- removal of CO_2 from the atmosphere through biological assimilation by land ecosystems; and
- removal of CO_2 from the atmosphere using chemical and physical mechanisms.

In connection with the coming into force of the Kyoto Protocol aimed at preventing climate warming due to the greenhouse effect of anthropogenic emissions of CO_2, an urgent need has arisen to specify models of carbon circulation in the environment in order to obtain more objective estimates of the degree and character of this impact. This came about because of the fact that existing ideas of the role of atmospheric CO_2 in observed changes of climate are based on the rather inaccurate and inadequate schemes describing the carbon fluxes between its main reservoirs on the planet. One of them is development of a balanced scheme of global carbon fluxes. About 27% of the carbon sink from the atmosphere in available schemes remains unexplained.

Studies by Kondratyev *et al.* (2004a, b) showed that consideration of the spatial heterogeneity of sinks and sources of atmospheric carbon and specification of the parameters of its fluxes at the atmosphere–land and atmosphere–ocean boundaries raised the accuracy of estimates, but did little to remove either imbalances or differences between carbon fluxes and the dynamics of the change in CO_2 partial pressure in the terrestrial atmosphere.

Unfortunately, the program of carbon flux control within the Global Carbon Project (GCP) ignored this contradiction. This reduces considerably the confidence in existing scenarios of possible natural cataclysms caused by the melting of Arctic and Antarctic ice and distorts the pattern of anthropogenic impact on climatic processes. A most serious shortcoming of the GCP program is that it disregards the geological component of the present carbon cycle.

From available, though approximate, estimates, about 10^{23} g of carbon-containing gases are concentrated in the rocks of the Earth's crust and mantle (lithosphere) (Korstenshtein, 1984; Sokolov, 1971). This mass of carbon exceeds by approximately 10^4 times the amount present today in the biosphere (over the Earth surface). Between the biosphere and lithosphere there is a constant, very intensive exchange of carbon that is self-regulatory. From the data of Barenbaum (2000, 2002), due to the Le Chatelier principle (Krapivin *et al.*, 1982), the content of mobile carbon in the system tries to attain a stable relationship:

$$n_i/\tau_i = C = \text{const}, \tag{3.1}$$

where n_i and τ_i are, respectively, total amount and average time of residence of mobile carbon (in every form) in the ith reservoir of the system; C is the constant characterizing the cycle of the rate of carbon in the system. For the present state of the carbon cycle in the biosphere, $C = (2.7 \pm 0.05) \cdot 10^{17}\ \mathrm{gCO_2\ yr^{-1}}$.

If Condition (3.1) is valid, removal of carbon from any reservoir of the system due to the cycle is replenished by its input from other reservoirs. If it is not valid, uncompensated flows of matter appear in the system, which return it to equilibrium.

In the process of the global cycle, mobile carbon repeatedly crosses the Earth's surface. Over the surface, playing the role of the "geochemical barrier", it circulates mainly in the oxidized form (CO_2), and under the surface mainly in the restored form (CH_4). This fact requires a study of the global cycles of CO_2 and CH_4.

Between all the factors governing a re-distribution of carbon above (and below) the planetary surface, two processes of mainly regional character play the most

important role: notably, (1) carbon transport by meteogenic water and (2) human economic activity. Due to the first factor, excess carbon in continents mixes with meteogenic water under the Earth surface, where reduced as hydrocarbons (HCs) they take part in the processes of present-day oil–gas formation (Barenbaum, 2004). As a result, industrial deposits of oil and gas are located: first, within large deposit basins that drain vast territories, and second, they gravitate toward zones where there are crust fractures. The presence of fractures, on the one hand, makes easier the penetration of meteogenic water under the surface and, on the other hand, promotes a release from such water of the carbon transported by them (Barenbaum, 2002).

Actual data show that oil and gas deposits are remarkably replenished during a period of 10–50 years. Such a short time period for deposit formation is determined by the rapid transport of carbon by water above the Earth's surface. From measurements that are likely underestimated, this rate on a global scale constitutes $\sim 5 \cdot 10^{15}\,\mathrm{gC\,yr^{-1}}$ (Voitov, 1999). This process is rather non-uniform (Syvorotkin, 2002). The basic mass of carbon descends onto the continents and their outskirts and moves upward around mid-oceanic ridges, along the continental fractures, and during numerous volcanic eruptions at the ocean bottom. Unfortunately, quantitatively these upward and downward carbon fluxes in the continents and especially in the ocean have been studied inadequately. What all this means is that the GCC cannot be studied separately from the global cycle of water.

The anthropogenic factor of carbon re-distribution between surface and underground reservoirs shows itself in the extraction and consumption of oil ($4 \cdot 10^9\,\mathrm{t\,yr^{-1}}$) and natural gas ($350 \cdot 10^{12}\,\mathrm{m^3\,yr^{-1}}$). Hence, the total mass of the consumed fossil carbon constitutes $\sim 7 \cdot 10^{15}\,\mathrm{gC\,yr^{-1}}$, which is comparable with the amount received by the surface due to natural circulation. Therefore, human activity closely connected with these volumes of HC utilization, along with the impact on climate, can also affect strongly the regional processes of oil and gas generation in the bowels of the Earth.

In the GCP project this fact should be taken into account, too. The present-day practice of oil and gas transportation over many thousands of kilometers from the places of extraction can lead to substantial re-distribution of the world resources of hydrocarbons in the nearest decades. Those industrial countries intensively consuming oil and gas will accumulate HCs in their territories, while those countries specializing in extraction and export of oil and gas, will rapidly drain their resources.

Bearing this in mind, a general scheme for the carbon cycle, supplemented by a geological unit that facilitates removal of the uncertainty present in the studies of the GCC connected with the so-called "missing sink", can serve as the basis for more accurate study of the greenhouse effect. This scheme, along with a description of the main CO_2 fluxes in the biosphere, considers the possibility of mobile carbon accumulating under the surface, thereby becoming closed and balanced.

Nadelhoffer *et al.* (1999) showed that the missing sink can be explained neither by the contribution of the ocean nor carbon assimilation by boreal forests of the Northern Hemisphere. It was shown that the existing uncertainty about the volume of carbon sink in forests cannot be reduced by more than $0.25 \cdot 10^{15}\,\mathrm{gC\,yr^{-1}}$. In

general, four basic versions for removal of this uncertainty are possible at the expense of the specified role of the biosphere:

- underestimation of carbon input to the ocean cannot not be excluded;
- the role of wetlands in CO_2 assimilation is underestimated (Mitsch, 2005);
- a warming-induced increase in the carbon sink in boreal forests is possible; and
- the role of nitrogen in boreal forests is underestimated.

The temporal scale of carbon circulation between its reservoirs differs by orders of magnitude:

- the surface biosphere stores and emits CO_2 on a temporal scale of tens and hundreds of years;
- oceans contain huge supplies of mobile CO_2, and the time period of its cycle in ocean ecosystems can vary from days to thousands of years; and
- the mineral deposits of carbonates and geological supplies of carbon bury CO_2 for thousands and even millions of years.

The IPCC (2005) report gives a general characteristic of various aspects of the GCC emphasizing the special features of individual regions and highlighting unsolved problems. The report notes that at the present state of humankind development the basic anthropogenic CO_2 sources are:

- fossil fuel burning for energy production and its use in the chemical production of various goods;
- oil-refining plants;
- large-scale industrial enterprises, cement production; and
- biomass fermentation.

Our goal is to analyze future achievements in studies of the GCC and to discuss the problems of raising the accuracy of assessment of the greenhouse effect due to anthropogenic CO_2 emissions. However, we do not discuss the problem of biotic regulation of the environment closely connected with the GCC problem (Kondratyev *et al.*, 2003b).

3.1.2 Global Carbon Project and reality

The first report on the GCP (Canadel *et al.*, 2003) contained a formulated strategy for international cooperation within the framework of the many environmental problems considered in the context of the interaction of the global nature–human system with emphasis on the need to develop methods and information technologies for analysis of the carbon–climate–society system (CCSS). The basic goal was to consider the following five aspects of the general GCC problem, including

- study of the GCC by integrating natural and anthropogenic components by analyzing the interactions between energy systems based on fossil fuel, the biogeochemical carbon cycle, and the physics of climate;

- development of new methods of analysis and numerical modeling of the integrated carbon cycle;
- global studies of the carbon cycle by taking the results of national and regional programs on the study of carbon fluxes between its reservoirs into account;
- one strategic objective of the international project should be to find ways of sustainable regional development to achieve stable CO_2 concentration in the atmosphere;
- the division according to advances in technology of all countries into developed and developing by the GCP foresaw a respective division into industrial, economic, and energy sectors of the NSS by their power as sources of anthropogenic CO_2 emissions.

The carbon cycle is closely connected with climate, the cycles of water and biogenic substances, and the products of photosynthesis on land and in the oceans. Therefore, all studies of the GCC that disregard the totality of such connections are unavoidably flawed and, naturally, cannot give even approximately reliable estimates of the consequences of anthropogenic carbon emissions to the environment. For this reason, many international projects studying the greenhouse effect and its impact on climate, as well as the Kyoto Protocol regulating CO_2 emissions, are equally flawed. Therefore, the GCP instills hope of achieving some progress as a result of planning interdisciplinary studies of the GCC. The subject matter of these studies can be divided into

(1) formation of a strategy for GCC study and assessment of its variability;
(2) analysis of cause-and-effect relations in when studying the mechanisms of interactions between natural and anthropogenic sources and sinks of CO_2 and the environment;
(3) identification and quantitative estimation of the evolutionary processes in the CCSS.

The first report of the GCP put forward the goal in the next decade of GCC study to conceptually unite the previously isolated programs IGBP, IHDP, and WCRP (Steffen *et al.*, 2005). Perhaps, for the first time, at least internationally, the authors of this report substantiated the need for an expanded scheme of cause-and-effect relations between climate–biosphere system components and emphasized the necessity for them to be considered together in order to raise the level of reliability of estimates and predictions of the climatic impact of CO_2. All these problems have been widely discussed (Kondratyev, 2004a, b; Kondratyev *et al.*, 2003a–c). Unfortunately, the first GCP report continues to underestimate the role of anthropogenic GHGs whose contribution in the near future may well exceed the role of CO_2. The list of GHGs, such as nitrous oxide, sulfur hexafluoride, methane, hydrofluorocarbons, and chlorofluorocarbons, is growing with time. The total emissions recalculated for CO_2 in 1990 constituted 3.6 $GtCO_2$; by 2010 this is expected to be 4.0 $GtCO_2$. By 2010, anthropogenic CO_2 emissions are estimated to be 6.0 GtC yr^{-1}–6.7 GtC yr^{-1}, while their level in 1950 was 1.6 GtC yr^{-1}. According

to EPA (2001), the levels of human emissions of some GHGs to enhancement of the greenhouse effect from the beginning of the industrial revolution constituted: CO_2 55%, CH_4 17%, O_3 14%, N_2O 5%, and others 9%.

This means that the continued (rather primitive in most cases) description of the GCC and the practical absence of parameterization for other GHGs cannot lead to reliable estimates of possible future climate change due to anthropogenic activity in the NSS. The means of identifying situations and the capacities of CO_2 sources and sinks on land and in the World Ocean declared by the first GCP report was not supported by serious and substantiated motivation of the development of new information technologies for complex analysis of the Earth's radiation balance.

Nevertheless, it should be noted that the main postulate of the GCP substantially improves our understanding of the GCC, directing the conceptual base of its studies at combining the natural and anthropogenic components using developed methods, algorithms, and models. The basic structure of the carbon cycle is determined by fluxes between its main reservoirs, including carbon in the atmosphere (mainly in the form of CO_2), in the oceans (divided up as surface, intermediate and deep layers, and bottom deposits), in land ecosystems (vegetation, litter, and soil), in rivers and estuaries, and in fossil fuels. These reservoirs should be studied by considering their spatial non-uniformity and dynamics under the influence of natural and anthropogenic factors on the basis of accumulated knowledge, according to which (Canadel *et al.*, 2003)

- Anthropogenic carbon emissions have grown constantly ever since industrial development, reaching 5.2 GtC in 1980 and 6.3 GtC in 2002.
- The content in the atmosphere of basic GHGs (CO_2, CH_4, and N_2O) has increased from 1750 by 31%, 150%, and 16%, respectively. About 50% of the CO_2 emitted to the atmosphere due to fuel burning has been assimilated by vegetation and oceans.
- The observed distribution of atmospheric CO_2 and oxygen/nitrogen ratios show that the land sink of carbon prevails in northern and middle latitudes over the ocean sink. In tropical latitudes, considerable emissions of CO_2 to the atmosphere as a result of the Earth's resources being exploited can be observed.
- Interannual oscillations in CO_2 concentration in the atmosphere correspond to changes in the use of fossil fuels. The intra-annual variability of atmospheric CO_2 correlates to a greater extern with the dynamics of land ecosystems and to a lesser extent with the dynamics of ocean ecosystems.
- Regional transfer of carbon in 2000 due to production of and trade in crops, wood, and paper constituted 0.72 GtC yr^{-1}. The pure global carbon flux at the atmosphere–ocean boundary in 1995 was estimated at 2.2 GtC ($-19\% \pm +22\%$) with an interannual variability of about 0.5 GtC. The greatest extent of CO_2 flux oscillations in the system can be observed in the equatorial Pacific.
- The approximate distribution pattern of ocean sources and sinks of atmospheric CO_2 is known: the tropical basins of the oceans are mostly sources of CO_2, and high-latitude basins are sinks of CO_2. The role of rivers is reduced mainly to the transport of carbon to the coastal zone of the World Ocean ($\sim$1 GtC yr^{-1}).

The most important aspect of the GCP is the global environmental monitoring and accumulation of detailed information about biome production, CO_2 fluxes at the atmosphere–ocean boundary, and the volumes of anthropogenic carbon emissions. A special role is played by remote satellite measurements of CO_2 using AIRS at the satellite observatory EOS-Aqua (launched by NASA on March 4, 2002 at an altitude of 750 km), and IASI (Infrared Atmospheric Sounder Interferometer) carried onboard the satellite METOP (METeorological Operational Polar) (Nishida *et al.*, 2003). Other functioning or planned-to-be-launched space vehicles will be used to evaluate CO_2 fluxes from the data of indirect measurements of environmental characteristics. In particular, these are the satellite TIROS-N (Television Infrared Observational Satellite-Next) and the apparatus SCIAMACHY (Scanning Imaging Absorption Spectrometer for Atmospheric Cartography). The latter spectrometer launched in 2002 ensures the high spectral resolution of absorption bands of greenhouse gases such as CO_2, CH_4, H_2O (1% accuracy), and N_2O, CO (10% accuracy) with the surface resolution from 30 km to 240 km depending on latitude.

Traditionally, ground observations will be continued with the main goal, as before, to substantiate national strategies of the use of the Earth resources including the development of forestry and agriculture, including stock-breeding and field crop cultivation.

The GCP program foresees the extended study of the physical, biological, biogeochemical, and ecophysiological mechanisms behind carbon flux formation in the environment. A deeper understanding of these mechanisms and their parameterization will make it possible to specify GCC models and related climate change. Accumulation of such a database of knowledge will enable the following available information about these mechanisms to be specified (Canadel *et al.*, 2003):

- Atmosphere–ocean carbon exchange is much controlled by physical processes, including mixing of the surface and deep layers of the ocean across the thermocline. Biological processes favor the movement of carbon from the surface layer to deep layers and down to bottom sediments. The biological "pump" functions as a result of phytoplankton photosynthesis.
- The complex of feedbacks controls interactive exchange with energy, water, and carbon between the atmosphere and the Earth's surface causing a response of these fluxes to disturbances such as transformation of land cover or pollution of the World Ocean with oil. Substantial feedbacks are physiological responses of vegetation communities to changes in temperature and humidity of the atmosphere and soil.
- The NH carbon sink depends on the growth of forest, climate change, soil erosion, fertilization, and carbon accumulation in freshwater systems. Unfortunately, the processes taking place at the same time have been poorly studied, and experimental information is all but absent. The power of the land sink of carbon can grow if climate change follows a given path. As soon as 550 ppm atmospheric CO_2 concentration is exceeded, many processes in land ecosystems will experiencing a deficit of biogenes and water, and therefore the

photosynthetic accumulation of carbon by land vegetation will become physiologically saturated.

- The number of key factors determining directions and amplitudes of CO_2 fluxes between the atmosphere and land ecosystems are limited by several factors:
  (1) Extreme climatic phenomena such as droughts, large shifts of seasonal temperatures, change of solar radiation due to the large-scale input of aerosols to the atmosphere (e.g., by volcanic eruptions or by the large-scale fires that took place in Iraq in connection with recent military operations).
  (2) Forest and other fires which contribute large-scale and long-term changes to characteristics of the carbon cycle (of th eglobal pure primary production of $\sim 57\,\mathrm{GtC\,yr^{-1}}$, approximately 5%–10% is emitted to the atmosphere due to wood burning).
  (3) Use of soils that changes biome boundaries and their types (substitution of coniferous forests for evergreen, pastures for forests, forested territories for meadows, etc.).
- Phenomena such as El Niños or thermocline circulation in the North Atlantic lead to global instability in the processes of energy and matter exchange, which should be reflected by parameterizing non-linear feedbacks.

The future dynamics of carbon exchange in the surface–atmosphere system will be determined by the strategy adopted for the interaction of natural and anthropogenic factors which, on the one hand, is apparent, but, on the other hand, is still to be discussed, since the problem of the greenhouse effect cannot be resolved within the framework of the GCP because this program is treated separately from other thematic sections of global ecodynamics. A broader approach to this problem was developed in the works of Kondratyev *et al.* (2002a, b, 2003a, 2004a) which, unfortunately, have so far been ignored by GCP elaborators.

3.1.3 A new approach to the study of the global carbon cycle

In some recent works (Bartsev *et al.*, 2003; Degermendzhy and Bartsev, 2003; Krapivin and Kondratyev, 2002; Kondratyev *et al.*, 2002a, b, 2003b, 2004a; Tarko, 2003, 2005) it was suggested that the GCC be considered in the context of its connections with other processes in the NSS. As these works point out, the carbon cycle correlates with a multitude of natural and anthropogenic factors whose interaction forms the dynamics of key processes in the NSS. For CO_2, these are the exchanges at the boundaries of the atmosphere with land cover and sea and ocean basins. Clearly, the analysis of CO_2 dynamics in the biosphere is possible with the available data on the spatial distribution of its sinks and sources. The present level of knowledge enables us to estimate the climatic impact of the greenhouse effect and to narrow down, thereby, the uncertainty in estimates of future climate change. However, the GCC model used here should reflect not only the spatial mosaics of its reservoirs, sinks, and sources—but also provide a dynamic calculation of their capacities. Earlier calculations using GCC models inadequately considered information about the state and classification of land cover, and even more so about World

Ocean basin variability. Therefore, formation of the scheme of spatial distribution of soil–vegetation formations and quasi-homogeneous World Ocean basins will make it possible to overcome such shortcomings in other models. A system of balance equations for this scheme is as follows:

$$\frac{\partial \alpha_S^i(\varphi,\lambda,z,t)}{\partial t} + V_\varphi \frac{\partial \alpha_S^i(\varphi,\lambda,z,t)}{\partial \varphi} + V_\lambda \frac{\partial \alpha_S^i(\varphi,\lambda,z,t)}{\partial \lambda} + V_z \frac{\partial \alpha_S^i(\varphi,\lambda,z,t)}{\partial z} = \sum_{j\in\Omega_S} H_{jS} - \sum_{m\in\Omega_S} H_{Sm} \quad (i=1,\ldots,N);$$

where S is the carbon reservoir in the ith cell (pixel) of spatial structure; φ is latitude; λ is longitude; z is depth; t is time; H_{jS} is carbon flux from the jth reservoir to reservoir S; H_{Sm} is the carbon sink from the reservoir S to the mth reservoir; Ω_S is the multitude of carbon reservoirs bordering reservoir S; N is the number of carbon reservoirs; $V(V_\varphi, V_\lambda, V_z)$ is the rate of exchange between reservoirs. Here rate V and fluxes H are the non-linear functions of environmental parameters. The form of these functions was described in detail, for instance, in the work of Krapivin and Kondratyev (2002). Here they will only be specified. First of all, the elements of the biocenotic unit of the global model must be specified. To do this, the global land surface should be covered by a homogeneous grid of geographic pixels $\sum_{ij} = \{(\varphi,\lambda) : \varphi_{i-1} \le \varphi < \varphi_i; \lambda_{j-1} \le \lambda < \lambda_j\}$ with boundaries in latitude $(\varphi_{i-1}, \varphi_i)$ and longitude $(\lambda_{j-1}, \lambda_j)$, and area σ. The number of pixels is determined by the available database; that is, by the choice of grid sizes $(\Delta\varphi, \Delta\lambda)$: $i = 1,\ldots,n$; $n = [180/\Delta\varphi]$; $j = 1,\ldots,k$; $k = [180/\Delta\lambda]$. As a rule, the choice of pixels for computer calculations is oriented according to the structure of the land surface, and in the case of the atmosphere at one of three scales of atmospheric processes. To parameterize synoptic-scale processes, a pixel 1,000 km^2 in size is chosen. For other situations, meso-scales and micro-scales are used with characteristic spatial scales of 1 km^2–1,000 km^2 and <1 km^2, respectively. Each pixel can cover N types of surface, including types of soil–vegetation formations, water system basins, and anthropogenic objects. The dynamics of vegetation cover of the s-type follows the law:

$$\frac{dB_s}{dt} = R_s - M_s - T_s,$$

where R_s is photosynthesis; M_s and T_s are losses of biomass B_s due to its dying off and evapotranspiration, respectively.

The right-hand components of this equation are functions of the environmental characteristics: light, temperature, atmosphere and soil humidity, and CO_2 concentration in the air. There are various ways and forms of parameterizing these functions. One of them is the model of Collatz *et al.* (1990, 1992, 2000) which serves as the basis for the global biospheric model SiB2 (Sellers *et al.*, 1996). Temperature, humidity, and rate of moisture evaporation in the vegetation layer and soil are interconnected with biometric parameters and energy fluxes in the atmosphere–vegetation–soil system. By analogy with electrostatics, the notion of "resistance" is introduced, and fluxes are calculated with a simple formula: flux = potential

difference/resistance. The SiB2 model considers the fluxes of sensible and latent heat through water vapor evaporation for vegetation and soil, and CO_2 fluxes are divided into classes C_3 and C_4, which substantially raises the accuracy of parameterizing functions in the right-hand part of the above equation for the biomass dynamics of vegetation cover. According to Collatz *et al.* (1992), three factors regulate the function R_s: efficiency of the photosynthetic fermentation system, the amount of photosynthetic active radiation (PAR) assimilated by cellulose chlorophyll, and the ability of a plant species to assimilate and deliver to the environment photosynthesis products. Application of the Libich principle and consideration of data on the distribution of the types of vegetation covers by pixels $\{\Sigma_{ij}\}$, partial pressures of CO_2 and O_2, air temperature and density, and illumination level enables us to calculate fluxes H in the equation of carbon balance for all land pixels.

The model of the carbon cycle in the atmosphere–ocean system was described in detail in the work of Kondratyev *et al.* (2003b). It was based on the same grid of geographic pixels but combined with a zonal principle according to the classification of Tarko (2001, 2003). Ocean thickness is considered to be a unique biogeocenosis in which the basic combining factor is the flux of organic matter produced in surface layers, which then penetrates down to maximum depths in the ocean. The regulator of carbon fluxes in this medium is the carbonate system, a parametric description of which was given in the work of Kondratyev *et al.* (2004a). As Follows *et al.* (2006) showed, the accuracy of CO_2 flux assessment depends on how the ocean carbonate system is parameterized. Follows *et al.* (2006) proposed a simplified method to describe the local carbonate system using 3-D biogeochemical models of the ocean based on parameterization of acidity with a minimum of interacting elements. Based on this approach, it was shown that failing to take regional changes in concentrations of dissolved inorganic phosphorus and silic acid in the surface layer of the ocean into account can lead to substantial systematic errors in the estimates of CO_2 fluxes at the atmosphere–ocean boundary. To some extent, this approach had something in common with the ideas of Bartsev *et al.* (2003) about the necessity to use simplified models to describe global biospheric processes.

Many parameters of the GCC model can be measured by satellite monitoring, which makes it possible to apply an adaptive scheme for calculation of greenhouse effect characteristics (Kondratyev *et al.*, 2004a). Such a scheme enables us to gain experience of the model as corrections to its structure and parameters proceed. Satellite measurements in the visible and near-IR regions provide operative estimates of PAR and such vegetation characteristics as vegetation canopy greenness, area of living photosynthetically active elements, soil humidity and water content in vegetation cover elements, CO_2 concentration on the surface of leaves, etc. Different ways of predicting vegetation cover biomass in each pixel Σ_{ij} and comparison with satellite measurements make it possible to correct some parts of the model (e.g., by doubling its units or their parametric adjustment in order to minimize a discrepancy between predictions and measurements). In particular, to calculate primary production there are a number of semi-empirical models which can be used by separate units in different pixels. There is a certain freedom of choice in estimating evaporation given off by vegetation cover (Wange and Archer, 2003).

Thus, theoretical analysis of the dynamics involved in the GCC shows that it is determined by a complicated totality of feedback mechanisms of timescales from decades to centuries and longer. Here are some of them:

- A change of CO_2 concentration in the atmosphere affects through feedbacks the carbon fluxes at the boundaries of natural media. The efficiency of carbon assimilation from the atmosphere by the ocean decreases with growing atmospheric CO_2 concentration due to the decreasing buffer capacity of its carbonate system.
- An increase of CO_2 concentration in the atmosphere does not determine substantial fertilization of marine bioproductivity—but does lead to pH decrease. As temperature grows, CO_2 assimilation by the ocean decreases, but CO_2 emissions due to upwellings are reduced and the transport of excess carbon to deep layers of the ocean diminishes. The anthropogenically induced input of nutrients to the oceans through river run-off and deposition of atmospheric aerosols (especially nitrate and iron as elements of atmospheric aerosols) can affect bioproductivity.
- Due to bioproductivity processes, carbon is transported from the surface to deep layers of the ocean, where it is re-mineralized. This process maintains the inorganic carbon concentration gradient and preservation of CO_2 concentration in the atmosphere at a level which is $(100–200) \cdot 10^6$ lower than it would be without bioproductivity.
- The assimilation of CO_2 on land is determined by net biome productivity (NBP), which is the balance between net primary productivity ($NPP \approx 56.4 \cdot 10^9\ tC\ yr^{-1}$) and carbon losses due to heterotrophic respiration and burning processes. According to observational data for many ecosystems, with increasing CO_2 concentration the NPP should grow with a gradual transition toward saturation at reaching a CO_2 concentration in the atmosphere of 800 ppm–1,000 ppm.
- The efficiency of the carbon sink on land depends on the transformation of carbon compounds into forms characterized by having a long lifetime (wood, soil). An enhancement of carbon sink due to increasing NPP can manifest itself only as a result of the inertia of these slow reservoirs of carbon in the process of land cultivation. At present, global pure production in agriculture is estimated at $8 \cdot 10^9\ tC\ yr^{-1}$.
- In the case of short timescales of atmospheric warming the rate of heterotrophic respiration on land will grow, but the degree of the impact of this process on long-term processes of CO_2 exchange remains unclear. Warming and regional changes in the spatial distribution of precipitation and clouds can cause changes in the structures of land ecosystems, their geographic distribution, and primary production. The total impact of such forcings should depend on special features of the regional structures of climate changes.
- The carbon cycle in land ecosystems is strongly affected by how land is used (e.g., agriculture, deforestation, and afforestation).
- Biotic regulation in atmosphere–land CO_2 exchange in tropical rainforests that demonstrate a vast biodiversity of species is still poorly studied (Bampfylde *et al.*, 2005).

3.1.4 Greenhouse effect and natural disasters

Problems as a result of the greenhouse effect have been discussed in detail in many publications (Boehmer-Christiansen, 2000; Demirchian and Kondratyev, 1999; Kondratyev, 1996, 2003, 2004a; Kondratyev and Demirchian, 2001; Krapivin, 2000a; Sorochtin, 2001; Chen *et al*., 2000; Pervaniuk and Tarko, 2001; Parchomenko and Tarko 2002; Tarko, 2005). However, other than a few publications, the interaction between the GCC state and natural disasters remains unstudied. Predicted climate warming in the range 2.5°C–5.0°C due to an increase of CO_2 concentration in the atmosphere can lead to large-scale catastrophic phenomena such as a rise in World Ocean level by 0.6 m–1.0 m, which would create serious problems for the densely populated regions of continental coasts and for gas and oil enterprises in lowland zones of most of the coasts of northern Russia. Moreover, a considerable breakdown of regional water balances could take place with a possible extension of deserts and disappearance of permafrost zones. Clearly, such predictions are based on incorrect climate models; nevertheless, humankind must find information technologies that study global processes in the NSS accurately and efficiently. At present, such technologies are being created by modifying climate models through including additional parameters, which should raise their adequacy, but might make them less stable, or through synthesizing simple model units, which parameterize direct connections and feedbacks in the climate system by using a small set of well-determined characteristics (Bartsev *et al*., 2003; Degermendzhy and Bartsev, 2003).

The problem of possible global climate warming due to anthropogenic sources of GHGs is important primarily for understanding real trends in global ecodynamics. Is there a direct dependence between a change of GHG concentrations in the atmosphere and natural disasters? This is one of the most important aspects of the present science of the environment, whose study will make it possible to more reliably predict many destructive natural phenomena that inevitably lead to the loss of life and economic damage. World statistics on natural disasters reveals a four-fold increase of large-scale catastrophes during the last 50 years, with a nine-fold increase of economic losses. These disasters mainly relat to climate characteristics. Basic natural disasters can be divided into four groups: hurricanes, floods, earthquakes, and storms. The relationship between them in different global regions is characterized by strongly differing indicators. On the whole, earthquakes constitute about 15% of natural disasters, and large-scale storms constitute 35%. However, the levels of damage are disproportionate to those indicators. A detailed analysis of natural disasters was carried out in the works of Grigoryev and Kondratyev (2001a, b). Here we shall only mention the (practically ignored) effect of carbon removal from forests by hurricanes, a characteristic process in the U.S.A. (McNulty, 2002). On average, 93% of powerful hurricanes occurring in the U.S.A. fall on the southern coast, 55% of which is covered with forests. In addition to economic damage, these hurricanes strongly damage forests, transforming the living biomass either into detritus or into fuel. In other words, hurricanes remove carbon from the cycle in the area of damaged forest transforming it into other fluxes. For instance, in September 1989 Hurricane Hugo (the most powerful hurricane for the last 100 years) reached a speed of 250 km

hr^{-1} and removed 20 TgC from forests near the U.S. coast, 1% of which from torn-off leaves and 5% from fallen pine needles. Along with removed carbon ~0.36 Gt of nitrogen were returned to the soil.

The consequences of natural disasters, their evaluation, and how they can be overcome are complicated functions of many socio-economic parameters. It is known that about 30% of the population in developing countries face economic difficulties, and 18% live in poverty. Therefore, developing countries find it difficult to efficiently resist natural disasters. But poverty can be liquidated by developing industry and agriculture, which judging by KP recommendations is impossible. Hence, it is vitally important to reliably assess the future dynamics of the atmospheric CO_2 concentration. Of course, to solve the theoretical and practical problems inherent in this, all available means should be used and even the most fantastic hypotheses should be taken into account (Walker, 2003).

Licki *et al.* (2003) showed that consideration of more accurate data on moderate and boreal forests makes it possible to raise the accuracy of assessment of their role as sinks of atmospheric carbon. Recent data were used about forests in 55 countries. Moderate and boreal forests cover about half the global wooded area. Estimates showed that the transition of atmospheric carbon to wood constitutes 0.71 GtC yr^{-1}–1.1 GtC yr^{-1}, disregarding the role of soil ecosystems. Saleska *et al.* (2003) measured CO_2 fluxes in the forests of the Amazon and found that the carbon balance in them is characterized by considerable intra-annual variations the extent of which depends much on the age of the forest, CO_2 concentration in the surface air, and moisture supply in soil. In particular, in El Niño years the carbon flux from an old forest to the atmosphere enhances considerably. On the whole, characteristic quantities of carbon fluxes in the forests of the Amazon are 0.10.5 tC ha^{-1} yr^{-1} for assimilated CO_2 and 0.1 tC ha^{-1} yr^{-1}–0.4 tC ha^{-1} yr^{-1} for emitted CO_2. In some areas of the forest, CO_2 sinks of 1.0 tC ha^{-1} yr^{-1}–5.9 tC ha^{-1} yr^{-1} were recorded. About 25%–30% of the Amazon is characterized by a binary climatic regime with a 7-month rainy season (rains >100 mm mo^{-1}) and an annual mean rain rate of 1,920 mm yr^{-1}. In such territories, CO_2 sinks are characterized by quantities ranging between 150 kgC ha^{-1} mo^{-1} and 700 kgC ha^{-1} mo^{-1}, and carbon losses due to forest biomass dying off constitute 2.0 ± 1.6 tC ha^{-1} yr^{-1}. This means that sinks and sources of CO_2 in forest territories should be thoroughly estimated, by keeping a detailed consideration of the spatiotemporal characteristics of forest ecosystems in mind. Unfortunately, there are no such estimates, and obtaining them was not foreseen in the GCP.

Climate change and related unfavorable variations of the environment are determined, to a great extent, by GHG content, among which N_2O plays an important role. From the viewpoint of the biospheric balance between carbon and nitrogen, there is a certain regularity in the C/N ratio that should be reflected in the GCP model to improve its accuracy. Average C/N quantities are 200 for trees and 15 for soils. Therefore, for reliable estimation of natural sinks and sources of CO_2, it is necessary to model C/N dynamics by taking into account the nitrogen supplies in biospheric reservoirs. In other words, the prediction of natural disasters requires details of the factors involved in phytocenosis evolution with consideration of the natural and

anthropogenic disturbances introduced and subsequent effects on nearby areas. The doubtless complexity of this problem implies that any existing GCC models that disregard at the very least the basic forms of vegetation dynamics cannot make—let alone claim—reliable conclusions about future climate change. The growing complexity of global models observed earlier and their resulting instability also require development of new non-traditional methods of modeling. A possible way of simultaneous simplification and specification of global models is a reasonable spatial representation of NSS elements. It can be realized by using the traditional landscape structure of the land.

The increasing number of natural disasters observed in recent decades is directly connected with energy production globally as the main reason for enhanced emissions of GHGs to the atmosphere. In this regard, detection of anthropogenic climate change requires introduction of special climatic indicators capable of sensing the approach of extreme SAT changes (Grigoryev and Kondratyev, 2001a, b). As for the anthropogenic enhancement of the atmospheric greenhouse effect, at present it constitutes $2\,W\,m^{-2}$, whereas other energy fluxes that determine climate formation are about 1.5–2 orders of magnitude greater, which, of course, seriously complicates recognition of the "greenhouse signal" in climate change, bearing in mind that the numerical modeling of global climate is at an early stage of its development. Even if we assume the greenhouse-warming hypothesis, it turns out that in many global regions the warming will positively affect agricultural productivity. Therefore, the correlation between possible increase in average planetary temperature and natural disasters is ambiguous and needs to consider the special features of the region.

3.1.5 Catalog of biospheric sources and sinks of carbon dioxide

Carbon dioxide circulates in the environment between its reservoirs, which are listed in Table 3.1. In general, the diverse compounds of carbon continuously form, change, decompose, and from all this diversity, natural and anthropogenic CO_2 fluxes are formed in the processes of respiration and decomposition of vegetation and humus, the burning of carbon-containing substances, rock weathering, etc. Some of the CO_2 dissolves in the World Ocean releasing carbonic acid and the products of its dissociation. The content of carbon in its reservoirs and estimates of its fluxes between them are the most important problems facing global CO_2 cycle analysis. Numerous schemes of this cycle, drawn from analysis of global interactions of living organisms and their physical and chemical media, as well as estimates of carbon supplies accumulated during the historical period serve as the basis for predictions of the dynamics of CO_2 concentration in the Earth's atmosphere, which has been the subject of vehement disputes in connection with assessments of the role of CO_2 in climate warming.

An important stage in understanding the processes of CO_2 exchange between biospheric reservoirs is study of the laws of the development of various ecosystems in pre-industrial epochs, when there was little human involvement. Natural carbon fluxes between the atmosphere, oceans, land ecosystems, and inland water bodies

Table 3.1. Global carbon reservoirs.

Reservoir	*Amount of carbon* (GtC)
Atmosphere	720
World Ocean	38,400
Total inorganic carbon	37,400
Surface layer	670
Deep layers	36,730
Total organic carbon	1,000
Lithosphere	
Carbonate sedimentary rocks	>60,000,000
Kerogens	15,000,000
Land biosphere	2,000
Living biomass	600–1,000
Dead biomass	1,200
Biosphere of inland waters	1–2
Burnt fuel	4,130
Coal	3,510
Oil	230
Natural gas	140
Others (peat, etc.)	250

are strongly variable both in space and in time (from year to year and seasonally). Analyses of ice cores from Greenland and the Antarctic have reliably shown variations of atmospheric CO_2 in the past. Eight thousand years ago the CO_2 concentration in the atmosphere constituted 200 ppmv. By the beginning of the pre-industrial epoch this quantity varied between 275 ppmv and 285 ppmv ($\pm$10 ppmv). By 1985 the concentration of CO_2 in the atmosphere reached $\sim$345 ppmv. But, in 1998 it was already 366 ppmv–367 ppmv (Bolin and Sukumar, 2000). The total amount of carbon in atmospheric CO_2 is estimated today at about 700 billion tC. The natural CO_2 budget is estimated at $\sim$150 billion tC emitted annually in the processes of respiration and decomposition and assimilated in photosynthesis both on land and in the ocean, as well as by CO_2 dissolving in the World Ocean.

To analyze the dynamics of CO_2 in the biosphere, it is important to take into account the maximum possible number of its reservoirs and fluxes as well as their spatial distribution. It is in this that numerous global models of the carbon cycle differ. The present level of these studies does not allow us to answer the principal question as to how extensive is information in the database about the supplies and fluxes of carbon. Therefore, many authors analyzing the dynamic characteristics

of the global CO_2 cycle rather arbitrarily utilize fragmentary information from databases on the distribution of the carbon sinks and sources.

A key component of the global CO_2 cycle is its anthropogenic emissions to the environment. The principal problem studied by most investigators consists in assessing the biospheric ability to neutralize excess amounts of CO_2. It is here that all predictions of the consequences of the greenhouse effect are wide open to criticism. All models of the global CO_2 cycle are based on scenarios that describe the dynamics of extraction and burning of fossil fuels. Hence, models of the energy–economy system require detailed parameterization of the geopolitical structure of the world. So far, among the most widely used models of this type is one developed by IIASA, in which the globe is divided into nine regions differing in the level of per capita energy consumption and other parameters. The regional structure is shown in Table 3.2. With this scenario of socio-economic structure we can attribute to it the development strategies of each region and assume possible consequences of future behavior of individual regions for the environment. Most similar scenarios use such an indicator as the rate of acceleration of energy consumption. This parameter varies from 0.2% to 1.5% per year. Various combinations are considered when choosing a source of energy among oil, gas, nuclear and solar energy, hydroelectric power stations, and solid waste burning. Naturally, we have to take into account the demographic, technical, political, and macro-economic factors. The size of population in most scenarios is assumed to grow at a rate that would reach by 2025 and 2075 the levels

Table 3.2. Characteristics of the growth of economic effectiveness and population dynamics in different regions of the world according to the IIASA scenario. From Oostenrijk *et al*. (2006).

Region	*P*	*Population* (millions)		
		2025	*2050*	*2075*
Australia and Japan	2.3	160	150	150
Africa	1.6	1,600	2,200	2,700
Canada and Europe	1.6	520	540	540
China	1.9	1,600	1,700	1,700
Latin America	1.9	720	850	900
Russia and C.I.S. countries	1.3	470	500	510
Middle Asia	1.9	280	360	410
U.S.A.	1.2	290	290	290
South-East Asia	1.8	2,600	3,100	3,400

P = annual increase in labor productivity (%).

of 7.9 and 10.5 billion people, respectively. If all these assumptions in the scenario are assumed to be true, we can calculate the anthropogenic emissions of CO_2 and other GHGs. Then, it would be necessary to determine the total temperature impact ΔT_Σ of these gases (Mintzer, 1987).

The anthropogenic constituent in the global CO_2 cycle causes changes in the reservoirs of the CO_2 sink. Maximum changes are connected with urbanization, deformed structures of soil–plant communities, and hydrospheric pollution. The rates of change in forest masses for pasture and cultivated lands are estimated at $0.05 \cdot 10^6\,\mathrm{km^2\,yr^{-1}}$. Dense tropical forests are transformed into plantations at a rate of $10^5\,\mathrm{km^2\,yr^{-1}}$. This process increases the rate of desertification ($5 \cdot 10^4\,\mathrm{km^2\,yr^{-1}}$), which increases the amount of emitted carbon ($\sim 0.1\,\mathrm{GtC\,yr^{-1}}$).

The general pattern of the present level of atmospheric CO_2 fluxes has been well studied. Due to the burning of solid and liquid fuels, about $20 \cdot 10^6\,\mathrm{tCO_2}$ are emitted every year (1:1 ratio). Burning of gas fuel contributes about $4.5 \cdot 10^6\,\mathrm{tCO_2}$ to the atmosphere. The contribution of the cement industry is estimated at $750 \cdot 10^6\,\mathrm{tCO_2}$. Individual regions and countries contribute to these fluxes rather non-uniformly.

Biomass burning in the tropics is one of the main sources of the input of minor gas components and aerosol particles to the troposphere. The share of the tropics is about 40% of the global land area and about 60% of global primary productivity. The types of vegetation in the tropics are much more diverse than other regions. However, at present, tropical forests and savannahs are being transformed into agricultural land and pasture at a rate of about 1% per year. This transformation is mainly caused by biomass burning which strongly affects the chemical composition of the atmosphere and, hence, climate.

As shown from analysis of satellite data, the share of the tropics constitutes about 70% of the biomass burnt, about half being concentrated in Africa, with most biomass burning in the annual course (in the dry season) observed north of the equator. Savannahs and forests in the tropics also emit to the atmosphere a large number of biogenic compounds. In connection with widely spread fires in savannahs and their strong impact on the environment, Nielsen (1999) analyzed special features of the spatiotemporal distribution of fires in the region (central Africa) during the field experiment EXPRESSO (Experiment for Regional Sources and Sinks of Oxidants), using data from AVHRR carried onboard NOAA meteorological satellites in the dry seasons from November 1994 to December 1997. Fire variability can be described as:

(1) Fire probability at a given point.
(2) Probability of repeated fires at a given point during a certain time period.
(3) The spatial extent and the temperature reached by savannah fires.

The processing of satellite imagery has shown that fires are not accidental. Fire probability increases, for instance, with fires in the neighborhood of the point considered. Combined analysis of the characteristics of the spatiotemporal variability of fires has made it possible to substantiate 12 typical regimes for fires as well as the dependence of special features of fires on those of the vegetation cover. Though there

is no doubt that, as a rule, savannah fires are caused by humans and not by other factors, specific causes of fires as a function of human activity remain unclear. From the viewpoint of temporal variability, it is expedient to classify fires relative to the beginning of the fire season, their development rate, and the duration of the fire season. In this context, the following types of fires can be identified: fast, late, or long.

The contribution of savannah fires exceeds 40% of the global level of biomass burning as a result of which the atmosphere receives minor gas components, such as non-methane hydrocarbons, carbon monoxide, methane, etc., as well as aerosols. According to available estimates for the period 1975–1980, 40%–70% of savannahs were burnt every year, about 6% of such fires took place in Africa. In 1990 about $2 \cdot 10^9$ t of vegetable biomass were burnt, and as a result 145 TgCO got into the atmosphere, which constituted about 30% of anthropogenic CO emissions.

Forest fires have serious impacts on the global carbon cycle. Though forest fires can occur naturally (e.g., lightning strikes), nevertheless, human contribution to their occurrence is constantly growing. A forest fire due to a lightning strike is only possible if it strikes standing wood or, in the case of open woodland, if it strikes soil covered with moss or litter. The electrical resistance of standing wood is known to be almost 100 times greater than that of growing trees; therefore, when lightning strikes a living tree, there is little evidence of the tree being charred. Therefore, monitoring of the fire danger in forests gives reliable estimates of the probability lightning-caused forest fires. A more complicated problem is predicting anthropogenic causes for forest fires. More than 90% of forest fires known to occur in a 10 km zone around populated areas are caused by humans. Hence, the fire load on forests has a strong correlation with the spatial distribution of population density. Of course, the intensity and frequency of occurrence of fires depend on climatic dryness in a given territory, on forest thickness, and their health. Therefore, to evaluate the role of a forest in the biogeochemical cycle of chemical compounds, of great importance are afforestation design, and control of soil erosion and its water balance, which can be realized by using models of the spatial structure of forests (Baskent and Keles, 2005).

A forest fire is dangerous not only because it is a source of pollutants for the atmosphere but also because its consequences are dangerous. Fires change the forest microclimate; in particular, illumination and heating of the soil increase, and the hydrological regime of the forest area changes. Moreover, over the scorched territory of forest fires the bioproductive ability of biocenoses deteriorates and, hence, the role of this territory in biogeochemical cycles changes. It is well known that in a region with a dry climate, fire-destroyed forests take time to restore naturally, and the area has to be re-forested. Therefore, it is important to understand the laws of interaction of forest fires and the biocenosis of its territory. For instance, fires in boreal forests contribute no more than 2% to carbon emissions to the atmosphere, but they seriously affect chemical processes in the high-latitude troposphere and atmospheric radiative properties. This can lead to global climatic consequences.

In general, for different reasons, biomass burning is a complex anthropogenic source of the atmospheric pollution and of the global impact on the biosphere as a whole. Estimates obtained by many authors show that the radiative forcing on climate determined by aerosols from biomass burning constitute about $-1.0\,\mathrm{W\,m^{-2}}$

(in the case of the pure scattering of aerosols uncertainty in the estimates ranges between $-0.3\,\mathrm{W\,m^{-2}}$ and $-2.2\,\mathrm{W\,m^{-2}}$).

3.1.6 Biospheric resources and the carbon cycle

The dynamics of global carbon dioxide flux is determined by natural and anthropogenic factors. The natural factors form in the process of biospheric evolution, and their dynamics depends on the interaction between natural ecosystems. The level of anthropogenic forcing on the global CO_2 cycle is determined by the relationship of natural forces with numerous aspects of humankind development: political, demographic, cultural, religious, economic, etc. All this diversity of anthropogenic origin in the present world is limited by the amount of biospheric resources, which eventually determine these aspects. Estimates of some biospheric resources given by Kondratyev *et al.* (2004b) suggest that despite the omnipotence of the human mind, which seems to believe nature can be destroyed with impunity, resources are limited by many circumstances. Humankind contaminates the environment by using mineral resources or by changing one ecosystem for another. In both cases humankind sooner or later enters a conflict with nature, and reaches the limiting factors in the global dynamics of destruction: depletion of resources, worsening of living conditions, etc.

A human (just like other elements in nature), when forming his or her environment, is mainly interested in the sources of material production: mineral resources. With growing scientific–technical progress the rate of mineral resource consumption is constantly increasing, and will approach sooner or later a critical level. Though the late 20th and early 21st centuries have been characterized by a broad spectrum of mineral deposits for industrial purposes, nevertheless, no serious alternative to oil, coal, and gas has yet been found. The increase in energy resource consumption is confined by the fact that almost half of known fuel resources used by humankind ($\sim$90 billion t) was consumed during the last 25–30 years.

By the end of the 20th century about 200 billion t of mineral deposits had been extracted. There are no reliable estimates of the global supplies of mineral resources. Therefore, the scenarios of carbon emissions to the atmosphere used by many authors should be considered conditional and disputable (Watson *et al.*, 2000; Houghton *et al.*, 2001). Nevertheless, there are undisputable relationships between the volumes of emitted CO_2 and national production. This relationship differs by a factor of 30 between developing and developed countries, which means considerable constraint should be used when working out an optimal strategy for formation of the profile of the global curve of CO_2 emissions to the atmosphere.

The World Ocean is a poorly mustered source of mineral resources. Along with maximizing access to seafood products, humankind is gradually mastering ways of mining the mineral fuel supplies lying beneath the seafloor and, especially those on marginal shelves. Oil, gas, and coal are already being extracted in large volumes from marine deposits, but of course there exist economic and technical limitations. On the whole, from preliminary estimates of the 180 oil and gas-bearing basins discovered by geologists in the World Ocean, the potential supplies of oil and gas can be estimated, respectively, at $300 \cdot 10^9\ \mathrm{m^3}$ and $150 \cdot 10^{12}\ \mathrm{m^3}$.

Human activity in changing the land cover is one of the many factors of the anthropogenic forcing on global carbon cycle dynamics that is difficult to assess. During the 20th century, humankind strongly affected the global distribution of vegetation, an important sink for atmospheric CO_2. This was caused by human engineering, construction, and mining activity, creation of new types of land formations, biological re-cultivation, etc. Especially dangerous for the environment are the processes of deforestation and desertification. For instance, Watson *et al.* (2000) stated that realization of the IPCC scenario for afforestation and re-forestation by the year 2050 will mean an additional 60 GtC–87 GtC (70% tropical forests, 25% temperate-zone forests, 5% boreal forests) will be removed from the atmosphere. An important parameter of this scenario is the rate of tree growth. For instance, if a forest grows at a rate of $3\,\mathrm{tC\,ha^{-1}\,yr^{-1}}$, then 1 tC can be attributed to the effect of atmospheric CO_2 assimilation. In general, the control of land biocenoses can markedly affect the biogeochemical carbon cycle. It is important to discover whether this control was planned or spontaneous. In any event, humans create anthropogenic landscapes on the Earth surface to improve their habitat. The appearance of artificial seas, recreation zones, cities, and other anthropogenic landscapes reduces the ability of land cover to evolve naturally. In other words, the human activity by changing landscapes can strongly affect the dynamics of atmospheric CO_2.

The main source of changing land cover is agricultural activity. The impact of agricultural activity on anthropogenic landscape formation propagates to other zones of the biosphere where the processes of transformation of inorganic masses intensify food production. The ability of humankind to affect the global carbon cycle has its limits here as well. But, nobody knows the limit to the consequences of these transformations. To understand the level of such trends, note that, according to chronicles of the late 16th–early 17th centuries, the population density in Europe was 1–2 people per square kilometer, 4 years later the population density increased by more than a factor of 50. During this time period forested areas decreased by a factor of 3, being substituted mainly by agriculture. This trend continues into the 21st century because, on the whole, agricultural activity improves the lot of human beings, though there is a negative side to it. To improve the conditions for agriculture, changes are introduced in geological, geochemical, and hydrogeological processes, and this eventually leads to irreversible changes in the global biogeochemical cycles of chemical elements. These changes include such processes as wind and water erosion of soils, leaching of the fertile soil layer and its transport to the World Ocean.

3.1.7 Eutrophication and greenhouse cycling

Eutrophication is caused by the growth in the ecosystem of chemical nutrients, with nitrogen and phosphorus being typical representatives. In general, eutrophication is followed by intensive growth of algae and intensive decomposition, which leads to prevalence of weeds and deterioration of the quality of water. In principle,

eutrophication can take place for both natural and anthropogenic reasons. Humankind, as a result of the development of agriculture, has managed to increase the rate of cycling, for instance, of phosphorus in the biosphere by four-fold.

Anthropogenic activity increases the flux of nitrogen to rivers, lakes, and estuaries provoking eutrophication. The processes of nitrification and denitrification in natural waters and bottom sediments transform dissolved inorganic nitrogen into nitrogen gas and nitrous oxide resulting in their entering the atmosphere, where they participate in global biogeochemical cycles. In this process estuaries play an important role where, along with river run-off and shore spillway, go large amounts of nitrogen and organic carbon, natural sources of CH_4. On the whole, the process of eutrophication is but one element of the complicated system of the processes of transformation of energy and matter in the biosphere (Galbraith *et al.*, 2006).

Eutrophication reduces the O_2 content and increases the presence of NH_4^+ in freshwater. These changes can affect the processes of transformation of carbon and nitrogen giving CH_4 and N_2O, which are emitted to the atmosphere. Liikanen and Martikainen (2003) studied these processes in Finland and showed that in the case of a eutrophicated lake the bottom sediment can emit up to 7.9 $mmol\,m^{-2}\,da^{-1}$ of CH_4 and 7.6 $\mu mol\,m^{-2}\,da^{-1}$ of N_2O, with oxygen being a key factor in the regulation of these fluxes through NO_3^- formation.

By the character of their ecological state, water systems can be divided into five basic categories, the consideration of which in the GMNSS makes it possible to raise the accuracy of evaluation of the greenhouse effect, which was not even discussed in IPCC (2007):

- *Oligotrophic water*. This is a relatively pure water basin with a small amount of organic matter or bottom sediment and low biological productivity because of limited biogenic elements.
- *Mesotrophic water*. A water basin with a moderate amount of nutrients ($0.3\,mgN \cdot L^{-1}$–$0.65\,mgN \cdot L^{-1}$; $0.01\,mgP \cdot L^{-1}$–$0.03\,mgP \cdot L^{-1}$) and middling biological productivity.
- *Eutrophic water*. A water basin with a very high content of nutrients and increased biological productivity ($75\,gC\,m^{-2}\,yr^{-1}$–$750\,gC\,m^{-2}\,yr^{-1}$). Some elements of the trophic pyramid are suppressed for lack of oxygen.
- *Hypereutrophic water*. Heavily polluted and highly productive water close to the state of wetland water. Many living elements of the ecosystem are at the point of extinction. The rate of CH_4 emission reaches $10\,mmol\,m^{-2}\,da^{-1}$–$46\,mmol\,m^{-2}\,da^{-1}$.
- *Dystrophic water*. As a rule, these are shallow-water basins with a small content of nutrients and oxygen, with the characteristic large content of dissolved organic matter and increased acidity.

3.1.8 A new mechanism for carbon dioxide loss in the geosphere

The complexity of the global cycle of carbon, one of the important elements of the biogeochemical processes on planet Earth, is determined by the variety of its

reservoirs and fluxes, many of which are often disregarded when evaluating the greenhouse effect of CO_2. Barenbaum (2002) was perhaps the first to describe the complete scheme of the carbon cycle in nature. This scheme reflects the carbon flux reaching the Earth extraterrestrially and selects three main cycles for carbon circulation: one biospheric and two lithospheric (i.e., fast and slow). The biospheric (the most thoroughly studied) carbon cycle includes the atmosphere, living substances, the World Ocean, and soils. The lithospheric carbon cycle covers the rocks of the Earth's crust and upper mantle. Detailing the carbon cycle in this way enables us to take into account the difference in timescales between the various sub-cycles of carbon. If the characteristic time of the biospheric cycle of carbon is $600 \cdot 10^3$ years, the time spent by the carbon cycle in the Earth's crust and mantle constitutes $(1.0–1.1) \cdot 10^6$ and 10^9 years, respectively.

Mobile carbon in the lithosphere circulates at a rate of $7 \cdot 10^{16}$ g yr^{-1}. Apart from mobile carbon, the lithosphere contains slow-moving carbon combined in carbonates or in sedimentary rock, from which it moves to the Earth's bowels and, as far as current timescales are concerned, is effectively removed from the cycle. Barenbaum (2004) connected these movements of carbon with the process of formation of oil and gas deposits, substantiating the mechanism of multiple transport of mobile carbon through the Earth surface in the process of the meteogenic water cycle. Another important point is that if carbon circulates mainly in its oxidized form of CO_2, under the surface it will be in its restored form (CH_4). Consideration of this fact in the global model of the carbon cycle by introducing the processes of Earth degassing makes the scheme in Figure 3.3 more correct.

3.2 CONCEPTUAL SCHEME FOR A MODEL OF THE GLOBAL BIOGEOCHEMICAL CARBON CYCLE

The reliability of assessment of the role of CO_2 in the greenhouse effect depends on detailed consideration in the models of the global biogeochemical cycle of carbon and on the accuracy of estimates about its characteristics. Diagrams showing the global cycle of carbon in the form of CO_2 are few and far between. We shall consider some of them in order to analyze them and understand the limits to such a detailed description of carbon cycle elements, beyond which it is impossible to get further knowledge of this cycle and, hence, of the CO_2-induced greenhouse effect. Note that all studied diagrams of the global cycle of CO_2 are divided into two classes: point (globally averaged) and spatial (locally averaged). All these diagrams divide the biosphere into the atmosphere, oceans, and land ecosystems. Many diagrams divide carbon into organic and inorganic forms. As a rule, the time step used to average all processes and carbon reservoirs is assumed to be equal to one year, and therefore the atmospheric reservoir is considered uniformly mixed (point). The World Ocean and land ecosystems are thoroughly detailed. This detailing, though, is limited by available databases about the reservoirs of carbon. As a rule, the final results of studies of the diagrams are either methodical in character or the CO_2 concentration in the atmosphere is predicted within a certain scenario of anthropogenic activity.

An idea of the size of carbon supplies in reservoirs is schematically shown in Figure 3.1, as proposed in the work of Bolin and Sukumar (2000). The quantities in this scheme differ widely from the data of other authors (Fierer *et al.*, 2003; Siegenthaler and Sarmiento, 1993). Figure 3.1 summarizes some of the published estimates. Nevertheless, their ratio and order of magnitude coincide in most cases. As can be seen, the maximum supply of carbon is concentrated in the World Ocean. The minimum is in the atmosphere.

The natural processes determining the dynamics of the GCC are characterized by various timescales. Some, such as burying dead organic matter at the bottom of the oceans, have characteristic timescales of the order of hundreds and thousands of years. Other processes (e.g., the biological carbon cycle on land) have a period of several tens of years. Therefore, consideration of the ratio of timescales in the biospheric carbon cycle is an important stage of studies of the dynamics of CO_2 content in the atmosphere. Here it is also important to take into account the fact that the characteristic time of complete mixing of the atmosphere is from several months to 2 years. During a year, according to results from routine measurements of CO_2 concentration at different monitoring stations, it varies widely. The difference between maximum and minimum values of atmospheric CO_2 concentration changes from 1 ppm at the South Pole to 15 ppm at high latitudes of the Northern Hemisphere. This spatial heterogeneity is determined by the large seasonally photosynthesizing vegetation communities present in the Northern Hemisphere. Boden *et al.* (1994) give some estimates of the latitudinal distribution of CO_2 in the atmosphere. The increased content of CO_2 in the NH atmosphere is mainly connected with the impact of human activity through direct CO_2 emissions and due to the impact on vegetation cover. Almost 90% of all carbon emissions in organic fuel burning fall in the zone between 30°N and 60°N. From the data of Boden *et al.* (1994) it follows that conceptual schemes of the global biogeochemical CO_2 cycle should take into account the spatial heterogeneity of atmospheric processes, too.

An important constituent of most conceptual schemes of the GCC is the structure of carbon fluxes in the World Ocean. As follows from Table 3.1, there is a certain informational possibility in the oceans to select several vertical layers and to distinguish the spatial heterogeneities in the structure of the ocean surface. Most authors consider the vertical structure of the oceans as two or three layers covering the photic layer and deep ocean. In the photic layer, the layers above and below the thermocline can be distinguished. The spatial heterogeneity of the oceans is expressed by upwellings and latitudinal zones with different rates and directions of CO_2 exchange between the oceans and the atmosphere. More detailed GCC schemes take into account heterogeneities in the carbonate system of the oceans, which makes it possible to considerably improve the accuracy of the respective models. Two widely used schemes of this type are given in the work of Kondratyev *et al.* (2003b).

The role of the World Ocean in the global cycle of CO_2 is mainly manifested through the process of its exchange at the atmosphere–ocean boundary. The intensity of ocean–atmosphere gas exchange is determined by the dynamic and diffusive behavior of the turbulent layers of water and air near the interface. Here numerous physical schemes appear which reflect the situations of wave formation, their collapse, and the

formation of foam and various films. As a result, carbon dioxide either dissolves in the ocean providing the input of CO_2 needed for photosynthesis or is emitted from the ocean to the atmosphere. This binary situation at the air–water boundary is explained by the different partial pressures of CO_2 in the atmosphere and CO_2 dissolved in water. In fact, this directed transport of CO_2 at the atmosphere–ocean boundary is more complicated. Its study requires expensive field experiments and a detailed classification both of synoptic and physico-geographic situations on the ocean surface. In programs of GCC study the emphasis is placed on the role of land ecosystems in GCC utilization (Houghton *et al.*, 2001). In the process of photosynthesis plants assimilate carbon dioxide and, in contrast, the decomposition of dead plants gives off carbon dioxide to the atmosphere. Thus, in the land biosphere continuous CO_2 exchange takes place between living and dead organic matter and the atmosphere. There are a multitude of conceptual diagrams which formalize this exchange and serve as the basis for global models of the carbon cycle. Clearly, the accuracy of estimates of carbon fluxes in the land biosphere is a function of detailed discretization of the types of soil–plant formations and the accuracy of biocenotic process parameterization. In this connection, global maps of vegetation and soils have been charted, their areas have been evaluated, many parameters of the biological production of land ecosystems have been determined, data on the vital activity of soil micro-organisms have been accumulated, and technologies for monitoring terrestrial landscapes have been worked out. Unfortunately, there are no balanced estimates of the limits to detailing soil–plant formations which would provide the required accuracy for estimating carbon fluxes. To solve this problem, a global model of carbon flux reflecting the hierarchy of significant (according to expert estimates) biospheric elements and processes of carbon transportation needs to be found. The list of carbon fluxes in this model is given and characterized in Table 3.3. Simulation experiments using this model facilitate carrying out comparative assessments of the consequences of complication of its various elements and in this way gradually approach the level of optimal spatial discretization.

GCC models have been developed by many authors (Chen *et al.*, 2000; Nitu *et al.*, 2004; Krapivin, 2000c; Tarko, 2005). Most models used data for the pre-industrial period and predicted CO_2 concentration for the next decade. For instance, Demirchian *et al.* (2002) discovered the linear dependence of the anthropogenic part of CO_2 concentration $K_a = P_a - 270$ (ppm) on the size of population G (billion) by reducing the formula to its simplest form, $K_a \approx 15G$. The G can be calculated using one of the many demographic models (Logofet, 1993, 2002; McVean, 2003). Demirchian *et al.* (2002) proposed an approach that reduced the formula to its simplest form, $G = a_1 + a_2 \operatorname{arctg}[(t - t_0)/a_3]$, where a_i and t_0 are functions of the prognostic estimate of global population size in 2100.

In these models the increase in the number of factors considered is clearly observed, as is the respective increasing adequacy that accompanies them. One of the first and sufficiently complete models of the global CO_2 cycle is the model proposed by Bjorkstrom (1979) which takes into account the dynamic interaction between carbon reservoirs in the biosphere and fluxes between them. For the first time, a unit for the World Ocean was realistically represented. In this unit the ocean is

Table 3.3. Reservoirs and fluxes of carbon as CO_2 in the biosphere in a simulation model of the global biogeochemical cycle of carbon dioxide as shown in Figure 3.6.

CO_2 reservoirs and fluxes	*Identifier in the model*	*Average estimate of the reservoir* (10^9 t) *and flux* (10^9 t/yr)
Carbon		
Atmosphere	C_A	650–750
Photic layer of the ocean	C_U	580–1,020
Deep layers of the ocean	C_L	34,500–37,890
Soil humus	C_S	1,500–3,000
Emission due to burning		
Vegetation	H_8^C	6.9
Fossil fuel	H_1^C	3.6
Desorption	H_2^C	97.08
Sorption	H_3^C	100
Rock weathering	H_4^C	0.04
Volcanic emanations	H_5^C	2.7
Assimilation by land vegetation	H_6^C	224.4
Respiration		
Plants	H_7^C	50–59.3
People	H_{10}^C	0.7
Animals	H_{11}^C	4.1
Emission		
Decomposed soil humus	H_9^C	139.5
Plant roots	H_{15}^C	56.1
Vital functions		
Population	H_{12}^C	0.3
Animals	H_{13}^C	3.1
Vegetation decay	H_{14}^C	31.5–50
Sedimentation to bottom deposits	H_{16}^C	0.1–0.2
Solution of marine sediments	H_{17}^C	0.1
Decomposition of detritus		
Photic layer	H_{22}^C	35
Deep layers of the ocean	H_{18}^C	5
Uplifting with deep waters	H_{19}^C	45

(*continued*)

Table 3.3 (*cont.*)

CO_2 reservoirs and fluxes	*Identifier in the model*	*Average estimate of the reservoir* (10^9 t) *and flux* (10^9 t/yr)
Lowering with surface waters and due to gravitational sedimentation	H_{20}^C	40
Photosynthesis	H_{21}^C	69
Underground sink	H_{23}^C	0.5
Surface sink	H_{24}^C	0.5-0.6
Breathing of living organisms in the ocean	H_{25}^C	25
Geospheric sink of carbon	H_{BG}	70
Geospheric source of carbon	H_{GB}	17

considered as a multi-layer composition of uniformly mixed reservoirs, the CO_2 exchange between them being described by linear laws. Models of the type of unit have been analyzed by many authors, which has provided the stimulus for successful division of the Earth's biogeosystem into homogeneous compartments and the creation of respective box models. Using the property of carbon to reside long in the atmosphere, which allows the atmosphere to be presented in the form of a point model, Bacastow (1981) developed a global four-reservoir model which made it possible to accurately approximate the dynamics of CO_2 exchange between Northern and Southern Hemispheres.

Each GCC model differs in the set of assumptions made and therefore concentrates on different effects. For instance, a simple numerical model of the gas exchange at the ocean–atmosphere boundary in the case of wind-driven roughness of the sea at wind speeds of $7\,m\,s^{-1}$ makes it possible to formulate, in the global model, a unit to calculate the persistent CO_2 flux between the water surface and the atmosphere. This can be exemplified by models of the ocean carbonate system described by many authors. Also, there are other models of the CO_2 cycle in natural systems (Riedo *et al.*, 2000; Zonneveld, 1998).

All models of the CO_2 cycle need improvement in the way they detail the spatial distribution of soil–plant formations and in the way they specify exchange processes in the ocean and at the atmosphere–ocean boundary. Accurate parameterizations of all studied elements of the biogeochemical carbon cycle should be synthesized into a single system. Such an attempt was made in the block scheme of the model shown in Figure 3.6. The main sources of CO_2 are the day-to-day activity of land and marine animals, photochemical reactions, decomposition of dead organic

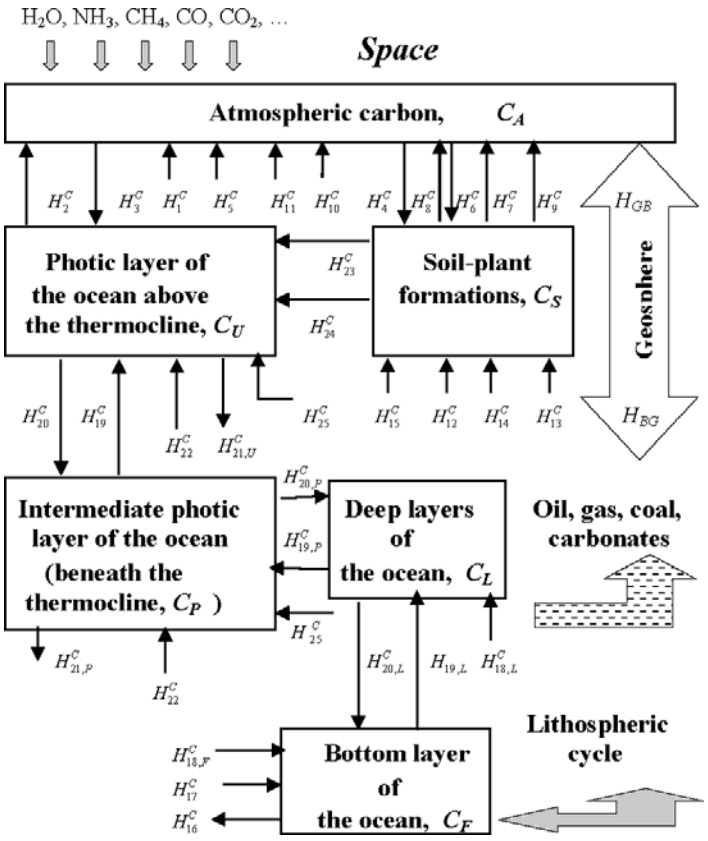

Figure 3.6. A block diagram of the global biogeochemical cycle of carbon on Earth. Carbon reservoirs and fluxes are described in Table 3.3.

matter, and anthropogenic activity. The time it takes CO_2 to migrate to the upper layers of the atmosphere is considered to be substantially less than the model's time step.

3.3 CARBON EXCHANGE PROCESSES IN THE ATMOSPHERE–OCEAN SYSTEM

3.3.1 World Ocean and carbon cycle

Knowledge of the exchange processes between the atmosphere and the ocean is very important in assessing the greenhouse property of CO_2. The intensive gas exchange between the ocean and the atmosphere ($\sim 90\,\mathrm{GtC\,yr^{-1}}$) rapidly equalizes CO_2 concentrations in the atmosphere and the surface layers of seawater (Cosca *et al.*, 2003).

The concentration of total dissolved inorganic carbon increases at depths below 300 m, exceeding substantially the equilibrium concentration at the ocean surface. Two processes determine the increased concentration of inorganic carbon within the ocean: the *solubility pump* and the *biological pump* (Grebmeier *et al.*, 2003). The efficient functioning of the solubility pump depends on the special features involved in thermohaline circulation as well as on spatiotemporal variations in ocean ventilation. Biological pump functioning is controlled by phytoplankton photosynthesis and decreases CO_2 concentration down to 150 ppm–200 ppm.

There are four ways in which the biological fixation of carbon can affect atmosphere–ocean CO_2 exchange:

- change of the biogenic composition of the ocean connected with removal or input of elements that can limit primary production;
- use of excess biogenic elements in areas with a low content of chlorophyll;
- participation of specific organisms in changing the ratio between organic and inorganic carbon; and
- change in the species composition of organisms which brings about the transport of carbon to deep layers of the ocean.

In most models of the global CO_2 cycle the relationship between the partial pressure of CO_2 dissolved in water (p_c) and the general concentration C_U of inorganic carbon in surface waters is calculated based on the buffer coefficient:

$$\xi = (p_c - p_{c,0})C_{U,0}(C_U - C_{U,0})^{-1}/p_{c,0},$$

where the "0" index refers to the pre-industrial period. However, numerous observations show that using this coefficient when calculating fluxes H_2^C and H_3^C will only give rough estimates if the effect of many other factors is not taken into account.

One of the first attempts to consider the spatial heterogeneity of the World Ocean and to simulate the impact of temperature gradients on CO_2 exchange between the upper layer of the ocean and the atmosphere was made by Bjorkstrom (1979). The idea to divide the World Ocean basins into two parts corresponding to warm and cold waters was later developed by numerous authors (e.g., Nefedova and Tarko, 1993). The most complete study of the physical mechanisms of CO_2 transport under different conditions of the water–air interface was carried out by Alekseev *et al.* (1992). Here for the first time CO_2 fluxes were measured in detail and their dependence on parameters of the state of the interface in the atmosphere–ocean system were analyzed, taking into account wind–wave mixing, foam formation on the water surface, wave collapse, and pollution. Parametric descriptions of the process involved in ocean–atmosphere gas exchange were proposed at each stage of the changing conditions in the water–air interface. For instance, it was shown that as roughness and foam formation increase, the rate of gas exchange grows considerably. For example, with a 5 cm thick foam layer the rate of gas exchange exceeds the gas

exchange through a free surface (i.e., one without foam) by 2.4 times. This fact is important for understanding the characteristics of gas exchange in inshore zones and in areas of heavy storms where foam bands are several centimeters thick. The presence of surface active substances (SASs) in the upper layer of the ocean is also of interest. When SASs reach about $7.8 \cdot 10^{-4}$% (volume), other conditions being equal, the rate of gas exchange reduces to 60%. However, where there is foam formation this effect decreases substantially.

On the whole, in the World Ocean the estimates of CO_2 flux between the atmosphere and the upper layer of the ocean vary between $16\,\text{mol} \cdot \text{m}^{-2}\,\text{yr}^{-1}$ and $1{,}250\,\text{mol} \cdot \text{m}^{-2}\,\text{yr}^{-1}$. Such a vast variability means that any global model of the CO_2 biogeochemical cycle needs to consider each individual feature in detail.

Under normal conditions the hydrosphere and atmosphere are in equilibrium with respect to CO_2 exchange, which is broken by fluctuations intemperature, ocean surface level, vertical circulation regime, etc. The amount of CO_2 assimilated and emitted in the process of exchange between the ocean and the atmosphere constitutes $55.6 \cdot 10^9\,\text{tC}\,\text{yr}^{-1}$. Algae assimilate $16.7 \cdot 10^9\,\text{tC}\,\text{yr}^{-1}$ from the atmosphere. These values are non-uniformly distributed over the water surface and vary strongly in time. For example, during the period 1980–1989 the flux of carbon between the ocean and the atmosphere varied from $-1.9\,\text{PgG} \cdot \text{yr}^{-1}$ to $2.9\,\text{PgG} \cdot \text{yr}^{-1}$. CO_2 exchange is characterized well by the Arctic Ocean, where low temperatures determine the high absolute content of CO_2 dissolved in the surface layer in any season. On average, in summer, Arctic waters assimilate CO_2 and emit O_2 to the atmosphere, and in winter, in contrast, they emit CO_2 and assimilate O_2. This clearly expressed seasonal change reduces in the basins of North Atlantic seas where the decrease in ice cover, increase in the period of photosynthetic activity, and the existing fall–winter vertical convection lead to gas exchange with the atmosphere intensifying toward prevalence of the H_3^C flux. Of the amount of CO_2 assimilated from the atmosphere, carbon constitutes $0.18 \cdot 10^9\,\text{tC}\,\text{yr}^{-1}$. Compared with total assimilation of CO_2 by the World Ocean estimated at $5.2 \cdot 10^9\,\text{tC}\,\text{yr}^{-1}$–$6.6 \cdot 10^9\,\text{tC}\,\text{yr}^{-1}$, the contribution of Arctic water basins to the removal of excess carbonic acid from the atmosphere is small (Table 3.4). However, this assessment is underestimated, when considering the results obtained by Kelley (1987). Average estimates show that the partial pressure of CO_2 in the atmosphere exceeds that in Arctic seas by 110 ppm. The CO_2 deficit in the marine medium happens mainly in the period of the springtime algal bloom and is estimated at $\sim 450\,\text{gC}\,\text{m}^{-2}$. This means that the CO_2 flux from the atmosphere to the marine medium can vary from $1.5\,\text{gC}\,\text{m}^{-2}\,\text{da}^{-1}$ to $4.0\,\text{gC}\,\text{m}^{-2}\,\text{da}^{-1}$. This assessment changes considerably as a function of longitude. For instance, the Norwegian Sea has a deficit in CO_2 partial pressure between 20 ppm and 50 ppm. For the Bering Sea, $\Delta p_{CO_2} \cong 70$ ppm. Between the CO_2 content in seawater and its temperature a clear linear correlation is observed with the proportion coefficient of $10\,\text{ppm}\,CO_2/^\circ\text{C}$.

All of this suggests the conclusion that Arctic waters remove carbon dioxide from the atmosphere. Therefore, once again a detailed study of this process is needed before a global model of carbon cycle can be specified, thereby improving the accuracy of estimation of the greenhouse effect due to emissions of anthropogenic CO_2.

Table 3.4. Annual budget of CO_2 exchange with the atmosphere for water bodies of the Arctic Basin and northern seas (10^6 tC/yr).

Region of the ocean	*Summer*			*Winter*			*Year*
	Assimilation	*Emission*	*Balance*	*Assimilation*	*Emission*	*Balance*	
Arctic basin	4.4	0.0	+4.4	—	—	—	+4.4
Arctic seas							
East Siberian	1.0	2.1	−1.1	0.0	0.7	−0.7	−1.8
Kara	11.4	2.4	+9.0	0.0	0.2	−0.2	+8.8
Laptev	2.4	3.6	−1.2	0.0	2.9	−2.9	−4.1
Chukchi	11.2	0.0	+11.2	0.0	0.6	−0.6	+10.6
Total	*26.0*	*8.1*	*+17.9*	*0.0*	*4.4*	*−4.4*	*+13.5*
North Atlantic seas							
Barents	71.9	0.0	+71.9	0.0	0.0	0.0	+71.9
Greenland	19.1	0.0	+19.1	8.7	0.0	+8.7	+27.8
Norwegian	64.8	0.0	+64.8	0.0	6.0	+6.0	+5.8
Total	*155.8*	*0.0*	*+155.8*	*8.7*	*6.0*	*+2.7*	*+158.5*
Arctic Ocean on the whole	186.2	8.1	+178.1	8.7	10.4	−1.7	+176.4

On the whole, when synthesizing a global model of the CO_2 biogeochemical cycle, the unit to simulate that part of the cycle spent in the ocean must describe how the ocean carbonate system works. Alekseev *et al.* (1992), analyzing the system CO_2–HCO_3–CO_3^{2-} and the distribution of pH values in ocean waters, discovered that more than 80% of dissolved carbon dioxide is in the form of hydrocarbonate ion of HCO_3. This means that when synthesizing a model of the ocean carbonate system only the first stage of the dissociation of carbonic acid can be reliably considered. As a result, the H_3^C flux of CO_2 dissolved in the upper layer of the ocean can be calculated by the formula

$$H_3^C = \psi(T_L)\sqrt{p_a}/(1 + 0.5C_S),$$

where $\psi(T_L)$ is a function of the effect of temperature on CO_2 solubility; and C_S is water salinity. Expression of the ψ function has been studied inadequately. There are just a few experimental estimates (Alekseev *et al.*, 1992). Nevertheless, there have been many approaches to determination of the direction of CO_2 fluxes at the atmosphere–ocean border. In the simplest case, fluxes H_2^C and H_3^C can be considered mutually exclusive. That is, a "valve" is supposed to exist on the atmosphere–ocean border, which switches on and off according to the pH parameter. A critical level of pH is about 8.11. At $pH \leq 8.11$ the ocean assimilates CO_2, and at $pH > 8.11$ the ocean emits CO_2.

On global scales, flux H_3^C prevails in World Ocean regions with cold waters (northern latitudes, upwelling zones) and flux H_2^C does so in warm waters. The dynamics of this regime is maintained by reactions in the hydrosphere between CO_2 and water resulting in the formation of carbonic acid:

$$HCO_3 + H_2O \Leftrightarrow H_2CO_3 + OH^-,$$

$$CO_3^{2-} + 2H_2O \Leftrightarrow H_2CO_3 + 2OH^-.$$

Saltwater contains dissolved carbon dioxide, non-dissociated molecules of H_2CO_3, anions of HCO_3, and CO_3^{2-}. They all are in equilibrium:

$$CO_2 + H_2O \Leftrightarrow H_2CO_3 \Leftrightarrow HCO_3^- + H^+ \Leftrightarrow CO_3^{2-} + 2H^+.$$

The equilibrium state between carbonic acid bicarbonate and carbonate ions is established rapidly. The solution of CO_2 and formation of H_2CO_3 take place over a longer period. However, since many authors dispute the availability of H_2CO_3, a summarized concentration of CO_2 and H_2CO_3 should be considered by denoting it as $[CO_2]$. Let us introduce some notations to characterize the total concentration of intermediate components:

$$\sum C = [CO_2] + [H_2CO_3] + [HCO_3^-] + [CO_3^{2-}]. \tag{3.2}$$

Another characteristic of the hydrosphere that needs to be parameterized is alkalinity:

$$A = [HCO_3^-] + 2[CO_3^{2-}] + [H_2CO_3] + [OH^-] - [H^+], \tag{3.3}$$

where $[Ca^{2+}]$ and $[H^+]$ are concentrations of ions of calcium and hydrogen, and $[HCO_3^-]$ and $[CO_3^{2-}]$ are concentrations of bicarbonate and carbonate ions.

Using these notations, let us formulate the equilibrium conditions:

$$K_0 p_c = [CO_2], \qquad [HCO_3^-] = K_1[CO_2]/[H^+], \tag{3.4}$$

$$[CO_3^{2-}] = K_2[HCO_3^-]/[H^+], \tag{3.5}$$

$$[Ca^{2+}] = L_p[H^+]^2/(K_1K_2[CO_2]), \tag{3.6}$$

where K_0 is the indicator of CO_2 solubility ($=250$ μmol/L atm at 30°C and 640 μmol/L atm at °C); L_p is the solubility indicator for $CaCO_3$; K_1 and K_2 are the first and second apparent coefficients of dissociation of carbonic acid (they depend on temperature and pressure).

From (3.2)–(3.6) we obtain:

$$\sum C = [CO_2](1 + K_1/[H^+] + K_1K_2/[H^+]^2),$$

$$A = [CO_3^{2-}](K_1/[H^+] + 2K_1K_2/[H^+]^2).$$

Eriksson (1963), using a differentiation operator δ, calculated relative changes in $[CO_2]$, $[Ca^{2+}]$, p_c, and A. Let us denote any of these components as U and taking

$\Delta U = \delta U/U$, we obtain:

$$\Delta p_c = \Delta[CO_2] - \Delta K_0, \tag{3.7}$$

$$\Delta[Ca^{2+}] = \Delta L_p + 2\Delta[H^+] - \Delta K_1 - \Delta K_2 - \Delta[CO_2], \tag{3.8}$$

$$\Delta\Sigma C = \Delta[CO_2] + F_1\Delta K_1/F_0 + a_2\Delta K_2/F_0 - F_2\Delta[H^+]/F_0, \tag{3.9}$$

$$\Delta A = \Delta[CO_2] + \Delta K_1 + 2a_2\Delta K_2/F_2 - F_3\Delta[H^+]/F_2, \tag{3.10}$$

where

$$F_0 = 1 + a_1 + a_2, \qquad F_1 = a_1 + a_2, \qquad F_2 = a_1 + 2a_2, \qquad F_3 = a_1 + 4a_2,$$
$$a_1 = K_1/[H^+], \qquad a_2 = K_1K_2/[H^+]^2.$$

Based on relationships (3.7) through (3.10) and taking experimental data into account, Eriksson (1963) showed that with a 1°C increase in temperature of the upper layer of the marine medium the partial pressure of CO_2 in the atmosphere can grow by 4.2%–5.8%, and with a 1% decrease in the water volume the partial pressure of CO_2 in the atmosphere grows by 3%, with 1% of carbon dioxide in the water medium precipitating as $CaCO_3$. With variations of the equilibrium state in deep layers of the hydrosphere a 1% output of CO_2 in the form of gas is followed by a 1% sediment of CO_2 in the form of $CaCO_3$. Moreover, variations in the CO_2 partial pressure correlate with changes in the concentration of phosphorus P, so that a decrease of P in deep layers by 1% leads to an increase of p_c by 5.6%.

Eriksson (1963) found that a 1% increase in alkalinity causes a 2.26% decrease in CO_2 partial pressure in the atmosphere and a 98% reduction of total CO_2 supply in the hydrosphere. Under conditions where there is no external input of Ca into the hydrosphere, a 1% increase in alkalinity causes an increase in the rate of $CaCO_3$ deposition (i.e., total alkalinity decreases by 0.92%). Thus, a 1% increase in water alkalinity is equivalent to a 0.5 increase in pH.

Equilibrium between various components of the hydrospheric carbonate system depends on temperature and pressure, a combination of which correlates with pH so that, at a given temperature and pressure, equilibrium is only a function of $pH = -\lg[H^+]$. The effect of temperature on pH in the first approximation can be described by the equation (Ivanov, 1978), $\Delta pH = -0.0111\Delta T$, valid when $pH \in [7.5, 8.4]$, $T \in [1–30]$°C, and salinity from 10‰ to 40‰. The dependence of pH on pressure p_c follows the dependence, $pH = d\Delta p_c$, where, on average, $d = -0.0254$. A more accurate presentation of this law is given in Table 3.5.

The connection between the equilibrium condition of CO_2 exchange and pH on the atmosphere–ocean border is such that when the CO_2 pressure in the atmosphere

Table 3.5. Empirical dependence of pH on atmospheric pressure. From Ivanov (1978).

pH at atmospheric pressure	7.5	7.7	7.9	8.1	8.3
ΔpH with pressure increasing by 1,000 dbar	−0.035	−0.028	−0.023	−0.021	−0.02

reaches $330 \cdot 10^{-6}$ atm, equilibrium occurs at 20°C for pH = 8.16 and at 0°C for pH = 8.11. At a lower pH value the ocean will assimilate CO_2, and at a higher pH it will emit CO_2. Hence, to describe the functions of fluxes H_2^C and H_3^C at the atmosphere–ocean border, the structure of the ocean carbonate system needs to be thoroughly studied. A simplified description of these fluxes is usually based on comparison of the partial pressures of CO_2 in the atmosphere and in the ocean. According to the data in Alekseev *et al.* (1992), fluxes H_2^C and H_3^C are approximated well by the function $H_i^C = k_i(p_a - p_c)^{1/2}$, where p_a and p_c are the partial pressures of CO_2 in the atmosphere and in the ocean, respectively. The partial pressure of CO_2 in the atmosphere at sea level can be calculated with the formula:

$$p_a = 0.421542 \cdot 10^{-18} M_C(273.15 + T),$$

where M_C is CO_2 mass in tons; and T is the air temperature in °C.

According to Bjorkstrom (1979), the functional dependence of p_c on parameters of the ocean carbonate system can be presented in the form $p_c = [CO_2]/K_0$. From the condition of chemical equilibrium, according to (3.4) and (3.5), it follows that

$$[CO_2] = [H^+] \sum C/a,$$

where $a = [H^+]^2 + [H^+]K_1 + K_1K_2$; $\sum C = C_U/W_U$; and W_U is the volume of an elementary reservoir. Let us denote

$$K_W = [H^+][OH^-], \qquad K_B = [H^+][B(OH)_4^-]/[B(OH)_3],$$
$$B_T = [B(OH)_3] + [B(OH)_4^-].$$

Then we obtain from (3.3):

$$A = K_W[H^+]^{-1} + K_BB_T(K_B + [H^+])^{-1} + C_U([H^+]K_1 + 2K_1K_2)/(aW_U) - [H^+]$$

or

$$A = [CO_2]\left(\frac{K_1}{[H^+]} + \frac{2K_1K_2}{[H^+]^2}\right) + \frac{B_T}{1 + [H^+]/K_B} + \frac{K_W}{[H^+]} - [H^+]. \tag{3.11}$$

The solution of this equation relative to $[H^+]$ enables us to determine p_c as a function of C_U. From the estimates by Bjorkstrom (1979), $K_B = 2 \cdot 10^{-9}$ and $K_W = 10^{-14}$.

The right-hand sides of Equations (3.3) and (3.11) imply consideration has been given of all the weak acids in saltwater. The ions of other compounds are taken into account through the dependence of equilibrium constants on salinity or chlorine content. The characteristic parameter of equilibrium in the carbonate system is a variable:

$$X = \frac{(K_1K_2)^{1/2}}{[H^+]} = \left[\frac{[CO_3^{2-}]}{[CO_2]}\right]^{1/2}.$$

In the terms of this parameter we have:

$$\sum C = (1 + KX + X^2)[\mathrm{CO_2}], \tag{3.12}$$

$$A = (KX + 2X^2)[\mathrm{CO_2}] + W(X), \tag{3.13}$$

where $K = \sqrt{K_1/K_2}$,

$$W(X) = B_T/\{1 + [K_1K_2]^{1/2}X^{-1}\}/K_B + K_W X[K_1K_2]^{-1/2} - [K_1K_2]^{1/2}X^{-1}.$$

Let us exclude $[\mathrm{CO_2}]$ from (3.12) and (3.13):

$$(2C - A')X^2 - K(A' - C)X - A' = 0, \tag{3.14}$$

where $A' = A - W(X)$.

Since $W(X) \ll A$, to solve Equation (3.14) the following iterative procedure can be used, beginning with an estimation of $X = X_1(\cong 1)$:

$$A'_i = A - W(X_i), \qquad X_i = 0.5[-b + (b^2 - 4ac)^{1/2}]/a \quad (i \geq 2),$$

where $a = 2C - A'_{i-1}$, $b = K(A'_{i-1} - C)$.

The exchange processes taking place at the atmosphere–ocean border were experimentally studied by Kiseleva (1990) and Zaitsev (1988), among others. They showed that at high wind speeds the rate of gas exchange sharply increases. This is connected with the mechanism of foam formation on wave crests as well as the intense activity of air bubbles being trapped and held beneath the water surface. The dependence of the amount of spray Q on height over the water surface can be approximated well by a linear function. For instance, at a wind speed of $V = 11.1$ m/s this approximation is (Kiseleva, 1990):

$$Q = \begin{cases} Q' \exp\{-14.5z + 0.684\} & \text{without wave breaking} \\ Q' \exp\{-7.48z + 0.842\} & \text{with wave breaking,} \end{cases}$$

where $Q'[1/(\mathrm{cm^2 s})]$ is the dimensional multiplier.

Experimental estimates of the net gas transport due to the droplet mechanism showed that the CO_2 flux between water and air can vary from 1.44 $\mathrm{mgCO_2\,m^{-2}\,hr^{-1}}$ in the absence of wave breaking to 26.6 $\mathrm{mgCO_2\,m^{-2}\,hr^{-1}}$. The rate of gas exchange at the atmosphere–ocean border is markedly affected by foam formation on the ocean surface. In this case the rate of gas exchange can increase up to 28%. All this suggests the conclusion that detailed modeling of the mechanisms involved in atmosphere–water CO_2 transport is needed. Satellite World Ocean monitoring allows us to identify the zones of foam formation and, hence, along with the modeling of the processes of foam formation, to perform direct measurements of the areas of the foam-covered basins.

The mechanism underlying air bubble behavior in the upper layer of the ocean has been poorly studied. The available theoretical results are based, as a rule, on a number of suppositions, which in many cases can drastically distort ideas about the real processes of gas exchange between the atmosphere and the ocean. Among these suppositions the following have been used most often:

- air bubbles in the upper layer of the ocean practically instantly acquire the temperature of the environment, since the molecular coefficient of heat conductivity exceeds that of gases by 2–3 orders of magnitude;
- air bubbles in water do not affect its dynamics;
- air bubbles do not merge in water.

The size of air bubbles in water varies constantly because they gradually dissipate. Gas flux through the bubbles is described by the relationship:

$$Q = 4\pi RD|\Delta p|S \cdot Nu,$$

where $|\Delta p|$ is the difference in the partial pressures of gas in the water and in the atmosphere; and R is the bubble radius,

$$Nu = \begin{cases} 1 + 0.5Pe + 0.5Pe^2 \ln(2Pe) & \text{for } R \leq 20\ \mu\text{m}, \\ \sqrt{2/3\pi}Pe^{1/3} & \text{for } 20\ \mu\text{m} < R \leq 200\ \mu\text{m}, \\ 0.45Pe^{1/3}Re^{1/3} & \text{for } 200\ \mu\text{m} < R \leq 400\ \mu\text{m}, \end{cases}$$

where Re is the Reynolds number ($Re = 2vR/D$); Pe is the Pekle number ($Pe = vR/\nu$); ν is water viscosity; v is the velocity of bubble motion; and D is the coefficient of gas molecular diffusion.

Of course, ocean surface condition substantially affects its gas exchange with the atmosphere. The size of basins covered in foam or white caps depends directly on a combination of parameters, such as wind speed, water temperature, and sea currents. Analysis of the statistical characteristics of the patchy pattern of the ocean surface made by many experts makes it possible to describe the percentage distribution of areas covered in foam (S_f) and white caps (S_l) with the following binary functions of wind speed V (at a height of 10 m):

$$S_f = \begin{cases} 0 & \text{for } V < 5\ \text{m/s}, \\ 0.65\{1 + 4.76 \cdot 10^{-2}(V - 5^2)\} & \text{for } V \geq 5\ \text{m/s}, \end{cases}$$

$$S_l = \begin{cases} 0 & \text{for } V < 5\ \text{m/s}, \\ 0.015\{1 + 2.2 \cdot 10^{-2}(V - 5^3)\} & \text{for } V \geq 5\ \text{m/s}. \end{cases}$$

According to Kiseleva (1990), the relationship between S_f and S_l at $V \geq 5$ m/s obeys the following rule:

$$S_f/S_l = 50 - 3.4(V - 5).$$

It is clear that the structure of the atmosphere–ocean border can affect the gas exchange within widely varying values of fluxes H_2^C and H_3^C (see Figure 3.6). Unfortunately, the current level of knowledge of the laws behind changes in the structure of the atmosphere–ocean border as a function of synoptic situations does not facilitate clear estimation of the limits to detailing the processes taking place at this border, to obtain values of the fluxes H_2^C and H_3^C that are close to real ones. This means that at this stage of synthesizing a global model of the CO_2 cycle some uncertainty still exists.

Observations in the equatorial band of the Pacific Ocean revealed in the period 1980–1990 a strong change in CO_2 partial pressure (pCO_2) in surface waters and in atmosphere-to-ocean CO_2 flux. During the 1980s there was a much slower increase in pCO_2 with time than during the 1990s. The trend intensified near 1990 and coincided with the supposition that the main factor of the impact of atmosphere–ocean CO_2 exchange was natural long-term climatic variability (Bratcher and Giese, 2002).

3.3.2 A zonal model for the carbon cycle in the atmosphere–ocean system

Let us consider one of the versions of parameterizing the dynamics of global carbon dioxide in the atmosphere–ocean system proposed and studied by Nefedova (1994). The spatial heterogeneity of the World Ocean can be approximated in a zonal scheme in accordance with the latitudinal dependence of climatic processes and the processes of mixing in the atmosphere and in the oceans. There are 14 latitudinal zones 10° in size. In the vertical, there are three layers in the World Ocean: the upper quasi-homogeneous layer (UQL) has a time-dependent thickness, thermocline, and deep ocean. As a result, the World Ocean can be divided into 42 volume parts. An upwelling is assumed to exist between 40°N and 40°S along with a downwelling at higher latitudes. In the UQL the water flows poleward from the equator, and in deep layers the water flows in the opposite direction (Kondratyev *et al.*, 2003a, b). Over each water basin, the atmosphere can be simulated by a point model. The carbon exchange between different zones of the atmosphere takes place due to advection H_i^a and turbulent diffusion H_i^d:

$$H_i = H_i^a + H_i^d \quad (i = \overline{1,14}),$$

$$H_i^a = 2\pi R_0 h_a V_i^* (C_i^a - C_{i+1}^a) \cos\phi_i,$$

$$H_i^d = [2\pi R_0 A_h h_a / \Delta\phi_i](C_i^a - C_{i+1}^a) \cos\phi_i,$$

where $C_i^a = M_i^a / V_i^a$ is the concentration of carbon in the ith zone of the atmosphere; M_i^a is the carbon mass in the ith zone of the atmosphere; V_i^a is the volume of the ith zone of the atmosphere; R_0 is the Earth's radius; ϕ_i is the latitude of the southern boundary of the ith zone; h_a is the altitude of the atmosphere (10 km); V_i^* is the average velocity of the meridian transport of air masses in the atmosphere (0.2 m/s–1.0 m/s); and A_h is the coefficient (10^5 m^2/s).

CO_2 exchange at the atmosphere–ocean border is described by the traditional law:

$$H_i^{a0} = k(u_i)(P_i^0 - P_i^0),$$

where

$$P_i^a = k_a M_i^a R T_i^a S_i^{-1} \mu^{-1},$$

where $k(u_i)$ is the proportion coefficient depending on wind speed; P_i^0 and P_i^0 are the partial pressures of CO_2 in the ith zone of the atmosphere and the ocean, respectively; k_a is the share of the 100 m air column mass in the mass of a 10 km column ($\approx$0.01602); R is the universal gas constant (8.31451 J/(mol · K); T_i^a is the air temperature at the level of the ocean in the ith zone ($T_i^a = T_i^{as} + \Delta T_i^a$); T_i^{as} is the seasonal

temperature component; and ΔT_i^a is the average annual change of air temperature caused by increased CO_2 content in the atmosphere.

An SST change is assumed to take place in phase with a change in air temperature by the same value:

$$T_i^0 = T_i^{0s} + \Delta T_i^a.$$

The partial pressure of CO_2 dissolved in surface waters is proportional to its concentration in the water and inversely proportional to its solubility. This dependence is established by solving the system of Equations (3.12) and (3.13), which describe the functioning of the ocean carbonate system. For the quantitative solution of this system we can use, for instance, the secant method. As a result, we obtain $[CO_2]$ and P_i^0. Based on data on the temperature dependence of the equilibrium constants for the respective chemical reactions, we find:

$$P_i^0 = P_i^0(C_i^1, T_i^0) \quad (i = \overline{1,14}).$$

The turbulent fluxes of carbon at the lower boundary of the UQL (H_{UPL}) and the upper boundary of the thermocline (H_T) are described by the functions:

$$H_{UPL} = \begin{cases} (C_i^1 - C_i^2)(V_i + dh_i/dt) & \text{for } dh_i/dt + V_i > 0, \\ 0 & \text{for } dh_i/dt + V_i \le 0, \end{cases}$$

$$H_T = \begin{cases} (C_i^1 - C_i^2)(V_i + dh_i/dt) & \text{for } dh_i/dt + V_i \le 0, \\ 0 & \text{for } dh_i/dt + V_i > 0, \end{cases}$$

where C_i^1 and C_i^2 are the concentrations of inorganic carbon in the UQL and thermocline, respectively; h_i is the UQL depth of the ith zone of the ocean (depends on the season); and V_i is the speed of water lifting (upwelling) or lowering (downwelling) (0.001 cm/s–0.1 cm/s).

The turbulent fluxes of carbon on the thermocline–deep ocean border is considered to be proportional to the coefficient k_T of the difference in carbon concentrations in the bordering layers:

$$H_{TF} = k_T(C_i^3 - C_i^2) \quad (i = \overline{1,14}),$$

where C_i^3 is the concentration of inorganic carbon in the deep ocean of the ith zone.

Production and circulation of organic carbon in the ocean have been studied in detail and parameterized by many authors (Nitu *et al.*, 2000a, b, 2004; Krapivin and Kondratyev, 2002; Kondratyev *et al.*, 2004a). In the model by Nefedova and Tarko (1993) the following approximations were assumed:

$$B_i^p = B_i^0\{1 + (\delta_i - 1)/(\delta_i + 1) \cdot \sin(wt - \pi/2)\}$$
$$\text{for } \varphi \in [60^\circ\text{N}, 90^\circ\text{N}] \cup [60^\circ\text{S}, 90^\circ\text{S}] \quad (i = 1, 14);$$

$$B_i^p = B_i^0\{1 + (\delta_i - 1)/(\delta_i + 1) \cdot \sin(2wt - \pi/2)\}$$
$$\text{for } \varphi \in [10^\circ\text{N}, 60^\circ\text{N}] \cup [10^\circ\text{S}, 60^\circ\text{S}] \quad (i = 2\text{–}6, 9\text{–}13);$$

$$B_i^p = B_i^0, \quad \text{for } \varphi \in [0^\circ\text{N}, 10^\circ\text{N}] \cup [0^\circ\text{S}, 10^\circ\text{S}] \quad (i = 7, 8);$$

where B_i^0 is the average annual production of phytoplankton (150-550 $\cdot 10^9$ t/yr); and δ_i is the ratio of maximum and minimum values of the rate of organic matter production.

Organic matter produced in the UQL decomposes and descends to deeper layers. Let B_i^{1d}, B_i^{2d}, and B_i^{3d} be the rates of organic matter decomposition in the UQL, thermocline, and deep ocean, respectively; γ the ratio of the average annual amount of organic matter decomposing in the UQL to the average annual production of phytoplankton; τ the lag time in organic matter decomposition; D the average depth of the ocean (3,653 m–3,795 m); and H the depth of the thermocline bottom (30 m–200 m). Then

$$B_i^{1d} = \gamma B_i^p(t-\tau) \quad (i = \overline{1,14}),$$

$$B_i^{2d} = (1-\gamma)(H-h_i)/(D-h_i)\langle B_i^{1p}\rangle,$$

$$B_i^{3d} = (1-\gamma)(D-H)/(D-h_i)\langle B_i^{1p}\rangle.$$

Here the angle brackets "$\langle\rangle$" denote calculation of the average value for the annual cycle.

So, the seasonal model of the global carbon cycle developed in the works by Nefedova and Tarko (1993) and Nefedova (1994) can be simulated by a system of 56 ordinary differential equations with periodic coefficients ($i = 1, \ldots, 14$):

$$\frac{d}{dt}C_i^1 h_i - \left(\frac{dh_i}{dt} + V_i\right)C_i^1 = H_i^{a0} - H_{UPL} + L_i^1 - B_i^p + B_i^{1d},$$

$$\frac{d}{dt}C_i^2(H-h_i) + \left(\frac{dh_i}{dt} + V_i\right)C_i^2 = H_T + H_{TF} + B_i^{2d},$$

$$\frac{d}{dt}C_i^3(D-H) + V_i C_i^3 = L_i^3 - H_{TF} + B_i^{3d},$$

$$\frac{dM_i^a}{dt} = \gamma_i^a + V_i^a(H_i - H_{i-1}) - 0.012 S_i H_i^{a0},$$

where γ_i^a are the anthropogenic carbon emissions in the ith zone of the atmosphere.

3.4 CARBON CYCLE IN THE WORLD OCEAN

3.4.1 The World Ocean as a complex hierarchic system

To increase the reliability of assessing the role of the World Ocean in the global carbon cycle, a more detailed description is needed of the production processes in ocean ecosystems. Along with the physical and chemical processes of transformation and motion of carbon in the ocean medium, the biological processes play an important role. In particular, phytoplankton, just like the nutrient elements, assimilates dissolved CO_2 from saltwater. As a result, an organic substance is formed that partially goes to the nutrient chains of the trophic pyramid of a given basin of the World Ocean and partially descends to bottom sediments. The totality of all the

processes involved in carbon motion in the ocean medium creates a gradient of CO_2 concentration between the surface and deep waters. Therefore, a study of the structure and functioning of ocean ecosystems has become one of the most important and rapidly developing directions for marine biology. Its various aspects are being developed in many countries within the framework of the International Biological Program. In particular, the international program JGOFS (Joint Global Ocean Flux Study) is dedicated to the study of biochemical processes in the ocean to obtain a deeper knowledge of how the ocean responds to external forcings. One of the goals of studies is to predict the system's behavior as a result of changes to some of its parameters. However, due to the unique nature and broad spatial extent of the World Ocean, it is difficult to quantitatively estimate all the elements of the system at different moments of its development and in different regions of the World Ocean and, moreover, to assess the effect of their change on how the system functions overall.

The ocean covers 71% of the planet's surface and is the source of a substantial amount of foodstuffs consumed by humans (around 1% of total food consumption), the remaining 99% of food is obtained from cultivated land. At the same time, the total amount of organic matter produced in the ocean is approximately equal to that produced by land vegetation. By rough estimates, the total biomass of nekton constitutes $5.3 \cdot 10^9$ t. The catch of fish and other species from the World Ocean is estimated at $70 \cdot 10^6$ t/yr, which constitutes 20% of the protein consumed by humans. The catch of traditional species is close to the limit for their sustainability ($\sim 90 \cdot 10^6$ t/yr–$100 \cdot 10^6$ t/yr). However, it is not a limit to the industrial ability of ocean ecosystems in general, since the supplies of krill and other biological objects are still used little.

This disproportion between the role of land and ocean ecosystems in food production is explained, primarily, by the fact that agriculture has been intensively developed, whereas in the seas and oceans development has been poor by comparison. Possible ways of increasing ocean bioproductivity have not been considered beyond catching animals at the end of the trophic chains of natural communities of the World Ocean (i.e., fish and whales). Each successive trophic level gains about 0.1% of the share of energy accumulated at a previous level. On land, two levels of organisms (vegetation and herbivores) are used, but in the ocean and in the seas there are up to five levels. The direct use of non-fish species will make it possible to sharply increase the amount of protein obtained from the ocean.

Second, the question arises about the transition from free fishing to cultivated methods of economy in the World Ocean (i.e., the question of artificially increasing the productivity of the biological communities of the ocean). To do this, it is necessary, first of all, to study the methods of controlling the output of the final product in the biological systems of the World Ocean. To determine rational ways of affecting ocean communities, it is necessary to study their structure and the way they function, to understand the production processes, transformations of matter, and energy flux at different trophic levels of ocean ecosystems. It is necessary to develop a theory of control in the biological systems of coastal waters and the open ocean, which differ both in natural hydrophysical and biogeochemical parameters as well as in the extent of anthropogenic impacts.

Marine communities are complicated biological systems of populations of individual species. As a result of their interaction, communities are in dynamic development. Their spatial structure is mostly determined by the composition of numerous biotic and abiotic factors, which depend on the totality of oceanic parameters. The latter are determined by the laws of general circulation of ocean waters, including tides and ebbs, zones of convergence and divergence, wind, and thermohaline currents.

In the late 20th century the urgent problem arose of predicting the dynamics of ocean systems in conditions of increasing anthropogenic impacts (chemical poisoning, elimination of living organisms, environmental changes) as well as assessing their role in the dynamics of the whole biosphere. In recent studies of the climatic impact of greenhouse gases it was shown that the role of the World Ocean in this process has been underestimated. In particular, Kondratyev and Johannessen (1993) provided data on the role of the Arctic basins in the formation of the global CO_2 cycle, from which it followed that previous assessments of this role were incorrect. This was connected with the fact that an account of biological and gravitational processes playing the combined role of a pump that sucked in carbon dioxide from the atmosphere to deep layers of the ocean was inadequate in earlier models of the global biogeochemical carbon cycle. Therefore, specific models of the working regime for this pump with climatic zones taken into account may be important in predicting estimates of the greenhouse effect.

The impact of ocean ecosystems on biogeochemical cycles is manifested through the atmosphere–water border and is usually parameterized based on observational data. However, what is important in this impact is the vertical structure of the processes taking place in the ocean medium. The nature of these processes depends much on external factors. For instance, according to Legendre and Legendre (1998), in the Arctic zones of the World Ocean the patchy structure of the springtime bloom of phytoplankton is determined by the winter conditions of ice formation and subsequent ice melting. In other zones these external factors are pollutions of the atmosphere and ocean surface, changes in phytoplankton living conditions, and functioning of the carbonate system.

Phytoplankton is at one of the initial levels of the trophic hierarchy of the ocean system. As field observations have shown, the World Ocean has a patchy structure formed by a combination of non-uniform spatial distributions of insolation, temperature, salinity, concentration of nutrient elements, hydrodynamic characteristics, etc. The vertical structure of phytoplankton distribution is less diverse and possesses rather universal properties. These properties are manifested by the existence of one to four vertical maxima of phytoplankton biomass.

Variability of the patchy topology and vertical structure is connected with seasonal cycles and has been well studied experimentally in many climatic zones of the World Ocean. The typical qualitative and quantitative indicators of this variability have been found. The combined distributions of abiotic, hydrological, and biotic components of the ocean ecosystems have been studied. Vetrov and Romankevich (2004) analyzed conditions for the carbon cycle formation in the Barents, White, Kara, East-Siberian, and Chukchi Seas, considering the relationships between

the sources of organic carbon and taking into account the role of phytoplankton, zooplankton, bacterioplankton, and zoobenthos.

The complexity and mutual dependence of all the processes in the ocean substantially hinder discovery of the laws of formation of phytoplankton spots and establishing correlations between the various factors that regulate trophic relationship intensity in ocean ecosystems. For instance, many studies revealed a close relationship between primary production and phytoplankton amount. At the same time, this relationship breaks down depending on the combination of synoptic situation and insolation. It turns out that the extent of this breakdown depends much on the combination of groups of phytoplankton (Legendre and Legendre, 1998).

Analysis of the accumulated observation data on assessments of the produce of seas and oceans and the attempts of many authors to discover the laws of produce formation characteristic of various water basins have revealed various laws in local relationships between productivity and environmental parameters.

An efficient way of studying the vertical structure of ocean ecosystems is to numerically model them based on measurements of their characteristics (Kuck *et al.*, 2000). To derive the model, it is necessary to know the structure of the trophic relationships in ecosystems, specific features of hydrological conditions, and information about other characteristics of the environment. Experience in such modeling has pointed up a possibility for efficient prediction of the dynamics of World Ocean communities. Examples of such models include a 3-D model of the ecosystem of the Peruvian current (Krapivin, 1996), of the Okhotsk Sea (Aota *et al.*, 1993), and others. In all these models the main task was parameterizing a unit for the vertical structure of the ecosystem.

3.4.2 Spatial model of the carbon cycle in the ocean

Along with the physico-chemical processes of transformation of carbon compounds in the hydrosphere mentioned above, the general circulation in the World Ocean plays an important role in their long-range transport. According to the available estimates, about 80% ($\sim$1.7 Gt) of organic matter formed in the process of photosynthesis descends to deeper layers and oxidizes giving CO_2. This process is balanced by a slow upwelling of water, and thereby a situation for stable CO_2 exchange arises. However, in local situations there are strong deviations from stable conditions, which can be described only by a scheme of the spatiotemporal structure of ocean water motion. The block scheme of this structure identifies the surface, intermediate, deep, and bottom waters as well as the current topography on every horizon. In the scientific literature, models simulating World Ocean circulation vary widely; therefore, the development of this part of the global model unit is not difficult.

Following Nitu *et al.* (2000b), ocean depth z can be divided into four basic layers: photic to well-heated ($\Omega_U = U[z_i, z_{i+1}]$, $z_0 = 0$; $i = 0, 1, \ldots, m-1$); intermediate ($\Omega_P = U[z_i, z_{i+1}]$, $i = m, \ldots, m+n-1$); deep ($\Omega_L = U[z_i, z_{i+1}]$, $i = m+n, \ldots, m+n+l-1$), and bottom Ω_F. According to their hydrophysico-ecological characteristics, layer Ω_U as a function of latitude φ, longitude λ, and season t can be attributed to warm or cold waters; layer Ω_P is photic but always

with low water temperatures; in layer Ω_L phytoplankton are not produced; and, finally, layer Ω_F plays the role of a boundary layer.

On average, layer Ω_U has an area $360 \cdot 10^{12}\,\mathrm{m}^2$ and a depth $z_m \cong 75\,\mathrm{m}$, its warm waters covering an area of $240 \cdot 10^{12}\,\mathrm{m}^2$. Layer Ω_P is located at depths from z_m to $z_{m+n} \cong 200\,\mathrm{m}$. In the model realizations given in Krapivin and Kondratyev (2002) the following assumptions were made: $m = 10$, $n = 2$, $l = 8$.

Vertical CO_2 transport in the ocean is determined by advective fluxes $H^C_{19,ij}$ and gravitational sedimentation of dead organic matter (flux $H^C_{20,ij}$). Advective transport from the ith to the jth reservoir of the ocean is considered proportional to the concentration of carbon in the respective reservoirs: $H^C_{19,ij} = \lambda_{2,ij} C_{a,i}$ $(a = U, P, L)$, where $\lambda_{2,ij} = V_{ij}/V_i$, V_{ij} is the water volume transported per unit time from the ith reservoir to the jth reservoir; and V_i is the volume of the ith reservoir.

The following algorithm is widely used to parameterize the process of carbon sedimentation. The flux under a unit area of the ocean is supposed to decrease exponentially with depth. If we denote the inflow of organic matter in the ith reservoir as g_i and the net outflow of organic matter from the water surface as $H_{20,T}$, we obtain:

$$H^C_{20,1} = H_{20,T}; \qquad H^C_{20,i} = g_{i-1}(\sigma_i/\sigma_{i-1}) \exp[-(z_i - z_{j-1})/D_s] \quad (i = 2, \ldots, m+n+l);$$

where σ_i is the area of the ith reservoir; and D_s is the characteristic time of organic matter particle sedimentation before their decomposition. The rate of decomposition in each reservoir is equal to:

$$R_{D,i} = H^C_{20,j} - H^C_{20,i+1} \quad (i = 1, \ldots, m+n+l); \qquad R_{D,F} = H^C_{20,m+n+l} - H^C_{16}.$$

However, if the transition time of organic matter particles from one layer to another is short compared with D_s, then it is better to take $H^C_{20,i} = \lambda_1 C_{a,i}$, $H^C_{16,i} = \lambda_4 C_{F,i}$. In addition to these fluxes we should take into account the fluxes of detritus decomposition, solution of bottom sediments, and carbon consumption in the process of photosynthesis:

$$H^C_{17,i} = \text{const}, \qquad H^C_{18,i} = \lambda_3 D_{L,i}, \qquad H^C_{22,i} = \lambda_3 D_{U,i}, \qquad H^C_{21,i} = C_{31} R_{\Phi,i}.$$

Estimates of modeled parameters of particular oceanic processes of the carbon cycle range widely. For instance, from the data of various authors the estimates of assimilation of carbon from the hydrosphere in the process of photosynthesis range from 10 GtC/yr to 155 GtC/yr. The value 127.8 GtC/yr is most widely used. However, because of large variations in these estimates, calculation of the C_{31} coefficient is fraught with great uncertainty; therefore, specifying it requires numerical experiments using other, more accurate data.

Finally, let us suppose that the surface layers of the ocean are filled with carbon due to its run-off from the land $H^C_{24,i} = C_7 W_{si0}$, $H^C_{23,i} = C_8 W_{Hi0}$, where W_{si0} and W_{Hi0} are river and underground run-offs into the World Ocean, respectively.

Considering the notations in Figure 3.6, the balance equations to describe the global carbon cycle are written as:

$$\frac{\partial C_A}{\partial t} = H_5^C - V_\varphi \frac{\partial C_A}{\partial \varphi} - V_\lambda \frac{\partial C_A}{\partial \lambda} + \begin{cases} -H_2^C + H_3^C, & (\varphi,\lambda) \in \Omega_0; \\ H_1^C + H_4^C - H_6^C + \sum_{i=7}^{11} H_i^C, & (\varphi,\lambda) \in \Omega \setminus \Omega_0; \end{cases}$$

$$\frac{\partial C_{S1}}{\partial t} = H_6^C - H_7^C - H_8^C - H_{14}^C - H_{15}^C;$$

$$\frac{\partial C_{S2}}{\partial t} = \sum_{i=1}^{4} H_{i+11}^C - H_4^C - H_9^C - H_{23}^C - H_{24}^C;$$

$$\frac{\partial C_U}{\partial t} + v_\varphi^U \frac{\partial C_U}{\partial \varphi} + v_\lambda^U \frac{\partial C_U}{\partial \lambda} = Q_U + H_{22}^C + H_{25}^C - H_{21,U}^C - H_3^C + H_2^C + H_{19,U}^C - H_{20,U}^C;$$

$$\frac{\partial C_P}{\partial t} + v_\varphi^P \frac{\partial C_P}{\partial \varphi} + v_\lambda^P \frac{\partial C_P}{\partial \lambda} = H_{19,P}^C - H_{19,U}^C + H_{20,U}^C - H_{20,P}^C - H_{21,P}^C + H_{22}^C + H_{25}^C;$$

$$\frac{\partial C_L}{\partial t} + v_\varphi^L \frac{\partial C_L}{\partial \varphi} + v_\lambda^L \frac{\partial C_L}{\partial \lambda} = H_{18,L}^C + H_{19,L}^C - H_{19,P}^C + H_{20,P}^C - H_{20,L}^C;$$

$$\frac{\partial C_F}{\partial t} + v_\varphi^F \frac{\partial C_F}{\partial \varphi} + v_\lambda^F \frac{\partial C_F}{\partial \lambda} = H_{17}^C - H_{16}^C + H_{18,F}^C - H_{19,L}^C + H_{20,L}^C.$$

Flux Q_U is formed from H_{23}^C and H_{24}^C. Let $Q_U = 0$ for the pelagic regions Ω_{OP} of the World Ocean. Let us describe the formation of Q_U on marginal shelves by a simple algorithm with the supposed uniform distribution of the sink from the Kth region to the Mth water basin:

$$Q_U = \begin{cases} 0, & (\varphi,\lambda) \in \Omega_{OP}, \\ (H_{23}^C + H_{24}^C)\sigma_{OP}/\sigma_L, & (\varphi,\lambda) \in \Omega_O \setminus \Omega_{OP}, \end{cases}$$

where σ_{OP} and σ_L are the areas of the water basins Ω_{OP} and Ω_L, respectively.

3.4.3 The organic carbon cycle in the ocean ecosystem

Each element of ocean ecosystem A can be described by a number of parameters, and the connection between elements can be presented as that between the respective parameters. Then, on the whole, ecosystem A can be described by N time-dependent parameters $x^*(t) = \{x_j(t), j = 1, \ldots, N\}$. The structure $|A(t)|$ and behavior $\overline{A}(t)$ of ecosystem A, which can be observed in more or less detail, are functions of these parameters. Therefore, the ecosystem itself $A(t) = \{|A(t)|, \overline{A}(t)\}$, as a combination of structure and behavior, is a function of these parameters:

$$A(t) = F(x^*(t)). \tag{3.15}$$

Hence, according to (3.15), with a change in time t, ecosystem A will be characterized by a trajectory in $(N+1)$-dimensional Euclidian space. Let us consider the following abstract formation as a model of ecosystem $A(t)$:

$$A_M(t) = F_M(x^{*,M}), \tag{3.16}$$

which depends on $M \leq N$ components of the vector $x^*(t)$ ($\{x^{*,M}(t)\} \in \{x^*(t)\}$) and considers all the connections existing between them.

The nearer M is to N and the more completely the connections between the components of vector $x^{*,M}(t)$ are taken into account, the less is the disagreement between the trajectories of ecosystem $A(t)$ and its model $A_M(t)$. The latter can be measured by any natural measure (e.g., by the maximum absolute difference of all the respective coordinates of trajectories or by the integral of absolute difference of all respective coordinates for a final time period). In other words, let us introduce a goal functional

$$V = Q(\{x_i(t)\}) \tag{3.17}$$

on the trajectory of ecosystem $A(t)$. The form of Q function is determined by the requirements made by system A on the environment. The natural evolutionary process is considered to lead to an optimal system, and therefore system $A_{opt,M}(t)$, which ensures an extremum of the functional (3.17), can be considered an optimal model of ecosystem A.

The extent of disagreement between the trajectories of ecosystem A and an optimal model $A_{opt,M}(t)$ is affected by the degree of correspondence of the goal functional V chosen by the relationship (3.17) to the real goal $\underline{A}$ of ecosystem A. The set $\underline{G} = \{\underline{A}_1, \ldots, \underline{A}_r, \ldots, \underline{A}_m\}$ of possible reliable goals $\{\underline{A}_r\}$ of the ecosystem can be derived on the basis of experience accumulated by oceanologists. Then, determining:

$$A_{opt,M,r} = g_r(\underline{A}_r), \quad \underline{A}_r \in \underline{G},$$

we obtain a limited assembly of possible optimal systems $A_{opt,M,r}$ ($r = 1, \ldots m$), whose trajectories together with the trajectory of ecosystem A are within the space of possible trajectories. If we find $A_{opt,M,r0}$, whose trajectory has a minimum disagreement with $A(t)$, then, based on this, we can find the most reliable goal of the ecosystem

$$\underline{A}_{r0} = (g_r)^{-1}(A_{opt,M,r0}(t)).$$

According to the principles mentioned above, the derivation of a numerical model of ocean ecosystem A requires either a detailed description of its states or derivation of an adequate complex of numerical models of energy exchange between the trophic levels taking place in A, as well as the interactions of biotic, abiotic, and hydrophysical factors. Of course, in this case an availability of a certain set of hypotheses is assumed concerning the character of the balanced relationship in ecosystem A.

The basic hypothesis is that in ecosystem A the only original source of energy and matter for all forms of life is solar radiation energy (E). According to numerous theoretical and experimental studies, sunlight penetration into deep layers of the

ocean follows an exponential law:

$$E = uE_0 \exp\left[-\int_0^z \{\delta p(\varphi, \lambda, x, t) + \beta d(\varphi, \lambda, x, t) + \nu Z(\varphi, \lambda, x, t)\}\, dx - \alpha z\right] + (1-u)E_0 \exp(-\zeta z), \tag{3.18}$$

where $E_0 = E(\varphi, \lambda, 0, t)$ is light reaching the ocean surface; α is the coefficient of light absorption as it filters through seawater; δ, β, and ν are the coefficients of light attenuation due to phytoplankton (p), detritus (d), and zooplankton (Z), respectively; u and ζ are the parameters chosen in a given situation to bring $E(\varphi, \lambda, z, t)$ closer to the real pattern of illumination changing with depth. Note that here the impact of the biomass of other trophic levels on water transparency is considered to be negligibly small.

Illumination affects the rate of photosynthesis R_p. The R_p parameter as a function of E has a maximum at some optimal value of E_{max}, which drifts from this critical value when illumination increases or decreases. The maximum R_p at various latitudes φ is located at depths that vary as a function of season (i.e., sun elevation). Thus, in tropical zones this variability with depth is most pronounced. On average, the photosynthesis maximum is located at depths of 10 m–30 m, and in open water bodies it can be observed at depths below 30 m. Here $E_{max} = 65\,\text{cal}\,\text{cm}^{-2}\,\text{da}^{-1}$–$85\,\text{cal}\,\text{cm}^{-2}\,\text{da}^{-1}$. At depths where $E = 20\,\text{cal}\,\text{cm}^{-2}\,\text{da}^{-1}$–$25\,\text{cal}\,\text{cm}^{-2}\,\text{da}^{-1}$, photosynthesis decreases in proportion to E. An apparent suppression of phytoplankton by light is observed at $E > 100\,\text{cal}\,\text{cm}^{-2}\,\text{da}^{-1}$. These estimates are quite different in northern latitudes, where the photosynthesis maximum is located, as a rule, at the surface.

The rate of photosynthesis at depth z depends on water temperature T_W, concentration of nutrient salts n, and phytoplankton biomass p, as well as on other factors, which are not considered here. To express this dependence, various equations are used, which reflect the limiting role of elements E, n, and p. Considering that $\partial p/p\,\partial z \to 0$ at $n \to 0$ as $\partial p/p\,\partial z \to$ const with increasing n, let us take the following function as the basic one to describe photosynthesis intensity at depth z:

$$R_p(\varphi, \lambda, z, t) = k_0(T_W) K_T f_2(p) f_3(n), \tag{3.19}$$

where

$$K_T = Af_1(E), \qquad A = kA_{max}/E_{max}, \qquad f_1(E) = E \cdot \exp[m(1 - E/E_{max})],$$
$$f_2(p) = [1 - \exp\{-\gamma_1 p\}], \qquad f_3(n) = [1 - \exp\{-\gamma_2 n\}]^{\theta}, \tag{3.20}$$

where k is the proportion coefficient; $k_0(T_W)$ is the function characterizing the dependence of photosynthesis rate on water temperature T_W; A_{max} is an assimilation number in the region of maximum photosynthesis (increment per unit weight of phytoplankton organisms); γ_1, γ_2, θ, and m are constants, the choice of which can determine the species characteristics of phytoplankton elements. For A_{max} the following estimates are valid: $A_{max} = 5.94E_{max}$ in the region of the photosynthesis minimum and $2.69E_{max}$ for other regions. According to these estimates, assimilation by the number of tropical phytoplankton in the region of maximum

photosynthesis averages $11\,\mathrm{mgC\,hr^{-1}}$–$12\,\mathrm{mgC\,hr^{-1}}$. Thus, for the Peru upwelling $A_{max} = 6.25\,\mathrm{mgC\,hr^{-1}}$. The light saturation of photosynthesis in equatorial regions is reached at $9\,\mathrm{cal\,cm^{-2}\,da^{-1}}$.

As for the dependence of $k_0(T_W)$, the specific intensity of phytoplankton photosynthesis first increases as temperature change increases, reaching at some point an optimal value for p, and then, as temperature further increases it begins to decrease. Near the maximum the following approximation is often used:

$$k_0(T_W) = \exp\{(T_W - T_{W,opt})\ln(\theta_0)\}, \quad 0 < \theta_0 \leq 2.$$

The dependence of the rate of photosynthesis on the concentration of nutrient elements $n(\varphi, \lambda, z, t)$ (phosphorus, silicon, nitrogen, and others), expressed in Formula (3.19) by the exponential term, is, of course, more complicated. Nutrient elements are among the most important parts of the ecosystem, since they regulate the energy flux in the ecosystem. Nutrient element supplies are spent in the process of photosynthesis at a rate R_n, usually approximated by the expression $R_n = \delta R_p$, where δ is the proportion coefficient. Nutrient element supplies are replenished due to their uplift from deep waters, where they build up as a result of the chemical processes of dead organic matter decomposition. This process is controlled by several abiotic conditions characteristic of various climatic zones of the World Ocean. The vertical flux of nutrient elements is determined by conditions of water mixing. In tropical zones, where the vertical structure of the water has a clear three-layer configuration in one of which the temperature leaps suddenly (the thermocline), the vertical motion of nutrient elements is confined to this layer. In water bodies where the thermocline is located at depths of 40 m–100 m, the upper layer is usually poor in nutrient elements, and their input to this layer takes place only in upwelling zones. In this case the average rate of uplift of vertical water beneath the thermocline varies from 10^{-3} cm/s to 10^{-2} cm/s, and in upwelling zones (where it breaks through the thermocline) it can reach $0.1\,\mathrm{cm\,s^{-1}}$.

The whole volume of oceanic water is considered as a single biocenosis in which the flux of organic matter produced in surface layers then descending to the bottom of the ocean is the main connecting factor. All model parameters are assumed to be able to change as functions of place and time, and their parametric description is made by average characteristics (i.e., deterministic models).

Let us suppose the food bonds between trophic levels are adequately described by the Ivlev model (i.e., the consumption of various kinds of food by the ith trophic level is proportional to the efficiency of their biomasses). Taking into account the diagram of food bonds developed by Kondratyev *et al.* (2003b) and the structure of the trophic pyramid of a typical ocean ecosystem, we can consider each trophic level in detail.

Bacterioplankton b play an important role in the trophic chains of the ocean. According to available estimates, no fewer than 30% of bacterioplankton are in natural masses exceeding 3 μ–5 μ in size, therefore acting as good for filtrates. This fact must be taken into account when deriving a model of the ecosystem, since in many regions of the World Ocean bacteria production is comparable with the production of phytoplankton. Bacteria, occupying a special place in the trophic pyramid, differ by variable exchange, strongly decreasing with the shortage of food,

which is followed by respective decrease in the rate of their growth. The food for bacteria consists mainly of detritus d and the dissolved organic matter g emitted by phytoplankton. As a result, food for bacteria can be described by the Ivlev formula:

$$R_b = k_b b[1 - \exp(-k_{1,d} d - k_{1,g} g), \tag{3.21}$$

where k_b, $k_{1,d}$, and $k_{1,g}$ are coefficients determined experimentally.

The equation describing the dynamics of the bacterioplankton biomass is written in the form:

$$\begin{aligned}\partial b/\partial t + V_\varphi\, \partial b/\partial\varphi + V_\lambda\, \partial b/\partial\lambda + V_z\, \partial b/\partial z \\ = R_b - T_b - M_b - \sum_{s\in\Gamma_b} C_{bs} R_s + k_{2,\varphi}\, \partial^2 b/\partial\varphi^2 + k_{2,\lambda}\, \partial^2 b/\partial\lambda^2 + k_{2,z}\, \partial^2 b/\partial z^2,\end{aligned} \tag{3.22}$$

where T_b and M_b are losses in bacterioplankton biomass due to energy exchange with the environment and dying-off; Γ_b is the trophic level subordinate to bacterioplankton (in a typical case Γ_b is an element of Z); and $C_{b,s}$ is the share of bacterioplankton in the food ration of the sth element of the ecosystem. The parameters T_b and M_b are described by the following relationships:

$$T_b = t_b b, \tag{3.23}$$

$$M_b = \max\{0, \mu_b (b - \underline{B}_b)^\xi\}, \tag{3.24}$$

where t_b is the specific expenditure as a result of exchange with the environment; μ_b is the rate of bacteria dying off; $\underline{B}_b$ and ξ are constants that determine the dependence of the intensity of bacteria dying off on their concentration. The coefficient $k_2 = (k_{2,\varphi}, k_{2,\lambda}, k_{2,z})$ determines the process of the turbulent mixing of ocean waters.

The dynamic equation for the phytoplankton biomass is:

$$\begin{aligned}\partial p/\partial t + V_\varphi\, \partial p/\partial\varphi + V_\lambda\, \partial p/\partial\lambda + V_z\, \partial p/\partial z \\ = R_p - T_p - M_p - \sum_{s\in\Gamma_p} C_{ps} R_s + k_{2,\varphi}\, \partial^2 p/\partial\varphi^2 + k_{2,\lambda}\, \partial^2 p/\partial\lambda^2 + k_{2,z}\, \partial^2 p/\partial z^2,\end{aligned} \tag{3.25}$$

where Γ_p is the trophic level subordinate to phytoplankton; C_{ps} is the share of the phytoplankton biomass in the food ration of the elements of the sth trophic level of the ecosystem; T_p is expenditure as a result of energy exchange with the environment; M_p is the dying-off of phytoplankton cells. The latter parameters are determined by the following relationships:

$$M_p = \max\{0, \mu_p (p - \underline{p})^\theta\}, \tag{3.26}$$

$$T_p = t_p p, \tag{3.27}$$

where t_p is the specific expenditure on respiration of the phytoplankton cells; μ_p is the coefficient of phytoplankton dying off; $\underline{p}$ and θ are coefficients characterizing the dependence of the rate of the phytoplankton cell dying off on their concentration.

Zooplankton are an important trophic element in the ocean ecosystem presented at an integral level Z which implies the presence of a large number of sub-levels with untersecting trophic bonds. Zooplankton feed on phytoplankton and bacterioplankton, and are themselves food for nekton r and detritophages D.

Let us describe the zooplankton ration by the Ivlev formula:

$$R_z = k_Z(1 - \exp[-\nu\overline{B}]), \tag{3.28}$$

where $\overline{B}$ is the biomass of accessible food ($\overline{B} = \max\{0, B - B_{min}\}$); k_Z is the maximum ration with plenty of food; ν is the coefficient characterizing the level of starvation. Maximum ration is assumed to be equal to the need for food, which, in turn, is determined by exchange intensity T_1 and maximum possible increment P_1 at a given intensity of exchange. The latter two parameters are related to the coefficient $q_2 = P_1/(P_1 + T_1)$, so that we obtain:

$$k_Z = T_1 u(1 - q_{2,max}),$$

where $1/u$ is food assimilation; and $q_{2,max} = \max q_2$.

Formula (3.28) implies that with a small amount of food the zooplankton ration grows in proportion to the amount of food, then, as the ration approaches its maximum of k_Z, its dependence on B diminishes. Since one trophic level never totally consumes another, there is a limitation in (3.28) that establishes $R_Z = 0$ at $B \leq B_{min}$, where B_{min} is the minimum unconsumed food biomass. In (3.26) the $\underline{p}$ parameter plays the same role but this time in the process of the dying-off of phytoplankton cells.

Thus, a change in zooplankton biomass follows the law described by the following differential equation:

$$\begin{aligned}\partial Z/\partial t + V_\varphi\, \partial Z/\partial\varphi + V_\lambda\, \partial Z/\partial\lambda + V_z\, \partial Z/\partial z \\ = R_Z - T_Z - M_Z - H_Z \sum_{s\in\Gamma_Z} C_{Zs}R_s + k_{2,\varphi}\, \partial^2 Z/\partial\varphi^2 + k_{2,\lambda}\, \partial^2 Z/\partial\lambda^2 + k_{2,z}\, \partial^2 Z/\partial z^2,\end{aligned} \tag{3.29}$$

where Γ_Z is the trophic level subordinatte to zooplankton; C_{Zs} is the share of the zooplankton biomass in the food ration of the sth trophic level; H_Z, T_Z, and M_Z are the losses in zooplankton biomass due to unconsumed food, expenditures on respiration, and dying-off, respectively. Let us describe the latter three parameters by the relationships:

$$H_Z = h_Z R_Z, \qquad T_Z = t_Z Z, \qquad M_Z = (\mu_Z + \mu_{Z,1} Z)Z, \tag{3.30}$$

where the coefficients h_Z, t_Z, μ_Z, and $\mu_{Z,1}$ are determined empirically for a given species of zooplankton.

As seen from (3.29), zooplankton are considered passive elements of the ecosystem subject to physical processes of transference in space as a result of water movement. However, zooplankton are known to migrate mainly in the vertical direction. In the given model we can use a simple mechanism to simulate the process of vertical migration of zooplankton. For this purpose, we divide the whole water thickness into two layers: $0 \leq z \leq z_0$ and $z_0 < z \leq H$. Let us suppose that zooplank-

ton migration between these layers depends on food availability; that is, some of the zooplankton from the layer $[z_0, H]$ can satisfy their need of food in the layer $[0, z_0]$. This means that by taking B_{min} into account the whole vertical profile $B(\varphi, \lambda, z, t)$ is considered.

Let us determine the coefficients C_{as} $(a = p, Z)$ in Formulas (3.25) and (3.29) by supposing that the consumption of various kinds of food in the sth trophic level is proportional to the efficiency of their biomasses:

$$C_{as} = k_{sa}\overline{B}_a \left[\sum_{a \in S_z} k_{sa}\overline{B}_a\right]^{-1}, \tag{3.31}$$

where $\overline{B}_a$ is the efficiency of the biomass at consuming ath food; S_s is the trophic level subordinate to the sth component; and k_{sa} is the proportion coefficient that determines the significance of the sth constituent in the food ration of the ath element.

The equations to describe the dynamics of the biomass of nekton, detritovores, detritus, dissolved organic matter, and nutrient salts will be

$$\partial r/\partial t = R_r - H_r - T_r - M_r - \sum_{s \in \Gamma_r} C_{rs}R_s, \tag{3.32}$$

$$\partial D/\partial t = R_D - H_D - T_D - M_D - \sum_{s \in \Gamma_D} C_{Ds}R_s, \tag{3.33}$$

$$\begin{aligned}\partial d/\partial t + V_\varphi\,\partial d/\partial\varphi + V_\lambda\,\partial d/\partial\lambda + V_z\,\partial d/\partial z = {} & M_b + M_D + M_r + M_p + M_Z \\ & + H_Z + H_r + H_D - \mu_d d - C_{dD}R_D \\ & + k_{2,\varphi}\,\partial^2 d/\partial\varphi^2 + k_{2,\lambda}\,\partial^2 d/\partial\lambda^2 \\ & + k_{2,z}\,\partial^2 d/\partial z^2,\end{aligned} \tag{3.34}$$

$$\begin{aligned}\partial n/\partial t + V_\varphi\,\partial n/\partial\varphi + V_\lambda\,\partial n/\partial\lambda + V_z\,\partial n/\partial z = {} & \mu_d d - \delta R_p + k_{2,\varphi}\,\partial^2 n/\partial\varphi^2 + \rho_g g \\ & + k_{2,\lambda}\,\partial^2 n/\partial\lambda^2 + k_{2,z}\,\partial^2 n/\partial z^2,\end{aligned} \tag{3.35}$$

$$\begin{aligned}\partial g/\partial t + V_\varphi\,\partial g/\partial\varphi + V_\lambda\,\partial g/\partial\lambda + V_z\,\partial g/\partial z = {} & T_p + T_b + T_r + T_D + T_Z - C_{gb}R_b \\ & + k_{2,\varphi}\,\partial^2 g/\partial\varphi^2 + k_{2,\lambda}\,\partial^2 g/\partial\lambda^2 \\ & + k_{2,z}\,\partial^2 g/\partial z^2,\end{aligned} \tag{3.36}$$

where $H_a = (1 - h_a)R_a$ is the unassimilated food of the ath element $(a = r, D)$; $T_a = t_a a$ is the expenditure on energy exchange; $M_a = (\mu_a + \mu_{a,1}a)a$ is dying-off; ρ_g is the indicator of the rate of replenishing the supplies of nutrient elements as a result of decomposition of dissolved organic matter; and δ is the coefficient of consumption of nutrient elements in the process of photosynthesis.

As follows from (3.32) and (3.33), a supposition is made in the model that nekton and detritophages do not move in space with the motion of water masses. These elements are assumed to migrate independently of the hydrophysical conditions of their environment. Consider two possible versions of modeling the processes of

migration. The first version is connected with addition to the right-hand sides of Equations (3.32) and (3.33) of terms describing turbulent mixing by coefficients $k_2^* > k_2$. In other words, the process of migration is identified with the process of intensified turbulent mixing (i.e., it is accidental). However, the process of fish migration manifests some expediency in the choice of direction of movement. According to the biological principle of adaptation, the migration of fish is subject to the principle of complex maximization of the food ration, with environmental parameters keeping within the conditions of their habitat. Hence, the motion of fish in space at characteristic velocities ensures their locations in regions where at that moment in time food and other abiotic conditions (temperature, salinity, dissolved oxygen, chemical concentration) are most favorable. This means that fish migrate in the direction of a maximum gradient of accessible food with the preserved limitations of environmental parameters.

3.5 CARBON EXCHANGE PROCESSES AT THE ATMOSPHERE–LAND BOUNDARY

The interaction between two carbon reservoirs, the atmosphere and land, is expressed by carbon fluxes formed as a result of ecological, geophysical, and geochemical processes, including photosynthesis, respiration of plants and animals, decomposition of dead organic matter, vegetation, and fuel burning, volcanic emanations, rock weathering, etc. Which of these processes prevails depends on many factors, such as wind direction and strength (Wang *et al.*, 2005). Therefore, in the scheme of Figure 3.7 and in Table 3.3 they are all taken into account.

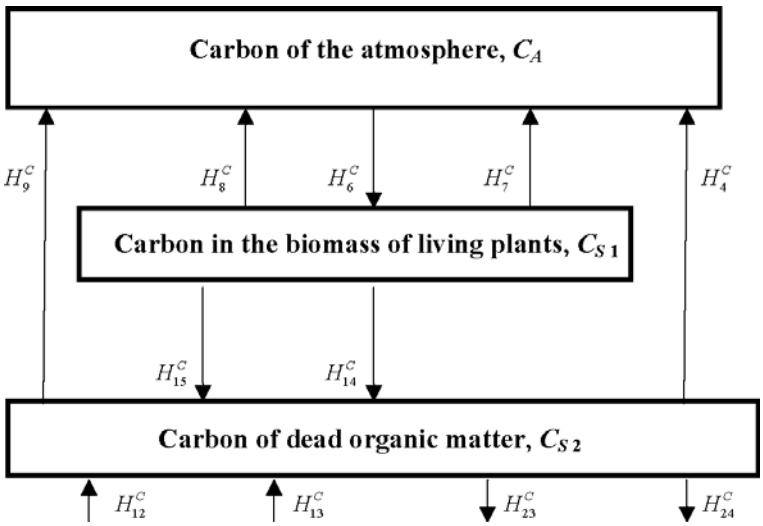

Figure 3.7. The scheme for carbon fluxes in the model of the atmosphere–vegetation–soil system.

The most important aspect in studying the global carbon cycle is the contribution of the interaction between surface vegetation and the atmosphere to CO_2 exchange. This dependence is based on the fact that all plants create their biomass by assimilating atmospheric constituents C, O_2, H, N, S, P, K, Ca, Mg, Fe, among which the most important are carbon, oxygen, nitrogen, and sulfur. Clearly, in a detailed analysis of the process of photosynthesis we should take into account the kinetics of CO_2, CH_4, H_2O, H_2S, NH_3, and NO_2. A minimum requirement for ensured CO_2 assimilation is the availability of CO_2, H_2O, light, chlorophyll, and proper environmental conditions (temperature and humidity). Therefore, the complex assimilation formula can be written as follows:

$$\underset{\substack{\text{moles 6}\\ 246\,\text{g}}}{CO_2} + \underset{\substack{\text{moles 12}\\ 216\,\text{g}}}{H_2O} + \underset{\text{Sun energy}}{675\,\text{kcal}} \rightarrow \underset{\substack{\text{moles 11}\\ 180\,\text{g}}}{C_6H_{12}O_6} + \underset{\substack{\text{moles 6}\\ 192\,\text{g}}}{O_2} + \underset{\substack{\text{moles 6}\\ 108\,\text{g}}}{H_2O}$$

This formula can be used to calculate the balance between plants and the atmosphere for CO_2 exchange, but cannot be used for water, since water is a limiting factor for photosynthesis. The plants use much more water because of transpiration. In global models the process of carbon assimilation should be detailed carefully to avoid violating a balanced description of other processes. Usually this is brought about by introducing the needed corrections (Krapivin and Kondratyev, 2002). For instance, possible losses in the balanced relationship for photosynthesis are taken into account. These losses are assumed to be 20%–30%; that is, on average, 6 mol CO_2 give 0.75 mol of glucose.

It is also necessary to consider the spatial heterogeneity of the Earth land covers, which differ in biomass density and the intensity of organic matter formation. On average, 90% of the total biomass ($\approx$830 GtC) are forests ($\approx 50 \cdot 10^6\,\text{m}^2$), 50% of this value constituting tropical forests ($\approx 24.5 \cdot 10^6\,\text{m}^2$), and only 10% ($\approx$84 GtC) refer to scrub, savannahs, meadows, deserts, semi-deserts, marshes, and cultivated lands. The process of organic matter formation is highly inhomogeneous: forests produce 33 GtC/yr, the remaining vegetation 20 GtC/yr. These heterogeneities lead to mosaic patterns in bioproductivity and therefore should be taken into account when synthesizing a model. For instance, from estimates of Saito *et al.* (2005), in a rice field in the period of maximum development of leaves, CO_2 assimilation from the atmosphere can reach 39 $\text{gCO}_2\,\text{m}^{-2}\,\text{da}^{-1}$, with high variability during the vegetation period. On the whole, the vegetation period in a rice field in central Japan lasts for about 100 days, from late May to late August. And during the remaining 70% of the year the rice fields serve as a CO_2 sink. The ratio of net primary production to losses from respiration in the rice fields constitutes 1.53 in the vegetation period and 0.43 in the post-harvest period. Knowledge of such details for other ecosystems is a necessary condition for accurate assessment of their role in the global biogeochemical carbon cycle.

The relationship between the global CO_2 cycle and land vegetation is manifested by the dependence of primary production and the rate of dead biomass decomposition on temperature and CO_2 concentration in the atmosphere. Temperature dependence is most apparent in northern latitudes where global mean temperature

variations can range up to 85°C, and the vegetative period of plants changes from 2 to 7 months. On the whole, the frequency of high air temperatures has increased in recent decades, and this should bring about changes in pure production in temperate and boreal forests, which affects the atmosphere–land exchange of CO_2 and solar energy (Granta *et al.*, 2005).

Nalder and Wein (2006) proposed a model of the carbon dynamics in a boreal forest in the west of Canada. The model was based on the algorithm of forest litter decomposition used in the model "Century", which parameterizes the dynamics of soil organic matter and at the same time taking its stratified structure into account. In the case considered, the forest litter and reservoirs of carbon in mineral-rich soil were discretized in accordance with the age structure of trees. It was shown that to improve the model description of the carbon cycle in a forest ecosystem, specified data are needed on the dynamics of dying-off of the root system and trees themselves, as well as the nitrogen balance of this system. Again, this conclusion confirms that available estimates of the CO_2 sink and sources on land are far from ideal, and their specification is only possible within the framework of the GMNSS (Kondratyev *et al.*, 2003b).

Ito *et al.* (2005) developed a model to simulate diurnal fluxes of CO_2 in a cool-temperate deciduous forest at one of the 25 sites of the AsiaFlux network in Japan (near Takayama). The proposed model was based on modifying the Sim-Cycle model of the carbon cycle to specify the seasonal and interannual variations of physiological processes. Also, the modification predicted selection of 12 reservoirs of carbon at a chosen site, including the canopy of fallen trees, evergreen undergrowth, litter, and mineral-rich soil. The model took into account the dependence of primary production on temperature, soil moisture, and CO_2 concentration. Calculations showed that at one forest site there were considerable seasonal oscillations in CO_2 fluxes. In particular, in late autumn, the forest ecosystem became a source of CO_2 delivering to the atmosphere $1\,gC\,m^{-2}\,da^{-1}$. On average, during the period of studies 1999–2002, the forest test site was a sink of atmospheric CO_2 ($206\,gC\,m^{-2}\,da^{-1}$). This study showed that in modeling the biogeochemical cycle of carbon in deciduous forests, it is necessary to describe in more detail the seasonal dynamics of forest ecosystems. Kitao *et al.* (2007) emphasized the importance of considering the vertical profiles of a forest ecosystem's base elements.

Lee *et al.* (2005) estimated CO_2 fluxes in a forest near Takayama on the basis of root system respiration using the polynomial constituent of the regression model, which took into account the temperature and moisture of the soil and reflected the hourly regime of soil respiration. It was shown that the contribution of the forest root system to soil CO_2 flux ($1.06\,kgC\,km^{-2}\,yr^{-1}$) constitutes 45% ($0.48\,kgC\,km^{-2}\,yr^{-1}$). This highlights the importance of reflecting the role of the root system in models of forest ecosystems as an independent element of the ecosystem.

Within the framework of the AsiaFlux program, Saigusa *et al.* (2005) measured the CO_2 fluxes since 1993 in the forest ecosystem of Takayama using an aerodynamic method to estimate the vertical gradient of CO_2 concentration and a vortex divergence method to calculate the coefficient of diffusion over the forest canopy. Also, measurements were made of vortex fluxes of sensible heat, water vapor, and CO_2.

Pure production in the forest ecosystem in 1999, 2000, and 2001 constituted 198–251 $gC\,m^{-2}\,yr^{-1}$, 309–376 $gC\,m^{-2}\,yr^{-1}$, and 290–342 $gC\,m^{-2}\,yr^{-1}$, respectively. The uncertainty in these estimates was probably caused by nighttime periods either being considered or ignored when calculating plant production. Pure production averaged over the period 1994–2002 constituted $237 \pm 92\,gC\,m^{-2}\,yr^{-1}$. The highest level of productivity of the forest was recorded in 1998 ($329\,gC\,m^{-2}\,yr^{-1}$) and in 2002 ($346\,gC\,m^{-2}\,yr^{-1}$) mainly due to the high rate of CO_2 assimilation in the first half of each year, when springs were warm due to El Niño.

The impact of atmospheric CO_2 on the growth of plants depends on many factors. There are two basic types of plants classified by the form of their reaction to changes in the partial pressure of atmospheric CO_2. The first, most widespread type of plants (type C_3) is characterized by photorespiration brought about by fermentation, which can simultaneously assimilate and emit CO_2 and O_2. This process has a so-called compensation point Γ, when the balance of all functions of the plant with respect to CO_2 concentration (C_a) is optimal. This point is characterized by the value $\Gamma \cong 50\,mmol\,mol^{-1}$ at 25°C, grows with growing temperature, is proportional to the value $(C_a - \Gamma)$ up to the level $1{,}000\,mmol\,mol^{-1}$, and has an efficiency in the initial use of light that increases with increasing CO_2 in proportion to $(C_a - \Gamma)/(C_a + \Gamma)$ (Goudrian *et al.*, 1990).

Plants of the other type (C_4), such as tall tropical grass (maize, sugar cane, millet, sorgo), assimilate CO_2 from the atmosphere independently of O_2 concentration, so that Γ remains practically constant and at a low level $\cong 5\,mmol\,mol^{-1}$. These plants react weakly to changes in the concentrations of carbon dioxide.

Numerous laboratory studies of the response of plants of both types to a change in the quantity C_A (Bazzaz, 1986) testify to the wide range of quantitative estimates of photosynthesis variations for the C_3 type. On average, plants respond to a change in CO_2 concentration after a 1-month delay. Doubled CO_2 concentration causes a doubling of the rate of photosynthesis. Further increase of C_A up to 400% leads to the effect of photosynthesis saturation for some plants (i.e., there can be a 20% addition to the rate of photosynthesis), and in some cases (e.g., *Setaria lutescens*) photosynthesis is suppressed. In fact, plants of the C_4 type even with the present quantity of C_A are in a state of photosynthesis saturation.

Hattas *et al.* (2005) studied the impact of changes in atmospheric CO_2 concentration on subtropical grass ecosystems, considering plants of both types (C_3 and C_4) and showed that the content of various elements in plants change non-uniformly with the growing content of atmospheric CO_2. The C/N and C/P ratios in both types of plants grow as CO_2 increases. From estimates obtained in Jones *et al.* (2005), the role of grass ecosystems in regulating the greenhouse effect was strongly underestimated, especially in the case of controlled meadows/pastures. It was shown that fluxes of CO_2, N_2O, and CH_4 depend strongly on the type of fertilizers applied. In the case of inorganic fertilizers, a meadow emits N_2O ($388\,gN_2O\text{–}N\,ha^{-1}\,da^{-1}$), and organic fertilizers increase the N_2O flux up to $3{,}488\,gN_2O\text{–}N\,ha^{-1}\,da^{-1}$.

There are many effects of CO_2 on plants that manifest themselves by changes in the nutrient regime of photosynthesis. Table 3.6 exemplifies this effect. Of course, the elemental composition of a plant's body varies. It includes C, O, H, N, S, P, K, Ca,

Table 3.6. Changing content of nutrient elements in trees as a result of a 2-year impact of changed CO_2 concentrations for *Acer pseudoplatanus* (A) and *Fugus sylvatica* (F). From Bazzaz (1986).

Chemical element	*CO_2 concentration* (mmol/mol)					
	370		520		670	
	A	*F*	*A*	*F*	*A*	*F*
N	1	1	1.09	1.11	1.17	1.21
P	1	1	1.10	1.33	1.20	1.50
K	1	1	1.15	1.21	1.27	1.33
Ca	1	1	1.17	1.13	1.25	1.23
Mg	1	1	1.14	1.22	1.29	1.22
Mn	1	1	1.00	1.08	1.07	1.25
Fe	1	1	1.43	1.17	1.54	1.50

Mg, Fe, and the exchange processes in the plant–atmosphere system include chemical compounds, such as CO_2, CH_4, H_2O, H_2S, NH_3, and NO_2. A living plant consists of 50%–95% of water, and the remaining part, the so-called dry substance, includes 70%–98% of organic substances that can burn. In other words, each plant on Earth plays a role of its own in the global biogeochemical cycle of CO_2 and other chemical elements. Therefore, all the existing models of the CO_2 cycle based on rough classifications of soil–plant formations are incorrect, and their reliability can hardly be assessed from the available data bases on vegetation cover and its parameters.

Dufrêne *et al.* (2005) developed a model called "Castanea" of a forest ecosystem consisting of *Castanea savita* and took into account the presence in the forest of the multi-layer physiological processes connected with carbon fluxes. The model describes the photosynthesis and transpiration of the forest canopy as well as the division of assimilators between leaves, branches, trunks, and roots as a function of evapotranspiration, heterotrophic respiration of soil, and soil balance of water and carbon. Net primary production (NPP) was calculated as the difference between general photosynthesis and plant respiration. The net ecosystem exchange (NEE) between the plant–soil system and the atmosphere was calculated as the difference between general photosynthesis and summed respiration (soil + plant). Input parameters for the model were global radiation, precipitation, wind speed, air temperature, and humidity. The "Castanea" model needs 150 input parameters. Uncertainty in the modeling results constituted 30% by NEE. This means that the model of the forest ecosystem "Castanea" is able to describe fluxes of CO_2 and N_2O in the atmosphere–plant–soil system to a rather high accuracy. The problem remains

to reproduce to the same accuracy the spatial distribution of vegetation and calculate the input parameters for the model (Davia *et al.*, 2005).

Dan *et al.* (2005) developed the AVIM model which combines the physical and biological components of the gas and energy exchange between the atmosphere and vegetation cover. The model has a spatial resolution of $1.5^\circ \times 1.5^\circ$ over the surface and selects in the atmosphere pixels 7.5° by longitude and 4.5° by latitude. The model gives stable results and can be used as a GMNSS unit.

Tundra and forest tundra biocenoses, which occupy about 4% of the global land surface, are quite special. Their role in the assimilation or emission of CO_2 is seasonal in character. Tundra with its marshes, water basins, and lakes is a source of CO_2 for the Arctic atmosphere. The soils of the Arctic tundra play a special role in this process. When snow melts they emit carbon monoxide (CO), and above the soil surface the CO partial pressure can reach 100 ppm with a mean annual value of 0.05 ppm (Kelley, 1987). The CO concentration in air bubbles produced in water bodies and lakes with a decaying biomass is estimated at 5 ppm–20 ppm. In spring, at the level of tundra plants the CO partial pressure in the air reaches 40 ppm, markedly decreasing by the end of summer. As a result, in spring, the CO_2 partial pressure in the near-surface atmosphere of the Arctic tundra can reach 2,100 ppm. What happens in winter to the CO_2 exchange at the atmosphere–tundra border is practically unknown. But there are data on photosynthesis and the respiratory activity of tundra vegetation, from which it follows that this activity continues even with illumination at $5\,W\,m^{-2}\,da^{-1}$–$7\,W\,m^{-2}\,da^{-1}$ and a temperature below zero. This means that the tundra vegetation in late summer and early winter can serve as a sink for atmospheric CO_2. The sink of CO_2 from the atmosphere due to assimilation by tundra vegetation is estimated at $146\,g\,m^{-2}\,da^{-1}$.

Large carbon supplies (about 400 GtC–500 GtC) are concentrated in northern soils and permafrosts which will escape in response to global warming. This necessitates an analysis of the carbon balance dynamics in these territories. In particular, the process of carbon storage by ecosystems in Alaska's tundra, which functioned as a sink of carbon (due to low temperature and sufficiently high soil moisture content, which favors a reduction in the rate of organic matter decomposition), changed direction as a result of global warming and climate dehydration in the early 1980s, and led to considerable losses of carbon. But, surprisingly, there are no reliable estimates of changes in the elements of the regional balance of carbon taking place in northern territories (Oechel *et al.*, 2000).

The role of tropical ecosystems in the global carbon cycle is rather uncertain, which is largely connected with the inadequately studied climatic impacts on carbon fluxes in these latitudes. Ichii *et al.* (2005) undertook an attempt to narrow these uncertainties by analyzing carbon fluxes for the period 1982–1999 in the Amazon, Africa, and Asia, using the Biome-BGC model developed at NCEP in the U.S.A. It was established that the observed interannual change in tropical ecosystem productivity is mainly caused by changes in solar radiation, temperature, and precipitation. It was shown that an increase in atmospheric CO_2 concentration leads to an increase in NPP, with solar radiation playing the dominating role in increasing the CO_2 sink of tropical forests.

Forest ecosystems in the Mediterranean basin play an important role in GCC regulation (Chiesi *et al.*, 2005). Therefore, many international programs on remote studies of land covers in these latitudes pay special attention to the formation of databases on the parameters and structures of vegetation in countries bordering the Mediterranean.

To assess the role of soil–plant formations in the global cycle of CO_2, models should have their spatial classification more detailed than is given, for example, in Figure 3.8. Unfortunately, current databases lack such information in a form acceptable for inclusion in the GMNSS. Therefore, published estimates of the role of soil–plant formations in the global model of the CO_2 cycle cannot be considered sufficiently accurate. However, the estimates of the role of land vegetation in Russia in assimilating excess CO_2 given in the work of Krapivin (1993) on the basis of this classification seem realistic.

Let $R_\kappa(\varphi, \lambda, t)$ be the photosynthesis production for vegetation of type κ at latitude φ and longitude λ at time moment t. Then, the CO_2 flux from the atmosphere to the living biomass can be described as

$$H_6^C(\varphi, \lambda, t) = C_{23} R_\kappa(\varphi, \lambda, t),$$

where the coefficient C_{23} reflects the efficiency of the mechanism of the photosynthesis response, which, on average, is estimated at $C_{23} \cong 0.549$. Bjorkstrom (1979) estimated the assimilation of CO_2 by vegetation with the formula:

$$H_6^C = k_b(1 + \beta \ln[C_A/C_A^*])C_\kappa,$$

where the parameter $\beta \in [0, 1]$ is the measurement of the ability of the vegetation system to react to an increase in atmospheric CO_2 partial pressure; C_k is the carbon content in the biomass of the kth type of vegetation; k_b is the coefficient of the amount of CO_2 that depends on temperature and the type of vegetation; and C_A^* is the concentration of carbon dioxide in the atmosphere in the pre-industrial period.

Various authors estimate flux $H_6^C(\varphi, \lambda, t)$ between 16.7 GtC/yr and 35 GtC/yr. This scatter of estimates is small enough to enable reliable estimation of the coefficients for approximating H_6^C. A more detailed description of H_6^C requires construction of an additional model unit, one that takes into account the relationship between CO_2 concentration and the functioning of surface biomes in a given territory. Such specifications were made in publications by Krapivin and Vilkova (1990), Nefedova and Tarko (1993), and Krapivin *et al.* (1996a, b). Empirical dependences have been used to specify function R_κ, as exemplified in Tables 3.7 and 3.8. The database of the modeling system contains similar information as well as data on the parameters for soil–plant formation. Of course, global data on the CO_2 balance in the biosphere are contradictory and incomplete. In Krapivin and Kondratyev (2002) regression formulas are given that enable calculation of productivity $F(T_a, W)$, humus supply $H(T_a, W)$, and phytomass supply $B(T_a, W)$ as a function

Table 3.7. Dependence of annual production ($kg\,m^{-2}\,yr^{-1}$) on mean global temperature and total precipitation amount, $F(T_a, W)$.

Precipitation, W (mm/yr)	*Atmospheric temperature,* T_a (°C)											
	−14	−10	−6	−2	2	6	10	14	18	22	26	30
3,125							3.4	3.5	3.7	3.8	3.9	4.0
2,875							3.2	3.3	3.5	3.6	3.7	3.8
2,625							3.0	3.2	3.3	3.4	3.5	3.6
2,375							2.8	2.9	3.0	3.1	3.2	3.3
2,125							2.5	2.6	2.7	2.9	2.9	3.0
1,875						1.6	2.3	2.3	2.4	2.5	2.6	2.7
1,625				0.4	0.6	1.3	2.0	2.1	2.1	2.2	2.3	2.4
1,375		0.2	0.3	0.4	0.7	1.1	1.7	1.9	1.9	2.1	2.1	2.0
1,125	0.2	0.3	0.3	0.4	0.6	1.0	1.6	1.8	1.9	1.8	1.8	1.7
875	0.2	0.3	0.4	0.5	0.8	0.9	1.5	1.4	1.3	1.3	1.2	1.2
625	0.3	0.3	0.5	0.6	0.9	0.9	0.9	0.8	0.8	0.7	0.7	0.7
375	0.4	0.4	0.5	0.7	0.6	0.6	0.6	0.5	0.5	0.5	0.4	0.4
125	0.1	0.3	0.3	0.2	0.2	0.2	0.2	0.2	0.2	0.1	0.1	0.1

of atmospheric temperature T_a (°C) and precipitation W (mm/yr):

$$F(T_a, W) = 4.25 \cdot 10^{-4} T_a^3 - 8.76 W^3 - 1.99 T_a^2 W + 4.29 T_a W^2 + 2.29 T_a^2 + 19.05 W^2 - 8.79 T_a W + 4.56 T_a - 14.16 W + 4.18;$$

$$H(T_a, W) = -5.16 T_a^3 - 161.4 W^3 - 9.41 T_a^2 W + 6.79 T_a W^2 - 9.47 T_a^2 + 199.51 W^2 - 4.37 T_a W + 7.47 T_a - 44.17 W + 4.93;$$

$$B(T_a, W) = -9.02 T_a^3 + 225.79 W^3 + 1.11 T_a^2 W - 29.39 T_a W^2 - 5.87 T_a^2 - 511.72 W^2 + 41.29 T_a W - 11.37 T_a + 356.97 W - 62.94.$$

The interaction of vegetation and the atmosphere is characterized by the CO_2 flux H_7^C that results from the process of respiration. Therefore, if T_κ denotes the loss of gross production by vegetation of type k in the process of respiration, then $H_7^C = C_{26} T_\kappa$. As a first approximation we can take $T_\kappa = \gamma B_\kappa$, where B_κ is the

Table 3.8. Dependence of humus content (kg/m^2) in a 1 m layer of soil on mean annual temperature and total precipitation amount $H(T_a, W)$.

Precipitation, W (mm/yr)	*Temperature, T_a* (°C)										
	−14	−10	−6	−2	2	6	10	14	18	22	26
3,000							21.9	21.8	21.2	21.1	19.8
2,750							22.4	22.4	22.4	21.2	20.3
2,500							22.5	22.5	22.4	21.3	20.6
2,250							22.6	22.6	22.5	21.5	20.7
2,000							22.7	22.7	22.7	21.5	20.9
1,750							22.8	22.7	22.7	21.6	21.1
1,500						15.6	22.8	22.8	22.7	21.6	21.3
1,250				6.0	6.1	16.2	23.2	23.0	22.9	21.7	21.4
1,000		5.0	5.0	6.5	6.1	16.9	25.8	24.1	23.1	22.5	22.2
750	1.0	5.5	6.0	11.0	21.5	35.1	25.1	24.0	23.1	23.1	22.3
500	1.0	6.1	7.4	9.1	19.1	58.3	45.1	23.3	19.2	14.3	18.2
250	1.1	6.1	7.5	11.0	13.5	14.3	10.1	5.2	3.4	1.1	1.0

vegetation biomass, and the product γC_{26} reflects the share of organic carbon emitted per unit time at the surface of the vegetation cover to the atmosphere.

The functioning of the atmosphere–land border in the process of CO_2 exchange includes other fluxes H_9^C, H_{14}^C, and H_{15}^C, which play an important role in the carbon balance of the biosphere. Bjorkstrom (1979) used the following relationships to describe these fluxes in his model of the biospheric balance of CO_2:

$$H_9^C = B_\kappa/\theta_9, \qquad H_{14}^C + H_{15}^C = B_\kappa/\theta_{14,15},$$

where θ_9 characterizes the carbon cycle in thesoil; and $\theta_{14,15}$ is the characteristic time for carbon in a living biomass to transit to the soil (about 1,000 years). If R_Q denotes the rate of humus decomposition and M_κ is the rate of vegetation decay, then $H_9^C = C_{30}R_Q$, $H_{14}^C = C_{18}M_\kappa$, $H_{15}^C = C_{15}B_\kappa$.

With the carbon supply in forest litter equal to 421.1 t/km^2, from which 12.95 t/km^2 are annually leached into the soil, with 82.5% of this amount remaining in the upper soil layer (which can be up to 8 cm thick), we get $C_{18} = 0.31$.

Flux H_9^C has a more complicated dependence on environmental parameters such as soil temperature and humidity. In the global model H_9^C is assumed to be a linear

increasing function. The non-linear effects are considered to be due to heterogeneity of the types of soils manifested through the process of oxidation of organic matter. The most inert system is peat which covers about $4.3 \cdot 10^6$ km^2 and contains 860 Gt of organic carbon. Under stable conditions the organic substance of the soil in the process of oxidation emits CO_2 and accumulates the same amount of carbon in the process of plant decay:

$$(H_9^C = H_{14}^C + H_{15}^C + H_{12}^C + H_{13}^C).$$

For peat bogs and tropical forests this balance is not observed. The soil in tropical forests emits CO_2 at a rate almost twice as high as the rate of CO_2 input to the soil from dead plant matter.

To complete a model of the atmosphere–soil CO_2 exchange, it is necessary to take into account the geophysical and demographic aspects of the formation of additional carbon fluxes. They include volcanic emanations (H_5^C), rock weathering (H_4^C), day-to-day living activity of animals (H_{11}^C, H_{13}^C), and humans (H_{10}^C, H_{12}^C), as well as vegetation burning (H_8^C). Though some of these nowadays do not play a substantial role in the total balance of CO_2, an account of them is necessary to improve model response under conditions of stress simulation. In models, flux H_5^C is usually assumed to be a function of time, and have spatial coordinates φ and λ. Fluxes H_i^C ($i = 10, \ldots, 13$) are considered to be proportional to the size of population G and animals F: $H_{10}^C = C_3 G$, $H_{11}^C = C_2 F$, $H_{12}^C = C_{22} G$, $H_{13}^C = C_{21} F$.

With respect to flux H_4^C, in the process of weathering of silicate rocks the rate of CO_2 extraction from the atmosphere is negligible compared with the similar process for carbonate rocks. Therefore, let us consider the contribution of such rocks to flux H_4^C. Under equilibrium conditions the relationship $[Ca^{2+}][HCO_3]^2/p_a = \text{const}$ is valid. Usually, $2[Ca^{2+}] = [HCO_3]$, and therefore we have $([HCO_3]/[HCO_3] = (\Delta p_a/p_a + 1)^{1/3} - 1$.

Flux H_8^C reflects anthropogenic interference with the global cycle of carbon dioxide. The formation of industrial CO_2 can be described rather precisely as follows:

$$H_1^C + H_8^C = \gamma_0 [\exp(rt)]^6,$$

where $r \approx 0.029\ \text{yr}^{-1}$.

The land carbon cycle is, of course, more complicated. Hence, the many carbon fluxes in Table 3.3 should be considered as characterizing the more detailed structure of carbon exchange in the atmosphere–plant–soil system. Detailing the land carbon cycle can be done by dividing the body of plants and soil into constituents. This process requires extensive knowledge of biogeochemical parameters, which, on a global scale, is only possible in the form of average estimates of phytomass, biomass of stems and roots, and supplies of organic matter in leaf litter and humus. Of course, information on the extent of soil erosion is important. For instance, in Afghanistan about 80% of the soil is eroded. And though this process is natural, the anthropogenic impact on soils accelerates it. The FAO estimates the global loss of productive land through erosion at $(5\text{–}7) \cdot 10^6\ \text{ha yr}^{-1}$. Therefore, consideration in the GMNSS of such data over all regions will make it possible to raise the accuracy of estimates of the CO_2 sink on land.

3.6 GLOBAL CARBON CYCLE MODEL AND NUMERICAL RESULTS

3.6.1 The role of vegetation in assimilation of carbon dioxide from the atmosphere

Land biota is a sink of atmospheric CO_2. Change in the structure of land cover is a critically important and dangerous anthropogenic process. In fact, the NPP ratio between various vegetation communities can change by as much as 45 times. For instance, swapping tropical rainforest for savannah or deciduous temperate forest for temperate grassland can decrease the sink of atmospheric CO_2 in these territories by a factor of 3 and 1.7, respectively. In the case of swapping tropical rainforest for desert, the sink of CO_2 is reduced by a factor of 4.5. Such changes are currently taking place in many regions of the globe and their consequences have already been estimated (Maddox, 1999; Terborgh. 1992; Wilson, 2002). For example, in Brazil, during the period 2000–2006 the size of forest reduced by more than 150,000 km^2. Unfortunately, available data and knowledge of the processes of plant respiration make it possible to obtain only rough integrated quantities of CO_2 fluxes in the vegetation cover. In fact, the role of plants in the daily assimilation of atmospheric CO_2 varies abruptly and is a complex function of such environmental factors as temperature, illumination, and air humidity. Nevertheless, parameterizations of the functions of vegetation carried out in Kondratyev and Krapivin (2004a) help assessment of the role of all types of soil–plant formations in CO_2 assimilation, as given in Table 3.9.

Figure 3.9 shows the role of forest vegetation in CO_2 dynamics. In addition to these results, note that experiments with global models make it possible to trace the dependence of the composition of atmospheric gas on the structure of planetary forest cover. From the available estimates, the total area of forests for $t_0 = 1970$ can be estimated at $\sigma_{L0} = \sigma_L(t_0) \approx 40.3\text{–}41.84 \cdot 10^6\ km^2$ (Watson *et al.*, 2000), 1% constituting national parks and forest reserves. With the formulated scenario, let us assume $t_L = 2050$, $\sigma_{X0} = \sigma_X(t_0) = 19.5 \cdot 10^6\ km^2$. As can be seen from Figure 3.6, the increasing rate of deforestation raises considerably the concentration of CO_2 in the atmosphere. Even with a 10% reduction of forest areas by 2050 compared with 1970 (i.e., $\sigma_{L1}/\sigma_{L0} = 0.9$), atmospheric CO_2 can increase by 44% by the end of the 21st century. In contrast, a 10% increase in forested areas decreases the concentration of atmospheric CO_2 by 15%. With a 50% increase in forested areas by 2050, the decrease of atmospheric CO_2 by 2100 will constitute 60% relative to its possible value, with the scale of impacts on the forest ecosystems observed at the end of the 20th century preserved. Hence, variations in the size the forested areas in the biosphere even within $\pm 10\%$ can substantially change the dynamics of numerous components of the global ecosystem.

Table 3.10 exemplifies the calculation of CO_2 sinks into the vegetation cover of Russia. Such calculations using the GMNSS demonstrate the dynamics of the CO_2 flux mosaic in the atmosphere–plant–soil system. Knowledge of this mosaic makes it possible to assess the role of specific types of soil–plant formations in the regional balance of carbon, and on this basis to calculate the global fluxes of carbon dioxide across the atmosphere–land border. Similar calculations are also possible for the atmosphere–ocean system.

Table 3.9. Identifiers of the types of soil–plant formations in Figure 3.8. From Bazilevich and Rodin (1967).

Type of soil–plant formation	*Identifier*
Arctic desert and tundra	A
Alpine desert	B
Tundra	C
Mid-taiga forest	D
Pampas and grass savannah	E
North taiga forest	F
South taiga forest	F
Sub-tropical desert	G
Sub-tropical and tropical grass–tree scrub of tugai type	I
Tropical savannah	J
Saline land	K
Forest tundra	L
Mountain tundra	M
Tropical xerophytic open woodland	N
Aspen–birch sub-taiga forest	O
Sub-tropical broadleaved and coniferous forest	P
Alpine and sub-alpine meadow	Q
Broadleaved coniferous forest	R
Sub-boreal and saltwort desert	S
Tropical desert	T
Xerophytic open woodland and shrub	U
Dry steppe	V
Moderately arid and arid (mountain included) steppe	W
Forest steppe (meadow steppe)	X
Variably humid deciduous tropical forest	Y
Humid evergreen tropical forest	Z
Broadleaved forest + sub-tropical semi-desert	&
Sub-boreal and wormwood desert	@
Mangrove forest	#
Lack of vegetation	*

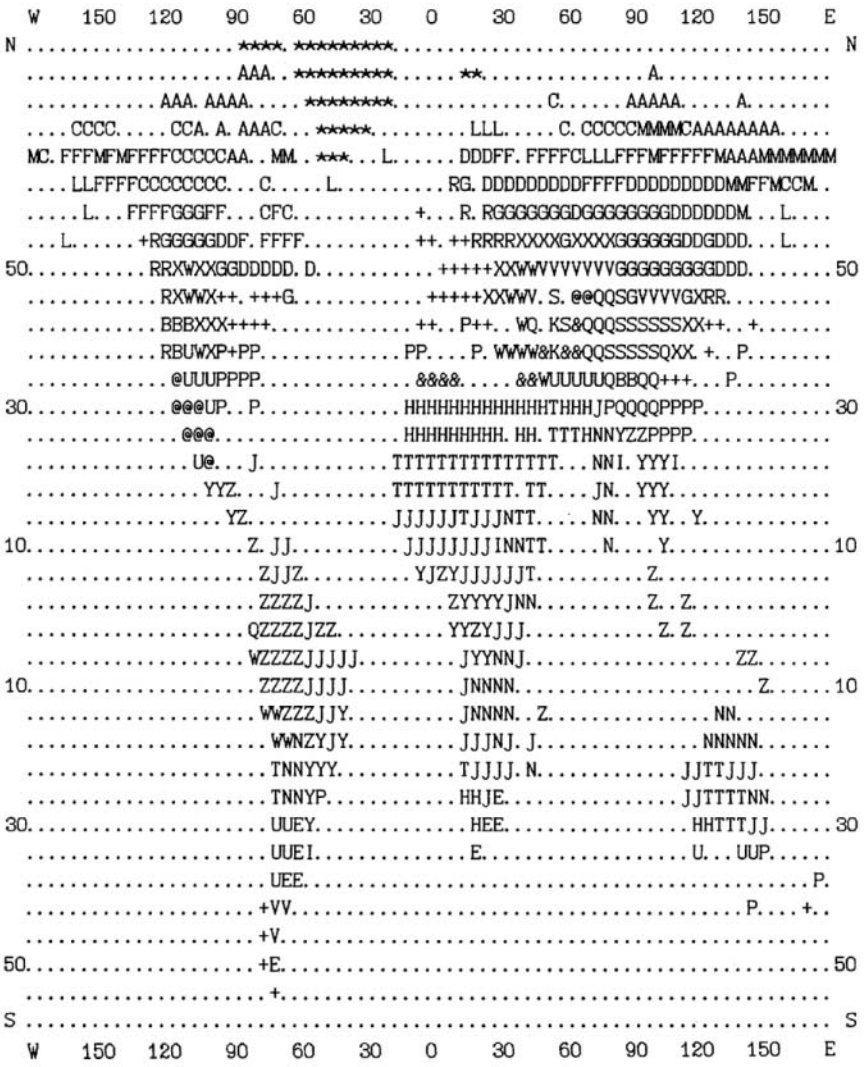

Figure 3.8. The spatial distribution of soil–plant formations over the $4^\circ \times 5^\circ$ geographical grid and their representation by pixels in the GMNSS spatial structure. Identifiers of the types of soil–plant formations are explained in Table 3.9.

Table 3.11 demonstrates the consequences of changing the global structure of soil–plant formations for the dynamics of CO_2 assimilation by vegetation. As can be seen, anthropogenic change in the vegetation cover substantially changes the balance of components in the global carbon cycle. Clearly, such experiments require thorough analysis of the data on the consequences of transforming vegetation cover by taking climatic zones and biocenological consistency into account. Nevertheless, such hypothetical experiments are useful for general assessment of the possible range of

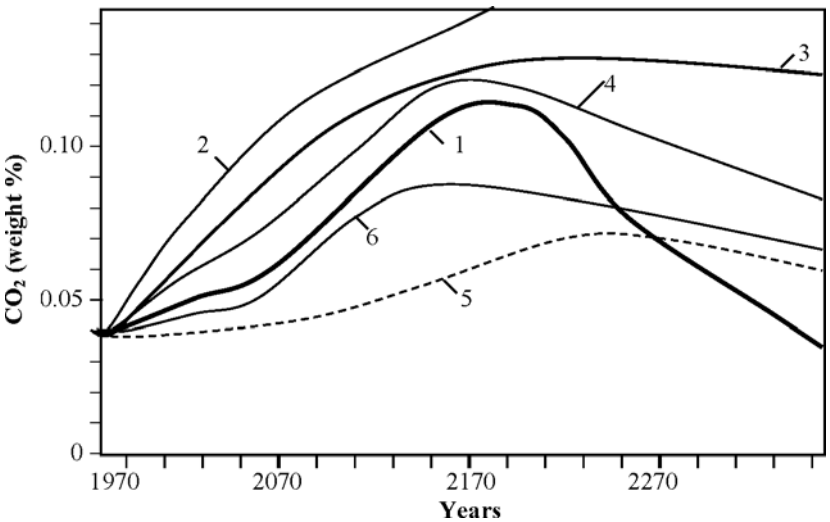

Figure 3.9. The dynamics of CO_2 concentration for different scenarios of changing forest areas: 1, rates of changes in forest areas remain at the 1970 level; 2, by 2050 all forests will have gone; 3, by 2050 the area of forest is reduced by 50%; 4, by 10%; 5, by 2050 the area of forest increases by 50%; 6, by 10%. From Demirchian *et al.* (2002).

anthropogenic impacts on the global carbon cycle. For instance, natural and anthropogenic cataclysms as a consequence of forest fires introduce annually considerable changes to this cycle, especially in the numerous fluxes and supplies of carbon over large territories. Tables 3.12–3.14 give estimates of deviations in the content of carbon in the basic biospheric reservoirs as a result of forest fires in different zones. Large-scale impacts on land biota are damped during 60–100 years. The biosphere turns out to be more resistant to impacts on forests in southern latitudes and more sensitive to violations of forest areas in temperate latitudes. Hence, Northern Hemisphere forests up to 42°N play an important role in stabilizing the carbon cycle in the biosphere.

The scenario of forest destruction, as typified in the works of many authors, evokes great interest in studies of the global carbon cycle and associated climate change. The range of possible real situations in the transformation of land cover is so large that it is impossible to assess all the consequences. Nevertheless, note that destruction of all northern taiga and mid-taiga forests (types F, D) in the next 50 years would lead to a 53% increase in atmospheric CO_2 with subsequent negative consequences for flux H_6^C. Similar consequences follow after the loss of all wet evergreen and deciduous tropical forests (types Z, Y). But in this case the indicated increase of atmospheric CO_2 would be reached 20 years later.

Structural changes to the land cover are not exclusively due to human activity. In some regions of the globe, hurricanes introduce considerable changes in the carbon balance of forest ecosystems. For example, in the U.S.A. two hurricanes happen on average every three years, which accelerates the transition of the living biomass of

Table 3.10. The dynamics of CO_2 assimilation by plants in Russia. The emission of carbon to plants in this territory in 1990 is assumed to be 1.6 GtC/yr with the annual change following Keeling's scenario. From Krapivin and Vilkova (1990).

Vegetation formation (see Table 3.9)	*Rate of CO_2 assimilation* (10^6 tC/yr)				
	1990	*2000*	*2050*	*2100*	*2150*
A	2.6	2.8	6.7	7.1	6.9
C	3.7	4.6	10.9	12.0	12.1
M	4.0	5.1	12.4	14.5	13.8
L	3.2	3.9	9.2	10.3	10.4
F	11.2	14.8	43.6	47.2	44.2
D	31.6	39.9	110.6	121.9	109.3
G	23.3	29.2	72.2	73.4	70.5
R	5.2	6.2	13.1	13.8	10.7
W	4.7	5.1	8.2	8.8	7.9
V	0.7	0.7	0.9	1.1	0.8
@	2.4	2.6	3.7	3.9	2.9
S	0.6	0.7	1.2	1.4	1.0
Q	1.5	1.6	2.2	2.3	1.8
Total	*94.7*	*206.1*	*294.9*	*317.7*	*292.3*

trees into dead organic matter. If 20 TgC are removed from U.S. forests every year, then 10%–15% of this is the result of a single hurricane (McNulty, 2002). Hence, hurricanes accelerate the return of carbon to the atmosphere, and their global inventory is needed to more accurately estimate the many components of the global carbon cycle.

3.6.2 The role of the World Ocean in carbon dioxide assimilation from the atmosphere

Estimation of the extent to which the World Ocean assimilates CO_2 from the atmosphere, as in the case of land, is only possible by spatially integrating the difference between fluxes H_3^C and H_2^C. Table 3.15 gives average estimates of this difference. Even with these rough estimates, we can see the mosaic character of the role of various

Table 3.11. The dynamics of the ratio of integral rates of (H_6^C) CO_2 assimilation by vegetation cover from the atmosphere with the natural distribution of soil–plant formations (Figure 3.8) and with its transformation according to the scenario in the second column.

Scenario		H_6^C *(changed Figure 3.8)*/H_6^C *(Figure 3.8)*		
Figure 3.8	*Changed Figure 3.8*	*2003*	*2020*	*2050*
A	L	2.79	2.40	1.97
C	L	0.96	0.94	0.95
M	L	1.67	1.15	1.01
F	D	1.68	1.57	1.11
G	D	2.11	1.67	1.45
R	D	3.98	3.70	2.87
P	Z	3.17	2.68	2.43
U	Z	22.52	20.73	17.95
W	Z	23.12	19.44	16.32
E	Z	100.14	77.75	68.54
H	Z	194.56	155.50	138.39
Q	Z	799.14	777.50	751.26
Y	Z	1.43	1.39	1.23
N	Z	69.98	62.20	56.59
J	Z	5.89	5.09	4.67
T	Z	26.54	25.92	23.58
I	Z	17.88	16.37	14.91
#	Z	0.91	1.12	0.97

basins of the World Ocean for atmospheric CO_2 assimilation. The water basins in northern latitudes and in the zone of upwellings are of key importance. Coldwater basins in southern latitudes remain little known, despite (as in the Arctic Ocean) large territories being covered with ice. From available estimates, $\Delta H_{32} = 0.006$ GtC/yr for ice-covered water basins and 0.022 GtC/yr for ice-free water bodies.

Some ideas about the role the World Ocean plays in CO_2 assimilation from the atmosphere can be obtained from the data in Figures 3.10 and 3.11. Figure 3.12 gives

Table 3.12. Model estimates of the deviation in carbon content in the event of all coniferous forests in the Northern Hemisphere (up to 42°N) being destroyed by fire.

Years after impact	*Deviations in carbon content* (Gt)			
	Atmosphere	*Soil*	*Upper ocean*	*Deep ocean*
0	140.9	−5.4	15.5	0.1
10	104.8	−33.1	29.8	3.1
20	83.1	−44.1	21.5	7.4
30	63.4	−43.5	19.0	8.5
40	47.2	−39.7	14.6	10.4
50	34.2	−34.6	11.6	11.7
60	24.1	−29.4	8.3	12.7
70	16.3	−24.7	6.2	13.5
80	10.2	−20.5	4.5	14.0
90	5.6	−17.1	3.3	14.3
100	2.1	−14.2	2.3	14.5
200	−9.0	−3.4	−0.8	13.5

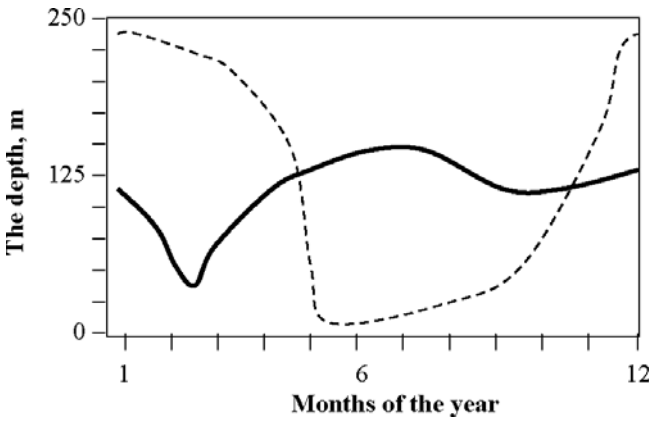

Figure 3.10. Distribution of the depth of the upper quasi-homogeneous layer of the World Ocean at latitudinal zones 0°–10°N (solid curve) and 60°N–70°N (dashed curve).

Table 3.13. Model estimates of the deviation in carbon content in the event of all forests in the Northern Hemisphere (up to 42°N) being destroyed by fire.

Years after impact	*Deviations in carbon content* (Gt)			
	Atmosphere	*Soil*	*Upper ocean*	*Deep ocean*
0	230.8	−7.9	24.9	0.1
10	173.2	−30.9	47.9	4.9
20	138.9	−67.6	39.2	10.0
30	107.9	−89.3	31.1	13.8
40	82.0	−64.3	24.1	16.8
50	60.9	−56.9	18.4	19.1
60	44.2	−49.0	13.9	20.7
70	31.1	−41.6	10.3	21.9
80	20.9	−35.0	7.5	22.8
90	12.9	−29.4	5.4	23.3
100	6.9	−24.7	3.7	23.6
200	−12.7	−5.9	−1.7	21.7

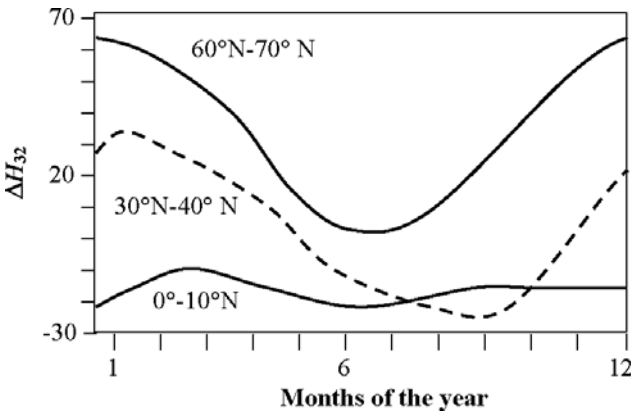

Figure 3.11. The annual distribution of carbon flux across the atmosphere–ocean border in different latitudinal zones.

Table 3.14. Model estimates of the deviation in carbon content in the event of all tropical forests being destroyed by fire.

Years after impact	*Deviations in carbon content* (Gt)			
	Atmosphere	*Soil*	*Upper ocean*	*Deep ocean*
0	396.0	−20.0	42.2	0.2
10	261.6	−93.7	73.9	8.0
20	162.2	−84.8	48.0	14.9
30	90.6	−38.6	28.2	19.1
40	45.3	−36.5	15.0	21.3
50	18.3	−21.6	7.5	22.4
60	2.9	−12.4	3.0	22.8
70	−5.8	−7.0	0.5	22.8
80	−10.6	−4.2	−0.9	22.6
90	−13.2	−2.6	−1.7	22.5
100	−14.5	−1.9	−2.1	21.8
200	−13.2	−2.3	−1.9	17.7

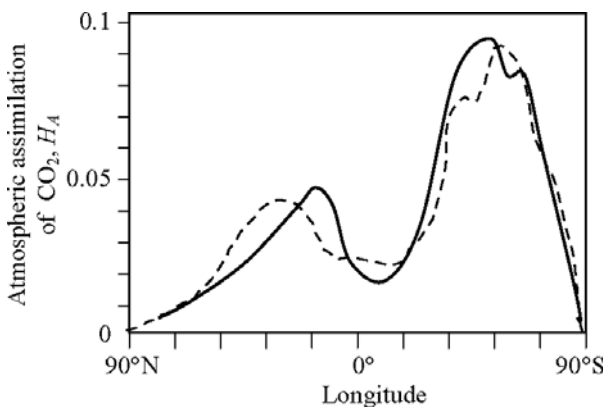

Figure 3.12. Longitude-averaged rates of atmospheric CO_2 assimilation by both land and ocean ecosystems with two scenarios of anthropogenic emissions of carbon: 6.26 GtC/yr (dashed curve, 2000) and 10.6 GtC/yr (solid curve, predicted for 2020). Notation: $H_A = \Delta H_{32} + H_6^C + H_4^C - H_8^C - H_7^C - H_9^C$ $(\mathrm{GtC} \cdot \mathrm{yr}^{-1})$.

Table 3.15. The spatial distribution of $\Delta H_{32} = H_3^C - H_2^C$ (GtC/km^2/solar year) estimated from averaged values of the assimilation and emission of CO_2 at the atmosphere–ocean border since the beginning of industrialization (σ is the area of the World Ocean basin, 10^6 km^2).

Water basin	σ	ΔH_{32}
South Atlantic Ocean	28.80	0.00138
Equatorial Atlantic Ocean	32.38	−0.00285
North Atlantic Ocean	26.01	0.01025
South Pacific Ocean	49.85	0.00531
Equatorial Pacific Ocean	88.81	−0.00323
North Pacific Ocean	32.45	0.00846
South Indian Ocean	49.63	0.00538
Equatorial Indian Ocean	32.85	−0.00592
Arctic Ocean	7.47	0.00131
The World Ocean	*348.23*	*0.00154*

the spatial distribution of CO_2 assimilated from the atmosphere which accounts for the combined role of land and ocean ecosystems. We can see that the general role of the environment in stabilizing the CO_2 content in the atmosphere only slightly varies while the amount of carbon increases considerably. This means that the natural medium preserves persistent feedbacks and the level of variability in the way land and ocean systems react to a marked increase in anthropogenic loads on the atmosphere remains stable. Detailed analysis of such reactions shows that a 60% increase in anthropogenic carbon flux during the next 20 years will result in a 4.8% increase of CO_2 flux from the tropical water basins of the World Ocean to the atmosphere, but the absorptivity of the ecosystems in northern latitudes will increase by 12.3%. The role of land ecosystems in assimilating excess carbon from the atmosphere will increase by 11.4%, and the role of Arctic waters by 13.2%. As a result, in 2020 the following amounts of carbon will be assimilated from the atmosphere: $25.7 \cdot 10^6$ tC by the south taiga forests; $35.1 \cdot 10^6$ tC by the mid-taiga forests, and $10.7 \cdot 10^6$ tC by tundra ecosystems.

3.6.3 Long-term memory effect in atmospheric CO_2 concentration

3.6.3.1 Introduction

A very important aspect of the climate problem consists in recognizing anthropogenically induced changes caused by increased CO_2 emissions to the atmosphere. In

this connection, highly uncertain quantitative estimates of anthropogenic impacts on global climate deserve special attention (Berger and Dameris, 1993; Hein *et al*., 2001; Dameris *et al*., 2005).

Recent years have been marked by the undoubtedly growing interest (among the media, politicians, and the general public) in the complex study of atmospheric CO_2 and the need to obtain reliable estimates of the CO_2 (both natural and anthropogenic) impact on global climate. The global climate numerical simulation performed recently which considered not only anthropogenically induced growth of greenhouse gas (GHG) concentrations, but also the increasing content in the atmosphere of anthropogenic sulfate aerosol revealed a much more complicated pattern of climate formation than was previously thought: aerosol-induced climate cooling compensates greenhouse warming to a certain extent (Kondratyev and Varotsos, 1995; Varotsos, 2002).

One of the main uncertainties and difficulties in assessing the role of atmospheric CO_2 in climate change has to do with the absence of adequate information about its temporal variability, and, in particular, whether CO_2 observations remain residually correlated with one another even after many years (long-range dependence).

In an attempt to address these questions, a modern method of statistical physics was recently applied by Varotsos *et al*. (2007) to CO_2 observations made at Mauna Loa, Hawaii. The necessity to employ a modern method of CO_2 data analysis stems from the fact that most atmospheric quantities obey non-linear laws, which usually generate non-stationarities. These non-stationarities often conceal existing correlations between the examined time series and therefore, instead of applying the conventional Fourier spectral analysis to atmospheric time series, new analytical techniques capable of eliminating non-stationarities in the data should be utilized (Hu *et al*., 2001; Chen *et al*., 2002; Grytsai *et al*., 2005).

Wavelet techniques (Koscielny-Bunde *et al*., 1998) and detrended fluctuation analysis (DFA) (Peng *et al*., 1994) are among the most recently used tools along these lines. Recently, much attention has been paid to DFA, because it has already proved its usefulness in a wide variety of complex systems (e.g., Stanley, 1999; Talkner and Weber, 2000; Varotsos *et al*., 2003a, b, 2005; Chen *et al*., 2005; Varotsos and Kirk-Davidoff, 2006). More information about the DFA method is given in Section 3.6.3.2.

3.6.3.2 Methodology and data analysis

The data employed by Varotsos *et al*. (2007) have been continuouslly collected at Mauna Loa Observatory, Hawaii (19°32′N, 155°35′W) since 1958. Four air samples are collected each hour and are analyzed by infrared spectroscopy for CO_2 concentrations. The Mauna Loa site is considered one of the most favorable locations for measuring undisturbed air because any possible local influences as a result of vegetation or human activities on atmospheric CO_2 concentrations are minimal and any influences from volcanic vents may be excluded from the records. The methods and equipment used to obtain these measurements have remained essentially unchanged during the 47-year monitoring program (Keeling and Whorf, 2005). The averaged

mean monthly values of CO_2 concentrations are now analyzed by employing the DFA method, which is briefly described below.

According to the DFA method, the time series $y(t)$ is first integrated and then divided into boxes of equal length, Δt. In each box, a least squares line (or polynomial curve of order l, DFA-l) is then fitted, in order to detrend the integrated time series by subtracting the locally fitted trend in each box. The root-mean-square (rms) fluctuation $F_d(\Delta t)$ of this integrated and detrended time series is calculated over all timescales (box sizes).

More specifically, the detrended fluctuation function $F(\tau)$ is calculated as follows:

$$F^2(\tau) = \frac{1}{\tau} \sum_{t=k\tau+1}^{(k+1)\tau} [y(t) - z(t)]^2, \quad k = 0, 1, 2, \ldots, \left(\frac{N}{\tau} - 1\right),$$

where $z(t) = at + b$ is the linear least squares fit to the τ data points contained in a class.

For scaling dynamics, the averaged $F^2(\tau)$ over N/τ intervals with length τ is expected to obey a power law, notably

$$\langle F^2(\tau) \rangle \sim \tau^{2a}$$

and the power spectrum function scales with $1/f^{\beta}$, with $\beta = 2a - 1$ (Kantelhardt *et al.*, 2002).

The slope a of the line on a log-log plot relating the average fluctuation and the box size indicates the plausible presence of power law scaling. A slope $a \neq \frac{1}{2}$ implies the existence of long-range correlations, while $a = \frac{1}{2}$ corresponds to the classical random walk. If $0 < a < 0.5$, power law anticorrelations are present (antipersistence). If $0.5 < a \leq 1.0$, long-range power law correlations prevail; the case $a = 1$ corresponds to so-called $1/f$ noise. In addition, when $1 < a < 1.5$, long-range correlations are again present (but are stronger than in the previous case) (e.g., Talkner and Weber, 2000).

It is worth recalling that a time series is said to exhibit long-range correlations when some of its properties at different times are correlated and its correlation function decays much slower than exponential decay (e.g., power law decay). It would be of interest to mention that wavelet-based estimators of self-similarity or of a long-range dependence scaling exponent lead to larger (smaller) mean squared errors for short (long) time series compared with DFA that is not wavelet-based (Chen *et al.*, 2005).

3.6.3.3 Application of DFA to the CO_2 time series

According to Varotsos *et al.* (2007) we begin the analysis of the time series (shown in Figure 3.13) by investigating whether the CO_2 concentration at different times is actually correlated. The motivation for this investigation stems from the observation that many environmental quantities have values which remain residually correlated with one another even after many years (long-range dependence).

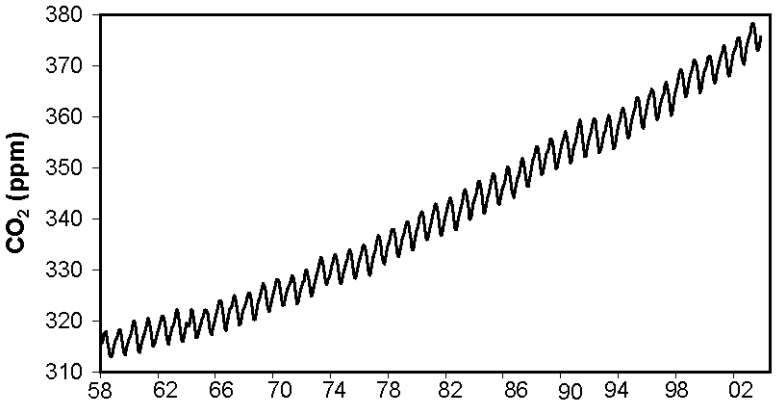

Figure 3.13. Time series of CO_2 concentration observed at Mauna Loa Observatory, during 1958–2004.

It is a truism that the standard tool to address this question is to derive the correlation function and the corresponding power spectrum (or frequency spectrum spectral density) of the time series, which is simply the Fourier transform of the autocorrelation function. Usually, short-range correlations are described by the autocorrelation function, which declines exponentially with a certain decay time. In contrast, long-range correlations (long-range dependence) imply that the autocorrelation function declines as a power law in time rather than exponentially. The latter has the following meaning: a correctly rescaled subset of the original time series resembles the original time series. However, direct calculation of the autocorrelation function is usually not appropriate due to noise superimposed on the collected data and due to underlying trends of unknown origin. Furthermore, in practice, we do not know the appropriate scaling transformation factors, in advance, or whether they exist. To this end, we analyze the data following the steps of DFA (described in Section 3.6.3.2).

The application of DFA-1 to the deseasonalized and detrended CO_2 concentration time series reveals $a = 1.05 \pm 0.04$ (Figure 3.14) for timescales between 4 months to 11 years. The same results are also found by using a polynomial fit of order l (DFA-l) to the same time series of CO_2 concentrations. More specifically, going from DFA-1 to DFA-5, the a-value was found to range from 0.98 to 1.08. Therefore, the fluctuations in CO_2 concentrations exhibit $1/f$-type long-range persistence. The strong persistence found signifies that the fluctuations in CO_2 concentration, from small time intervals to larger ones (up to 11 years) are positively correlated in a power law fashion. In other words, persistence refers to the memory or internal correlation within the CO_2 concentration time series. For example, there is a tendency for an increase in CO_2 concentration to be followed by another increase in CO_2 concentration at a different time in a power law fashion. The latter conclusion illustrates that the correlations between the fluctuations in CO_2 concentration do not obey classical Markov-type stochastic behavior (decrease exponentially with time), but exhibit more slowly decaying correlations.

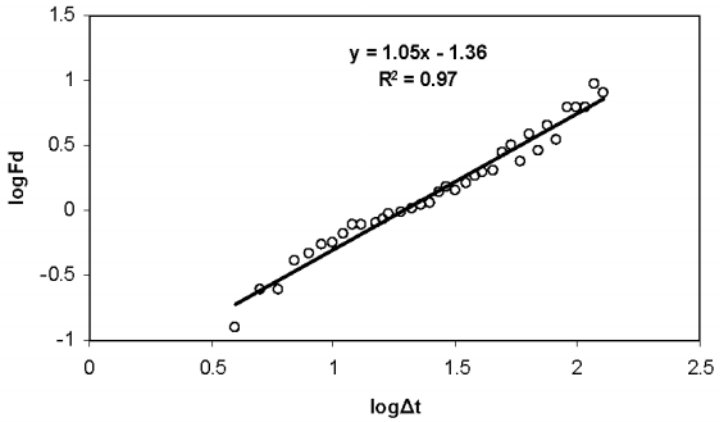

Figure 3.14. Log-log plot of the DFA function vs. the temporal interval Δt (in months) for detrended and deseasonalized CO_2 concentrations, during 1958–2004.

It is worthwhile clarifying at this point that the persistence found above provides, in principle, a forecast for CO_2 concentration, which assumes that the value of the CO_2 concentration in the following time interval (up to 11 years) will be the same as in the corresponding current time interval. This obviously has a different meaning from the conventional forecast in climatology, which assumes that the value of CO_2 concentration in the following, say, 11 years will be the same as the overall climatological CO_2 concentration mean.

Finally, Varotsos *et al.* (2007) investigated whether the persistence found in CO_2 concentration time series stems from their own values of CO_2 concentrations and not from their time evolution. Therefore, they shuffled the deseasonalized and detrended CO_2 concentrations. If the shuffled CO_2 values follow the random walk, then the persistence found above comes not from data, but from their time evolution. Indeed, application of the DFA-1 to the shuffled CO_2 data gives $a = 0.49 \pm 0.02$, which reveals that shuffled deseasonalized and detrended CO_2 data are practically uncorrelated (Figure 3.15). Therefore, the power-law relationship derived from the real measurements of carbon dioxide concentrations eventually stems from their time evolution. The latter could also be used to test the scaling performance of climate prediction models under different scenarios of carbon dioxide levels (Ebel, 2001; Govindan *et al.*, 2002).

3.6.3.4 Conclusions

Long-range correlations of the fluctuations of CO_2 concentrations measured at Mauna Loa, Hawaii during 1958–2004 were investigated by applying the DFA method. The main finding is that fluctuations in CO_2 concentrations exhibit $1/f$-type long-range persistence, which means that the fluctuations in CO_2 concentrations, from small time intervals to larger ones (up to 11 years), are positively correlated in a power law fashion. In other words, persistence refers to the memory or internal correlation within the CO_2 concentration time series up to the timescale of the

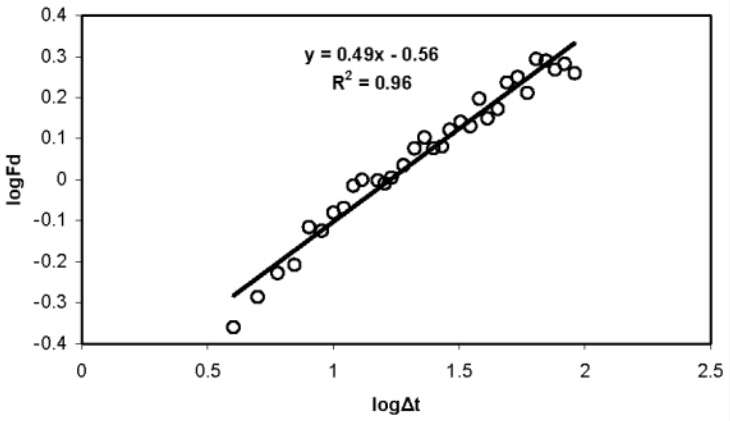

Figure 3.15. Log-log plot of the DFA function vs. temporal interval Δt (in months) for detrended and deseasonalized CO_2 concentrations, during 1958–2004.

11-year solar cycle. This scaling comes from time evolution and not from the values of carbon dioxide data. Scale invariance and $1/f$ noise are considered to be the signatures of complex systems. The scaling property detected in real observations of CO_2 concentrations could be used to test the scaling performance of the leading global climate models under different scenarios of CO_2 levels and to improve the performance of atmospheric chemistry transport models.

4

Modeling the interactive cycles of greenhouse gases and other chemicals

4.1 BIOGEOCHEMICAL CYCLES AND THE GREENHOUSE EFFECT

The stability of the biosphere as a global ecosystem and its self-regulating ability are determined by the cyclic character of the processes of exchange between matter, energy, and information that take place within it and are brought about as a result of incoming solar energy and the activity of living substances. These processes manifest themselves through the following three basic forms:

(1) The *biological cycle* covers all biophyllic elements and vitally important micro-elements and is characterized by selection of the lightweight isotopes of carbon, hydrogen, nitrogen, and sulfur from heavier forms.
(2) The *water cycle in the biosphere* determines the planetary transitions of various components such as aerosols, micro-organisms, and dissolved and suspended substances.
(3) The *processes of erosion, chemical denudation, transition, sedimentation, and accumulation* of mechanical and chemical deposits on land and in the ocean provide the global circulation of matter and energy.

Therefore, any discussion of the greenhouse effect cannot be constructive without complex consideration of the feedbacks of the CO_2 cycle and the biogeochemical processes in the presence of other elements such as nitrogen, sulfur, phosphorus, methane, ozone, water, and others (Fasham, 2003; Stevenson and Cole, 1999; Melillo *et al.*, 2003; Wang *et al.*, 2005a, b). The processes of CO_2 assimilation from the atmosphere are affected by numerous natural and anthropogenic factors manifested through a long chain of cause-and-effect bonds. For instance, acid rain affects the state of the vegetation cover and the latter affects CO_2 exchange at the atmosphere–land boundary. The use of nitrogen ($\approx 90 \cdot 10^6$ tN yr^{-1}) and phosphorus fertilizers in agriculture means cultivated plants assimilate atmospheric CO_2 differently, and

affects the rates of decomposition of soil organic matter. Moreover, manure used in agriculture is an important source of greenhouse gases such as CH_4 and N_2O. Park *et al*. (2006) studied the fluxes of CH_4 and N_2O from supplies of liquid pig manure under cold-climate conditions at an annual mean temperature below 10°C at farms in Ontario (Canada) for the period 2000–2002. At an annual mean air temperature of 8.4°C the manure temperature was, on average, higher by 4°C, and the average content of dry matter in the manure and decomposition potential ranged between 0.6%–3% and −232 mV–333 mV. Average fluxes of N_2O changed depending on the farm from 0 $\mu g\,m^{-2}\,s^{-1}$ to 337.6 $\mu g\,m^{-2}\,s^{-1}$ in summer and to 101.8 $\mu g\,m^{-2}\,s^{-1}$ in winter. Monthly mean fluxes of CH_4 ranged between $4.6 \cdot 10^{-3}$–1.05 $mg\,m^{-2}\,s^{-1}$. If we had such data for the globe we would be able to specify the structure of the biogeochemical cycle of GHGs.

However, the complexity of the biogeochemical cycles of GHGs and estimates of how well they are understood indicate the necessity of caution when predicting global changes and the development of new information technologies to study these cycles in correlation with other global processes. Developed countries are spending vast amounts on creating information bases capable of providing reliable predictions of climate change. But, practically all international programs targeting this are investigating parts of the overall scheme. For instance, the scientific priorities of the Joint Global Ocean Flux Study (JGOFS) program include

- determining how changes in basin-scale forcing affect the dynamics of the North Pacific Drift Current and how these dynamics affect the nutrient and carbon-trapping capacity of the California Current System;
- understanding the imbalance between nitrogen fixation and denitrification (the marine nitrogen cycle) and its relationship to the ability of the oceanic biological pump to sequester anthropogenic carbon dioxide;
- quantifying how regime shifts interact with seasonal and stochastic variability to produce extreme events such as the recent coccolithophorid bloom in the Bering Sea and basin-scale hypoxia (Murata and Takizawa, 2002; Weeks *et al*., 2004).

Unfortunately, even a complex program such as the GCP cannot resolve the problem of accessing enough information for reliable prediction of global change. However, one technology capable of constructively resolving this problem is the GIMS (Kondratyev *et al*., 2000, 2002b, 2004a; Nitu *et al*., 2004; Krapivin *et al*., 2006).

On the whole, many chemical elements, especially GHGs, getting into the environment from anthropogenic sources, become the object not only of biogeochemical analysis but also of economic consideration. Such a multi-purpose analysis in connection with CH_4 was carried out at the *Second International Conference* in Novosibirsk in 2000 (Bazhin, 2000; Byakola, 2000). Similar analyses to that of CH_4 need to be done with other GHGs, and then all should be thoroughly systematized and parameterized. Otherwise, it is impossible to speak about any reliable assessment of the role of the biosphere in assimilating excess CO_2 from the atmosphere. Complex studies in this direction are being carried out, for instance, in several laboratories in

the U.S.A. and Europe (Friedrich, 2001). Measurements of the spatiotemporal distributions of gases related to the global CO_2 cycle are being taken onboard flying laboratories and on specialized stationary platforms. The accumulation of such data will make it possible to reveal the dependences needed for the global model. However, the U.S.A. has taken an irreconcilable stand with respect to the Kyoto Protocol despite the fact that CO_2 emissions from their territory are responsible for almost 25% ($541 \cdot 10^7\ tCO_2\ yr^{-1}$) of all global anthropogenic sources. In March 2001, President Bush said he wouldn't be ratifying the Kyoto Protocol because it could significantly damage the country financially. He was also concerned about the pressure on "industrialized" countries to cut back on carbon dioxide, while developing countries weren't expected to cut theirs back too. Emissions in America have continued to rise and are now 11% higher than in 1990, even though when they did temporarily sign up to Kyoto, they promised a 6% reduction.

All this confirms the fact that fragmentary studies of the global carbon cycle (i.e., not based on a complex global model such as that described in Krapivin and Kondratyev, 2002) will always raise doubts. For global conclusions, like those made in the Kyoto Protocol recommendations, we need to be sure that the predicted global consequences are accurate. Nevertheless, such conclusions and assessments are necessary. Unfortunately, most international programs on the subject are not aimed at the development of global modeling technology and do not encourage specialists to formulate numerical NSS models.

Existing global models are simple and inadequately supported by databases. Three directions for global modeling to follow were described in the works of Kondratyev *et al.* (2002b) and Boysen (2000). In each of them one or several components are absent, but on the whole, conceptually they are mutually additive. This makes it possible to combine them and, hence, to derive a global model that takes into account the most important processes in the nature–society system. One of them is the gas exchange between the atmosphere and vegetation cover (described in global models at a very high level). Nevertheless, models of the land ecosystem have recently appeared, such as Biome-GCP, Forest-GCP, or TsuBiMo (Wang *et al.*, 2005; Alexandrov *et al.*, 2005) which simulate the supplies and fluxes of energy, water, hydrogen, and nitrogen in the vegetation cover, leaf litter, and soil, which enables us to specify the role of land in regulating the radiation balance of the atmosphere–plant–soil system. In particular, Wang *et al.* (2005a, b) studied the fluxes of H_2O, CO_2, and nitrogen in the plains of north China from data on vegetation and soils for 2002 and showed that the Biome-GCP model reliably assesses the response of land ecosystems to anthropogenic interference with the natural balance of water, carbon, and nitrogen. Without any interference these ecosystems are in a balanced state with regard to these elements, but interference intensifies the fluxes of CO_2 and H_2O, and excess nitrogen gets into the soil and neighboring water basins, contaminating them.

Clearly, systematization of the models of land ecosystems and their introduction to the GMNSS as alternative units, regulated by available databases, will make it possible to markedly reduce the level of uncertainty in the estimates of CO_2 sinks and sources. Such a study was carried out by Alexandrov *et al.* (2005) in which calibration of TsuBiMo by the database of the Osnabrück Center for Environment and

Technology (Germany) is demonstrated. The proposed calibration scheme consists of four stages:

(1) Reduction of the number of unspecified parameters of the model by introducing a generalized parameter.
(2) Evaluation of generalized parameters from the available database.
(3) Formation of an empirical model relating generalized parameters to climate.
(4) Establishing a relationship between the global multitude of generalized parameters and global fields of climatic variables.

Applying this scheme of calculation to the TsuBiMo model, Alexandrov *et al.* (2005), from measurements of CO_2 fluxes in the neighborhood of Takayama (Japan), constructed an empirical model to calculate monthly mean temperatures and showed that the accuracy of calculations of the inter-annual and intra-annual variability of biome productivity can be substantially increased at the local level.

The photochemical system of the atmosphere has been poorly studied and is not considered in global models. Knowledge of the laws of how incoming radiation intensity changes the effects of its assimilation by gases and aerosols will make it possible to raise the accuracy of greenhouse effect estimates. Most important here is the role of molecular nitrogen, ozone, water vapor, nitric oxide, sulfur dioxide, nitrogen dioxide, CH_4, CO_2, and other gases. Greenhouse gases, other than CO_2, may play an unpredictable role in formation of the Earth radiation balance. Therefore, some models are proposed here which will enable us to parameterize some of these elements.

4.2 GLOBALIZATION OF THE SULFUR CYCLE

An increase in the intensity and spatial distribution of anthropogenic processes during recent decades can be seen by the increased propagation of sulfur compounds into the biosphere. This effect is confirmed by comparing it with the pre-industrial period, which shows that sedimentation of sulfur over the continents and oceans has increased by 162.5% and 24.6%, respectively. Emissions of sulfur to the atmosphere have now reached $93 \cdot 10^6$ tS yr^{-1}. The anthropogenic flux of sulfur in the form of SO_2 is easily estimated, assuming $3.1 \cdot 10^{12}$ kg of coal is globally burnt every year, with the average content of sulfur in it being 2.5% (by weight).

Any improvement of the global model of the biosphere can only be achieved by extending our knowledge of the biogeochemical cycles involved in it. The need to parameterize a unit describing sulfur fluxes in natural systems is dictated by the dependence of biotic processes on the content of sulfur in biospheric compartments. The available data on the supplies and fluxes of sulfur compounds in the atmosphere, soils, vegetation cover, and hydrosphere, enable formulation of mathematical relationships to describe the global sulfur cycle.

Sulfur compounds strongly affect the health of the environment and its role in regulating the greenhouse effect. For instance, in December 1952 a fog consisting of a

mixture of smoke and coal dust covered London. As a result, during one week more than 2,000 people died from illnesses connected with air pollution. These events had happened before, but had not been recorded. Measurements carried out at St. Bartholomew's Hospital showed that the concentration of particles of smoke and SO_2 exceeded several milligrams per cubic meter. In general, London at that time depended on the use of coal for heating and energy production, and since that event attempts were made to remove sulfur from coal before its burning. Nevertheless, in 1962 the tragedy recurred with 800 victims succumbing to smog.

Since 1970, in OECD countries the problem of air quality has become the subject of studies at many scientific centers. Oil from the Middle East became the main source of energy. The content of sulfur in oil constitutes 2.5%–3%. In 1985 some European countries signed the CLRTAP protocol on a 30% reduction of sulfur emissions. As a result, present day levels of SO_2 emissions have decreased by more than 50% compared with 1980. Of course, this was possibly largely due to Europe going over to the use of Russian gas.

It should be mentioned that, along with the formation of acid rain, sulfur compounds directly bring about decreases in the greenhouse effect. For instance, a sulfate ion has the opposite effect to a change of air temperature than CO_2 and, hence, reduces the effect of climate warming.

The global sulfur cycle consists of a mosaic structure of local fluxes of its compounds with other elements formed due to water migration and atmospheric processes. Conceptual schemes of the global and regional cycles of sulfur have been described in detail by many authors (Nitu *et al.*, 2000b; Xu and Carmichael, 1999; Stein and Lamb, 2000; Howarth *et al.*, 1992). However, existing models were developed for restricted usage, which makes it difficult to include them in a global model without substantial changes to their parameters. The model of the global sulfur cycle proposed here was derived as a unit with inputs and outputs, which enables it to be matched with other units of the global model via their inputs and outputs.

In contrast to hydrogen, sulfur compounds cannot be attributed to long-lived elements of the biosphere. For example, the lifetime of sulfur oxide in the atmosphere does not exceed 15 days. Therefore, when calculating a unit for sulfur the spatial digitization of its natural and anthropogenic reservoirs should be planned to reflect the local distributions of sulfur in the vicinity of its sources and to facilitate estimation of the intensities of inter-regional fluxes of sulfur compounds. The version of the sulfur unit proposed here, in contrast to the known hydrodynamic models of long-distance transport, takes into account the fluxes of sulfur compounds between the hydrosphere, atmosphere, soil, and biota. The model does not consider the vertical stratification of the atmosphere. The characteristics of sulfur fluxes averaged vertically are calculated for both the land and ocean (Fasham, 2003; Sanets and Chuduk, 2005; Stevenson and Cole, 1999). The spatial digitization of the biosphere and the World Ocean corresponds to the scheme of Figure 3.8. The elements in the block scheme of the model of the sulfur biogeochemical cycle are described in Tables 4.1 and 4.2. This scheme is realized in every cell Ω_{ij} of the Earth's surface and in every compartment Ω_{ijk} of the World Ocean. Interaction between the cells and

Table 4.1. Sulfur reservoirs and sulfur recovery factor.

Sulfur reservoir	*Sulfur storage*	*Lifetime of sulfur in the reservoir*
Atmosphere	4.8 MtS	8–25 days
Lithosphere	20 PtS	10^8 years
World Ocean	3 PtS	Million years
Marine biota	30 MtS	1 year
Lakes	300 MtS	3 years
Soils	0.3 TtS	1,000 years
Sediments	300 TtS	Million years

compartments is organized through the climate unit of the global model. Therefore, equations for the sulfur unit lack terms reflecting the dynamic pattern of the spatial transformation of sulfur reservoirs. According to the notation in Tables 4.2 and 4.3, the equations describing the balance relationships between the reservoirs of sulfur compounds can be written in the form:

$$\frac{dAH2SL}{dt} = C_1 + C_2 + C_3 - C_4 + C_{21}, \tag{4.1}$$

$$\frac{dASO2L}{dt} = C_4 + C_5 + C_6 - C_7 - C_8 - C_9, \tag{4.2}$$

$$\frac{dASO4L}{dt} = C_9 + C_3 + C_{20} - C_{11} - C_{12}, \tag{4.3}$$

$$\frac{dS}{dt} = C_{17} - C_{16} - C_{19}, \tag{4.4}$$

$$\frac{dSO4L}{dt} = C_{10} + C_{11} + C_{12} + C_{16} - C_3 - C_{13} - C_{14}, \tag{4.5}$$

$$\frac{dFIX}{dt} = C_7 + C_{15} - C_{17} + C_{22}, \tag{4.6}$$

$$\frac{dH2SOL}{dt} = C_8 - C_{18} - C_{21} - C_{22}, \tag{4.7}$$

$$\frac{dAH2SO}{dt} = H_1 + H_3 + H_4 + H_{26} - H_2, \tag{4.8}$$

$$\frac{dASO2O}{dt} = H_2 + H_5 + H_6 - H_7 - H_8 - H_{24}, \tag{4.9}$$

$$\frac{dASO4O}{dt} = H_8 + H_9 + H_{12} - H_{10} - H_{11}, \tag{4.10}$$

Table 4.2. The characteristics of the land and hydrospheric fluxes of sulfur in the biosphere. Numerical estimates of the fluxes ($mg\,m^{-3}\,day^{-1}$) are obtained by averaging over respective territories.

Sulfur flux	*Land*		*Hydrosphere*	
	Identifier	*Estimate*	*Identifier*	*Estimate*
Volcanic invasions H_2S SO_2 SO_4^{2-}	 C_1 C_5 C_{20}	 0.018 0.036 0.035	 H_3 H_5 H_9	 0.0068 0.0073 0.0074
Anthropogenic emissions H_2S SO_2 SO_4^{2-}	 C_2 C_6 C_{10}	 0.072 0.92 0.47	 H_1 H_6	 0.00076 0.038
Oxidation of H_2S to SO_2	C_4	1.13	H_2	0.3
Oxidation of SO_2 to SO_4^{2-}	C_9	1.35	H_8	0.16
Dry sedimentation of SO_4^{2-}	C_{12}	0.37	H_{11}	0.11
Fallout of SO_4^{2-} with rain	C_{11}	1.26	H_{10}	0.38
Biological decomposition and emission of H_2S into the atmosphere	C_3	1.03	H_4	0.31
Assimilation of SO_4^{2-} by biota	C_{15}	0.41	H_{13}	1.09
Biological decomposition and formation of SO_4^{2-}	C_{16}	1.13	H_{17} H_{23}	0.43 0.12
Sedimentation and deposits	C_{18} C_{19}	0.22 0.11	H_{15} H_{16} H_{19} H_{25}	0.98 0.55 0.0076 0.036
Wind-driven return to the atmosphere	C_{13}	0.25	H_{12}	0.33
Replenishing sulfur supplies due to dead biomass	C_{17}	0.86	H_{14}	1.1
Assimilation of atmospheric SO_2	C_7	0.46	H_7	0.18
Leaching of SO_2 from the atmosphere	C_8	0.27	H_{24}	0.061
River run-off of SO_4^{2-} to the ocean	C_{14}	1.17		
Transition of gas-phase H_2SO_4 to H_2S	C_{21}	0.018	H_{26}	0.0076
Assimilation of the leached part of atmospheric SO_2 by biota	C_{22}	0.036	H_{27}	0.015
Oxidation of H_2S to SO_2 in water medium			H_{18} H_{22}	0.045 0.19
Advection of SO_2			H_{20}	0.38
Advection of H_2S			H_{21}	0.37

Table 4.3. Some estimates of the sulfur reservoirs that can be used as initial data.

Reservoir	*Identifier in Equations (4.1)–(4.18)*	*Quantitative estimate of the sulfur reservoir* (mg/m^2)
The atmosphere over the oceans		
H_2S	*AH2SO*	10
SO_2	*ASO2O*	5.3
SO_4^{2-}	*ASO*40	2
The atmosphere over land		
H_2S	*AH2SL*	36.9
SO_2	*ASO2L*	17.9
SO_4^{2-}	*ASO4L*	12.9
Land		
SO_4^{2-}	*SO4L*	11.2
Biomass	*FIX*	600
Soil	*S*	5,000
Photic layer of the World Ocean		
H_2S	*H2SOU*	1.9
SO_4^{2-}	*SO4OU*	19×10^7
Biomass	*FI*	66.5
MOB	*DU*	730
Deep layers of the World Ocean		
H_2S	*H2SOD*	$2 \cdot 10^6$
SO_4^{2-}	*SO4OD*	3.4×10^9
MOB	*DD*	13,120

$$\frac{\partial SO4OU}{\partial t} + v_z \frac{\partial SO4OU}{\partial z} + k_z \frac{\partial^2 SO4OU}{\partial z^2} = H_7 + H_{10} + H_{11} + H_{20} + H_{22} + H_{27} + C_{14} - H_{12} - H_{13}, \tag{4.11}$$

$$\frac{\partial H2SOU}{\partial t} + v_z \frac{\partial H2SOU}{\partial z} + k_z \frac{\partial^2 H2SOU}{\partial z^2} = H_{21} + H_{23} - H_4 - H_{22}, \tag{4.12}$$

$$\frac{\partial H2SOD}{\partial t} + v_z \frac{\partial H2SOD}{\partial z} + k_z \frac{\partial^2 H2SOD}{\partial z^2} = H_{17} - H_{18} - H_{21}, \tag{4.13}$$

$$\frac{\partial SO4OD}{\partial t} + v_z \frac{\partial SO4OD}{\partial z} + k_z \frac{\partial^2 SO4OD}{\partial z^2} = H_{18} - H_{19} - H_{20}, \tag{4.14}$$

$$\frac{\partial DU}{\partial t} + v_z \frac{\partial DU}{\partial z} + k_z \frac{\partial^2 DU}{\partial z^2} = H_{14} - H_{15} - H_{23}, \tag{4.15}$$

$$\frac{\partial DD}{\partial t} + v_z \frac{\partial DD}{\partial z} + k_z \frac{\partial^2 DD}{\partial z^2} = H_{15} - H_{16} - H_{17}, \tag{4.16}$$

$$\frac{\partial FI}{\partial t} + v_z \frac{\partial FI}{\partial z} + k_z \frac{\partial^2 FI}{\partial z^2} = H_{13} - H_{14}, \tag{4.17}$$

$$\frac{\partial BOT}{\partial t} = H_{16} + H_{19}, \tag{4.18}$$

where v_z is the velocity of vertical water motion in the ocean, $\mathrm{m\,da^{-1}}$; and k_z is the coefficient of turbulent mixing, $\mathrm{m^2\,da^{-1}}$.

Equations (4.1) through (4.18) are supplemented in each cell of the spatial division of the ocean surface with initial conditions (Table 4.3). The boundary conditions for Equations (4.11) through (4.18) are zero. The calculation procedure to estimate sulfur concentration consists of two stages. First, at each time moment t_i, for all cells Ω_{ij}, Equations (4.1)–(4.18) are solved by the quasi-linearization method, and all reservoirs of sulfur are estimated for $t_{i+1} = t_i + \Delta t$, where time step Δt is chosen from the convergence state of the calculation procedure. Then, at moment t_{i+1} using the climate unit of the global model these estimates are specified with account of the atmospheric transport and ocean currents over time Δt.

Sulfur supplies in reservoirs are measured in $\mathrm{mgS\,m^{-3}}$ (sulfur fluxes are measured in $\mathrm{mgS\,m^{-3}\,da^{-1}}$). The sulfur supplies in water are calculated by taking the volumes in compartments Ω_{ijk} into account. To estimate sulfur supplies in the atmosphere, it is assumed that an effective thickness of the atmosphere h is an input parameter either introduced into the model by the user or prescribed as constants from Table 4.3, or received from the climate unit of the global model. Quantitative estimates of the fluxes in the right-hand sides of Equations (4.1) through (4.18) are obtained in different units of the global model. The anthropogenic fluxes of sulfur H_1, H_6, C_2, C_6, and C_{10} are simulated in the unit of scenarios. The fluxes H_3, H_5, H_9, C_1, C_5, and C_{20} are prescribed either by the climate unit or formed in the unit of scenarios. The accuracy of different functional presentations of the fluxes in Equations (4.1) through (4.18) corresponds to the accuracy of similar fluxes of the biogeochemical cycles of hydrogen, phosphorus, and nitrogen. The rate of emission of H_2S into the atmosphere as a result of humus decomposition is described by the linear function $C_3 = \mu_1(\mathrm{pH}) \cdot SO4L \cdot T_L$, where μ_1 is the proportion coefficient depending on soil acidity, $\mathrm{da^{-1} \cdot K^{-1}}$, and T_L is the soil temperature, °K . The initial value of $SO4L$ in Equation (4.5) is estimated from the humus supply by considering the content of sulfur in humus prescribed by the parameter a_g, %. According to the available observations of the input of H_2S into the atmosphere from the ocean, the flux H_4 varies widely from low values to high values on transition from stagnant water to zones of upwellings. Flux H_4 is assumed to be a function of the ratio of the rates of H_2S oxidation in the photic layer to the rate of vertical uplifting of water. Therefore, to describe the H_4 flux, let us use the parameter t_{H2SU}, which reflects the lifetime of H_2S in water: $H_4 = H2SU/t_{H2SU}$. Let us determine the value of t_{H2SU} as a function of the rate of vertical advection v_z and concentration of oxygen O_2 in the upper layer Z_{H2S} thick: $t_{H2SU} = H2SOU \cdot v_z(\theta_2 + \mathrm{O_2})/[\mathrm{O_2}(\theta_1 + v_z)]$, where constants θ_1 and θ_2

are determined empirically, and the value of O_2 is either calculated by the oxygen unit of the global model or prescribed from the global database.

The reaction of oxidation of H_2S to SO_2 in the atmosphere, on land, and over the water surface is characterized by the rapid process of the reaction of hydrogen sulfide with atomic and molecular oxygen. At the same time, the reaction of H_2S with O_3 in the gas phase is slow. It is impossible to describe within the global model the diversity of the situations appearing here; however, inclusion of fluxes H_2 and C_4 into the unit of sulfur enabled us to take into account the correlation between the cycles of sulfur and oxygen. These fluxes are parameterized using the indicator t_{H2SA} of the lifetime of H_2S in the atmosphere: $C_4 = AH2SL/t_{H2SA}$, $H_2 = AH2SO/t_{H2SA}$. The mechanism to remove SO_2 from the atmosphere is described by the fluxes H_7, H_8, H_{27}, C_7, C_8, and C_9. Schematically, this mechanism consists of a set of interconnected reactions of SO_2 with atomic oxygen under the influence of various catalysts. A study of the succession of reaction enables us to estimate the lifetime of SO_2 for oxidation over land t_{SO2L} and water surface t_{SO2A1}, making it possible to assume the following parameterizations of the fluxes H_8 and C_9: $H_8 = ASO2O/t_{SO2A1}$, $C_9 = ASO2L/t_{SO2L}$.

Sulfur dioxide is assimilated from the atmosphere by rocks, vegetation, and other Earth covers. Over the water surface this assimilation is connected with the intensity of turbulent gas fluxes and surface roughness. We describe a dry deposition of SO_2 over the vegetation by the model $C_7 = q_2 RX$, where $q_2 = q_2' \cdot ASO2L/(r_{tl} + r_s)$, r_{tl} is the atmospheric resistance to SO_2 transport over the vegetation of l type, da m^{-1}, r_s is the surface resistance of s type to SO_2 transport, da m^{-1}, RX is the production of vegetation of X type, mg m^{-2} da^{-1} (calculated by the biogeocenotic unit of the global model), and q_2' is the proportion coefficient. The parameters r_{tl} and r_s are functions of the types of soil–vegetation formations and estimated, respectively, at 0.05 and 4.5 for forests, 0.9 and 3 for grass cover, 0.5 and 2 for bushes, 0.8 and 1 for bare soils, 1.9 and 0 for water surfaces, and 2 and 10 for snow cover.

The leaching of SO_2 from the atmosphere with changing phase to H_2SO_4 and a subsequent neutralization on the surface of the l type is described by the function: $C_8 = q_{1l} W \cdot ASO2L$ with the Langmuir coefficient (Mon *et al.*, 2006) q_{1l} and precipitation intensity $W(\varphi, \lambda, t)$. The interaction of acid rain with Earth surface elements is reflected in Table 4.2 by fluxes C_{18}, C_{21}, and C_{22} for land and H_{25}, H_{26}, and H_{27} for water surface. To parameterize these fluxes, assume the hypothesis that the reservoirs of $H2SO4L$ and $H2SO4O$ are spent in proportion to the outfluxes, and the coefficients of this proportion are the controlling parameters of the numerical experiments: $C_{18} = h_1 \cdot H2SO4L$, $C_{22} = h_2 \cdot RX \cdot H2SO4L$, $C_{21} = h_3 T_a \cdot H2SO4L$, $H_{25} = h_6 \cdot H2SO4O$, $H_{26} = h_4 T_a \cdot H2SO4O$, $H_{27} = h_5 \cdot RFI \cdot H2SO4O$, $h_1 + h_2 \cdot RX + h_3 T_a = 1$, $h_4 T_a + h_5 \cdot RFI + h_6 = 1$, where $T_a(\varphi, \lambda, t)$ is the air surface temperature. Let us parameterize the fluxes H_7 and H_{24} by the relationships $H_7 = ASO2O/t_{SO2A2}$ and $H_{24} = q_{1l} W \cdot ASO2O$, where t_{SO2A2} is the lifetime of SO_2 over the water surface.

Sulfates interacting with the ecosystems and establishing the interaction of the sulfur cycle with other biogeochemical processes are one of the most important elements in the global cycle of sulfur. Numerous complicated transformations of sulfates in the environment are described by the set of fluxes H_7, H_8, H_{10}, H_{11},

H_{12}, C_9, C_{11}, C_{12}, C_{13} for the atmospheric reservoir and fluxes H_{13}, H_{18}, H_{19}, H_{20}, H_{22}, C_3, C_{14}, C_{15}, C_{16} for land and the World Ocean.

The physical mechanisms for the transport of sulfates from the atmosphere to the soil and water medium are connected with dry and wet sedimentation. An efficient model of the wet removal of particles and gases from the atmosphere was proposed by Langmann (2000): substituting the mechanism of the aerosols and gases by a simplified binary model enables us to match it with other units of the global model: $H_{10} = \mu W \cdot ASO4O$, $H_{11} = \rho v_{\mathrm{O}} \cdot ASO4O$, $C_{11} = b_3 W \cdot ASO4L$, and $C_{12} = d_1 v_a \cdot ASO4L$, where v_{O} and v_a are the rates of aerosol dry deposition over the water surface and land, respectively, μ, b_3, ρ, and d_1 are constants.

The return of sulfates from the soil and water medium to the atmosphere is connected with rock weathering and spray above a rough water surface: $C_{13} = d_2 \cdot RATE \cdot \mathrm{SO_4}L$, $H_{12} = \theta \cdot RATE \cdot SO4U$, where $RATE(\varphi, \lambda, t)$ is the wind speed over the surface, m/s, and d_2 and θ are empirical coefficients.

Flux C_{14} relates to the surface and water reservoirs of sulfur. Let σ be the share of the river system area on land and d_3 the proportion coefficient, then $C_{14} = d_3 W \cdot SO4L + (C_{11} + C_{12})\sigma$.

The surface part of the sulfur cycle is connected with the functioning of the atmosphere–vegetation–soil system. Plants adsorb sulfur from the atmosphere in the form of $\mathrm{SO_2}$ (fluxes C_7 and C_{22}) and assimilate sulfur from the soil in the form of $\mathrm{SO_4^{2-}}$ (flux C_{15}). In the hierarchy of soil processes, two levels can be selected defining the sulfur reservoirs as "dead organics" and "$\mathrm{SO_4^{2-}}$ in soil". The transitions between them are described by flux $C_{16} = b_2 ST_L$, where the coefficient $b_2 = b_{2,1} b_{2,2}$ reflects the rate $b_{2,1}$ of transition of sulfur contained in dead organics into the form assimilated by vegetation The coefficient $b_{2,2}$ indicates the content of sulfur in dead plants.

The fluxes of sulfur in the water medium according to studies by Bodenbender *et al.* (1999) depend on the biological processes in water bodies and constitute an isolated part of the global cycle of sulfur that contains only the fluxes that connect it with atmospheric and surface cycles. Rough estimates show that the rates of the sulfur cycle in the water of seas and oceans do not play a substantial role for the remaining parts of its global cycle. Despite this fact, for the purity of the numerical experiment, in the proposed model the internal hydrospheric fluxes of sulfur compounds are separated in space and parameterized with the same details as other fluxes of sulfur in the atmosphere and on land. This excessiveness is important for other units of the global model as well. In particular, it is important for the parameterization of photosynthesis whose rate *RFI* affects the closure of other biogeochemical cycles. Finally, let us assume $H_{13} = \gamma \cdot RFI$, $H_{14} = b \cdot MFI$, $H_{15} = f \cdot DU$, $H_{16=p \cdot DD}$, $H_{17} = q \cdot DD$, $H_{18} = H2SOD/t_{H2SOD}$, $H_{19} = u \cdot SO4D$, $H_{20} = a_1 v_D \cdot SO4D$, $H_{21} = b_1 v_D \cdot H2SOD$, $H_{22} = H2SOU/t_{H2SOU}$, and $H_{23} = g \cdot DU$, where *MFI* is the mass of dead phytoplankton, t_{H2SOU} and t_{H2SOD} are the time of complete oxidation of $\mathrm{H_2S}$ in seawater at the photic and deep layers, respectively, and γ, b, f, p, q, u, a_1, b_1, and g are constants.

Anthropogenic input to the sulfur unit comes about through fluxes C_2, C_6, C_{10}, H_1, and H_6 as functions of spatiotemporal coordinates.

4.3 GLOBALIZATION OF THE PHOSPHORUS CYCLE

In contrast to nitrogen, the main reservoir of phosphorus in the biosphere is not the atmosphere but the rocks and other deposits formed in the past geological epochs, which, being subject to erosion, emit phosphates. Moreover, there are other mechanisms for the return of phosphorus to the biospheric cycle, but, as a rule, they are not that efficient. One of these mechanisms is fishing, returning to land from the hydrosphere about $60 \cdot 10^3\,\mathrm{tP\,yr^{-1}}$; another is the extraction of phosphorus-containing rocks estimated at $(1\text{–}2) \cdot 10^6\,\mathrm{tP\,yr^{-1}}$. The present cycle of phosphorus is closed by its fluxes to the bottom deposits in the World Ocean where it mixes with sewage, as well as with coast and river run-off. Estimates of the amount of phosphorus and its fluxes given by different authors are contradictory. In Table 4.4 we attempt to bring these estimates together. In addition, it should be noted that, when modeling biogeochemical cycles, information about the residence time of chemical elements in respective media is needed. For phosphorus the complete cycle takes 53 hours in the atmosphere, 47.2 years in land biota, 2,000 years in the soil, 48 days in ocean biota, and 26 and 1,500 years in surface and deep layers of the ocean, respectively. Such indicators in a model are important for model verification purposes.

The elements involved in flux in a model of the global phosphorus cycle are presented in Figure 4.1 and Table 4.4, according to which the balance system of equations will be:

$$\frac{\partial P_A}{\partial t} + V_\varphi \frac{\partial P_A}{\partial \varphi} + V_\lambda \frac{\partial P_A}{\partial \lambda} = H_1^P + H_{19}^P + \begin{cases} -H_{16}^P, & (\varphi, \lambda) \in \Omega_0; \\ H_7^P - H_8^P, & (\varphi, \lambda) \in \Omega \setminus \Omega_0; \end{cases}$$

$$\frac{\partial P_U}{\partial t} + v_\varphi \frac{\partial P_U}{\partial \varphi} + v_\lambda \frac{\partial P_U}{\partial \lambda} + v_z \frac{\partial P_U}{\partial z} = H_{11}^P + H_{15}^P + H_{16}^P - H_9^P - H_{10}^P;$$

$$\frac{\partial P_L}{\partial t} + v_\varphi \frac{\partial P_L}{\partial \varphi} + v_\lambda \frac{\partial P_L}{\partial \lambda} + v_z \frac{\partial P_L}{\partial z} = H_{12}^P + H_{14}^P - H_{13}^P - H_{15}^P;$$

$$\frac{\partial P_S}{\partial t} = H_2^P + H_8^P + H_9^P + H_{10}^P - H_6^P - H_7^P - H_{11}^P,$$

where $P_U = P_{U_1} + P_{U_2} + P_{U_3}$, $P_S = P_{S_1} + P_{S_2}$. By detailing this in such a way we get:

$$\frac{\partial P_{U_1}}{\partial t} + v_\varphi \frac{\partial P_{U_1}}{\partial \varphi} + v_\lambda \frac{\partial P_{U_1}}{\partial \lambda} + v_z \frac{\partial P_{U_1}}{\partial z} = H_{17}^P - H_9^P - H_{10}^P - H_{20}^P;$$

$$\frac{\partial P_{U_2}}{\partial t} + v_\varphi \frac{\partial P_{U_2}}{\partial \varphi} + v_\lambda \frac{\partial P_{U_2}}{\varphi \lambda} + v_z \frac{\partial P_{U_2}}{\partial z} = H_{20}^P - H_{18}^P;$$

$$\frac{\partial P_{U_3}}{\partial t} + v_\lambda \frac{\partial P_{U_3}}{\partial \varphi} + v_\lambda \frac{\partial P_{U_3}}{\partial \lambda} + v_z \frac{\partial P_{U_3}}{\partial z} = H_{11}^P + H_{18}^P - H_{17}^P;$$

$$\frac{\partial P_{S_1}}{\partial t} = H_3^P - H_4^P - H_5^P;$$

$$\frac{\partial P_{S_2}}{\partial t} = H_2^P + H_4^P + H_5^P + H_8^P - H_3^P - H_6^P - H_7^P.$$

Table 4.4. The characteristics of fluxes (10^6 t/yr) and reservoirs (10^6 t) of phosphorus in the biosphere.

Reservoirs and fluxes of phosphorus	*Identifier*	*Estimate*
Phosphorus supplies		
In the atmosphere	P_A	3
On land	P_S	1,546
In the photic layer of the World Ocean	P_U	2×10^4
In deep layers of the World Ocean	P_L	12×10^4
Volcanic emissions	H_1^P	0-2
Fertilizer	H_2^P	19
Assimilation by plants	H_3^P	45.34
Input with dead plants	H_4^P	39.34
Input of the day-to-day lives of organisms		
On land	H_5^P	5
In the World Ocean	H_{20}^P	81.5
Transition to a form that cannot assimilate	H_6^P	2.9
Weathering	H_7^P	5
Falling out with precipitation		
On land	H_8^P	1.8
On the oceans	H_{16}^P	2
Removal with fish catch	H_9^P	0.06
Removal by birds	H_{10}^P	0.04
Leaching and sink into the World Ocean	H_{11}^P	4–14
Input due to detritus lysis in the oceans		
Photic layer	H_{18}^P	550
Deep layers	H_{12}^P	159
Exchange between photic and deep layers of the ocean		
Lifting	H_{15}^P	96.1
Descending	H_{14}^P	22
Precipitation	H_{13}^P	13–83.9
Rock weathering	H_{19}^P	1
Photosynthesis	H_{17}^P	630–1,300

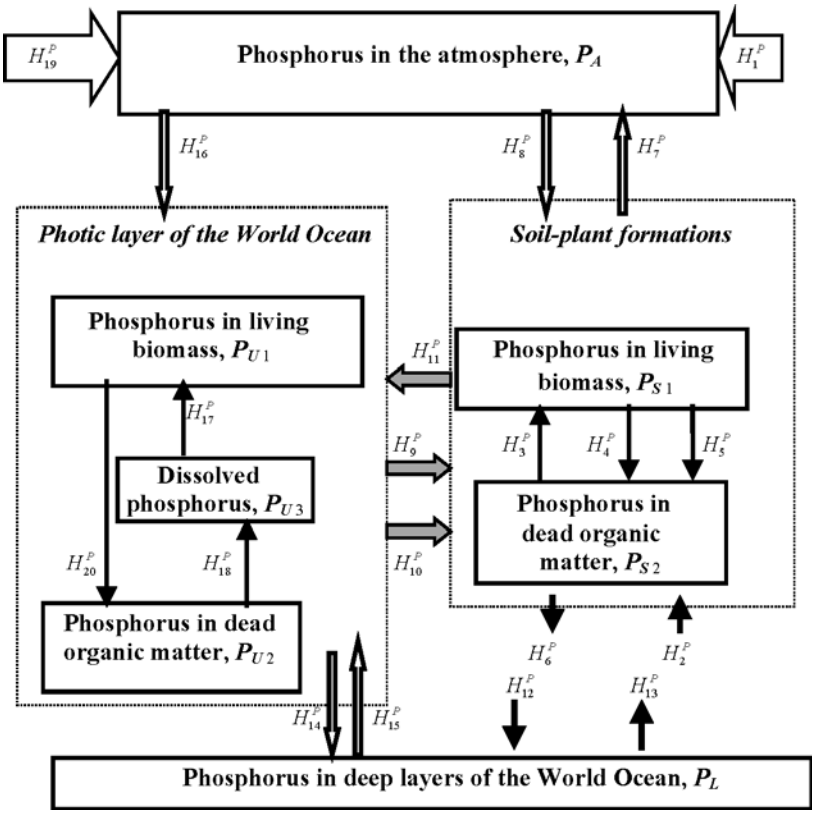

Figure 4.1. The scheme of phosphorus fluxes in the biosphere. Notations are given in Table 4.4.

Let us now determine the functional and dynamic characteristics of the fluxes of phosphorus (Table 4.4) based on analysis of existing ideas about their nature. The atmospheric cycle is governed by rock weathering, volcanic eruptions, and by the leaching of phosphorus by precipitation. From available estimates, the content of phosphorus in the lithosphere constitutes 0.093%, and the processes of weathering deliver annually to the atmosphere from $0.67\,\mathrm{mgP\,cm^{-3}\,yr^{-1}}$ to $5.06\,\mathrm{mgP\,cm^{-3}\,yr^{-1}}$. Every year, volcanic eruptions contribute to the atmosphere about $0.2 \cdot 10^6$ tP. Since these processes are complicated and stochastic in nature and their models are absent, as a first approximation fluxes H_1^P and H_{19}^P can be considered constant.

The continental cycle of phosphorus is determined by ten fluxes (Figure 4.1) closed by a single component P_S indicating the phosphorus supplies on land in soil–vegetation formations and in animals. The supplies of phosphorus in soils are replenished due to fluxes H_l^P $(l = 2, 4, 5, 8, 9, 10)$. The loss of phosphorus from the soil is determined by fluxes H_j^P $(j = 3, 6, 7, 11)$. As the detailing of surface reservoirs of phosphorus and consideration of more ingenious effects in the interaction between these reservoirs gets more complicated, so the classification of the surface fluxes of

phosphorus becomes more complicated as well. In detailing the surface reservoirs of phosphorus the following functional presentations of fluxes $\{H_i^P\}$ can be considered:

$$H_2^P = p_1 GMG_0^{-1}M_0^{-1}; \qquad H_3^P = p_V R_V; \qquad H_4^P = p_4 M_L; \qquad H_5^P = p_5 H_F;$$
$$H_6^P = p_6 P_{S_2}/P_{S_{2,0}}; \qquad H_9^P = p_3 I; \qquad H_7^P = p_7 \theta^{\Delta T} P_{S_2}/P_{S_{2,0}};$$
$$H_{11}^P = p_2 P_{S_2}[1 - \exp(-k_{su} W_{so})]/P_{S_{2,0}},$$

where p_V is the content of phosphorus in the living biomass of plants; p_4 and p_5 is the content of phosphorus in organic matter of vegetable and animal origin, respectively; I is the production of seafood from the ocean; G is the population; M is mineral resources; R_V is food production from crops; H_F is the biomass of unassimilated food of animals; $M_L = \mu_V L$; μ_V is the rate at which vegetation dies off; L is the vegetation biomass; θ is the temperature coefficient of the rate at which dead organic matter decomposes on land; ΔT is SAT variation with respect to a control value; W_{so} is the volume of river run-off into the oceans; and p_i ($i = 1, \ldots, 7$) are constants. The index "0" in G_0, M_0, and $P_{S2,0}$ attributes these parameters to some control time moment t_0, when all parameters in the model are known.

Let us describe the hydrochemical cycle of phosphorus by the totality of its fluxes H_k^P ($k = 9$–18, 20): $H_{12}^P = p_{14} R_{DL}$, $H_{13}^P = p_8 P_L/P_{L,0}$, $H_{14}^P = p_9 P_U/P_{U,0}$, $H_{15}^P = p_{10} P_L/P_{L,0}$, $H_{16}^P = p_{12} R_{WO} P_A/P_{A,0}$, $H_{17}^P = p_{13} R_\Phi$, $H_{18}^P = p_{15} R_{DU}$, $H_{20}^P = p_{16} M_\Phi$, where R_D is the rate at which dead organic matter decomposes; R_{WO} is precipitation over the ocean; R_Φ is the production of phytoplankton and other living organisms in the ocean; M_Φ is the rate at which living biomasses die off; and p_i ($i = 8$–16) are proportion constants.

4.4 GLOBALIZATION OF THE NITROGEN CYCLE

A model of the global nitrogen cycle (MGNC) needs a unit simulating the fluxes of nitrogen in the environment for several indisputable reasons: nitrogen compounds can affect environmental conditions, change the quality of food, affect the climate, and transform hydrospheric parameters. The abundant use of nitrates leads to water pollution and deteriorates the quality of food products. It is well known that intensive exploitation of soils that disregards the consequences of the misuse of nitrogen fertilizers breaks the stability of agri-ecosystems and and has concomitant effects for human health. Moreover, nitrogen protoxide (N_2O), nitrogen dioxide (NO_2), and nitrogen oxide (NO), being minor gas components of the atmosphere, substantially affect the formation of absorption processes of optical radiation in the atmosphere. Small deviations in their concentrations can cause significant climatic variations near the Earth surface (Kondratyev, 1999a; Stockwell *et al.*, 1999).

The nitrogen cycle is closely connected with the fluxes of hydrogen, sulfur, and other chemicals (Smith *et al.*, 1998; Dimitroulopoulou and Marsh, 1997; Chapin *et al.*, 2002; Rhee *et al.*, 2005; Stevenson and Cole, 1999). Nitrogen and hydrogen react under great pressure and temperature in the presence of a catalyst to make ammonia. The study of correlations between the cycles of these elements is necessary to improve

estimates of the greenhouse effect and helps in our understanding of the mechanisms involved in dynamic process formation as a result of the participation of reactive nitrogen (NO_y, NH_x) and sulfate (SO_x) in the environment.

4.4.1 The nitrogen cycle and sustainable development

Nitrogen is key to the production of food for people, fodder for animals, and fiber. The global production of nitrogen fertilizers constitutes about $90 \cdot 10^6$ tN yr^{-1}, and the volume of nitrogen fixed in natural ecosystems is estimated at approximately $150 \cdot 10^6$ tN yr^{-1}. In recent decades an increase in the availability of nitrogen for plants as a result of using fertilizers was stimulated by the growth in population size and the need for improved living standards. As a result, the anthropogenic impact on the natural nitrogen cycle is now global in scale. As Bhatti *et al.* (2006) noted, the problem of nitrogen cycle control has become a first-priority task for the Scientific Committee on Problems of the Environment (SCOPE) and International Geosphere-Biosphere Program (IGBP), which in 2002 within the framework of the World Summit on Sustainable Development in Johannesburg started the International Nitrogen Initiative (INI).

Being a vitally important element, nitrogen plays a substantial role in all proteins and deoxyribonucleic acid (DNA). There are two nitrogen pools on Earth: the atmosphere and that held within various compounds. In the atmosphere there resides the gas fraction of nitrogen (N_2). The chemical compounds of nitrogen along with other elements such as carbon, hydrogen, and oxygen are collectively called "reactive nitrogen". This includes inorganic reduced forms (e.g., ammonia and ammonium), inorganic oxidized forms (e.g., NO_x, HNO_3, N_2O, NO_3^-, and NO_2^-), and organic compounds (e.g., urea, amines, proteins, and nucleic acids). The nitrogen found in humus is of interest as it can only be attributed to the category of "reactive" conditionally, as a result of its long lifetime in soil processes. In all these forms, nitrogen circulates across the boundaries between the atmosphere, hydrosphere, biosphere, and pedosphere (the Earth's soil layer). Among these reservoirs of nitrogen, agricultural ecosystems play a growing role and, perhaps, are the decisive factor in achieving NSS sustainable development.

The growing need for food and other agricultural products, as pointed out by Wood *et al.* (2004), stimulates an increase in the rate of production and application of nitrogen fertilizers. For example, the average 2.4% annual growth in food production in the period 1961–2001 was followed by the growing use of nitrogen fertilizers reaching 4.5% per year. Of course, there is a large reservoir of nitrogen that can be used to raise the efficiency of agricultural production, fortunately with reduced loads on the nitrogen cycle due to the use of closed technologies in the application of fertilizers as well as through improvement of the structures of agricultural ecosystems. The need for nitrogen in the near future is likely to increase by 18%, from 90.0 MtN in 2005/2006 to 99.4 MtN in 2010/2011 (Heffer and Prud'homme, 2006; Mosier *et al.*, 2004).

An important indicator of the level of need for food is the size of population. According to FAO (2006) estimates, the observed dynamics of food consumption can

be quantified as 2,552 kcal per capita per day in 1979–1981 and 2,803 kcal per capita per day in 1997–1999. If this trend persists until 2030 it will lead to levels of food consumption reaching 2,940 kcal per capita per day in 2015 and 3,050 kcal per capita per day in 2030. Of course, these quantities are possible with a growth in GDP in developed countries of not less than 4% per year.

There is an adverse side to correlations between the process of sustainable development and the global cycle of nitrogen that relates to the burning of fossil fuels. Solution of problems related to NO_x emissions is the objective of many international agreements both at the intergovernmental level and within the framework of the U.N. The related results demonstrate the presence of linear correlations between the burning of carbon-containing fuels and fluxes of emitted nitric oxides. Therefore, achievement of a balance in the impacts on the nitrogen cycle may well be possible using a global model that takes into account all sources and sinks of nitrogen in its different forms.

4.4.2 Numerical models of the global nitrogen cycle

4.4.2.1 Conceptual schemes of the nitrogen cycle in nature

The global cycle of nitrogen (nitrogen being a nutrient element) takes on a mosaic structure with the local processes of its compounds the results of water migration and atmospheric processes. The present-day nitrogen cycle is strongly subject to anthropogenic forcings manifested through interference with the nitrogen cycle both directly and via the influence on related processes. Therefore, construction of an adequate model of the nitrogen cycle in nature should be based on description of the whole complex of natural processes and those initiated by humans. A general description of supplies and fluxes of nitrogen is schematically given in Figures 4.2–4.6.

The natural sources of nitrogen oxides are connected with the vital functions of bacteria, volcanic eruptions, and several atmospheric phenomena (e.g., lightning discharges). The biogeochemical cycle of nitrogen includes such processes as fixation, mineralization, nitrification, assimilation, and dissimilation. The structural schemes of these processes have been described in detail by many authors. Their complexity level is determined by the goal of the study in question, availability of data on the rates of transformation of nitrogen-containing compounds and their supplies, by the level of detail required, etc.

Nitrogen moves in the biosphere by the complicated meandering structure of its fluxes consisting of the hierarchy of cycles at various levels of life on Earth. From the atmosphere, nitrogen enters the cells of micro-organisms, through which it enters the soil, eventually reaching higher plants, animals, and humans. As living organisms die nitrogen returns to the soil, from which it either goes to plants and living organisms once again or is emitted to the atmosphere. There is a similar scheme for the cycling of nitrogen oxide that is inherent to the hydrosphere. The characteristic feature of these cycles is the ease with which nitrogen is taken up from the biosphere by rocks, from which it returns at a much slower rate. Taking into account the nature of the nitrogen

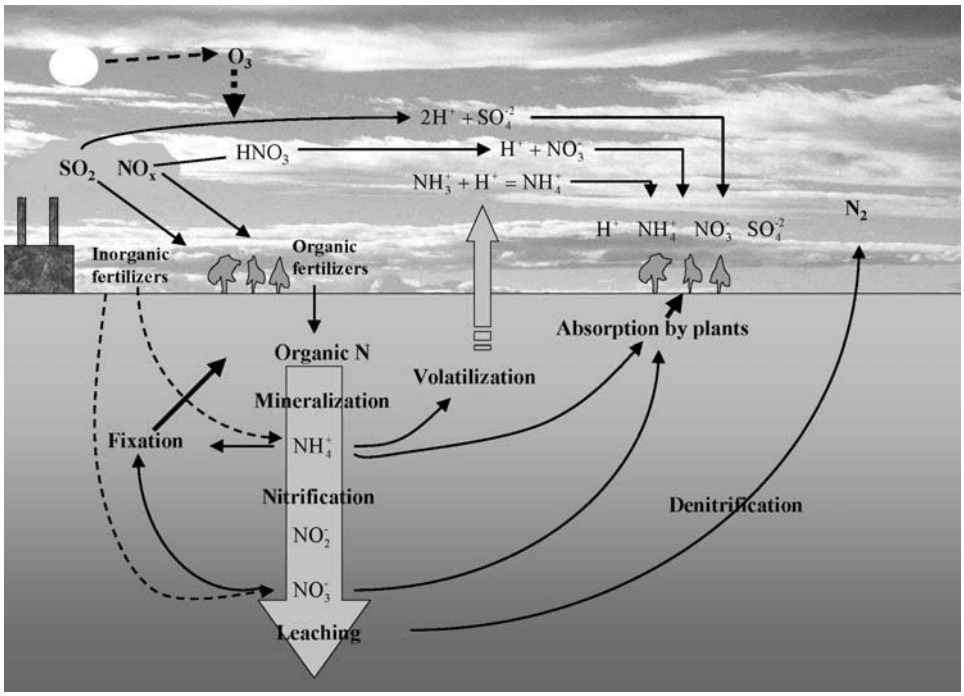

Figure 4.2. A scheme for the circulation of sulfur and nitrogen with the formation of acid precipitation.

cycle in the biosphere and its reservoir structure means we can formulate a global scheme of nitrogen fluxes.

4.4.2.2 A block diagram of the model of the global nitrogen cycle in the biosphere

Analysis of the model schemes of the flux diagrams of nitrogen compounds in nature proposed by various experts means we can construct a block diagram like that in Figure 4.6. Here the atmosphere, soil, lithosphere, and hydrosphere are considered as nitrogen reservoirs. The first three reservoirs are described by 2-D models, and the hydrosphere is described by a 3-D multi-layer model. The characteristics of nitrogen fluxes between these reservoirs are given in Table 4.5. The equations of the model are written as

$$\frac{\partial N_A}{\partial t} + V_\varphi \frac{\partial N_A}{\partial \varphi} + V_\lambda \frac{\partial N_A}{\partial \lambda} = H_1^N + \begin{cases} H_{20}^N - H_{16}^N, & (\varphi, \lambda) \in \Omega_0; \\ H_7^N + H_{19}^N - H_8^N - H_9^N + H_{22}^N - H_2^N - H_{10}^N, & (\varphi, \lambda) \in \Omega \setminus \Omega_0; \end{cases} \tag{4.19}$$

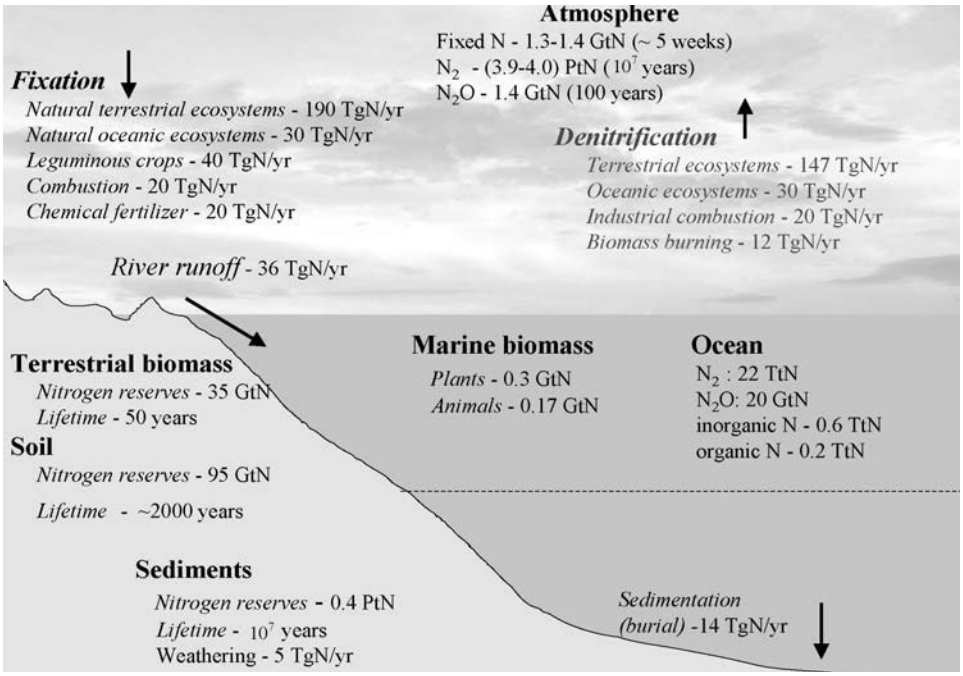

Figure 4.3. Reserves, fluxes, and cycling times of nitrogen in the atmosphere–biosphere–geosphere system. From Harrison *et al*. (2005) and Vitousek (2004). Notation: $\mathrm{Pt} = 10^{-15}$ tons, $\mathrm{Tg} = 10^{-12}$ grams, $\mathrm{Gt} = 10^{-9}$ tons.

$$\frac{\partial N_{S_1}}{\partial t} = H_8^N + H_6^N - H_3^N, \tag{4.20}$$

$$\frac{\partial N_{S_2}}{\partial t} = H_2^N + H_3^N + H_5^N + H_9^N - H_6^N - H_7^N - H_{11}^N - H_{21}^N \tag{4.21}$$

$$\frac{\partial N_U}{\partial t} + v_\varphi \frac{\partial N_U}{\partial \varphi} + v_\lambda \frac{\partial N_U}{\partial \lambda} = H_{16}^N + H_{4,U}^N + H_{18,U}^N + H_{11}^N - H_{17,U}^N - H_{20}^N - H_{14,UP}^N - H_{15,UP}^N \tag{4.22}$$

$$\frac{\partial N_P}{\partial t} + v_\varphi \frac{\partial N_P}{\partial \varphi} + v_\lambda \frac{\partial N_P}{\partial \lambda} = H_{18,P}^N + H_{4,P}^N + H_{14,UP}^N + H_{15,PL}^N - H_{17,P}^N - H_{14,PL}^N - H_{15,UP}^N \tag{4.23}$$

$$\frac{\partial N_L}{\partial t} = Q_L + H_{12,L}^N + H_{14,PL}^N + H_{15,LF}^N - H_{14,LF}^N - H_{15,PL}^N \tag{4.24}$$

$$\frac{\partial N_F}{\partial t} = Q_F + H_{12,F}^N + H_{23}^N + H_{14,LF}^N - H_{13}^N - H_{15,LF}^N \tag{4.25}$$

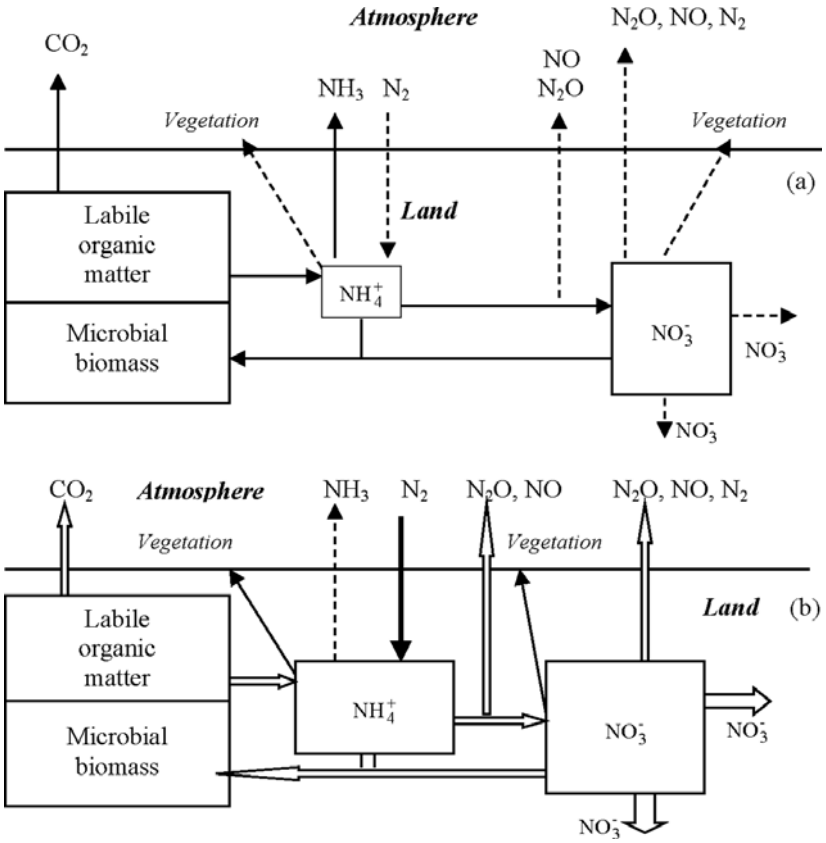

Figure 4.4. Block diagram of biogeochemical cycles of C and N in water-limited ecosystems. From Austin *et al.* (2004). (a) Dry season. (b) Wet season.

where $V(V_\varphi, V_\lambda)$ is the wind speed; $v(v_\varphi, v_\lambda)$ is current velocity in the ocean; and Q_L and Q_F are functions describing the mixing of deep water in the ocean.

To simplify the calculation scheme presented in Figure 4.6, the advective processes in Equations (4.19) through (4.25) can be described by superposition of fluxes H_{14}^N and H_{15}^N. Computer realization of the equations of the MGNC unit introduces some corrections to Equations (4.19)–(4.25) to get an agreement between the dimensions of variables and the spatial digitization of Ω. Therefore, the estimates of fluxes H_i^N given below, when considering them for inclusion in the MGNC, should be corrected following this criterion.

4.4.3 Atmospheric components of the nitrogen cycle

The atmospheric part of the nitrogen cycle is a good example of the complicated mechanism of transformation of gas substances that are characterized by an intricate set of fluxes at the borders between the basic reservoirs of nitrogen. Nevertheless, the

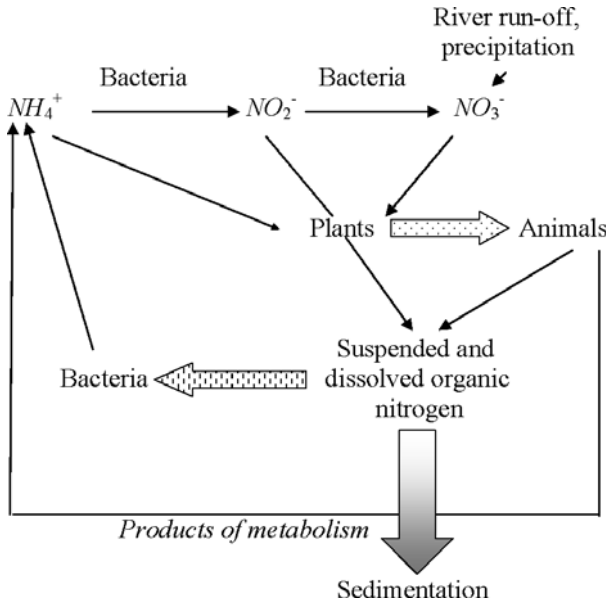

Figure 4.5. The scheme of nitrogen fluxes in the marine medium.

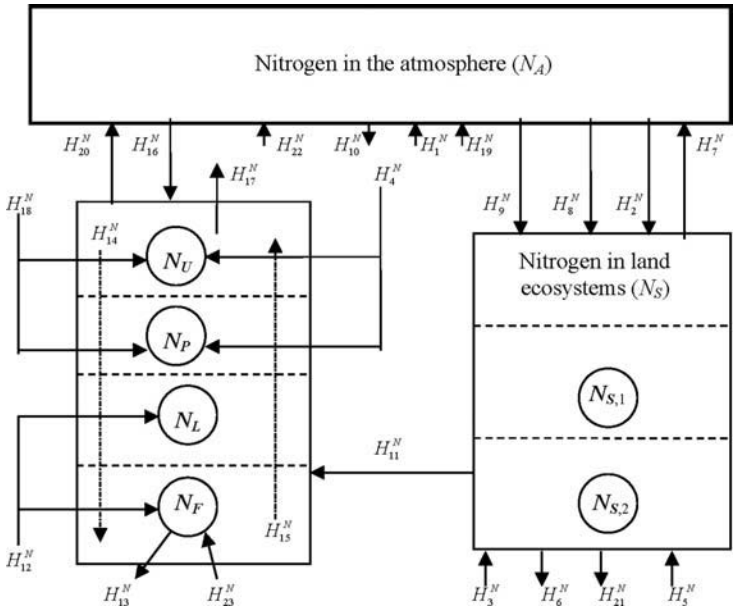

Figure 4.6. The scheme of nitrogen fluxes in nature (see Table 4.5).

Table 4.5. Characteristics of the reservoirs and fluxes of nitrogen in the biosphere (Figure 4.6).

Reservoirs (Gt) *and fluxes* (10^6 t/yr)	*Identifier*	*Estimate*
Nitrogen supplies		
Atmosphere	N_A	$(3.9–4) \times 10^5$
Soil	N_S	280–950
Photic and intermediate layer of the ocean	$N_U + N_P$	2,800
Deep and bottom layer of the ocean	$N_L + N_F$	36,400
Natural sources of the hydrosphere	H_1^N	0.392
Technogenic accumulation		
In fuel burning	H_2^N	22.8
In fertilizer production	H_9^N	41.8
Input from dead organisms		
On land	H_3^N	42.2
In the upper layers of the World Ocean	H_{18}^N	5
In deep layers of the World Ocean	H_{12}^N	7.8
Input from the day-to-day life of organisms		
On land	H_5^N	0.1
In the World Ocean	H_4^N	0.3
Biological fixation		
On land	H_6^N	20.3
In the World Ocean	H_{17}^N	10
In the atmosphere	H_{10}^N	40
Denitrification		
On land	H_7^N	52
In the World Ocean	H_{20}^N	49.8
Atmospheric fixation		
Over land	H_8^N	4
Over the World Ocean	H_{16}^N	3.6
Run-off from land into the World Ocean	H_{11}^N	38.6
Precipitation	H_{13}^N	0.5
Vertical exchange processes in the oceans		
Descending	H_{14}^N	0.2
Lifting	H_{15}^N	7.5
Anthropogenic emissions to the atmosphere	H_{19}^N	15
Removal of nitrogen from the cycle due to sedimentation	H_{21}^N	0.2
Input of nitrogen to the atmosphere in the process of weathering of rocks	H_{22}^N	0.217
Input of nitrogen to water by sediments dissolving	H_{23}^N	0.091

results obtained by many experts mean we can formulate clear ideas about the flux diagram of nitrogen compounds in the atmosphere. In particular, many international programs, such as GOME, EDGAR, TRACE-P, and CORP, are dedicated to studies of tropospheric NO_2 in connection with ozone (Ma *et al.*, 2006).

Nitrogen resides in the atmosphere both in a free state (N_2) and as various compounds, such as ammonia (NH_3), nitrogen protoxide, nitrogen oxide, nitrogen dioxide, and other nitrogen oxides (NO_3, N_2O_3, N_2O_4, N_2O_5), which play an intermediate role in chemical reactions. From available estimates, the active part of atmospheric nitrogen constitutes $3.92 \cdot 10^{12}$ t (i.e., $N_A = 0.77 \cdot 10^4\ \mathrm{t\,km^{-2}}$). Detailing the atmospheric reactions of nitrogen is still incomplete because the sources and behavior of various forms of ammonia have not been studied adequately. The most important reactions in the atmosphere are the following:

$$\mathrm{NO_2} \rightarrow \mathrm{NO} + \mathrm{O}, \qquad \varphi K_a = 0\text{–}25\ \mathrm{h^{-1}};$$
$$\mathrm{O_3} + \mathrm{NO} \rightarrow \mathrm{NO_2} + \mathrm{O_2}, \qquad K_1 = 1{,}320\ \mathrm{ppm^{-1}\ h^{-1}}.$$

Photochemical equilibrium is described by the relationship:

$$(\mathrm{NO})(\mathrm{O_3})/(\mathrm{NO_2}) = \varphi K_a / K_1.$$

The time of relaxation in this case constitutes 16 s, and therefore the equilibrium between NO, NO_2, and O_3 in the atmosphere can be considered stable. However, the equilibrium $N_2 + O_2 \leftrightarrow 2NO$ under anthropogenic conditions relates to NO transforming into NO_2 over several hours. Therefore, from the viewpoint of global modeling, the separate consideration of the components NO and NO_2 is unnecessary here as well. In other words, we shall consider atmospheric nitrogen as a generalized component of the global model.

4.4.3.1 Atmospheric fixation

Nitrogen fixation is the process by which the relatively inert molecular form (N_2) in the atmosphere is converted into ammonia, nitrate, and nitrogen dioxide, which take part in other chemical processes. As a result of the various physico-chemical processes taking place in the atmosphere, free nitrogen can move from the atmosphere to soil and water bodies. Fixation of atmospheric nitrogen due to electrical charges and photochemical processes constitutes annually no more than $0.035\ \mathrm{t\,km^{-2}}$ (arguably more accurate estimates show it to be $0.027\ \mathrm{t\,km^{-2}}$ for land and $0.01\ \mathrm{t\,km^{-2}}$ for the oceans). Since nitrogen fluxes due to atmospheric fixation are mainly determined by meteorological conditions, it is quite natural to consider them independently for each region of land and each water body of the World Ocean as functions of temperature and precipitation.

Flux H_{16}^N of nitrogen fixed in the atmosphere over any ocean basin is described by the relationship:

$$H_{16}^N = [\lambda_1(\theta_1)^{\Delta T} + \lambda_2 R_W] N_A,$$

where ΔT is atmospheric temperature variation; θ_1 is the indicator of temperature dependence of the rate of atmospheric fixation of nitrogen; R_W is precipitation; and λ_1 and λ_2 are coefficients.

The equation of atmospheric fixation over a land site Ω_{ij} is written by analogy to H_{16}^N:

$$H_{8,ij}^N = [\lambda_3(\theta_1)^{\Delta T} + \lambda_4 R_{W,ij}]N_A,$$

where λ_3 and λ_4 are coefficients.

To estimate coefficients λ_i $(i = 1, \ldots, 4)$, as a first approximation we can use average data on nitrogen fluxes and precipitation. If we assume $H_{16}^N = 9.96 \cdot 10^{-3}\,\mathrm{t\,km^{-2}\,yr^{-1}}$, $H_8^N = 0.027\,\mathrm{t\,km^{-2}\,yr^{-1}}$, and estimate local precipitation over the ocean and land at $1.01\,\mathrm{m\,yr^{-1}}$ and $0.24\,\mathrm{m\,yr^{-1}}$, respectively, and convective precipitation over the ocean and land at $0.19\,\mathrm{m\,yr^{-1}}$ and $0.116\,\mathrm{m\,yr^{-1}}$, respectively, we obtain $\lambda_1 = 0.00498$, $\lambda_2 = 0.00458$, $\lambda_3 = 0.0135$, and $\lambda_4 = 0.0285$. These estimates are easily specified by taking onboard local data at a fixed time moment for smaller regions and water bodies.

4.4.3.2 Geospheric sources of nitrogen

The flux of nitrogen H_1^N is determined by the geothermal activity of the Earth. Estimates of H_1^N testify to the necessity for this constituent to be considered in the global model. For instance, in the nitrogen fumaroles of Vesuvius the content of nitrogen by weight constitutes 98%, in gases of the lavas of Hawaiian volcanoes nitrogen constitutes only 5.7%, and over the globe the input of juvenile nitrogen averages $0.4 \cdot 10^6\,\mathrm{t\,yr^{-1}}$. Let H_1^N be a function of time approximating a statistical series of observations. A more strict account of this flux of nitrogen in the model can be realized by using algorithms to parameterize random processes (e.g., by using evolutionary modeling). However, within the global model, oriented toward describing processes in time steps of decades, it is enough to use average annual data.

Flux H_1^N can be, to some extent, interpreted as compensating for fluxes H_{13}^N and H_{21}^N.

4.4.4 The land surface part of the biospheric nitrogen cycle

The nitrogen supplies on land consist of the assimilable nitrogen in the soil $N_{S2} \approx 0.19 \cdot 10^4\,\mathrm{t\,km^{-2}}$, in plants $(12 \cdot 10^9\,\mathrm{t})$, and living organisms $(0.2 \cdot 10^9\,\mathrm{t})$. A diversity of nitrogen fluxes is formed here of the processes of nitrification, denitrification, ammonification, fixation, and river run-off. The intensities of these fluxes depend on climatic conditions, temperature regime, moisture, as well as the chemical and physical properties of soil. Many qualitative and quantitative characteristics of these dependences have been described in the literature (Hellebrandt *et al.*, 2003). Let us consider some of them.

4.4.4.1 Nitrification

Nitrification is the biological oxidation of ammonia (by oxygen) producing nitrites followed by the oxidation of these nitrites into nitrates. Nitrification is an important step in the nitrogen cycle in the soil. Nitrification involves the oxidation of nitrogen by specialized bacteria (*Nitrosomonas*, *Nitrobacter*, etc.).The return of nitrogen to the cycle due to the day-to-day life of micro-organisms is a stabilizing natural process. To simplify the whole process of the ammonia salt transformation into nitrates, let us present the activity of heterotrophic micro-organisms and saprophages as a generalized process for organic matter decomposition. The rate of organic matter decomposition and nitrification increases with increasing temperature, reaching its optimal value at $T_a = 34.5^{\circ}\mathrm{C}$. Therefore, for flux H_3^N an approximation $H_3^N = \lambda_{N_\kappa} M_\kappa$ can be assumed, where M_κ is the rate at which component κ dies off, and λ_{N_κ} is the content of nitrogen in component κ.

4.4.4.2 Denitrification

Denitrification takes place in anoxic environments where nitrate and nitrite act as electron acceptors (oxidizers) and nitrification reactions then reverse: $NO_3^- \Rightarrow NO_2^- \Rightarrow NO$. The processes of denitrification (H_7^N) on land are important channels for nitrogen to get into the atmosphere. The intensity of these processes depends on temperature, humidity, pollution of soils with poisonous chemicals, and pH. The quantitative and functional characteristics of these dependences have been well studied. The global model need only take into account temperature and humidity:

$$H_7^N = \lambda_6 \theta_2^{\Delta T} W_S \frac{N_S}{k_1 + N_S},$$

where W_S is soil moisture; θ_2 is the temperature coefficient; and λ_6 and κ_1 are empirical parameters. If we assume $H_7^N = 0.318\,\mathrm{t/km^2/yr}$, then $\lambda_6 = 0.496$ and $k_1 = 0.556$.

4.4.4.3 Biological fixation

In the biological cycle of nitrogen of importance are the processes of its fixation by micro-organisms and plants whose intensity is estimated at $148 \cdot 10^6\,\mathrm{t\,yr^{-1}}$. The rate of fixation, depending on the character of the medium, can vary reaching $3 \cdot 10^9\,\mathrm{t\,yr^{-1}}$ in highly productive regions. Nitrogen flux H_{10}^N depends on the distribution of vegetation cover and can be described by the equation $H_{10}^N = \sigma_\kappa \lambda_\kappa R_\kappa / \sigma_{ij}$, where σ_κ is the parcel of land under vegetation of κ type in territory Ω_{ij} of area σ_{ij}, R_κ is the productivity of plants of κ type, and λ_κ is the coefficient.

The fixation of nitrogen by plants directly from the soil via the root systems (flux H_6^N) occupies a principle place in the nitrogen cycle, especially in areas that are cultivated. For instance, an increase in the yield of legumes in agriculture can raise H_6^N up to $35\,\mathrm{t\,km^{-2}\,yr^{-1}}$. Therefore, consideration of this flux in the model is

necessary and can be realized in the following form:

$$H_6^N = \sigma_\kappa R_\kappa \mu_\kappa / \sigma_{ij}, \tag{4.26}$$

where μ_κ is the constant.

The rate of assimilation of nitrogen by the roots of plants is known to depend much on the soil temperature regime, decreasing a little as temperature lowers to 8°C–10°C and dropping dramatically at temperatures below 5°C–6°C. The movement of nitrogen from the roots to the upper parts of the plants slows down, too. Formula (4.26) reflects this regularity through the respective reactions of plant productivity (time lag is disregarded).

On land, plants assimilate annually about $30 \cdot 10^6$ tN from the atmosphere and more than $5.3 \cdot 10^6$ tN directly from the soil. Approximate estimates of the productivity of various types of vegetation average $R_\kappa = 710\,\mathrm{t\,km^{-2}\,yr^{-1}}$–$3{,}243\,\mathrm{t\,km^{-2}\,yr^{-1}}$. Hence, from (4.26) we have $\mu_\kappa = 0.134 \cdot 10^{-5}$–$0.506 \cdot 10^{-4}$.

4.4.4.4 The loss of nitrogen through leaching from soils

On global scales, one means of nitrogen migration includes the transport of its compounds between land and oceans due to water run-off. The annual input of nitrogen from land into the World Ocean is estimated at $38.6 \cdot 10^6$ t. Let the total sink to the ocean from land be described by the function W_{SO}, then the nitrogen flux H_{11}^N can be approximated by the expression

$$H_{11}^N = \lambda_N N_{S_2}[1 - \exp(-k_N W_{SO})],$$

where λ_N and k_N are coefficients. The functional form foresees nitrogen flux from the land to the ocean as equal to zero in the absence of run-off and its stabilization at level λ_N, with the run-off volume considerably increasing. To estimate the parameters λ_N and k_N, it is necessary to take into account the spatial heterogeneity of the types of soil–vegetation formations, relief, and other geophysical parameters. In particular, the content of nitrogen compounds in water differs as a function of run-off territory. River water in forest regions with a temperate climate contain $0.4\,\mathrm{mg\,L^{-1}}$ of nitrates; for arid areas this value is $1.45\,\mathrm{mg\,L^{-1}}$. The concentration of nitrates increases sharply in the drainage water of irrigation systems ($5.5\,\mathrm{mg\,L^{-1}}$), in the river water of thickly populated regions ($25\,\mathrm{mg\,L^{-1}}$), and reaches a maximum in the soil solutions of salty irrigated soils ($200\,\mathrm{mg\,L^{-1}}$). Ground water contains from $10\,\mathrm{mg\,L^{-1}}$ to $100\,\mathrm{mg\,L^{-1}}$ of nitrates. The total run-off of water into the World Ocean reaches $50 \cdot 10^3\,\mathrm{km^3}$, 30% of which is underground run-off; hence, the total flux of nitrogen per unit area of the ocean is $0.107\,\mathrm{t\,yr^{-1}}$. Assuming $W_{SO} = 0.337$ m and that a 95% level of sink saturation is reached at a five-fold increase of W_{SO}, we obtain $k_N = 0.367$ and $\lambda_N = 0.708$.

The land surface part of the nitrogen cycle involves the constant process of nitrogen removal from the biosphere into deposits (in particular, as a result of accumulation of saltpeter on the Earth surface through erosion and alkalification). From the available estimates, $H_{21}^N \approx 3.9 \cdot 10^{-4}\,\mathrm{t/km^2/yr}$, with $H_{21}^N < H_{22}^N$, but $H_{21}^N + H_{13}^N \cong H_1^N + H_{22}^N + H_{23}^N$. This relationship follows from the fact that during

the Holocene the loss of nitrogen was balanced by its input. Of course, in the present biosphere, with the changing intensity of most of the fluxes enumerated in Table 4.5, this balance is breaking down as a result of increasing fluxes H_9^N and H_{19}^N.

Finally, we must mention the fact that in connection with the persistent C/N ratio for different types of soils and climatic zones for nitrogen fluxes it is important to find correlations between factors that regulate biogeochemical cycles at a regional level. Arid regions where soils are poor in micro-organisms and the moisture cycle is determined by division into dry and wet seasons are important here. In this connection, Austin *et al.* (2004) showed that the episodic nature of water availability in arid and semi-arid ecosystems has significant consequences on below-ground carbon and nutrient cycling. Pulsed water events directly control the C/N of microbially available substrate. The level of this control depends on the spatiotemporal heterogeneity of vegetation cover, topographic position, and soil texture. The seasonal distribution of water pulses eventually leads to a change in biogeochemical cycling in water-limited ecosystems. A schematic outline of the biogeochemical cycles of C and N in arid and semi-arid ecosystems in dry seasons, and after rainfall is given in Figure 4.4.

4.4.5 The hydrosphere and its role in the dynamics of the nitrogen cycle

In seawater, nitrogen is present as dissolved gas, ions of ammonium NH_4^+, nitrite NO_2^-, nitrate NO_3^-, and as various organic compounds. Inorganic nitrogen compounds are assimilated by algae and phytoplankton and thus transfer into organic forms that serve as food for living organisms. The expenditure of inorganic nitrogen supplies is compensated by atmospheric precipitation, river run-off, and mineralization of organic remains in the process of the day-to-day lives of organisms and their dying-off. According to Ivanov (1978), nitrogen fluxes in seawater can be schematically shown (see Figure 4.5). Of course, not all nitrogen fluxes available in nature have been taken into account. The diversity of ways in which nitrogen transforms in water have been studied inadequately, though the available information may well be sufficient for the global model. Processes, such as the replenishing of nitrogen supplies in water due to the lysis of detritus and the functioning of living organisms, the nitrogen exchange between photic and deep layers of the ocean, and nitrogen fixation at photosynthesis and denitrification, have been thoroughly studied and described in the literature. Also, there are rough estimates of nitrogen supplies in the ocean, according to which we can assume, on average, that $N_U = N_P = 0.77 \cdot 10^4\,\mathrm{t\,km^{-2}}$ and $N_L = N_F = 10^5\,\mathrm{t\,km^{-2}}$. More detailed spatial distributions of nitrogen supplies in the hydrosphere can be calculated from data on biomass, dissolved organic matter, and concentration of dissolved oxygen. The volume relationships of dissolved nitrogen are related to the volume of oxygen as $\mathrm{mLN_2/L} = 1.06 + 1.63\,\mathrm{mLO_2/L}$.

Nitrogen supplies in water bodies are replenished due to the bacterial decomposition of organic sediments and dissolved organic matter. Let us consider component D as the content of dead organic matter in water. On such a basis, we can write $H_{18}^N = \lambda_D D(\varphi, \lambda, z, t)$, where λ_D is the indicator of the nitrogen content and

the rate of detritus lysis. The free nitrogen supplies in water are also replenished as organisms live their lives. By accounting for phytoplankton Φ and nekton r, we have:

$$H_4^N = H_r^N + H_\Phi^N; \qquad H_r^N = \lambda_r T_r; \qquad H_\Phi^N = \lambda_\Phi T_\Phi,$$

where T_r and T_Φ are characteristics of the metabolic processes, respectively, in nekton and phytoplankton; and λ_r and λ_Φ are coefficients. To determine average values for these coefficients, let us assume $T_r = 0.194\,\mathrm{t\,km^{-2}\,yr^{-1}}$, $T_\Phi = 0.125\,\mathrm{t\,km^{-2}\,yr^{-1}}$, and $H_r^N = H_\Phi^N = 0.83 \cdot 10^{-3}\,\mathrm{t\,km^{-2}\,yr^{-1}}$. Then $\lambda_r = 0.00428$ and $\lambda_\Phi = 0.00664$.

The process of denitrification in water delivers considerable amounts of nitrogen to the atmosphere: $H_{20}^N = \lambda_5(\theta_2)^{\Delta T} N_U(\varphi, \lambda, z, t)$, where λ_5 and θ_2 are constants.

The biological fixation of nitrogen in water is about $10 \cdot 10^6\,\mathrm{t\,yr^{-1}}$, reaching $20.7 \cdot 10^6\,\mathrm{t\,yr^{-1}}$ in the photic layer of the ocean, and $(36\text{–}1{,}800) \cdot 10^4\,\mathrm{t\,km^{-3}\,yr^{-1}}$ in small lakes. For the World Ocean, $H_{17}^N = 0.0277\,\mathrm{t\,km^{-1}\,yr^{-1}}$, on average. Assuming $H_{17}^N = \lambda_R R_\Phi$, where R_Φ is the production by phytoplankton averaging $168.8\,\mathrm{t\,km^{-2}\,yr^{-1}}$, we obtain $\lambda_R = 0.164 \cdot 10^{-3}$.

The characteristic feature of the nitrogen cycle in water is its transport due to gravitational sedimentation, vertical convection, turbulent diffusion, and convergence. The processes of nitrogen transport by migrating animals are almost negligible and can be neglected in the global model. The simplest way of describing the vertical fluxes of nitrogen can be reduced to the model $H_{14}^N = \lambda_\kappa \Delta N_\kappa$, $H_{15}^N = \lambda_\rho \Delta N_\rho$, where $\kappa = (U, P, L)$ and $\rho = (P, L, F)$.

4.4.6 Anthropogenic factors affecting the biospheric nitrogen cycle

The present contribution of human activity to the general biospheric cycle of nitrogen has reached a level when the consequences of changes have become unpredictable and probably catastrophic. Epidemiological studies testify to the growth of respiration diseases in areas with high concentrations of nitrogen and sulfur oxides as well as photochemical oxidizers. The harmful effect of nitrogen oxides on living organisms starts to manifest itself when the $940\,\mu\mathrm{kg\,m^{-3}}$ level is exceeded. In general, the consequences of nitrogen pollution of the biosphere are more complicated. For instance, on the one hand, technogenic accumulation of nitrogen from the atmosphere for fertilizer production plays a positive role by raising the productivity of land and water ecosystems, and, on the other hand, it causes the undesirable eutrophication of water basins. Removal of nitrogen from the atmosphere for industrial and agricultural needs is compensated for by technogenic input of nitrogen into the atmosphere through the burning of solid and liquid fuel. A considerable share is contributed by the transport sector, which emits nitrogen oxides reaching, for instance, in the U.S.A., $11.7 \cdot 10^6$ t per year. However, even this physical equilibrium cannot restore the chemico-biological balance. Therefore, in this multi-functional hierarchical set of global fluxes of nitrogen, the most vulnerable breaks and linkages should be highlighted, which is only possible within a well-planned numerical experiment.

Quantitative estimate of the main stages of the nitrogen cycle that takes into account the human factor enables us to see the overall effect of breaking the global

balance of nitrogen. Tables 4.5 and 4.6 demonstrate the size of this imbalance. However, from available data on the global distribution of violations of the nitrogen cycle it is impossible to reliably estimate the contribution of the industrial synthesis of nitrogen compounds and their scattering over the globe into its biogeochemical cycle. In the final years of the 20th century, industry increased the total amount of nitrogen circulating in the biosphere by 50%. As a result, the natural equilibrium between the processes of nitrification and denitrification turned out to be out of balance to the tune of $9 \cdot 10^6$ t.

Preliminary estimates of increasing anthropogenic pressure on the nitrogen fluxes between biospheric elements suggest the hypothesis of the existence of a strong correlation between fertilizer production H_9^N and population density G, technogenic accumulation of nitrogen from the burning of fuel H_2^N and mineral resource expenditure R_{MG}, anthropogenic input of nitrogen into the atmosphere H_{19}^N, and the intensity of emissions of general pollution Z_{VG}. The quantitative characteristics of these dependences can be obtained from known trends. From some estimates, the amount of nitrogen oxide emitted to the atmosphere is proportional to the weight of the fuel used with a 4% annual increasing trend. The scales of industrial fixation of nitrogen for the last 40 years increased by a factor of 5, reaching a value that could have been fixed by every ecosystem on Earth before the advent of current agricultural technology. In 1968, global industry was responsible for about $30 \cdot 10^6$ t of fixed nitrogen and in 2000 this value reached 1 billion.

Let us formalize these correlations as the following models:

$$\left.\begin{aligned} H_9^N &= \min\{U(K)\overline{G}(K,t); N_A\sigma_K/\sigma\}, \\ H_2^N &= \lambda_{AG}R_{MG}, \qquad H_{19}^N = \lambda_{GA}Z_{VG} \end{aligned}\right\} \tag{4.27}$$

where K is the number allocated to an economic region; $\overline{G}$ is the average population density of region K; and σ_K is the area of region K. The coefficients U, λ_{AG}, and λ_{GA} are determined from analysis of available information about the processes in (4.27). If we assume that $H_2^N = 0.154\,\mathrm{t\,km^{-2}\,yr^{-1}}$, $H_{19}^N = 0.102\,\mathrm{t\,km^{-2}\,yr^{-1}}$, and $H_9^N = 0.283\,\mathrm{t\,km^{-2}\,yr^{-1}}$, then at $\overline{G} = 24.4$ people $\mathrm{km^{-2}}$, $R_{MG} = 30.5$ oil units $\mathrm{km^{-2}\ yr^{-1}}$, and $Z_{VG} = 3.39\,\mathrm{t\,km^{-2}\,yr^{-1}}$, we obtain $U = 0.283$, $\lambda_{AG} = 0.504 \cdot 10^{-2}$, and $\lambda_{GA} = 0.03$.

Anthropogenic interference with the nitrogen cycle can also have medico-biological consequences expressed, for instance, through increasing mortality with growing amounts of NO_2 at $190\,\mu\mathrm{g\,m^{-3}}$–$320\,\mu\mathrm{g\,m^{-3}}$, if living organisms experience this level for one hour more than once a month. From the data of the World Health Organization the natural background concentration of NO_2 over continents constitutes $0.4\,\mu\mathrm{g\,m^{-3}}$–$9.4\,\mu\mathrm{g\,m^{-3}}$.

Finally, human impact on the nitrogen cycle can affect the structure and intensity of biospheric energy exchange. As can be seen in Table 4.7, there are possibilities of considerable shifts in such an exchange depending on intensification of one or another reaction.

Table 4.6. Estimates of some parameters of the global biogeochemical cycle of nitrogen in the biosphere.

Parameter	*Estimate*
Nitrogen content in the atmosphere (%)	
By volume	78.084
By weight	75
Nitrogen content in some biospheric components (%)	
Soil humus	6
River water	1.5×10^{-3}
Sewage	2.5
Vegetation decomposition	1
Marine organisms	5
Content of dissolved nitrogen in seawater (mL/L)	
Near the equator	14.1
High latitudes	8.2
Average content of nitrogen in seawater (g/m^3)	0.3
Content of nitrates in river water (t/km^3)	
Arid regions	1.45
Densely populated regions	25
Temperate climate forests	0.4
Concentration of nitrates (t/km^3)	
Drainage water of irrigation systems	5.5
Soil solutions of salty irrigated soils	200
Ground water	10–100
Fallout of fixed nitrogen onto the land (10^6 t/yr)	
Through precipitation	25
Aerosols	15
Assimilation of nitrogen by land plants (10^6 t/yr)	
From the atmosphere	30
From the soil	5.3
Input of nitrogen to the ocean due to detritus lysis (10^6 t/yr)	5
Intensity of nitrogen movement from the photic layers of the oceans to deep layers with descending water, sedimentary algae, and animal carcasses (10^6 t/yr)	0.2
Global production of nitrogen fertilizers (10^6 t/yr)	31.6–90.1
Removal of nitrogen from the soil by growth of crops (10^6 t/yr)	90–200

Parameter	*Estimate*
Emissions of nitrogen oxides in some countries (10^6 t/yr)	
U.S.A.	22.8
Japan	2.4
U.K.	2.43
The Netherlands	0.32
Concentration of NO_2 in the stratosphere at altitudes (ppb)	
10 km	0.2–0.5
30 km	4–12
Background value of N_2O concentration in the atmospheric layer up to 16 km (ppm)	325
Observed variations in background N_2O concentration in the atmospheric layer up to 16 km (ppm)	0.08–0.35
NO concentration near the Earth surface (ppb)	
Over oceans	0.004
Over industrial regions	1
Background content of NO in the atmosphere (ppb)	
In the layer up to 7 km	0.03–0.06
At altitudes 35 km–45 km	5–20
NO_2 concentration in the surface air layer (ppb)	
Over oceans	0.1–2.6
Over continents	0.8–16

4.5 BIOSPHERIC BUDGET OF OXYGEN AND OZONE IN THE CONTEXT OF GLOBALIZATION PROCESSES

The oxygen cycle in nature is composed of characteristic biogeochemical transitions between the reservoirs of basic constituents circulating in the biosphere (Lane, 2003). Therefore, a block scheme of oxygen exchange resembles those of sulfur, nitrogen, carbon, and phosphorus (Figure 4.7 and Table 4.8). However, oxygen has the widest spread of constituents across the globe, which makes it one of the substantial components of the biogeochemical cycles. Its amount in the Earth's crust, including the hydrosphere, reaches 49% by mass. The lithosphere (without the ocean and the atmosphere) contains 47.2% of oxygen and 88.89% of water. In ocean water, oxygen constitutes 85.82% and living organisms contain 65% by mass. These estimates testify to the significance of oxygen for the biosphere, the appearance and existence

Table 4.7. Basic reactions of the global biogeochemical cycle of nitrogen and their energy output. From Delvich (1972).

Reaction	*Reaction formula*	*Energy output* (kcal)
Ammonification	$CH_2NH_2COOH + \frac{3}{2}O_2 \rightarrow 2CO_2 + H_2O + NH_3$	176
Nitrification	$NH_3 + \frac{1}{2}O_2 \rightarrow HNO_2 + H_2O$ $KNO_2 + \frac{1}{2}O_2 \rightarrow KNO_3$	66 17.5
Fixation	$N_2 \rightarrow 2N$ $2N + 3H_2 \rightarrow 2NH_3$	-160 12.8
Respiration	$C_6H_{12}O_6 + 6O_2 \rightarrow 6CO_2 + 6H_2O$	686
Denitrification	$C_6H_{12}O_6 + 6KNO_3 \rightarrow 6CO_2 + 3H_2O + 6KOH + 3N_2O$ $5C_6H_{12}O_6 + 24KNO_3(3OCO_2 + 18H_2 + 24KOH + 12N_2$ $5S + 6KNO_3 + 2CaCO_3 \rightarrow 3K_2SO_4 + 2CaSO_4 + 2CO_2 + 3N_2$	545 570 132

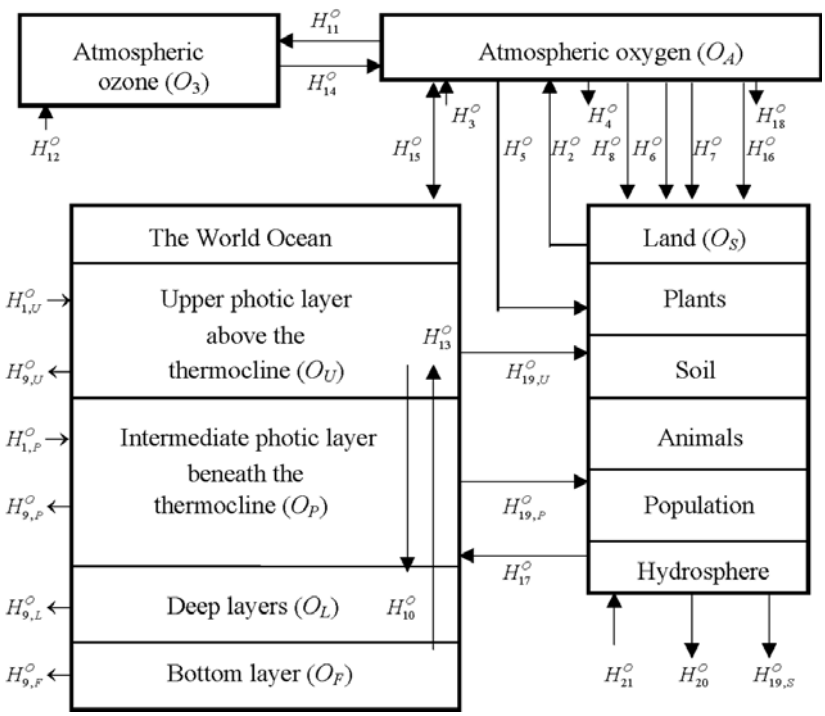

Figure 4.7. Oxygen fluxes in the biosphere.

Table 4.8. Estimates of the reservoirs and fluxes of oxygen and ozone used to adjust the GMNSS unit. From Kondratyev and Varotsos (2000).

Reservoirs (t/km^2), *fluxes* ($t\,km^{-2}\,yr^{-1}$)	*Identifier*	*Estimate*
Oxygen in the upper photic layer of the World Ocean	O_U	0.8×10^8
Oxygen in the transition layer of the ocean	O_P	0.7×10^9
Oxygen in deep ocean	O (?)	3×10^4
Oxygen in the bottom layer of the ocean	O_F	9×10^3
Oxygen in the atmosphere	O_A	0.24×10^7
Oxygen in the surface part of the hydrosphere	O_S	0.6×10^8
Ozone	O_3	0.23
Photosynthesis in the ocean	H_1^O	108–388
Photosynthesis on land	H_2^O	70-100
Photodecomposition of water in the atmosphere	H_3^O	0.008
Oxidation processes in the atmosphere	H_4^O	0.009
Respiration of plants	H_5^O	0.07–0.1
Respiration of animals	H_5^O	50–60
Respiration of humans	H_7^O	70–80
Oxidation–restoration processes in soil	H_8^O	1
Oxidation processes in the World Ocean	H_9^O	164
Descent in oxygen-saturated waters	H_{10}^O	190
Decomposition and destruction of O_2 in the atmosphere	H_{11}^O	
Formation of O_3 from NO_2	H_{12}^O	0.23–22.2
Lifting of dissolved oxygen in upwelling zones	H_{13}^O	36
Decomposition and destruction of ozone in the atmosphere	H_{14}^O	1.48–1.66
Exchange at the atmosphere–ocean border	H_{15}^O	18–140
Exchange at the atmosphere–inland water body border	H_{16}^O	18–140
Transport of oxygen to the ocean by river run-off	H_{17}^O	50
Anthropogenic consumption of oxygen	H_{18}^O	60–90
Expenditures of O_2 on metabolism by aquatic animals	H_{19}^O	0.2
Oxidation processes in continental water bodies	H_{20}^O	90–200
Photosynthesis in continental water bodies	H_{21}^O	100–400

of which are determined by the presence of oxygen (Lane, 2003). Today about $39 \cdot 10^{14}\,tO_2$ circulate in the biosphere, $37 \cdot 10^{18}\,molO_2$ reside in the atmosphere; the oceans and long-lived biota contain $219 \cdot 10^{15}\,molO_2$ and $180 \cdot 10^{15}\,molO_2$, respectively. The timescale of the complete cycle of oxygen varies from $3 \cdot 10^6$ years for the atmosphere to 22 days for the surface waters of the World Ocean. On the whole, for oceans and long-lived biota, oxygen completes its cycle in 500 and 50 years, respectively.

Oxygen is present in the biosphere in the form of molecular oxygen (O_2), ozone (O_3), atomic oxygen (O), and as a constituent of various oxides. On the one hand, oxygen maintains life on the Earth due to the process of respiration and formation of the ozone layer, and, on the other hand, is itself the product of the day-to-day living of organisms. This fact hinders a description of its cycle, since it requires synthezing various processes. An attempt was made to describe the cycle and derive a model of the global oxygen cycle (MGOC) as a unit of the GMNSS (Kondratyev *et al.*, 2004b).

Many authors believe that in the short term nothing threatens the stability of the global biogeochemical cycle of oxygen. This statement is not valid for ozone, whose concentration and spatial distribution suffered serious changes in recent decades. According to Kondratyev and Varotsos (2000), available observations of the vertical profile of atmospheric ozone show a very complicated spatiotemporal variability that depends on many characteristics of the nature–society system. The MGOC unit that parameterizes ozone fluxes follows the numerical model by Aloyan (2004) and Arutiunian *et al.* (2004), with the needed correction taken into account. This correction consists in substituting some functional dependences for scenarios reflecting the dynamics of the changes in concentrations of the chemicals which are not described in the global model of the carbon cycle.

4.5.1 Oxygen sources and sinks

4.5.1.1 Oxygen sources

Nowadays and in the geological past there have been two sources of oxygen: endogenic and photosynthetic. Without dwelling on the respective scientific discussions and all existing concepts, we shall try to describe the sources of oxygen in the present biosphere, following numerous studies in this field.

The basic source of atomic oxygen is the photosynthesis of plants, whose equation has the form:

$$2H_2O + CO_2 \xrightarrow[\text{chlorophyll}]{\text{light}} COH + H_2O + O_2$$

Photosynthesis annually produces above $50 \cdot 10^9$ t of oxygen (i.e., an order of $3.3 \cdot 10^{14}$% of its supply in the atmosphere). Hence, we can see that only by means of photosynthesis can the oxygen supplies in the atmosphere be totally renewed during a time period of 300,000 years. About 80% of the total amount of oxygen produced

by photosynthesis results from the day-to-day activity of phytoplankton, and land vegetation communities produce only 20%. If we denote by $R_\Phi(\varphi, \lambda, t)$ and $R_\kappa(\varphi, \lambda, t)$ the production by phytoplankton Φ and the land surface of κ type at an Earth surface point (φ, λ) at a time moment t, then oxygen fluxes to the hydrosphere and from land to the atmosphere can be described by the relationships:

$$H_1^O = a_\Phi R_\Phi, \qquad H_2^O = a_\kappa R_\kappa, \qquad H_{21}^O = a_s R_\Phi,$$

where the coefficients a_Φ, a_κ, and a_S depend on phytoplankton species and the type of vegetation. To average them out we use data on fluxes: $H_1^O = 140\,\mathrm{tO_2\,km^{-2}\,yr^{-1}}$, $H_2^O = 70\,\mathrm{tO_2\,k^{-2}\,yr^{-1}}$, $H_{21}^O = 600\,\mathrm{tO_2\,km^{-2}\,yr^{-1}}$, $R_\Phi = 401.3\,\mathrm{t\,km^{-2}\,yr^{-1}}$, and $R_\kappa = 102.4\,\mathrm{t\,km^{-2}\,yr^{-1}}$. Then $a_\Phi = 0.35$, $a_\kappa = 0.68$, and $a_S = 1.49$. Of course, these estimates have a considerable spatiotemporal scatter. In particular, using data on the productivity of some oceans, we obtain values for the coefficient a_Φ: the Atlantic Ocean 0.53; the Indian Ocean 0.25; the Arctic Ocean 11.1; and the Pacific Ocean 0.64.

Apart from photosynthesis, photolysis can be a source of oxygen in the atmosphere (i.e., the decomposition of water vapor under the influence of UV radiation in the upper layers of the atmosphere). However, the intensity of this source under present conditions is negligible. Nevertheless, let us denote this flux by $H_3^O = a_H W_A$, where W_A is water vapor content in the atmosphere; and a_H is an empirical coefficient. If we assume that in the upper layers of the atmosphere a constant share of W_A can reside, then at $H_3^O = 0.0039\,\mathrm{tO_2\,km^{-2}\,yr^{-1}}$ and $W_A = 0.025\,\mathrm{m}$, we have $a_H = 1.56 \cdot 10^{-7}$ per year.

Vernadsky (1944) considered rock metamorphism, basaltic volcanism, and underground radioactive waters as possible sources of oxygen. However, there are no sufficiently reliable estimates of these fluxes and therefore it is impossible to parameterize them.

4.5.1.2 Processes of oxygen assimilation

The oxidation process both on land and in water is the basic consumer of oxygen on Earth. The ability of oxygen to react with many elements of the Earth crust forms the fluxes of oxygen leaving biospheric reservoirs. The balance between the income and expenditure fluxes of oxygen was reached in the course of the biospheric evolution.

Oxygen is spent on respiration by plants, animals, humans, and on dead organic matter decomposition both in the hydrosphere and on land. To parameterize the income parts of oxygen balance, we use the following models: $H_5^O = a_1 T_\kappa$, $H_6^O = a_2 T_F$, $H_7^O = a_3 T_G$, $H_{19}^O = a_6 T_R$, $H_8^O = a_Q R_D$, and $H_{20}^O = a_5 R_S$, where T_m is the energy expenditure on respiration ($t = \kappa, F, G, R$); and R_ζ is the rate of dead organic matter decomposition ($\zeta = Q, D, S$).

4.5.2 Indicators of the status of the ozone layer

Atmospheric ozone constitutes $0.64 \cdot 10^{-6}$ of the atmospheric mass and belongs to the class of optically active gases. It absorbs UV solar radiation in the range 200 nm–300 nm, strongly affecting thereby the thermal regime of the stratosphere. Moreover,

ozone has a number of vibration–rotation bands of absorption in the IR spectral region (9.57 μm) and partially absorbs visible radiation in the Chappuis band (0.6 μm) (Angione *et al.*, 1976). The formation and destruction of ozone have been described in detail (Kondratyev and Varotsos, 2000; Kondratyev, 1999a).

Ozone forms in the upper stratosphere from molecular oxygen under the influence of UV solar radiation. In the lower stratosphere and troposphere, the source of ozone is the decomposition of nitrogen dioxide under the influence of UV and visible radiation. The formation of the vertical profile of ozone concentration is connected with its meridional and vertical transport. The general characteristic of this profile is the total amount of ozone measured by the thickness of its layer given in Dobson units (1 DU = 0.001 cm).

Ozone was first measured in the mid-19th century. For instance, at that time over Europe and in the region of the Great Lakes ozone maximums varied within 17 ppbv–23 ppbv. At present, the ozone layer over western regions of North America in April–October is characterized by quantities of 30 ± 5 ppbv. Due to the rapid economic growth of many Asiatic regions followed by increased volumes of consumed fossil fuels and respective increases in NO_x and SO_2 emissions (5% per year, on average), there is an increasing trend in monthly mean ozone concentration of 2 ppbv–6 ppbv per year which is likely to continue until at least 2010. This is despite the attempts undertaken in Europe and North America to reduce emissions to the atmosphere of chemical compounds by 8%–10%. Therefore, local measures for ozone layer stabilization on the global scale have no prospects of success.

Ozone destruction involves a complex set of photochemical reactions and participation of compounds of hydrogen, nitrogen, and chlorine. From the available estimates, 50%–70% of ozone is destroyed by nitrogen compounds, 20%–30% by oxygen (O), 10%–20% by water-containing particles of HO_x, and less than 1% by chlorine compounds. The predominant role of nitrogen compounds in ozone destruction has been confirmed (Wauben *et al.*, 1997) for all latitudes. The equation of photochemical equilibrium between concentrations of ozone and nitrogen oxides is $[NO] \cdot [O_3]/[NO_2] = \mu$, where the equilibrium constant μ depends on solar radiation intensity and can range from 0 to 0.02.

There are various approaches to parameterizing the process of formation and destruction of the ozone layer. The difficulty of deriving dynamic models of the ozone cycle in the atmosphere has to do with the participation in the cycle of more than 75 chemical reactions, a qualitative and quantitative description of which is impossible without deriving detailed models of the many minor gas components of the atmosphere. Nevertheless, there are empirical models of the ozone layer, which make it possible, under the present climatic situation, to obtain adequate spatial distributions of ozone. For instance, Bekoryukov and Fedorov (1987) derived a simple empirical model of total ozone content confirmed by observational data for the Southern Hemisphere:

$$O_3(\varphi, \lambda) = \sum_n \sum_{n \le m} P_n^m(\varphi)[a_{n,m} \cos(m\lambda) + a_{n,-m} \sin(m\lambda)], \tag{4.28}$$

where P_n^m are non-normalized spherical functions of degree n and order m; and $a_{n,m}$

and $a_{n,-m}$ are empirical coefficients whose values are given in Bekoryukov and Fedorov (1987) and in Krapivin and Kondratyev (2002).

There are also static models to describe the vertical profile of ozone density distribution. One such model is the Krüger formula:

$$O_3(h) = 51.4 \exp[-(h - 40)/4.2] \quad (\mu g/m^3).$$

By combining static and prognostic models it is possible to predict the levels of O_3 concentration in real time. However, in this case it is necessary to describe photochemical reactions with other components of the atmosphere and, to a greater extent, by taking NO_2 into account (Agirre-Basurko *et al.*, 2006). Some other ozone models were reviewed by Kondratyev and Varotsos (2000).

The simplest dynamic model of the ozone layer can be written in the form of a balance equation that reflects its income–expenditure components. Ozone supplies are replenished by reactions between UV radiation on oxygen ($H^O_{11} = e_3 O_A$) and nitrogen dioxide ($H^O_{12} = e_2 N_A$). The ozone layer is curently being destroyed at a rate $H^O_{14} = O_3/T_3$, where T_3 is the lifetime of ozone molecules depending on atmospheric pollution: $T_3 = T^O_3 - e_1 B$. The lifetime T^O_3 of ozone molecules in a perfect atmosphere averages 50–60 days. Participating nitrogen oxides, in contrast to the H^O_{12} cycle of ozone destruction, contribute much to the magnitude of B.

4.5.3 Anthropogenic impacts on the oxygen and ozone cycles

4.5.3.1 Oxygen cycle and anthropogenic processes

Studies of the history of biospheric evolution reveal a close correlation between oxygen production intensity and the development of life on Earth. And although the expected relative oscillations of the oxygen concentration in the near future do not exceed 10%, the considered impacts on the biosphere do not cover all potential anthropogenic trends, and therefore cannot be considered reliable. Therefore, let us analyze the constituents of possible mechanisms for violation of the natural balance of oxygen. Naturally, our concern is not only for an increase but also a decrease of the oxygen content in the atmosphere.

The oxygen cycle is complicated by its ability to take part in a lot of chemical reactions giving a multitude of epicycles. This fact makes the oxygen cycle sufficiently stable but hinders assessment of its stability.

Anthropogenic forcing on numerous epicycles of oxygen manifests itself both directly through its involvement in other cycles of substances at fuel burning and production of various materials, and indirectly through environmental pollution and biospheric destruction. Therefore, parameterization of the anthropogenic impact on the oxygen balance is realized within other units of the global model. Flux H^O_{18}, taken into account in Figure 4.7, completely covers the direct consumption of oxygen both in industry and in agriculture. Let us assume $H^O_{18} = y_1 R_{MG}$, where R_{MG} is the rate of natural resource expenditure; and y_1 is a coefficient ($\approx$0.084).

Fluxes H^O_{15} and H^O_{16} are strongly affected by anthropogenic forcings. Their variations are caused by the discharge of high-temperature industrial sewage

containing considerable numbers of oxidizers, as well as by oil-polluted water bodies. The quantitative characteristics of the change in oxygen dissolved in water as a function of temperature have been studied comprehensively. The empirical formula to calculate the concentration of seawater-dissolved oxygen has the form (Ramad, 1981): $[O_2 \text{ dissolved}] = 80/(0.2T_O - 7.1)$, where $[O_2]$ is expressed in mg/L and T_O in °C. The estimates of oxygen solubility in water are well known (Krapivin and Kondratyev, 2002).

Fluxes H_9^O and H_{19}^O, which balance the oxygen fluxes into water under natural conditions, as a result of anthropogenic forcing increase, as a rule, due to more active aerobic bacteria and the increasing metabolic needs of animals. For instance, a 10°C increase in water temperature increases the oxygen expenditure on respiration of marine animals by a factor of 2.2.

One of the negative manifestations of anthropogenic impact on the oxygen cycle is depletion of the ozone layer, especially marked in polar regions. There are various hypotheses on the causes of sharply changing concentrations of ozone, as well as discussions on the so-called "ozone hole" over the Antarctic. The main cause of all violations is connected with progressive human activity accompanied by the growing volumes of long-lived components emitted to the atmosphere (e.g., freons). The consequences of these violations are very serious, and the real scale of danger threatening life on Earth can only be estimated using a global model of the nature–society system.

The diversity of anthropogenic impacts on the global biogeochemical cycle of oxygen is determined by direct and indirect causes of breaking the natural balance of oxygen. According to the equation of photosynthesis, the gram-molecular amounts of assimilated CO_2 and emitted O_2 are equal. Also equal are the gram-molecular amounts of assimilated O_2 and emitted CO_2 for dead organic matter decomposition and fuel burning. Hence, for time periods of tens and hundreds of years, the change in CO_2 amount in the atmosphere is accompanied by the same change in O_2, but in the opposite direction. For instance, a doubling of CO_2 in the atmosphere leads to a decrease in the amount of O_2. But, since the volume concentration of CO_2 in the atmosphere is now estimated at 0.031% and that of O_2 at 20.946%, in this case a decrease of O_2 will constitute only 0.15% of the total O_2 content in the atmosphere.

Imagine the following situation. Let the total biomass of the biosphere ($\sim 9.6 \cdot 10^{11}$ tC), all the organic matter of soil ($\sim 14 \cdot 10^{11}$ tC), and all the fossil chemical fuel, the known deposits of which constitute $128 \cdot 10^{11}$ t of conditional fuel ($64 \cdot 10^{11}$ t C), be burnt. Then, the amount of CO_2 in the atmosphere would increase by a factor of 12.5, and that of O_2, respectively, would decrease—but only by 1.75%. Hence, the amount of oxygen over hundreds of years has to be practically constant.

However, it should be borne in mind that the region of excess anthropogenic emissions of CO_2 and, hence, O_2 assimilation is concentrated over a relatively small area, comprising cities and forest fires. Since concentrations in the atmosphere do not equalize instantly, the gradient of O_2 concentrations can be given for these sites, early warning of insufficient oxygen provision for animals and humans. Therefore, the model of the global oxygen cycle (MGOC unit) reflecting spatial heterogeneities in the distributions of O_2 concentrations, enables us to identify such dangerous territories.

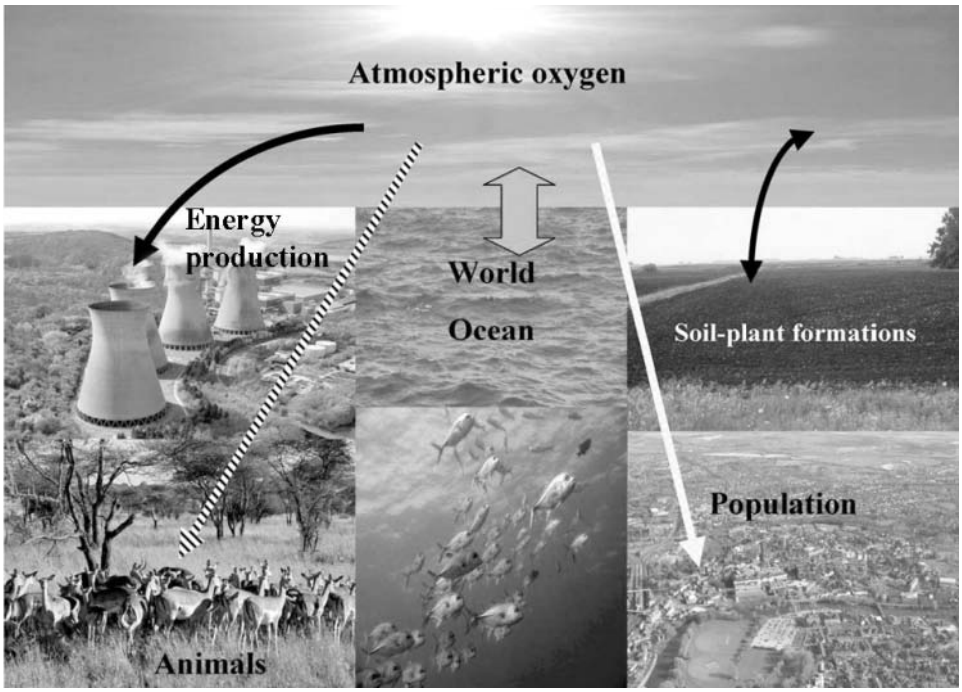

Figure 4.8. Simplified scheme of the biogeochemical oxygen cycle in the biosphere.

The interaction between the cycles of oxygen, nitrogen, sulfur, phosphorus, and carbon manifests itself through the processes of oxidation and decomposition. The level at which global model units are detailed does not permit reflection of all the diversity of these processes. Therefore, in the simplest case, when only averaged characteristics of the oxygen cycle elements are taken into account, the scheme in Figure 4.7 of global O_2 fluxes can be presented as the schemes in Figures 4.8 and 4.9. The indicated stability of O_2 concentration in the atmosphere makes it possible to simplify the description of the MGOC unit, using a single balance equation:

$$\frac{\partial O}{\partial t} + V_\varphi \frac{\partial O}{\partial \varphi} + V_\lambda \frac{\partial O}{\partial \lambda} = k_0 R_F + k_L R_L - \nu_L T_L - b_G G - \nu_F T_F - \nu_G T_G - \mu_Q R_Q,$$

where k_0 and k_L are indicators of the rate of O_2 emission due to photosynthesis in the ocean and on land, respectively; ν_s is the indicator of the role of respiration of land vegetation ($s = L$), animals ($s = F$), and humans ($s = G$) in the removal of oxygen from the atmosphere; and μ_Q is the rate of O_2 consumption at the decomposition of the dead organic matter in the soil.

4.5.3.2 Assessment of the role of aviation in ozonosphere change

The problem of monitoring and predicting the dynamics of the ozone layer is just as important as the problem of the atmospheric greenhouse effect (Varotsos and

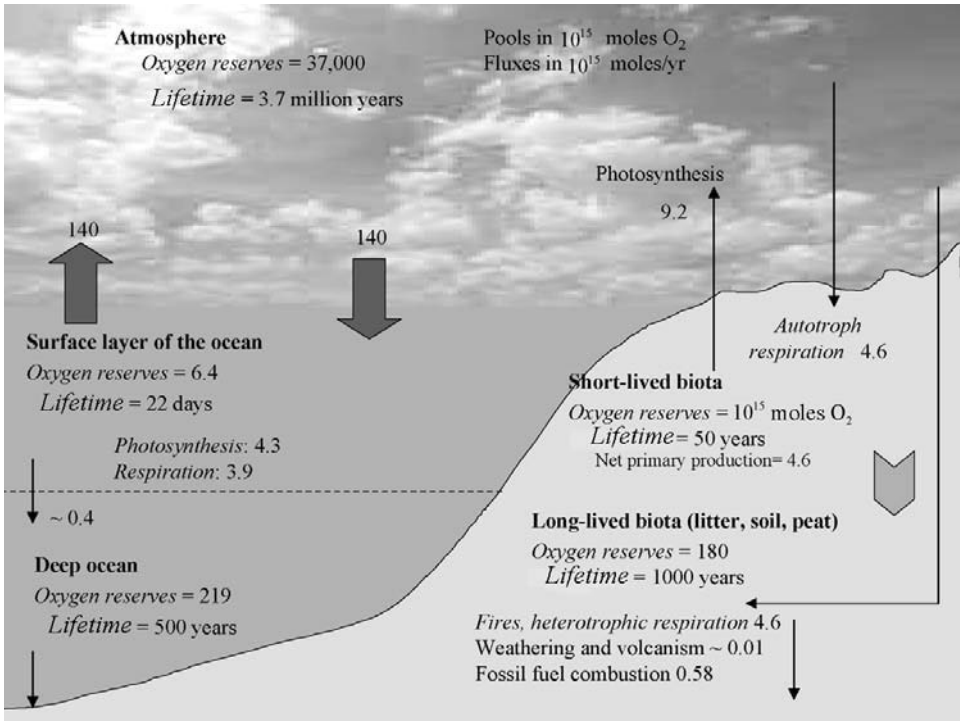

Figure 4.9. Reserves, fluxes, and lifetimes of oxygen in its basic reservoirs.

Kondratyev, 1998a, b; Popovicheva *et al.*, 2000). In both cases there are contradictory estimates of the causes of ecological danger at the observed levels of ozone concentration, ozone destruction, or greenhouse gases. Despite such contradictory estimates, often displaying a political awareness (Zuev, 2000), these problems attract the attention of experts from the various fields of natural sciences, who are trying to create information technologies to ensure a high level of objectivity and reliability of estimates of the consequences of anthropogenic interference with the global biochemical cycles of ozone, carbon dioxide, methane, water vapor, and other minor gas components (MGCs). Let us now consider the narrow—but important—problem of ozone layer changes over small areas caused by aviation flightpaths over this territory. This problem has recently attracted growing attention. The impact of flights of subsonic (altitudes 9 km–13 km) and supersonic (16 km–20 km) aircraft on the ozonosphere has become substantial, at least, on a regional scale. The more so because the volumes of global air transportation are increasing by almost 5% annually, and the amount of emitted nitrogen oxides, sulfur compounds, and other MGCs is increasing by about 4% annually. According to average global estimates, NO_x emissions ($NO + NO_2$) now constitute about $500\,\mathrm{ktN\,yr^{-1}}$, with their predicted increase up to $1{,}100\,\mathrm{ktN\,yr^{-1}}$ by 2015.

The substances ejected by aircraft to the atmosphere include H_2SO_4, HNO_3, HNO_2, HNO, Cl, NO_3, ClO_2, CO, CO_2, CH_4, N_2O, H_2O, SO_2, SO_3, N_2O_5, CH_3Cl, Cl_2, CH_3NO_2, CH_3NO_3, $BrONO_2$, HNO_4, $ClONO_2$. Many of these are responsible for the formation of polar stratospheric clouds, affect markedly the aerosol composition of the atmosphere, and intensify the greenhouse effect.

Analysis of the distribution of these components in the atmosphere requires an understanding of photochemistry and atmospheric dynamics. Unfortunately, current ideas about the rates of reactions in which these substances participate, about the coefficients of micro/macro-turbidity, and about local synoptic characteristics are limited by data averaged in time and space. As a result many authors have found ways of simplifying matters to overcome these information uncertainties.

Atmospheric ozone chemistry has been well studied (Kondratyev and Varotsos, 2000). Nevertheless, this knowledge is insufficient to derive a model of the biogeochemical cycle of ozone that would satisfy everyone. The main problem relates to the time-dependent nature of environmental processes. Unfortunately, neither simple nor complicated climate models (which take into detailed account the compounds involved in the atmospheric chemistry of ozone) give acceptable results. Therefore, an approach needs to be found that will raise the reliability of estimates of the state of the ozone layer over a given territory. Application of technology that combines measurements and modeling and takes into account expert estimates would constitute such an approach. In this case, to assess the vertical profile of ozone, all available information (scientific and empirical) can be used on ozone formation and destruction, and the additional background information about anthropogenic and natural processes can be obtained from established correlations or scenarios.

One of the difficulties in synthesizing a model of ozone dynamics and observational data is the necessity to adequately describe the location of the tropopause. There is uncertainty in the flightpaths of subsonic aircraft regarding accurate determination of the height of the tropopause. This is very important since, depending on whether the flight path is below the tropopause or in the stratosphere, photochemical reactions with ozone differ. With supersonic aviation, there is no problem as all flightpaths lie in the stratosphere. Therefore, to exclude instability from the model, we assume the hypothesis of seasonal change in tropopause altitude following a binary law: in spring and summer Z_1, and in autumn and winter Z_2.

This approach excludes the instability of using estimates. Nevertheless, there have been many successful attempts at modeling ozone photochemistry. A number of Lagrange-type models are efficient and some take into account up to 75 chemical elements and compounds. The 3-D model MOZART (Model for OZone And Related chemical Tracers) is also efficient (Kondratyev and Varotsos, 2000).

In this section the difficulty of estimating the vertical profile of the ozone concentration in the atmosphere over small areas is considered by taking into account only one of many anthropogenic sources that have an effect on the ozonosphere, aviation. Since the range of substances ejected by aircraft is large, the consequences of aircraft flight over these areas include numerous changes in both the gas and aerosol composition of the atmosphere. Of course, the scale of these changes is determined by the intensity of aircraft flights and the density of flight corridors. We now propose a

method of integrating these causes and develop an information system, which can be used for regional and national monitoring. Moreover, the presentation of the input information and the spectrum of chemical reactions have been limited so that aircraft operators can substitute their own lists of substances contained in exhaust gases.

Units of the Simulation System to Control the Regional Ozonosphere (SSCRO) are enumerated in Table 4.9. The territory in question Ω is covered by a geographical grid with steps $\Delta\varphi$ and $\Delta\lambda$ representing latitude and longitude, respectively. Over each cell $\Omega_{ij} = \{(\varphi, \lambda)\colon \varphi_i \le \varphi \le \varphi_{i+1};\ \lambda_j \le \lambda \le \lambda_{j+1};\ i = 1, \ldots, N;\ j = 1, \ldots, M\}$ the possible location (altitude and time) of the flight corridor is determined. For this purpose, in the database for SSCRO an indicator is formed of the flight load on Ω (type of engine, fuel, velocity, and flight altitude). The background concentration of ozone and the meteorological situation are assumed to be taken from the data of regional, national, and global systems of environmental monitoring.

Ozone concentration as a function of spatial coordinates and time is calculated by the formula:

$$\frac{\partial O_3(\varphi, \lambda, z, t)}{\partial t} = Q + S + U - P - R, \tag{4.29}$$

where z is the altitude, and the functionals in the right-hand side of Equation (4.29) describe the following processes of ozone formation: Q is the change in ozone concentration due to atmospheric motion and gravitational sedimentation; P and U are the photochemical destruction and formation of ozone outside the passageway, respectively; and R and S are the photochemical destruction and formation of ozone within the flight corridor.

Equation (4.29), with initial data for time moment $t = t_0$, is solved by taking account of the mosaic of flight corridors. Functionals R and S are calculated for $\Omega_{i,j,k} = \{(\varphi, \lambda, z)\colon (\varphi, \lambda) \in \Omega_{ij};\ z_k \le z \le z_{k+1}\}$ at time moment t only in the presence of aircraft. Three zones are considered in the interaction of the products of fuel combustion in the contrails of an aircraft engine: (1) immediately behind all engines (time duration Δt_1); (2) when exhaust gases mix with the atmosphere (Δt_2); and (3) on the mixture's ways of penetrating large-scale reservoirs (Δt_3). Hence, after the aircraft transits there exists a passageway for a time period $\Delta t = \Delta t_1 + \Delta t_2 + \Delta t_3$, after which $R(\varphi_i, \lambda_j, z, k, t) = S(\varphi_i, \lambda_j, z, k, t) \equiv 0$ and according to Equation (4.29) the functionals Q, U, and P start working.

During time period Δt there are many transformation processes of substances ejected by aircraft engines within the flight corridor. The term "index of transformations in a jet" is an integral estimate of the concentrations of these substances as a function of time. Let us suppose that exhaust took place at moment t_0 (the moment of aircraft transit over a given point of the Earth surface). Then, the index of transformation of chemicals in the contrail after the flight can be presented by a three-step function:

$$J_N(t) = \begin{cases} J_{N_1}, & \text{for } t_0 \le t < t_0 + \Delta t_1; \\ J_{N_2}, & \text{for } t_0 + \Delta t_1 \le t < t_0 + \Delta t_1 + \Delta t_2; \\ J_{N_3} & \text{for } t_0 + \Delta t_1 + \Delta t_2 \le t < t_0 + \Delta t_1 + \Delta t_2 + \Delta t_3. \end{cases} \tag{4.30}$$

Table 4.9. The characteristics of SSCRO units.

Unit	*Functions of the unit*
AADB	Algorithmic adaptation of the database to the structure of the controlled territory. A matrix structure is developed with elements reliably attaching environmental elements to geographical coordinates, configuration of the territory of the region, location on it of objects such as airports, and division of the territory into land and water.
IRDB	Information renewal of the database. A possibility is provided to operationally change the configuration and appearance of the territory described in AADB.
MIF	Management of information fluxes between SSCRO units. The dimensions of model parameters are coordinated; the dimensions of input data are coordinated with the scales assumed in SSCRO. For instance, the formula $1\,\text{ppmv} = 10^{-3}[M/(M_i\rho)]\,\mu\text{g}\cdot\text{m}^{-3}$, where M_i is the molecular weight of the ith chemical element. Formulas of the type $1\,\mu\text{g}O_3/\text{m}^2 \Rightarrow 0.467\times10^{-7}$ atm-cm are also re-calculated.
CFSU	Control of the functions of system units. Depending on the availability of needed information in the database about correlations between various processes, a version is selected from alternative versions that does not contradict the database.
PADB	Parametric agreement of the models and database. Signals of the user's interface are analyzed for an efficient removal from the database of the coefficients of models, or in case of disagreements the model is substituted for the scenario.
MPR	Modeling the photochemical reactions in the flight corridor with selection of three stages: (1) in the nearest zone after an ejection of fuel from the aircraft; (2) scattering the jet of fuel; (3) complete mixing with the surrounding atmosphere.
MPTO	Modeling the processing of propagation and transformation of ozone in the interaction between the contrail and the surrounding atmosphere.
MFDO	Modeling the formation and destruction of ozone by taking account of all flight corridors over the territory in question.
CCAB	Calculation of corrections for the atmospheric balance of ozone by considering the effects of land cover and sea surface.
FBLO	Formation of the background level of ozone either from data provided by a regional and global monitoring system or using a model.
FS	Formation of scenarios for the location of flight corridors and of their load.
MUII	Management of the user's information interface. Provision of computer experiments.

The values J_{N_i} $(i = 1, 2, 3)$ depend on the time of day, season, and on many other parameters (temperature, altitude, geographical coordinates). Empirical estimates of J_{N_i} are introduced to the system's database and used to calculate $J_N(t)$. With further improvement of SSCRO it will be expedient to include a unit to give theoretical estimates of J_{N_i}.

Since an aircraft flies at velocity V_a along the route $x(\varphi, \lambda, z)$, at time moment t_0 it is at some point x_0, and all its engines eject $V_M(t_0)$ of the substance of M type. Taking (4.30) into account we obtain:

$$V_M(t) = \begin{cases} L_1, & \text{for } t_0 \le t < t_0 + \Delta t_1; \\ L_2, & \text{for } t_0 + \Delta t_1 \le t < t_0 + \Delta t_1 + \Delta t_2; \\ L_3, & \text{for } t_0 + \Delta t_1 + \Delta t_2 \le t < t_0 + \Delta t, \end{cases}$$

where

$$L_1 = V_M(t_0) - \frac{t - t_0}{\Delta t_1}[V_M(t_0) - J_{N_1} V_M(t_0)],$$

$$L_2 = J_2 V_M(t_0) + \frac{t_0 + \Delta t_1 + \Delta t_2 - t}{\Delta t_2} V_M(t_0) \cdot (J_{N_1} - J_{N_2}),$$

$$L_3 = J_3 V_M(t_0) + \frac{t_0 + \Delta t_1 + \Delta t_2 - t}{\Delta t_3} V_M(t_0) \cdot (J_{N_2} - J_{N_3}).$$

After time Δt the effects of the aircraft flight are considered to cease and all processes involved in the transformation and destruction of ozone within the flight corridor after the flight return to normal. The zone of the contrail behind the flying aircraft has a circular section of diameter r, and during the time period $\tau = \Delta t_1 + \Delta t_2$ its interaction with the surrounding atmosphere can be considered negligibly small. At the third stage, this interaction begins with slight contact between the two media. At any rate, the interaction between the flight corridor and the surrounding atmosphere needs to be specified and developed by forming a set of scenarios.

NO_x is the most important component of exhaust gases. During the lifetime of an aircraft contrail NO_x gets oxidized by hydroxyl, present in the contrail, giving off HNO_3 and HO_2NO_2. As laboratory studies have shown, the processes of formation and destruction of ozone are also affected markedly by the heterogenic mechanisms of the impact on atmospheric chemistry. This impact manifests itself both within the flight corridor and in a free atmosphere. In particular, the reaction $N_2O_5 + H_2O_2HNO_3$ with sulfate aerosols, mainly resulting from aircraft flight, reduces the rate of ozone destruction due to the NO_x cycle, but raises the negative role of Cl_x and HO_x in O_3 destruction.

The second important component of exhaust gases is SO_2, the ejection of which by engines doubles the area occupied by sulfate particles in the atmosphere of the flight corridor, which leads to an increase of O_3 losses. In a number of field experiments (Kraabol and Stordal, 2000) onboard an F-16 and in laboratory experiments of the F-100 engine using several types of aviation fuel with high (~1,150 ppmS), moderate (~170 ppmS–300 ppmS), and low (~10 ppmS) content of sulfur, the SO_2 emission changed from $2.49\,gSO_2\,kg^{-1}$ for fuel with a high sulfur content to

0.01 $gSO_2\,kg^{-1}$ for fuel with a low sulfur content. For these experiments the following relationship was derived:

$$0.02 \leq \frac{[SO_3]}{[SO_2]+[SO_3]} \leq 0.14.$$

The results of studies carried out by Weisenstein *et al.* (1998) show that the ways in which the composition of engine exhaust gases evolve as they interact with the atmosphere have been poorly studied; hence, the importance of further development of kinetic models describing the role of aircraft flights in changing the atmosphere.

The functional Q in (4.29) is written following the traditional scheme

$$Q = -v_\varphi \frac{\partial O_3}{\partial \varphi} - v_\lambda \frac{\partial O_3}{\partial \lambda} - v_z \frac{\partial O_3}{\partial z} + \frac{\partial}{\partial \varphi}\left(D_\varphi \frac{\partial O_3}{\partial \varphi}\right) + \frac{\partial}{\partial \lambda}\left(D_\lambda \frac{\partial O_3}{\partial \lambda}\right) + \frac{\partial}{\partial z}\left(D_z \frac{\partial O_3}{\partial z}\right),$$

where $V(V_\varphi, V_\lambda, V_z)$ is the wind speed; and $D(D_\varphi, D_\lambda, D_z)$ is the coefficient of eddy diffusion.

The units CCAB, MFDO, and MPTO divide the functional Q by taking the output information from the unit AADB into consideration (see Table 4.9). As a result, air mass mixing is realized at two stages:

(1) mixing of the atmospheric zone of aircraft flight with the environment; and
(2) mixing of the cells $\{\Omega_{i,j,k}\}$ selected by the AADB unit. As a first stage the volumes and location of the zone of effect of aircraft are calculated:

$$\omega = \{(\varphi, \lambda, z) : \varphi_0 \leq \varphi \leq \varphi_1; \lambda_0 \leq \lambda \leq \lambda_1; z_0 \leq z \leq z_1\},$$

where $\varphi_1 = \varphi_0 + V_{a\varphi}\Delta t/k_\varphi$; $\lambda_1 = \lambda_0 + V_{a\lambda}\Delta t/k_\lambda$; $\Delta z = z_1 - z_0$ is the diameter of the zone of the impact of aircraft ($\Delta z = r$); φ_0 and λ_0 are the latitude and longitude of the aircraft location at time moment t_0; κ_φ and κ_λ are the number of kilometers within 1° of latitude and longitude, respectively; and z_1 and z_0 are the lower and upper boundaries of the flight corridor.

If the obtained space ω agrees with the adjacent multitude of atmospheric units $\{\Omega_{ijk}\}$, then the ozone content is averaged over ω and the adjacent compartments $\{\Omega_{ijk}\}$ with their volumes taken into account.

The second stage realizes a two-step procedure that re-calculates the ozone concentration over the whole space $\Xi = \{(\varphi, \lambda, z) : (\varphi, \lambda) \in \Omega; 0 \leq z \leq z_H\}$, where z_H is the altitude of the atmospheric boundary layer ($z_H \sim 70$ km), whose consideration is important in estimating the state of the regional ozonosphere. These two steps correspond to the vertical and horizontal constituents of atmospheric motion. This division is made for convenience, so that the user of the expert system can choose a synoptic scenario. According to the available estimates (Karol′, 2000; Kraabol *et al.*, 2000; Meijer and Velthoven, 1997), the processes involved in vertical mixing prevail in the dynamics of ozone concentration. It is here that, due to uncertain estimates of D_z, there are serious errors in model calculations. Therefore the units CCAB, MFDO, and MPTO (see Table 4.9) provide the user with the principal possibility to choose various approximations of the vertical profile of the eddy diffusion coefficient (D_z).

The database of SSCRO contains versions of estimates of D_z (m^2/s) already used by many authors in the models of ozone dynamics $\approx 3 m^2/s^{-1}$; $\approx 0.5(V_\varphi + V_\lambda)$:

$$D_z \approx \begin{cases} 10\,m^2\,s^{-1} & \text{for } 0 \le z \le 10\,km; \\ 10 + 2.57(10 - z) & \text{for } 10 < z \le 13\,km; \\ 70 - 1.22(70 - z) & \text{for } 13 < z \le 70\,km. \end{cases}$$

Since model retrieval of the background situation over a given territory has numerous versions that require information on regional and global processes, the SSCRO foresees the possibility of applying different models of the dynamics of ozone. But the scenario is deliberately intended to be basic, and under the control of an aircraft operator using data from the regional or global ozonometric network. The operator can prescribe a discrete function $O_{3,i,j,k,s} = Q_3(\varphi_i, \lambda_j, z_k, t_s)$, *a priori* considering the value of $O_{3,i,j,k,s}$ an average estimate of the function $Q_3(\varphi_i, \lambda_j, z_k, t_s)$ in space Ω_{ijk} for time period $t_{s-1} \le t \le t_s$.

Possibilities are foreseen to choose various versions of approximation of the O_3 function over the whole territory by a number of latitudinal and meridional distributions.

In this case only the ozone–air mixing ratio can be prescribed. From this ratio the O_3 function can be reconstructed, provided the SSCRO database contains information on the vertical profile of air density at any point $(\varphi, \lambda) \in \Omega$. The respective computer dialog procedure makes this choice automatic.

One of the important elements of how the SSCRO functions is the way in which the database is updated as it adapts to the conditions of a given region: the database includes information about the flight timetable over the region and other characteristics of the engines, cruising altitude, airspeed, location of airports, air route, etc.

All background information is concentrated in the form of matrix structures, such as $F = \|f_{ij}\|$, $D = \|d_{ij}\|$, $C = \|c_{ij}\|$, $B = \|b_{ij}\|$, where f_{ij} is a vector whose components contain all the needed information for the ith arrival flight (f_{i_1} time of landing, f_{i_2} arrival direction, f_{i_3} type of engine, f_{i_4} airspeed, f_{i_5} cruising altitude, f_{i_6} and f_{i_7} latitude and longitude of the airport of entry), and other possible characteristics; the d_{ij} vector contains similar information about departing aircraft, the c_{ij} vector describes information about air routes and transit aircraft, and, finally, the b_{ij} vector decodes the f_{i_3} component, giving the volume of fuel burnt, its type, and the composition of exhaust gases. Transit flights, with intermediate flight breaks at airports in the region, are taken into account by identifiers F and D separately, before landing and after take-off.

Model estimates of the impact of aircraft on the atmosphere and climate, which can be obtained using the SSCRO, will make it possible with available synoptic information to solve the problem of optimizing flight corridors and flight timetables. Considering various scenarios of the aircraft load on the regional ozonosphere using the SSCRO, it is possible to determine the location of flight corridors that, in other similar conditions, will reduce the consequences of this load. There is also the

possibility of specifying the compounds of other biogeochemical processes that participate in greenhouse gases.

4.5.4 Numerical model of the global oxygen cycle

Assuming the scheme of oxygen fluxes in nature (shown in Figure 4.7) to be balanced, let us write the equations of the model in the following traditional form of balanced relationships (Table 4.8):

$$\frac{\partial O_A}{\partial t} + V_\varphi \frac{\partial O_A}{\partial \varphi} + V_\lambda \frac{\partial O_A}{\partial \lambda} = H_2^O + H_3^O + H_{14}^O + H_{15}^O + H_{16}^O - \sum_{i=4}^{8} H_i^O - H_{11}^O - H_{18}^O;$$

$$\frac{\partial O_3}{\partial t} + V_\varphi \frac{\partial O_3}{\partial \varphi} + V_\lambda \frac{\partial O_3}{\partial \lambda} = H_{11}^O + H_{12}^O - H_{14}^O;$$

$$\frac{\partial O_S}{\partial t} = H_{21}^O - H_{16}^O - H_{17}^O - H_{19,S}^O - H_{20}^O;$$

$$\frac{\partial O_U}{\partial t} + V_\varphi \frac{\partial O_U}{\partial \varphi} + V_\lambda \frac{\partial O_U}{\partial \lambda} = H_{1,U}^O + H_{13,PU}^O + H_{17}^O - H_{9,U}^O - H_{10,PU}^O - H_{15}^O - H_{19,U}^O;$$

$$\frac{\partial O_P}{\partial t} + V_\varphi \frac{\partial O_P}{\partial \varphi} + V_\lambda \frac{\partial O_P}{\partial \lambda} = H_{1,P}^O + H_{10,PU}^O + H_{13,PL}^O - H_{9,P}^O - H_{10,PL}^O - H_{13,PU}^O - H_{19,P}^O;$$

$$\frac{\partial O_L}{\partial t} = Q_L + H_{10,PL}^O + H_{13,LF}^O - H_{9,L}^O - H_{10,LF}^O - H_{13,PL}^O;$$

$$\frac{\partial O_F}{\partial t} = Q_F + H_{10,LF}^O - H_{9,F}^O - H_{13,LF}^O.$$

Here Q_L and Q_F denote the oxygen fluxes resulting from mixing of the deep and bottom layers of the ocean. The oxygen exchange between the hydrosphere and the atmosphere (fluxes H_{15}^O and H_{16}^O) depend on its partial pressures at the water–air border. The directions of fluxes H_{15}^O and H_{16}^O depends on the relationship between temperatures T_a, T_U, and T_S. Due to high concentrations of oxygen in the atmosphere, the partial pressure varies negligibly, and therefore the fluxes H_{15}^O and H_{16}^O can be considered to depend only on oscillations in the concentrations of O_U and O_S: $H_{15}^O = k_{OU}(T_U - T_a)O_U$; $H_{16}^O = k_{OS}(T_S - T_a)O_S$. If we assume $O_U = 5.5\,\text{mL/L}$ and $O_S = 2.1\,\text{mL/L}$, then at $T_U - T_a = T_S - T_a = 2^\circ\text{C}$, $H_{15}^O = 18\,\text{t}\,\text{km}^{-2}\,\text{yr}^{-1}$, and $H_{16}^O = 140\,\text{t}\,\text{km}^{-2}\,\text{yr}^{-1}$ we obtain $k_{OU} = 0.5 \cdot 10^{-4}\,\text{km}/^\circ\text{C/yr}$ and $k_{OS} = 0.1 \cdot 10^{-2}\,\text{km}/^\circ\text{C/yr}$.

The ocean layers exchange oxygen by circulation processes, and as a result, depending on latitude, longitude, and season, the intensity of fluxes H_{10}^O and H_{13}^O can sharply change. In any case, this intensity mainly depends on the velocities v_A of vertical water uplifting and v_H of its lowering. In the zones of upwellings the flux H_{13}^O prevails and, in contrast, the flux H_{10}^O prevails in convergence zones. The velocities v_A and v_H range from 0 m/s to 0.1 m/s. The most characteristic values of these velocities range from 10^{-2} m/s to 10^{-4} m/s. For instance, near California $v_A \approx 0.77 \cdot 10^{-5}$ m/s,

and in Bangladesh uplifting $v_A = 0.25\,\mathrm{m/s}$. Thus, for fluxes H_{10}^O and H_{13}^O we use the following approximations $H_{10}^O = \lambda_{\kappa\gamma}(O_\kappa - O_\gamma)$ and $H_{13}^O = \mu_{\gamma\kappa}(O_\gamma - O_\kappa)$, where $\lambda_{\kappa\gamma}$ and $\mu_{\gamma\kappa}$ are the coefficients of local mixing ($\kappa = U, P, L$; $\gamma = P, L, F$).

In the marginal shelves of the ocean, oxygen balance formation is much affected by the run-off from continents. Despite the complexity of this process, the following simple parameterization can be accepted for this case:

$$H_{17}^O = n_{SU}(O_S - O_U).$$

4.6 THE ROLE OF WATER IN THE GLOBAL CARBON CYCLE

4.6.1 The role of precipitation

The transport and transformation of CO_2 in land ecosystems are closely connected with the heat and water regime of the atmosphere–plant–soil system. These processes are functions of the hydrometeorological and actinometric characteristics of the vegetation ecosystem. An important element in the specification of the global model of CO_2 cycle in the biosphere is consideration of the role of the process of its leaching from the atmosphere with precipitation. Although this process is unilateral, it has been inadequately studied. Nevertheless, there is direct experimental evidence of CO_2 assimilation by rain drops (Egan *et al.*, 1991). In particular, one confirmation of the fact that precipitation leaches CO_2 from the atmosphere is the presence in rain of a considerable amount (up to $15\,\mathrm{mg \cdot L^{-1}}$) of the hydrocarbonate ion HCO_3^-. A combined analysis of precipitation amount and variations in atmospheric CO_2 concentration over the same territory, using the data of the global observational network, made it possible to reveal the persistent correlation between these processes. Figure 4.10 shows curves of change in average monthly precipitation and concentra-

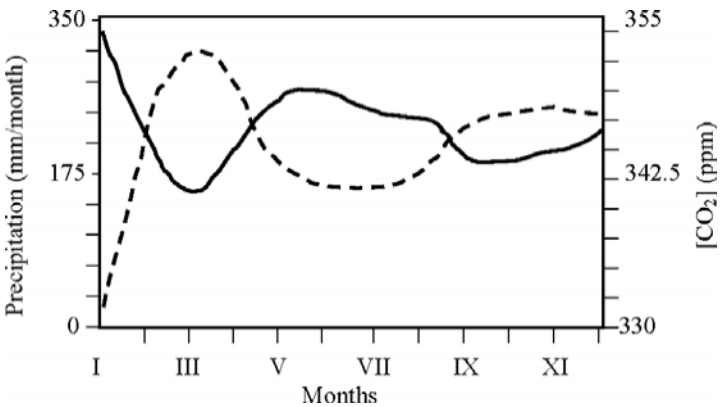

Figure 4.10. Variations of precipitation amount (solid curve) and CO_2 concentration in the atmosphere (dashed curve). Estimates from integrated data of the observatory observations within the framework of the Global Carbon Project (GCP).

tion of atmospheric CO_2. We see that the dependence between changes in atmospheric CO_2 and precipitation is sufficiently stable. Detailed analysis of this dependence for various latitudinal belts or for other configurations of smaller territories reveals similar patterns independent of geophysical coordinates. We should point out here the high sensitivity of the correlation between the duration and type of precipitation. For instance, during a shower the HCO_3^- concentration in precipitation can either double or halve depending on the presence or lack of thunderstorms. Moreover, this ratio depends strongly on the duration of the precipitation period. Observations showed that with the increasing duration of rain the concentration of HCO_3^- ions decreases. In other words, the interaction between CO_2 concentration and moisture content in the atmosphere is an important component of the global carbon cycle.

Formalization of the role of rain in the global CO_2 cycle requires a model of CO_2 absorption by water droplets falling at velocity u. The most widely used version of such a model is an equation of gas balance on the surface of rain droplets:

$$\frac{dC}{dz} = \frac{3\Delta}{ur^2}(1 + 0.3\sqrt{Re^3}\sqrt{Sc})(C_A - C^*),$$

where Δ is the coefficient of CO_2 diffusion in the air; r is the droplet radius; C^* is the balanced concentration of CO_2 in a droplet; C_A is the CO_2 concentration in the atmosphere; z is altitude; $Sc = \nu/\Delta$ is the Schmidt number; ν is the kinematic viscosity; and $Re = 2ru/\nu$ is the Reynolds number.

The diversity of forms of precipitation over the globe complicates consideration of their role in the global CO_2 cycle. This problem can be solved in two ways. The first is formal numerical description of the totality of the processes of precipitation formation. The second is connected with the use of the present means of global observation of precipitation. In both cases the forms of rain should be clearly classified as functions of meteorological situations. The rain rate can range widely from $1\,\text{mm}\,\text{hr}^{-1}$ to $8\,\text{mm}\,\text{hr}^{-1}$ and, in exceptional cases, even more. What is more, there is a certain correlation between precipitation rate and size of rain droplet. With low-intensity rain $r \in [0.1; 0.5]$. A shower can be characterized by the formation of droplets up to $r \sim 6\,\text{mm}$.

Thus, the problem of assessing the role of precipitation in leaching CO_2 from the atmosphere is urgent, and to solve it the global model should separately take into account the change in hydrological cycles over the World Ocean and over land, since these regions of the planet differ in their interaction with the atmosphere.

4.6.2 Water budget in the atmosphere–land system

Land–atmosphere exchange processes include the evaporation of soil moisture, from the leaf surface, stems, and trunks of plants, as well as transpiration, precipitation, and evaporation off the surface of unstable water accumulations low in the ground (Figure 4.11). The water flow from the soil through the plant is the least studied link in this chain. The importance of the process of transpiration in the global water cycle cam be judged from available estimates, according to which the process of

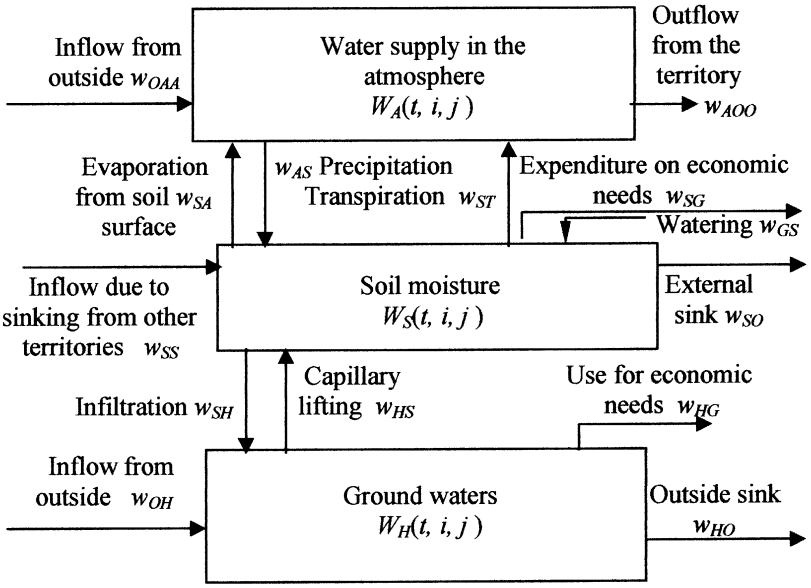

Figure 4.11. Water fluxes across the border of a small land territory.

transpiration takes more water than photosynthesis. For instance, from average estimates, to grow a 20 t yield (wet mass), plants extract from the soil about 2,000 t of water, with only 3 t of the used water being atomic hydrogen bound to atomic carbon in photosynthesis.

A model description of the process of transportation requires an understanding of the role played by the physical and physiological factors in this process. A simplified idea about this role can be reduced to the following. If the plant roots are in sufficiently wet soil, then the rate of transpiration is a function of temperature, humidity, wind speed, and insolation. Beyond some threshold of soil moisture, when the water supply in soil dries up, the role of these physical factors sharply diminishes, being inferior to the physiological factors: the type of plants, the construction of roots, phase of development, type of soil, and soil layer thickness. This threshold can vary from 5 cm to 50 cm of the precipitable water. At any rate, if, for a given type of plant, water is not a limiting factor (i.e., water is not limited), then, as a first approximation, the total growth of plants can be considered proportional to total potential transpiration for the whole period of growth. The latter is proportional to the amount of incoming solar radiation.

At present about 12% of total evaporation from the Earth's surface is used by plants in the process of photosynthesis. In this process about 2,250 km^3 of water participate annually with a return coefficient of 0.75. Therefore, the simplest description of transpiration is $w_{ST}(t,i,j) = \beta_{ij} W_S(t,i,j)$, where β_{ij} depends on vegetation productivity. The values of β_{ij} are 0.67 for forests, 0.44 for grassland, and 0.25 for agricultural crops. However, in real situations W_S is a limiting factor in the more

complicated dependence of the impact on transpiration rate by the rate of photosynthesis R_p. In other words, $w_{ST} = k_p R_p$, where k_p is the transpiration coefficient for the plants of p type. As a first approximation, we can use $R_p = \varepsilon_p r_p$, where ε_p is the share of solar energy, assimilated by the pth type of plants in the process of photosynthesis. The value ε_p depends on the presence of water accessible for plants:

$$\varepsilon_p = \varepsilon_{p,0}[1 - \exp(-\varepsilon_{p,1} W_S(t,i,j))],$$

where $\varepsilon_{p,0}$ is the value of ε_p when there is sufficient water; and $\varepsilon_{p,1}$ is the coefficient reflecting the reduction of solar energy assimilated by plants when the amount of accessible water is decreasing. On average, $\varepsilon_{p,0}$ is reached at $W_S = 10$ mm. Assuming $\varepsilon_p/\varepsilon_{p,0} = 0.9$, we have $\varepsilon_{p,1} = 0.23$. In this case $r_p = 9.6\,\mathrm{kg\,km^{-2}\,da^{-1}}$ of dry substance (or 37 kg of wet phytomass). Coefficient k_p is estimated for each type of plants. Coefficient k_p is equal to 368 for maize, 397 for sugarbeet, 435 for wheat, 636 for potatoes, 462 for cotton ($\mathrm{kgH_2O/kg}$ of pure substance).

One of the models in the process of transpiration can be written as $w_{ST} = Y_S(24a + b$, where Y_S is the return of water; a is the rate at which ground water rises (cm/hr); and b is the average daily change in ground water level (cm).

Within the GMNSS, to describe the process of the atmosphere–land interaction, fluxes w_{SA}, w_{ST}, and w_{AS} are used, the parametric descriptions of which serve as the basis for this unit. Information on precipitation w_{AS} is usually included in the information bulletins (weather forecasts) of hydrometeorological services. The history of the distribution of precipitation in the form of a set of matrices $W_{AS}(\theta) = \|w_{AS}(\theta,i,j)\|$, where $(i,j) \in \Psi$, θ are given time moments of precipitation recorded by hydrometeorological services, is used to derive the functional $w_{AS}(t,i,j) = F(W_{AS}(\theta_1), \ldots, W_{AS}(\theta_N), t)$. This is carried out by means of extrapolation and evolutionary modeling. Such an approach requires data on precipitation over a given geographical grid $\Delta\varphi \times \Delta\lambda$. However, this database can also be modeled by simulating the global cloud field, thus ensuring precipitation. The simplest parameterization of clouds consists in prescribing threshold $W_{A,max}$, beyond which excess atmospheric moisture transforms into water and precipitates. To reduce the inevitable errors (mainly caused by overestimation of precipitation), it is expedient to introduce a threshold matrix $W_{max} = \|W_{A,max}(i,j)\|$, $(i,j) \in \Psi$. Then,

$$w_{AS}(t,i,j) = \begin{cases} 0, & \text{for } W_A(t,i,j) \le W_{A,max}; \\ W_{A,max} - W_A(t,i,j), & \text{for } W_A(t,i,j) > W_{A,max}. \end{cases}$$

If value $W_{A,max}(i,j)$ corresponds to the real critical value of the moisture content in the atmosphere over Ω_{ij}, then w_{AS} has been overestimated. It is assumed here that at $W_A(t,i,j) > W_{A,max}$ cloud fills the whole cell Ω_{ij}, which does not always correspond with reality. Moreover, the fact that a considerable amount of moisture, even exceeding the critical level, can remain in the cloud and evaporate is disregarded. Therefore, to take these special features into account, the adaptive coefficient $\alpha_W < 1$ should be introduced.

Let us divide precipitation into two basic types: solid and liquid. This division can be made by means of the thermal principle or by seasons. The thermal principle is preferable due its flexibility in the event of sudden climate change and possible shifting of seasonality. Synoptic division of the seasons that experience different precipitation is justified in various regions of the globe. The average daily temperature at the onset of solid precipitation (snow) is below zero, ranging from -4°C to -7°C. On the border of this division the precipitation of a different type is observed. The relationship between the types of precipitation is described by the formula $x_T = a - bT$, where x_T is the share of solid precipitation; T is temperature; and a and b are empirical coefficients. For the Atlantic climatic zone $a = 50$ and $b = 5$.

To parameterize the process of evaporation from land, numerous formulas are used. Here a simple dependence is assumed:

$$w_{SA}(t,i,j) = \rho_{ij}[1 - \exp(-\delta_{ij}/\rho_{ij})]/\sigma_{ij},$$

where δ_{ij} is a maximum possible rate of evaporation in the region; and ρ_{ij} is the total amount of moisture getting into the soil per unit time.

The choice of model to simulate the evaporation process is determined by the character of the database used. Evaporation from the soil surface substantially depends on the type of vegetation cover. Evaporation in forests and in fields differs by 30%–40%. This is connected with the heterogeneous impacts on the water regime within various vegetation covers of such factors as the freezing of soil, the melting intensity of soil, soil structure, radiation budget, among others. To calculate the dependence of the rate of evaporation from land on temperature T_{ij}, the character of vegetation cover, and the properties of soil, the following formula is used:

$$w_{SA}(t,i,j) = \delta^*(T_{ij}/\overline{T}_{ij})[1 - \lambda \exp(-\lambda_1 A_{ij}/\overline{A}_{ij})][1 - \lambda_2 \exp(-\lambda_3 X_{ij}/\overline{X}_{ij})],$$

where $\overline{T}_{ij}$ is the surface air temperature in region Ω_{ij}, averaged over the period considered; $\overline{A}_{ij}$ and $\overline{X}_{ij}$ are the average depth of the soil layer and the density of vegetation cover, respectively; and $\delta^*, \lambda, \lambda_1, \lambda_2$ are empirical coefficients.

Detailed analyses of possible models of evaporation from the land surface that consider the different types of vegetation cover and changes of climatic parameters is given in the works by Bras (1990), Chock and Winkler (2000), and Karley *et al.* (1993). In particular, there are formulas to calculate evaporation as a function of the height and density of vegetation cover, wind speed, and temperature. For instance, the following dependence is proposed for the rate of complete evaporation:

$$E_T = \begin{cases} (\Delta Q_N + m\gamma L_j)/[\Delta + (1+n)\gamma + I(1-C)], & \text{for } T < 0^{\circ}\text{C}; \\ (\Delta Q_N + \gamma L_j)/[\Delta + \gamma], & \text{for } T \geq 0^{\circ}\text{C}, \end{cases}$$

where Δ is the rate of change in the pressure of saturated vapor as a function of temperature; Q_N is the amount of energy reaching the evaporating surface; γ is the psychometric coefficient ($\approx 0.66\,\text{mb} \cdot \text{K}^{-1}$); I is the share of complete evaporation due to precipitation retained by foliage; and C is the compensation coefficient due to transpiration. Coefficients m, n, and C are functions of height h and type r_s of

vegetation:

$$m = 53\ln^2(20/h + 2.5); \qquad C = (\Delta + \gamma)/[\Delta + (1+n)\gamma];$$
$$n = r_s[m(1 + U/100]/250.$$

The indicator of the type of vegetation r_s (m/s) for some types is estimated at 40 (sunflower and alfalfa), 70 (barley and potatoes), 250 (citrus plants), 130 (cotton), 80 (maize and rice), 50 (sugarbeet), 60 (wheat), 400 (tundra), 200 (subtropical meadows), 100 (temperate-zone meadows), 100–300 (tropical forests), 200–300 (coniferous forests), and 100–150 (deciduous forests in mid-latitudes). Typical values of the parameters n, m, and I are: for grass ecosystems $n \approx 2.5$, $m \approx 3.5$, $I \approx 0.2r$; for woodland $n \approx 30$, $m \approx 5$, $I \approx 0.3r$ (temperate latitudes), and $I \approx 0.15r$ (tropics), where r is precipitation.

Albedo is an important parameter when calculating the amount of solar radiation energy participating in the process of evaporation. The relationship between the height of plants and albedo, as a first approximation, can be described by their linear dependence. With the height of plants reaching ~20 m, albedo decreases from 0.25 to 0.1.The albedo values for some types of land cover are known: heather 0.14; ferns 0.24; natural pastures 0.25; shrubland 0.21; savannah 0.17; deciduous forests in mid-latitudes 0.1; coniferous forests and orange groves 0.16; eucalyptus forests 0.19; wet tropical forests 0.13; and waterlogged forests 0.12. The albedo of agricultural fields varies from 0.15 (sugarcane and fruit trees) and 0.26 (sugarbeet, barley, cucumbers).

The surface's role in land–atmosphere water exchange deals with the subdivision of the phase space into at least two levels: soil and ground water. The soil level plays the role of a buffer zone between precipitation and ground water. The simplest parameterization of fluxes between these levels is reduced to their linear dependences: $w_{SH}(t,i,j) = \lambda_{ij}W_S(t,i,j)$ and $w_{HS}(t,i,j) = \mu_{ij}W_H(t,i,j)$. However, a more strict description of the soil level is dictated by the natural heterogeneity of the structure of Ω_{ij}, where small water bodies and land sites of a given relief can be located. According to the landscape hydrological principle, to simulate Ω_{ij} it is necessary to choose the facies and sites of water surface, which can be done by identifying the background flora, the concrete condition of which is determined by micro-relief, types and properties of soil, surface moisture, depth of ground water, and other factors. It is possible to choose the m_{ij} of facies and the n_{ij} of water bodies. In this case, soil moisture forms not only as a result of the fluxes shown in Figure 4.11, but also due to leakage and filtration of water from the water bodies and aqueducts located in Ω_{ij}.

An important factor of the surface's role in the water balance is infiltration of precipitation into the soil both during rainfall and in run-off. The rate of water take-up by soil w_{SH} is described by the formula $w_{SH} = k_S l$, where k_S is the coefficient of filtration, and l is the hydraulic slope. Let us denote the volume mass of the soil as κ, which, on average, varies from 1.4 g/cm^3 to 1.5 g/cm^3, then for k_S it is convenient to use the Azizov formula: $k_S = 256.32\kappa^{-7.28}$–$1.27\kappa^{1.14}$ (cm/da). The parameter l can be calculated using formula $l = (z_0 + z_1 + z_2)/z_0$, where z_0 is the depth of the column that leaches out, z_1 is the capillary pressure, and z_2 is the height of the

water layer on top of the soil surface. At $z_0/z_1 \leq 2$ an approximation $w_{SH} = k_S + t^{-1/2}(0.5k_S z_1 D)^{1/2}$ is valid, where D is the soil moisture deficit, and t is time. Other approximations of the function w_{SH} are known, such as the Horton empirical formula $w_{SH} = [w_{SH}(t_0, i, j) - k_S]\exp(-\beta t) + k_S$, the Popov formula $w_{SH} = r \cdot \exp(-rt/D) + k_S$, and the Kostiakov formula $w_{SH} = k_S + \alpha t^{-n}$, where α, n, and β are calibration parameters, and r is rain intensity.

The interaction between regions of the grid of the biosphere surface $\{\Omega_{ij}\}$ can be simulated by fluxes w_{OAA}, w_{AOO}, w_{SS}, w_{SO}, w_{OH}, and w_{HO}. Functional presentations of the land–atmosphere water fluxes are usually chosen on the basis of available data and knowledge. In particular, the available estimates of water renewal time facilitate and simplify getting such approximations. The renewal times for the atmosphere, soil moisture, and rivers as basic water reservoirs are known to constitute 7–10 days, 270–290 days, and 12–20 days, respectively. Of course, in each concrete region and even in a spatial pixel of a given land surface in the GMNSS it is necessary to have more accurate estimates of this parameter.

4.6.3 Water exchange processes in the atmosphere-ocean system

The processes of transport at the atmosphere–water surface border have been well studied. The transport of moisture from the surface of a water body into the atmosphere is one of the complicated physical processes of mass and energy exchange across the water–air interface (Figure 4.12). These processes are functions of many climatic parameters and, to a large extent, are regulated by eddy motions in the surface layer of the atmosphere determined by the wind field.

The possibility of estimating water transport from the water surface into the atmosphere consists in assessing the water content of the lower part of the surface layer of the atmosphere, which forms spray and water vapor. The eddy flux of water

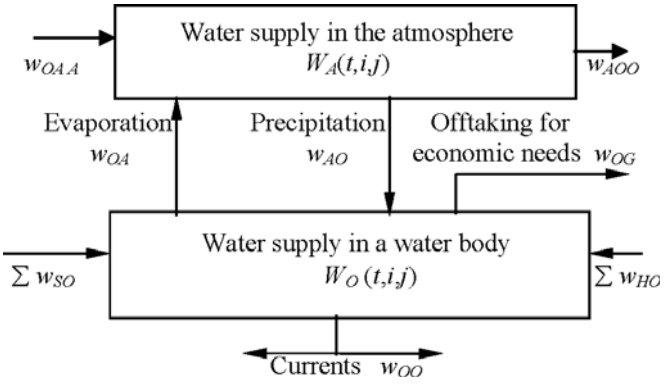

Figure 4.12. Water fluxes across the border of a small territory with a water body.

Table 4.10. The coefficient K_W (cm^2/s) of water vapor diffusion in the atmosphere at a pressure of 1,000 mb as a function of temperature T. From Roll (1968).

T (°C)	−20	−10	0	10	20	30	40
K_W	0.197	0.211	0.226	0.241	0.257	0.273	0.289

per unit surface can be described by the relationship:

$$W_V = -\rho K_W \frac{\partial q}{\partial z} = -(\rho w)' q' \approx -\rho \langle w' q' \rangle,$$

where W_V is the vertical eddy flux of water vapor ($g\,cm^{-2}\,s^{-1}$); K_W is the coefficient of the eddy transport of water vapor (cm^2 s) (Table 4.10); q is the specific air humidity ($g\,g^{-1}$); ρ is air density ($g\,cm^{-3}$); z is the vertical coordinate; w is the vertical constituent of wind speed ($cm\,s^{-1}$); and w' and q are fluctuations in w and q values, respectively. If we let p be atmospheric pressure, then we can express q through average water vapor elasticity e: $q = 0.621e/p$.

Evaporation from a water body surface depends on air temperature and can be described by the function $w_{SA} = w^* T^{\omega}$, where w^* and w are empirical parameters. If measurements are made of wind speed θ (m/s), saturated water vapor pressure at the temperature of the evaporating surface E_1, and atmospheric pressure p (mmHg), then we can use the Dalton law to estimate the rate of evaporation, $w_{SA} = A(E_1 - e)/p$, as well as the Shuleikin formula $w_{SA} = C\theta(E_1 - e)$, where A and C are parameters related as $A = C\theta/p$ ($C = 0.45 \cdot 10^{-6} g\,cm^{-3}\,mb^{-1}$). The models by Horton (1937) and Kohler (1954) are also efficient.

4.6.3.1 Simulation of water fluxes in the atmosphere

The atmospheric processes of moisture transport that are directly connected with the temporal variations of meteorological elements, play an important role in the global water cycle. Global atmospheric circulation can be described by the Monin model (Monin and Krasnitsky, 1985):

$$\frac{\partial v_\delta}{\partial t} + V_z \frac{\partial v_\delta}{\partial z} + V_\delta R^{-1} \frac{\partial v_\delta}{\partial \delta} + V_\lambda R^{-1} \sin^{-1} \delta \frac{\partial v_\delta}{\partial \lambda} = R^{-1} (V_\lambda)^2 \operatorname{ctg} \delta + 2\Omega V_\lambda \cos \delta + (R\rho)^{-1} \frac{\partial p}{\partial \delta} + f_\delta,$$

$$\frac{\partial v_\lambda}{\partial t} + V_z \frac{\partial v_\lambda}{\partial z} + V_\lambda R^{-1} \frac{\partial v_\lambda}{\partial \delta} + V_\delta R^{-1} \sin^{-1} \delta \frac{\partial v_\lambda}{\partial \lambda} = -R^{-1} V_\delta V_\lambda \operatorname{ctg} \delta - 2\Omega V_\delta \cos \delta - (R\rho \sin \delta)^{-1} \frac{\partial p}{\partial \lambda} + f_\lambda,$$

where Ω is the angular rate of Earth's rotation; $\delta = \pi/2 - \varphi$ is an addition to latitude; λ is longitude; V_z, V_δ, and V_λ are components of the velocity of atmospheric motion; R is the Earth's radius; and f_δ and f_λ are the components of acceleration due to

friction expressed by the friction stress tensor u_{sl}:

$$\rho f_\delta = \frac{\partial u_{\delta z}}{\partial z} + (R \sin \delta)^{-1} \left(\frac{\partial u_{\delta\delta}}{\partial \delta} + \frac{\partial u_{\delta\lambda}}{\partial \lambda} \right) - R^{-1} u_{\lambda\lambda} \operatorname{ctg} \delta,$$

$$\rho f_\lambda = \frac{\partial u_{\lambda z}}{\partial z} + (R \sin \delta)^{-1} \left(\frac{\partial u_{\lambda\delta}}{\partial \delta} + \frac{\partial u_{\lambda\lambda}}{\partial \lambda} \right) - R^{-1} u_{\lambda\delta} \operatorname{ctg} \delta,$$

Velocity field equations are closed by prescribing zero boundary conditions for the Earth's surface, that is parametrized by the function $z = h(\delta, \lambda)$ and by adding the equation of the state of humid air $p = \rho T[r_d + q(r_V - r_d)$, where $r_d = 0.287$ Joule/g K and $r_V = 0.46$ Joule/g K are the gas constant of dry and water vapor, and $q \approx 3\%$–4% is the specific humidity. The distribution of temperature $T(\delta, \lambda)$ and function $q(\delta, \lambda)$ can be described by the respective equations of evolution, and global archive data can substitute them for tabulated values.

The models of general atmospheric circulation were thoroughly described by Nicolis and Nicolis (1995). The description of the atmospheric part of the hydrological cycle can be simplified by the equation $\partial W_A/\partial t + \nabla Q = E - P$, where W_A is the vertically integrated specific air humidity in this column, and E and P are evapotranspiration and precipitation at the soil level, respectively.

Further simplification of models of the hydrological cycle can be done by selecting one of the three prevailing wind directions: western, eastern, and meridional. For such an approximation, data are used on the amplitude of wind speed oscillations and the number of days related with these directions. If the mass of water vapor in the air column over area σ_{ij} is $a = W_A \sigma_{ij}$, then, for instance, for the eastern orientation of the atmospheric circulation the water flux between the adjacent cells of the Earth's surface grid will be $w_{AO} = 2a\theta/d_{ij}$, where θ is the wind speed, and d_{ij} is the diameter of Ω_{ij}. Following this scheme, it is easy to re-calculate the moisture supplies at each point in time, since it is unnecessary to solve the problems of numerical integration of partial differential equations. Background information about W_A, σ_{ij}, θ, and d_{ij} is accumulated in the database from different sources. Function W_A is calculated by the balance equation or can be prescribed based on other data. In particular, as temperature T and the partial pressure of water vapor e change, so W_A can be estimated from the relationship $W_A = meh(1 + \alpha T)^{-1}$, where h is the height of the effective atmospheric layer, and m and α are the proportion coefficients ($m = 0.8$ and $\alpha = 1/273$ when measuring W_A in g m^{-2} and T in °C).

4.6.3.2 Simulation of water flows in the World Ocean

The World Ocean clearly occupies first place among all the water reservoirs on Earth. Its present volume exceeds 50-fold the volume of water in glaciers, which occupies second place. This comparison is important for understanding the correlation between the hierarchical steps of water basins and determining their structure in the model. Within *a priori* scenarios of anthropogenic activity and possible changes in the biosphere, the correlation between these steps is important. For instance, 1.6%

of the global supplies of water are accumulated in the Antarctic. By comparing these supplies with the volume of the Arctic Ocean where the water content is 20% less than in the Antarctic glacier cover, the inadequacy of any global model of the hydrological cycle that fails to take the role of the Antarctic into account is obvious (Keeling and Visbeck, 2001).

The hydrology and sea currents of the Southern Ocean along with the effects of glacier cover have been described in numerous monographs, and circulation models of different complexity and degree of detailing have been derived to simulate them. Such models for the World Ocean, on the whole, are based on configurations of the non-penetrating boundaries and topology of straits. Numerous numerical experiments using such models have made it possible to reveal the principal structure of global oceanic circulation as consisting of a hierarchy of closed ring circulations with the centers of lifting and descending waters. To describe water circulation in the Southern Ocean basin, it is necessary to take the Drake Passage into account. A scheme of the hydrological circulation in the World Ocean, acceptable for simulation, was proposed by Seidov (1987) and Chahine (1992). The model is a system of equations and boundary conditions that take into account the outline of shores, the bottom relief, as well as ice formation and melting. However, on a global scale, to simulate oceanic circulation, a simplified scheme is necessary, one that mainly reflects the role of straits. Such a scheme is shown in Figure 4.13. The quantitative characteristics of the constituents of this scheme are given in Table 4.11. The final unit responsible for modeling World Ocean circulation has the following form:

$$\sigma_{OF}\frac{dW_{OF}}{dt} = H_{OF} + R_F + I_{LF} + S_{LF} - S_{FL} - H_{FO} - A_{FI} + M_{IF} + D_{PF} + (w_{AOF} - E_{FA})\sigma_{OF} + A_F,$$

$$\sigma_{OI}\frac{dW_{OI}}{dt} = A_{FI} + C_{PI} + N_{PI} + K_I + R_I + (w_{AOI} - E_{IA})\sigma_{OI} - A_{IP} - M_{IF},$$

$$\sigma_{OP}\frac{dW_{OP}}{dt} = A_{IP} + R_P + (w_{AOP} - E_{PA})\sigma_{OP} + I_P - B_{PL} - D_{PF} - C_{PI} - N_{PI},$$

$$\sigma_{OL}\frac{dW_{OL}}{dt} = R_L + B_{PL} + (w_{AOL} - E_{LA})\sigma_{OL} + S_{FL} - I_{LF} - S_{LF},$$

$$\sigma\frac{dW_A}{dt} = (E_{PA} - w_{AOP})\sigma_{OP} + (E_{FA} - w_{AOF})\sigma_{OF} + (E_{IA} - w_{AOI})\sigma_{OI} + (E_{LA} - w_{AOL})\sigma_{OL}.$$

Within this large-scale approach to the formation of the MBWB ocean unit, the dependences of the fluxes of water in its different phases on environmental parameters remain uncertain. Apparently, the mass exchange between reservoirs s and l can be described by the simplest linear scheme $w_{sl} = |W_{OS}\sigma_{OS} - W_{OL}\sigma_{OL}|/T_{sl}$, where T_{sl} is the time it takes to equalize levels W_{OS} and W_{OL}, and σ_{OS} and σ_{OL} are the areas of

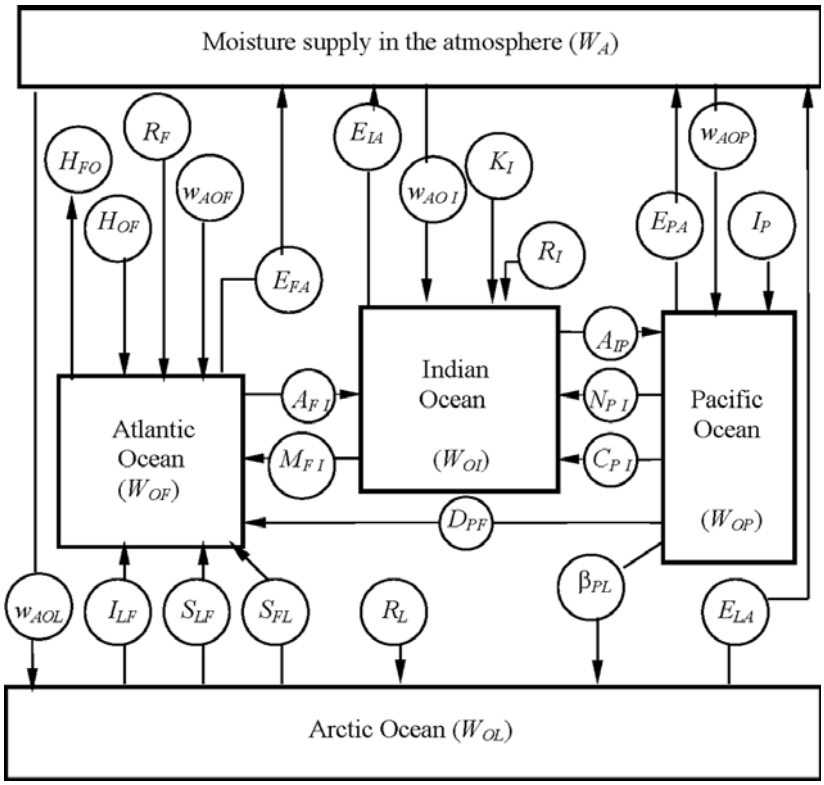

Figure 4.13. Elements of the global water balance with the role of the ocean taken into account. Notations: w_{AOL}, w_{AOF}, w_{AOI}, w_{AOP} precipitation; H_{FO}, H_{OF} Straits of Gibraltar; R_F, R_I, R_L rivers; E_{FA}, E_{IA}, E_{PA}, E_{LA} evaporation; A_{FI}, A_{IP} the Antarctic Current; M_{FI} the Cape Igolny Current; C_{PI} the East-Australian Current; β_{PL} Bering Strait; I_{LF} Arctic ice; D_{PF} Drake Passage; I_P Antarctic ice; N_{PI} Indonesian seas; S_{LF}, S_{FL} straits.

water basins s and l. For the scheme in Figure 4.13 we have:

$$A_{FI} = \max\{(V_{OF} - V_{OI})/T_{FI}, 0\}, \qquad M_{FI} = \max\{(V_{OI} - V_{OF})/T_{IF}, 0\},$$

$$A_{IP} = \max\{(V_{OI} - V_{OP})/T_{IP}, 0\}, \qquad N_{PI} = \max\{(V_{OP} - V_{OI})/T_{PI}, 0\},$$

$$C_{PI} = \max\{(V_{OP} - V_{OI})/T^*_{PI}, 0\}, \qquad D_{PF} = \max\{(V_{OP} - V_{OF})/T_{PF}, 0\},$$

$$S_{LF} = \max\{0, (V_{OL} - V_{OF})/T_{LF}\}, \qquad S_{FL} = \max\{0, (V_{OF} - V_{OL})/T_{FL}\},$$

$$\beta_{PL} = \max\{0, (V_{OP} - V_{OL})/T_{PL}\},$$

where $V_{OS} = W_{OS}\sigma_{OS}$ $(S = F, I, P, L)$.

To estimate flux K_I, we take into account information on the moisture balance in the region of the Red Sea. According to available estimates, the input of water to the

Table 4.11. Quantitative estimates of water fluxes in the scheme in Figure 4.7 (10^{-3} km^3 yr^{-1}).

Flux	*Estimate*	*Flux*	*Estimate*
w_{AOL}	3.6	I_{LF}	0.57
S_{LF}	436	S_{FL}	400
R_L	5.14	A_F	0.3
H_{OF}	23.97	R_F	19.33
w_{AOF}	72.5	E_{FA}	96.6
A_{FI}	6,780.24	M_{IF}	952
D_{PF}	5,771.09	C_{PI}	437
N_{PI}	66.86	I_{OI}	0.765
A_{IP}	6,338.74	E_{IA}	115.4
w_{AOI}	84	R_I	5.386
K_I	0.005	R_P	13.12
E_{PA}	200.4	w_{AOP}	206.7
I_P	0.975	E_{LA}	1.7
β	80.5		

Red Sea via the Suez Canal and by precipitation can be disregarded. Not a single river flows into the Red Sea. The main component of flux K_I through Bab el Mandeb is persistent. Hence, we can assume $K_I = \max\{0, w_{AK}\sigma_{KMP} - E_{KMA}\sigma_{KM}\}$, where w_{AK} and σ_{KMP} are the level and the area of mainland run-off to the Red Sea, respectively, and E_{KMA} is evaporation from area σ_{KM} of the Red Sea. The water expenditure through the Straits of Gibraltar $H_{FO}(H_{OF})$ is determined by the relationship between the levels of W_{OF} and the Mediterranean Sea. In order not to complicate the structure of the model, the level of water in the Mediterranean Sea is determined by its watershed and the difference between precipitation and evaporation. Since the intra-annual distribution of water inflow into the Atlantic Ocean varies within 20%, we can reliably assume $W_{FO} = -W_{OF} = \text{const}$.

4.6.4 Numerical model of global water balance

4.6.4.1 Modeling the global water cycle

Water is one of the substances most widely spread in nature (Table 4.12). It is present in various forms in practically all areas of the planet and plays an important role in

Table 4.12. Water in the biosphere.

Reservoir	*Volume* (10^3 km^3)	*Part of total volume* (%)	*Regeneration time*
World Ocean	137,000	97.61	3,100 years
Glaciers	29,000	2.08	16,000 years
Ground water	4,000	0.29	300 years
Fresh lakes	125	0.009	1–100 years
Saline lakes	104	0.008	10–1,000 years
Soil moisture	67	0.005	280 days
Rivers	1.2	0.00009	12–20 days
Atmosphere	14	0.0009	9 days

the energy and mass exchange between continents, oceans, atmosphere, and other, smaller land territories and water basins. This role in recent years is increasingly manifesting itself in the complex system of human–society–environment interactions necessitating creation of scientific principles for rational control of water resources. Human-induced changes in the global water cycle are now globally significant and are being modified without adequate understanding of how this cycle works. Therefore, the problem of evaluating the role of water in the global carbon cycle is but a small part of the general global problem of the interaction between nature and society.

Oceans, polar ice caps, glaciers, lakes, rivers, soils, and the atmosphere contain between them $1.4–1.5 \cdot 10^9$ km^3 of water. This mass is in constant dynamic interactions with other biospheric components and determines thereby the factors of environmental variability. The methods of numerical experiments that have been developed should be used to assess the role of these factors under current conditions and to show the significance of the water balance in stabilizing the many climatic and biogeocenotic processes. We have attempted here, by systematizing information about the water balance of the planet, to create a version of the model of biospheric water balance (MBWB) capable, within the general approach to modeling the carbon balance, to take into account the role of water fluxes.

An important block of the MBWB is the methods of determination of various parameters of the water cycle. Such methods are based on the use of surface, satellite, and airborne measurements. The MBWB used as a global model makes it easier to understand the role of the oceans and land in the hydrological cycle, to identify the main factors that control it, as well as to trace the dynamics of its interaction with plants, soil, and topographic characteristics of the Earth surface. It is based on the interaction between the elements of the water cycle, and takes natural and anthropogenic factors into account by means of information interfaces with other units of the global model (Krapivin and Kondratyev, 2002).

Let us consider a block scheme of global water exchange and write respective equations for it. The basic regularity of global water exchange is the invariability of water supplies on Earth over time periods of hundreds of years (i.e., we can reliably write the balance equation $W_E + W_S + W_O$, where W_E, W_S, and W_O are water supplies on Earth, on land and in the oceans, respectively). A compartment of the atmosphere is related to the respective region of water basin. Such a relationship is valid

$$\frac{dW_E}{dt} = \frac{dW_S}{dt} + \frac{dW_O}{dt} = 0$$

or $dW_S/dt = -dW_O/dt$. Hence, the trend in changes of water supplies on land is in direct contrast to the similar trend in the oceans.

With water supply in the atmosphere $W_A = W_{AO} + W_{AS}$, we obtain $W_E = W_A + W_{S1} + W_{O1}$, where W_{AO} and W_{AS} are water supplies in the atmosphere over the oceans and land, respectively; $W_{S1} = W_S - W_{AS}$ and $W_{O1} = W_O - W_{AO}$. The balance equation will be:

$$\frac{dW_E}{dt} = \frac{dW_A}{dt} + \frac{dW_{S1}}{dt} + \frac{dW_{O1}}{dt} = 0.$$

As can be seen, the structure of trends in the ratios of water supplies is complicated and to analyze it additional considerations are needed. This complication becomes considerable as we further subdivide the biosphere.

Within the MBWB, small corrections for the water exchange between the Earth and space are not taken into account. A model of the global water cycle can be based on describing the hydrology of comparatively large territories. In this case the basic unit of such a territory is compartment Ω_{ij} of the Earth surface of size $\Delta\varphi_i$ by latitude and $\Delta\lambda_j$ by longitude.

The state of the water component of compartment Ω_{ij} and its coordinates (φ_i, λ_j) can be characterized by the magnitude of an equivalent liquid water column per unit area. Possible water fluxes across the border of Ω_{ij} are shown in Figures 4.11 and 4.12. The intensities of these fluxes depend on the phase state of water, temperature, wind speed, and other geophysical and ecological factors. It is difficult to take into account the fine detail of these fluxes within the global model because their interactions have been studied inadequately. Therefore, the degree of detailing chosen here is oriented toward account of the most important components of their states. Water is considered in liquid, solid, and gas phases. Within compartment Ω_{ij} there is only one state; though in future, once the needed information becomes available, a vector parameter can be introduced to determine the share of precipitation over Ω_{ij} in the form of snow, granulated snow, pellets of ice, ice rain, rain, drizzle, wet snow, and others.

The global water balance consists of the mosaic structure of local balances at the level of Ω_{ij}. The proposed description of water fluxes enables us to trace their balance at any level of spatial digitization: region, water basin, continent, ocean, hemisphere, or biosphere. Clearly, the general balance of evaporation and precipitation at the level of the biosphere is maintained. In other cases, as the spatial size of the

selected unit of the biosphere decreases, we should expect to observe differences between the precipitation amount and evaporation. In such cases water transport through the atmosphere, river run-off, and sea currents will serve as an equalizer. Though the quantitative estimates of all these parameters are well known, the dynamics of the water cycle can only be described using a model. As a first approximation, to assess the role of precipitation in the global CO_2 cycle we use only components W_{AU} and W_{AS}. However, to account for the spatially heterogeneous distribution of CO_2, the entire biosphere needs to be digitized.

Using the notation in Figures 4.11 and 4.12, the balance equations of the water cycle at the level of Ω_{ij} are written as follows:

$$\frac{dW_S(t,i,j)}{dt} = w_{AS} + w_{GS} + w_{SS} + w_{HS} - w_{SO} - w_{SG} - w_{ST} - w_{SA} - w_{SH},$$

$$\frac{dW_H(t,i,j)}{dt} = w_{SH} + w_{OH} - w_{HO} - w_{HG} - w_{HS},$$

$$\frac{dW_O(t,i,j)}{dt} = \sum_{(k,n)\in I_{kn}} [w_{IO}(t,k,n) + w_{HO}(t,k,n)] + w_{AO} + w_O - w_{OA} - w_{OG} - w_{OR} - w_T,$$

$$\frac{dW_A(t,i,j)}{dt} = w_{OAA} - w_{AOO} + w_{SA} + \begin{cases} w_V, & \text{for water surface;} \\ w_{ST}, & \text{for land.} \end{cases}$$

Detailing the right-hand sides of these equations with changing parameters of the environment will determine the qualitative and quantitative reliability of the model. In particular, the model can be simplified by approximating the average value of W_O:

$$\overline{W}_O = \begin{cases} 2{,}500 + 350\sqrt{t}, & \text{for } 0 \le t \le 70, \\ 6{,}400 - 3{,}200\exp(-t/62.8), & \text{for } t > 70, \end{cases}$$

where the average depth of the World Ocean is measured in meters, and the age of the ocean t is calculated in millions of years. Variations in the ocean volume can also be approximated by the formula $\Delta V = \Delta W_O A_O + 59.5(\Delta W_O)^2$, where $A_O = 361.06 \cdot 10^6$ km^2.

Let us consider the scheme in Figure 4.14 as the basis for modeling the hydrological regime of a small territory Ω_L, home to the water ecosystem under study. The territory has a river network, water bodies, and land. According to the hydrological principle of landscapes, to derive a model to simulate how a hydrological system functions, it is necessary to select the facies that typifies the background flora, the concrete appearance of which is determined by the micro-relief, type and properties of the soil, surface moistening, depth of ground waters, and other factors. In general, territory Ω_L is characterized by the presence of m facies, and the water network has n heterogeneous sites. Bearing this in mind, according to Figure 4.14, the closed system of balance equations has the form:

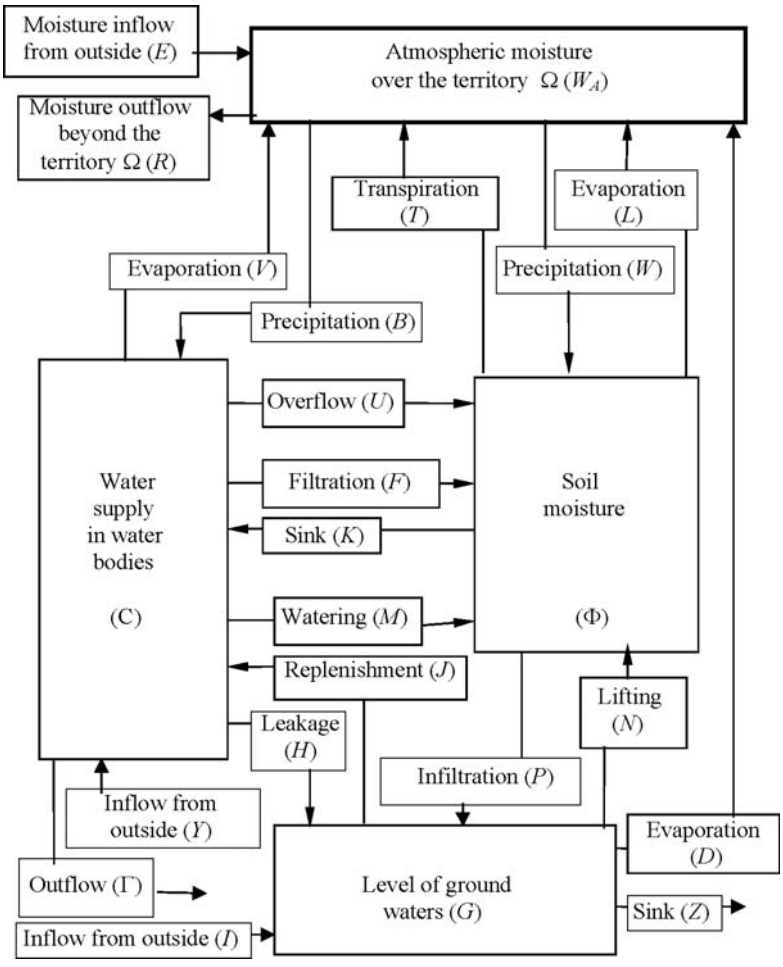

Figure 4.14. The block scheme of the sample model of water balance in a small territory.

$$\sigma_{ij}\frac{dW_{A,ij}}{dt} = E_{ij} - R_{ij} + \sum_{k=1}^{n}(V_k - B_k S_k) + D_{ij} + \sum_{l=1}^{m}(L_l + T_l - W_l\sigma_l),$$

$$S_k\frac{dG_k}{dt} = Y_k - V_k + B_k S_k - H_k + J_k + \sum_{l=1}^{m}(K_{lk} - F_{kl} - V_{kl} - M_{kl}) - \Gamma_k + S_k(C_{k-1}V_{k-1}/\Delta_{k-1} - C_k V_k/\Delta_k),$$

$$\sigma_l\frac{d\Phi_l}{dt} = \sum_{k=1}^{n}(F_{kl} + V_{kl} + M_{kl}) + \sum_{k=1}^{m}\psi_l^k\theta_l - L_l - T_l - P_l - \theta_l + N_l + W_l\sigma_l,$$

$$\sigma_{ij}\frac{dG_{ij}}{dt} = I_{ij} - Z_{ij} - D_{ij} + \sum_{k=1}^{n}(H_k - J_k) + \sum_{l=1}^{m}(P_l - N_l).$$

In these formulas the following notations are assumed: σ_{ij}, σ_l, and S_k are the areas of the territory Ω_{ij} of the lth facies and the kth compartment of the river network, km^2, respectively; Δ_k is the linear size of the kth compartment of the river network, km; $W_{A,i,j}$, G_k, and Φ_l are, respectively, the levels of water in the atmosphere, in the kth compartment of the river network, and the lth facies on the territory Ω_{ij}; θ_{ij} is the level of ground water, m; ψ_l^k is the share of the run-off of the kth facies that reaches the territory of the lth facies; the remaining notations are given in the scheme in Figure 4.14.

Application of the model to other regions is realized via variables E, R, Y_i, Γ_i, I, Z. Moreover, when analyzing the concrete situation, the configuration of the waterway and the level of the water table are taken into account. The needed equations are written like those above, proceeding from the condition of the water volume balance. Functionally, all fluxes in the scheme in Figure 4.14 can be described according to the laws of hydrodynamics and with account of available observational information. The inflow E_{ij} and outflow R_{ij} of moisture can be determined by data from remote sensing. Between measurements, the information used about wind speed V_{ij} and the functions E_{ij} and R_{ij} are calculated by the formulas $E_{ij} = E_{H,ij}$ and $R_{ij} = W_{A,ij}l^*/(l^* + k_1 V)$, where $l^* = 2\sqrt{\sigma}/H$, E_H is atmospheric moisture at the windward border of the region, and k_1 is a constant coefficient reflecting the contribution of wind to the circulation of precipitation.

Such information on precipitation and run-off is inserted into the data catalogs of hydrometeorological services. Based on these data, respective model units can be derived. Assuming that the distribution of precipitation is proportional to relevant areas, we obtain:

$$B_k = W_{A,ij}\sigma_k/\sigma_{ij}; \qquad W_l = W_{A,ij}\sigma_l/\sigma_{ij}.$$

A model of river run-off should take into account the watershed topography and the spatial distribution of characteristics of its soil as well as special features of vegetation covers. Let $\theta_l = (g_l + K_l \exp[-a_l X_l - C_l A_l])\sigma_l$, where X_l and A_l are, respectively, the vegetation density (m/km^2) and the soil layer thickness (m) over the area σ_l; g_l is the coefficient of the relief run-off in the lth facies; k_l is the coefficient of water penetration through vegetation and soil covers over area σ_l; a_l and C_l are the coefficients of precipitation retained by plants or soil in the lth facies, respectively. Parameters for this dependence can be determined from field measurements that establish, for a given type of soil and plants, the connection between precipitation intensity, the rate of water take-up by the soil, and the water resistance of its structure. For instance, run-off is equal to precipitation in takyrs.[1] Such a rough approximation can be specified, since radiometric methods make it possible to classify soil moisture in at least three types: firmly bound, loosely bound, and free water. Bound water is the film of moisture adsorbed by the surface of ground particles and has a thickness of 6–8 molecular layers. The content of bound water is estimated at 2%–3% in sands, and 30%–40% in clay and loess. Bound water cannot be assimilated by plants and does not dissolve salts. In the models considered these

[1] A takyr is a flat hollow in the desert.

specific features are taken into account when determining the respective coefficients of evaporation and transpiration.

Run-off θ_l is distributed between facies, and in the form of return water K_{lk} flows into the river. In a general form this is reflected through the coefficients of run-off distribution $\psi_s^l \left(\sum_{s=1}^{m+2} \psi_s^l = 1 \right)$, where ψ_{m+1}^l is the share of run-off from the lth facies that leaves the region, ψ_{m+2}^l is the share of run-off from the lth facies that enters the river. The coefficients $\omega_{lk} \left(\sum_{k=1}^{n} \omega_{lk} = 1 \right)$ characterize the run-off distribution from the lth facies to river compartments and are determined by the landscape relief and the spatial location of the facies and waterway compartments. Thus, $K_{lk} = \omega_{lk} \psi_{m+2}^l \theta_l$.

Evaporation from the soil surface can be described by the formulas of Hitchcock, Horton, Weissman, and others (Bras, 1990). For instance, the formula by Priestley and Taylor (1972) for the latent heat of evaporation q_E is $q_E = \alpha S(q^* - q_i)/(S + \gamma)$, where q_i is soil heat flux, W/m^2; q^* is net radiation flux, W/m^2; $\gamma = 0.066 \cdot 10^3$ Pa/K is a psychometric constant; and S is the slope of the curve of temperature dependence of saturated moisture pressure (Pa/K),

$$\alpha = \begin{cases} 1.06, & \text{for wet soil;} \\ 1.04, & \text{for dry soil;} \\ > 1.26, & \text{at warm air advection over a wet surface.} \end{cases}$$

The Horton formula gives

$$V = 0.36[(2 - \exp\{-0.44\theta\})l_V - l_a] \quad \text{(mm/da)},$$

where θ is the wind speed (m/s); l_V is the vapor pressure near the water surface; and l_a is water vapor elasticity.

The Rower formula is written as

$$V = 0.771(1.465 - 0.007\rho)(0.44 + 0.26\theta)(l_V - l_a) \quad \text{(mm/da)},$$

where ρ is atmospheric pressure (mmHg).

The diversity of forms to parameterize the dependence of the rate of evaporation from the soil surface on environmental parameters facilitates adapting the model of water balance to the information base.

Flux T in Figure 4.14 reflects the impact of vegetation cover on the hydrological regime of a territory. A simple model of transpiration is the following dependence:

$$T = y(24\alpha^* + \beta^*) \quad \text{(cm/da)},$$

where y is the specific water return of the soil; α^* is the rate at which ground water rises (cm/hr); and β^* is the daily change in the level of ground waters (cm).

Let us determine the constituents of the block scheme in Figure 4.14 characterizing the processes of leakage and filtration of water from the river. Both leakage and

filtration depend on the quality of the riverbed and water level. Let

$$H_i = \begin{cases} \mu_i C_i S_i, & \text{for } 0 \le C_i \le C_{i,min}; \\ \mu_i C_{i,min}, & \text{for } C_i > C_{i,min}, \end{cases}$$

where μ_i is the coefficient of water penetration through the riverbed. Filtration F_i increases as C_i increases between two critical values: $C_{i,min}$ when there is no filtration, and $C_{i,max}$ when it is at a maximum; hence

$$F_{i,max} = \begin{cases} 0, & \text{for } 0 \le C_i \le C_{i,min}; \\ \mu_i(C_i - C_{i,min})S_i, & \text{for } C_{i,min} < C_i < C_{i,max}; \\ \mu_i(C_{i,max} - C_{i,min})S_i, & \text{for } C_i \ge C_{i,max}. \end{cases}$$

The distribution of water filtering from the river between facies depends on the distance r_{ij} between the ith compartment and the jth facies, as well as on the structure of the soil and landscape relief. In particular, this dependence can be described by the function $F_{ij} = F_{i,max}\chi(r_{ij})$, where $\chi(r_{ij})$ is the decreasing function satisfying the condition

$$\sum_{j=1}^{m} \chi(r_{ij}) = 1.$$

Evaporation from the river surface depends on the environmental temperature and can be described by the formula $V_i = V_i^* T^{\omega}$ or by the relationship $V_i = \mu(\theta)(\rho_V - \rho_2)$, where $\mu(\theta)$ is a function reflecting the impact of the wind; ρ_V is the water vapor pressure at the temperature of the evaporating surface, mb; and ρ_2 is absolute air humidity at a height of 2 m, hPa .

The volume of overflow is determined by the binary regime within a maximum possible water level $C_{i,max}$, so that

$$V_i^* = \begin{cases} 0, & \text{for } 0 \le C_i \le C_{i,max}; \\ C_i - C_{i,max}, & \text{for } C_i > C_{i,max}. \end{cases}$$

The distribution of U_i^* between facies depends on the landscape relief, characterized by the matrix of relief run-off $\Psi = \|\Psi_{ij}\|$, and is written as

$$\sum_{j=1}^{m} \Psi_{ij} = 1, \Psi_{ij} \ge 0.$$

As a result, $U_{ij} = \Psi_{ij} U_i^*$.

Taking water for agriculture from the ith compartment of waterway is an anthropogenic factor, and should be considered as a free parameter $M_i^* = \sum_{j=1}^{m} M_{ij}$. To take into account any possible heterogeneity in the distribution of M_i^* between facies, it is necessary to introduce the matrix of the coefficients of the distribution of watering $\nu = \|v_{ij}\|$ $(\nu_{ij} \ge 0, \ \sum_{j=1}^{m} \nu_{ij} = 1, \ i = 1, \ldots, n; \ j = 1, \ldots, m)$ such that $M_{ij} = \nu_{ij} M_i^*$.

The relationship between surface water fluxes and ground water strongly depends on the flux of water infiltrating downward through the soil layer. This flux, called infiltration, accounting only for the vertical heterogeneity of the soil can be described in a general form by the equation:

$$\frac{\partial P}{\partial t} = \frac{\partial}{\partial z}\left[p(P)\frac{\partial P}{\partial z} + K_z(P)\right]. \tag{4.31}$$

Bras (1990) gave various versions of solutions to this equation. For practical use the following solution can be recommended:

$$f = f_c + (f_0 - f_c)\exp(-Pl^2 t),$$

where $f = (P_i - P_0)P/(\pi t)^{-1}$; f_c is the asymptotic value of the rate of filtration; and f_0 is the initial value of the rate of filtration.

The processes of infiltration and evaporation of ground water depend strongly on the vertical profile of the soil layer. The following soil layers can be selected: saturated and unsaturated. The saturated layer usually covers depths >1 m. The upper unsaturated layer includes soil moisture around plants' roots, the intermediate level, and the level of capillary water. Water motion through these layers can be described by the Darcy (1856) law, and the gravitation term $K_z(P)$ in Equation (4.31) can be calculated by the equation:

$$K_z(P) = 256.32\delta_s^{-7.28} - 1.27\delta_s^{1.14} \quad \text{(cm/da)},$$

where δ_s is the volume mass of soil ($\mathrm{g\,cm^{-3}}$).

Thus, any system of equations for the regional water budget that has these functional descriptions of water fluxes in the region under study, at initial values of $W(t_0)$, $G(t_0)$, $C_i(t_0)$, $\Phi_j(t_0)$ prescribed for time moment t_0, facilitates calculation of the characteristics of the water regime of the whole region for $t \geq t_0$. Initial values are provided by the monitoring system. The regularity of surveys depends on the required accuracy of prognosis and can be realized by planning the monitoring regime. Based on how the model is synthesized and the remote-sensing system, the monitoring of any irrigated agri-ecosystem can in practice be carried out. However, problems do appear in tallying airborne measurements with the values of geophysical, ecological, and hydrological parameters. An example of successful solution of such problems (Vinogradov, 1983) was determination of the dependence between the coefficient of spectral brightness $\tau_J = \tau_z + (\tau_0 - \tau_z)\exp(-\alpha W^c) + dW^n$, where τ_0 is the coefficient of dry soil brightness, τ_z is the coefficient of brightness of soil that has a moisture content close to the minimum field moisture capacity (when there is no free water in the soil); α, c, d, and n determine the type of soil ($\alpha, d, n < 1$; $c > 1$; for achromatic loamy soils we have $\tau_z = 0.09$, $\tau_0 = 0.28$, $\alpha = 0.01$, $c = 2.3$, $n = 0.9$, $d = 0.0001$). Getting estimates of these is an important problem facing remote sensing of the environment.

Finally, note that the deterministic approach to modeling the water cycle in zone Ω_L described here cannot be considered the only one possible. Such an approach gives only average trends in changes of the water cycle components. Their distribution and probabilistic prognosis can be obtained only on the basis of dynamic-stochastic

models of the water balance. In modeling the global carbon cycle this approach facilitates taking into account the sink of atmospheric CO_2 over the region due to leaching.

4.7 CARBON CYCLE AND METHANE

Methane like carbon dioxide is another greenhouse gas. The spectrum of its natural and anthropogenic sources is wide, and its greenhouse effect exceeds 20 times that of CO_2 though its concentration ($\sim$1.6 ppm) in the atmosphere is about 200 times less than that of CO_2 (Dementyeva, 2000; Panikov and Dedysh, 2000; Arneth *et al.*, 2002; EPA, 2001). It occupies second place to carbon dioxide in the greenhouse effect. Methane also affects ozone content in the stratosphere and plays a key role in transforming chemically active Cl into less active HCl. Before human interference, the natural cycle of methane was balanced with respect to climate. By extracting natural combustible gases consisting of 90%–95% of methane, humankind has contributed instability and uncertainty to this cycle. On the whole, during the last 200 years anthropogenic contribution to the input of CH_4 to the atmosphere has doubled. The situation has now arisen when the difference between methane concentrations at the poles has reached 150 ppb. Most authors estimate the level of the global emission of methane into the atmosphere at $535 \cdot 10^6\ tCH_4\ yr^{-1}$, of which $375 \cdot 10^6\ tCH_4\ yr^{-1}$ is of anthropogenic origin ($50 \cdot 10^6\ tCH_4\ yr^{-1}$ from rice paddies). The anthropogenic input of methane is expected to grow within the next 20–30 years, though in some developed regions, measures are being taken to reduce anthropogenic emissions of methane into the atmosphere. Nevertheless, the concentration of methane in the present atmosphere is increasing seven times faster than the growth of CO_2 concentration, so that its amount is increasing annually by 2%; that is, by 2020 the amount of methane in the atmosphere can double compared with 2000, which, from numerous estimates, will lead to a global warming of 0.2°C–0.4°C. As in the case of CO_2, these estimates will remain rather doubtful and contradictory until a global model like the one mentioned above is synthesized. However, at the level of current knowledge, only the initial steps can be taken to model the features of the global cycle of CH_4.

The sources of methane include oil, sedimentary and ejected (volcanic) rocks, bottom sediments of lakes, seas, oceans, and other objects of the hydrosphere, as well as soil, peatbogs, rice paddies, and many more. Principal among which are

- natural gas and oil extracting and refining systems;
- vital functions of animals;
- landfills of solid waste;
- coal mining;
- processing of stockbreeding waste;
- sewage processing;
- anaerobic decomposition of organic matter in rice paddies;
- fossil fuel burning;

- burning of agricultural waste, biomass, rubbish, and savannah fires; and
- various industrial processes.

The basic reaction of methane formation due to anaerobic fermentation or mineralization of organic matter is as follows:

$$C_6H_{12}O_6 \rightarrow 3CO_2 + 3CH_4.$$

Sinks for tropospheric methane are:

- reaction with hydroxyl radical (~90%);
- transport to the stratosphere (~5%); and
- oxidation in dry soil (~5%).

Ways of methane transformation, as shown in Table 4.13, include numerous processes that are 70%–80% of biogenic origin mostly affected by humans (Girnis *et al.*, 2003). Of course, the significance of these processes varies depending on many natural and anthropogenic parameters. Relationships between the individual

Table 4.13. Sources of the input of CH_4 into the terrestrial atmosphere.

Source of CH_4	*Area of the source* (10^6 km^2)	*Rate of CH_4 formation* (g m^{-2} yr^{-1})	*Average rate of CH_4 formation* (10^6 t/yr)
Rice paddies	1.35	206	280
Marshes	2.6	50–100	130–260
Freshwater lakes	2.5	50–100	1.25–25
Arid soils	30	0.44	10
Woodland	44	0.01–0.09	0.4
Tundra	8	10	0.8–8
Oceans	361	0.012	4–6.7
Marginal shelves	1.4	5-10	0.07–1.4
Animals			101–220
Termites			150
Fossil fuels			100
Slag heaps			20–40
Sewage			30–40

elements correlation the cycles of CO_2, CH_4, and other chemicals vary, too. At any rate, it is clear that depending on the strategy adopted for the nature–society system, in due course the composition of the terrestrial atmosphere will change substantially. Suffice it to say that the burning of just $1\,m^3$ of methane extracts from the atmosphere $2\,m^3 O_2$. From open slag heaps and municipal and industrial sewage, the atmosphere receives annually about 2% of anthropogenic methane ($\sim 270–460 \cdot 10^6$ tC). These integral estimates do not permit calculation of the actual distribution of CH_4 flux in the atmosphere. A certain contribution detailing the spatial distribution of the sources of methane was made at the *Second International Conference on the Problems of Methane* held in Novosibirsk in 2000. The proceedings of this conference contain concrete data on the sources of methane in many regions of the globe. For instance, according to Byakola (2000), within the framework of the international UNEP/GDP project, an inventory of the sources and sinks of CO_2 and CH_4 was made for Uganda ($236 \cdot 10^3\,km^2$). In Uganda, the basic anthropogenic sources of methane are agriculture, municipal sewage, and biomass burning. In 1990, stockbreeding and rice paddies in Uganda contributed to the atmosphere $205.45 \cdot 10^3$ t and $23.45 \cdot 10^3$ tCH_4, respectively. Agricultural waste burning added $3.55 \cdot 10^3$ tCH_4.

Naturally, Uganda needs to reduce GHG emissions, but the threshold at which such emissions must not be exceeded is unknown. Of course, stockbreeding and rice production in Uganda will develop in future, increasing thereby the volumes of CH_4 emitted to the atmosphere. Hence, a balanced correlation should be sought between the economy of the country and the state of the environment. This problem can be solved with the new technologies of nature use (Krapivin and Kondratyev, 2002). In particular, one of the ways to reduce CH_4 emissions is secondary utilization of organic waste (e.g., in paper production). In Uganda, up to 16% of urban waste is used in paper production.

Gas transport systems are one of the powerful anthropogenic sources of CH_4. The work of Coconea (2000) contains information about methane emissions from pipelines in Romania, the country that signed the Lisbon Protocol in 1994 and now supports the Kyoto Protocol. Romania was the first country in Europe to install a pipeline to transport natural gas; this took place in 1917 and the pipeline was 50 km long. At present, natural gas constitutes 36% of the energy resources of the country, the share of oil and coal constituting 32.6% and 15.2%, respectively. Therefore, the problem of anthropogenic input of CH_4 from the territory of Romania to the atmosphere is urgent. Here, like Uganda, saving technologies play an important role, reducing by 38.9% the leakage of methane from pipelines during the last 20 years, constituting 55.35% in 1994 with respect to the leakage in 1987. On the whole, both extraction and distribution of coal, oil, and gas in Romania are responsible for 56% of the total amount of CH_4 emitted from this territory. Agriculture takes second place with 29%.

One of the significant sources of CH_4 is Russia, which contributes to the atmosphere about $47 \cdot 10^6$ t$CH_4\,yr^{-1}$, and this flux is expected to reach $78 \cdot 10^6$ t$CH_4\,yr^{-1}$ by 2025. This increase will be caused by the developing infrastructure of the gas, oil, and coal industry. On global scales, these trends will be practically observed in all countries. In Table 4.14 the contribution of the coal industry to CH_4 production is

Table 4.14. Emissions of methane by the coal industry in various countries. From Gale and Freund (2000), IEA (2007a, b).

Country	*Coal reserves* (Gt)	*Coal production* (Gt of oil equivalent/yr)	*CH_4 emissions* (10^6 t/yr)	*Specific rate of CH_4 emision* ($kgCH_4$/t coal)
Australia	78,500	203.1	0.8	3.5
U.K.	220	11.3	0.5	7.4
Germany	6,739	50.3	1.0	3.6
India	93,445	209.7	0.4	1.5
China	114,500	1212.3	7.7	6.7
Poland	14,000	67.0	0.6	3.0
Russia	157,010	144.5	4.5	8.3
U.S.A.	246,643	595.1	4.3	5.0
Czechoslovakia	5,552	23.7	0.3	3.4
South Africa	48,750	144.8	1.0	0.5
Total world	*909,064*	*3079.7*	*21.7*	*4.9*

estimated for various global regions. These estimates are determined by technologies used in the coal industry. On average, the contributions of various sources to the coal industry itself constitute 70% underground ventilation in coalmines, 20% underground drainage, 5% surface loading and unloading operations, 4% opencast mining of deposits, and 1% derelict mines.

The global cycle of methane, just like the other cycles, has not been studied sufficiently well, and therefore its modeling faces a lot of unsolved problems. CH_4 fluxes from waterlogged territories have been studied best. These fluxes constitute about 20% of the total input of methane to the atmosphere from all sources (Tables 4.14 and 4.15). Note that almost 80% of the sources of methane are biological in nature, but anthropogenic interference with its natural cycle is also possible through violation of various biospheric processes. In particular, in waterlogged territories, methane forms only due to biological processes. The hydrospheric sources of methane can be presented as a multi-layer model (Figures 4.15 and 4.16). This scheme describes the vertical structures of most water bodies. Methane forms in bottom deposits as a byproduct of bacteria, and in the zone with oxygen, methane is partially oxidized giving off carbon dioxide $CH_4 + 2O_2 \rightarrow CO_2 + 2H_2O + E$. The bacteria that take part in methane oxidation use released energy E for organic matter synthesis. The remaining methane gets into the atmosphere and, in contrast to CO_2, practically

Table 4.15. Methane emissions from different sources recalculated for carbon equivalent. From EPA (2001). Estimates of methane fluxes are given in 10^6 tC per year.

Anthropogenic source of methane	*1990*	*1995*	*2000*	*2005*	*2010*
Output of natural gas and oil	181.1	177.0	185.2	186.9	190.2
Animal vital functions	157.4	143.4	144.0	149.5	150.8
Landfill sites	136.9	131.4	133.9	134.4	135.5
Coal mining	82.8	62.6	59.0	59.3	59.0
Processing of stockbreeding waste	27.9	26.8	28.1	29.2	29.8
Sewage processing	10.1	9.8	9.8	10.4	10.4
Other sources connected with agriculture	7.9	8.2	8.5	8.2	8.2
Industrial and municipal sectors	15.0	13.9	13.7	13.9	14.8

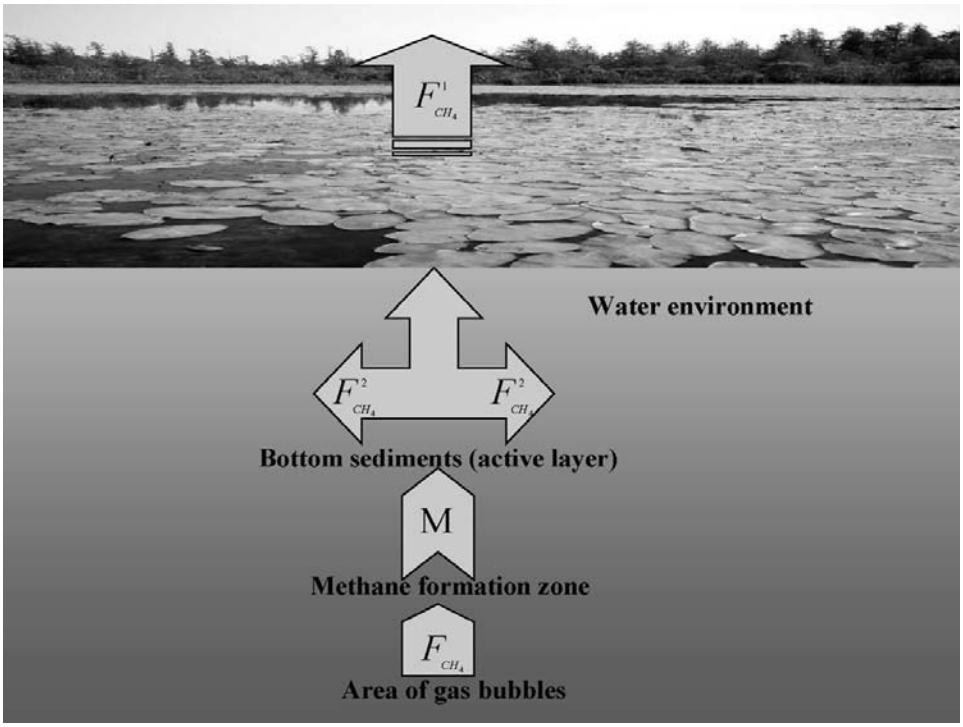

Figure 4.15. Block diagram for formation and transport of methane in waterlogged country. Notation: $F^1_{CH_4}$ is the methane flux across the atmosphere/water body interface; $F^2_{CH_4}$ is the oxidation of methane in aerobic zones; F_{CH_4} is the intensity of the methane source; M is methane concentration.

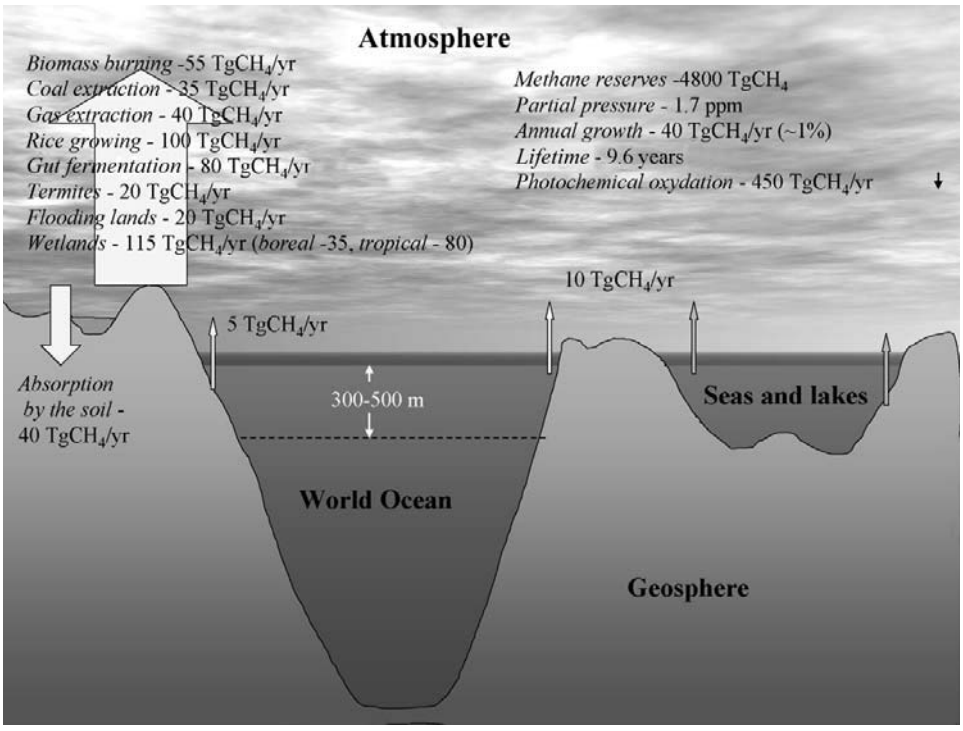

Figure 4.16. Reserves and fluxes of methane in the atmosphere–ocean–land system. From Fung *et al.* (1991). Notation: $\mathrm{Tg} = 10^{12}$ g.

never returns to the water medium. This is somehow connected with the fact that CH_4 solubility in water is almost 40 times lower than that of CO_2. The lifetime τ_H of methane in the atmosphere is estimated at about 5 years. Its extraction from the atmosphere takes place due to the participation of methane in photochemical reactions, resulting in methane oxidation first to CO, and then to CO_2. The cycle CO–OH–CP_4 plays an important role in the methane cycle:

$$\mathrm{OH} + \mathrm{CH_4} \rightarrow \mathrm{CH_3} + \mathrm{H_2O},$$
$$\mathrm{OH} + \mathrm{CO} \rightarrow \mathrm{CO_2} + \mathrm{H}.$$

Participating OH radicals form in the atmosphere during water vapor photolysis. As a result, the simplest diagram of methane oxidation in the atmosphere is the following:

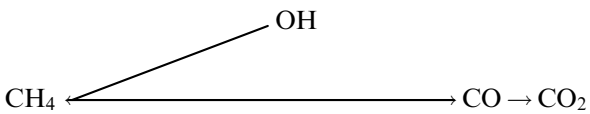

Human interference with the processes described by this diagram breaks the natural stability of the balance $CH_4/CO/CO_2$. In particular, the reclaiming of marshes is one such destabilizing factor. For instance, the drainage of 20% of marshes leads to a natural reduction of CH_4 emissions from the marshes by 20%, and on the whole, the amount of methane is reduced by 4%, which practically does not influence climate, but causes changes in the biogeochemical cycles of ozone and carbon dioxide with unpredicted consequences. These estimates are important to reach a final conclusion about the level of the overall greenhouse effect. However, solution of this problem is connected with many factors, disregarding which will lead to serious errors. For instance, the CH_4 flux at the atmosphere–marsh border depends on the vertical profile of the temperature in the marsh body. In the simplest case, if we denote as $T_W(z, t)$ the temperature at time moment t at depth z and write the equation of heat conductivity as

$$\frac{\partial T_W(z,t)}{\partial t} = a^2 \frac{\partial^2 T_W(z,t)}{\partial z^2}, \tag{4.32}$$

where $a^2 = Kc^{-1}\rho^{-1}$, K is the coefficient of heat conductivity, c is specific heat capacity, and ρ is the medium density, then estimation of flux F^1_{CH4} as a time function becomes dependent on the multitude of poorly assessed characteristics of the environment.

Let the marsh surface temperature vary cyclically with frequency ω and amplitude A, decreasing with depth $T_W(0, t) = A(z) \cdot \cos(\omega t)$, where

$$A(z) = A(0) \cdot \exp\left(-\sqrt{\frac{\omega}{2a}}z\right).$$

The solution to Equation (4.32) enables us to trace temperature variations $T_W(z, t)$ and suggests the conclusion that in this case these variations weakly depend on $T_W(0, t)$. Even if $T_W(0, t)$ increases by 2°C, then according to (4.32), the amplitude of temperature changes with depth will rapidly decrease to 0.97°C, 0.33°C, and 0.01°C at depths 40 cm, 2 m, and 3 m, respectively. Hence, with a 2°C increase in the average global atmospheric temperature, flux F^1_{CH4} will increase by no more than 1.4%.

Comparing the global significance of the CO_2 and CH_4 cycles in the atmosphere–marsh system, note that the CO_2 cycle promotes climatic stabilization, whereas the CH_4 cycle intensifies climate change. With climate warming, marshes assimilate some CO_2 from the atmosphere and reduce thereby the greenhouse effect. In contrast, when the climate warms due to increasing F^1_{CH4}, the greenhouse effect intensifies.

The western Siberian region of Russia is characterized by numerous intensive natural and anthropogenic sources of methane formation. These are marshes, tundra, permafrost, oil and gas deposits. In this region, flux F^1_{CH4} varies widely both during the year and shorter time periods. From measurements carried out by Jagovkina *et al.* (2000) on the Yamal coastline in June 1996, the CH_4 concentration in the atmosphere

at a height of 2 m varied from 1.83 ppmv on June 18 to 1.98 ppmv on June 23, with an average daily variance of 0.032 ppmv.

The peatbogs of Siberia are quite special in the global cycle of methane. They play a unique role in the biogeochemical cycles of methane and carbon dioxide. On the one hand, they are a non-anthropogenic source of CH_4 and CO_2, but on the other hand, they are intensive assimilators of carbon from the atmosphere and extract it from the natural cycle for a long time. The marshes of west Siberia, for instance, contain 20%–30% of global carbon supplies. The intensity of CH_4 emissions from the marshes is, on average, almost 2,000 times weaker than that of CO_2. Between 35% and 50% of all methane emitted from Russia falls on marshes. West Siberian marshes emit to the atmosphere no more than $1.7 \cdot 10^6\,tCH_4yr^{-1}$, which does not exceed 1% of the global CH_4 flux. The spatial heterogeneity of flux F^1_{CH4} is high, which is determined by different characteristics of the marsh ecosystems. In particular, the upper oligotrophic coniferous–shrubby sphagnum swamps emit $0.9\,mgC\,m^{-2}\,hr^{-1}$–$10\,mgC\,m^{-2}\,hr^{-1}$ (Dementjeva, 2000). This estimate is rather approximate, since the scattering of such estimates by many authors constitutes hundreds of percent. For instance, a traditional drained sphagnum swamp can emit $142\,gC\,m^{-2}\,hr^{-1}$–$204\,gC\,m^{-2}\,hr^{-1}$, and rush–sphagnum bogs $83.5\,mgC\,m^{-2}\,hr^{-1}$–$309\,mgC\,m^{-2}\,hr^{-1}$.

The main mechanism for the formation of methane in a marsh is connected with the functioning of special groups of micro-organisms. Some methane due to diffusion is emitted to the atmosphere, but most remains in the peat layer and is gradually emitted to the atmosphere.

By remaking nature, humankind interferes with the natural biogeochemical balance of greenhouse gases practically everywhere in the world. One of the aspects of this remaking is the reduction in the areas of marshland and their transformation into agricultural fields. Diverse human agricultural activities add to the atmosphere 20% of all the anthropogenic flux of greenhouse gases. For instance, in the U.S.A. this is 30%. Stockbreeding contributes considerably to this flux. In California and Wisconsin each hectare of pasture emits annually $502\,kgCH_4$ (or $10{,}511\,kgCO_2$) and $134\,kgCH_4$ (or $2{,}814\,kgCO_2$), respectively. In New Zealand such emissions of CH_4 are estimated at $291\,kgCH_4$ (or $6{,}110\,kgCO_2$) (Johnson and Ulyatt, 2000).

Among the Kyoto Protocol signatories, the U.K. occupies ninth place by the volume of reduced emissions of greenhouse gases. The decreasing trend of methane emissions is part of the general reduction of emissions of six greenhouse gases (CO_2, CH_4, N_2O, hydrofluorocarbons, perfluorocarbons, sulfur hexafluoride) from 1990. In 2000 greenhouse emissions decreased by 15% compared with 1990. By 2010, CH_4 emissions will constitute $20{,}134\,t\,yr^{-1}$. This reduction will be reached mainly due to new technologies in the processing of waste and in the coal industry. On the whole, in the U.K., according to the developed scenario, emissions of methane by 2010 will decrease by 14% in agriculture, by 82% in the coal industry, by 29% in the oil and gas industry, and by 73% in waste processing. The possibility of realization of this scenario is confirmed by the CH_4 decreasing trend in 1998 compared with 1990. For instance, during this period, emissions of methane in the coal industry decreased by 64%, and in waste processing by 29%. In 1990, the share of waste processing in the

U.K. constituted 32% of all CH_4 emissions, only 3% of which were connected with sewage processing.

In agriculture, emissions of CH_4 in the U.K. constituted $1{,}037 \cdot 10^3$ t in 1990 and $998 \cdot 10^3$ t in 1998. The scenario of reduction of flux F^1_{CH4} from the U.K. due to improved technologies in agriculture foresees emissions of $902–983 \cdot 10^3$ tCH_4 in 2010. CH_4 emissions from the burning the agricultural wastes are expected to be zero and, in stockbreeding, emissions of methane are expected to reduce by 8% compared with 1990.

The coal industry in the U.K. was responsible for emissions of methane in 1990 of $819 \cdot 10^3$ t with the main contribution to this flux made by underground operations. This constituted 24% of the whole flux of methane from the U.K. In 1998, flux F^1_{CH4} decreased to $264 \cdot 10^3$ t and by 2010 it should decrease to $218 \cdot 10^3$ t. A similar decreasing trend in methane emissions from the U.K. is expected in the oil and gas industry, too. According to the scenario, the contribution of these sectors as a result of energy production to flux F^1_{CH4} will decrease from $540 \cdot 10^3$ t in 1990 to $349–464 \cdot 10^3$ t in 2010 (Meadows, 2000).

According to Bazhin (2000), flux F^1_{CH4} in every water basin that has a vertical stratiform structure forms in an active layer beneath the water surface. Practically all water geosystems have such a structure. The layer where methane forms has two areas. In the bottom area located at depth h, methane takes the form of bubbles. Above this layer, due to diffusion, the concentration of methane decreases, and bubbles disappear. Let us denote as $D_{CH4}(z)$ the coefficient of methane diffusion at depth z, then the stationary behavior of the whole system shown in Figure 4.15 is described by the equation:

$$\frac{d}{dz}\left[D_{CH4}(z)\frac{d}{dz}M(z)\right] - F_{CH4}(z) + F^1_{CH4} + F^2_{CH4} = 0.$$

Model calculations and field measurements carried out by Bazhin (2000) show, for instance, that in rice paddies $h_b = 1.3$ m, $F_{CH4} = (1.3–1.7) \cdot 10^{-12}$ mol $\cdot$ cm^{-3} s^{-1}. According to Khalil *et al.* (2000), rice paddies play a significant role in the gas balance of the atmosphere due to emissions of CH_4, CO, N_2O, H_2, and $CHCl_3$. For instance, Chinese rice paddies deliver these gases to the atmosphere at the following rates (mg/m^2 hr): CH_4 900–50,000; CO 80–100; H_2 5–30; N_2O 50–1,000; CHCl 1–8. The wide scatter of these estimates is explained by the highly unstable fluxes of these gases due advances in rice-growing technology. For instance, the use of sulfates on rice paddies increases emissions of methane by 12.0%–58.9% subject to other characteristics of these paddies (Liping *et al.*, 2000).

Thus, estimation of flux F^1_{CH4} as a function of a given territory with account of the natural and anthropogenic processes taking place there requires first of all a detailed inventory of methane sources as well as natural and technogenic systems functioning on this territory. Examples of such an inventory as the one given above serve as the basis for development of studies in this direction.

The dynamics of the CH_4 content H_A in the atmosphere can be parameterized by a simple balance relationship:

$$\frac{\partial H_A}{\partial t} + V_\varphi \frac{\partial H_A}{\partial \varphi} + V_\lambda \frac{\partial H_A}{\partial \lambda} = F^1_{CH4}(t, \varphi, \lambda, \Xi) - \frac{H_A(t, \varphi, \lambda)}{\tau_H},$$

where Ξ is the identifier of the type of natural or technogenic system.

On the whole, the fluxes of methane in the environment are rather diverse. The scheme in Figure 4.15 and data in Figure 4.16 reflect, to some extent, this diversity.

5

Monitoring the cycles of chemical substances in the environment

5.1 OBSERVATIONAL SYSTEMS FOR BIOGEOCHEMICAL CYCLES

Organization of the monitoring of GHG concentrations in the atmosphere has been aimed at recording the rate of their increase and evaluating the power of their sources and sinks, which will make it possible to determine more accurately a strategy of controlling possible climate change due to the impact of GHGs on the Earth's radiation balance. To achieve this goal, the CCGG group was organized at NOAA in 1992. The task of this group was to carry out ground and aircraft measurements of the GHG content in the atmosphere. In September 2005, in Boulder (Colorado) the *13th Meeting of Experts* was held on CO_2 concentration and related methods of measurement, at which results of the CCGG group's work were summarized. A multi-branched information network created in the U.S.A. assesses the content in the atmosphere of CO_2, CH_4, N_2O, CO, H_2, and SF_6 (Chédin *et al.*, 2002; Krapivin and Potapov, 2006). Measurements gathered by this network are used to identify long-range transport, estimate seasonal changes, and calculate the spatial distribution of gases that regulate the carbon cycle. To accomplish the program of measurements, a network of specialized towers (>400 m) was equipped with instruments to measure the speed and direction of wind, temperature, and relative air humidity. Since October 1994, these towers carried a four-channel gas chromatograph (GC) capable of measuring the products of burning CO, CH_4, H_2, and other gases of anthropogenic origin (CFCs, methyl chloroform, carbon tetrachloride, chloroform, sulfur hexafluoride, perchloroethylene).

Reliable assessment of the constituent elements of the global GHG cycle, especially CO_2, is impossible without organizing observations of vegetation cover. In this connection, the *Working Meeting* held in March 1995, in Italy, and dedicated to developing a strategy for long-term study of CO_2 and water balance in land ecosystems, recommended carrying out the European project EuroFlux and getting American experts to participate who had experience in the parallel project

AmeriFlux. As a matter of fact, over North and South America 25 ecosystems have been recorded, including forests, meadows, tundra, cropland, and pastures. By considering their distribution, it should be possible to assess the gas, energy, and water exchanges in the atmosphere–land biosphere system. Satellite measurements using AVHRR data should give information about changes in land cover. Information about the global productivity of ocean ecosystems can be obtained from measurements using MODIS.

Most satellites provide daily images of vegetation cover except of course on cloudy days. Despite the seemingly high accuracy, daily averaged data cannot reflect the actual variability of CO_2 fluxes at the atmosphere–vegetation boundary, since this can happen in just a matter of hours. Therefore, Sims *et al.* (2005) proposed an algorithm to get the data of satellite monitoring of CO_2 fluxes to agree with various periods of averaging. This algorithm is based on calculating CO_2 fluxes using ratios between photosynthesis and photosynthetically active radiation in the form of a model of the efficiency of light assimilation by plants.

In the U.S.A., the USGCRP agency was set up to collect data on the long-term trends of environmental systems and to record them for subsequent studies in an attempt to evaluate global changes. As a result, the spaceborne system NPOESS was created and the strategic plan IGOS was developed which, together with subject-oriented systems GCOS, GTOS, and GOOS, can monitor practically all ecosystems over the globe, and deliver data not only for estimation of the components of the global carbon cycle but also for broader investigations using a GMNSS. The generalized characteristics of some systems and programs of environmental monitoring are given in Tables 5.1 through 5.4.

Among efficient means of observing the components of biogeochemical cycles components we should point out the GOME and SCIAMACHY spectrometers which cover a broad spectral band, and therefore can measure the characteristics of O_3, BrO, OClO, ClO, SO_2, H_2CO, NO, NO_2, NO_3, CO, CO_2, CH_4, H_2O, N_2O, aerosols, radiation, and the height of clouds and their upper layer. SCIAMACHY was created to broaden global knowledge, get a deeper understanding of the chemistry and physics of the atmosphere (troposphere, stratosphere, and hemisphere), and forecast potential changes in natural phenomena caused by anthropogenic interference. It is primarily directed at collecting data on such natural phenomena and processes as

- stratospheric ozone (behavior of ozone holes and ozone in mid-latitudes);
- pollution of the troposphere as a result of industrial activity and biomass burning;
- exchange processes at the troposphere–stratosphere boundary;
- volcanic eruptions, and regional and global phenomena connected with solar activity.

The spectral interval of SCIAMACHY ranges from the UV to near-IR (240 nm–2,380 nm). This spectrometer provides information about the composition, dynamics, and radiation balance of the atmosphere, making it possible to measure MGCs in the

Table 5.1. Some systems for environmental observation and their equipment.

System	*Characteristic of the system*
GEOSS	Global system incorporating all Earth-observing systems. It combines basic spaceborne systems of observations of the atmosphere, hydrosphere, and land.
ADEOS	An improved, satellite Earth-observing system equipped with modernized radiometer of the visible and near-IR intervals (AVNIR), ocean color and temperature scanner (OCTS), and radiometer POLDER to carry out global systematic measurements of polarization and spectral characteristics of solar radiation reflected by the Earth–atmosphere system. The satellite ADEOS-2/ Midori-2 was launched on December 14, 2002 by the Japan Space Agency and is an ideal means of global monitoring.
ESA ERS-1, 2	European satellites for remote sounding of the environment used under the ESA program, equipped with spectrometers to measure the characteristics of aerosols, ozone, NO_2, SO_2, and other GHGs. GOME-type instruments record reflected solar light in the UV, visible, and near-IR intervals (Chance, 2005).
EOS	The Earth-observing system including Terra, Aqua, Aura, AM-1, and other satellites. It is equipped with sensors to record data on clouds and ERB, altimeter, acoustic atmospheric lidar, laser wind gauge, and gives information about volcanic eruptions.
UARS	Satellite launched by NASA in 1991 to study the upper atmosphere.
MOS	Satellites of the Japan National Space Agency to observe the seas, equipped with radiometers of visible and IR intervals and scanning microwave radiometer.
ENVISAT	Orbital polar ESA satellite to study the atmosphere, oceans, land, and ice, launched on March 1, 2002 and equipped with the spectrometer SCIAMACHY. It has ten measuring systems to monitor global warming, ozone holes, and to detect zones of desertification.
ERBS	NASA satellite to observe the ERB.
GMS	Geostationary meteorological satellite.
GOES	Geostationary satellite to monitor the environment.
LandSat	Series of NASA satellites. The first was launched in April 1972. The most improved satellite LandSat-7 was launched in April 1999 in a 750 km orbit. It has eight spectral intervals with spatial resolutions 15 km, 30 km, and 60 km with a 185 km swathwidth.

(*continued*)

Table 5.1 (*cont.*)

System	*Characteristic of the system*
JERS	Satellite of Japan Space Agency to study the Earth's natural resources.
GMS-1	Meteorological satellite launched on August 28, 2002, designed for cloud cover mapping and ERB estimation.
METSAT-1	Meteorological satellite launched on September 12, 2002, equipped with a scanning radiometer that has a resolution of 2×2 km to measure clouds, temperature, and water content in the atmosphere.
TAO/TRITON	Buoys anchored in the tropical Pacific with instruments to measure the characteristics of the atmosphere and ocean.
Aqua (NASA-EOS)	Spaceborne observatory launched on May 4, 2002 by NASA to study components of the global hydrological process, equipped with the six sensors characterized in Table 5.3.

troposphere and stratosphere, as well as aerosols. The GOME spectrometer has four channels: 240 nm–295 nm, 290 nm–405 nm, 405 nm–605 nm, and 590 nm–790 nm. The modified GOME-2 consists of two spectrometers, one recording the components of light reflected from the Earth's atmosphere toward the satellite within the band 240 nm–790 nm with a resolution of 0.24 nm–0.53 nm, the other providing polarization measurements with a resolution of 2.8 nm at 312 nm and 40 nm at 790 nm.

Many national programs on environmental studies are aimed at studying and understanding the causes of the regional changes observed in land cover, water basins and ground water quality, and in the atmosphere. After all, many changes take place at a regional level without any anthropogenic interference. This is of special concern in regions with increasing desertification. For instance, the U.S. National Council for Science and the Environment (NCSE) specializes in programs that foster collaboration between diverse institutions, communities, and individuals. NCSE organizes an annual National Conference on Science, Policy, and the Environment. NCSE provides information on the causes, consequences, and location of desertification. The *Asian Conference on Remote Sensing* (ACRS) proposed efforts be made to consolidate the national programs of Asian countries on studies of the environment. Japan plays an important role in this. In America and Europe, these problems are being looked at at a higher organizational level. For instance, in Europe, a consortium has set up GEMS which includes

- more than a dozen regional centers for atmospheric monitoring;
- ten leading research laboratories dealing with the study and modeling of atmospheric chemistry;
- two leading European laboratories ECMWF and EU JRC to provide weather forecasts and to study global processes.

Table 5.2. Some programs to study the environment.

Program	*Characteristic of the program*
AAOE	Airborne experiment to study the ozone layer in the Antarctic.
ACC	Program to study anthropogenic climate change.
ASHOE	Airborne experiment to study the ozone layer in the Southern Hemisphere.
BIBEX	Experiment to study the process of biomass burning.
CEPEX	Experiment to study the central equatorial sectors of the Pacific Ocean.
CLIVAR	Program of studies of the variability and predictability of climate with anthropogenic factors and interactions in the ocean–atmosphere–land system taken into account.
WOCE	Experimental studies of World Ocean circulation.
WCRP	Study of the global climate system.
UNEP	U.N. program to study the environment.
STIB	Study of interactions in the stratosphere–troposphere–biosphere system.
STEP	International program to study solar energy fluxes in land ecosystems.
GOFS	Program to study global fluxes in the World Ocean.
GORC	Study of the global carbon cycle in the World Ocean.
IHP	UNESCO program to study hydrological processes.
TOGA	Experimental program to study the global atmosphere and tropical zones of the World Ocean.
TEMIS	Part of the general ESA DUP program aimed at delivery of information about the long-range transport of aerosols, O_3, NO_2, and SO_2.

The European project GEMS foresees creating a system for global satellite monitoring of atmospheric chemistry aimed at monitoring European territory. The major executors of the project are two leading European laboratories ECMWF and EU JRC, with their rich experience in environmental diagnostics. The main goal of the project is to monitor greenhouse gases and other chemically active gases and aerosols covering the troposphere and stratosphere, considerating processes at both the regional and global scale. The main goals of the project are

- Global retrospective analysis of the dynamics and composition of the atmosphere, which also takes specific compositions of the troposphere and stratosphere into account.
- Short-range (1–3 day) and medium-range (3–7 day) forecasts of atmospheric air quality to indicate zones potentially dangerous for human health.

Table 5.3. Instrumental equipment carried by the space observatory Aqua. From Parkinson (2003).

Measuring system	*Characteristics of the measuring system*
Atmospheric Infrared Sounder (AIRS)	It has 2,382 high-resolution channels, 2,378 channels measuring IR radiation in the range 3.7 μm to 15.4 μm, other channels cover visible and near-IR regions (0.4 μm–0.94 μm).
Advanced Microwave Sounding Unit (AMSU)	It is a 15-channel gauge to measure upper atmosphere temperature, radiation in the range 50 GHz to 60 GHz and at frequencies 23.8 GHz, 34.4 GHz, and 89 GHz, water vapor, and precipitation. Spatial resolution of 40 km–45 km.
Humidity Sounder for Brazil (HSB)	HSB is a four-channel microwave device measuring humidity (183.31 GHz) and radiation (150 GHz). Horizontal resolution of 13.5 km.
Clouds and the Earth's Radiant Energy System (CERES)	CERES is a broadband three-channel scanning radiometer. One channel measures reflected solar radiation in the range 0.3 μm–5.0 μm. Two other channels (0.3 μm–100 μm and 8 μm–12 μm) measure reflected and emitted radiant energy at the top of the atmosphere.
Moderate Resolution Imaging Spectro-radiometer (MODIS)	MODIS is a 36-channel scanning radiometer in the visible and IR ranges (0.4 μm–14.5 μm), aimed at obtaining biological and physical information about the atmosphere–land system.
Advanced Microwave Scanning Radiometer for EOS (AMSR-E)	AMSR-E is a 12-channel scanning passive radiometer to record land cover radiation at frequencies 6.9 GHz, 10.7 GHz, 18.7 GHz, 23.8 GHz, 36.5 GHz, and 89.0 GHz with regard to the horizontal and vertical polarization of the signal. The antenna's diameter is 1.6 m, scanning period is 1.5 s.

- Development of models and algorithms from the combined use of satellite and *in situ* measurements to prepare basic information to make forecasts.
- Creation of an automated system to assess and predict the composition and dynamics of the atmosphere at global and regional (50 km) scales, and giving 3-D distributions of its characteristics at 60 levels in the troposphere and stratosphere (up to 65 km), including estimates of the key elements:
  (1) greenhouse gases (CO_2, CH_4, N_2O, SF_6, radon);
  (2) chemically active gases (O_3, NO_2, SO_2, CO, formaldehyde, and a gradually widening set of other elements); and
  (3) aerosols (up to 30 parameters).
- Development of methods to forecast "chemical weather" and to assess the air quality over Europe, which also takes the impact of global climate change into account.

Table 5.4. The GOOS subsystems of obtaining data on some parameters of the World Ocean from spaceborne monitoring. From IGOS (2001, 2004).

Parameter to be measured	*Satellite systems measuring the parameter*
Ocean surface level	TOPEX/Poseidon, Jason-1, ERS-2, ENVISAT. ENVISAT is equipped with synthetic aperture radar ASAR, altimeter RA-2, microwave radiometer MWR, interferometer MIPAS, system of positioning DORIS, and system to record ozone layer characteristics GOMOS.
Ocean surface temperature	AVHRR, ATSR-2/ERS-2, AATSR/ENVISAT, MODIS/EOS-Terra/Aqua, AMSR-E/EOS-Aqua, OCTS/ADEOS. Spaceborne system EOS/Terra is equipped with radiometer ASTER to measure thermal radiation and its reflection from the ocean surface, spectrometers MODIS and MISRC, as well as MOPITT and CERES instruments to record pollutant and energy fluxes, respectively.
Wind field characteristics	Seawinds/QuickSCAT, ERS-2, Seawinds/ADEOS-2, SSM/I. Spaceborne system ERS-2 is equipped with scatterometer WS, synthetic aperture radar SAR, microwave radiometer MWR, altimeter RA, scanning radiometer ATSR, and the system GOME to measure ozone.
Ocean surface layer salinity	SMOS (planned for launch in the future), an ESA satellite to observe soil moisture and ocean salinity, equipped with microwave radiometer MIRAS.
Sea ice	SSM/I, ERS-2, ASARE/ENVISAT, MODIS/EOS-Terra/Aqua. Data of SSM/I can be used to study wind speed trends at a height of 10 m, water vapor, cloud water content, and rain rate, and to assess the state and movement of ice.
Ocean coloration	SeaWIFS, MODIS/EOA-Aqua, MERIS/ENVISAT, OCTS/ADEOS.
Precipitation	TRMM, SSM/I. The TRMM system is equipped with radar PR to measure precipitation at a frequency 13.8 GHz with horizontal resolution 5 km and vertical resolution 250 m, scanner VIRS (0.63 μm, 1.61 μm, 3.75 μm, 10.8 μm, and 12 μm with spatial resolution of 2.5 km, microwave image recorder TMI (10.7 GHz, 19.3 GHz, 21.3 GHz, 37 GHz, 85.5 GHz), and solar light recorder LIS.
Cloud cover	Meteosat, the ESA geostationary satellite.
Aerosols	ENVISAT, POLDER-2/ADEOS-2. ENVISAT is the European satellite equipped with ten optical and radiometric sensors including radiometer MERIS for continuous monitoring of land, oceans, and the atmosphere.

- Development of algorithms to assess the sources and sinks of MGCs and aerosols by considering their intra-continental transport.
- Preparing key information for analysis of the fulfillment of the Kyoto and Montreal Protocols and the U.N. Convention on Long-Range Transboundary Air Pollution.
- Coordination of such a system for atmospheric monitoring over Europe with the existing infrastructure of meteorological services in Europe.

The accomplishment of many stages of such plans depends in many respects on the development of an information-measuring means of remote sounding and, in particular, spaceborne means. For example, El-Askary *et al.* (2003) analyzed several remote-sounding instrument capabilities in monitoring dust storms including MODIS, TRMM, and TMI. It was shown that in the optical part of the spectrum, dust storms have a very high albedo and hence appear quite bright. Therefore, we can look for high reflectance and anomalous water vapor to serve as indicators of dust storms. In the longer wavelength microwave region, dust storms respond strongly to scattering and this leads to reduced brightness temperatures. Combined optical and microwave sounding has brought about a high probability of detecting dust storms.

Of particular concern is the recently observed uncertainty in assessments of the atmosphere–ocean gas exchange. The main reason for this uncertainty is that distributions of inorganic and organic carbon in oceans are governed by a wide range of processes whose spatiotemporal variability is studied on the basis of spatially fragmentary and temporally episodic measurements from research ships. To narrow this uncertainty, the *16th Session of the IOC Assembly* decided that in March 1991 work should start on creating the global ocean observing system (GOOS) on the basis of numerous projects and programs such as PIRATA, CPR, SOOP, and others, within the framework of which autonomous anchored platforms with measuring systems are being created such as TAO/TRITON. Though these systems are subject-oriented at measuring the characteristics of the atmosphere–ocean system being used to assess climate change, they can of course be used to study global biogeochemical cycles.

A system of anchored ocean buoys is the basis for TAO/TRITON (Figure 5.1). Buoys are mainly located in the band 8°N–8°S between 137°E and 95°W. Among the many characteristics of the atmosphere–ocean system measured by this system, of importance for studies of the carbon biogeochemical cycle are the temperature of the atmosphere and ocean, wind direction and speed, precipitation rate, incoming shortwave and longwave radiation, salinity and conductivity of water, relative air humidity, pH, content of dissolved inorganic carbon, acidity of the medium, partial pressure of CO_2, oxygen content, and many characteristics of the ocean–carbonate system (Buesseler *et al.*, 2000; Ando *et al.*, 2005; Jiang *et al.*, 2005). Together with other measuring systems, developed within the framework of projects such as TOGA, JGOFS, GOOS, CLIVAR, ECOHAB, RIDGE, OASIS, OOS, and others, TAO/TRITON provides routine measurements of important parameters and helps to obtain data about the dynamics of those elements of the World Ocean whose role in the CO_2 global biogeochemical cycle has been evaluated inadequately. The TAO/

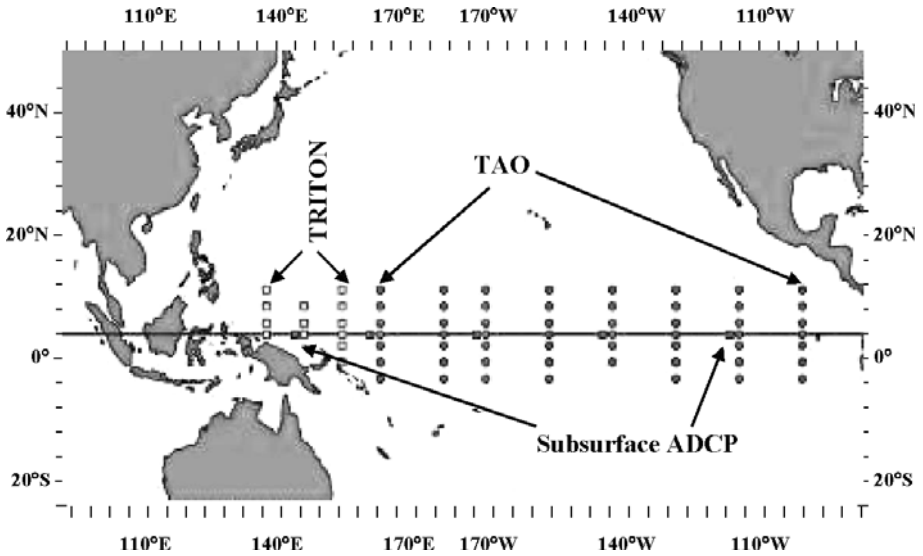

Figure 5.1. TAO/TRITON (*http://www.clivar.ucar.edu/organization/other/images/tao_new.jpg*).

TRITON system is being enhanced by allocation of new buoys (e.g., along the equator in the Indian Ocean). Together with data obtained using BATS, HOT, OFP, and other components of the autonomous anchored stations to monitor different basins of the World Ocean, an information database is being accumulated for more reliable estimation of GMNSS input parameters.

GOOS is a comprehensive, full-scale, environmental monitoring system aimed at solving a wide spectrum of problems (Holland and Nowlin, 2001; GOOS, 2002). The history and prospects for GOOS development are reflected in the dynamics of its structure and functions. For example, in 2000 deployment of its equipment constituted only 30% of the level planned for the following decade, but by 2009 all its planned levels look likely to be allocated and equipped with the necessary instruments to measure a wide range of characteristics of the World Ocean and the atmosphere.

The main principles of GOOS consist in the following (Holland and Nowlin, 2001):

- Maximum involvement of all countries in creating the GOOS system with subsequent development of an information service to help the climate change studies of individual scientists or groups of experts on a global scale.
- Emphasis on development of local expertise to inform decision-makers about the sustainable development of marine resources and preservation of the marine domain.
- Achievement of goals set by regions or countries.
- Active involvement of the scientific community of the participating countries in finding the best way of developing the system.

- Provision of regional cooperation to maximize the use of the system's resources by creating efficient regional sub-systems.
- Creation of a mechanism to interact with local, regional, and global systems, without which the successful functioning of GOOS cannot be realized.
- Stability through a partnership between organizations and countries.
- Provision of thorough support to GOOS by governments, international organizations, and other structures interested in preserving the environment and maintenance of NSS sustainable development.
- Making the necessity to support GOOS at both national and international levels clear to the population and politicians.
- Preservation of an ongoing strategy and long-term goals for the system.
- Information support and public demonstration of the efficiency of GOOS goals.

The basic operational modules of GOOS are

- A network of remote-sounding means including both ground and spaceborne oceanographic systems.
- Integration of all oceanographic models which provide parameterization of the processes and their prediction for the coastal and open basins of the World Ocean.
- A network of information sub-systems to collect and accumulate measurement data with the subsequent formation of oceanographic databases.

However, despite the availability of such powerful information systems, the problem remains of the statistical reliability of observational data, especially in the summer in the tropics, when the instability of environmental characteristics remains high (Barnett, 2003).

5.2 DATA AND KNOWLEDGE BASES ON ENVIRONMENTAL BIOGEOCHEMISTRY

To obtain more reliable information on the global field of CO_2 concentration in a free (unpolluted) atmosphere above a region of the South Pacific basin, in August–October 1996 Vay *et al.* (1999) carried out aircraft (NASA flying laboratories DC-8 and P3-B) measurements of CO_2 concentration within the framework of the PEM-Tropics program (data obtained cover the atmospheric layer 0.1 km–12 km). Analysis of the data showed that CO_2 concentration in the Southern Hemisphere is determined by the prevailing impact of inter-hemispherical transport coupled with the marked influence of regional processes. Comparison of data on the measured concentration of CO_2 and other MGCs has led to the conclusion that the level of CO_2 concentration is mainly determined by contributions from continental sources. Within the lower and middle troposphere above distant regions of the Pacific Ocean large-scale plumes of highly concentrated CO_2 due to biomass burning have been observed. Vay *et al.* (1999) discovered a source of CO_2 in the band 15°N–15°S from

the data of ground observations and from aircraft data for the lower troposphere in the band 8°N–8.5°S and a further zone of increased CO_2 concentration in the band 6.5°N–1°S. The observational data suggest the presence in the region of the SH ocean of a CO_2 sink located south of 15°S, with two distinct zones with opposite phases in the annual change of concentration.

Of particular interest among MGCs is carbon monoxide, CO, the annual cycle of which is estimated at 2.3×10^{15} g. In distant regions of the Southern Hemisphere CO concentrations vary within 40 mmol mol^{-1} and 65 mmol mol^{-1}, and in the Northern Hemisphere in the presence of powerful CO_2 sources, its concentration varies from 90 mmol mol^{-1} to 200 mmol mol^{-1}. Since November 1981, systematic studies of this concentration have been carried out as part of the Shuttle program. The MAPS experiment on remote sounding of global atmospheric pollution was undertaken. The success of this experiment determined its continuation during two 10-day periods in April and October 1994 using improved MAPS equipment, the nadir-directed radiometer with a gas filter functioning at 4.67 μm within the basic CO_2 absorption band. This radiometer is based on the principle of selective modulation. The measured signal is the difference between signals after passing through two gas cuvettes, one of which is filled with the studied gas, the other is either empty or contains a gas that does not absorb radiation. Analysis of the results obtained has shown that the error of retrieval of CO_2 content in the atmosphere does not exceed 10%.

During the flights of the Space Shuttle orbiter *Endeavour* on April 2–19 and October 30–November 11, 2004, measurements were made of CO content simultaneously with those from aircraft. Latitudinal and longitudinal distributions of CO drawn from these measurements revealed a considerable change in CO content in the atmosphere, which reflects the geographical location and changes in the intensity of CO sources and sinks. For instance, in April, maximum CO concentrations averaged over the atmospheric thickness constituting about 120 ppbv were observed in the Northern Hemisphere with a gradual decrease of concentration (down to 40 ppb–60 ppb) toward middle and high latitudes of the Southern Hemisphere. A radical change in CO distribution took place in October, when there was a change in sign of the meridional gradient of concentration compared with April. In October, maximum values of CO concentration (>135 ppb) were located in the tropical band covering the central part of South America, southern Africa, Indonesia, and northern Australia. In these regions there were intensive fires as a result of biomass burning.

The sphere of science that assesses the atmospheric composition of aerosols of different scales and characters has advanced greatly. Henderson and Chýlek (2005), based on data from satellite measurements using MTI, AVHRR, MODIS, MISR, AATSR, and POLDER considered the problem of estimating aerosol optical depth (AOD) as a function of the spatial resolution of the sensors applied and established that in the range of pixels of the Earth's surface from $40 \times 80\,m^2$ to $2{,}040 \times 4{,}080\,m^2$, NDVI is a great way of estimating AOD. Along with the optical depth of aerosols in the atmosphere, the radius of cloud drops, character of heterogeneity, and profile of clouds are important characteristics too. Knowledge of these characteristics makes it possible to parameterize the radiation properties of clouds. Bréon and Doutriaux-Boucher (2005) analyzed *in situ* observations of clouds from flying laboratories and

satellites and showed that the average radius of cloud drops over the continents is less than that over NH oceans, and that maximum sizes of cloud drops are observed over the open ocean. The data-processing algorithm used was based on the supposition that cloud drop size has a gamma distribution. It was shown that in measurements of the optical depth and efficient radius of cloud drops over land, ocean, and snow cover, the most informative channels are 0.65 μm, 0.86 μm, and 1.2 μm, respectively. Especially efficient was the polarization method based on calculation of Stokes vector components.

Another important factor in the global biogeochemical cycle of substances is the long-range transport of dust particles from Asia and Africa. "Seas" of Saharan dust are the most dynamic part of the global flux of dust through the atmosphere. As numerous studies have shown, efficient assessment of their motion is possible, in the case of polarization observations, by two sensors SSM/I and TMI at frequencies 19 GHz and 37 GHz. The dust storms that often occur in the Nile delta and move toward the Mediterranean Sea have been known to reach North America, India, and Arctic latitudes (Franzen *et al.*, 1994). Facts on long-range dust transport from Africa were first recorded in 1970 by the Nimbus satellite. El-Askary *et al.* (2003) showed that efficient monitoring of fluxes of dust and sand in the atmosphere is possible with the combined use of satellite measurements in the visible (MODIS), infrared (TOMS), and microwave (TMI) intervals. Apart from wind erosion there are other, no less important mechanisms of dust input to the atmosphere, many of which are connected with soil cultivation. Nevertheless, the structure of dust flux monitoring should cover other objects of the NSS and processes in the environment.

Detection and quantitative estimation of clouds of volcanic ashes or smoke from biomass burning should be considered in the many national and international geoinformation-monitoring programs. Ash can represent a serious danger for aviation, and therefore mapping of clouds of volcanic ash should be made in real time. This is only possible using spaceborne means coordinated with ground weather radars. Marzano *et al.* (2006) analyzed the possibilities for this and suggested an algorithm to estimate the size of particles and their concentration based on the microphysical model of volcanic ash reflectivity. Detection of smoke from the sources of biomass burning is possible from satellite measurements using the GOME-type sensors carried by the ESA ERS-2 satellite and makes it possible to measure the concentrations of ozone, NO_2, H_2CO, BrO, OClO, and SO_2.

Global estimation of the sources and sinks of greenhouse and other gases as well as the chemical elements actively participating in biogeochemical cycles is possible only by combining ground and satellite measurements with numerical models. Good examples of such studies are Choi *et al.* (2005), Jaeglé *et al.* (2004, 2005), and Liu *et al.* (2006). Choi *et al.* (2005) analyzed the distributions of NO_2 using a GOME spectrometer and CO using a MOPITT sensor of observations made over North America and adjacent basins of the World Ocean in 2000 and showed that use of the RCTM model enables reliable estimation of the contribution of lightning to sources of NO_2 in the lower atmosphere, and to calculate the output of CO from the lower troposphere due to downward air fluxes. The MOPITT sensor provides a spatial resolution of 22×22 km and has eight channels to record radiation in the IR.

Jaeglé *et al.* (2004, 2005) studied the efficiency of combining satellite and ground observations of NO_x both on a global scale and over the territory of Africa using the GOME-CHEM model. This study aimed at narrowing the uncertainty in the estimates of fluxes of nitrogen oxides from sources in forest fire and biomass-burning zones. Indeed, available estimates of anthropogenic NO_x emissions are characterized by the following values. The contribution from fossil fuel burning is estimated at $20\,TgN\,yr^{-1}$–$24\,TgN\,yr^{-1}$, biomass burning gives $3\,TgN\,yr^{-1}$–$13\,TgN\,yr^{-1}$, and exchange in the atmosphere–soil system constitutes $4\,TgN\,yr^{-1}$–$21\,TgN\,yr^{-1}$. This high uncertainty in the estimates of anthropogenic NO_x input hinders reliable assessment of the ozone layer, acid rain, and eventually, climate change. The existing methods of calculating NO_x fluxes are mainly based on statistics that characterize the trade in energy resources, on information about fires in forests and savannahs, and on data on the amount of burnt biomass in agriculture. Another source of uncertainty in the biogeochemical cycle of nitrogen is the microbiological process in soils, which can only be estimated from individual local measurements of nitrogen fluxes at the atmosphere–soil boundary. Studies carried out under the GOME program using the ERS-2 satellite made it possible to obtain the global pattern of NO_x source distribution and to assess the vertical distribution of NO_x in the troposphere. Jaeglé *et al.* (2005) showed that the space-derived inventory of biomass-burning areas has made it possible to narrow uncertainty in the estimate of NO_x fluxes to the atmosphere. Data on the distribution of NO_x sources were put in the 3-D model of tropospheric chemistry (GEOS-CHEM) with a horizontal resolution of 2° lat. $\times$ 2.5° long. and 30 levels in the vertical, which made it possible to halve uncertainty in the estimate of the global flux of anthropogenic nitrogen to the atmosphere (from $\pm 80\%$ to $\pm 40\%$).

Jaeglé *et al.* (2004), based on satellite measurements in 2000, charted maps of the sources of NO_x over the territory of Africa, marked in the dry season by fires and biomass burning when the atmosphere–soil gas exchange varies widely. Ground observations within the information network IGAC/DEBITS/IDAF in western Africa provided data on the microbiological processes in soils, which combined with satellite observations enabled, for 40% of Africa, assessment of the NO_x fluxes to the atmosphere due to processes in soils ($3.3 \pm 1.8\,GtN\,yr^{-1}$) and biomass burning ($3.8 \pm 2.1\,GtN\,yr^{-1}$). Model extrapolation enabled estimation of the contribution of biogenic processes in the soils of Africa to the input of nitrogen to the atmosphere at $7.3\,GtN\,yr^{-1}$.

Liu *et al.* (2006) studied the global mapping of the ozone layer to reveal details of its spatiotemporal evolution and found that the layer of tropospheric ozone grows in the latitudinal band 20°N–30°S in the southern spring, and over latitudes 25°N–45°S during the boreal spring and summer. It was shown that the 3-D model of tropospheric chemistry GEOS-CHEM efficiently parameterizes the seasonal variability of the ozone layer over most regions, especially in the Southern Hemisphere. By numerous comparisons between real satellite measurements and model calculations it was shown that, by combining the results of both, the global estimate of the state of the ozone layer can be given to within ± 5 DU. A study carried out by Choi *et al.* (2005) confirmed these conclusions and showed that using a spaceborne spectrometer to

study the laws of solar spectrum absorption in the terrestrial atmosphere facilitates the use of atmospheric chemistry models to retrieve the distributions of concentrations of various gases, especially SO_2 and NO_2, and to estimate the albedo of the atmosphere–land system. In particular, at solving the problem of the profile retrieval of ozone, NO_2, OClO, temperature, and water vapor content of the atmosphere, spaceborne instruments such as GOME, GOMOS, and SCIAMACHY are efficient.

As Haszpra *et al.* (2005) demonstrated, assessment of the carbon balance over a small territory can be done by measurements from stationary systems. A measuring system was mounted on an 82 m radio/TV tower in an area with mixed vegetation cover (agricultural fields and small areas of forest). Observations were made between 1997 and 2004, and it was found that in the daytime $1.4\,mgCO_2\,m^{-2}\,s^{-1}$–$1.5\,mgCO_2\,m^{-2}\,s^{-1}$ was assimilated from the atmosphere, and at night the atmosphere received $0.1\,mgCO_2\,m^{-2}\,s^{-1}$–$0.3\,mgCO_2\,m^{-2}\,s^{-1}$. On the whole, the CO_2 sink constituted $107 \pm 48\,mgC\,m^{-2}\,s^{-1}$. Such measurements make it possible to substantially increase the accuracy of estimating CO_2 sources and sinks and to calculate thereby the global role of a given territory in climate change.

The methods of remote sounding of CO_2 fluxes are mainly based on NDVI measurements (Burgheimer *et al.*, 2006; Myeong *et al.*, 2006) using various satellite technologies as well as *in situ* measurements with SCIAMACHY carried by satellites of the ESA series. The surface resolution of SCIAMACHY constitutes 320 km, and the frequency of measurements is 36 hours.

5.3 ALGORITHMS FOR OBSERVATIONAL DATA PROCESSING

Geoinformation-monitoring data are characterized by their spatiotemporal inadequacy. The measurements of environmental parameters from the ground or by flying laboratories give only fragmentary information about the elements involved in the biogeochemical system. The use of GIS technology to process this information gives a possibility to have its cartographic presentation. However, many fragments in this pattern remain unidentified. To reconstruct them, algorithms for spatiotemporal interpolation have been proposed that are characterized by their varying claims to accuracy (Krapivin and Potapov, 2002; Kondratyev *et al.*, 2002a, b; Denzer *et al.*, 2005). In particular, Denzer *et al.* (2005) described the goals and problems of the GIMM12 project (a satellite was launched in April 2002) which aimed at creating, on the basis of open systems, an information network using GIMS technology (Krapivin *et al.*, 2006; Chukhlantsev, 2006). GIMS technology realizes the formula GIMS = GIS + model (Krapivin *et al.*, 2006; Wainwright and Mulligan, 2003).

5.3.1 A spatiotemporal interpolation algorithm based on the differential approximation method

The database of an environmental monitoring system does not always meet the requirement of parametric saturation demanded by GIMS technology. Therefore, an algorithm to parameterize the functions of the system of a selected territory, which

avoids the need to make demands on a database would be of great interest. Suppose that in the monitoring regime measurements are made of N characteristics of the system x_i $(i = 1, \ldots, N)$ at time moments t_s $(s = 1, \ldots, M)$. The formal dependence between $x_i(t)$ will be presented as a system of differential equations with coefficients $\{a_{ijk} b_{ij}\}$ known:

$$\frac{dx_i}{dt} = \sum_{k,j=1}^{N} [a_{ijk} x_j(t) x_k(t) + b_{ij} x_j(t)]. \tag{5.1}$$

Under initial conditions:

$$x_i(0), \qquad i = 1, \ldots, N. \tag{5.2}$$

The problem of retrieving the $x_i(t)$ values at any time moment in the interval of observations $[0, T]$ is reduced to a simple Cauchy problem for the system of standard equations. The only obstacle to its solution is the uncertainty of coefficients a_{ijk} and b_{ij}. In this case we follow a traditional course; that is, we measure the deviation between calculated $x_i(t_s)$ and measured $\hat{x}_i(t_s)$ values:

$$E = \sum_{s=1}^{M} \left\{ \sum_{i=1}^{N} [x_i(t_s) - \hat{x}_i(t_s)]^2 / N \right\} \Big/ M, \tag{5.3}$$

where $0 \leq t_1 \leq \cdots \leq t_M \leq T$.

Then a set of coefficients $\{a_{ijk}, b_{ij}\}$ can be determined by solving the following optimization problem:

$$E_0 = \min_{\{a_{ijk}, b_{ij}\}} E. \tag{5.4}$$

The search for the minimum function E in (5.4), according to methods described in Bellman and Roth (1966), can be reduced to a problem of dynamic programming. Suppose that coefficients $\{a_{ijk}, b_{ij}\}$ are functions of time.

Let us denote:

$$Y(t) = \begin{Vmatrix} x_1(t) \\ \vdots \\ x_N(t) \\ a_{111}(t) \\ \vdots \\ a_{NNN}(t) \\ b_{11}(t) \\ \vdots \\ b_{NN}(t) \end{Vmatrix}. \tag{5.5}$$

Without violating generality, it can be assumed that $a_{ijk} = a_{ikj}$. Then the Cauchy problem can be written in the following form:

$$\frac{dY}{dt} = G(Y), \tag{5.6}$$

where the function G has the following components:

$$\left.\begin{aligned} &G_i(Y) = 0 \quad \text{for } i = N+1, \ldots, N_c, \\ &G_i(Y) = \sum_{k,j=1}^{N} [a_{ijk} x_j(t) x_k(t) + b_{ij} x_j(t)] \quad \text{for } i = 1, \ldots, N; \end{aligned}\right\} \tag{5.7}$$

with $a_{ijk}(0) = \bar{a}_{ijk}$, $b_{ij}(0) = \bar{b}_{ij}$, and $N_c = N + N^2 + N^2(N+1)/2$.

Note that, by using the quasi-linearization method, the solution of a non-linear problem can be reduced to solution of a succession of linear problems. The method is a further development of the Newton–Raphson method (Dulnev and Ushakovskaya, 1988) and its generalized version.

Let us introduce a succession of functions $Y^{(1)}(t), \ldots, Y^{(n)}(t)$ so that $Y^{(1)}(t)$ is a first approximation to solution of system (5.6). Then the nth approximation is found by solving the following linear system:

$$\frac{dY_i^{(n)}(t)}{dt} = G_i[Y^{(n-1)}(t)] + \sum_{j=1}^{N_c} \left\{ \frac{dG_i[Y^{(n-1)}(t)]}{dY} \right\} [Y_j^{(n)} - Y_j^{(n-1)}]. \tag{5.8}$$

As shown in Bellman and Dreifus (1962), the iterative process (7.8) converges following the square law. Solution of (5.8) in a general form is written as

$$Y^{(n)}(t) = P(t) + \sum_{k=1}^{N_c} C_k H^{(k)}(t), \tag{5.9}$$

where $P(t)$ is a partial solution to system (7.8); and $H^{(k)}(t)$ is the vector solution of a homogeneous system. To determine $P(t)$, we solve (7.8) under initial conditions $Y_i(0) = 0$ $(i = 1, \ldots, N_c)$. Functions $H^{(k)}(t)$ are found by solving the Cauchy problem:

$$\frac{dY_i^{(n)}(t)}{dt} = \sum_{j=1}^{N_c} \left\{ \frac{dG_i[Y^{(n-1)}(t)]}{dY} \right\} [Y_j^{(n)} - Y_j^{(n-1)}] \quad (i = 1, \ldots, N_c), \tag{5.10}$$

$$H^{(1)}(0) = \begin{Vmatrix} 1 \\ 0 \\ \vdots \\ 0 \\ 0 \end{Vmatrix}, H^{(2)}(0) = \begin{Vmatrix} 0 \\ 1 \\ \vdots \\ 0 \\ 0 \end{Vmatrix}, \ldots, H^{(N_c)}(0) = \begin{Vmatrix} 0 \\ 0 \\ \vdots \\ 0 \\ 1 \end{Vmatrix}. \tag{5.11}$$

It follows from (5.8)–(5.11) that constants C_k are unknown initial conditions of the system of equations (5.7). Therefore, at each iteration in the process of finding

either a partial solution or full solutions to homogeneous equations, constants C_k are found in order to obtain the solution of $x^{(n)}$ that best agrees with observational results in the sense of the least squares method:

$$E = \min_{\{C_k\}} \sum_{s=1}^{M} \sum_{i=1}^{N} \left[P_i(t_k) + \sum_{k=1}^{N_c} C_k H_i^{(k)}(t_s) - \hat{x}_i(t_s) \right]^2. \tag{5.12}$$

Let

$$\frac{\partial E}{\partial C_k} = 0 \quad \text{for } k = 1, \ldots, N_c. \tag{5.13}$$

It follows from (5.12) and (5.13) that

$$\sum_{k=1}^{N_c} A_{km} C_k + B_m = 0, \quad m = 1, \ldots, N_c, \tag{5.14}$$

where

$$A_{km} = \sum_{s=1}^{M} \sum_{t=1}^{N} H_t^{(k)}(t_s) H_t^{(m)}(t_s),$$

$$B = \sum_{s=1}^{M} \sum_{t=1}^{N} [P_1(t_s) - \hat{x}_1(t_s)] H_t^m(t_s).$$

Thus, at each iteration of (5.8), system (5.14) should be solved. The rate of convergence of this procedure depends on the correct choice of initial conditions. The method of differential approximation refers to universal approaches in the function approximation theory to the analysis of dynamic systems. Under remote monitoring conditions, the use of this method can be justified by allowing aircraft and satellite measurements to be spaced in time with respect to the objects to be monitored and, hence, in processing the readings from measuring instruments it is necessary to take into account possible changes in the object between moments of measurement.

5.3.2 Method of self-organizing models

The problem of spatiotemporal recovery of monitoring data can be solved using the inductive method of model self-organization developed in Ivachnenko *et al.* (1984). The idea behind this approach is the traditional function approximation theory.

Let an object or process be described by model $\Psi = f(a_1, \ldots, n)$, where parameters $\{a_i\}$ reflect the quantitative, functional, and structural sections of the phenomenon under study. The multitude of possible types of function f can be determined on the basis of expert estimation with consideration of *a priori* information and a heuristic set of partial descriptions of the phenomenon. The training sequence $\{f_i\}$ is constructed which serves the basis for multi-row selection of the model of optimal complexity and acceptable accuracy. The first level of selection consists in calculating row $\{y_s\}$, where $y_s = g(a_{i-1}, a_i)$ $(s = 1, \ldots, L = C_n^2; i = 1, \ldots, n)$. The second level of selection gives row $\{z_p\}$, where $z_p = g(y_{j-1}, y_j)$

($p = 1, \ldots, C_L^2$; $j = 1, \ldots, L$). The process of selection is continued until the most regular mathematical description of the phenomenon under study is obtained. Estimation of the accuracy of the model obtained and the choice of moment for the process of selection to end depend on the chosen criterion of discrepancy between the theoretical and empirical image of the phenomenon. The rms deviation criterion is most often used, and a polynomial serves as function f. The procedure for model selection consists in a gradual complication of the polynomial approximation.

The method of self-organizing models was described in detail in the work of Ivachnenko *et al.* (1980, 1984), in which various modifications of the method are given accompanied by examples of how best to use them in solving applied problems.

5.3.3 Harmonic function method

The process of heat propagation in a flat homogeneous medium G with constant thermal-physical properties (ρ is density, c is specific heat capacity, and K is the coefficient of heat conductivity; $\rho, C, K = \text{const} > 0$) is described by

$$\frac{\partial T}{\partial t} = a^2 \left(\frac{\partial^2 T}{\partial \varphi^2} + \frac{\partial^2 T}{\partial \lambda^2} \right), \tag{5.15}$$

where $T = T(\varphi, \lambda, t)$ is the temperature at point $(\varphi, \lambda) \in G$ at time moment t; and $a^2 = K/\rho c$ is the coefficient of heat conductivity for G. If the process of heat transfer is stationary, then (5.15) becomes the standard Laplace equation:

$$\text{div} \cdot \text{grad}\, T = \frac{\partial^2 T}{\partial \varphi^2} + \frac{\partial^2 T}{\partial \lambda^2} = 0. \tag{5.16}$$

In this case T is a harmonic function of spatial coordinates φ and λ. Together with the temperature field $T(\varphi, \lambda, t)$ let us consider the field of self-radiation of G in the microwave range, whose intensity in accordance with the Rayleigh–Jeans approximation (Chinlon, 1989) at a local thermodynamic equilibrium is characterized by brightness temperature $T_J(\varphi, \lambda, \eta, \theta, t)$, where η is the wavelength of the electromagnetic interval, and θ is the observation angle. Assume that for a sufficiently small area V_M of any point $M \in G$ the following condition is satisfied:

$$T_J(\varphi, \lambda, \eta, \theta, t) = A_M + B_M T(\varphi, \lambda, t); \qquad (\varphi, \lambda) \in V_M; \quad (A_M, B_M = \text{const}). \tag{5.17}$$

The form of (5.17) follows from theoretical and experimental estimates of T_J. Thus, for a medium that is homogeneous in depth and limited by a flat surface, the following equation is valid $T_J = \kappa T_0$, where $\kappa = \kappa(\eta, \theta, \varepsilon)$ is the emissivity coefficient of the medium, ε is the dielectric permeability of the medium, and T_0 is the thermodynamic temperature. According to experimental estimates (Shutko, 1987), at wavelengths $\eta \geq 5\,\text{cm}$–$8\,\text{cm}$ and T_j for freshwater practically linearly dependent on T_0, the steepness of this dependence constitutes $0.35^\circ\text{K}/^\circ\text{C}$–$0.5^\circ\text{K}/^\circ\text{C}$. An increase in salinity S from 0‰ to 13‰–16‰ is followed by a decrease in sensitivity of the radiation field to temperature variations in a wide range of decimeter waves from 10 cm to 5 cm. In cases of relationships $\eta S \cong 700$, $0 \leq T_0 \leq 30^\circ\text{C}$, $0 \leq S \leq 180‰$,

and $0 \le \theta \le 25^\circ$ radiation field sensitivity to variations in T_0 is at a minimum. It follows from (5.17) that T_J at each point $M \in G$ follows the relationship:

$$T_J(\varphi, \lambda, \eta, \theta, t) = (2\pi)^{-1} \int_0^{2n} [A_M + B_M T(\varphi + r\cos a, \lambda + r\sin a, t)\, da$$

$$= (2\pi)^{-1} \int_0^{2\pi} T_J(\varphi + r\cos a, \lambda + r\sin a, \eta, \theta, t)\, da$$

for any $r \in (0, r_M)$, from which it follows that T_J is harmonic in G and, hence, satisfies (5.16). A typical boundary value problem for (5.16) is the Dirichlet problem. At boundary Γ of medium G a continuous function $\tilde{T}_J = \tilde{T}_J(u)$ is prescribed, where $u = \varphi + i\lambda$ is the complex coordinate of point $(\varphi, \lambda) \in \Gamma$. Function T_J should be found to be harmonic within G, assuming given values of $\tilde{T}_J$ on Γ. This function, according to the complex derivative function theory is a real part of some analytical function $\Phi(z)$, which is found as the Cauchy integral:

$$\Phi(z) = \frac{1}{2\pi i} \int_\Gamma \frac{\mu(\zeta)}{\zeta - z} d\zeta \tag{5.18}$$

with the real density $\mu(\zeta)$, where $\zeta \in \Gamma$; $z = \varphi + i\lambda$ is a random point in G. Directing z to some point u of contour Γ and taking into account relationships $\mathrm{Re}\, \varphi(u) = \tilde{T}_J(u)$ and $\mathrm{Im}(d\zeta/(\zeta - u) = -\cos(r, n)\, d\sigma/r$, where r is the distance from ζ to u (the direction is chosen from ζ to u), $d\sigma$ is the length element on Γ, and n is the external normal to Γ. From (5.18) we obtain for $\mu(u)$ the Fredholm integral equation:

$$\mu(u) - \frac{1}{\pi} \int_\Gamma \mu(\zeta) \frac{\cos(r, n)}{r} d\sigma = 2\tilde{T}_J(u)$$

with the continuous core $\cos(r, n)/r$, which can be solved from any right-hand side. Having solved this equation, we find $\varphi(z)$ and, hence,

$$T_J(\varphi, \lambda, \eta, \theta, t) = \mathrm{Re}\, \varphi(z).$$

When G is a circle $|z - z_0| < R$, the solution

$$T_J(\varphi, \lambda, \eta, \theta, t) = T_J(r, \psi, \eta, \theta, t) \qquad (\varphi + i\lambda = z_0 + re^{i\psi}, r < R, 0 \le \psi \le 2\pi)$$

of the Dirichlet problem can be obtained in the form of a Poisson integral:

$$T_J(\varphi, \lambda, \eta, \theta, t) = \frac{1}{2\pi} \int_0^{2\pi} \tilde{T}_J(a) \frac{R^2 - r^2}{R^2 + r^2 - 2Rr\cos(\psi - a)} da,$$

where $\tilde{T}_J(a) = \tilde{T}_J(z_0 + Re^{ia})$ $(0 \le a \le 2\pi)$.

Without breaking integrity, we apply this method together with the method of differential approximation to the procedure of data retrieval from the route measurement and mapping of territory G at time moment t^*. Let remote measurements be made in the time interval $[t_0, t_L]$ at a discrete number of points A_i $(i = 1, \ldots, N)$ at boundary Γ. Assume that during the time of measurements Δt the level of time dependence of observational data is negligibly small; that is, the whole series of

measurements can be divided into $M = |[t_L - t_0]/\Delta t|$ statistically reliable sites $[t_j, t_{j+1}]$ $(j = 1, \ldots, M)$, and all measurements can be presented in the form of matrix $\|T_J(i,j)\|$. The method of differential approximation makes it possible to reduce all lines in this matrix to moment t^* and then, following the method described above to retrieve T_J in territory G.

5.3.4 Method of evolutionary modeling

Remote measurements of environmental parameters are often characterized by sets of rows that have highly unstable properties. In this case using methods like that above or other methods of traditional statistics becomes impossible. The method of evolutionary modeling makes it possible under conditions of unavoidable instability to retrieve true estimates of environmental characteristics. This method consists in successive selection of models according to indicators of the reflective quality of these models of the process under study. The model resulting from this selection is assumed to accurately represent the object of monitoring and is used to calculate the necessary characteristics. Various problem-oriented realizations of this method and the necessary computer procedures are described in Bukatova *et al.* (1991).

The method of evolutionary modeling is based on a principally new approach to intellectual technologies, one that ensures transformation of knowledge about a strategic resource. Particular important here are intellectual information technologies based on knowledge oriented at solving intellectual problems. Their function consists in support by means of human–machine systems of the use of knowledge considered in an abstract way as being scattered, dissolved in the individual experience of other people, models of the world, and knowledge accumulated in the course of the evolutionary development of individual sciences (natural, public, and technical). Intellectual technologies are constructed according to the following principle: some part of knowledge is in a way abstracted from the general information pattern of the world, and then, because of its ability to provide new knowledge, returns to the user, transforming into a meta-technology for certain kinds of human activity. When selecting the necessary level of knowledge for decision-making. Thus, prerequisites appear for penetration of information technologies into new spheres: global ecology, synthesis of complicated technical systems, medicine, geology, etc., in which rational solutions cannot be adequately formalized.

The complexity of problems to be solved here brings forth the unique problem of creating computerized tools of intellectual technologies. The latter are determined not by initial computer properties—but by providing a computer with the characteristics needed to adjust problematic conditions and requirements for their solution. These requirements cannot be simplified in the way that traditional calculation technologies are (i.e., based on the triad: mathematical model, discrete model oriented at numerical solution of the problem, and software corresponding to the structure of algorithmic provision). The kinds of characteristics can be determined from general features of the problems of intellectual technologies such as problem orientability, system character, peculiar input, conditionality in decision-making because of the

complexity of systems, their multi-factor character, and internal dynamism. In this connection, the computer should be able:

- to operate with unreliable data or incomplete data;
- to accumulate unreliable knowledge (i.e., knowledge that is fragmentary, controversial, subjective, and poorly structured);
- to synthesize, based on non-formal principles, dissimilar scientific knowledge; and
- to search in the hypothetic space for alternatives bound to a given problem.

These properties could not result from the evolutionary development of computer techniques, because they are based on the functioning of successive principles, which reflect the Cartesian ideal of Mind, when formal judgements are subjected to traditional cognitive science (Valera, Thompson, and Rosch, 1991). That's why, for a qualitative leap, ideas are needed from "outside the box", outside the global direction of development of computer techniques including an improvement of architecture, hardware logic, methods of programming, and database control. To solve the problems of global ecodynamics connected with a search of strategies for NSS sustainable development, a certain understanding is needed of the necessity to take into account the human factor because of the presence of informal stages in problem solution and the possibility to meet the formalization requirements by using heuristics-intuitive knowledge.

Knowledge engineering is the means of constructing expert systems as a kind of intellectual technology. Here the gap between the problems of intellectual technologies and the proper content of artificial intelligence as a scientific and technical discipline has been removed:

- heuristic search methods have been improved for solving complex optimization problems (Rayward-Smith *et al.*, 1996);
- methods of presenting knowledge have been developed (with consideration of their functions) to describe concrete fragments of specialized subject knowledge of experts;
- methods of working with experts have been developed to fill the base of knowledge with non-controversial fragments; and
- expert systems themselves have been provided with the ability to iterate and evolve (i.e., to correct the content of bases of knowledge in the process of work with the user).

This brief description testifies to the fact that scientists have managed in an abstract way to extrapolate of capabilities of artificial intelligence. However, embedding concrete expert systems into a weakly structured human medium has revealed so-called "narrow places". These are the prescribed bases of knowledge, problem of extracting knowledge from the expert, and the antithesis to specialized and universal strategies of problem solution. This does not deny the significance of the attempts of

specialists to develop these principles of artificial intelligence, since for a certain set of problems such means are sufficient. For instance, various architectures of expert systems have appeared designed to solve problems about the structure of a problem, types of data, etc. (Jackson, 1999). In particular, in the problems of global eco-dynamics, the fact–conclusion bond is always postulated, which is manifested through the use of sets of partial models, such as balance, statistical, optimization, neuronet models, etc. Here the problem arises of the choice of model (Bartsev *et al.*, 2003). Kondratyev *et al.* (2002a, b) proposed a technology to synthesize such a model on the basis of numerous partial models of different types, whose structure is adjusted by pre-history and adapted to data of real-mode monitoring. Thus, a procedure is being developed of renewable adaptation of the model and the monitoring regime to NSS dynamics, due to which situations of irremovable uncertainty can be overcome.

5.3.5 Approximate method for the inverse problem solution to identify the parameters of a monitored object

In the process of monitoring, a multitude of data series is formed, the use of which needs the establishment of correlations between the parameters of the object under study. Consider a situation that occurs under conditions of radio-physical monitoring. Let, at time moment t_i at the output of each measuring device (radiometer), the values Z_{ij} $(i = 1, \ldots, M; j = 1, \ldots, \eta)$ be fixed so that $Z_{ij} = T_j + \xi_{ij}$. Here $T_j$is the real value of the jth parameter (radio brightness temperature at wavelength λ_j), and ξ_{ij} is the noise constituent. Search for the correlation is reduced to determination of the dependence

$$T_j = f_j(X), \tag{5.19}$$

where $X = (x_1, \ldots, x_m)$ are geophysical parameters.

There are many approaches to finding function f. As a rule, mean square deviation is used as the criterion for agreement (Borodin and Krapivin, 1998). However, this criterion cannot reflect the dispersive characteristics of the noise constituent in measurements. Therefore, let us consider the problem from this point of view. Let function (5.19) be linear, and then we obtain the system $n \geq m$ of equations:

$$\|A_{ij}\|X = T + \Xi. \tag{5.20}$$

A solution for (5.20) should be found so that its dispersion is at a minimum. It is assumed that $\Xi = \{\xi_1, \ldots, \xi_n\}$ has a zero average and dispersion $\{\sigma_1^2, \ldots, \sigma_n^2\}$. Such a solution for $\{x_1^*, \ldots, x_m^*\}$ is called a σ-solution.

Multiply the ith equation of system (5.19) successively by magnitudes $c_{1i}, \ldots, c_{mi}$ $(i = 1, \ldots, m)$ and let

$$\sum_{i=1}^{n} c_{ji} A_{il} = \sigma_{jl}; \tag{5.21}$$

$$\delta_{jl} = \begin{cases} 1, & j = l; \\ 0, & j \neq l; \end{cases} \quad (l, j = 1, \ldots, m). \tag{5.22}$$

With conditions (5.21) and (5.22) satisfied we obtain

$$x_1^0 = \sum_{i=1}^{n} c_{1i} T_i. \tag{5.23}$$

Similar relationships are written for x_j^0 $(j = 2, \ldots, m)$. Substituting T for Z in (5.23) (i.e., proceeding to system (5.20)), we have

$$\tilde{x}_1 = \sum_{i=1}^{n} c_{1i}(T_i + \xi_i). \tag{5.24}$$

From (5.24) we calculate the dispersion

$$D[\tilde{x}_1] = \sum_{i=1}^{n} c_{1i}^2 \sigma_i^2. \tag{5.25}$$

Since the $\tilde{x}_1$ and x_1^0 averages coincide by definition, to solve the posed problem it is necessary to find a minimum of dispersion (5.25) with conditions (5.22) satisfied. Let us use the method of uncertain Lagrangian multipliers and form an auxiliary expression:

$$\varphi(c_{11}, \ldots, c_{1k}) = \sum_{i=1}^{n} c_{1i}^2 \sigma_i^2 + \mu_1 \left(\sum_{i=1}^{n} c_{1i} A_{i1} - 1 \right) + \sum_{j=2}^{m} \mu_j \sum_{i=1}^{n} c_{1i} A_{ij}. \tag{5.26}$$

Equalizing the first derivatives of function (5.26) to zero, we obtain:

$$2c_{1k}\sigma_k^2 + \sum_{j=1}^{m} \mu_j A_{kj} = 0 \quad (k = 1, \ldots, n). \tag{5.27}$$

Relationships (5.27) and conditions (5.22) constitute a system $(m + n)$ of equations whose solution makes it possible to determine the optimal values of c_{ij}^* we are looking for. Analysis shows that $D[x_j] = -\mu_j/2$. The values of μ_j can be found from the system of equations:

$$\sum_{j=1}^{m} \mu_j \sum_{i=1}^{n} \frac{A_{ij} A_{i1}}{\sigma_i^2} = -2; \qquad \sum_{j=1}^{m} \mu_j \sum_{i=1}^{n} \frac{A_{ij} A_{il}}{\sigma_j^2} = 0; \quad l = 2, \ldots, m.$$

Quantitative estimates show that the σ-solution is preferable to that obtained by the criterion of mean square deviation. Let us consider the case $m = 2$ and $n = 3$, where x_1 is the thermodynamic temperature, and x_2 is the mineralization degree. From (5.27) we have

$$c_{1k}^* = \frac{1}{\Delta\sigma_k^2} \left(A_{k1} \sum_{i=1}^{n} \frac{A_{i2}^2}{\sigma_i^2} - A_{k2} \sum_{i=1}^{n} \frac{A_{i1} A_{i2}}{\sigma_i^2} \right); \quad k = 1, \ldots, n; \tag{5.28}$$

$$c_{2k}^* = \frac{1}{\Delta\sigma_k^2} \left(A_{k2} \sum_{i=1}^{n} \frac{A_{i1}^2}{\sigma_i^2} - A_{k1} \sum_{i=1}^{n} \frac{A_{i1} A_{i2}}{\sigma_i^2} \right); \quad k = 1, \ldots, n; \tag{5.29}$$

where

$$\Delta = \sum_{i=1}^{n} \frac{A_{i1}^2}{\sigma_i^2} \sum_{i=1}^{n} \frac{A_{i2}^2}{\sigma_i^2} - \left(\sum_{i=1}^{n} \frac{A_{i1} A_{i2}}{\sigma_i^2} \right)^2.$$

Optimal estimate of x_j^* can be determined from the relationship

$$x_j^* = \sum_{i=1}^{n} c_{ji}^* Z_i \quad (j = 1, 2).$$

The dispersion of the x_j^* estimate is as follows:

$$D[x_1^*] = \Delta^{-1} \sum_{i=1}^{n} \frac{A_{i2}^2}{\sigma_i^2}; \qquad D[x_2^*] = \Delta^{-1} \sum_{i=1}^{n} \frac{A_{i1}^2}{\sigma_i^2}. \tag{5.30}$$

Compare this estimate with that by the method of least squares. Let

$$\|A_{ij}\| = \begin{Vmatrix} 1 & 1 \\ 1 & 2 \\ 1 & 3 \end{Vmatrix}.$$

Then, from formulas (5.30) we obtain

$$c_{11}^* = (6\sigma_2^{22} + 2\sigma^3)/\Delta_1; \qquad c_{12}^* = (3\sigma_1^2 - \sigma_3^2)/\Delta_1; \qquad c_{13}^* = -2(\sigma_1^2 + \sigma_2^2)/\Delta_1;$$
$$c_{21}^* = -(2\sigma_2^2 + \sigma_3^2)/\Delta_1; \qquad c_{22}^* = (-\sigma_1^2 + \sigma_3^2)/\Delta_1; \qquad c_{23}^* = -(\sigma_1^2 + 2\sigma_2^2)/\Delta_1,$$

where $\Delta_1 = \sigma_1^2 + 4\sigma_2^2 + \sigma_3^2$.

Then, we have

$$D[x_1^*] = (9\sigma_1^2\sigma_2^2 + 4\sigma_1^2\sigma_3^2 + \sigma_2^2\sigma_3^2)/\Delta_1;$$
$$D[x_2^*] = (\sigma_1^2\sigma_2^2 + \sigma_1^2\sigma_3^2 + \sigma_2^2\sigma_2^2)/\Delta_1.$$

Let $\hat{x}_1$ and $\hat{x}_2$ be estimates of the parameters x_1 and x_2, obtained by the method of least squares (i.e., be solutions of the minimization problem):

$$\min_{x_1, x_2} \left(\sum_{i=1}^{n} (T_i + \xi_i - A_{i1} x_1 - A_{i2} x_2)^2 \right)^{1/2} = \left(\sum_{i=1}^{n} (T_i + \xi_i - A_{i1} \hat{x}_1 - A_{i2} \hat{x}_2)^2 \right)^{1/2}.$$

We have

$$\sum_{k,j=1}^{N} = 4(T_1 + \xi_1)/3 + (T_2 + \xi_2)/3 - 2(T_3 + \xi_3),$$

$$\hat{x}_2 = -(T_1 + \xi_1)/2 + (T_3 + \xi_3)/2,$$

$$D[\hat{x}_1] = (16\sigma_1^2 + \sigma_2^2 + 4\sigma_3^2)/9; \qquad D[\hat{x}_2] = (\sigma_1^2 + \sigma_3^2)/4.$$

It can be seen that $D[\hat{x}_1] \geq D[x_1^*]$ and $D[\hat{x}_2] \geq D[x_2^*]$. Hence, the σ-solution is preferable to estimates obtained by the method of least squares.

5.3.6 Randomization algorithm for linear fractional approximation

Measurements of the environmental parameters in the monitoring regime provide sets of series of quantitative characteristics for the system of data processing, which cannot be analyzed because of their stationarity. There are many ways to overcome time dependence and thereby remove the contradiction between the applicability of statistical methods and the level of observational data stationarity. One such way consists in partitioning a series of noise-loaded measurements into quasi-stationary parts (Borodin *et al.*, 1996; Krapivin *et al.*, 2004).

Let the results of measurements be presented by a succession of magnitudes Z_{ij}, where $i = 1, \ldots, N$ is the number of time intervals, $j = 1, \ldots, M$ is the number of the measuring device (i.e., the information channel). It is assumed that

$$Z_{ij} = T_{ij} + \xi_{ij}, \tag{5.31}$$

where T_{ij} and ξ_{ij} are the determinate and stochastic constituents, respectively, with ξ_{ij} having a zero average and dispersion σ_j^2.

The problem of sampling the piecewise constant of a random succession (5.31) is reduced to classification of distribution functions with identical averages. To approximate sample $\{Z_{ij}\}$ by a linear, broken, randomized function, we perform the following operations. First, we find the difference

$$\Delta Z_{kj} = Z_{k+1,j} - \frac{1}{k}\sum_{l=1}^{k} Z_{lj} = \Delta T_{kj} + \frac{1}{k}\sum_{l=1}^{k} \Delta\xi_{lj}.$$

If magnitudes Z_{kj} and $Z_{k+1,j}$ belong to samples with similar averages, then $\Delta T_{kj} = 0$. Otherwise, $\Delta T_{kj} \neq 0$. Let us ssume that Z_{kj} and $Z_{k+1,j}$ belong to a sample from distributions with similar averages if

$$|\Delta Z_{kj}| \leq a_{kj}, \tag{5.32}$$

where $a_{kj} = d\sigma_j$, d is an adaptation coefficient (usually $d = 3 - (1 + 1/k)^{1/2}$). Beginning with $k = 1$ and continuing to successively calculate ΔZ_{kj} and check the condition (5.32), we find the quasi-stationary section of succession $\{Z_{ij}\}$. If condition (5.32) is not satisfied simultaneously for $Z_{(k+1),j}$ and $Z_{(k+2),j}$, then the element Z_{kj} is considered the last in the sub-multitude whose elements satisfy the condition of quasi-stationarity. The subsequent sub-multitude of the series $\{Z_{ij}\}$ begins from $Z_{(k+1),j}$ as a first element. The sub-multitude where the average is not a constant value (i.e., the condition (5.32) is never satisfied) is formed as a sub-multitude of random values, whose average changes, following the linear law. In this case, at all stages of the procedure can the values $\Delta Z_{(k+m),j} = Z_{(k+m+1),j} - Z_{(k+m),j}$ $(m = 1 \div s)$ be calculated. The linear approximation of the section of series $\{Z_{ij}\}$ is constructed between the values $Z_{(k+1),j}$ and Z_{sj}. The equation for the straight line we are looking for can be written as:

$$Z - \bar{Z}_{\bar{t}_{sj}} = \overline{\Delta Z}_{sj}(t - \bar{t}_{sj}), \tag{5.33}$$

where t is the time identified at the very moment the measurements were recorded:

$$\bar{t}_{sj} = 0.5(s-k-2), \quad \overline{\Delta Z}_{sj} = \frac{1}{N-1}\sum_{i=1}^{N-1} \Delta Z_{(k+1),j}, \quad N = 2\bar{t}_{sj}, \quad \bar{Z}_{sj} = \frac{1}{N}\sum_{i=1}^{N} Z_{(k+i),j}.$$

Checking the stability of the angle of the straight line slope (5.33) as it is formed can be carried out by analyzing the value

$$\Delta\tilde{Z}_{lj} = \Delta Z_{lj} - \frac{1}{l}\sum_{i=1}^{l} \Delta Z_{(k+1),j},$$

calculated at each step l. Single violations of this stability (i.e., when $|\Delta\tilde{Z}_{lj}| \geq 6\sigma_j(1 + l^{-1})^{1/2}$) are considered accidental releases and either are excluded from consideration or substituted with average values.

5.3.7 Statistical classification of the thermal fields of land cover

The developed remote-sounding technology, based on the radiofrequency region of electromagnetic waves, intensively introduced in the systems of nature monitoring requires the development of algorithms for the data processing of measurements based on the retrieval of qualitative characteristics. Non-stationarity is one of the characteristic indicators of $T_j(t)$ data rows recorded at the end of measurements $[t_1, t_2]$ for each radiometer in the wavelength region λ_j. T_j values during single time intervals $[t^j_{1l}, t^j_{2l}] \in [t_1, t_2]$ are determined by the spatial features of characteristics of the proper radiation of natural and anthropogenic fields of brightness U_j located at respective sectors of the measurement line (e.g., from flying laboratories).

The process representing the time function $T_j(t)$ of the spatial distribution of dielectric, thermodynamic, and relief features of land covers is essentially the same process of linear averaging of the brightness field within the main antenna lobe, with the addition of the proper noise of the radiometer to the obtained result $\tilde{T}_j(t)$.

$$T_J(t) = (1/\alpha_J)\int_0^t \tilde{T}_j(z)\exp[-(t-z)/\alpha_J]\,dz + \xi(t), \tag{5.34}$$

where α_J is the time constant of integration of the RC chain,

$$\xi(t) = (1/\alpha_j)\int_0^t [\eta_j(z) + \beta_j(z)]\exp[-(t-z)/\alpha_j]\,dz.$$

Here β_j is the time function resulting from averaging the brightness field over the side lobes of the radiometer antenna of range λ_j.

These assumptions facilitate use of the theory of linear transformation of determinate, fluctuating, and pulse processes both to ascertain function $T_j(t)$ in (5.34) with U and η given, and to identify field U_j from the results of radiometric measurements.

The type of U_j field corresponds to the type of cover:

- smooth backgrounds give (as radiometer output) $T_j(t)$ values with single-type (in a statistical sense) properties like the measurements over an isotropic field with a given function of correlation (quiet water bodies, landing strips, etc.);
- quasi-homogeneous covers give single-type realizations of T_j, like those obtained in measurements over the U_j field with a given function of correlation (rough sea surface, barkhan[1] sands, etc.);
- anisotropic surfaces with bifurcations are characterized by rare but considerable changes in apparent temperature observed in measurements which determine T_j realizations with one or several extremes (forest and peatbog fires, conduit network, takyrs, etc.); and
- parti-colored (patchy) covers that show variations in their radiant characteristics take the form of pulses of different amplitude and duration (waterlogged forest, burned-out part of a forest fire, forest–marsh complexes, etc.).

To solve the problem of identification, classification, and determination of the radiophysical and geometrical characteristics of different objects of the environment by the output signal of the jth radiometer is reduced to the following chain of operations:

- selection of a given $\{T_j\}$ realization of time intervals $[\tilde{t}^j_{1l}, \tilde{t}^j_{2l}]$ within which $\{T_{j1}\}$ can be considered a quasi-stationary (locally homogeneous) process by the criterion of Borodin *et al.* (1978) with all readings in a given interval attributed to the distribution of similar averages and dispersions (single-range UHF phase);
- calculation of first moments $\{M_{j1}\}$ from the data of each $\{T_{j1}\}$ sample and cross-correlation functions from the data of different samples presented as brightness temperatures;
- determination of the left t^j_{1l} and right t^j_{2l} boundaries for each interval of quasi-stationarity by considering the transition processes caused by specific features of the directional diagram of radiometer antennas;
- approximation of $T_j(t)$ in the form of consecutive adjacent pulses q_{j1} whose leading and falling edges coincide in time with t^j_{1l} and t^j_{2l}, and the amplitude is equal to the average value of function $T_{jl}(t)$ in the time interval;
- revealing the parametric and non-parametric statistical features of $T_j(t)$ realizations as a sequence of random quantities $\{q_{jl}\}$ with averages $\bar{T}_{jl}$ and correlation matrix K^j_{lm}; and
- calculation of the point, interval, and non-parametric estimates of the reliability of distinguishing between objects q_{jl} and the characteristics of field U at respective sectors of the measurement line in terms of the assumed classification of the covers.

[1] Barkhan sands are the mobile sand dunes shaped like a crescent that are the typical image of desert landscapes.

Calculation of the spectral and polarization characteristics of field $\{U_j\}$ by the entire m-range and n-channel radiometric complex assumes

- specification and spatiotemporal combination of the boundaries of a single-range UHF phase;
- determination of the boundaries θ^n_{1k} and θ^n_{2k} of the existence of an m-range UHF phase Q^n_{jk} (i.e., of natural origin), where the set of averages, dispersions, and other moments does not vary (for each channel and range) within the interval $[\theta^n_{1k}, \theta^n_{2k}]$;
- revealing the parametric and non-parametric statistical features of all realizations of $\{T_j\}$ $(j = 1, \ldots, n)$ as a sequence of n-dimensional random quantities $\{Q^n_k\}$, according to their moments and correlation matrices;
- calculation of the point, interval, and non-parametric estimates of the reliability of distinguishing in the n-range UHF phase between respective estimates of the geophysical and geometrical characteristics of an object Q^n_k.

The whole procedure of identifying an environmental object ends with the component-by-component verification of its parameters according to the scheme in Figure 5.2.

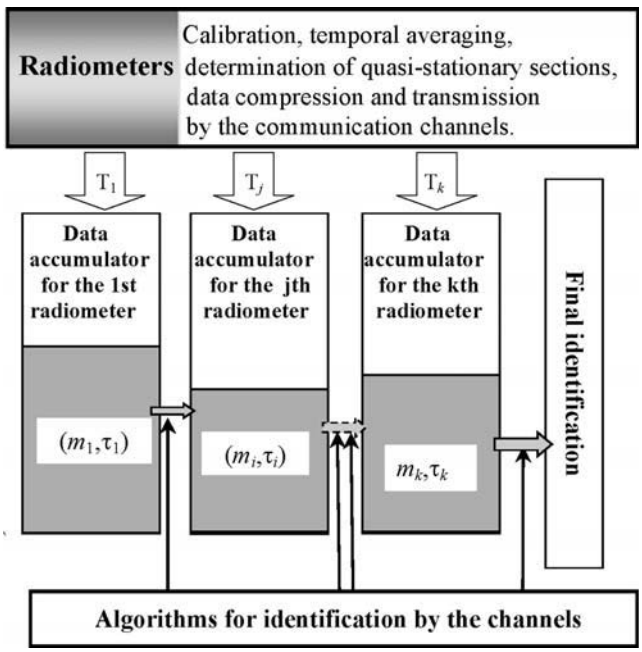

Figure 5.2. Schematic diagram of the consecutive, simultaneous, exhaustive procedure for statistical decision-making in a multi-channel microwave-monitoring system. Designations: m_j is the memory capacity for the jth channel, τ_j is the time delay interval in the jth channel, and T_i is the radiobrightness temperature.

5.3.8 Assessment of algorithm accuracy

The algorithms of spatiotemporal interpolation considered here are, of course, less accurate than model restorations of spatial patterns since the latter, in contrast to the former, take into account more detailed correlations between the elements and processes over the territory under study. But the former do have their advantages: they are universal and independent of the orientation of the monitored object. Therefore, when equipping monitoring systems, the complex use of these methods is expedient, making it possible for the user to choose between them on the basis of expert estimation or other algorithms. The results given in Tables 5.5 through 5.7 characterize to some extent the accuracy of these algorithms in the case of two natural objects.

The calculations given in Krapivin and Phillips (2001) to enable comparison of empirical and retrieved estimates of brightness contrasts showed that under stationary climatic conditions, the method of harmonic functions is more accurate. The method of group consideration of arguments is always less accurate than the method of differential approximation. However, without theoretical comparisons of these algorithms it is impossible to pick out the most accurate or to clearly classify them depending on the quality of experimental data rows. Further studies of these logarithms are needed. Clearly, they can supplement each other in attempts at realizing the adaptation process when choosing one of them.

5.3.9 Consistency of remote-monitoring information

Remote monitoring of the environment is an efficient and non-invasive method of obtaining information about the state of natural objects. This information is used to develop the methods and forms of interaction of humans with natural systems, to realize preventive measures for their protection from undesirable impacts, and to predict the consequences of accomplishment of anthropogenic projects. The results from application of remotely obtained information depend on how such data are accumulated, processed, and used. In other words, the real mechanism behind the use of information is based on construction of an empirical model that looks for dependences between numerous variables in a given sample of measurements. The expert component, which includes formation of the feature space and the use of *a priori* information, constitutes a large part of this process. It is here that distortions of mechanisms of interpretation and presentation of the knowledge obtained about the studied natural system occur. The main reasons for such distortion are connected with the noise loading of observational data, non-representativeness of data samples, total or partial lack of relevant arguments, the fragmentary character both in space and in time of the measurements themselves, and with the presence of irremovable information uncertainties.

The mathematical model is the basic instrument for learning and making decisions in environmental monitoring. Here, along with these reasons of information distortion, additional facts appear connected with a poor choice of model and inadequately studied mechanisms of the functioning of natural systems.

Table 5.5. Comparison of the accuracies of the Method of Self-Organizing Models (MSOM) and differential approximation algorithms from results of retrieval of water level oscillations at the boundary of the Nyok Ngot lagoon (South Vietnam) with the South China Sea. From Bui (2001). Notation: Δt is the time step, and ε is the error (%).

Measured values		*Calculated values*							
		MSOM				*Differential approximation*			
$\Delta t =$ 1 day	$\Delta t =$ 1 hour	$\Delta t =$ 1 day	ε	$\Delta t =$ 1 hour	ε	$\Delta t =$ 1 day	ε	$\Delta t =$ 1 hour	ε
12	1	13.44	12	1.06	6	10.92	9	1.17	7
17	−23	14.11	17	−18.86	18	15.64	8	−24.38	6
22	−41	21.78	1	−34.85	15	20.90	5	−37.72	8
22	−42	20.02	9	−40.74	3	22.66	3	−37.80	10
12	−28	9.36	22	−29.96	7	13.32	11	−30.52	9
1	−11	0.96	4	−12.21	11	0.87	13	−11.55	5
−15	−4	−16.05	13	-4.16	4	−13.65	9	-4.12	3
−23	−12	−24.61	7	−11.16	7	−25.53	11	−11.46	2
−34	−13	−27.54	19	−11.83	9	−30.60	10	−14.43	11
−36	2	−33.12	8	2.04	2	−33.58	7	1.92	4
−28	20	−33.04	18	21.20	6	−24.64	12	18.80	6
−15	26	−16.50	10	22.62	13	−16.65	11	23.92	8
−4	1	−4.12	3	0.91	9	-4.36	9	1.05	5
−1	11	−1.10	10	10.45	5	−1.10	10	10.56	4
Minimum error (%)			1		2		3		2
Average error (%)			10.5		7.8		8.5		5.9
Maximum error (%)			22		18		13		11

Therefore, in the sphere of information provision for monitoring, the principal problem is choice of an adequate model. There are various approaches to solution of this problem. The simplest class of models, based on approximation of *in situ* observations, are the polynomial models that are constructed using the method of regressive analysis, the method of group consideration of arguments, the method of

Table 5.6. Comparison of various algorithms for spatiotemporal interpolation with retrieved speeds of flows in Nyok Ngot lagoon.

Measured value (cm/s)	*Calculated value*					
	GMDH	*Error,* ε (%)	*Method of differential approximation*	*Error,* ε (%)	*Evolutionary method*	*Error,* ε (%)
12	12.4	0.030	12.29	0.024	12.61	5.1
16	15.9	0.006	16.37	0.023	16.74	4.9
31	30.1	0.003	30.41	0.019	27.90	10.0
39	38.7	0.008	38.30	0.018	38.49	9.3
41	40.9	0.002	40.02	0.024	37.43	8.7
39	40.7	0.044	41.07	0.053	43.84	12.4
52	50.2	0.035	50.28	0.033	45.92	11.7
49	47.3	0.035	46.89	0.043	43.46	11.3
44	43.0	0.023	42.64	0.031	48.79	10.9
42	42.1	0.002	41.08	0.022	41.92	4.8
35	35.2	0.006	35.63	0.018	36.19	3.4
15	12.6	0.160	16.37	0.091	16.08	7.2
10	8.0	0.2	10.08	0.008	9.97	0.3
1	1.2	0.2	1.12	0.119	9.88	1.2
14	14.3	0.021	14.03	0.002	12.95	7.5
29	30.8	0.041	28.45	0.009	26.42	8.9
31	33.3	0.074	30.63	0.012	34.47	11.2
31	32.9	0.061	30.57	0.014	33.82	9.1
24	23.1	0.038	24.53	0.022	24.86	3.6
19	17.2	0.095	19.34	0.018	18.16	14.4
27	26.6	0.015	26.54	0.017	24.44	9.5

(*continued*)

Table 5.6 (*cont.*)

Measured value	*Calculated value*					
	GMDH	*Error,* ε	*Method of differential approxi-mation*	*Error,* ε	*Evolu-tionary method*	*Error,* ε
(cm/s)		(%)		(%)		(%)
18	17.6	0.022	18.20	0.011	16.61	7.7
9	8.8	0.022	9.10	0.011	9.66	7.3
5	6.3	0.26	5.12	0.023	5.19	3.8
10	9.9	0.01	10.19	0.019	8.96	10.4
2	1.7	0.15	2.04	0.017	2.18	9.1
Minimum error		0.002		0.002		0.3
Average error		0.061		0.027		8.28
Maximum error		0.26		0.119		14.4

minimization of the middle class, the method of splain-approximation, etc. Each of these methods has a certain degree of information reliability.

The remote sounding of land covers is based on recording the properties of reflected and scattered electromagnetic radiation. Such a possibility to obtain information about land cover properties is connected here with the facts that the character of proper (thermal) radiation, and the mechanisms of scattering and reflection are closely connected with the physical and geometrical properties of the surface, inadequate knowledge of which can also lead to erroneous conclusions and, hence, is a source of controversy in the information space.

To parameterize the reasons for information instability that appear in problems of the remote sounding of the environment, we consider two types of models. The first refers to the class of expert structures, which reflects expert opinion. Expert models are ranged according to their efficiency. Each of these models, M, is characterized by structure $|M|$ and complexity C: $M = \{|M|, C\}$. The quality of the model M is assessed either by expert criterion τ or by objective criterion ζ. Let $A(\zeta)$ be the multitude of arguments present in the model's structure, the best by criterion ζ, and $A(\zeta, \tau)$ the multitude of arguments included in the model's structure, the best by both criteria ζ and τ. Then, the simplest empirical component of knowledge is the parameter:

$$\mu = 2|A(\zeta)| \cap A(\zeta, \tau)|/[|A(\zeta)| + |A(\zeta, \tau)|],$$

where $\mu \in [0, 1]$.

Table 5.7. Example of retrieval of brightness temperature measured over the Sarakamysh hollow (central Asia) from a flying laboratory using a microwave radiometer at the 1.35 cm wavelength.

Brightness temperature measured at 1.35 cm wavelength	*Retrieved brightness temperature and introduced error*			
	Method of differential approximation	*Error* (%)	*Method of harmonic functions*	*Error* (%)
247.72	324.29	31	210.67	15
249.35	316.58	27	212.06	15
150.00	172.50	15	174.01	16
229.00	190.07	17	256.48	12
243.92	217.19	11	209.92	14
139.25	164.27	18	157.76	9
234.14	203.72	13	229.46	2
248.28	196.20	21	230.92	7
152.50	181.38	19	172.26	13
223.59	268.19	20	245.89	10
234.64	194.86	8	260.38	11
223.59	279.34	25	234.74	5
235.80	188.86	20	274.65	9
244.82	198.46	19	257.02	5
258.69	181.29	30	240.63	7
141.88	164.44	16	157.39	11
252.00	264.69	5	221.76	12
262.08	288.28	10	222.78	15
252.63	272.79	8	229.95	9
146.60	175.82	19	162.66	11
249.27	199.47	20	256.74	3
257.34	226.50	12	236.78	8
258.00	221.88	14	283.81	10
Minimum error		8		2
Average error		17		10
Maximum error		31		16

Hence, function $\mu = \mu(|M|, C)$ uniquely characterizes the level of consistency of expert and empirical information. If $\mu \to 1$, then we can speak about the similarity between expert and experimental knowledge. With $\mu \to 0$ these two levels of knowledge become controversial. Actually, some optimal level of consistency μ_{opt} can be reached, if $|M| \in X$ and $C \in Y$:

$$\mu_{opt} = \max_{|M|,C} \mu(|M|, C),$$

where X and Y are the multitudes of possible structures and complexities.

In practice, the construction of function μ is connected with considerable limitations in the sphere of knowledge to which the subject of investigation refers. In the sphere of remote monitoring these limitations are explained by the presence of unsolved problems when optimizing the choice of the most informative wavelengths as well as by the absence of efficient methods to study non-stationary processes. Therefore, in the field of remote monitoring, both expert and empirical knowledge is combined at the level needed to study partial models for transition to a comparative analysis by criterion μ.

Study of the environment by radiophysical methods is a well-known field in remote monitoring. Here difficulties appear in estimating the accuracy of solutions to problems of identification, data recovery, and calculation of statistical characteristics. One of the important problems is to increase the accuracy of calculations of the spectral density of a random process, information about which is needed to reveal homogeneous patterns along the route of satellite or aircraft monitoring. First, the sectors of stationarity are revealed in the broad sense (i.e., in which average, dispersion, and correlation coefficients behave following the law of unbiasedness and independence). For example, in the work of Borodin and Gordina (1983) an algorithm was proposed to partition the successions of measurements made by radiophysical methods into sections of quasi-stationarity, which provides an automated regime when estimating differences between empirical and model levels of knowledge. As shown in Bukatova *et al.* (1991), there is a mechanism for collection and analysis of data without the procedure of partition of measurements into quasi-stationary sections. This mechanism is connected with the use of evolutionary model synthesis by selecting structures whose subject orientation cannot be determined beforehand. Finally, a future approach to development of statistical interpolation methods can be proposed in the form of construction of an empirical model for a stochastic variable

$$z(x) = m + \varepsilon(x),$$

where m is the constituent determined; ε is a random component; and x is a route variable. The essence of the method consists in presenting the $z(x)$ value at point $x = x_0$ as a linear combination

$$\tilde{z}(x_0) = \sum_{j=1}^{N} \lambda_j z(x_j),$$

where λ_j are coefficients independent of the measurement procedure satisfying the condition $\sum_{j=1}^{N} \lambda_j = 1$ and determined by minimization of the respective discrepancy.

In the microwave monitoring of the environment, when identifying objects, average values of brightness temperature often turn out to be important. The use of the Behrens–Fisher criteria to compare averages in two quasi-stationary zones of the variable x enablesus to identify natural objects according to standards (Pagurova, 1968; Dong, 2004). Let $\{T_{1,j}\}$ and $\{T_{2,j}\}$ be mutually independent random quantities following the normal distribution with unknown parameters (a_1, σ_1) and (a_2, σ_2), respectively. Such a criterion to check the hypothesis $a_1 - a_2 = \sigma$ is based on estimation of the quantity

$$v = \frac{d - \delta}{\sqrt{b_1 s_1^2 + b_2 s_2^2}},$$

where

$$d = \bar{T}_1 - \bar{T}_2, \qquad \bar{T}_i = \frac{1}{n_i} \sum_{k=1}^{n_i} T_{i,k}, \qquad b_i = \frac{1}{n_i}, \qquad s_i^2 = \frac{1}{n_i - 1} \sum_{k=1}^{n_i} (T_{i,k} - \bar{T}_{i,k})^2.$$

The diversity of models $\{M_k\}$ used in microwave monitoring is determined by the body of knowledge that has built up about microwave propagation in the environment and by various approaches to the choice of expert, empirical, and theoretical models. In particular, in the way they interpret microwave measurements of soil moisture, these models vary in accordance with the scenario of changes in the dielectric constant of soil with depth (Shutko, 1987; Mkrtchyan, 1982). Measurement of water surface temperature can efficiently be made using the method of module regulation (Kazansky and Filatov, 1987). The theoretical basis for modeling land vegetation reflectivity consists of two specially introduced indices $SR = a_N/a_V$ and $ND = (a_N - a_V)/(a_N + a_V)$, where a_N, a_V are surface reflectivity in the near-IR and visible wavelengths, respectively.

To verify the agreement between expert and empirical information, let us take a data sample $Y = \{y_i, x_{ij}; i = 1, \ldots, r; j = 1, \ldots, n\}$, where y is a function, and $\{x_j\}$ are arguments. Let us determine by $\varphi(m)$ the influence of argument x_m on y and range the arguments so that $\varphi(m_1) > \varphi(m_2) > \cdots > \varphi(m_n)$. Let us further suppose two models y_1 and y_2 are ε-close, as long as according to quality criterion ζ inequality $|\zeta(y_1) - \zeta(y_2)| < \varepsilon$ is valid. The influence of arguments m_1 and m_2 is assumed to be σ-equivalent if $|\varphi(m_1) - \varphi(m_2)| < \sigma$.

Let us consider the class of polynomial models:

$$y = a_0 + \sum_{i=1}^{m} a_i x_i + \sum_{i,j=1}^{m} b_{ij} x_i x_j + \cdots + \sum_{i_1,\ldots,i_s}^{m} c_{i_1,\ldots,i_s} x_{i_1,\ldots,i_s}$$

Let us introduce a symmetric binary ratio $\mathfrak{R} \in \Omega$, following the rule $(y_1, y_2) \in \mathfrak{R}$ only when structures y_1 and y_2 differ in one argument, to set of pairs of every possible

polynomial model Ω . During microwave experiments a search of $\Re$ is carried out by establishing correlations between the parameters of the object under study. Shifting by pairs in space $\Re$ simplifies the search for an optimal model, though there is a chance of missing the best model.

5.4 MONITORING AND PREDICTION OF NATURAL DISASTERS

5.4.1 Ecodynamics and natural disasters

As civilization continues to develop, the problems of forecasting future environment changes and relevant changes in people's living conditions have become most important. The main problem of interest is the origin and propagation of dangerous natural phenomena which lead to the loss of life and cause serious economic damage. Natural anomalies of different spatiotemporal scales are known to have played an important role in the evolution of nature as mechanisms for natural system regulation.

Natural disasters can be classified in different categories. Large-scale disasters include environmental phenomena that are responsible for the death of thousands of people, the destruction of their homes, and the accompanying economic damage to a given region. Hence, the scale of natural disasters depends on the level of economic development of the region in question, which determines the degree of protection from natural disasters. Therefore, studies of phenomena connected with natural catastrophes should be followed by analysis of the poverty level of the given region. The results of studies accumulated during the last 25 years show that in developing countries the scale of losses from natural catastrophes is much larger than in economically developed regions. Bearing in mind that during the last decade the number and scale of natural disasters has substantially increased, we should expect more of the same in the near future. Therefore, the forecast of and warning about potential crises on a global scale should be a subject of concern for all countries, independent of their economic development.

At present theories about environmental catastrophes and the analysis of risks are well developed (Potapov *et al.*, 2006). Using them to describe events and processes in the actual environment requires a study of the methods of system analysis to synthesize a global model of the NSS by means of spaceborne monitoring. Solution of the relevant problems is the subject matter of ecoinformatics, which entails combination of analytically simple semi-empirical and complex non-linear models of ecosystems in the latest global databases. Many international and national programs on environmental problems and space-oriented studies have recently raised the level of thematic coordination in order to reach the necessary degree of efficiency. For instance, this is true of the Global Carbon Project (GCP) and Earth Observing System (EOS) programs, within which the most efficient information and technical means of assessment and prediction of the dynamics of the NSS have been concentrated.

The development of constructive methods to predict natural catastrophes requires solution of some problems.

- Adaptation of ecoinformatics methods to the problem of diagnostics and prediction of natural catastrophes in all their variety and at all scales.
- Determination of the statistical characteristics of natural catastrophes in their historical aspect, selecting categories and determining spatiotemporal scales of catastrophic changes in habitats. Analysis of the history of disasters is important for understanding the present dependences of crises both in nature and in society. The statistical characteristics of the dynamics of natural disasters enable formulation of the basis for the mathematical theory of catastrophes and to determine top-priority directions of studies.
- Development of the concept and synthesis of the model of survival to assess the effect of natural disasters on human habitat.
- Study of the laws of interaction between various elements and processes in the global NSS in correlation with such notions as the biological complexity of ecosystems (biocomplexity), considering it as a function of biological, physical, chemical, social, and behavioral interactions between environmental subsystems including living organisms and their communities. The notion of biocomplexity is connected with the laws of biospheric functioning and consists of all ecosystems and natural-economic systems at different scales, from local to global. In this connection, it is necessary to give a combined formalized description of biological, geochemical, geophysical, and anthropogenic factors and processes taking place at a given level of the spatiotemporal hierarchy of units and scales. It is also important to assess the possibilities of using various indicators of an approaching natural catastrophe (e.g., biocomplexity).
- Study of relationships between vital activity, biocomplexity, and evolution of the NSS using global modeling technology. Development of units of the global model to describe the laws and trends in the environment that lead to the appearance of stress situations brought on by human economic or political activity.
- Consideration of demographic premises for the origin of natural disasters, and determination of mechanisms that govern the environment and hinder realization of these premises.
- Assessment of the information content from the current technical means of collecting data on the state of NSS subsystems and available global databases for their successful allocation in solving the problems of assessing conditions conducive to stress situations in the environment.

The role of natural disasters in the formation of global trends in the environment has been studied inadequately to make realistic predictions of possible consequences (e.g., for the regulation of biogeochemical cycles). As can be seen from the scheme in Figure 5.3, for an accurate estimation of CO_2 fluxes at the atmosphere–ocean boundary, it is necessary to have a great deal of data on the whole World Ocean basin. In the zones of tropical hurricanes, the characteristics of ocean ecosystems change drastically. It is also known that tropical hurricanes strongly affect hydrological cycle parameters over large territories, causing floods and facilitating the transport of chemical compounds over large distances. Avery *et al.* (2004) studied

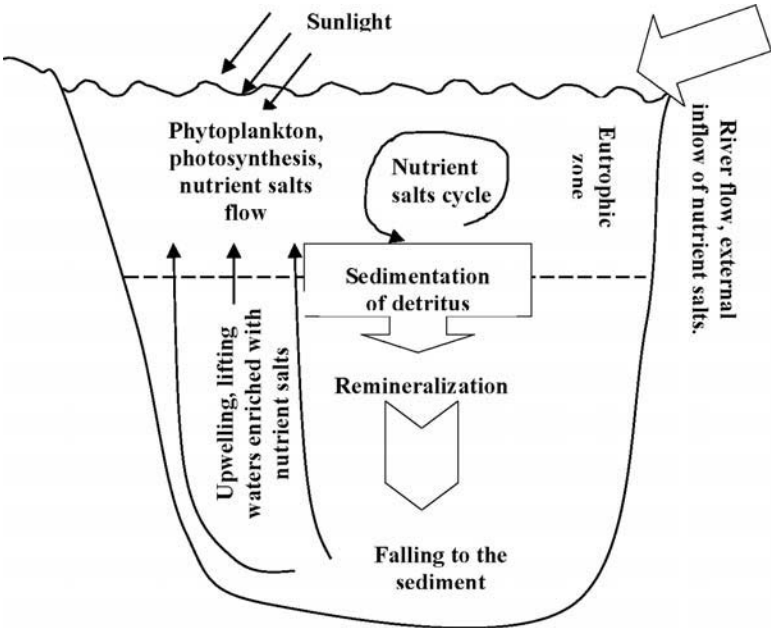

Figure 5.3. Schematic representation of the ocean biological pump. From Usbeck (1999).

the impact of hurricanes on the hydrological cycle in North Carolina and evaluated the respective changes in the river run-off of dissolved organic carbon (DOC) to the World Ocean. In particular, it was shown that an increase in biologically acceptable DOC by 3%–9% on average over 1–2 days after the hurricane leads to a short-term leap in productivity of the water basin's ecosystem as a direct result of the hurricane. Hanshaw *et al.* (2006) specified these estimates having analyzed the biological response of the ocean ecosystem to the impact of a hurricane and showed that the surface concentration of chlorophyll grows after the hurricane in proportion to its intensity, but this increase does not markedly affect the integral productivity of the ecosystem. This conclusion is explained by the fact that along the path of its movement the hurricane either intensifies existing upwellings or initiates new transient upwellings, which leads to enriching the ocean domain with biogenic salts. However, this deviation vanishes rapidly because of the return of the ocean domain to a stable state with pre-hurricane characteristics. Nevertheless, as Smitha *et al.* (2006) showed, using the Bay of Bengal as an example, primary productivity increases up to $3{,}800\,\mathrm{mgC\,m^{-2}\,da^{-1}}$.

On the whole, the problem of assessing the role of hurricanes in the formation of gas exchange at the atmosphere–ocean boundary remains to be studied. Clearly, in the tropical low-productive zone of the World Ocean, where atmospheric CO_2 assimilation is negligibly small, getting reliable estimates of the increase in ecosystem productivity during the passage of tropical hurricanes will make it possible to specify the role of the World Ocean in regulating climate.

5.4.2 Natural disaster as a dynamic category of environmental phenomena

Walker (2003) justly noted that the notion of natural catastrophe is rather vague, and its definition depends on many factors. Grigoryev and Kondratyev (2001a, b) define a natural catastrophe as an "extreme and calamitous situation in the vital activity of population caused by substantial unfavorable changes in the environment" or as "abrupt changes in the system as its sudden response to smooth changes of external conditions." The number of such critical situations in the environment grows. At present, natural catastrophes consist of floods, droughts, hurricanes, storms, tornadoes, tsunami, volcanic eruptions, landslides, mudflows, snow avalanches, earthquakes, forest fires, dust storms, severe frosts, heat waves, locust invasions, and many other natural phenomena (Kondratyev *et al.*, 2002b). In future, this list is likely to widen with the advent of new types of natural catastrophes, such as collisions with cosmic bodies and those caused by man (i.e., bio-terrorism, nuclear catastrophes), abrupt change in the Earth's magnetic field, plague, and others. Therefore, it is important to develop efficient quantitative technologies and criteria to give early warning with high reliability of a dangerous catastrophic natural phenomenon.

The notion of natural catastrophe is associated by many authors with the notion of ecological safety, a term coined for the necessity of assessing the danger for the population of a given territory of injury to health, buildings, or property as a result of changes in environmental parameters. These changes can be caused by fluctuations in natural processes connected with the changing ecological situation, epidemics, or natural disaster. In the latter case, danger appears to be a response of nature to human activity. For instance, such factors as reforestation and change in the vegetation cover amplify the instability in the region of these impacts. These factors have caused land resource degradation and increased the destruction of the natural environment at the expense of water flows. Field and Raupach (2004) and Abrahamson (1989) explain changes in the laws of natural catastrophe occurrence as a consequence of the growth of instability in the carbon–climate–human system. According to Field *et al.* (2002), this instability is likely to increase substantially in the next two decades due to changes in many characteristics of World Ocean ecosystems. Analyzing the history of various large-scale catastrophes, Milne (2004) gives a pessimistic prognosis for the fate of humankind, using emotive words like "doomsday".

In general, the threat of ecological danger in any territory stems from deviation from environmental parameters beyond limits where in the course of time living organisms mutate (i.e., change in a way that does not correspond to the natural process of evolution). As a matter a fact, the notion of "ecological danger" or "ecological safety" is connected with the notion of stability, vital activity, and integrity of the biosphere and its elements. Moreover, the NSS, being a self-organizing and self-structuring system that does so according to the laws of evolution, creates within itself ecological niches, the acceptability of which for the population of a given territory is determined, as a rule, by national criteria (ambient air standard, religious dogmas, national traditions, etc.).

When considering the prospects for life on Earth, we can only proceed from human assessment of the level of environmental degradation. In due course local and

regional environmental change will develop into global ones. The amplitude of these changes is determined by mechanisms of NSS functioning. Humankind is increasingly deviating from this optimality in the way it interacts with surrounding inert, abiotic, and biotic components of the environment. But, at the same time, humankind as an NSS element is attempting to understand the character of large-scale relationships with nature, directing the efforts of many sciences at this, and studying the cause-and-effect relations in this system.

5.4.3 Search for and detection of natural catastrophes

Let the approach of the moment of a natural disaster be characterized by vector $\{x_i\}$ that gets into some cluster of multi-dimensional phase space X_{ij}. In other words, converting our verbal portrait to quantitative estimation of this process, we introduce a generalized characteristic $I(t)$ of a natural disaster and identify it by calibrated scale Ξ, for which we postulate the presence of relationships of type $\Xi_1 < \Xi_2$, $\Xi_1 > \Xi_2$, or $\Xi_1 \equiv \Xi_2$. This means that there always exists a value of $I(t) = \rho$ which determines when a natural catastrophe of a given type can be expected: $\Xi \to \rho = f(\Xi)$, where f is conversion of the notion of "natural disaster" into a number. As a result, magnitude $\theta = |I(t) - \rho|$ determines the expected time interval before the catastrophe occurs.

Let us search for a satisfactory model to transform our verbal portrait of a natural catastrophe into notions and indicators subject to formalized description and transformation. With this aim in view, we select m elements of subsystems at the lowest level in the $N \cup H$ system, the interaction between which we determine using the matrix function $A = \|a_{ij}\|$, where a_{ij} is an indicator of the level of dependence of the relationships between subsystems i and j. Then, the $I(t)$ parameter can be estimated as the sum:

$$I(t) = \sum_{i=1}^{m} \sum_{j>i}^{m} a_{ij}.$$

In general, we have $I = I(\sim 0, a, t)$. For a small territory SZ with area a indicator I is defined as an average value:

$$I_\Omega(t) = (1/\sigma) \int_{(\varphi,\lambda)\in\Omega} I(\varphi, \lambda, t)\, d\varphi\, d\lambda.$$

The introduction of characteristic I_Ω makes it possible to propose the following scheme of monitoring and predicting natural disasters. Figure 5.4 demonstrates a possible structure for a monitoring system with functions that search, predict, and monitor a natural catastrophe. There are three levels in the system, recorder, decision-maker, and searcher, whose units have the following functions:

(1) regular monitoring of environmental elements to accumulate data about their state in the regime;
(2) recording of suspicious elements in the environment for which the value of indicator $I_\Omega(t)$ corresponds to the frequency of occurrence of a natural anomaly of a given type;

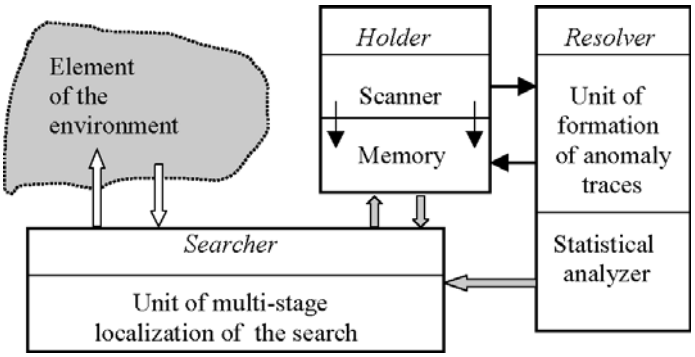

Figure 5.4. Block scheme of a monitoring system to detect anomalies in the environment.

(3) formation of a dynamic series $\{I_\Omega(t)\}$ for a suspicious element to make a statistical decision about its noise or signal, and in the latter case examination of the suspicious element by criteria of the next level of accuracy (getting vector $\{x_i\}$ into the cluster, etc.);
(4) making the final decision about the imminence of a natural catastrophe and transmitting such information to the respective environmental control services; and
(5) iterative procedure to locate an anomaly.

The efficiency of such a monitoring system depends on the measuring methods used and algorithms for observational data processing. Most important here is the model of the environment used in parallel with the formation and statistical analysis of series $\{I_\Omega(t)\}$ which is then adapted to the monitoring regime according to the scheme in Figure 5.5.

As can be seen from the criterion of an imminent natural catastrophe, the form and behavior of $I_\Omega(t)$ are special for each type of process in the environment. One complicated problem consists in determining these forms and their respective classification. For instance, such frequent dangerous natural events as landslips and mudflows have characteristic features, such as preliminarily changing relief and landscape, which can be successfully recorded from satellites in the optical range. This, together with data of aerial photography and surface measurements of relief slopes, exposure of slopes, and the state of the hydro-system, makes it possible to predict dangerous natural events several days beforehand. However, the restricted capabilities of the optical range under conditions of clouds or vegetation cover should be broadened by introducing systems of remote sounding in the microwave region of the electromagnetic spectrum. Then, in addition to the indicators of landslips and mudflows, we can add such information parameters as soil moisture and biomass, because an increase in soil moisture leads to landslips, while one in biomass testifies to the increased capability of the roots of vegetation cover to hold soil and rocks together to prevent rockfalls. This is especially important when assessing the likelihood of snow/stone or snow avalanches. Compiling a catalog of these indicators for

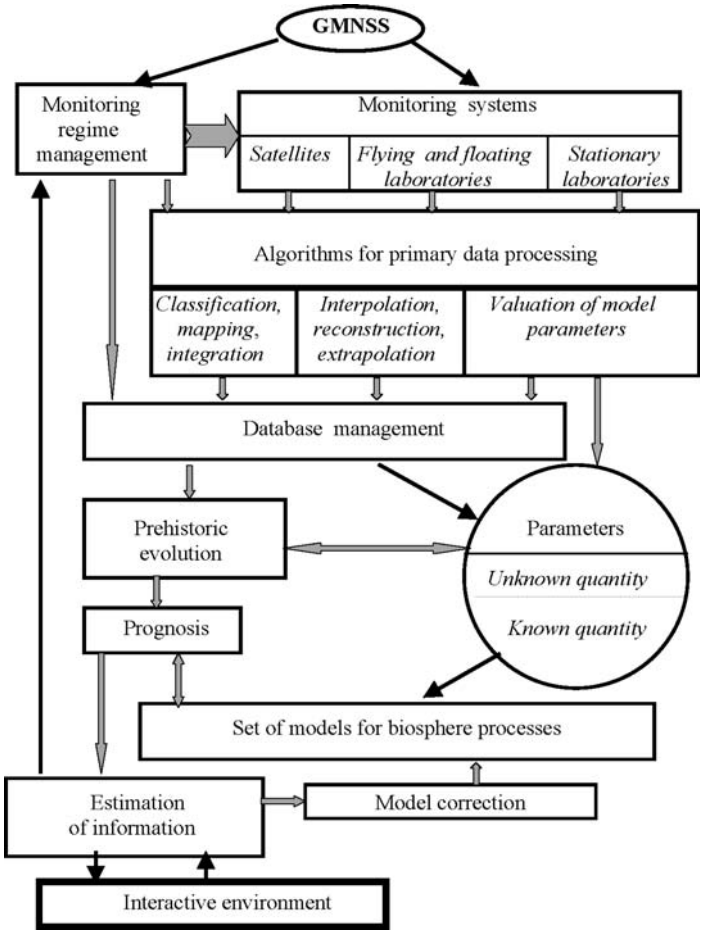

Figure 5.5. The concept behind adaptive adjustment of the GMNSS for geoinformation monitoring.

all possible natural disasters and making it an integral part of the information base of the monitoring system is a necessary stage to raising its efficiency.

Knowledge of the set of information indicators $\{x_i^j\}$ for a natural catastrophe of jth type and *a priori* determination of its cluster X^j in the space of these indicators makes it possible from spaceborne monitoring to calculate the rate v_2 at which point $\{x_i^j\}$ approaches the center of X^j and thus to calculate the time of catastrophe occurrence. Other algorithms for predicting natural disasters are also possible. For instance, a forest fire can be predicted using the dependence of a forest's microwave emission at different wavelengths on the moisture content of inflammable material in the forest. Knowledge of this dependence gives a real possibility to assess the fire risk in the forest by taking the moisture content the of vegetation cover and upper soil layer into account (Grankov *et al.*, 2006; Soldatov, 2007).

Many studies have shown that the possibility exists of assessing the fire risks of waterlogged and boggy forests by considering the water content of vegetation cover and the upper soil layer, using microwave sounding in the range 0.8 cm–30 cm. Multi-channel sounding makes it possible using cluster analysis algorithms to solve the problem of forest classification according to fire risk category. The efficiency of these methods depends on detailed simulation of the forest structure reflecting the state of the canopy and tree density. Undergrowth fires are the most dangerous and difficult to detect. In such a case the three-layer model of the soil–trunk–canopy system used with the fire risk indicator $I(\lambda_1, \lambda_2) = [T_b(\lambda_1) - T_b(\lambda_2)]/[T_b(\lambda_1) + T_b(\lambda_2)]$ is known to be efficient. For instance, at $\lambda_1 = 0.8\,\text{cm}$ and $\lambda_2 = 3.2\,\text{cm}$ indicator I changes approximately from -0.25 in zones where the risk of forest fire is absent to 0.54 in fire zones. In zones where first indicators appear of the litter catching fire, $I \approx 0.23$. The I value depends weakly on distribution in the layers of the forest of such inflammable materials as lichen, moss, grass thatch, dead pine-needles, and fallen leaves.

Realization of this three-layer regime for decision-making about an approaching natural disaster depends on the agreement between the spatiotemporal scales of the monitoring system and the respective characteristics of the natural phenomenon. Most difficult for decision-making are delayed action natural catastrophes which

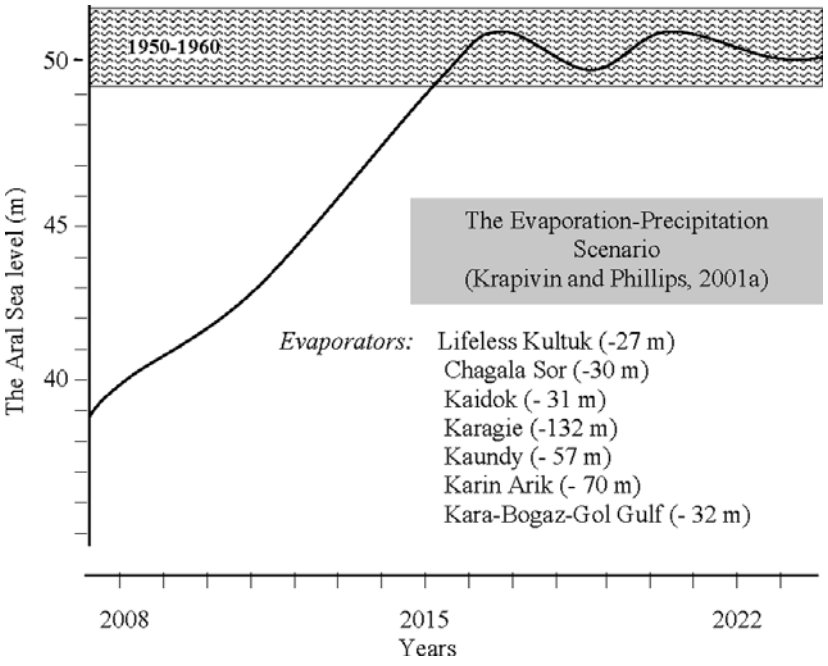

Figure 5.6. Possible dynamics of Aral Sea levels (in meters with respect to the World Ocean level) as a result of the impact of forced evaporators on the hydrological regime of the territory of the Aral–Caspian aquageosystem beginning from 2008.

may well take place decades later. Such disasters include ozone holes, global warming, desertification, reduced biodiversity, overpopulation of lands, and others. Solution of the basic problem of reliable prediction of the occurrence of such disasters or undesirable regional-scale natural phenomena initiated by them using the GMNSS has been proposed, the input data for which comprises information from constantly updated global databases and from ongoing satellite and surface measurements.

The use of the GMNSS in a number of studies has shown that this technology enables us not only to forecast delayed action disasters but also to propose scenarios for their prevention. An example is the scenario for reconstruction of the water regime of the Aral–Caspian system considered in Krapivin and Phillips (2001a). Figure 5.6 shows the final result of using the GMNSS to solve this problem. It can be seen that by realizing the suggested irrigation of some lowlands on the eastern coast of the Caspian Sea without subsequent anthropogenic interference can sharply change the hydrology of the territory between the Aral and Caspian Seas. Of course, this result is merely a demonstration of the GMNSS capability to evaluate the consequences of realizing scenarios of the impacts on the environment. Many problems crop up here in the organization of studies, but they can be solved within the complex scientific–technical program set up to monitor the zone of impact of the Aral and Caspian Seas.

6

Multi-dimensional analysis of interactivity between global ecodynamics and the Arctic Basin

6.1 KEY PROBLEMS FACING ARCTIC BASIN STUDY

Recent growing attention to the Arctic's environmental problems is motivated by a number of circumstances including

(i) the stronger sensitivity of high-latitude environments to various external forcings;
(ii) increasing understanding of the importance of numerous interactions and feedbacks between components of the Earth's system; and
(iii) growing need to use natural resources located at high latitudes (especially the Arctic Shelf).

It is fair to say that "the Arctic system constitutes a unique and important environment with a central role in the dynamics and evolution of the earth system" (Vörösmarty *et al.*, 2001).

Some important scientific results were pointed out in the ACIA Implementation Plan (ACIA, 2000):

- "There has been increased coastal erosion in the Bering Sea from storm surges resulting from reduced sea ice."
- "Sea ice extent in the Arctic has decreased Arctic-wide by 0.35% per year since 1979. During summer of 1998, record reduction of sea ice coverage was observed in the Beaufort and Chukchi Seas."
- "Sea ice thickness has also been reduced by between 1 m and 2 m in most parts of the Arctic Ocean and the sub-Arctic seas."
- "Streamflow discharge of major Siberian rivers into the Arctic Ocean has increased in recent years and is associated with a warmer climate and enhanced precipitation in the river basins."

- "Since 1970, the Arctic Oscillation, which is a measure of the strength of the circumpolar vortex, has strengthened. This has been found to be consistent with temperature change in the Arctic."
- "There has been an increased warming of the Arctic Ocean's Atlantic layer and an approximate 20% greater coverage of Atlantic water types."
- "Record low levels of ozone were measured in 2000 in the Arctic with increasing evidence that these levels are likely to continue for at least the next 20 years."
- "Ongoing studies indicate that the current UV levels can have a significant effect on fish larvae survival rates."
- "General warming of soils in regions with permafrost, derived primarily from Alaskan data, has been observed over recent years."

It was emphasized in ACIA (2000) that past assessments indicated the Arctic to be important to global-scale processes in at least four ways.

- "The thermohaline circulation dominated by the Arctic Ocean and Nordic Seas is responsible for a considerable part of the Earth's poleward heat transport and may also serve as a sink for CO_2. Alterations of this circulation, as have been observed during climatic changes of the past, can affect global climate and in particular the climate of Europe and North America."
- "The melting of the Arctic land ice sheets can cause sea level rise around the world. A compilation of studies suggests that a global warming of 1°C will lead to ~1 mm per year of sea-level rise from small ice caps and glaciers. The Arctic will supply over half of this total, with an additional 0.3–0.4 mm per year contributed from Greenland although uncertainties remain about the mass balance of the Greenland ice sheet."
- "Arctic soils can act as either sinks or sources of greenhouse gases depending on temperature and moisture changes within the Arctic. Moisture has opposing effects on the concentrations of the two major trace gases: CH_4 flux declines with soil drying while CO_2 flux initially increases. These changes can influence greenhouse gas warming globally."
- "Our current understanding of the Arctic climate system suggests that positive feedbacks in high-latitude systems, including the snow and ice albedo effect, amplify anthropogenically-induced atmospheric changes and that disturbances in the circumpolar Arctic climate may substantially influence global climate."

In the context of the health of the Arctic marine environment and the normal functioning of economically important ecosystems, Orheim (2000) asked a number of key questions:

- "How was the polar basin formed, where are the plate boundaries?"
- "What has been the detailed paleo-climatic history of the high Arctic Ocean during the last 1 million years?"
- "Do decreases in ice extent and upper stratification of the ocean signal a different sea ice regime?"

- "What is the stability of the sea ice cover, what are the effects of radiative feedback in the Arctic and how do they modulate global ocean circulation?"
- "What is the role of continental shelves in the cycling of C, N, Si and other chemicals?"
- "What is the productivity of the Arctic Ocean, and what is the structure and diversity of higher trophic levels?"
- "What are the effects of environmental change, both of climate and of pollutants and contaminants such as the introduction of persistent organic pollutants (POPs) into the food chain?"

Of particular interest is the dynamics of high-latitude climate. According to Weller and Lange (1999),

> "While considerable uncertainty still exists about the exact nature of the future impacts of global climate change, there can no longer be any doubt that major changes in the climate have occurred in recent decades in the Arctic, with visible and measurable impacts following the climatic changes. Greater impacts are likely in the future and while some of them will be positive, others will be detrimental to human activities."

Analysis of ice cores from the Arctic (Everett and Fitzharris, 2001) revealed large-scale and rapid paleo-climate changes. Rapid warming took place ~11,500 years ago, at the end of the last glacial period. The coldest parts of ice cores had been as much as 21°C colder than the present temperature in central Greenland; and temperatures increased by more than 10°C in a few decades. There is evidence of even more rapid change in the precipitation pattern, rapid reorganizations of atmospheric circulation, and periods of rapid warming during the past 20,000 years. Rapid warming of ~10°C in a few decades during the last glacial period in central Greenland was followed by periods of slower cooling over a few centuries and then a generally rapid return to glacial conditions. About 20 such intervals, each lasting between 500 and 2,000 years, occurred during the last glacial period.

Everett and Fitzharris (2001) emphasized that the polar systems are extremely sensitive to variability in temperature, and several aspects of these systems will be affected by any further climate change. The primary impacts will be on the physical environment, including ice, permafrost, and hydrology; on biota and ecosystems, including fisheries and terrestrial systems; and on human activities, including social and economic impacts on settlements, on resource extraction and transportation, and on existing infrastructure. Scenario predictions of potential future global warming indicate a necessity to particularly take into account various phenomena such as thermocarst erosion in lowland areas, thawing of permafrost accompanied by hydrological and climatic changes. Climate change will affect terrestrial ecological systems through changes in permafrost as well as direct climatic changes, including changes in precipitation, snow cover, and temperature. Terrestrial ecosystems are likely to change from tundra to boreal forests, although vegetative changes are likely to lag behind climatic change. Major shifts in biomass will be associated with changes in

microbiological (bacteria, algae, etc.) and insect communities (some may diminish while others may prosper).

Everett and Fitzharris (2001) pointed out that in the recent geologic past, the tundra was a carbon sink, but recent climatic warming in the Arctic, coupled with the concomitant drying of the active layer and the lowering of the water table, has shifted areas of the Arctic from sinks to sources of CO_2 (the existence of such a problem is, however, far from being proved). An important potential consequence of permafrost thawing is the emission of methane, a greenhouse gas. The levels of another greenhouse gas, tropospheric ozone, might increase due to warming of the troposphere (Kondratyev and Varotsos, 2000).

An interesting illustration of potential future surprises due to interactions and feedbacks was discussed by Stevenson *et al.* (2000) who obtained future estimates of tropospheric ozone radiative forcing and methane turnover in the context of the impact on climate change. (It should be pointed out that studies of the contribution of tropospheric ozone, O_{3T}, as a greenhouse gas as well as assessments of the potential impact of global warming on permafrost melting and methane emissions are still at the preliminary stage of development.) Interactive simulations of climate dynamics and O_{3T} changes during the time period 1990–2100 for scenarios of "high" (A2) or "middle" (B2) cases of CO_2 emissions resulted in tropospheric ozone radiative forcing (RF) equal to $+0.27(\text{A2})\,\text{W m}^{-2}$ or $+0.09(\text{B2})\,\text{W m}^{-2}$. However, if climate–ozone coupling was disregarded, then relevant RF values would be equal to $+0.43\ (+0.22)\,\text{W m}^{-2}$. With climate change included, CH_4 lifetime fell by 0%–5%. Hence, climate warming exerts a negative feedback on itself by increased destruction of O_{3T} and CH_4.

Three principal achievements have stimulated progress in studying the Arctic environment in recent years (Dickson, 1999):

(i) further development of observation programs using various observation means (including satellites and submarines);
(ii) declassification of the military Soviet–American archive of ocean "climatology" data;
(iii) discovery of the fact that the climatic forcing in the Arctic and northern seas in the 1990s has increased compared with that observed during the previous century. A similar situation also took place with respect to climate dynamics indicators such as the Arctic Oscillation (AO) and the North Atlantic Oscillation (NAO).

Overland and Adams (2001) pointed out that

> "decadal differences between the 1990s and 1980s in winter sea-level pressure and 300 hPa zonal winds have an Arctic-centered character with nearly equal contributions from the Atlantic and Pacific sectors. In contrast, the differences between positive and negative AO composites defined from monthly values of Principal Components from the same period have similar magnitudes in the Pacific and Arctic, but have additional large NAO signature in the Atlantic

sector. Thus Arctic changes of decadal scales are more symmetric with the pole than suggested by the standard AO index definition. Change point analysis of the AO shows that a shift in value near 1989 is an alternative hypothesis to a linear trend. Analysis of zonal and meridional winds by longitudinal sectors shows the importance of the standing wave pattern in interpreting the AO, which supplements the view of the AO as a simple zonal average (annular) mode.''

Thus. the Arctic Oscillation should be considered as a physical phenomenon connected with the enhancement of circumpolar vortex and relevant mass and temperature changes in the stratosphere.

By the end of the 1980s/beginning of the 1990s the very strong NAO increase resulted in powerful transport of warmer and fresher Norwegian Atlantic water to the north of the Fram Strait and the Barents Sea. Entering the Arctic, the sub-layer of Atlantic water was becoming thinner, warmer (by about 2°C), and increased its horizontal extent (~20%). At smaller depths, the cold haloclyne (which thermally isolates the sea ice cover from the warm Atlantic layer located below) shifted toward the Euro-Asiatic Basin, which resulted in substantial changes in the mass and energy balances of the ice cover surface. This and other phenomena have been studied within a number of recent programs (Aagard, 1998; Allison *et al.*, 2001; Orheim, 2000). Of particular interest is the climatic impact of polynyas[1] (Holland, 2001; Lemke, 2001).

Alekseev (1998) emphasized that the Arctic is in many respects key to the global climatic system, where the strongest natural fluctuations in climatic characteristics develop. The global impact of the Arctic is primarily accomplished through the Arctic Ocean, which is capable of changing the structure of its circulation regime under the influence of changes in freshwater and salt and heat exchange with the non-polar parts of the global system. The desalinated upper layer and sea ice located above it turn out to be most active components, with freshwater, heat, and salt transport being the major processes responsible for coupling between the high-latitude environment and its lower latitude parts.

Specific features of the Arctic atmosphere, such as Arctic Haze and extended cloudiness and radiation, were studied during the the First GARP (Global Atmospheric Research Program) Global Experiment, FGGE (Kondratyev, 1999a, b).

Important progress has been achieved in the field of Arctic climate diagnostics (Adamenko and Kondratyev, 1999; Gillett *et al.*, 2002; Lloyd and Fastie, 2002; Moritz *et al.*, 2002; Nagurny and Maistrova, 2002). The basic features of Arctic climate dynamics have also been demonstrated, such as the strong spatiotemporal variability of various scales. Nagurny and Maistrova (2002) showed, for instance, that as far as interannual lower troposphere variations are concerned, before the 1980s negative anomalies prevailed, while later on, for the whole troposphere, positive temperature anomalies were typical. Total polar atmosphere energy (potential plus internal) during the previous 40 years had not changed, however.

[1] A polynya is any non-linear area of open water surrounded by sea ice. It is used as a geographic term for areas of sea in Arctic or Antarctic regions which remain unfrozen for much of the year.

A much more difficult situation exists in the field of numerical modeling of high-latitude climate change. It was mentioned in IPCC (2001) that current estimates of future changes in the Arctic vary significantly. Model results disagree as to both the magnitude of changes and the regional aspects of these changes.

An important step forward in studying the Arctic environment is the Climate and Cryosphere (CliC) Project (Allison *et al.*, 2001). The term "cryosphere" describes those portions of the Earth's surface where water is in solid form. This includes all kinds of ice and snow and frozen ground such as permafrost. The cryosphere is an important part of the global climate system. It is strongly influenced by temperature, solar radiation, and precipitation, and, in turn, influences each of these properties. It also has an effect on the exchange of heat and moisture between the Earth's surface (land or sea) and the atmosphere, on clouds, on river flow (hydrology), and on atmospheric and oceanic circulation. Parts of the cryosphere are strongly influenced by changes in climate. The cryosphere may therefore act as an early indicator of both natural and human-induced climate change.

As a core project of the World Climate Research Program, the "Climate and Cryosphere" (CliC) Project encourages and promotes research into the cryosphere and its interactions as part of the global climate system. It seeks to focus attention on the most important issues, encourage communication between researchers with common interests in cryospheric and climate science, promote international co-operation, and highlight the importance of this field of science to policy-makers, funding agencies, and the general public. CliC also publicizes significant findings regarding the role of the cryosphere in climate, and recommends directions for future study.

CliC aims to improve understanding of the cryosphere and its interactions with the global climate system, and to enhance the ability to use parts of the cryosphere for detection of climate change. The scientific goals of CliC are to

- improve understanding of the physical processes through which the cryosphere interacts within the climate system;
- improve the representation of cryospheric processes in climate models;
- assess and quantify the impacts and consequences of past and future climatic variability on components of the cryosphere; and
- enhance the observation and monitoring of the cryosphere.

To attain these goals, CliC seeks to develop and coordinate national and international activities aimed at increasing the understanding of four main scientific themes:

- Interactions between the atmosphere and snow and ice on the land surface.
- Interactions between glaciers and ice sheets and sea level.
- Interactions between sea ice, oceans, and the atmosphere.
- Interactions of the cryosphere with the atmosphere and oceans on a global scale.

CliC encourages the use of observations, process studies, and numerical modeling within each of the above topic areas. In addition, CliC promotes the establishment of new cryospheric monitoring programs.

The cryosphere is also considered an indicator of climate variability and change. Allison *et al.* (2001) pointed out:

> ''Atmosphere–snow/ice–land interactions are concerned with the role of the terrestrial cryosphere within the climate system and with improved understanding of the processes, and of observational and predictive capabilities applicable over a range of time and space scales. Better understanding of the interactions and feedback of the land/cryosphere system and their adequate parameterization within climate and hydrological models are still needed. Specific issues include the interactions and feedback of terrestrial snow and ice in the current climate and their variability; in land surface processes; and in the hydrological cycle. Improved knowledge is required of the amount, distribution, and variability of solid precipitation on a regional and global scale, and its response to a changing climate. Seasonally-frozen ground and permafrost modulate water and energy fluxes, and the exchange of carbon, between the land and the atmosphere. How do changes of the seasonal thaw depth alter the land–atmosphere interaction, and what will be the response and feedback of permafrost to changes in the climate system? These issues require improved understanding of the processes and improved observational and modeling capabilities that describe the terrestrial cryosphere in the entire coupled atmosphere–land–ice–ocean climate system.
>
> Over a considerable fraction of the high-latitude global ocean, sea ice forms a boundary between the atmosphere and the ocean, and considerably influences their interaction. The details and consequences of the role of sea ice in the global climate system are still poorly known. Improved knowledge is needed of the broad-scale time-varying distributions of the physical characteristics of sea ice, particularly ice thickness and the overlying snow-cover thickness, in both hemispheres, and the dominant processes of ice formation, modification, decay and transport which influence and determine ice thickness, composition and distribution. We do not know how accurate present model predictions of the sea ice responses to climate change are, since the representation of much of the physics is incomplete in many models, and it will be necessary to improve coupled models considerably to provide this predictive capability.
>
> Key issues on the global scale are: understanding the direct interactions between the cryosphere and atmosphere, correctly parametrizing the processes involved in models, and providing improved data sets to support these activities. In particular, improved interactive modeling of the atmosphere–cryosphere surface energy budget and surface hydrology, including fresh-water runoff, is required.
>
> The scientific strategy for a CliC project is similar in each of the areas of interaction: a combination of measurement, observation, monitoring and analysis, field process studies and modeling at a range of time and space scales. A CliC modelling strategy must address improved parametrization in models of the direct interactions between all components of the cryosphere, the atmosphere, and the ocean. It will need to do this at a variety of scales from the regional to global; and with a hierarchy of models ranging from those of individual processes to fully

coupled climate models. It will also be essential to provide the improved data sets needed for validation of models and parametrization schemes.''

Table 6.1 characterizes the major components of the cryosphere (Allison *et al.*, 2001). Allison *et al.* (2001) said that the processes operating in the coupled cryosphere–climate system involve three timescales: intraseasonal–interannual, decadal–centennial, and millennial or longer. The longest timescale is addressed through the IGBP PAGES program, although abrupt climate shifts evidenced in ice core and ocean sediment records (Heinrich events, involving extensive deposition of ice-rafted detritus in the North Atlantic) are also highly relevant to CliC. The other two timescales are commensurate with WCRP interests, as manifested in ACSYS, GEWEX, and CLIVAR. In the space domain, cryospheric processes and phenomena need to be investigated over a wide range of scales from meters to thousands of kilometers.

The study of cryosphere dynamics is important for many applications. Table 6.2 illustrates some applications (Allison *et al.*, 2001).

Four overarching goals that address major concerns for the WCRP can be identified (Allison *et al.*, 2001).

(1) To improve understanding of the physical processes and feedbacks through which the cryosphere interacts within the climate system.
(2) To improve the representation of cryospheric processes in models to reduce uncertainties in simulations of climate and predictions of climate change.
(3) To assess and quantify the impacts of past and future climatic variability and change on components of the cryosphere and their consequences, particularly for global energy and water budgets, frozen ground conditions, sea level change, and the maintenance of polar sea ice covers.
(4) To enhance the observation and monitoring of the cryosphere in support of process studies, model evaluation, and change detection.

Specific questions that help define the primary tasks of CliC are:

(i) How stable is the global cryosphere?
    - How well do we understand and model the key processes involved in each cryospheric component of the climate system?
    - How do we best determine the rates of change in cryospheric components?
(ii) What is the contribution of glaciers, ice caps, and ice sheets to changes in global sea level on decadal to century timescales? And how can we reduce current uncertainties in these estimates?
(iii) What changes in frozen ground regimes can be anticipated on decadal to century timescales that would have major socio-economic consequences, either directly or through feedback on the climate system?
(iv) What will be the annual magnitudes, rates of change, and patterns of seasonal redistribution in water supplies from snow-fed and ice-fed rivers under climate changes?

Table 6.1. Areal and volumetric extent of major components of the cryosphere.

Component	*Area* (10^6 km^2)	*Ice volume* (10^6 km^2)	*Sea level equivalent*[a] (m)
Land snow cover[b]			
Northern Hemisphere			
Late January	46.5	0.002	
Late August	3.9		
Southern Hemisphere			
Late July	0.85		
Early May	0.07		
Sea ice			
Northern Hemisphere			
Late March	14.0[c]	0.05	
Early September	6.0[c]	0.02	
Southern Hemisphere			
Late September	15.0[d]	0.02	
Late February	2.0[d]	0.002	
Permafrost (underlying the exposed land surface, excluding Antarctica and Southern Hemisphere high mountains)			
Continuous[e]	10.69	0.0097–0.0250	0.024–0.063
Discontinuous and sporadic	12.10	0.0017–0.0115	0.004–0.028
Continental ice and ice shelves			
East Antarctica[f]	10.1	22.7	56.8
West Antarctica and Antarctic Peninsula[f]	2.3	3.0	7.5
Greenland	1.8	2.6	6.6
Small ice caps and mountain glaciers	0.68	0.18	0.5
Ice shelves[f]	1.5	0.66	—

[a] Sea level equivalent does not equate directly with potential sea level rise, as a correction is required for the volume of the Antarctic and Greenland ice sheets that are presently below sea level. The melting of 400,000 km^3 of ice is equivalent to a rise in global sea level of 1 m.

[b] Snow cover includes that on land ice, but excludes snow-covered sea ice.

[c] Actual ice areas, excluding open water. Ice extent ranges between approximately 7.0 and 15.4×10^6 km^2.

[d] Actual ice area excluding open water. Ice extent ranges between approximately 3.8 and 18.8×10^6 km^2. Southern Hemisphere sea ice is mostly seasonal and generally much thinner than Arctic sea ice.

[e] Data calculated using the Digital Circum-Arctic Map of Permafrost and Ground-Ice Conditions and the GLOBE 1 km Elevation Data Set.

[f] Ice sheet data include only grounded ice. Floating ice shelves, which do not affect sea level, are considered separately.

Table 6.2. Examples of socio-economic sectors affected by changes in the cryosphere.

Socio-economic component	*Cryosphere factor*
A. Direct effects	
Loss of coastal land and population displacement	
Transportation	Land ice melt contribution to sea level
Shipping	Iceberg hazard; sea ice extent, thickness
Barge traffic	Freshwater ice season
Tundra roads	Freshwater ice roads; frozen ground thaw
Road/Rail traffic	Freeze events; snowfall
Water resources	
Consumption	Snow/Glacier melt runoff
Irrigation	Snow/Glacier melt runoff
Hydropower	Snow/Glacier melt runoff
Agriculture	Moisture recharge extremes
Hydrocarbon and mineral resource development	Icebergs and sea ice; frozen ground duration and thickness
Wildlife population	Snow cover; frozen ground and sea ice
Recreation/safety	Snow cover; avalanches
B. Indirect effects	
Enhanced greenhouse	Thaw of clathrates
Traditional lifestyles (Arctic, sub-Arctic and high mountain)	Changes in sea ice and freshwater ice, snow cover, and frozen ground
Tourism/Local economies	Loss of glaciers; shorter snow season
Insurance sector	Changes in risk factor

(v) What will be the nature of changes in sea ice mass balance in both polar regions in response to climate change?
(vi) What is the likelihood of abrupt climate changes resulting from regime changes in ice shelf–ocean and sea ice–ocean interactions that impact oceanic thermohaline circulation?
(vii) How do we monitor cryospheric components as indicators of change in the climate system?

Monitoring cryosphere dynamics is a key aspect of high-latitude environmental studies (Kondratyev *et al.*, 1996; Kondratyev and Cracknell, 1998), especially because of the controversial information concerning ice cover dynamics. This is particularly

true, for instance, for ice thickness observations. Holloway and Sou (2001) pointed out that "while the range of numerical experiments indicate modest reduction in ice area, similarly to satellite-derived area reduction over 1979–1999, some experiments exhibit only moderate thinning. This contradicts the rapid thinning reported from submarine observations. Either the model results are systematically flawed or inferences previously drawn from submarine data are misleading. Exploring a wide range of model cases has not revealed systematic errors in model formulation. We turn to the question of whether we have been misled by the submarine data."

The exploration strategy for the Arctic region in a broad context of biospheric studies was discussed in detail by Matishov (1998, 2000) and Matishov and Matishov (2001), where the need for an ecosystem approach to studying land and marine biota was particularly emphasized and to studying conditions of socio-economic development in high-latitude regions. Aibulatov (2000) and Matishov and Matishov (2001) discussed general problems of high-latitude environmental dynamics with special emphasis on radioactive pollution as a left-over of the Cold War. Aibulatov (2000) analyzed the principal sources of artificial radioisotopes in the Russian Arctic seas such as atomic explosions at Novaya Zemlya, the global radionuclide background as a result of worldwide nuclear tests, Russian chemical and mining plants, the Chernobyl accident, West European radiochemical plants, solid and liquid radioactive waste dumping in the Barents and Kara Seas, the Northern Military Marine and its bases, atomic submarine construction and maintenance facilities, and Atomflot (the atomic fleet) of the Murmansk Shipping Company.

Studying the distribution of ^{137}Cs, ^{90}Sr, and ^{239,240}Pu in the water masses of the North, Norwegian, Barents, Kara, White and Laptev Seas has resulted in the following conclusions (Aibulatov, 2000).

(1) The general level of radioactive contamination of the waters of Arctic seas, except for several local areas, is characterized at the present time by little difference in comparison with the background level ($\sim$6 Bq/kg).
(2) Radioactive pollution of the water in the North and Norwegian Seas is entirely due to emissions from radiochemical plants located in Western Europe.
(3) The contamination of water in the Barents, White, Kara, and Laptev Seas is due to both local (Russian) sources and West European plants.
(4) Field observations in the Kara Sea in 1992–1995 have resulted in the conclusion that there have been no substantial emissions from radioactive burial sites in the area.
(5) The contribution of Ob′ and Yenisey River runoff to overall radioactive transport is not significant at the present time, except during extremely heavy floods, which happen very rarely.
(6) Compared with the open water of the Arctic Ocean, the shelf seas of the Russian Arctic are more heavily contaminated.

Aibulatov (2000) pointed out that, judging from the ^{137}Cs distribution patterns in the Kara Sea, it becomes evident that the Yenisey and Ob Rivers (less evident, however, in the latter case) should be considered as transport channels for inputs

of technogenic radionuclides to Arctic Ocean water. There are radioactive sources in the ocean as well. The ^{137}Cs activity level reached its maximum in 1984 and was equal to 245 Bq/kg (in the open sea); during the 1990s (1993) this level was found to be equal to 100 Bq/kg (in the Yenisey estuary).

Arctic fjords have been classified into categories of comparatively clean, contaminated, heavily contaminated, and potentially contaminated. Contaminated areas include, for instance, Kola Gulf and, probably, all the fjords of the northern Kola Peninsula west of Murmansk. The content of radionuclides in phytobenthos, in the coastal zone east of Murmansk, is low. Evidently, there has not recently been any serious radionuclide penetration into this area. The low gamma-nuclide level (1 Bq/kg–3 Bq/kg) is typical for the zoobenthos of the Barents Sea. This is also true for the Kara Sea.

The impact of all the sources of radioactivity in the zone of the Arctic coast on the local population has not been assessed reliably enough. It was particularly difficult to separate the natural and anthropogenic components of such an impact. Aibulatov (2000) discussed future research into Russian Arctic radioactive pollution, including

- Development of a coordinated Russian Arctic Sea radioactivity ecological monitoring program.
- Assessments of the impacts of different radioactive sources on contamination of the Arctic marine environment including water basins, land, and atmosphere.
- Studies of the detailed spatiotemporal variability of various long-lived technogenic radionuclides in bottom sediments.
- A detailed examination of all Novaya Zemlya fjords in connection with the dumping of radioactive waste.
- Research of the impact of radioactive pollution on the dynamics of the Arctic marine ecosystem.
- Studying the medical aspects of environmental pollution in the Arctic.

The fundamental study of radioactivity in Arctic and sub-Arctic marine ecosystems was undertaken by Matishov and Matishov (2001), which resulted in substantiation of a new branch of science: radiational ecological oceanology. Investigations were conducted into the level of artificial radionuclide concentration in both the environment and biota of bays and inlets (the Kola, the Chernaya, the West Litsa), where radioactively dangerous objects are located. In this context, a classification was suggested for coastal areas (bays, gulfs, fjords) in accordance with contamination levels for bottom sediments. The discovery of a biofilter in both the pelagic zone and the coastal zone during the processes of self-cleaning of water reservoirs and transport of radionuclides from water to bottom sediments is of major importance. For the first time the levels of ^{137}Cs, ^{90}Sr, and $^{239,240}Pu$ concentrations for different types and populations of sea organisms have been measured. In addition, migrations of radioisotopes along the trophic chains (from macrophytes and plankton to zoobenthos, fish, birds, seals, and whales) were studied. The assessments of comparative contributions of global, regional, and local sources of radioactive

environmental contamination since the time of nuclear tests up to the present day were analyzed and used as a source of information for environmental prediction. An important optimistic conclusion concerning the consequences of potential accidents is that for all prescribed scenarios of radioactive emissions, it is highly improbable that large-scale contamination of the Arctic Ocean will take place with ruinous impacts on marine bioresources. High biological assimilation capacity in combination with specific features of hydrodynamic and other processes is expected to serve as a barrier against dangerous pollution of the Arctic Ocean.

Kalabin (2000) accomplished a study of the environmental dynamics and industrial potential of the Murmansk region, the most urbanized and industrially developed trans-polar region on the planet. Under these conditions, certain features of environmental dynamics are affected by increased anthropogenic impacts. In this context, Kalabin (2000) analyzed critical environmental loads for some of the northern ecosystems and emphasized the need to investigate their assimilation (buffer) capacity as a principal aspect for the sustainable functioning of natural systems. The solution to regional problems of sustainable development requires a careful analysis of the interaction between ecodynamics and socio-economic development.

The progress achieved in studying Arctic environment variability is due to the accomplishment of a number of international research programs. Of particular importance is the Arctic Climate System Study (ACSYS) project set up in 1991 by the WCRP as a practicable program for the next decade to assess the role of the Arctic in the global climate. Five areas were emphasized:

(1) ocean circulation;
(2) sea ice climatology;
(3) the Arctic atmosphere;
(4) the hydrological cycle; and
(5) modeling.

The scientific goals of ACSYS, which started its main observational phase in January 1994 and will continue for a 10-year period, includes three main objectives (ACSYS, 1994):

(1) understanding the interaction between Arctic Ocean circulation, ice cover, and the hydrological cycle;
(2) initiating long-term climate research and monitoring programs for the Arctic; and
(3) providing a scientific basis for accurate representation of Arctic processes in global climate models.

The Arctic Ocean Circulation Program of ACSYS consists of four components:

(1) the Arctic Ocean Hydrographic Survey, to build up a high-quality hydrographic database that is representative of the Arctic Ocean;
(2) Arctic Ocean Shelf Studies, which are aimed at understanding how shelf processes partition saltwater and freshwater components and at defining the dynamics and thermodynamics of shelf waters as well as other processes;

(3) the Arctic Ocean Variability Project, designed to assess variability in the circulation and density structure of the Arctic Ocean; and
(4) the Historical Arctic Ocean Climate Database Project, aimed at establishing a universally available digital hydrographic database for the Arctic Ocean for analysis of climate-related processes and variability, and to provide a data set suitable for initialization and verification of Arctic climate and circulation models.

The ACSYS sea ice program includes three main components:

(1) establishing an Arctic Basin-wide sea ice climatology database;
(2) monitoring the export of sea ice through the Fram Strait; and
(3) Arctic sea ice process studies.

One of the main tasks of the ACSYS Arctic sea ice program is to establish the climatology of ice thickness and ice velocity. Data about this will be supplied by the WCRP Arctic Ice Thickness Project, the International Arctic Buoy Program, sonar profiling from naval submarines and unmanned vehicles, airborne oceanographic lidar, and polar satellites carrying appropriate instruments.

The Arctic atmosphere provides the dynamic and thermodynamic forcing underlying the circulation of the Arctic Ocean and sea ice. Key directions of research include such problems as cloud–radiation interaction, air–sea interaction in the presence of ice cover (impacts of polynyas and leads are of special interest), Arctic haze, etc.

The primary ACSYS efforts within the Hydrological Cycles project in the Arctic region are aimed at

(1) the documentation and intercomparison of solid precipitation measurement procedures used in high latitudes; and
(2) the development of methodologies for determining areal (regional) distributions of precipitation from station data.

There are two relevant data-archiving efforts: the Arctic Precipitation Data Archive (APDA) and Arctic Run-off Data Base (ARDB).

The principal purpose of the ACSYS Modeling Program is the simulation of climate variation in polar regions which arise from the interaction between atmosphere, sea ice, and ocean.

Apart from these ACSYS projects, a number of new research programs have been developed, such as the Study of Environmental Arctic Change (SEARCH), which is an interdisciplinary, multi-scale program dedicated to understanding the complex of interrelated changes that have been observed in the Arctic environment in the past few decades (Morison, 2001; Morison and Calder, 2001). SEARCH is envisioned as a long-term effort of observations, modeling, process studies, and applications with emphasis on five major thematic areas:

- human society;
- marine/terrestrial biosphere;
- atmosphere and cryosphere;
- ocean, and
- integrated projects/models/assessment.

The Arctic System Science (ARCSS) Program (ARCUS, 1998a, b) is an interdisciplinary program with the principal goals of (1) understanding the physical, geological, chemical, biological, and sociocultural processes of the Arctic system that interact with the global system and thus contribute to or are influenced by global change, in order to (2) advance the scientific basis for predicting environmental change on a seasonal to centennial timescale, and for formulating policy options in response to the anticipated impacts of global change on humans and societal support systems. The following four scientific thrusts are considered the central aims of ARCSS:

- to understand the global and regional impacts of the Arctic climate system and its variability;
- to determine the role of the Arctic in global biogeochemical cycling;
- to identify global change impacts on the structure and stability of Arctic ecosystems; and
- to establish the links between environmental change and human activity.

ARCSS has four linked ongoing components: Ocean/Atmosphere/Ice Interactions (OAII); Land/Atmosphere/Ice Interaction (LAII); Paleoenvironmental Studies, which include the Greenland Ice Sheet Project 2 (GISP2) and Paleoclimates of Arctic Lakes and Estuaries (PALE); Synthesis, Integration, and Modeling Studies (SIMS), and Human Dimensions of the Arctic System (HARC). Aagard (1998) discussed basic problems by taking a multidisciplinary look at the Arctic Ocean, including physical and chemical studies, biological studies, contaminant studies, measurement of the properties and variability of the ice cover and of the surface radiation budget, studies of atmospheric chemistry, and geological observations.

LAII research has three main goals:

(1) to estimate important fluxes in the region, including the amount of carbon dioxide and methane reaching the atmosphere, the amount of river water reaching the Arctic Ocean, and the radiative flux back to the atmosphere;
(2) to predict how possible changes in the Arctic energy balance, temperature, and precipitation will lead to feedback affecting large areas; this incorporates changes in water budget, duration of snow cover, extent of permafrost, and soil warming, wetting, and drying; and
(3) to predict how the land and freshwater biotic communities of the Arctic will change, and how this change will affect future ecosystem structure and function.

A major LAII research project is the Flux Study, whose principal purpose is a regional estimate of the present and future movement of material between the land, atmosphere, and ocean in the Kuparuk River basin in northern Alaska.

Of the 19 LAII projects 3 are part of the International Tundra Experiment (ITEX), which looks at the response of plant communities to climate change. Three others are concerned with atmosphere processes, including weather patterns affecting snowmelt, Arctic-wide temperature trends, and water vapor over the Arctic and its relationship with atmospheric circulation and surface conditions. Another project deals with the response of birds to climate and sea level change at river deltas, and yet another studies the balance and recent volume changes of McCall Glacier in the Brooks Range.

Synthesis, integration, and modeling studies are intended to foster linkages and system-level understanding. Research on both the past and contemporary relationship between humans and global climate change is thought to be critical to understanding the consequences of global change in the Arctic.

There are a number of ARCSS data projects that provide CDs. They include the LAII Flux Study Alaska North Slope (data sampler CD); OAII Northeast Water (NEW) Polynya project CD; Arctic solar and terrestrial radiation CD, etc.

A list of major OAII components includes the joint U.S./Japan Cruise, the Western Arctic Mooring project, and the Northeast Water Polynya project (mentioned above). Among other OAII projects the most notable are the U.S./Canada Arctic Ocean Section and the Surface Heat Budget of the Arctic Ocean (SHEBA) project.

An outstanding feat was accomplished in 1994 within the Canada/U.S. 1994 Arctic Ocean Section when two icebreakers entered the ice in the northern Chukchi Sea on July 26, 1994, reached the North Pole on August 22, and left the ice northwest of Spitsbergen on August 30, thereby completing the first crossing of the Arctic Ocean by surface vessels. This voyage greatly altered our understanding of biological productivity, the food web, ocean circulation and thermal structure, and the role of clouds in the summer radiation balance, as well as the extent of contamination and spreading pathways of radionuclides and chlorinated organics, and the extent and effects of sediment transport by sea ice.

In connection with the SHEBA project, the U.S. Department of Energy's Atmosphere Radiation Measurement (ARM) program indicated its intention to develop a Cloud and Radiation Testbed (CART) facility on the North Slope of Alaska. The principal focus of this program will be on atmospheric radiative transport, especially as modified by clouds (such transport impacts the growth and decay of sea ice), as well as testing, validation, and comparison of radiation transfer models in both the ice pack and Arctic coastal environment.

Another important project is the Russian–American Initiative on Shelf–Land Environments in the Arctic (RAISE) with the principal goal of facilitating ship-based research in the Russian Arctic (Cooper and Romanovsky, 2001). Earlier relevant land-based research projects under the RAISE umbrella included studies of

- organic material and nutrient fluxes from Russian rivers;
- seasonal flooding dynamics along rivers; and
- reconstruction of the late Pleistocene glacial and sea level history of Wrangel Island.

New scientific topics in the near-shore waters of the Russian continental shelf will include a broad range of studies: from the biogeochemical fate of organic material contributed to the Arctic Ocean by shoreline erosion and river run-off to the social and biological impacts of changes in sea ice distribution.

The Western Arctic Shelf–Basin Interactions (SBI) project, sponsored by the ARCSS Program and the U.S. Office of Naval Research, is investigating the Arctic marine ecosystem to improve our capacity to predict environmental change. The SBI Phase II Field Implementation Plan (2002–2006) (Grebmeier *et al.*, 2001) focuses on three research topics in the core study area:

- northward fluxes of water and bioactive elements through the Bering Strait input region;
- seasonal and spatial variability in the prediction and recycling of biogenic matter on the shelf slope area; and
- temporal and spatial variability of exchanges across the shelf slope region into the Canada Basin.

A meeting of the International Arctic Science Committee (IASC) identified the following four science priorities:

(1) Arctic processes relevant to global systems;
(2) effects of global change on the Arctic and its peoples;
(3) natural processes within the Arctic; and
(4) sustainable development in the Arctic.

The following areas in Arctic global change research were considered the most significant:

(1) terrestrial ecosystem;
(2) mass balance of glaciers and ice sheets;
(3) regional cumulative impacts; and
(4) human dimensions.

An important aspect of studying high-latitude environmental dynamics is assessment of the impact of potential anthropogenic climate warming. In this context Frederick (1994) formulated the key issues to be considered when integrating assessments of the impact of climate change on natural resources. Specific project objectives include

(1) characterizing the current state of natural science and socio-economic modeling of the impacts of climate change and current climate variability on forests, grassland, and water;
(2) identifying how current impact assessments can be used and how to undertake such assessments;

(3) identifying impediments to linking biophysical and socio-economic models as integrated assessments for policy purposes; and
(4) recommending research activities that will improve the state of the art and remove impediments to model integration.

The following questions need to be answered:

- How will the overall system (physical–biological–economic) respond to various imposed stresses?
- What effect(s) do uncertainties in the component models give to overall system response uncertainty?
- Is society made more vulnerable to extreme natural events either by changing those events or by reducing the human ability to respond with corrective action?
- How likely is it that the consequences of climate change will be severe or catastrophic?
- What is at risk and when is it at risk?
- What are the likely impacts on the landscape and the hydrological system?
- How might the boundary conditions and the overall productivity of forests, grassland, and other rangeland be affected?
- How might increasing carbon dioxide levels affect crops and food supplies for humans, livestock, and wildlife?
- What are the socio-economic consequences of these physical and biological changes?
- What are the likely consequences for ecosystems of mitigation actions?
- Can the costs associated with climate change be reduced through natural adaptation of ecosystems or policy-initiated adaptation?

Frederick (1994) emphasized that the accumulated results of many regional and local climate impact assessments may help provide informed answers to these questions. Nevertheless, the uncertainties surrounding both the nature and the impacts of any future climate change are likely to remain very large, precluding precise estimates of the net benefits associated with alternative policy responses. Even if the range of uncertainty were diminished, it might still be difficult to justify specific measures on narrow economic grounds because (as noted above) the impacts on natural resource systems are apt to be poorly reflected in standard benefit–cost analysis.

Mendelsohn and Rosenberg (1994) asked the following questions regarding global-warming effects on ecological and water resources:

- Do changes in ecosystems provide important feedbacks to the natural carbon, nitrogen, and methane cycles? For example, will the natural sinks or emitters be affected by changing precipitation, temperature, and CO_2 levels?
- What are the appropriate output measures of ecosystem component models? What are the ecological effects of climate change that policy analysts use to determine the importance of ecosystem change?
- What climate change–driven shifts in ecosystem boundaries can be predicted?

- Will these effects be subtle and small or large and dramatic and over what time frame and spatial dimensions?
- Will climate change cause a change in the productivity of valuable market or non-market species? For example, to what extent will some forests grow more quickly or more slowly. Will non-market species, such as bear, elk, and bald eagles, be more or less plentiful?
- What species could be lost with rapid climate change? How do vulnerable species break down by type and geographic distribution? How should conservation policies adapt to a world requiring change?
- How are ecosystems likely to change as the climate evolves over time? Will there be a large increase in early succession species and where?
- How will average flows in rivers change with greenhouse warming? How will these flows change over seasons? Will the probabilities of catastrophic events change?
- What values do people assign to changes in ecosystems by climate change? Which changes are important and which are minor? Can a value be assigned to non-use?
- How much should society be willing to pay to reduce the probability of losing specific species? If different scenarios favor different species, how should society trade between these outcomes?
- What impact does ecosystem change have on the economy? For example, how will climate change affect grazing, commercial fishing, timber, or commercial tourism?

Goldman (1999) suggested the following priority program areas and relevant projects:

(a) Impacts of global change on the Arctic region and its peoples:
  – regional cumulative impacts
  – effects of increased UV radiation.
(b) Arctic processes of relevance to global systems:
  – mass balance of glaciers and ice sheets
  – terrestrial ecosystems and feedback on climate change.
(c) Natural processes within the Arctic:
  – Arctic marine/coastal/riverine systems
  – disturbance and recovery of terrestrial ecosystems.
(d) Sustainable development in the Arctic:
  – sustainable use of living resources
  – dynamics of Arctic populations and ecosystems
  – environmental and social impacts of industrial development.

Future priorities of the ARCSS include the following research questions (ARCUS, 1998a, b): How will the Arctic climate change over the next 50 to 100 years? How will human activities interact with future global change to affect the sustainability of natural ecosystems and human societies? How will changes in Arctic biogeochemical cycles and feedbacks affect Arctic and global systems? How will

changes in Arctic hydrological cycles and feedbacks affect Arctic and global systems? Are predicted changes in the Arctic detectable?

Important perspectives are connected with the paleo-environmental studies by the Paleoenvironmental Arctic Science (PARCS) community (MacDonald *et al.*, 2001) which have the principal aim of answering the question: To what extent do recent observations of climate change in the Arctic reflect natural climate cycles? Relevant major topics include:

- the Medieval Warm Period (approximately AD 1000–1400) and Little Ice Age (approximately AD 1400–1850);
- high-amplitude Holocene climate cycles; and
- the possible connection between the onset of neoglacial (a mid-Holocene cooling, particularly evident at high northern latitudes) and shifts in the frequency and amplitude of such climate cycles.

According to the PARCS community, there are very warm past scenarios that can serve as analogs for future climate warming:

- the early Holocene, when the Arctic experienced high summer insolation anomalies; and
- the last interglacial period (Marine Isotope Stage 5), which appears as a very strong warming in the paleorecord approximately 125,000 years ago.

Key topics to investigate in relation to these periods are

- feedbacks and non-linear changes (surprises) as consequences of strong warming, particularly the role of sea ice, ice sheets, and land surface cover; and
- implications of strong warming for Arctic and global carbon budgets.

To summarize, despite the many recent Arctic environmental programs, it must be emphasized that relevant information cannot be considered exhaustive (IASC, 2001). An obvious conclusion is that the number of programs is too great. There is a clear need for better co-ordination of all ongoing efforts and their ''regularization''.

Vörösmarty *et al.* (2001) are right in their conclusion that

> ''understanding the full dimension of arctic change is a fundamental challenge to the scientific community over the coming decades and will require a major new effort at interdisciplinary synthesis. It also requires an unprecedented degree of international cooperation.''

Undoubtedly, there is an urgent need for a Second International Polar Year.

6.2 THE ARCTIC BASIN AND ITS ROLE IN GLOBAL CHANGES

The Arctic Basin plays a special role in the formation of global processes in the environment, determining numerous feedbacks in the Earth's climate system. Decreased temperatures, the high level of atmospheric circulation, and the presence of large ice-covered water bodies, all this distinguishes high latitudes from other latitudes of the globe.

The intensive development of the northern territories of Russia, Canada, the U.S.A., and the Scandinavian countries has led to a considerable change in the natural conditions of these regions. Development of the oil and gas industry in the Yamal Peninsula, Taymyr Island, and in northwestern Siberia, and coal mining and gold mining in Yakutia and Chukotka, as well as mining on the Kola Peninsula, make the northern territory of Russia one of the most dangerous territories for the Arctic environment.

Over some territories of the Arctic, vegetation cover has been violated; the areas and productivity of reindeer pasture have been reduced. The hydrological regime of Arctic rivers has markedly changed, too. Pollutants are taken with river run-off to the coastal zones of the northern Russia, which influences the functioning of Arctic Basin ecosystems.

Any further influence on vulnerable Arctic ecosystems will likely lead to negative consequences, possibly global in scale. Therefore, the problem of human development of the northern territories, especially in Russia, requires a thorough analysis of the dynamics of all types of ecosystems, formation of a database on their current state, and development of efficient ways of co-ordinating the development of both natural and anthropogenic processes. The following directions to be taken by any further development of the northern territories are now clearly seen:

(1) Intensive development and differentiation by territorial indicators of known and future deposits for mining and energy.
(2) Formation of reserves, national parks, and other forms of ecosystem protection in the northern territories.

Realizaton of these directions needs the development of a means of monitoring the system (e.g., a renewable database). The monitoring system should be able to trace violations of the ecosystem's balanced state and anthropogenically violated landscapes as well as assess the state of the habitat of animals and humans in the northern territories. In this connection, the following studies should be carried out first:

- the complex monitoring of land territories and sea basins to create a cadastre[2] of land resources and a database of the parameters of biocenoses and ecosystems;

[2] A registry of real estate.

- study of the social problems faced by nomadic people in the northern latitudes, and evaluation of the damage to their habitat;
- regioning the northern territories on the basis of the landscape–basin–administrative principle of settling nomadic people, but taking the migration of reindeer and reindeer farmers into account;
- revealing and ranging the functional problems facing the systems of nature protection.

First of all, all violations of land cover, landfill sites, polluted territories, routes taken by oil and gas pipelines, sources (known and hypothetical) of pollutants of soil, water, and atmosphere, zones of flooding as a result of anthropogenic activity should be brought to light and included in databases. Estimates of some parameters of the systems of the Arctic Basin are given in Tables 6.3 through 6.5.

These problems are considered from different aspects in the many international and national programs that are studying the environment. For example, in 1991 the U.S.A. launched the ARCSS program (Arctic Science System: Land/Atmosphere/Ice Interaction) as part of the Global Change international program initiated at the U.S. National Science Foundation (McCauley and Meier, 1991). The main goal of this program is to develop methods, technologies, algorithms, and software, to facilitate evaluation of the sensitivity of global oscillations in the NSS to changes in its Arctic

Table 6.3. Estimates of some parameters of the Arctic Basin.

Parameter	*Available estimate of the parameter*
Area of the Arctic basin (10^6 km^2)	16.23
Flows of water masses through straits (10^3 m^3 yr^{-1})	
Faroe–Shetland	+135; −45
Denmark	+30; −130
Bering	±1.8
Faroe–Iceland	+40
Ice salinity (‰)	
one-year (≈150 cm)	5
multi-year (≈3 m)	1
River run-off (km^3/yr)	
Yenisey	603
Ob′	530
Lena	520
Mackenzie	340
Pechora	130
Kolyma	132
Northern Dvina	110
Outflow from freshwater basins with ice (km^3/yr)	1,500

Table 6.4. Characteristics of Arctic Basin water bodies.

Water body	*Area* (10^3 km^2)	*Volume* (10^3 km^2)	*Depth*	
			Average	*Maximum*
Central Basin	4,977	12,442	2,500	4,000
Barents Sea	1,424	316	222	600
Greenland Sea	1,195	1,961	1,641	5,527
Norwegian Sea	1,340	2,325	1,735	3,970
White Sea	90	6	67	350
Baffin Bay			200	700
Kara Sea	893.4	101	113	600
Chukchi Sea	582	23	40	60
East Siberian Sea	944.6	18	20	30

sector. Essentially, the ARCSS program should provide understanding of the role of physical, geological, chemical, biological, and social processes taking place in the Arctic region, in global changes to the environment, and to create thereby the scientific basis for solution of the major problem of predicting such changes on different timescales, from annual to centennial. The U.S. Biocomplexity national program launched in 2000 supplements the goals above, extending them to the global scale. Within this program, plans are being made to study and understand correlations between the complexity of biological, physical, and social systems and trends in changes of the present environment. The complexity of the system, no matter how it interacts with the environment, is a phenomenon that occurs as a result of contact between living systems and their environment under global conditions.

Table 6.5. Characteristics of the freshwater balance of Arctic Basin water bodies.

Water body	*Area* (10^3 km^2)	*Supply of freshwater in ice* (km^3)	*Volume of melted freshwater* (km^3/yr)
Central Basin	4,977	13,000	1,990
North European Basin	4,065	2,470	1,170
Seas of the Siberian Shelf	3,025	5,330	2,260
Canadian Basin	2,632	4,700	1,800

Biocomplexity is a derivative of the biological, physical, chemical, social, and behavioral interactions of environmental sub-systems, including living organisms and the global population. As a matter of fact, the notion of biocomplexity in the environment is closely connected with the rules of biosphere functioning which unites ecosystems and natural–economic systems at different scales, from local to global (Kondratyev, 1999a, b). Therefore, to determine biocomplexity and to assess it, a combined formalized description is needed of the biological, geochemical, geophysical, and anthropogenic factors and processes taking place at a given level of the spatiotemporal hierarchy of units and scales.

Biocomplexity is a characteristic feature of all systems of the environment connected with life. The ways in which this is manifested are studied within the framework of the theory of stability and vitality of ecosystems. Note that biocomplexity includes indicators of the extent to which interacting systems modify each other, and this means that biocomplexity should be studied by considering both the spatial and biological levels of its organization. The difficulty of this problem is explained by the complicated behavior of the object under study, especially when the human factor is considered, due to which the number of stress situations in the environment is constantly growing. Within this study the Arctic systems are considered as NSS sub-systems.

The problem of routine monitoring of the northern territories and water bodies of the Arctic Basin is far from being solved. Understanding this, in 1992 the Institute of Marine Science (University of Alaska Fairbanks), the Environment and Natural Resources Institute (University of Alaska Anchorage), the Institute of Ecoinformatics (Russian Academy of Natural Sciences), the Institute of Radioengineering and Electronics (Russian Academy of Sciences), the Russian Institute for the Monitoring of Lands and Ecosystems, and the Insitute of Oceanology (Russian Academy of Sciences) developed a program to synthesize a system for geoinformation monitoring of the Arctic (Krapivin, 1999a, b; Kelley *et al*., 1992, 1999). In recent years, attempts have been made to consolidate the efforts of scientists from both countries to solve these problems. The results of these efforts have been reflected in joint publications, three international symposia, and two Russian–American ecological expeditions in Siberia (Krapivin *et al*., 1997; Phillips *et al*., 1997).

Understanding and prediction of correlations between the processes taking place in the Arctic environment and in other global regions is only possible within the complex scientific–technical approach to a study and analysis of these processes, by means of the balanced use of observational and theoretical studies and using satellite, aircraft, mobile and stationary measurements from the ground, such as GIS and GIMS technologies.

Interactions between the atmosphere, land, and marine ecosystems in the Arctic climate are characterized by a range of spatiotemporal scales; understanding the internal bonds at each level is the key objective of monitoring. Each scale is characterized by a certain type of Earth landscape: vegetation cover, topography, character of hydrological and synoptic structures, and the animal kingdom. Revelation of internal and external cause-and-effect bonds between these elements and other components of the global NSS will make it possible to form a database for any future

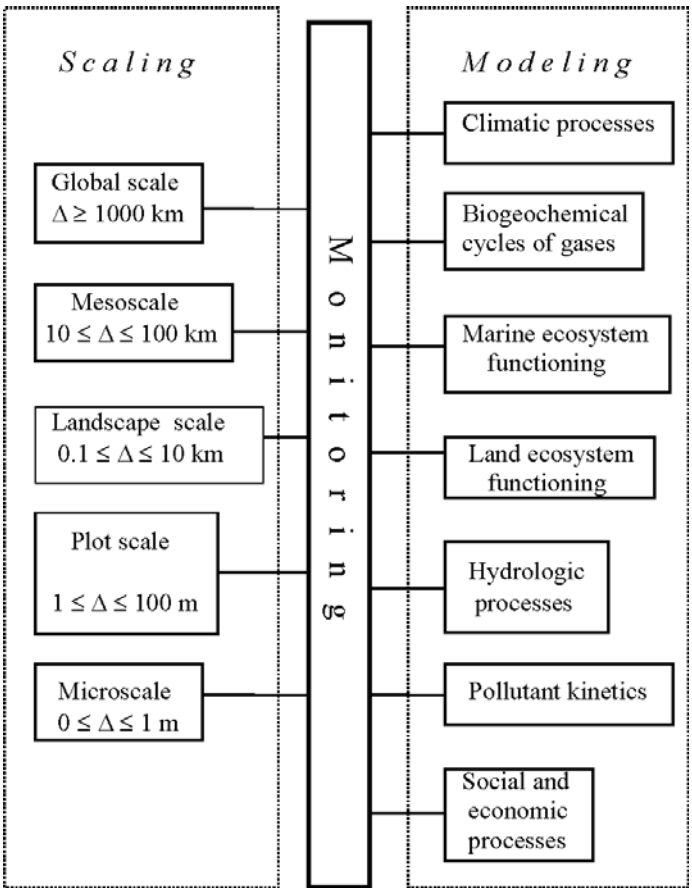

Figure 6.1. Conceptual scheme of environment monitoring for northern latitudes. It reflects the correlations between spatial scales and the problems facing studies attempting to understand the functioning of the Arctic.

geoinformation system aimed at monitoring the Arctic. Figure 6.1 explains the methodology behind the study of these bonds.

The methodology, which combines the means of remote and ground monitoring with numerical modeling of processes shown in the right-hand part of Figure 6.1, was proposed in the works of Russian and American scientists (Krapivin *et al.*, 1996a, b; Krapivin and Phillips, 2001a, b). Its application will make it possible to obtain more accurate assessments of the role of Arctic latitudes in global processes taking place in the NSS. The current practice of considering land and marine processes separately should not impede complex studies. Present-day numerical models of NSS functioning are capable of overcoming this separation. Such models will make it possible to synthesize the migration of chemical elements in Arctic latitudes and to assess the consequences of large-scale anthropogenic processes in the northern territories.

Revelation of critical situations and processes is another problem that faces the complex system of monitoring the Arctic region.

Essentially, this concerns formation of a software package. the input to which will be data on the spatial distribution of land and marine ecosystems, as well as sets of scenarios of anthropogenic processes and climatic trends. Such a database will be continuously updated and provide sequences of models to provide reliable forecasts of the dynamics of these ecosystems and will facilitate realization of hypothetic scenarios for Arctic environmental control.

The successful solution of some of these problems can be exemplified by the 3-D model that calculates the dynamics of radionuclide pollution of the Arctic Basin (Preller and Cheng, 1999) and the 2-D model of the ice condition of Arctic Ocean basins (Riedlinger and Preller, 1991).

6.3 ARCTIC BASIN POLLUTION PROBLEM

The purpose of this section is to develop and investigate a model to simulate the pollution dynamics in the Arctic Basin. There are many experimental and theoretical results giving estimates of the growing dependencies between the pollution dynamics in the World Ocean and that of the continental environment. The problem of Arctic Basin pollution is problematic for investigators (Krapivin and Phillips, 2001a, b). The ecosystems of the Arctic seas are known to be more vulnerable than the ecosystems of other seas. The processes that clean the Arctic Ocean are slower, and marine organisms of the Arctic ecosystem live under polar climate conditions where the vegetation period is restricted. Some feedback mechanisms operate with significant time delays and their capacity to neutralize the effects of human activity is feeble. In addition to these reasons the Arctic ecosystem has specific boundary conditions connected with the sea ice ergocline which reduce the survivability level of pollution.

In connection with this, the Arctic Basin is the object of investigation in many national and international environmental programs, such as the International Geosphere–Biosphere Program, U.S. Global Change Research, the international Arctic System Science program (ARCSS), the U.S. Arctic Nuclear Waste Assessment Program (ANWAP), and the International Arctic Monitoring and Assessment Program (AMAP). The research strategies of these programs include the theoretical and experimental study of tundra ecosystems, Siberian rivers, and near-shore and open Arctic waters. The main problems consist in identifying the most important priorities for immediate study, including

(1) *Transport modeling of pollutants in Arctic ecosystems.* From the experimental database, it is necessary to prepare a complete set of models and corresponding computer realizations to describe the processes of transfer and transformation of pollutants in the Arctic's natural ecosystems. This set includes the following models:
   - a model of the transformation of organic pollution in the ecosystems of freshwater basins and streams;

- models of the self-cleaning processes for oil, radionuclides, heavy metals, and other pollutants;
- a model of radionuclide and heavy metal accumulation in the river ecosystems of the Far North;
- a model of the transport of radionuclide, heavy metal, and organic pollution from river flows into the coastal zones of Arctic waters;
- a model of pollution leaching out during the spring season in tundra and forest–tundra zones;
- a model of the kinetics and transformation mechanisms for biospheric elements in water systems;
- a kinetics model of radionuclides and heavy metals in the foodchains of the land ecosystems for boreal zones;
- a model of the surface flow of chemical elements and compounds from territories in zones with open-cast mines under the climatic conditions of the Far North; and
- a model of the seasonal influence of pollution on phytoplankton and primary production in northern seas.

(2) *Modeling the exchange processes of carbon dioxide and methane between tundra ecosystems and the atmosphere*. The global interaction of Arctic ecosystems with the biosphere and with the Earth's climatic system is carried out in particular through the influence on the biogeochemical cycles of carbon dioxide and methane. Existing models of the global circulation of these greenhouse gases are incomplete in that they do not take into account this interaction. Present estimations of the gas exchange between Arctic ecosystems and the atmosphere confirm, however, the necessity of making such an account. To create a model set related to the gas exchange in the Arctic reservoirs it is necessary to compile a catalog of soil–plant formations, ice fields, and land-based and oceanic reservoirs. It is necessary also to put in the database estimations of evapotranspiration, dead vegetation decomposition rate, and the productivity of vegetation communities. With the aid of this model set it will be possible to evaluate the role of tundra ecosystems in forming the greenhouse effect.

(3) *Modeling the hydrological regime and estimation of the pollutant flows in the Arctic Basin*. It is necessary to prepare a set of models to describe the dynamics of separate aquatories[3] and of the whole hydrosystem of the Arctic Ocean, including:

- a complex model of the water circulation in the Arctic Basin;
- regional models of the water circulation in Arctic seas;
- a model of the kinetics of radionuclides, heavy metals, and organic pollutants in the trophic structures of Arctic marine ecosystems;
- a model of the spread of pollutant concentration from a point-like source in the near-coastal zone of the Arctic Basin;
- a model of the transfer of radionuclides, heavy metals, and organic pollutants due to vertical mixing of Arctic waters; and

[3] By "aquatory" we mean the restricted ocean (or sea) area that is the subject for study.

- a model of the conservation and release processes due to freezing and thawing of the ice cover.

(4) *Modeling Arctic ecosystems as a result of anthropogenic impacts*. Anthropogenic influence in the Arctic Basin and on adjacent territories is connected with local, regional, and global activities. Therefore, it is necessary to construct models/scenarios that simulate:
- the influence of radionuclides, heavy metals, and oil hydrocarbons on the dynamics of marine ecosystems under Arctic climate conditions;
- the limit of vegetation cover due to the different types of pollution that are brought to land ecosystems by precipitation and surface flows;
- the dynamics of vegetation covers subjected to physical influence;
- town and settlement structures under development; and
- the changes in area of traditional seasonal regions of the activity of nomadic peoples;
- the social development of the scattered peoples in the Far North.2

(5) *Modeling the biogeochemical carbon cycle in the atmosphere–Arctic Ocean system*. As was shown by from experience of modeling the carbon dioxide global cycle, estimations of the role of the World Ocean in redundant carbon absorption are rather rough. For models to be more precise they need to be reinforced by more reliable parameterizations of the physical processes related to the interaction between the bordering layers of the atmosphere and Arctic aquatories. According to numerous laboratory and natural observations, the directivity of these processes depends considerably on many factors. The most significant of these are the speed of the driving wind, the presence of ice cover, and the vertical distribution profile of the water temperature. The complex composition of these factors determines the variety of possible models and their details. One significant problem is explanation of the powerful growth of seaweed during the spring season and hence to construct a parameterization system for the dynamics of photosynthetic processes under conditions of snow and ice cover and when they thaw in spring.

(6) *Development of a complex model to simulate the functioning of the hydrologic and biogeochemical systems in the Arctic*. In addition to the set of models intended for local and fragmentary processes in Arctic ecosystems, as well as for understanding their global role, it is necessary to synthesize a single model for the whole complex of biogeochemical, biogeocenotic, and hydrologic processes that occur in boreal systems. Creation of such a model will make it possible to obtain a means of estimating the consequences of anthropogenic projects. Using this model we can estimate the consequences of forest cutting and fires, of the broadening of zones with disturbed land cover, of land and basin pollution by oil, of hydrogeological changes in adjacent territories due to deliberate flooding of land, of territorial pollution by waste material from mining, etc.

(7) *Estimation of the stability of Arctic systems under variable global climate conditions*. Human activities in the delicate ecosystems of the Far North need to be conducted with great care. In this regard, two questions spring to mind:

- How can the natural balance be safeguarded from the rising influence of human civilization with all its industrial might?
- How can the survival of these ecosystems be evaluated in different situations?

These and other questions need to be answered as part of the program outlined above.

An understanding of the environmental processes in Arctic regions, a prerequisite to finding scientific solutions to the problems arising there, can be found only by combining many disciplines, including ecology, oceanography, mathematical modeling, and system analysis. This section synthesizes many data sources and knowledge from various scientific fields and take the form of blocks in the Spatial Simulation Model of the Arctic Ecosystem (SSMAE). Separate blocks of the SSMAE were created earlier by many authors (Riedlinger and Preller 1991; Muller and Peter 1992; Legendre and Krapivin 1992). The sequence of these blocks in the SSMAE structure and the adaptation of it to the Spatial Global Model (SGM) can act as the technology for computer experiments (Krapivin, 1993, 1995; Kondratyev *et al.*, 2000).

This investigation solves one of the problems of the ARCSS Program. The present chapter describes a simulation system based on sets of computer algorithms for processing data from the monitoring of Arctic regions and for applying mathematical models of natural and anthropogenic processes.

The basic blocks of the SSMAE are aimed at describing the dynamics of any given pollutant. For consideration of a specific pollutant it is necessary to include in the SSMAE an additional block describing its physical and chemical characteristics. This procedure can be demonstrated by examples of blocks that simulate the characteristics of radionuclides, heavy metals, and oil hydrocarbons. The consideration of these pollutants is restricted to elements with averaged properties.

The boundaries of the Arctic Basin water area Ω studied in this chapter include the peripheral Arctic seas as well as the coastline and southern boundaries of the Norwegian and Bering Seas.

6.4 APPLICATION OF MODELING TECHNOLOGY TO THE STUDY OF POLLUTANT DYNAMICS IN THE ARCTIC SEAS

6.4.1 Spatial simulation model of the Arctic ecosystem

A conceptual diagram and the block contents of the SSMAE are shown in Figure 6.2 and Table 6.6. The functioning of the SSMAE is supported by the SGM and by the Climate Model (CM) (Sellers *et al.* 1996). The inputs to the SSMAE comprise data about the pollutant sources of the near-shore Arctic Basin, ice areas, and current maps. The SSMAE contains three types of blocks: mathematical models of the natural ecological and hydrophysical processes, service software and a scenario generator. The marine biota block (MBB) describes the dynamics of energy flows in the trophic chains of the Arctic Basin ecosystem. The hydrological block (HB)

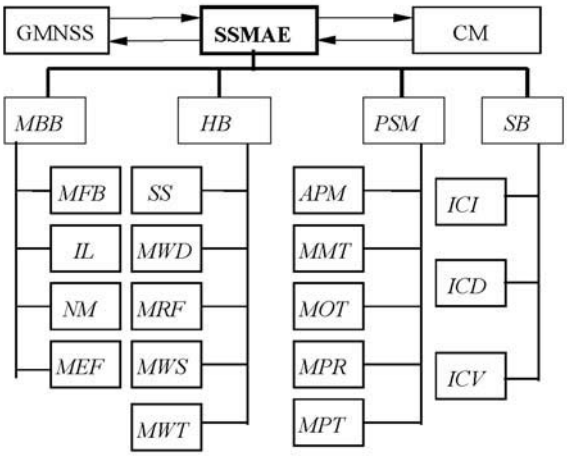

Figure 6.2. Block diagram of the SSMAE. Descriptions of the blocks are given in Table 6.6. CM is the climate model or the climate scenario.

describes the spatial discretization of Ω on water circulation in the Arctic. The pollution simulation model (PSM) contains anthropogenic scenarios and the service control block (SB).

Let us designate the Arctic Basin aquatory as $\Omega = \{(\varphi, \lambda)\}$ where φ and λ are latitude and longitude, respectively. Spatial heterogeneity of the Arctic Basin model is provided for by a set of cells $\Delta T_{CO_2}$with latitude and longitude steps $\Delta\varphi$ and $\Delta\lambda$, respectively. These cells are the basic spatial structure of Ω for the realization of computer algorithms. The cells Ω_{ij} are heterogeneous as to their parameters and functioning. There are a set of cells that are adjacent to river mouths (Ω_R) and to ports (Ω_P), bordering on land (Ω_Γ), in the Bering Strait (Ω_B) and on the south boundary of the Norwegian Sea (Ω_N). The water area Ω is divided in depth z by steps Δz. The distribution of depths is given as the matrix $H = \|h_{ij}\|$ where $h_{ij} = H(\varphi_i, \lambda_j)$, $(\varphi_i, \lambda_j) \in \Omega_{ij}$. As a result, the full water volume of Ω is divided into volumetric compartments

$$\Xi_{ijk} = \{(\varphi, \lambda, z) \,|\, \varphi_i \le \varphi \le \varphi_{i+1}; \lambda_j \le \lambda \le \lambda_{j+1}; z_k \le z \le z_{k+1}\},$$

with volumes $\sigma_{ijk} = \Delta\varphi_i \, \Delta\lambda_j \, \Delta z_k$. Within Ξ_{ijk} the water body is considered homogeneous in structure. The water temperature, salinity, density, and biomass of compartments Ξ_{ijk} are described by box models. The anthropogenic processes acting on water area Ω are described for the four seasons: τ_w winter, τ_s spring, τ_u summer, and τ_a autumn.

The procedure of spatial discretization is provided for via the ICI block of the SSMAE database, which includes a set of identifiers $A_k = \|a_{ij}^k\|$, where a_{ij}^k is the specific symbol that identifies a real element of Ω_{ij} in the computer memory. Identifier A_1 reflects the spatial structure of the Arctic Basin and adjoining territories ($a_{ij}^1 = 0$ for $(\varphi_i, \lambda_j) \notin \Omega$; $a_{ij}^1 = 1$ for $(\varphi_i, \lambda_j) \in \Omega$ when (φ_i, λ_j) belongs to the land (islands), and

Table 6.6. Description of the SSMAE blocks (Figure 6.2).

Block	*Description of the block*
MBB	Marine Biota Block, containing the set of models of energy flows in the trophic chains of the Arctic Basin ecosystem (Krapivin, 1995; Legendre and Legendre, 1998; Legendre and Krapivin, 1992).
HB	Hydrological Block, describing the water circulation in the Arctic seas and the movement of ecological elements (Krapivin, 1995, 1996).
PSM	Pollution Simulation Model of the Arctic Basin, including a set of anthropogenic scenarios (Krapivin, 1993, 1995).
SB	Service Block, to control the simulation experiment
APM	Air Pollution transport Model (Kondratyev and Varotsos, 2000; Krapivin, 1995; Muller and Peter, 1992).
MFB	Model of the Functioning of Biota under the conditions of energy exchange in the trophic chain of the Arctic Basin ecosystem (Legendre and Legendre, 1998; Legendre and Krapivin, 1992).
SS	Simulator of Scenarios, describing the ice fields, synoptic situations, and changes in hydrological regimes.
MWD	Model for the Water Dynamics of the Arctic Basin (Riedlinger and Preller, 1991).
MMT	Model for heavy Metal Transport through foodchains (Krapivin *et al*., 1998).
IM	The Illumination Model (Nitu *et al*., 2000b).
NM	The Nutrients Model (Legendre and Krapivin, 1992; Legendre and Legendre, 1998; Krapivin, 1996)
MPT	Model for Pollution Transport through water exchange between the Arctic Basin and the Atlantic and Pacific Oceans.
MOT	Model for the process of Oil hydrocarbon Transport to foodchains (Payne *et al*., 1991).
MPR	Model for the Process of Radionuclide transport to foodchains (Krapivin, 1995).
MRF	Model of River Flow to the Arctic Basin (Krapivin *et al*., 1998).
MWS	Model of Water Salinity dynamics (Nitu *et al*., 2000b).
MEF	Model for Energy Flow transport in the Arctic basin ecosystem.
MWT	Model for calculating Water Temperature (Nitu *et al*., 2000b).
ICI	Interface for Control of Identifiers.
ICD	Interface for Control of the Database.
ICV	Interface for Control of Visualization.

Table 6.7. Initial data for SSMAE on the distribution of pollutants over Arctic water bodies at moment t_0.

Water body	*Symbol*	*Concentration*			
		Radionuclides (Bq/L)		*Heavy metals*	*Oil hydrocarbons*
		^{137}Cs	^{60}Co	(mg/L)	(mg/L)
Greenland Sea	Γ	0.05	0.05	0.5	0.2
Norwegian Sea	N	0.05	0.05	0.7	0.4
Barents Sea	B	0.07	0.07	0.8	0.6
Kara Sea	K	0.10	0.10	1.0	0.4
White Sea	∇	0.10	0.10	1.1	0.4
Laptev Sea	Λ	0.05	0.05	0.9	0.5
East Siberian Sea	E	0.01	0.01	0.9	0.5
Bering Sea	S	0.02	0.02	0.8	0.7
Chukchi Sea	X	0.01	0.01	0.8	0.6
Beaufort Sea	Φ	0.05	0.05	0.7	0.2
Central Basin	U	0.00	0.00	0.1	0.1

a^1_{ij} equals the water area identifier symbol from the second column of Table 6.7 when (φ_i, λ_j) belongs to a given sea).

Identifier A_2 shows the position of cells Ω_R, Ω_P, Ω_N, Ω_S, Ω_Γ and describes the spatial distribution of pollutant sources. Other identifiers A_k are used to describe ice fields ($k = 3$), the spatial distribution of solar radiation ($k = 4$), and the dislocation of upwelling zones ($k = 5$).

The user of the SSMAE in free-running mode may choose different ways to describe the many input parameters. Blocks ICI and ICD activate online entry to A_k and to the database. For example, if the user has data about the spatial distribution of ice fields in Ω, he can form identifier A_3 with $a^3_{ij} = 0$ for an ice-free water surface, $a^3_{ij} = 1$ for new ice, and $a^3_{ij} = 2$ for old ice. In this case block SS enables the input of data from the climate model concerning ice fields.

The block structure of the SSMAE is provided for using a C++ program. Each of the blocks from Table 6.6 is a C++ function. The main function provides for interactions between the SSMAE, SGM, and CM. This functional specification supports overlapping of output and input streams of SSMAE blocks. In conversational mode the user can toggle the datastreams between the slave blocks.

The calculating procedure is based on sub-division of the Arctic Basin into grids $\{\Xi_{ijk}\}$. This is realized by means of a quasi-linearization method (Nitu *et al.*, 2000a). All differential equations of the SSMAE are substituted in each box Ξ_{ijk} by easily integrable ordinary differential equations with constant coefficients. Water motion and turbulent mixing are realized in conformity with current velocity fields which are defined on the same coordinate grid as the $\{\Xi_{ijk}\}$ (Krapivin *et al.*, 1998).

6.4.2 Marine biota block

The ice–water ergocline plays an important role in the biological productivity of northern seas. According to the hypothesis of Legendre and Legendre (1998), energy ergoclines are the preferential sites for biological production in the Arctic Ocean. Primary production in foodchains of Arctic Basin ecosystems is determined by phytoplankton productivity. This is connected with complex variations in the meteorological, hydrodynamic, geochemical, and energy parameters of the sea environment. The problem of parameterizing phytoplankton production in northern seas was studied by Legendre and Legendre (1998). Table 6.8 shows the seasonal composition of conditions affecting primary production in Ω. This scheme is applied to each Ξ_{ijk}.

Block MWT calculates the water temperature T_w by averaging the temperatures of mixed water volumes. In addition, the following correlations are applied:

$$T_g = T_r = T_f = \begin{cases} -0.024b + 0.76T_0 + 8.38, & \text{when } b \le 50 \text{ cm}; \\ -0.042b + 0.391T_0 - 0.549, & \text{when } b < 50 \text{ cm}. \end{cases} \tag{6.1}$$

where $b = g + r + f$; T_0 is the surface temperature; g is the snow depth; r is the thickness of floating ice; and f is the depth of submerged ice below the water surface. If we designate by ρ_g, ρ_r, and ζ the density of snow, ice, and seawater, respectively, we

Table 6.8. The vertical structure of the Arctic Basin's water bodies.

Layer (A)	Δz	*Parameters of the layer*				
		T_A	E_A	k_A	α_A	β_A
Surface		T_0	E_0			
Snow	g	T_g	E_g		α_g	β_g
Floating ice	r	T_r	E_r		α_r	β_r
Drowned ice	f	T_f	E_f		α_f	β_f
Water	$z - f$	T_W	E_W	k_W	α_W	β_W

Δz = layer thickness, T_A = temperature, E_A = illumination, k_A = turbulence coefficient, α_A = coefficient of illumination attenuation, and β_A = coefficient of light reflection.

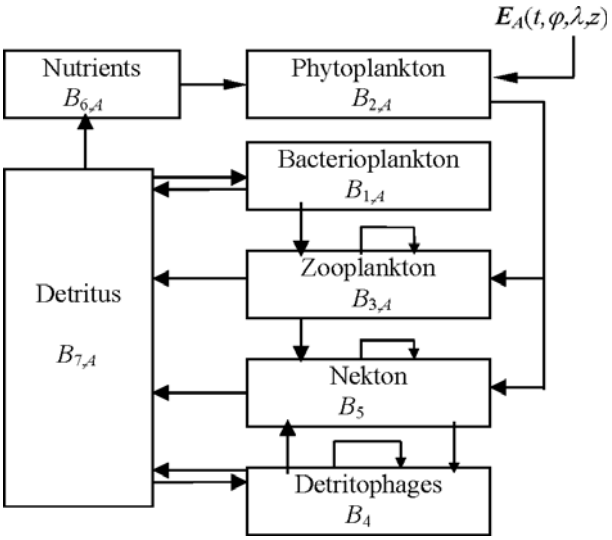

Figure 6.3. Block diagram of energy flows (cal m^{-3} da^{-1}) in the trophic pyramid of the Arctic Basin ecosystem. This is realized as block MEF. The boxes with elements denote the generalized trophic levels of the Arctic ecosystem. All of the elements are described by means of averaged parameters for the biological community of the northern seas. It is supposed that this trophic pyramid takes place in each of the Arctic Basin seas. The trophic relations between the elements of the model are described on the basis of the energy principle (Nitu *et al.*, 2000b). Biomasses, rates of production and exchange (respiration), and food rations are expressed in energy units. Total nitrogen serves as a "nutrient salts" prototype in the model.

obtain for the depth of ice beneath the surface:

$$f = (g\rho_g + r\rho_r)/(\zeta - \rho_r).$$

Figures 6.3 and 6.4 show a conceptual flowchart of the energy in an ecological system. The energy input during time interval t is provided by solar radiation $E_A(t, \varphi, \lambda, z)$, as is the upward transport of nutrients from deep-sea layers. The concentration of nutrients $B_{6,A}(t, \varphi, \lambda, z)$ at depth z is determined by photosynthesis R_{pA}, advection, and destruction of suspended dead organic matter B_7. The role played by hydrodynamic conditions relates to maintenance of the concentration of nutrients required for photosynthesis which occurs via transport from other layers or aquatories of the sea where the concentration is sufficiently high. Taking into account the designations of Table 6.7 we have

$$E(t,\varphi,\lambda,z)=\begin{cases} E_0(t,\varphi,\lambda), & \text{when } z \le -(g+r); \\ E_g(t,\varphi,\lambda,z)=(1-\beta_g)E_0\exp(\alpha_g z), & \text{when } z \in [-(g+r),-r]; \\ E_r(t,\varphi,\lambda,z)=(1-\beta_r)E_g(t,\varphi,\lambda,-r)\exp(\alpha_r z), & \text{when } z \in [-r,0]; \\ E_f(t,\varphi,\lambda,z)=(1-\beta_f)E_r(t,\varphi,\lambda,0)\exp(-\alpha_f z), & \text{when } z \in [0,f]; \\ E_w(t,\varphi,\lambda,z)=(1-\beta_w)E(t,\varphi,\lambda,f)\exp(-\alpha_w z), & \text{when } z > f. \end{cases}$$

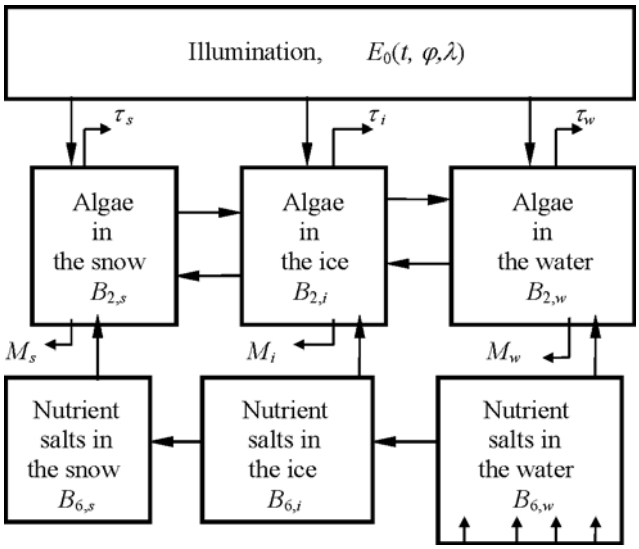

Figure 6.4. Block diagram of energy flows (cal m^{-3} da^{-1}) at the snow–ice–water interface.

where the values of α_A $(A = g, r, f, w)$ depend on the optical properties of the Ath medium. Irradiance E_0 arrives at surface Ω. The estimate of E_0 is obtained from monitoring or is calculated from the climatic model. The flow of E_0 is attenuated by snow, ice, and water according to Table 6.7. In each cell Ω_{ij} the structure of these layers is changed corresponding to the time of year. Within each layer, the attenuation of irradiance with depth is described by an exponential model (Legendre and Krapivin, 1992). Parameters α_A and β_A are functions of salinity, turbidity, temperature, and biomass. The form of this dependence is given as a scenario, otherwise standard functions are used (block IL).

As a basic scheme for the flow of nutrients in water, the scheme proposed by Krapivin (1996) is accepted, as adjusted to conditions in the Arctic Basin by Legendre and Legendre (1998). It is supposed that the spatial distribution of upwelling zones is given with seasonal variations. Block NUM realizes this scheme regarding the current structure of upwelling regions.

The dynamic equation for nutrients $B_{6,A}$ in the environment, where $A = \{S \text{ snow}, I \text{ ice}, W \text{ water}\}$, is given by

$$\frac{\partial B_{6,A}}{\partial t} + v_\varphi^A \frac{\partial B_{6,A}}{\partial \varphi} + v_\lambda^A \frac{\partial B_{6,A}}{\partial \lambda} + v_z^A \frac{\partial B_{6,A}}{\partial z} = Q_A + k_2^W \frac{\partial^2 B_{6,A}}{\partial^2 z} + \beta_V \frac{\partial B_{6,A}}{\partial z} + \rho_1 \sum_{i=1}^{5} T_i - \delta_1 R_{pA} + \varepsilon_1^A H_1^\varepsilon, \quad (6.2)$$

where $v_\varphi^A, v_\lambda^A, v_z^A$ are velocity projections of motion in the environment; Q_A is the input of biogenic elements to A resulting from the decomposition of detritus $(Q_A = \delta_n R_D^A)$ with $R_D^A = \mu_A B_7$; δ_n is the content of nutrients in dead organic matter;

μ_A is the rate of decomposition of detritus in environment A; k_2^W is the kinematical coefficient of vertical diffusion; δ_1 is the velocity of nutrient assimilation by the photosynthetic process per unit of phytoplankton production; ε_1^A is the proportional part of the εth radionuclide that is chemically analogous to $B_{6,A}$ on substrate A; H_1^ε is the rate of input flow of the εth radionuclide; T_i is the rate of exchange with the environment; ρ_1 is that part of biomass losses due to exchange that transforms into nutrients (Legendre and Legendre, 1998); and β_V is upwelling velocity. Equation (6.1) is the basic element of block NM.

Phytoplankton production R_{pA} in environment A is a function of solar radiation E_A, concentration of nutrients n_A, temperature T_A, phytoplankton biomass p_A, and concentration of pollutants ξ_A. There are many models that describe the photosynthesis process (Legendre and Legendre, 1998; Legendre and Krapivin, 1992). For the description of this function in the present study, an equation of Michaelis–Menten type is used (block MFB):

$$R_{pA} = a_A k_I^A p_{A,max}/(E_A + k_I^A), \tag{6.3}$$

where k_I^A is the irradiance level at which $R_{pA} = 0.5 \cdot R_{pA,max}$; and $p_{A,max}$ is the maximum quantum yield (Legendre and Legendre, 1998). The coefficient a_A reflects the dependence of phytoplankton production on environment temperature T and concentration of nutrients $B_{6,A}$. The block MFB realizes the following equation for calculation of a_A:

$$a_A = a_1 K_0(T,t)/[1 + B_{2,A}/(a_2 B_{6,A})], \tag{6.4}$$

where a_1 is the maximal rate of nutrient absorption by phytoplankton (da^{-1}); and a_2 is the index of the rate of saturation of photosynthesis, and

$$K_0(T,t) = a_3 \max\left\{0, \frac{T_c - T}{T_c - T_{opt}} \exp\left[1 - \frac{T_c - T}{T_c - T_{opt}}\right]\right\}, \tag{6.5}$$

where a_3 is a weight coefficient; and T_c and T_{opt} are the critical and optimal temperatures for photosynthesis, respectively (°C).

Equation (6.3) adequately fits laboratory data. Relationships (6.4) and (6.5) make the description of phytoplankton production more accurate for critical environmental conditions when the concentration of nutrients and the temperature fluctuate widely. The coefficients of these relationships are defined on the basis of estimates given by Legendre and Legendre (1998).

The dynamic equation for phytoplankton biomass in environment A takes the following form:

$$\frac{\partial B_{2,A}}{\partial t} + v_\varphi^A \frac{\partial B_{2,A}}{\partial \varphi} + v_\lambda^A \frac{\partial B_{2,A}}{\partial \lambda} + v_z^A \frac{\partial B_{2,A}}{\partial z}$$
$$= R_{pA} - \theta_p^A - M_p^A + k_2^A \frac{\partial^2 B_{2,A}}{\partial z^2} - [k_{Zp}^A R_{ZA}/\xi_Z^A + k_{Fp}^A R_{FA}/\xi_F^A] B_{2,A}, \tag{6.6}$$

where $R_{ZA}(\xi_Z^A)$ and $R_{FA}(\xi_F^A)$ are the production (the food spectrum) of zooplankton B_3 and nekton B_5, respectively; M_p^A is mortality; and θ_p^A is the rate of exchange. The

balance equations for the other ecological elements of Figure 6.3 are given by Krapivin (1995, 1996).

The energy source for the entire system is solar radiation $E_A(t, \varphi, \lambda, z)$, the intensity of which depends on time t, latitude φ, longitude λ, and depth z. The equation that describes the biomass dynamics of living elements is

$$\frac{\partial B_i}{\partial t} + \xi_i \left[V_\varphi \frac{\partial B_i}{\partial \varphi} + V_\lambda \frac{\partial B_i}{\partial \lambda} + V_z \frac{\partial B_i}{\partial z} \right]$$

$$= R_i - T_i - M_i - H_i - \sum_{j \in \Gamma_i} C_{ij} R_j + \xi_i \left[\frac{\partial}{\partial \varphi} \left(\Delta_\varphi \frac{\partial B_i}{\partial \varphi} \right) + \frac{\partial}{\partial \lambda} \left(\Delta_\lambda \frac{\partial B_i}{\partial \lambda} \right) \right.$$

$$\left. + \frac{\partial}{\partial z} \left(\Delta_z \frac{\partial B_i}{\partial z} \right) + \beta_V \frac{\partial B_i}{\partial z} \right] \quad (i = 1, 3, 4, 5); \tag{6.7}$$

where $V(V_\varphi, V_\lambda, V_z)$ are components of the water current velocity ($V_\varphi = v_\varphi^W$, $V_\lambda = v_\lambda^W$, $V_z = v_z^W$); R_i is production; M_i is mortality; H_i is non-assimilated food; and Γ_i is the set of trophic dependences of the ith component $C_{ji} = k_{ji} F_i \Big/ \sum_{m \in S_i} k_{jm} F_m$; S_i is the food spectrum of the jth component; k_{jm} is the index of satisfaction of the nutritive requirements of the jth component at the expense of the mth component biomass; $F_i = \max\{0, B_i - B_{i,min}\}$; $B_{i,min}$ is the minimal biomass of the ith component consumed at other trophic levels; $\Delta(\Delta_\varphi, \Delta_\lambda, \Delta_z)$ are components of the turbulent mixing coefficient (on the assumption of isotrophism of vertical mixing in the horizontal plane $\Delta_\varphi = \Delta_\lambda = v_H$); and β_V is upwelling velocity. Functions R_i, M_i, H_i and T_i are parameterized according to the models by Krapivin (1996) and Legendre and Krapivin (1992). The equations describing the dynamics of the abiotic elements are represented in conformity with Kondratyev and Krapivin (2001a, b). Functions M_4 and M_5 include biomass losses from fishing. Parameter ξ_i characterizes the subjection of the ith component relative to the current. It is supposed that $\xi_i = 1$ for $i = 1, 2, 3$ and $\xi_i = 0$ for $i = 4, 5$.

The inert components are described by the following equation (Krapivin, 1996):

$$\frac{\partial B_7}{\partial t} + V_\varphi \frac{\partial B_7}{\partial \varphi} + V_\lambda \frac{\partial B_7}{\partial \lambda} + V_z \frac{\partial B_7}{\partial z}$$

$$= \sum_{i=1}^{5} (M_i + H_i) - \mu_W B_7 - (v_* - \beta_V) \frac{\partial B_7}{\partial z} - (k_{1,7} R_1 / P_1 + k_{3,7} R_3 / P_3 + k_{4,7} R_4 / P_4$$

$$+ k_{5,7} R_5 / P_5) B_{7,min} + \frac{\partial}{\partial \varphi} \left(\Delta_\varphi \frac{\partial B_7}{\partial \varphi} \right) + \frac{\partial}{\partial \lambda} \left(\Delta_\lambda \frac{\partial B_7}{\partial \lambda} \right) + \frac{\partial}{\partial z} \left(\Delta_z \frac{\partial B_7}{\partial z} \right), \tag{6.8}$$

where $P_i = \sum_{j \in S_i} k_{i,j} B_{j,min}$; μ_W is the velocity of decomposition of detritus per unit biomass; v_* is the speed of settling due to gravity; and k_{ij} is a coefficient of the relation between the ith element and the jth element of the ecosystem.

Equations (6.2)–(6.8) can only be used for the complete volume when $(\varphi, \lambda, z) \in W$. In other cases (in the layers of ice or snow) these equations are automatically reduced in accordance with the scheme represented in Figure 6.4.

6.4.3 Hydrological block

The circulation of water in the Arctic Basin is a complex system of cycles and currents with different scales. Block HB simulates the dynamics of Arctic Basin water by the system of sub-blocks presented in Figure 6.2. The water dynamics in Ω is presented by flows between compartments Ξ_{ijk}. The directions of water exchanges are represented on every level $z_k = z_0 + (k-1)\Delta z_k$ according to Aota *et al.* (1992) in conformity with the current maps assigned as SSMAE input. The external boundary of Ω is determined by the coastline, the sea bottom, the Bering Strait, the southern boundary of the Norwegian Sea, and the water–atmosphere interface.

The hydrological data are synthesized via a four-level structure according to the seasons (block MWD). The velocity of current in the Bering Strait is estimated by the following binary function:

$$V(t) = \begin{cases} V_1, & \text{for } t \in \tau_u \cup \tau_a; \\ V_2, & \text{for } t \in \tau_w \cup \tau_s. \end{cases}$$

Water exchange through the southern boundary of the Norwegian Sea is V_3. The water temperature T^W_{ijk} in Ξ_{ijk} (block MWT) is a function of evaporation, precipitation, river flows, and inflows of water from the Atlantic and Pacific Oceans. Its change with time in Ξ_{ijk} is described by the equation of heat balance:

$$\zeta C \sigma_{ijk} \frac{\partial T^W_{ijk}}{\partial t} = \sum_{s,l,m} (W^{ijk}_{slm} + f^{ijk}_{slm}) - W_{ijk}, \tag{6.9}$$

where ζ is seawater density (g cm^{-3}); C is water thermal capacity, (cal $\cdot$ g^{-1} grad^{-1}); σ_{ijk} is the volume of Ξ_{ijk}; W^{ijk}_{slm} is heat inflow to Ξ_{ijk} from Ξ_{slm}; f^{ijk}_{slm} is heat exchange between Ξ_{slm} and Ξ_{ijk} caused by turbulent mixing; and W_{ijk} is total heat outflow from Ξ_{ijk} to bordering cells. Heat exchange with the atmosphere is calculated in accordance with empirical equation (6.1).

The dissipation of moving kinetic energy, geothermic flow on the ocean bed, heat effects of chemical processes in the ocean ecosystem, and freezing and melting of the ice are not considered to be global determinants of water temperature fields. Therefore, the SSMAE does not consider these effects.

The dynamics of water salinity $S(t, \varphi, \lambda, z)$ during time interval t are described by the balance equation as block MWS. Ice salinity is defined by a two-step scale: s_1 old, s_2 new. It is supposed that $S(t, \varphi, \lambda, z) = s_0$ for $z > 100$ m, $s_2 = k_s S(t, \varphi, \lambda, f)$ for $r + f > H_{max}$, and $s_1 = k_r s_2 H_{max}/(r+f)$ for $r + f < H_{max}$, where coefficients k_s and k_r are determined empirically and H_{max} is the maximal thickness of new ice. In accordance with estimations by Krapivin (1995), simulation experiments are realized for $H_{max} = 50$ cm, $k_s = k_r = 1$. River flows, ice fields, and synoptic situations

are described by scenarios given in the MRF and SS blocks and formed by the user of the SSMAE.

Snow layer thickness $g(t, \varphi, \lambda)$ may be described via statistical data with given dispersion characteristics $g = \bar{g} + g_0$, where the value $\bar{g}$ is defined as the mean characteristic for the chosen time interval, and function $g_0(t, \varphi, \lambda)$ gives the variation of g for the given time interval.

An alternative way of parameterizing the process of snow layer dynamics in the framework of the atmospheric process simulation algorithm (block APM) relates to the thickness of the growth and melting of the snow layer according to temperature and precipitation:

$$g(t + \Delta t, \varphi, \lambda) = g(t, \varphi, \lambda) + S_F - S_M,$$

where S_F is snow precipitated at temperatures close to freezing ($265\,\mathrm{K} \leq T_0 \leq 275\,\mathrm{K}$); and S_M is snow ablation (i.e., evaporation + melting).

Block SS gives the user the possibility of choosing between these algorithms. When statistical data on snow layer thickness exist, function $g(t, \varphi, \lambda)$ can be reconstructed for $(\varphi, \lambda) \in \Omega$ by means of the approximation algorithm at the time of polynomial interpolation in space (Krapivin, 2000a, b; Nitu *et al.*, 2000b).

6.4.4 Pollution block

The block PSM simulates the pollution processes over territory Ω as a result of atmospheric transport, river and surface coastal outflow, navigation, and other human activity (Mohler and Arnold, 1992; Muller and Peter, 1992). The variety of pollutants is described by three components: oil hydrocarbons O, heavy metals (e solid particles, ψ dissolved fraction), and radionuclides ε. It is supposed that pollutants only enter living organisms through the foodchain.

Rivers make a considerable contribution to the level of pollution of Arctic water. The concentration of pollutant κ in river γ is γ_κ. Pollutant κ enters compartment $\Omega_{ijk} \in \Omega_R$ with velocity c_γ reflecting the mass flow per unit time. Subsequently, the spreading of pollutant κ in Ω is described by other sub-blocks.

The influence of water exchanges between the Arctic Basin and the Pacific and Atlantic Oceans on the pollution level in Ω is described by block MPT. It is supposed that the watersheds of the Norwegian Sea Ω_N and the Bering Strait Ω_B are characterized by currents with varying directions given as a scenario.

The atmospheric transport of heavy metals, oil hydrocarbons, and radionuclides is described by many models (Phillips *et al.*, 1997; Payne *et al.*, 1991; Sportisse, 2000). Application of these models to the reconstruction of the pollution distribution over Ω makes it possible to estimate optimal values of $\Delta\varphi, \Delta\lambda$ and time steps Δt. The present level of the database for the Arctic Basin provides for use of a single-level Euler model with $\Delta t = 10$ days, $\Delta\varphi = \Delta\lambda = 1^\circ$ (block APM). It is supposed that pollution sources can be located at the Arctic Basin boundary. Detailed distributions of these pollution sources are given as SSMAE input. The transport of pollutants to the Arctic Basin and the formation of their spatial distribution are realized in conformity with the wind velocity field, which is considered as given (Krapivin and Phillips, 2001a, b).

It is postulated that oil hydrocarbons $O(t, \varphi, \lambda, z)$ are transformed by the following processes (Payne *et al.*, 1991): dissolution H_O^1, evaporation H_O^2, sedimentation H_O^3, oxidation H_O^4, biological adsorption H_O^5, bio-sedimentation H_O^6, and bacterial decomposition H_O^7. The kinetics equation that describes the dynamics of oil hydrocarbons in the Arctic Basin is given by

$$\frac{\partial O}{\partial t} + v_\varphi^w \frac{\partial O}{\partial \varphi} + v_\lambda^w \frac{\partial O}{\partial \lambda} + v_z^w \frac{\partial O}{\partial z} = Q_O + k_2^w \frac{\partial^2 O}{\partial z^2} - \sum_{i=1}^{7} H_O^i, \tag{6.10}$$

where Q_O is the anthropogenic source of oil hydrocarbons.

The process of diffusion of heavy metals in seawater depends on their state. The dissolved fraction of heavy metals (ψ) takes part in the biogeochemical processes more intensively than suspended particles (e). But unlike suspended particles, the heavy metals fall out more rapidly to the sediment. A description of the entire spectrum of these processes in the framework of this study is impossible. Therefore, block MMT describes processes that can be estimated. The transport of heavy metals in seawater includes absorption of the dissolved fraction ψ by plankton (H_Z^ψ) and by nekton (H_F^ψ), sedimentation of the solid fraction (H_1^e), deposition with detritus (H_D^ψ), adsorption by detritophages from bottom sediments ($H_L^{e\psi}$), and release from bottom sediments owing to diffusion ($H_a^{e\psi}$). As a result, the dynamic equations for heavy metals become:

$$\frac{\partial e_W}{\partial t} + v_\varphi^W \frac{\partial e_W}{\partial \varphi} + v_\lambda^W \frac{\partial e_W}{\partial \lambda} + v_z^W \frac{\partial e_W}{\partial z} = \sum_{i=1}^{3} \alpha_2^i Q_{e\Psi}^i - H_1^e + \alpha_1 H_a^{e\Psi}, \tag{6.11}$$

$$\frac{\partial \psi_W}{\partial t} + v_\varphi^W \frac{\partial \psi_W}{\partial \varphi} + v_\lambda^W \frac{\partial \psi_W}{\partial \lambda} + v_z^W \frac{\partial \psi_W}{\partial z} = (1-\alpha_1) H_a^{e\psi} + k_2^W \frac{\partial^2 \psi_W}{\partial z^2} - H_Z^\psi - H_F^\psi - H_D^\psi - H_a^\psi, \tag{6.12}$$

$$\frac{\partial e^*}{\partial t} = H_1^e - \alpha_1 (H_L^{e\psi} + H_a^{e\psi}), \tag{6.13}$$

$$\frac{\partial \psi^*}{\partial t} = H_D^\psi - (1-\alpha_1)(H_L^{e\psi} + H_a^{e\psi}), \tag{6.14}$$

where e_w, ψ_w and e^*, ψ^* are the concentrations of heavy metals in the water and in the bottom sediments as solid and dissolved phases, respectively; H_a^ψ is the output of heavy metals from the sea to the atmosphere by evaporation and spray; $Q_{e\psi}^i$ is the input of heavy metals to the sea with river water ($i = 1$), atmospheric deposition ($i = 2$), and ships' waste ($i = 3$); α_2^i is the part of suspended particles in the ith flow of heavy metals; and α_1 is the part of the solid fraction of heavy metals in bottom sediments.

Each radionuclide of εth type is characterized by its half-life τ^ε, the rate H_1^ε of input flow to water area Ω, the accumulation rate H_α^ε in living organisms $\alpha(p_A, B_A, Z, F, L)$, and the removal rate H_D^ε with dead elements of the ecosystem. As a result, the concentration Q^ε of radionuclide ε in Ω_{ijk} is described by the

following system of equations:

$$\frac{\partial Q^{\varepsilon}}{\partial t} + v_{\varphi}^{W}\frac{\partial Q^{\varepsilon}}{\partial \varphi} + v_{\lambda}^{W}\frac{\partial Q^{\varepsilon}}{\partial \lambda} + v_{z}^{W}\frac{\partial Q^{\varepsilon}}{\partial z} = \frac{\sigma_{ijk}}{\sigma}H_{1}^{\varepsilon} + k_{2}^{W}\frac{\partial^{2} Q^{\varepsilon}}{\partial z^{2}} - H_{\alpha}^{\varepsilon} - H_{D}^{\varepsilon} - \frac{\ln 2}{\tau^{\varepsilon}}Q^{\varepsilon} + H_{*}^{\varepsilon}, \tag{6.15}$$

$$\frac{\partial Q^{\varepsilon}}{\partial t} = H_{D}^{\varepsilon} - H_{*}^{\varepsilon} - \frac{\ln 2}{\tau^{\varepsilon}}Q_{*}^{\varepsilon}, \tag{6.16}$$

where Q_{*}^{ε} is the concentration of εth radionuclide in bottom sediments; and H_{*}^{ε} is the rate of output flow of the εth radionuclide from bottom sediments via desorption. The exchange of radionuclides between the water layers as a result of migration by living organisms is ignored as it has a small value in comparison with flow H_{D}^{ε}.

6.4.5 Simulation results

6.4.5.1 The assumptions

The SSMAE facilitates estimation of the pollution dynamics of the Arctic Basin under various *a priori* suppositions about the intensities of the flows of pollutants and under other anthropogenic impacts on the ecosystems of this region. In this section we consider some possible situations. The thermal regime of the Arctic Basin is given by a normal distribution with average temperatures and with dispersions on the aquatories as given by the SEDAAR (Strategic Environmental Distributed Active Archive Resource). The scheme of transport of pollutants in the atmosphere is adopted from Christensen (1997). The estimates of parameters for the blocks of Table 6.6 are given by literature sources or personal recommendations (Table 6.9). The vertical distribution of pollutants at initial moment t_0 is taken as homogeneous. The average diameters of solid particles are estimated to be in the range from 0.12 μm to 1,000 μm and the vertical velocity of sedimentation is 0.003 m/s. The concentration of nutrients in the ice and snow equals 0. Also it is supposed that the deep water temperature $Y(t, \varphi, \lambda) = 0^{\circ}\mathrm{C}$ and the surface ice temperature $f_1(t, \varphi, \lambda) = -3^{\circ}\mathrm{C}$ for $(\varphi, \lambda) \in \Omega$. It is further supposed that $\varepsilon_1^A = 0$ and that phytoplankton productivity in the ice layer is 2.5% of the primary production in the water column $[(R_{p,r} + R_{p,f})/R_{p,w} = 0.025]$.

Let the ratio between solid and dissolved phases of heavy metals at moment $t = t_0$ equal 1:2 (i.e., $e(t_0, \varphi, \lambda, z)/\psi(t_0, \varphi, \lambda, z) = 0.5$). The flows of heavy metals, H_Z^{ψ}, H_F^{ψ}, H_D^{ψ}, and H_L^{ψ}, are described by linear models, $H_1^e = 0.01 e_w$, $H_a^{e\psi} = 0$. The boundaries of the Norwegian and Bering Seas are approximated by lines at $\varphi_N = 62^{\circ}\mathrm{N}$ and $\varphi_B = 51^{\circ}\mathrm{N}$, respectively. The values of the other parameters are defined by Wielgolaski (1997), Wania *et al.* (1998), Valette-Silver *et al.* (1999), Preller and Cheng (1999), Bard (1999), and Rudels *et al.* (1991). The initial data are defined in Tables 6.7 and 6.10.

Table 6.9. The values of some parameters in simulation experiments using the SSMAE.

Parameter	*Estimate of the parameter*
Step of space digitized by	
Latitude, $\Delta\varphi$	1°
Longitude, $\Delta\lambda$	1°
Depth, Δz	
$z \leq 100$ m	1 m
$z > 100$ m	$h = 100$ m
Coefficient of ice heat conductivity, λ_1	2.21 W/m/°
Coefficient of water heat conductivity, λ_2	0.551 W/m/°
Coefficient of turbulent mixing, k_2^W	
For open water	0.5×10^{-4} m^2/s
For ice-covered water bodies	5×10^{-6} m^2/s
Characteristic heat of ice melting, q	334 kJ/kg
Content of biogenic elements in dead organic matter, δ_n	0.1
Intensity of detritus decomposition, μ_A	
$A = g, r, f$	0
$A = W$	0.01
Velocity of current in the Bering Strait, V_i	
$i = 1$	0.2 m/s
$i = 2$	0.05 m/s
Water heat capacity, C	4.18 kJ/kg/K
Ice salinity, s_i	
$i = 1$	5‰
$i = 2$	1‰
Water salinity at $z > 100$ m, s_0	34.95‰
Area of the Arctic Basin, σ	16,795,000 km^2
Half-life period of radionuclides, τ_ε	
$\varepsilon = {}^{60}$Co	5.271 yr
$\varepsilon = {}^{137}$Cs	30.17 yr
Critical temperature for photosynthesis, T_c	-0.5°C

6.4.5.2 The dynamics of Arctic Basin radionuclear pollution

The intensity of external flows through the boundaries of the Arctic Basin and the internal flows due to dead organisms H_D^ε, sediment H_*^ε, and living organisms H_α^ε can be described by linear models in accordance with Krapivin and Phillips (2001a, b).

Table 6.10. Input flows of radionuclides, heavy metals (suspended particles e and dissolved fraction ψ), and oil hydrocarbons O to Ω by water flows taken into account in the SSMAE.

Source	*Flow into the basin* (km^3/yr)	*Concentration of pollutant*				
		^{137}Cs (Bq/L)	^{60}Co (Bq/L)	e (mg/L)	ψ (mg/L)	O (mg/L)
Rivers:						
Yenisey	600	0.5	0.5	0.3	5.1	2.3
Ob′	400	0.1	0.1	0.4	6.9	4.7
Lena	500	0.0	0.0	1.1	8.8	6.9
Pechora	130	0.1	0.1	0.3	1.5	3.0
Northern Dvina	100	0.0	0.0	0.2	1.1	4.0
Other Siberian rivers	200	0.1	0.1	0.1	0.5	2.3
North America rivers	600	0.2	0.2	0.1	1.0	1.0
Evaporation	3,500	0.0	0.0	0.0	0.0	0.0
Precipitation	5,300	0.0	0.0	0.1	0.1	0.0
Southern boundary of the Norwegian Sea	12,000	0.1	0.1	0.6	2.2	2.4
Bering Strait	10,560	0.0	0.0	0.5	1.9	1.9

Some results of the simulation experiment are given in Figures 6.5 and 6.6. Figure 6.5 shows the tendency vs. time of the average content of radionuclear pollution on the whole Arctic water area. The distribution with depth is represented by a three-layer model, upper waters ($z < 1$ km), deep water ($z > 1$ km), and sediments. Bottom depth is taken as 1.5 km. More realistic depth representations of both shallow seas and the deeper Arctic Basin will be considered in a future refinement of the model. The curves describe the vertical distribution with time of the radionuclide content in two water layers and in sediments. The transfer of radionuclides from upper water to deep water occurs at a speed which results in the reduction of radionuclear pollution in upper water by 43.3% over 20 years. Such distributions for each Arctic sea are given in Table 6.11.

Local variations in the vertical distribution of radionuclides are determined by both hydrological and ecological conditions. The correlation between these conditions is a function of the season. Table 6.12 gives estimates of the role of ecological processes in the formation of the vertical distribution of the radionuclear pollution of Arctic seas. These estimates show that the biological community plays a minor role in radionuclide transport from upper layers to the deep ocean.

The aquatories of the White, Laptev, East Siberian, and Chukchi Seas are subject to visible variations in radionuclear pollution. The accumulation of radionuclides is observed in the Central aquatory of the Arctic Basin. The aquageosystems of the Greenland and Kara Seas have currently unknown factors that allow radionuclear

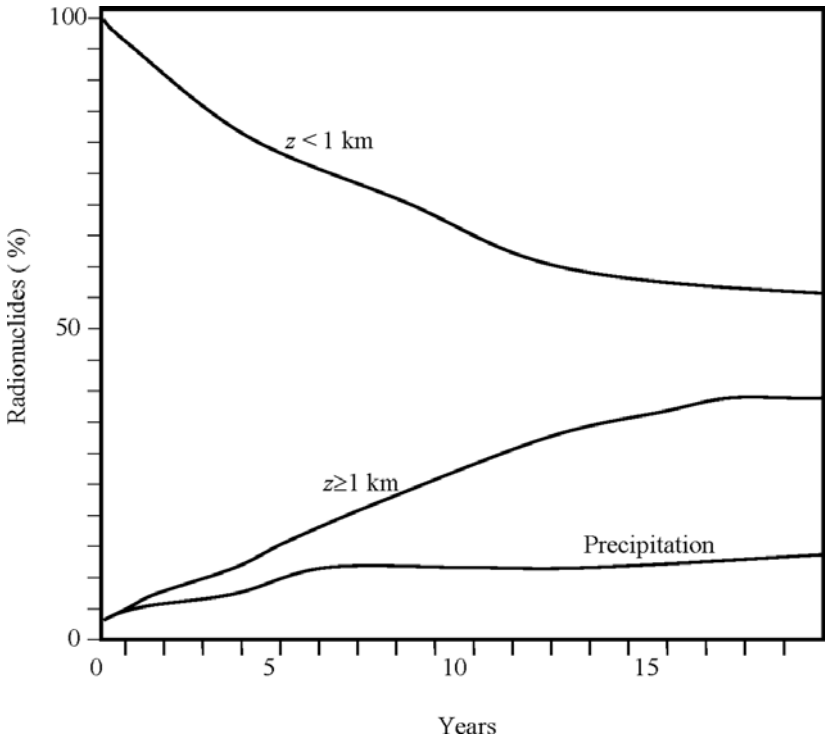

Figure 6.5. Dynamics of the radionuclide distribution in the Arctic Basin. It is assumed that at moment $t_0 = 0$ radionuclear pollutants (^{137}Cs, ^{60}Co; see Tables 6.7 and 6.10) can only be found in the upper water layer $z \leq 1$ km. The curves show the radionuclear pollutant distribution with time in the two water layers and in the sediments obtained by averaging the simulation results for all of the northern seas.

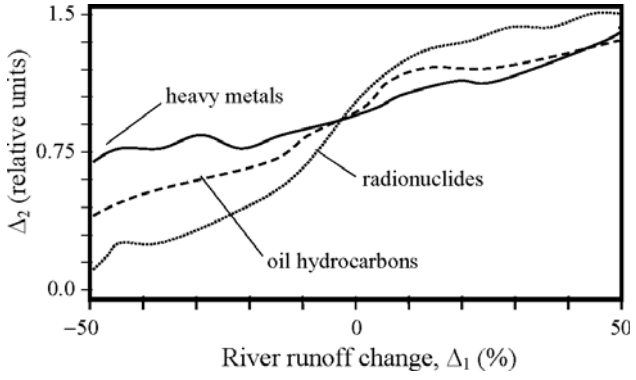

Figure 6.6. Influence of variations in river flow on Arctic Basin pollution level. Here Δ_1 is the percentage variation in river flow to Ω with respect to the value averaged on Ω_R in the last three years and Δ_2 is the content of pollutant averaged on all rivers in Ω_R and normalized to the initial data (such that $\Delta_2 = 1$ for $\Delta_1 = 0$).

Table 6.11. Distribution of radionuclear pollution in Arctic aquatories 30 years and 50 years later (%).

Aquatory (see Table 6.7)	Γ	*N*	*B*	*K*	∇	Λ	*E*	*S*	*X*	Φ	*U*
30 years after t_0											
$z \leq 1$ km	50	60	69	46	73	44	43	57	58	61	68
$z > 1$ km	49	39	29	52	26	54	54	39	39	34	29
Bottom	1	1	2	2	1	2	3	4	3	3	3
50 years after t_0											
$z \leq 1$ km	65	57	70	66	70	50	49	62	59	58	70
$z > 1$ km	30	38	24	27	21	47	46	32	37	34	26
Bottom	5	5	6	7	9	3	5	6	4	8	4

Table 6.12. Some simulation experiment results using the SSMAE to estimate the vertical distribution of radionuclides in the Arctic Basin. The contribution of ecological processes to formation of the vertical distribution in the radionuclide content of the water is represented by the parameter ξ (%). The average content of phytoplankton is represented by the parameter p_w (g/m^2).

Aquatory	*Seasons*							
	Winter		*Spring*		*Summer*		*Fall*	
	τ_w		τ_s		τ_u		τ_a	
	p_w	ξ	p_w	ξ	p_w	ξ	p_w	ξ
Greenland Sea	3.2	2	8.4	10	5.7	5	6.3	5
Norwegian Sea	2.9	2	7.8	9	5.9	5	6.7	6
Barents Sea	2.1	1	8.9	11	6.8	6	7.1	6
Kara Sea	2.4	1	9.2	12	5.3	5	6.0	5
White Sea	2.2	1	7.6	9	6.3	6	6.4	5
Laptev Sea	0.9	1	2.4	4	1.3	2	1.4	2
E. Siberian Sea	1.3	1	2.7	4	1.9	3	2.1	3
Bering Sea	2.5	2	7.1	9	3.9	4	5.3	4
Chukchi Sea	2.3	2	6.9	8	4.1	4	5.1	4
Beaufort Sea	1.9	2	5.7	7	4.8	4	4.9	4
Central Basin	1.0	1	1.7	2	1.5	2	1.6	2
Average value	*2.1*	*1.5*	*6.2*	*7.7*	*4.3*	*4.2*	*4.8*	*4.0*

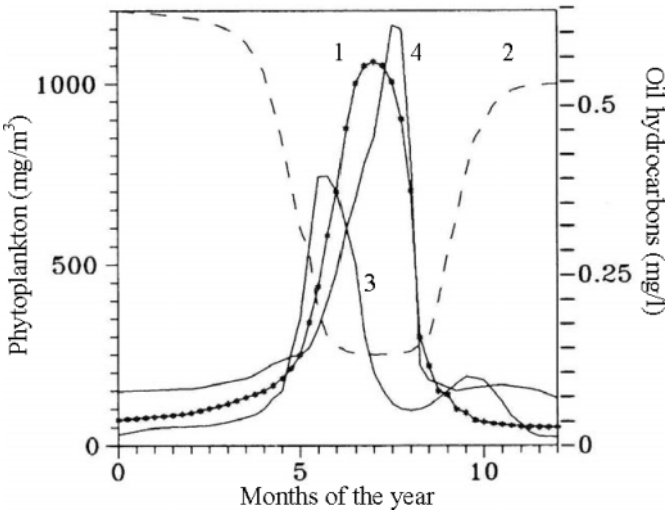

Figure 6.7. Influence of the Barents Sea ecosystem on the dynamics of oil hydrocarbons in seawater. Curves 1 and 2 show the simulation results for phytoplankton (solid curve) and oil hydrocarbons (dashed curve), respectively. Curves 3 and 4 show the yearly distribution of phytoplankton in the southwestern, northern and, northeastern aquatories of the Barents Sea, respectively. From Terziev (1992).

pollution to build up, while in the Norwegian Sea the pollution level actually decreases.

A degree of stability can be observed in the vertical distribution of radionuclides. This is generally achieved between 5 and 7 years following initial moment t_0 with the exception of the East Siberian, Laptev and Kara Seas where the stabilization processes of vertical distribution are delayed by 10–12 years.

The results of simulation experiments show that variations of the initial data by $\pm 100\%$ change the stabilization time by no more than 30%, so that the distributions take shape in 4–8 years. One unstable parameter is river flow into the Arctic Basin. Figure 6.7 shows variations in simulation results under a change in river flow to the Arctic Basin. Radionuclear pollution is reduced by 80% when river flow decreases by 50%. While river flow increases by 50% the radionuclear pollution of the Arctic basin increases by only 58%. Hence, a $\pm 50\%$ error in river flow estimate can cause a $<100\%$ deviation of the simulation results for radionuclear pollutants. As follows from the other curves of Figure 6.6, such deviations are less for heavy metals and oil hydrocarbons.

The SSMAE allows estimation of a wide spectrum of radionuclear pollution parameters. Thus, this study shows the dependence of the biological transformation mechanism on initial prerequisites. The biological transport of radionuclides downward from the mixed layer varies in a wide interval from months to scores of years. Vertical transport by biological elements is divided between 11% by the movement of living organisms and 89% for transport by dead organisms. Again, there is a degree

of stability here in that the lower trophic levels of the Arctic ecosystem have a greater concentration of radionuclides than higher trophic levels. But, it is evident that for a higher precision of block MPR the model of biological processes must consider separately each radioactive element and its interaction with plankton.

6.4.5.3 The dynamics of Arctic Basin pollution by heavy metals

The results of the simulation experiment are given in Table 6.13. We can see that the average content of heavy metals across the full water area of the Arctic Basin stabilizes after 3–5 years. Under this stable regime, the concentration of heavy metals in compartments $\Omega_R \cup \Omega_P$ (river mouths and ports) is six times higher than in the Central aquatory and twice as high in $\Omega_\Gamma \cup \Omega_B \cup \Omega_N$ (near-shore waters, the Bering Strait, and the southern boundary of the Norwegian Sea). The concentration of heavy metals in phytoplankton is 18% lower than in zooplankton and 29% lower

Table 6.13. Results of the simulation experiment on estimates of the parameters involved in pollution of Arctic waters by heavy metals. From Kondratyev *et al.* (2002a, b).

Parameter	*Estimate of the parameter after* Δt *years*					
	$\Delta t = 1$	$\Delta t = 3$	$\Delta t = 5$	$\Delta t = 10$	$\Delta t = 15$	$\Delta t = 20$
Average concentration of heavy metals in the biomass (ppm)						
Phytoplankton	0.011	0.012	0.016	0.024	0.036	0.037
Zooplankton	0.013	0.014	0.019	0.028	0.041	0.043
Nekton	0.015	0.017	0.022	0.04	0.07	0.07
Detritophages	0.033	0.037	0.048	0.088	0.15	0.16
Average content of heavy metals in Arctic waters (ppm)	0.022	0.027	0.036	0.037	0.038	0.038
Flow of heavy metals from the upper layer to deep layers ($mg\,m^{-2}\,da^{-1}$)						
Norwegian Sea	0.71	1.07	1.14	1.17	1.19	1.22
Barents Sea	0.72	1.08	1.25	1.19	1.24	1.16
Greenland Sea	0.26	0.62	0.71	0.82	0.76	0.89
White Sea	0.11	0.23	0.24	0.21	0.19	0.2
Kara Sea	0.34	0.47	0.57	0.61	0.63	0.64
Laptev Sea	0.55	0.78	0.81	0.89	0.74	0.77
East Siberian Sea	0.59	0.79	0.95	0.97	1.02	1.07
Chukchi Sea	0.88	0.83	1.54	1.49	1.31	1.44
Beaufort Sea	0.34	0.67	0.66	0.81	0.74	0.69

than in nekton. The process of accumulation of heavy metals in the upper trophic levels can be seen; moreover, the ratio of the concentration of heavy metals in phytoplankton to that of other trophic levels varies from 0.3 in $\Omega_R \cup \Omega_P$ to 0.5 in the open part of the Arctic Basin.

The distribution of heavy metals in seawater is characterized by more rapid accumulation in water areas adjoining the western coastline of Novaya Zemlya and situated at the boundary between the Jan–Mayen and East Iceland currents. The central water area of the Arctic Basin has a quasi-uniform distribution of heavy metal concentration. The vertical gradients of heavy metals vary in the interval from $0.11 \cdot m^{-2}da^{-1}$ to $1.54\ mg \cdot m^{-2}da^{-1}$. The vertical distributions of the dissolved fraction (ψ_W) and suspended particles (e_W) of heavy metals are not obviously expressed. The average ratio of the concentration of heavy metals in sediment and in water ($[\psi^* + e^*]/[\psi_W + e_W]$) varies over the area of the Arctic Basin from 1.9 to 5.7. For example, this ratio for the Bering Sea is 3.3. The contribution of the biosedimentation process to the vertical distribution of heavy metals varies from $0.23\,mg \cdot m^{-2}\,da^{-1}$ to $1.24\,mg \cdot m^{-2}da^{-1}$. The SSMAE provides the possibility of estimating the characteristics for separate types of heavy metals. An example of such calculations is given in Table 6.14.

Table 6.14. Estimates of heavy metal flows to and from the atmosphere. From Kondratyev *et al.* (2002b).

Heavy metal	*Parameter*	
	Atmospheric deposition, $Q^2_{e\psi}$ ($mg/m^2/h$)	*Evaporation and spray*, H^{ψ}_{α} (t/yr)
Ag	0.7	7
Cd	1.1	58
Co	0.3	5
Cr	1.8	188
Cu	15	169
Fe	599	894
Hg	0.6	3
Mn	4.2	283
Ni	5.5	60
Pb	48	5
Sb	0.05	123
Zn	109	4,471

6.4.5.4 *The dynamics of Arctic Basin pollution by oil hydrocarbons*

Spatial distributions forecast for oil hydrocarbons in Arctic water areas for 5 years after t_0 were obtained under the following restrictions: $O(t_0, \varphi, \lambda, z)$, $H_O^1 = 0.1\,\mathrm{mg \cdot m^{-3}\,da^{-1}}$, $H_O^2 = 0$ for $g(t) > 0$ and $H_O^2 = 0.01\,\mathrm{mg \cdot m^{-3}\,da^{-1}}$ for $g(t) = 0$ and $z \geq \Delta z_1$, $H_O^3 = 0.01\,\mathrm{mg \cdot m^{-3}\,da^{-1}}$, $H_O^4 = 0.01\,\mathrm{mg \cdot m^{-3}\,da^{-1}}$, $H_O^5 = k_D D_A^{1/3}$ (the adsorption coefficient $k_D = 0$ for $A = g, r, f$ and $k_D = 0.005\,\mathrm{da^{-1}}$ when $A = W$), $H_O^6 = k_Z Z^{1/4}$ (the biosedimentation coefficient $k_Z = 0$ when $A = g, r, f$ and $k_Z = 0.004\ \mathrm{da^{-1}}$ for $A = W$), $H_O^7 = k_B B_A$ (the bacterial destruction coefficient $k_B = 0.01\,\mathrm{da^{-1}}$ for $A = g, r, f$ and $k_B = 0.05$ when $A = W$). Simulation experiments show that the anthropogenic sources of oil hydrocarbons (Q_O) estimated by Mcintyre (1999) are transformed to other forms by 56% in surface snow, floating ice, and submerged ice and by 72% in water. Stabilization of the distribution of oil hydrocarbons is realized 3 years after t_0. The average level of oil pollution in the Arctic Basin reaches 0.005 mg/L. This is lower than the natural level of World Ocean pollution. In the zone of influence of the Gulf Stream and in Pacific waters an insignificant increase in this level is observed. The Barents and Kara Seas are the most polluted. Here the concentration of oil hydrocarbons reaches the value 0.03 mg/L. The average summary content of oil hydrocarbons in the Arctic Basin is 65,331 t (metric tons) with a dispersion of 32%. The hierarchy of flows H_O^i $(i = 1, \ldots, 7)$ (see Equation (6.10)) is estimated by the set $H_O^2 > H_O^4 > H_O^1 > H_O^5 > H_O^6 > H_O^7$. This set changes for each of the Arctic seas. The order of preponderance of destruction processes H_O^i of oil hydrocarbons is defined by seasonal conditions. Oxidation at the expense of evaporation of oil hydrocarbons (H_O^2) prevails over the other processes in summer.

In reality, oil hydrocarbons evaporated from the surface of Arctic seas return to the Arctic Basin from precipitation. These processes are simulated in blocks APM and PSM. The maximal destruction of oil hydrocarbons is $0.0028\,\mathrm{g \cdot m^{-2}\,da^{-1}}$. The flow H_O^7 due to bacterial decomposition averages $27\,\mathrm{t \cdot yr^{-1}}$. It has unequal values for different seas ($\mathrm{t \cdot yr^{-1}}$): Bering 3.7, Greenland 11, Norwegian 2.2, Barents 3.4, Kara 2.3, White 2.3, Laptev 2.8, East Siberian 2.8, Chukchi 3.4, Beaufort 2.5, and Central Basin 0.5.

The total estimate of the role of the Arctic Basin ecosystem in the dynamics of oil hydrocarbons can be traced for each Arctic sea. As an example, Figure 6.7 gives such results for the Barents Sea. The discrepancy between simulation results (solid curve 1) and the data of curves 2 and 3 (Terziev, 1992) is explained by the assumption that the trophic structures of different Arctic seas are described by means of the general scheme represented in Figure 6.3 and discrimination between the ecological elements in each Arctic sea is not taken into consideration in the SSMAE.

Figure 6.7 indicates that the vegetative period for phytoplankton in the Barents Sea lasts 4.9 months as shown by the ecosystem's contribution to the self-cleaning of oil hydrocarbons (dashed curve). In the case considered, the Barents Sea ecosystem neutralizes about 25% of oil hydrocarbons during the vegetative period. The rest of the time this value oscillates near 3%. Dispersion of these estimates with latitude reaches 53%. For example, in the northern part of the Barents Sea the vegetative

period lasts from 2.6 to 3.1 months, while in southern latitudes the variation is 5.3–5.8 months. Consequently the ecosystem's role in the self-cleaning of oil hydrocarbons is 8% and 36% for northern and southern water areas, respectively. Such estimates can be calculated for each cell $\Delta\varphi \times \Delta\lambda \times \Delta z$ of the Arctic Basin.

6.4.5.5 The dynamics of pollutants in the Arctic Basin

Determining and understanding the role of the various pollutant sources in forming the pollution levels for different Arctic Basin areas are important issues (McCauley and Meier, 1991). A major function of the SSMAE is to estimate the pollution dynamics in each of cells $\Omega_{ij} \subseteq \Omega$ as a function of time. The influence of pollutant sources on the Arctic ecosystem occurs through the boundary area $\Omega_R \cup \Omega_P \cup \Omega_B \cup \Omega_N \cup \Omega_\Gamma$ and through the atmosphere. A full picture of the spatial distribution of pollutants can be formed from local dynamic processes. The incompleteness of the Arctic database forces some scenarios to be considered and some assumptions to be made in an attempt to make indefinite Arctic system parameters concrete. Krapivin *et al.* (1998) estimated the flow of pollutants to the Kara Sea based on experimental measurements of radionuclear pollution and heavy metals in the Angara–Yenisey river system. Therefore, the SSMAE is used to estimate the flow of pollutants from the Kara Sea to the other water areas of the Arctic Basin.

The Ob′ and Yenisey Rivers are considered to be the main sources of radionuclear pollution, heavy metals, and oil hydrocarbons for the Kara Sea (Table 6.10). Figure 6.8 shows the influence of river flow on the volume of pollutants transported by the Kara Sea aquageosystem to the Central Basin. As shown by curves 1 and 2, the transfer of heavy metals and radionuclides from the Ob′ and Yenisey Rivers through the Kara Sea aquageosystem to the Central water areas of the Arctic Basin amounts to 2.1% when the river flow varies from 500 km^3/yr to 1,000 km^3/yr and after that it begins to grow linearly up to 7.6% for 2,000 km^3/yr. Hence, there is a critical level of pollution for the Kara Sea ecosystem beyond which it does not have time to dilute the flow of heavy metals and radionuclear pollutants. Similar estimations can be obtained for the other elements of set Ω_R using the rivers referred to in Table 6.10.

The SSMAE allows for estimation of the flow of pollutants between the different water areas of the Arctic Basin. For example, the transport of heavy metals and oil hydrocarbons from the Barents Sea to the Kara Sea is 631 $kg\,yr^{-1}$ and 473 $kg\,yr^{-1}$, respectively. The total flow of pollutants from the Russian coastline to Alaska varies in Table 6.10 between 0.3% and 0.9% of the initial flow. As is evident from curves 3 and 4 of Figure 6.8, the flow of the Ob′ and Yenisey Rivers has practically no influence on the pollution level of Arctic waters near Alaska. This effect does not change over time.

6.4.6 Summary and conclusions

We will discuss here three aspects of the SSMAE which are very important. The first concerns the incorporation of ecological, hydrophysical, climatic, and biogeochemical relationships in a model simulating the dynamics of Arctic Basin pollution.

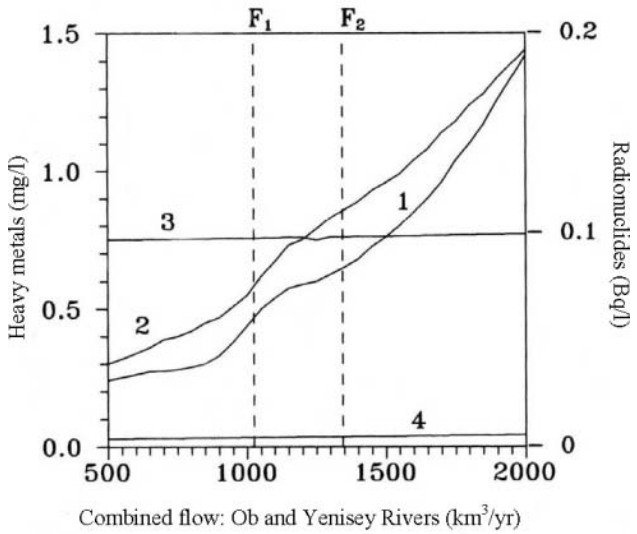

Figure 6.8. Dependence of the concentrations of heavy metals ($\psi + e$) and radionuclides ($\varepsilon = {}^{137}\mathrm{Cs} + {}^{60}\mathrm{Co}$) at different geographical points as a function of the flow (F) of the Ob′ and Yenisey Rivers to the Kara Sea. The interval $[F_1, F_2]$ between the dashed lines corresponds to the range of variations of F in the real world. Curves 1 and 2 show concentrations of the heavy metals and radionuclides, respectively, at the point $\varphi, \lambda = 75^\circ\mathrm{N}, 65^\circ\mathrm{E}$ in the northwestern part of the Kara Sea. Curves 3 and 4 show the concentrations of heavy metals and radionuclides, respectively, at the point $\omega, \lambda = 72^\circ\mathrm{N}, 150^\circ\mathrm{W}$ above the Alaskan north coast.

The main problem here is how to parameterize these relationships to achieve the requisite precision. The second concerns the key problem of database conformity to the model. In this case, the task lies in adapting the spatiotemporal scale to the database. The third concerns the user's ability to run the SSMAE in the scenario space.

This investigation shows that simulation experiments provide the possibility of studying both the common and spatial distributions of pollutant dynamics in the Arctic Basin. The precision of the results is a function both of the scenarios and the ways in which elements in Equations (6.1)–(6.16) are parameterized. It is obvious that the SSMAE is not effective when climate conditions reach a critical state or when the anthropogenic impacts are increased to a critical value. But, in the SSMAE the Arctic Basin acts as a stabilizing sub-system of the biosphere. When the atmospheric temperature reaches $-1^\circ\mathrm{C}$, there occurs an inverse connection in the water balance of the atmosphere–land–sea system, which acts to stabilize the estimates. Parameterization of such variations in the framework of the SSMAE is not convenient. Nevertheless, by connecting the SSMAE to a global database having estimates of such parameters as ice area, temperature, and albedo distributions, will allow the use of the SSMAE in the present form. The effectiveness of the SSMAE will increase using such models as the coupled ice–ocean model described in Riedlinger and Preller (1991). In general, many different modifications of the SSMAE are possible. But, it is

obvious that movement to the optimal SSMAE structure demands greater accuracy in pollutant types, ecosystem structure, water cycle, ice movement, and climate model. The main difficulty is optimal modification at the same time for each of the blocks of the SSMAE.

The pollution level of the Arctic Basin is formed mainly by river flows. Because of this, block MRF plays a very important role in the SSMAE. Regular monitoring of water flows and pollutant inputs by rivers to the SSMAE is impossible. Consequently, the study and measurement of these flows during scientific expeditions and the modeling of the results are necessary steps in the investigation of Arctic Basin pollution.

A good example of such a step is the U.S./Russian expedition of 1995 which obtained on-site measurements of pollution levels in the Yenisey and its tributary the Angara, in its attempt to investigate the likely origins of land-based sources contributing to pollution levels in the Yenisey estuary.

SSMAE verification is important. It will be possible to realize this after essential modifications to the SSMAE, using models of greater precision to account for hydrological, biogeochemical, ecological, and climatic processes. The present SSMAE structure is part of the new technology of Arctic Basin pollution monitoring. Greater accuracy in the SSMAE may be realized by means of simulation experiments in which model parameters are varied over wide intervals. However, that is beyond the scope of this chapter.

Let us now look at several results of this investigation. In the nuclear war scenario, for example, the SSMAE shows that Arctic environmental stability would be disturbed 3 months after the impact. From other scenarios, it follows that variations in the velocity of vertical advection from 0.004 cm/s to 0.05 cm/s does not affect the Arctic environmental state. An error of 32% in ice area estimate leads to a variation in simulation results of 36%. When this error is more than 32%, simulation results become less stable and can vary by several times. The problem exists of finding the proper criterion to estimate SSMAE sensitivity to variations in model parameters. As Krapivin (1996) showed, a survivability function $J(t)$ reflecting the dynamics of the total biomass of living elements would enable this sensitivity to be estimated. In this instance

$$J(t) = \frac{\sum_{i=1}^{5} \iint_{(\varphi,\lambda)\in\Omega} \int_0^{H(\varphi,\lambda)} B_i(t,\varphi,\lambda,z)\, d\varphi\, d\lambda\, dz}{\sum_{i=1}^{5} \iint_{(\varphi,\lambda)\in\Omega} \int_0^{H(\varphi,\lambda)} B_i(t_0,\varphi,\lambda,z)\, d\varphi\, d\lambda\, dz}.$$

Index $J(t)$ provides an estimate of the uncertainty associated with SSMAE parameters. Although a complete investigation of the influence of SSMAE parameter variations on model results should be done independently, various estimates are given here. Preliminary simulation results show that the SSMAE permits variations in the initial data between -70% to 150%. A great degree of uncertainty ($\pm 50\%$) is permitted in the value of such parameters as μ_A, δ_n, V_i, T_c, T_{opt}, ρ_1, and k_{ij}. The

correlation between variations in these parameters and model results is linear. However, high model sensitivity is observed under variations of β_A, α_A, E_0, and T_0. In general terms, the acceptable variation of these parameters is $\pm 20\%$. Moreover, the deviation in model results due to variations in these parameters is non-linear. For example, fluctuations of surface temperature T_0 within ± 5 K are not hazardous to the system, causing small variations in $J(t)$ by $\pm 10\%$, but fluctuations of T_0 by ± 7 K cause much larger variations ($\pm 30\%$) in the value of $J(t)$. Under such a scenario the time dependence of system dynamics to variations in parameters is diverse.

The SSMAE does not completely describe the processes taking place in the Arctic Basin. The optimal extension of SSMAE functions is possible using environmental monitoring to control parametric and functional model inputs. In this framework, prognosis of the Arctic aquageosystem state can be realized on the basis of the SSMAE and by processing observational data.

6.5 INTERACTIONS IN THE ARCTIC SYSTEM

The Arctic region is a mosaic of freshwater, terrestrial, and marine ecosystems intimately interactive with factors of the nature–society system. Interactions include many components such as ocean/atmosphere/ice, land/atmosphere/ice, and land/ocean/freshwater. An interpretation and prediction of correlations between the processes occurring in the Arctic environment is possible only in the framework of the complex approach to the study of these processes. This approach is based on GIMS technology (Kelley *et al.*, 1992, 1999; Kondratyev *et al.*, 2002a, b). The interaction between the atmosphere, land, and sea ecosystems under the Arctic climate is characterized by a series of spatiotemporal scales. An understanding of the interior correlations at every level is key to environmental monitoring. Each scale has a specific landscape, vegetation cover, topography, character of both hydrophysical and weather structures, and living elements. Discovery of the internal and external correlations between these elements and other elements of the NSS makes it possible to form a database for an Arctic Basin monitoring system.

Interactions between the Arctic components of the global NSS have been studied by many authors (McCauley and Meier, 1991; Trites *et al.*, 1999; Kondratyev and Johannessen, 1993; Riedlinger and Preller, 1991; Preller and Cheng, 1999; Kelley and Gosink, 1992). A good example of these interactions is the Angara/Yenisey river system in Siberia. The intensive industrial development of northern Russian territories has led to significant environmental changes in these regions (Morgan and Codispoti, 1995). Major quantities of pollutants are brought to the northern coast of Russia by rivers, thus threatening the balance of ecosystems of the northern seas. The Angara–Yenisey river system (AYRS) is no exception.

The Yenisey River flows northward to the Kara Sea along the boundary between the western Siberian floodplain and the central uplands, draining an area of about 2.6 million km^2 over its 4,100 km length. The flow rate of the Yenisey into the Kara Sea has large seasonal variations, averaging 19,800 m^3/s, reaching as much

as 130,000 m^3/s during the spring. The Angara, a major tributary, accounts for about one-fourth of the total flow. It flows swiftly northward from Lake Baikal for about one-third of its 1,850 km length, before turning westward toward its confluence with the Yenisey. Recognizing that major sources of the radionuclides found in the Kara Sea, as well as other environmental pollutants, might lie in the Siberian watersheds of the Yenisey and the Angara, a joint Russian–American expedition was undertaken in July and August of 1995. The region under study included the five hydroelectric dams at Krasnoyarsk and Sayano-Shushenskoye on the Yenisey and at Irkutsk, Bratsk, and Ust-Ilimsk on the Angara. The power output from these facilities fostered rapid industrial growth in this region. Krasnoyarsk is the major industrial city located on the upper reaches of the Yenisey. Nearby is the nuclear production and processing facility, Krasnoyarsk-26, which is situated approximately 270 km upstream of the Angara–Yenisey junction. Along the Angara River, there are five cities with major industrial activities: Irkutsk, Angarsk, Usolye-Sibirskoye, Svirsk, and Bratsk. These cities have facilities producing both radionuclides and chemical pollutants, possible pollutant sources in the two rivers.

Samples of Angara River water and sediment were taken near its source at Lake Baikal and at selected sites of interest downstream of its junction with the Yenisey River near the lumber-processing village of Strelka. Along the Yenisey sampling was conducted on both sides of the junction just upstream of the village of Kazachinskoye and continuing downstream to the town of Lesosibirsk.

As Krapivin (1995) showed, complex evaluation of the pollution level in the Arctic Basin as a whole is possible by synthesizing a mathematical model of pollutant transport by rivers from adjacent territories.

6.5.1 The Angara–Yenisey river system simulation model

Following Krapivin (1995), a block diagram of the AYRSSM (AYRS simulation model) is given in Figure 6.9. The AYRSSM has three levels of blocks (AYRSSM blocks are described in Table 6.15). The two blocks of the first level take control of the models of different processes and various regimes of the computer experiments. Block HYD simulates river flow and considers the correlation between the water regime and ecological, topographical, and synoptical parameters of the territory studied. Block CON brings together functions of the informational interface between the user and other AYRSSM blocks. The main function of CON is forming the database and identification of AYRS elements. The four blocks of the second level analyze input information and synthesize the AYRSSM structure. The 26 blocks of the third level bring about concrete models and processes during the computer experiment.

Let us suppose that the AYRS watershed has area Ω. The spatial structure of Ω is determined by the spatial discretization of the AYRS surface with a uniform geographic grid with latitude φ and longitude λ divided into steps of $\Delta\varphi$ and $\Delta\lambda$, respectively. In this study, we suppose $\Delta\varphi = \Delta\lambda = 0.1^\circ$. As a result, the area $\Omega = \bigcup_{i=1}^{N} \Omega_k$, where Ω_k is part of Ω of area $\sigma_k = \Delta\varphi\,\Delta\lambda$, $\left(\sum_{k=1}^{N} \sigma_k = \sigma\right)$. The cells Ω_k

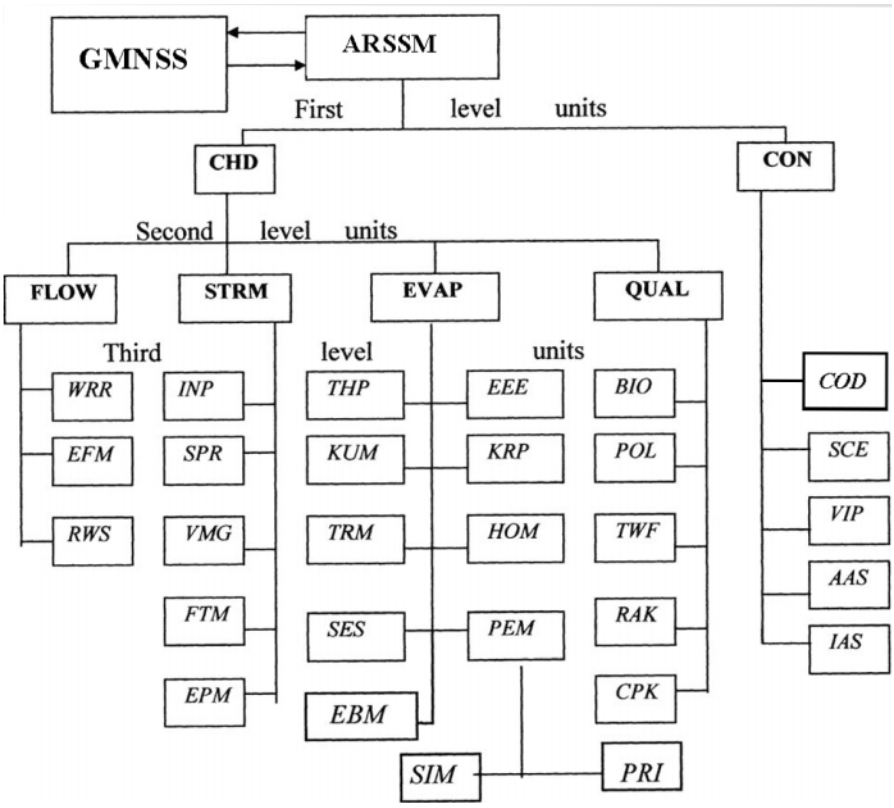

Figure 6.9. Structure of the AYRSSM.

are situated along the AYRS beginning with Ω_1 at the Angara River source up to Ω_N in the Yenisey River mouth. The procedure of spatial discretization is provided for by the IAS block by including in the AYRSSM database the set of identifiers $A_k = \|a_{ij}^k\|$, $k = 1, \ldots, 5$. The hydrology regime of the AYRS is described by the schematic diagram of Figure 6.10. Equations for this scheme can now be written in the form of balance correlations for each of the Ω_k ($k = 1, \ldots, N$):

$$\sigma_k\left(\frac{\partial W}{\partial t} + \xi_\varphi \frac{\partial W}{\partial \varphi} + \xi_\lambda \frac{\partial W}{\partial \lambda}\right) = V - B\sigma_k + D + T + L, \tag{6.17}$$

$$\rho_k\sigma_k\left(\frac{\partial C}{\partial t} + \mu \frac{\partial C}{\partial x}\right) = \rho_k\sigma_k B + J + K - V - U - F - M - R, \tag{6.18}$$

$$(1-\rho_k)\sigma_k \frac{d\Phi}{dt} = U + F + M + N + (1-\rho_k)\sigma_k B - T - L - K - P, \tag{6.19}$$

$$\sigma_k\left(\frac{\partial G}{\partial t} + v_\varphi \frac{\partial G}{\partial \varphi} + v_\lambda \frac{\partial G}{\partial \lambda}\right) = R + P - J - N - D, \tag{6.20}$$

Table 6.15. List of blocks of the AYRSSM, whose scheme is presented in Figure 6.9.

Identifier of the block	*Description of the unit*
CHD	Takes control of parameterizing hydrophysical and hydrological processes in the AYRS.
CON	Interface control of the computer experiment..
FLOW	Model of river run-off.
STRM	Simulation procedure that reflects water mass motion in the AYRS.
EVAP	The choice of model to parameterize the process of evaporation.
QUAL	The choice of criterion to assess water quality.
WRR	Model of the water regime in a water body.
EFM	An empirical model of river run-off.
RWS	Model to simulate how river run-off spreads beyond the riverbed.
INP	Model of infiltration.
SPR	Model of the sink taking into account the effect of vegetation and soil covers.
VMG	Model of the vertical uplifting of ground water in evaporation, feeding, and exfiltration.
FTM	Model of filtration.
EPM	An empirical model of precipitation.
THP	A specified model of transpiration.
RUM	The Kuzmin model (Kuzmin, 1957).
TRM	A simple model of transpiration.
SES	Model of snowmelt and evaporation from snow surface.
EBM	Parameterization of evaporation using the method of energy balance.
PEM	The Penman model (Penman, 1948).
PRI	The Penman model as specified by Priestley (Bras, 1990).
KRP	The Penman model as specified by Kohler and Richards (1962).
SIM	A simplified version of the Penman model.

Identifier of the block	*Description of the unit*
EEE	Empirical models of evaporation.
KOH	The Kohler model (Bras, 1990).
HOM	The Horton model (Bras, 1990).
BIO	A simulation model of sedimentation and biological assimilation of pollutants.
POL	A simulation model of the formation of anthropogenic fluxes of pollutants.
TWT	Model of the process of water temperature formation.
RAK	Model of kinetics of the radionuclide pollution of water.
CPK	Model of kinetics of the chemical pollution of water.
COD	Database correction.
SCE	The choice and formation of scenario for the simulation experiment.
VIP	Visualization of simulation experiment results.
AAS	Adaptation of the AYRSSM to the scenario of the simulation experiment.
IAS	Referencing the AYRSSM to spatiotemporal scales.

where ξ_φ and ξ_λ are projections for the wind speed; ρ_k is the part of area Ω_k occupied by the river; μ is the speed at which the river flows; v_φ and v_λ are speed projections for ground water motion; x is the direction of river flow; and t is time.

The functions on the right-hand side of Equations (6.17)–(6.20) are described by mathematical expressions in accordance with Krapivin *et al.* (1996a, b) and Bras (1990). Appropriate models are given in Table 6.15. There are various realizations of these functions. This provides the user of the AYRSSM with the possibility of forming scenarios for computer experiments. The values of ξ, μ, and v were estimated using the Irkutsk Scientific Center database. It is possible for the user to vary these parameters during the calculation process. In this study, average values of these parameters are estimated by $\xi = 3.3\,\text{m/s}$, $\mu = 1.7\,\text{m/s}$, and $v = 0$. Variations in parameter μ are realized by adapting the left part of Equation (6.18) to the empirical data illustrated in Figure 6.10. Boundary conditions for Equations (6.17)–(6.20) are formed by the global model (Krapivin, 1993). Soil moisture transport between cells Ω_k is disregarded. Synoptic situations are described by a discrete scheme with temporal parameters t_i $(i = 1, \ldots, 4)$, where t_1 is the beginning of summer, t_2 is the start of winter, t_3 is the end of winter, and t_4 is the time of the spring thaw when snow and ice are melting. Between these times the synoptic situation does not change.

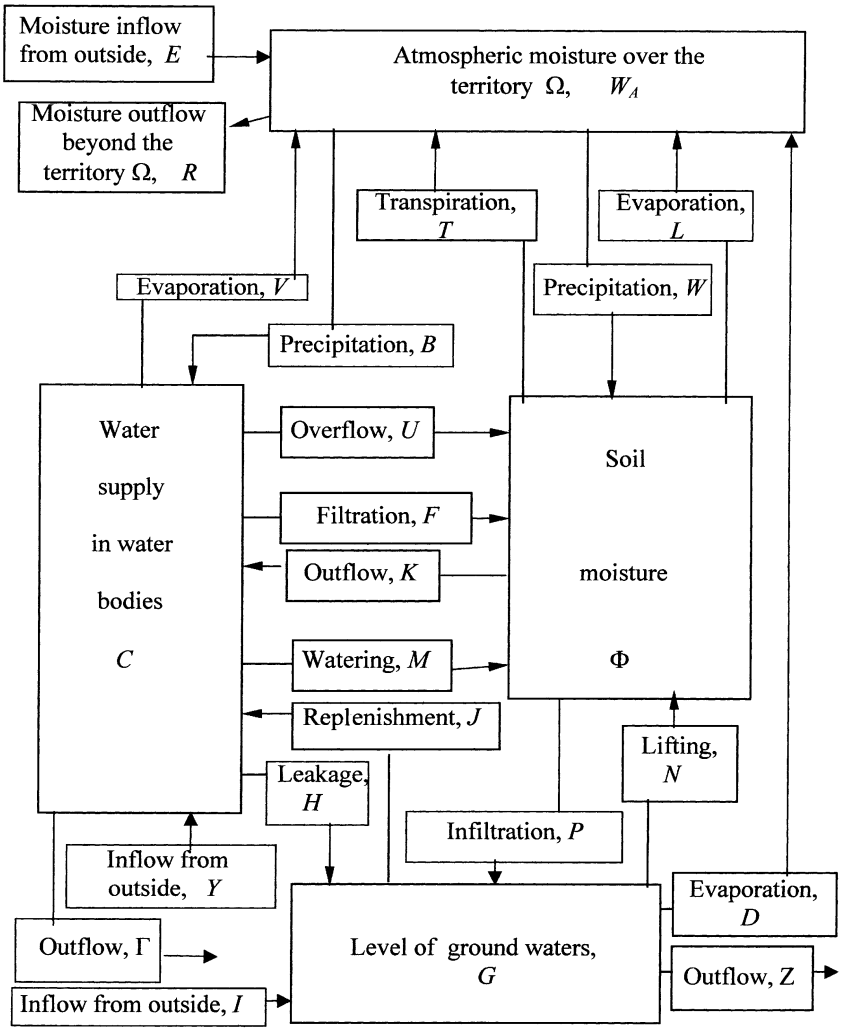

Figure 6.10. Block diagram of the AYRS water regime on area Ω_k ($k = 1, \ldots, N$). The functions W, B, C, G, and Φ are given in meters. All the other functions are in cubic meters per day.

In the common case, the vertical structure of the river water area in Ω_k ($k = 1, \ldots, N$) is described by block SES (Krapivin, 1995). A snow layer of thickness g_k is formed at the expense of flow B_k according to:

$$\frac{dg_k}{dt} = \begin{cases} 0, & \text{when } t \notin [t_2, t_3]; \\ B_k, & \text{when } t \in [t_2, t_3]. \end{cases} \tag{6.21}$$

For $t \in [t_3, t_4]$ the value of $g_k(t, \varphi, \lambda)$ decreases linearly from $g_k(t_3, \varphi, \lambda)$ to $g_k(t_4, \varphi, \lambda) = 0$. The functional representation of the other blocks from Table 6.15

is realized at times t_i ($i = 1, \ldots, 4$) by values which are given by the user for scenario realization. The dynamics of pollutants in the AYRS is determined by the structure of its hydrological regime, which takes into account the transport of pollutants by water motion and their accumulation in sediments, ice, snow, and the living biomass. Pollutant types are divided into radionuclear elements and heavy metals. The set of radionuclear pollutants is described by index ν. The set of heavy metals is divided into particles (index e) and the dissolved fraction (index ψ).

The νth radionuclide is characterized by its half-life t_ν, by the rates $H_{k\nu}$ of input to and output from area Ω_k ($k = 1, \ldots, N$), and by the concentrations of Q_ν, E_ν, Ξ_ν, and S_ν in the water, soil, sediment, and ground water, respectively. As a result the main balance equations of the RAK block can be written in the form:

$$\Delta_k\left(\frac{\partial Q_{k,\nu}}{\partial t} + \mu_k \frac{\partial Q_{k,\nu}}{\partial x}\right) = H_{1,\nu} + H_{2,\nu} + H_{3,\nu} - H_{4,\nu} - H_{5,\nu} + H_{6,\nu} - H_{7,\nu} + \rho_k H_{12,\nu} - \frac{\ln 2}{t_\nu}\Delta_k Q_{k,\nu}, \tag{6.22}$$

$$\delta_k \frac{\partial E_{k,\nu}}{\partial t} = H_{8,\nu} + H_{4,\nu} + H_{9,\nu} - H_{10,\nu} + (1-\rho_k)H_{12,\nu} - \delta_k E_{k,\nu}\frac{\ln 2}{t_\nu}, \tag{6.23}$$

$$\psi_k \frac{\partial \Xi_{k,\nu}}{\partial t} = H_{5,\nu} - H_{6,\nu} - \psi_k \Xi_{k,\nu}\frac{\ln 2}{t_\nu}, \tag{6.24}$$

$$y_k\left(\frac{\partial S_{k,\nu}}{\partial t} + v_\varphi \frac{\partial S_{k,\nu}}{\partial \varphi} + v_\lambda \frac{\partial S_{k,\nu}}{\partial \lambda}\right) = H_{7,\nu} + H_{10,\nu} - H_{2,\nu} - H_{9,\nu} - H_{11,\nu} - y_k S_{k,\nu}\frac{\ln 2}{t_\nu}, \tag{6.25}$$

where $H_{1,\nu}$ is the rate of radionuclide leaching from the soil with flow K; $H_{2,\nu}$ is the radionuclide input to the river from ground water with flow J; $H_{3,\nu}$ is the transport of radionuclides to area Ω_k through the boundary of Ω by AYRS tributaries; $H_{4,\nu}$ is the radionuclides carried out with flows U, F, and M; $H_{5,\nu}$ is radionuclide sedimentation at the river bottom by gravitation and with the dead biomass of the river ecosystem; $H_{6,\nu}$ is the leaching of radionuclides from sediments; $H_{7,\nu}$ is the radionuclide leakage to ground water with flow R; $H_{8,\nu}$ is the anthropogenic source of radionuclides; $H_{9,\nu}$ is radionuclide input to the soil from ground water by flow N; $H_{10,\nu}$ is radionuclide leaching from the soil to the ground water by P flow; $H_{11,\nu}$ is the radionuclide loss by sedimentation in ground water; and $H_{12,\nu}$ is radionuclide input by rain. The quantities $\Delta_k = \rho_k \sigma_k C_k$, $y_k = \sigma_k G_k$, $\delta_k = l_k(1-\rho_k)\sigma_k$, and $\psi_k = r_k \rho_k \sigma_k$, where l_k is the thickness of the efficient soil layer on area Ω_k, and r_k is the thickness of the sediment layer.

Flows $H_{i,\nu}$ ($i = 1, \ldots, 12$) can be parameterized by linear models according to Krapivin (1995) and Nitu *et al.* (2000a). The BIO and CPK blocks are described by similar balance models in analogy with the models described by Somes (1999) and Kram (1999). AYRS biology is given in the form of a scenario or is described by

the model of Legendre and Krapivin (1992). The flows of heavy metals include the assimilation of dissolved fractions by plankton (H_{ψ}^{Z}) and by nekton (H_{ψ}^{F}), the sedimentation of solid fractions (H_{e}^{1}), the absorption from sediments by living elements ($H_{e,\psi}^{L}$), sedimentation with dead organic matter (H_{ψ}^{D}), and the discharge from sediments ($H_{e,\psi}^{a}$) by erosion, diagenesis, turbulence, and anthropogenic impacts. The balance equations taking these flows into account have the same form as Equations (6.22)–(6.25):

$$\Delta_k\left(\frac{\partial e_w}{\partial t}+\mu_k\frac{\partial e_w}{\partial x}\right)=\sum_{i=1}^{3}\alpha_2^i Q_{e,\psi}^i-H_e^1+\alpha_1 H_{e,\psi}^a, \tag{6.26}$$

$$\Delta_k\left(\frac{\partial \psi_w}{\partial t}+\mu_k\frac{\partial \psi_k}{\partial x}\right)=(1-\alpha_1)H_{e,\psi}^a-H_{\psi}^Z-H_{\psi}^D, \tag{6.27}$$

$$\psi_k\frac{\partial e^*}{\partial t}=H_e^1-\alpha_1(H_{e,\psi}^L+H_{e,\psi}^a), \tag{6.28}$$

$$\psi_k\frac{\partial \psi^*}{\partial t}=H_{\psi}^D-(1-\alpha_1)(H_{e,\psi}^L+H_{e,\psi}^a), \tag{6.29}$$

where (e_w, e^*) and (ψ_w, ψ^*) are heavy metal concentrations in water, sediments as solid and dissolved phases, respectively; $Q_{e,\psi}^i$ is the heavy metal input from AYRS tributaries ($i=1$), from atmospheric precipitation ($i=2$), and from industrial waste ($i=3$); α_1 is the solid fraction part in bottom sediments and α_2^i is the solid particle part in the ith flow of heavy metals. The removal of heavy metals from water by evaporation and sprays is disregarded.

Approximate solutions to the initial value problem for Equations (6.17)–(6.29) are realized by means of the quasi-linearization method (Nitu *et al.*, 2000b).

6.5.2 *In situ* measurements

To get data for the AYRSSM database, the joint U.S./Russian expedition to Siberia's Angara and Yenisey Rivers was conducted in the summer of 1995 (Phillips *et al.*, 1997; Krapivin *et al.*, 1998). Sampling began at the town of Bolshaya Rechka on the Angara near Lake Baikal and continued past the cities of Irkutsk, Angarsk, and Bratsk, with a side trip on the Kitoy River, near Angarsk. The expedition then proceeded to the Yenisey–Angara junction. Sampling began near the village of Kulakovo upstream on the Angara and continued downstream to the junction with the Yenisey at the logging town of Strelka. On the Yenisey, sampling began near the village of Kazachinskoye above the junction and continued downstream past the industrial complex at Lesosibirsk below the junction. Figure 6.11 shows points of measurements during this expedition. The water balance of the AYRS was calculated with the data given in Figure 6.12. Some results from this expedition are given in Tables 6.16–6.19. A mobile radionuclide analysis system consisting of a mechanically cooled germanium gamma-ray spectrometer in a lead shield was set up on-site in Irkutsk. The results of this analysis are given in Table 6.16. An X-ray-fluorescent spectrometer (XRF) was also set up on-site and used to screen samples for heavy

Table 6.16. Results of measurements of the content of radionuclides in river bottom sediments made in July 1996 (averaged data of isotopic activity, Bq/kg of dry weight). Places of sampling are marked in the map in Figure 6.12 and are listed in Table 6.17.

Place of sampling	^{60}Co	^{137}Cs	^{152}Eu	^{235}U	^{238}U
Angara					
Upstream of the Irkutsk dam	<2.0	2.2 ± 1.0	<3.1	<1.9	<280
Downstream of the Irkutsk dam	<3.5	<3.6	<5.3	27.2 ± 4.6	720 ± 300
Angarsk (technical canal)	<2.0	<1.8	<3.1	<1.7	<320
Upstream of Angarsk	<4.1	25.2 ± 3.1	<6.0	<4.2	<630
Upstream of the Bratsk dam	<2.3	<2.3	<3.9	<2.2	<420
Downstream of the Bratsk dam	<2.6	3.4 ± 1.2	<4.0	<2.5	<440
Before the confluence of the Angara with the Yenisey	<1.9	2.2 ± 1.0	<2.8	<1.7	<290
Yenisey					
Upstream of Kazachinskoye	8.6 ± 1.9	22.9 ± 2.3	6.7 ± 3.0	<2.7	<500
Kazachinskoye	241 ± 11	392 ± 12	151 ± 27	<8.2	<1,340
Downstream of Kazachinskoye	30.1 ± 3.0	203 ± 5	42.3 ± 9.5	<3.8	<680
Confluence of the Angara with the Yenisey (the settlement Strelka)				<4.5	<840
Downstream of Lesosibirsk	96.9±5.1 <5.7	211±6 27.1 ± 3.8	55.7±13.5 <8.2	< 6.4	< 860

metals. After the expedition, samples were sent to a commercial laboratory for element analysis. The results of this analysis are given in Tables 6.18 and 6.19. Results for each of these two categories of pollutants are discussed below.

6.5.2.1 Radionuclides in river sediment

The synthetic radioisotope ^{137}Cs (which has a 30-year half-life) was detected in all samples analyzed above the Irkutsk dam, with concentrations ranging from 2 Bq kg^{-1} to 12 Bq kg^{-1} (dry weight). These values are consistent with background levels expected due to global fall-out as a residual from atmospheric nuclear testing. Below the Irkutsk dam in the vicinity of the cities of Irkutsk and Angarsk, measured ^{137}Cs concentrations ranged from <4 Bq kg^{-1} to 30 Bq kg^{-1}, indicating that some of the

Table 6.17. Results of on-site radionuclide measurements in river sediment.

Sample ID	*Weighted average isotopic activity* (Bq/kg of dry weight)*				
	^{60}Co	^{137}Cs	^{152}Eu	^{235}U	^{238}U
Angara River					
I1	<2.0	2.2 ± 1.0	<3.1	<1.9	<280
I2	<3.5	< 3.6	<5.3	27.2 ± 4.6	720 ± 300
I3	<3.7	30.6 ± 2.6	<5.1	<3.7	<580
A1	<2.0	< 1.8	<3.1	<1.7	<320
A2	<4.1	25.2 ± 3.1	<6.0	<4.2	<630
B1	<2.3	< 2.3	<3.9	<2.2	<420
B2	<2.6	3.4 ± 1.2	<4.0	<2.5	<440
J1	<1.9	2.2 ± 1.0	<2.8	<1.7	<290
Yenisey River					
J2	8.6 ± 1.9	22.9 ± 2.3	6.7 ± 3.0	<2.7	<500
J3	241 ± 11	392 ± 12	151 ± 27	<8.2	<1340
J4	96.9 ± 5.1	211 ± 6	55.7 ± 13.5	<4.5	<840
J6	<5.7	27.1 ± 3.8	<8.2	<6.4	<860
J7	30.1 ± 3.0	203 ± 5	42.3 ± 9.5	<3.8	<680*

* Errors given are ±2 standard deviations. The sign "<" indicates less than the minimum detectable concentration, which is given at the 90% confidence level. Sample J7 was taken in the floodplain of the Yenisey River above the junction. The locations of the other samples are given in Table 6.17.

samples contained ^{137}Cs concentrations significantly higher than the average global background. For samples taken near Bratsk, only background levels of ^{137}Cs activity were detected.

^{137}Cs concentrations in samples taken on undeveloped reaches of the Angara River upstream of the AYRS junction at Strelka were determined to have lower than background levels, about 2 Bq kg^{-1}, of dry river sediment. Downstream of the junction with the Yenisey, the ^{137}Cs concentration in samples ranged from 3 Bq kg^{-1} to 27 Bq kg^{-1}. The latter value is significantly above activity levels detected on the Angara River upstream of the junction.

In samples drawn from the Yenisey River at and upstream of the junction, levels of the neutron activation product ^{60}Co (5.27-year half-life) and of the fission products ^{137}Cs and ^{152}Eu (13.3-year half-life) were much higher than background: ranging

Table 6.18. Laboratory analysis of the concentrations of heavy metals in sediments and in water measured in July 1996 during the American–Russian hydrophysical expedition (Krapivin *et al.*, 1998). Places of sampling are marked in the map in Figure 6.12. Measurement error did not exceed one sigma.

Place of sampling	As	Cd	Cr	Cu	Ni	Pb	Zn
Samples of river bottom sediments (ppm)							
Grand River	7.2	<0.52	26	19	25	15	64
Upstream of the Irkursk dam	5.0	<0.51	41	22	44	11	55
Downstream of the Irkutsk dam	4.5	<0.51	20	11	21	9	17
Angarsk (technical canal)	0.9	<0.50	7.0	11	9.3	7.9	31
Upstream of Angarsk	4.3	<0.51	48	38	40	14	86
Kitoy River	2.4	<0.50	27	20	37	7.8	40
Upstream of the Bratsk dam	<0.5	<0.50	6.4	9	12	2.3	22
Downstream of the Bratsk dam	3.4	<0.50	31	210	39	6.1	50
Angara (upstream of the confluence with the Yenisey)	3.2	<0.50	14	13	18	4.5	31
Confluence of the Angara with the Yenisey (the settlement Strelka)	5.1	<0.51	47	35	37	14	100
Downstream of Lesosibirsk	6.9	<0.51	34	31	36	17	100
Kazachinskoye	5.8	<0.51	54	43	390	18	150
Upstream of Kazachinskoye	2.2	<0.50	18	8.2	20	3.9	47
Water samples (ppm)							
Downstream of the Irkutsk dam	12	<0.50	<10	<20	<20	<5.7	<5.7
Upstream of the Irkutsk dam	10	<0.50	<10	<20	<20	<5.7	<5.7
Angarsk	12	<0.50	<10	<20	<20	<5.7	<5.7
Upstream of the Bratsk dam	16	<0.50	<10	<20	<20	<5.7	<5.7
Angara (just before the confluence with the Yenisey)	12	<0.50	<10	<20	<20	<5.7	<5.7
Downstream of Lesosibirsk	13	<0.50	<10	<20	<20	<5.7	<5.7
Kazachinskoye	8.6	<0.50	<10	<20	<20	<5.7	<5.7

Table 6.19. Comparison of results (ppm) of the laboratory analysis of materials from the 1996 expedition on Angara water quality (Analytical Services Center of Ecology and Environment, Inc., New York).

Type of data	*Data of the Irkutsk Ecological Service on Angara water quality control*						*Results of water samples analysis*	
Year	*1978*		*1979*		*1980*		*1996*	
Season	*T1*	*T2*	*T1*	*T2*	*T1*	*T2*	*August*	
The Ershov water collector (upstream of the Irkutsk dam)							Map ID #I15	Map ID #I11
Mg	3.2	3.0	3.3	3.1	3.4	3.3	3.5	4.9
Fe	na	na	0.01	nm	na	na	<0.05	<0.05
As	na	na	na	na	na	na	0.0063	0.012
Zn	na	na	na	na	na	na	0.15	0.12
Cu	0.002	0.002	0.003	0.002	0.001	0.003	<0.02	<0.02
Mn	0.001	0.001	0.003	0.005	0.003	0.006	<0.01	<0.01
Al	0.005	0.005	0.018	0.008	0.004	0.007	<0.1	<0.1
Co	nm	na	nm	na	na	na	<0.02	<0.02
Ni	na	na	nm	0.003	0.001	0.002	<0.02	<0.02
V	na	na	na	na	na	na	<0.02	<0.02
Pb	na	na	na	na	na	na	<0.0057	<0.057
The water collector near the Sukhov station upstream of Angarsk							Map ID #A14	
Mg	3.4	3.4	3.7	3.5	3.3	3.4	3.2	
Fe	0.02	0.3	0.07	0.001	na	na	<0.05	
As	na	na	na	na	na	na	0.012	
Zn	na	na	0.0053	na	na	na	0.24	
Cu	0.001	0.002	0.004	0.007	0.004	0.008	<0.02	
Mn	0.011	nm	0.018	0.007	0.012	0.011	0.028	
Al	na	0.015	0.02	0.028	0.013	0.012	<0.01	
Co	nm	na	0.004	0.002	na	na	<0.02	
Ni	nm	0.001	0.003	0.002	0.002	0.0005	<0.02	
V	na	na	na	na	0.001	na	<0.02	
Pb	na	na	na	na	na	na	<0.0057	

Type of data	*Data of the Irkutsk Ecological Service on Angara water quality control*						*Results of water samples analysis*
Year	*1978*		*1979*		*1980*		*1996*
Season	*T1*	*T2*	*T1*	*T2*	*T1*	*T2*	*August*
The water collector 0.5 km downstream of the Bratsk dam							Map ID #B2
Mn	4.4	3.8	4.4	3.9	4.8	5.2	4.9
Fe	na	na	0.02	0.13	na	na	<0.05
As	na	na	na	na	na	na	0.016
Zn	na	na	na	na	na	na	0.087
Cu	na	na	na	na	na	na	<0.02
Mn	na	na	0.004	0.001	0.002	0.001	<0.01
Al	nm	0.002	na	0.002	0.003	nm	<0.1
Co	na	na	na	na	na	na	<0.02
Ni	nm	na	na	na	na	na	<0.02
V	na	na	na	0.001	0.001	0.15	<0.02
Pb	na	na	na	na	na	na	<0.0057

from 9 Bq kg^{-1} to 240 Bq kg^{-1} for ^{60}Co, from 14 Bq kg^{-1} to 400 Bq kg^{-1} for ^{137}Cs, and from 7 Bq kg^{-1} to 150 Bq kg^{-1} for ^{152}Eu. These are unmistakable indications of reactor products and are consistent with releases from the plutonium production reactors at Krasnoyarsk-26, which is approximately 270 km upstream on the Yenisey River. The large variations in measured activities were due to sampling location: the higher values came from a dead-end backwater channel with thick sediment (J3) and from a floodplain area with thick mud deposits (J7) while the lower values came from sandy sediment (J2) where the current was swift and deposits were more likely to be washed away.

Above background levels of ^{235}U and ^{238}U were observed in several samples taken just below the dam at Irkutsk. However, the measured concentrations of ^{238}U had large uncertainties due to the relatively weak gamma-ray emission from this radionuclide. The ratios observed for ^{235}U/^{238}U were larger than the natural abundance of 0.7% and were outside statistical uncertainties. However, these were no more than counting errors and did not include uncertainties in the interference between the overlying 186 keV gamma rays of ^{235}U and ^{226}Ra and possible errors

from self-attenuation due to non-uniformity in the samples. These samples were taken in an area undergoing active landfill. As a result, uranium-containing fills could have been brought in from elsewhere.

6.5.2.2 Heavy metals in river sediments

Using the XRF unit as a screening instrument, a number of heavy metals were identified in all riverbank and river sediment samples collected during the expedition. After the expedition, 21 river sediment and 8 river water samples were sent for trace element analysis to an EPA-certified commercial laboratory. Some of the analytical results are shown in Tables 6.18 and 6.19. Five heavy metals (Cd, Cr, Cu, Ni, and Pb) were identified in all the samples at concentrations which were within the usual ranges of worldwide background levels. Two heavy metals, As and Zn, were identified in the river water samples at concentrations much higher than the median for natural freshwater (Lal and Stewart, 1994). In fact, the Zn concentration in four of the samples exceeded the normal range for natural freshwater. These water samples were collected near to or downstream from industrial complexes on both the Angara and Yenisey Rivers. Table 6.19 compares the 1995 U.S./Russian expedition results with archived 1978–1980 water quality data taken from the Angara at Irkutsk, Angarsk, and Bratsk, carried out by the Irkutsk Medical Inspection Service (private communication with G.M. Svender and A.A. Krechetov, Chemical Department, Irkutsk State University, Russia). The measurements indicate a significantly higher Zn concentration in water collected above Angarsk than was measured previously.

6.5.3 Experiments using the Angara–Yenisey river system simulation model

The AYRSSM database includes estimates of model coefficients, initial information for climatic and anthropogenic scenarios, and a set of identifiers $\{A_i\}$ describing the boundaries of area Ω, thus giving the structure of the land–water surface. The CON block provides an interface with the database and allows the user to modify its elements.

Let us assume that the vertical distribution of pollutants in river water is homogeneous, the pollution in the soil and plants is negligible, and the cleaning process of the atmosphere has an exponential character with half-life τ_a ($\tau_a = 10$ days when $t \in [t_1, t_2]$, $\tau_a = 20$ days when $t \in [t_2, t_4]$). Let us further assume that the pollution sources located in Ω support a constant level of distribution of pollutants. The distribution function is uniform in the intervals shown in Table 6.19. The values of ξ, μ, and ν were determined by average estimates for the last three years on the base of published data (Rovinsky *et al.*, 1995) and data of the Irkutsk Scientific Center. The AYRS slope is taken equal to 0.21 m/km. Ecological elements of the AYRS are considered as having unique levels, with biomass $\beta(t)$ a constant value at each of the intervals $[t_i, t_{i+1}]$ $(i = 1, 2, 3)$. The equation for $H_{5\nu}$ is written in the form $H_{5\nu} = [g_1 + m_1 m_2 \beta] Q_{k\nu} \Delta$, where g_1 is the gravitation coefficient ($0.05\,\mathrm{da}^{-1}$), m_1 is the mortality coefficient ($0.01\,\mathrm{da}^{-1}$), and m_2 is the pollutant capture coefficient ($0.03\,\mathrm{kg}^{-1}$).

Table 6.20. Relative concentrations of ^{137}Cs in water (γ_w) and in bottom sediments (γ_d) normalized for values at $x = 0$.

Distance from Lake Baikal (km)	*Time from the beginning of the simulation experiment* (days)							
	30		60		90		120	
x	γ_w	γ_d	γ_w	γ_d	γ_w	γ_d	γ_w	γ_d
0	1.0	1.0	1.0	1.0	1.0	1.0	1.0	1.0
250	8.2	20.4	6.7	18.7	7.4	17.8	8.3	17.1
500	9.5	14.4	9.4	12.3	9.3	15.3	8.4	14.9
1,000	10.3	4.1	8.8	9.8	7.8	11.6	7.9	10.3
1,500	9.7	3.0	10.2	5.2	6.3	8.5	4.8	7.6
2,000	8.9	2.9	6.9	2.9	4.9	4.1	4.5	2.8
2,500	6.5	2.3	5.9	2.2	3.1	2.4	3.1	1.8
3,000	3.2	1.9	2.7	1.7	2.9	1.9	3.0	1.4
3,500	2.5	1.6	1.8	1.1	1.8	1.2	2.4	1.1
4,000	1.7	1.1	1.6	0.9	1.8	1.2	1.4	1.1

Table 6.20 uses the AYRSSM to estimate ^{137}Cs distribution in Ω where cells Ω_{ij} are situated along the AYRS at discretization steps of $\Delta x = 10$ km. The ^{137}Cs distribution along the river system has a single maximum which changes in value and coordinate over time. A similar picture can be observed for other radionuclides in Table 6.16. Such a result cannot only be explained by the location of sources of radionuclear pollutants. It is possible that variations in the value and position of maximal ^{137}Cs concentration are caused by high turbulence in the river system and by the existence of reservoirs and eddies. The AYRSSM gives only averaged results. Fourth-level blocks in the AYRSSM structure are necessary to describe hydrological processes with $\Delta x < 100$ m.

Computer experiments show that the input of radionuclear pollution to the Kara Sea from the Yenisey River is stable with a dispersion equal to $\pm 32\%$. The role of the AYRS ecosystem in transforming radionuclear pollution is disregarded because it is negligible ($<3\%$). Vertical transport by organisms varies from 0.1% to 0.7%. Such calculations can be carried out for different scenarios.

Figure 6.13 shows the distribution of heavy metal concentrations along the AYRS constructed by means of a computer experiment. We see that there are three maxima of heavy metal concentrations located at distances from Lake Baikal of 200 km, 1,200 km, and 2,000 km. This is the result of the distribution of pollution sources along the river system. The AYRS neutralizes pollutants over a distance of

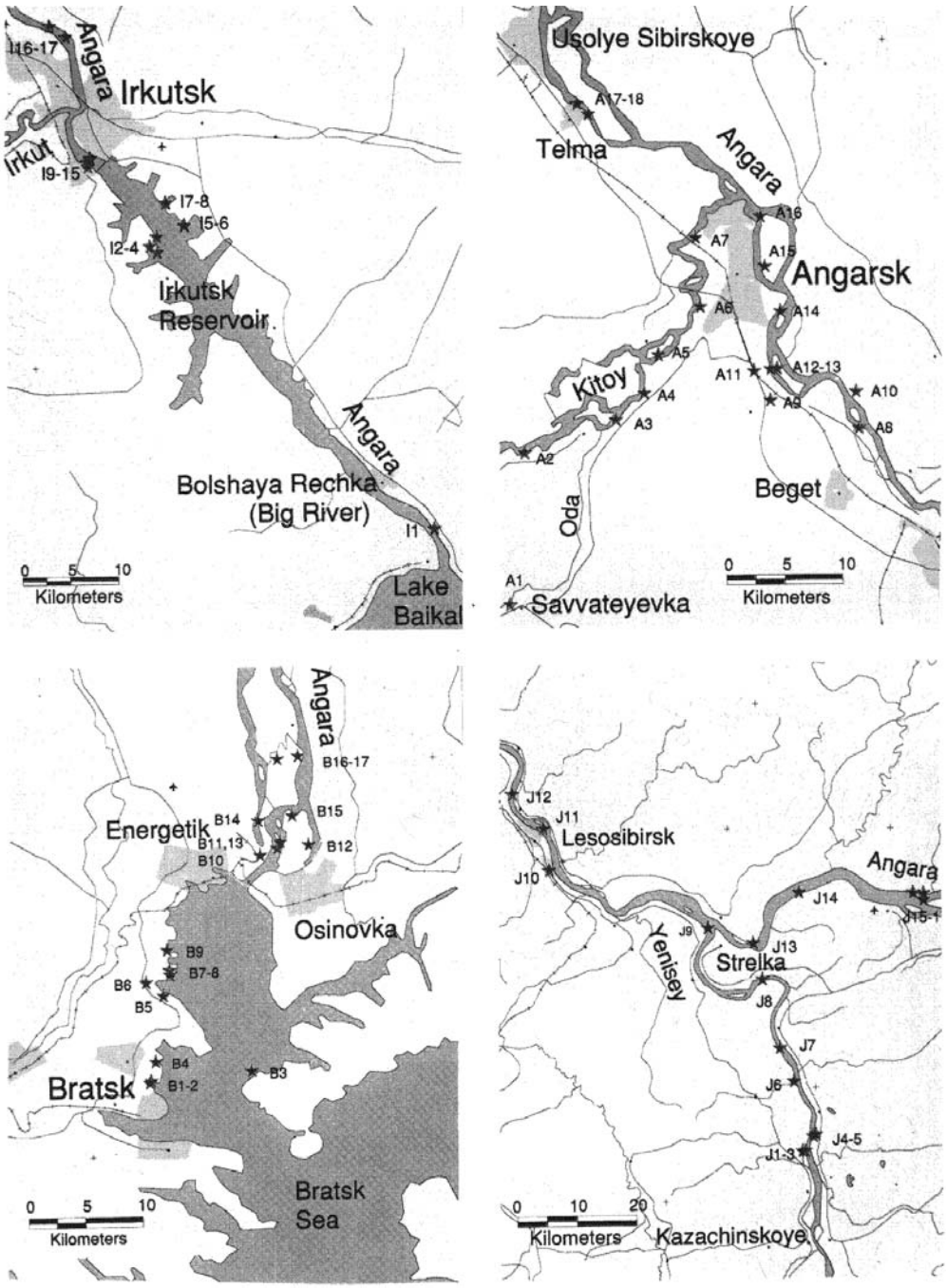

Figure 6.11. Maps of sample locations (marked by stars) during the American–Russian ecological expedition of 1996. From Krapivin *et al.* (1998).

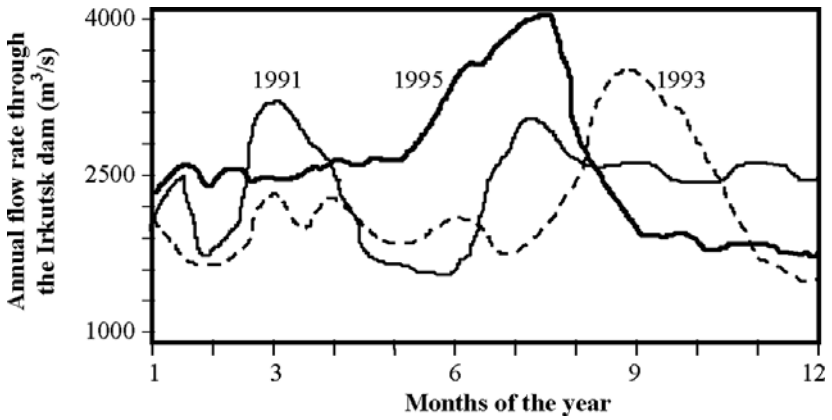

Figure 6.12. Annual flow rate through the Irkutsk dam for the years 1991–1995.

600 km–1,000 km from the source. The locations of maxima vary as a function of river flow rate. For the flow data of Figure 6.12 this variation is 150 km. The river system transforms the pollutant flow in such a way that input into the Kara Sea is estimated at a pollution level which is less than 2% of the maximal concentration of pollutant in the AYRS.

The AYRSSM allows us to estimate the dependence of pollution level in the AYRS estuary as a function of anthropogenic activity. Suppose that the intensity of sources of heavy metals is such that their concentration in the water near Angarsk, Irkutsk, Krasnoyarsk, Bratsk, and Ust-Ilimsk can be described by a stationary function, supporting heavy metal concentrations at level h at each of these cities. Computer experiments show that there is a stable correlation between h, the heavy metal concentration in the AYRS estuary, and the water flow rate μ. An increase in h of 10% leads to a rise of pollution input to the Kara Sea by 2.5%. An increase in h of 1% leads to a rise of pollution input to the Kara Sea by 0.7%. These results are correct only when variances in values μ and h are close to their average estimates. Near their critical values the estimates are unstable and more detailed models are required.

In conclusion it is necessary to note that this study demonstrates the possibility of using modeling technology to solve complex environmental problems that demand combined knowledge from different scientific fields. The AYRSSM is a good example of such a combination. It provides the typical elements necesssary to synthesize a simulation model to look into Arctic Basin pollution.

The results given in this section illustrate the functional features of a simulation experiment. Clearly, the strategy of any modeling technology depends on a balance between model calculations and on-site experiments. In the case considered, such a strategy has an economical benefit as it reconstructs the distribution of pollutants along the AYRS and provides estimates of environmental consequences should the chosen scenarios be realized.

The joint U.S./Russian expedition to Siberia's Angara and Yenisey Rivers detected synthetic contaminants in water and sediment samples from industrial regions and wilderness areas. On-site analysis using sensitive instrumentation revealed radionuclides, heavy metals, and volatile organic compounds. The results indicate that the nuclear production facility near Krasnoyarsk on the Yenisey River has introduced radioactive contamination far downstream and is a probable source of previously detected radioactivity in the Yenisey estuary at its outlet into the Kara Sea.

The AYRSSM is a complex system which treats natural and anthropogenic elements hierarchically. This study of the AYRS was the first time that simulation results were based on large-scale on-site measurements. The method proposed in this chapter can be used to investigate other Siberian river systems. However, to expand the experimental base, remote-sensing technology must be used (Sellers *et al.*, 1995). Remote monitoring can give more precise data on the structure of identifiers A_2 and A_3, which describe the spatial distribution in the Arctic of pollutants and ice fields, respectively. The authors hope for continuation of this study. Based on the database created, it is planned to prepare a complete set of models and corresponding software to describe the process of transfer and transformation of pollution substances in Arctic natural ecosystems. This will demand the synthesis of models for the kinetics of radionuclides and chemical compounds in the foodchains of the water and land ecosystems for boreal zones, modeling the hydrological regime, and estimating pollutant flows in the Arctic Basin.

The ultimate aim of these investigations is the development of an environmental technology as a result of co-operative scientific work directed toward evaluating the state of the Arctic ecosystem. The modeling system should be provided with a comprehensive database and have at its disposal a ramified informational measuring network and a complete set of computer models for the main biogeochemical, climatic, and biogeocenotic processes.

6.6 BIOCOMPLEXITY IN THE ARCTIC SYSTEM

Biocomplexity can be described as the result of dynamic interactions between the physical, biological, and social components of the biosphere–society system (BSS). Investigations of the processes involved in this interaction are, as a rule, targeted at understanding and estimating the consequences of such interactions. The reliability and precision of such estimates depend on criteria founded on conclusions, expertise, and recommendations. At present, there is no unified methodology for selecting a criterion due to the absence of a common science-based approach to the ecological standardization of anthropogenic impacts on the natural environment. Moreover, the precision of ecological expertise for the functioning and planning of anthropogenic systems, as well as the representativeness of the global geoinformation monitoring data, depend on these criteria.

6.6.1 Biocomplexity indicator

Processes that have their origin in the environment can be presented as a combination of interactions between its sub-systems. The human sub-system is a part of the environment, and therefore it is illogical to divide the environment into separate sub-systems such as biosphere and society. What is needed is a methodology to describe existing correlations between nature and humanity that reliably reflects dynamic tendencies in the BSS system. Unfortunately, the part of the BSS system that is responsible for the quality of modeling climatic processes introduces instability in the modeling results. This is the reason we suggest below that the BSS climatic component be replaced by a scenario describing stable climatic trends during the time of investigation. Then, what is actually studied is the biosphere–society system.

Let us introduce a scale Ξ of biocomplexity ranging from the state when all interactions between environmental sub-systems cease to the state when they correspond to natural evolution. This gives us an integrated indicator of the environmental state including bioavailability, biodiversity, and survivability. It reflects the level of all types of interactions between environmental sub-systems. In reality, specific conditions exist when these interactions change and transform. For example, under the biological interaction of type "consumer–producer" or type "competition for energy resources" there exists a minimal level of food concentration when contacts between interacting components cease. In the common case, physical, chemical, and other types of interactions in the environment depend on specific critical parameters. Environmental dynamics is regulated by these parameters and the main task is to parameterize them. Biocomplexity reflects this dynamics.

All of this corroborates the fact that biocomplexity is related to categories that are difficult to measure empirically and express quantitatively. However, we will try to transfer truly verbal tautological reasoning to formalized quantitative definitions. For transition to gradations of scale Ξ that has quantitative positions it is necessary to postulate that relationships between two values of Ξ are of type $\Xi_1 < \Xi_2$, $\Xi_1 > \Xi_2$ or $\Xi_1 \equiv \Xi_2$. In other words, there always exists a value of scale ρ that defines a biocomplexity level $\Xi \to \rho = f(\Xi)$, where f is a certain transformation of the biocomplexity concept to a number. Let us attempt to search for a satisfactory model to reflect the verbal biocomplexity image onto the field of conceptions and signs, subordinating it to formal description and transformation. With this purpose in mind m sub-systems of the BSS are selected. The correlations between these sub-systems are defined by the binary matrix function $X = \|x_{ij}\|$, where $x_{ij} = 0$ if subsystems B_i and B_j do not interact and $x_{ij} = 1$ if they do. Then, any one point $\xi \in \Xi$ is defined as the sum $\xi = \sum_{i=1}^{m} \sum_{j>i}^{m} x_{ij}$. Certainly, there arises the need to overcome uncertainty, for which it is necessary to complicate scale Ξ (e.g., to introduce weight coefficients for all BSS sub-systems). The origin of these coefficients depends on the type of sub-system. This is the reason three basic sub-system types are selected: living sub-systems, non-living sub-systems, and vegetation. Living sub-systems are characterized by their density, estimating by numbers of elements or by biomass value per unit area or

volume. Vegetation is characterized by the type and portion of occupied territory. Non-living sub-systems are measured by their concentration per unit square or volume of the environment. In the common case, certain characteristics $\{k_i\}$, corresponding to the significance of sub-systems $\{B_i\}$, are assigned to every sub-system B_i $(i = 1, \ldots, m)$. As a result we get nearer to definition of the formula to move from the biocomplexity concept to the scale Ξ of its indicator:

$$\xi = \sum_{i=1}^{m} \sum_{j>i}^{m} k_j x_{ij}.$$

It is clear that $\xi = \xi(\varphi, \lambda, t)$, where φ and λ are geographical latitude and longitude, respectively, and t is the current time. For territory Ω the biocomplexity indicator is defined as a mean value:

$$\xi_\Omega(t) = (1/\sigma) \int_{(\varphi,\lambda)\in\Omega} \xi(\varphi, \lambda, t)\, d\varphi\, d\lambda,$$

where σ is the area of Ω.

Thus, indicator $\xi_\Omega(t)$ is the generalized characteristic of BSS complexity reflecting the individuality of its structure and behavior at each time t in space Ω. According to natural evolution laws a decrease (increase) in ξ_Ω will correspond to an increase (decrease) of biocomplexity and the survivability of nature–anthropogenic systems. Since a decrease in biocomplexity disturbs the exclusiveness of biogeochemical cycles and leads to a decrease in stress on the non-renewal of resources, then the binary structure of matrix X changes in direction to intensify resource impoverishment technologies. The vector of energy exchange between BSS sub-systems is moved to the position where the survivability level of the BSS is reduced.

The global simulation model is oriented to spatial discretization of the Earth's surface with $\Delta\varphi$ in latitude and $\Delta\lambda$ in longitude. In other words, the BSS space Ω is divided into a set of cells

$$\Omega_{ij}\left(\Omega = \bigcup_{(i,j)} \Omega_{ij}; \Omega_{ij} = \{(\varphi, \lambda); \varphi_i \le \varphi < \varphi_{i+1}; \lambda_j \le \lambda < \lambda_{j+1};\right.$$
$$\left. i = 1, \ldots, N; j = 1, \ldots, M; N = [180/\Delta\varphi]; M = [360/\Delta\lambda]\}\right).$$

Each cell Ω_{ij} has its own biocomplexity indicator value:

$$\xi_\Omega(i, j, t) = (1/\sigma_{ij}) \int_{(\varphi,\lambda)\in\Omega_{ij}} \xi(\varphi, \lambda, t)\, d\varphi\, d\lambda. \tag{6.30}$$

The value $\xi_\Omega(i, j, t)$ calculated by Formula (6.30) reflects the topological structure of matrix $X(i, j, t)$. Consequently, there exist $n = N \cdot M$ matrices and biocomplexity indicators to characterize BSS biocomplexity. Within the computer experiment a set of numerical characteristics of the BSS biocomplexity arises, distributed in space and time. Integrated BSS biocomplexity indicators can be calculated for any arbitrary

area $\omega \in \Omega$:

$$\xi_\omega(t) = (1/\sigma_\omega) \sum_{(\varphi_i,\lambda_j)\in\omega} \xi_\Omega(i,j,t). \tag{6.31}$$

This can be the average BSS biocomplexity by zone of longitude or latitude, by ocean or sea aquatory, by country or state territory, etc.

6.6.2 The biosphere–society system biocomplexity model

The BSS consists of sub-systems B_i $(i = 1, \ldots, m)$ the interactions of which are formed over time as functions of many factors. BSS biocomplexity reflects the structural and dynamic complexity of its components. In other words, BSS biocomplexiry is formed under the interaction of its sub-systems $\{B_i\}$. In due course, sub-systems B_i can change their state and, consequently, change the topology of relations between them. The evolutionary mechanism that adapts sub-system B_i to the environment supports the hypothesis that each sub-system B_i, independently of its type, has structure $B_{i,S}$, behavior $B_{i,B}$, and goal $B_{i,G}$ such that $B_i = \{B_{i,S}, B_{i,B}, B_{i,G}\}$. The strivings of sub-system B_i to achieve certain preferable conditions are represented by its goal $\hat{A}_{i,G}$. The expedience of structure $B_{i,S}$ and the purposefulness of behavior $B_{i,B}$ for sub-system B_i are estimated by the effectiveness with which goal $B_{i,G}$ is achieved.

As an example, we consider the process of fish migration. The investigations of many authors revealed that this process is accompanied by the external appearance of purposeful behavior. From these investigations it follows that fish migrations are subordinated to the principle of complex maximization of effective nutritive rations, given the preservation of favorable environmental conditions (temperature, salinity, dissolved oxygen, pollution level, depth). In other words, the travel of migrating species takes place at characteristic velocities in the direction of the maximum gradient of effective food, subject to adherence to ecological restrictions. This is the reason we can formulate goal $B_{i,G}$ of the fish sub-system as directed toward increasing their food rations, and behavior $B_{i,B}$ consists in defining the trajectory needed to secure its goal $B_{i,G}$.

Since interactions between sub-systems B_i $(i = 1, \ldots, m)$ are connected with chemical and energy cycles, it is natural to suppose that each sub-system B_i can bring about the geochemical and geophysical transformation of matter and energy to remain in a stable state. The formalism of approach to this process consists in supposing that interactions between BSS sub-systems are represented as a process in which systems exchange a certain quantity V of resources spent for a certain quantity W of resources consumed. This process is called "(V, W)-exchange".

The goal of the sub-system is to find the most advantageous (V, W)-exchange (i.e., it tries to get maximum W in exchange for minimum V). Quantity W is a complex function of the structure and behavior of interacting sub-systems, $W = W(V, B_i, \{B_k, k \in K\})$, where K is the space of sub-system numbers interacting with sub-system B_i.

Let us designate $B_K = \{B_k, k \in K\}$. Then, the following (V, W)-exchange is the result of interactions between sub-system B_i and its environment B_K:

$$W_{i,0} = \max_{B_i} \min_{B_K} W_i(V_i, B_i, B_K) = W_i(V_i, B_{i,opt}, B_{K,opt}),$$

$$W_{K,0} = \max_{B_K} \min_{B_i} W_i(V_K, B_i, B_K) = W_K(V_K, B_{i,opt}, B_{K,opt}).$$

Hence, it follows that some range of the goal of sub-system B_i exists which defines the levels of V_i and V_K. Since limiting factors are in force in nature then in this case it is natural to suppose that some level $V_{i,min}$ exists when sub-system B_i ceases to spend its energy resource to get the external resource (i.e., if $V_i \leq V_{i,min}$, then sub-system B_i transfers to regeneration of its internal resource). In other words, when $V_i \leq V_{i,min}$ a decrease in biocomplexity indicator $\xi_\Omega(t)$ is realized at the expense of breaking off interactions of sub-system B_i with other sub-systems. Commonly, the structure of $V_{i,min}$ is a checkered function (i.e., the change-over of x_{ij} from state $x_{ij} = 1$ to state $x_{ij} = 0$ is not realized for all j at the same time). Actually, in any trophic pyramid of living sub-systems the relationships of producer–consumer type cease when consumer biomass concentrations fall below some critical level. In other cases, interactions between sub-systems $\{B_i\}$ can be stopped at the expense of various combinations of its parameters. Parametric description of possible situations of interactions of sub-systems $\{B_i\}$ can be realized in the BSS simulation model.

6.6.3 Biocomplexity problem related to fisheries in the Okhotsk Sea

The Okhotsk Sea has high ecosystem productivity which functions under a rigorous climate. The structure of the spatiotemporal fields of basic hydrological and ecological characteristics of the Okhotsk Sea is heterogeneous. The chemical, physical, and biological processes occurring in seawater have been studied by many authors to assess its bioproductivity. According to Terziev *et al.* (1993), the following structural discretization of the Okhotsk Sea can be realized. Five ecological layers exist. Layer 1, of maximal photosynthesis, is situated above the thermocline and has a depth of about 20 m–30 m. In fact, it corresponds to the wind-mixed layer. Layer 2 occupies the water space from 30 m to 150 m in depth. It has low temperatures and oxygen saturation of about 80%–90%. Layer 3, characterized by low oxygen saturation (15%–20%), lies between the depth of 150 m to 750 m. Layer 4 extends from 750 m down to a depth of 1,500 m. This layer has minimal oxygen saturation (10%–15%). Lastly, layer 5 is situated deeper than 1,500 m. It is characterized by oxygen saturation of 25%–30%.

The Okhotsk Sea aquatory is divided into zones having specific ecological features (Suzuki, 1992). The spatial distribution of the fish biomass depends on seasonal conditions and to a great extent correlates with the layers outlined above. The use of sea biological resources is a function of this distribution. Fishing intensity essentially depends on knowledge of the biomass distribution in zones with specific environmental conditions. Many authors (Plotnikov, 1996; Aota *et al.*, 1992) have tried to solve this task by means of models simulating ecosystem dynamics. However,

modeling results do not always turn out to be sufficiently representative or reflect the classification of sea zones by their productivity scale. The biocomplexity indicator is one such simple form to identify these zones. In fact, many investigators have indicated that Okhotsk Sea zones with high productivity are characterized by complex multi-level trophic charts (Terziev *et al.*, 1993). This effect is not seen in other seas. For instance, the Peruvian current ecosystem has high productivity in zones where the trophic chain is short (Krapivin, 1996). These situations are distinguished by migration processes. This is the reason the biocomplexity of these ecosystems forms in various ways.

Let us consider the following components of the Okhotsk Sea ecosystem mentioned in Table 6.21. The trophic pyramid $X = \|x_{ij}\|$, where x_{ij} is a binary value equal to 1 or 0 under the existence or absence of a nutritive correlation between the ith and jth components, respectively. Let us define the biocomplexity as a function:

$$\xi(\varphi, \lambda, z, t) = \sum_{i=1}^{20} \sum_{j=1}^{19} x_{ij} C_{ij},$$

where φ and λ are geographical latitude and longitude; t is the current time; z is the depth; and $C_{ij} = k_{ji} B_{i,*} / \Sigma_{j+}$ is the nutritive pressure of the jth component on the ith component:

$$\Sigma_{i+} = \sum_{m \in S_i} k_{im} B_{m,*}$$

is the actual food available to the ith component; $k_{im} = k_{im}(t, T_W, S_W)$ $(i = 1, \ldots, 17)$ is the index of satisfaction of nutritive requirements of the ith component at the expense of the mth component biomass; k_{im} $(i = 18, 19)$ is the transformation coefficient from the mth coponent to the ith component; k_{i20} is the characteristic anthropogenic influence on the ith component; $S_i = \{i : x_{ij} = 1, j = 1, \ldots, 19\}$ is the food spectrum of the ith component; T_W is water temperature; S_W is water salinity; and $B_{m,*} = \max\{0, B_m - B_{m,min}\}$.

$$x_{i,j} = \begin{cases} 1, & \text{if } B_m \geq B_{m,min}; \\ 0, & \text{if } B_m < B_{m,min}. \end{cases}$$

where $B_{m,min}$ is the minimal biomass of the mth component consumed by other trophic levels.

Let us designate the water area of the Okhotsk Sea by $\Omega = \{(\varphi, \lambda)\}$. The value of the biocomplexity indicator for any area $\omega \in \Omega$ is determined by $\xi_\omega(z_1, z_2, t)$, where $[z_1, z_2]$ is the water layer located between depths z_1 and z_2. The maximal value of $\xi = \xi_{max} (\approx 20)$ is reached during the spring–summer period when nutritive relations in the Okhotsk Sea ecosystem are extended, the intensity of energy exchanges is increased, and horizontal and vertical migration processes are stimulated. In the wintertime the value of ξ is reduced to near $\xi_{min} (\approx 8)$. The spatial distribution of ξ reflects the local variability in components of the food spectrum. Table 6.22 shows an example of such a distribution. Comparison of this distribution with the distribution

Table 6.21. Trophic pyramid of the Okhotsk Sea ecosystem considered in calculations of the biocomplexity indicator.

Consumers of energy and matter	*Sources of energy and matter*																		
	B_1	B_2	B_3	B_4	B_5	B_6	B_7	B_8	B_9	B_{10}	B_{11}	B_{12}	B_{13}	B_{14}	B_{15}	B_{16}	B_{17}	B_{18}	B_{19}
Phytoplankton, B_1	0	0	0	0	0	0	0	0	0	0	0	0	0	0	0	0	0	1	0
Bacterioplankton, B_2	0	0	0	0	0	0	0	0	0	0	0	0	0	0	0	0	0	0	1
Microzoa, B_3	1	1	0	0	0	0	0	0	0	0	0	0	0	0	0	0	0	0	1
Microzoa, B_4	1	1	0	0	0	0	0	0	0	0	0	0	0	0	0	0	0	0	0
Carnivores, B_5	0	1	1	1	1	0	0	0	0	0	0	0	0	0	0	0	0	0	1
Zoobenthic animals, B_6	1	1	1	1	1	0	0	0	0	0	0	0	0	0	0	0	0	0	1
Flatfish, B_7	0	0	0	0	0	1	1	1	1	1	1	1	1	1	1	1	1	0	0
Coffidae, B_8	0	0	0	0	1	1	1	1	1	1	1	1	1	1	1	1	1	0	0
Ammodytes hexapterus, B_9	0	0	0	0	0	1	1	0	0	1	1	1	0	0	0	1	0	0	0
Mallotus, B_{10}	0	0	0	0	1	1	1	0	0	0	1	0	0	0	0	0	0	0	0
Theragra chalcogramma, B_{11}	0	0	0	0	1	0	0	0	0	1	1	1	0	0	0	0	0	0	0
Salmonidae, B_{12}	0	0	0	0	0	1	1	0	0	1	1	1	1	0	0	1	0	0	0
Coryphaenoides, B_{13}	0	0	0	0	1	1	1	1	1	1	1	1	1	1	1	1	1	0	0
B_{14}	0	0	0	0	1	1	1	1	1	1	1	1	1	1	1	1	1	0	0
B_{15}	0	0	0	0	1	1	0	0	0	0	0	0	0	0	1	0	0	0	0
Crabs, B_{16}	0	0	0	0	0	1	0	1	1	1	0	1	0	0	0	1	1	0	0
Laemonema longipes, B_{17}	0	0	0	0	1	1	0	0	0	0	0	0	0	0	0	0	1	0	0
Biogenic salts, B_{18}	0	0	0	0	0	0	0	0	0	0	0	0	0	0	0	0	0	0	1
Detritus, B_{19}	1	1	1	1	1	1	1	1	1	1	1	1	1	1	1	1	1	0	0
People, B_{20}	1	1	1	1	1	1	1	1	1	1	1	1	1	1	1	1	1	1	1

B_{14} = *Reinhardti ushippoglossoi des matsuura*; B_{15} = *Clupeapallasi pallasi* Val.

Table 6.22. Estimates of the biocomplexity indicator ξ^* for different layers in the spring–summer season and in winter.

Season	*Layers*				
	1	*2*	*3*	*4*	*5*
Spring–Summer	0.89	0.93	0.62	0.34	0.21
Winter	0.31	0.49	0.71	0.39	0.22

of zones with industrial fish accumulations (Terziev *et al.*, 1993) shows that there is a correlation between these distributions.

In the common case, indicator ξ reflects the level of complexity of the Okhotsk Sea ecosystem. A change in ξ is realized as a consequence of migration processes and of variability in nutritive interactions. Sub-system B_{20} plays the role in these processes of an external source of change in other components. These changes are interpreted in terms of fishing and other impacts causing variations in component biomasses.

Calculations show that basic variability in $\xi^* = \xi/\xi_{max}$ is caused by migration processes, under which quick redistribution of the interior structure of matrices X and $\|C_{ij}\|$ occurs. For instance, according to Terziev *et al.* (1993) many fish species during springtime migrate to the shelf zone, and during wintertime they move to the central aquatories of the sea. Therefore, we get the value $\xi^* \to 1$ during spring and $\xi^* \to 0.6$ during winter for the shelf zone. This means that the biocomplexity of the Okhotsk sea ecosystem in the shelf decreases by 40% in winter in comparison with spring. For the central aquatories the value ξ^* changes little during the year. Such stability in the biocomplexity indicator is explained by the balance between nutritive correlations and productivity during the spring, summer, and winter seasons.

It can be established that the variability in ξ^* reflects the changes of fish concentrations which are controlled by environmental conditions. Specifically, during the springtime *Clupeapallasi escapes* occupy the area with $T_W < 5^\circ$C. Other fishes have a preferred depth for their feeding and spawning (Terziev *et al.*, 1993). All these processes exert an influence on the variability of ξ^*. A more detailed investigation of the correlations between the value of ξ^* and the structural and behavioral dynamics of the Okhotsk Sea ecosystem requires additional studies.

This section introduced a methodology to move from a verbal description of biocomplexity to its numerical representation. In future studies it will be necessary to take into consideration bottom relief, climate trends, ice field dynamics, detailed components of the trophic pyramid, bottom sediments, and the structure of currents. Also, it will be necessary to add to Formula (6.31) elements describing anthropogenic impacts on the ecosystem considered in a socio-economic sense.

6.7 CARBON CYCLE DYNAMICS IN THE ARCTIC SYSTEM

Studies of the climate-forming processes in the Arctic, characterized by isolation of the ocean from the atmosphere by the ice cover, have long been of particular concern.

The most important impacts of sea ice on climate, as revealed through numerical modeling, are the following:

(1) maximum climate warming (with increasing CO_2 concentration in the winter) due to increased heat input from the ocean through the thinner ice as a result of warming;
(2) the effect of albedo on the atmospheric temperature of the more extended sea ice 18,000 years ago, which is compatible with the impact of continental glaciers; and
(3) possible reversal of the conventional relationship between the amplitude of the annual change of temperature and the depth of the oceanic mixed layer when sea ice dynamics are taken into account. A thinner mixed layer favors the strengthening of wintertime sea ice, which causes a delay in springtime melting and produces a colder summer. The latest data of numerical modeling have confirmed, on the whole, these conclusions (Kondratyev and Johannessen, 1993).

When discussing the role of the polar regions in the formation of global changes, we need to keep in mind the two aspects of global ecology that are of paramount importance:

(1) anthropogenically induced redistribution of the components of the heat balance of the Earth as a planet (with emphasis on the atmospheric greenhouse effect and its climatic impact); and
(2) anthropogenically induced breaking of global biogeochemical cycles (primarily, this refers to carbon, nitrogen, and sulfur).

This is the reason polar regions are given special consideration as components of the global ecosystem. These aspects are not taken into account completely by existing global models of the nature–society system. A new approach to the synthesis of geoinformation monitoring systems, proposed by Kondratyev *et al.* (2000) overcomes this shortfall. In this approach the interchange of CO_2 between high-latitude vegetation, the northern seas, and the atmosphere is considered part of the global biogeochemical cycle described by the Global Simulation Model (GSM) (Krapivin, 1993). The GSM comprises blocks that parameterize the following:

(1) the global hydrological balance;
(2) productivity of soil–plant formations, with 30 types defined;
(3) photosynthesis the ocean ecosystems taking into account depth and surface inhomogeneity;
(4) demographic processes; and
(5) anthropogenic changes.

The GSM makes it possible to compute the dynamics of industrial CO_2 distribution between the oceans, terrestrial biota, and the atmosphere. The GSM describes the World Ocean as a spatial four-layer model with due regard for water chemistry. Spatial heterogeneity of the World Ocean is represented by the structural

distribution of surface temperature applied to upwelling and convergence zones. Sea ice in polar regions is considered using CIESIN data (Yohe *et al.*, 2006). The biogeochemical cycle of CO_2 is described by balance equations in accordance with Figures 3.3 and 3.4. The GSM carbon dioxide block takes into consideration the dependence of flows H_2 and H_3 from water surface processes (wind–wave mixing, rough seas, foam as a result of wave action). Simulation experiments have shown that these flows vary from $16\,\mathrm{mol\,m^{-2}\,yr^{-1}}$ to $1{,}250\,\mathrm{mol\,m^{-2}\,yr^{-1}}$. In the Arctic Ocean during the June–September period the partial pressure p_a of CO_2 in the atmosphere exceeds the partial pressure of CO_2 in seawater by 20 ppm–110 ppm. These variations in the partial pressure of CO_2 have specific distributions for Arctic seas. For instance, the Norwegian Sea and Bering Sea have CO_2 deficits of 18 ppm–54 ppm and 33 ppm–69 ppm, respectively. The average CO_2 deficit reaches $450\,\mathrm{gC\,m^{-2}}$. Flow H_3 changes between $1.5\,\mathrm{gC\,m^{-2}\,da^{-1}}$ and $4.1\,\mathrm{gC\,m^{-2}\,da^{-1}}$. In addition, linear correlations between the partial pressure of CO_2 and water temperature T are observed, with a proportionality coefficient equal to 9.8 ppm/°C.

Flow H_3 is calculated by the formula $H_3 = \psi(T)p_a^{-1/2}(1 + 0.5S)$, where S (‰) is the water salinity, and the Weis function ψ describes the influence of water temperature T (°K) on carbon dioxide solubility in seawater (Weis *et al.*, 1982).

The greenhouse effect is discussed by many authors within the framework of different anthropogenic scenarios (Kondratyev, 1998b; Gorshkov *et al.*, 2000). The main conclusion is that global climate change brought about through CO_2 dynamics will be insignificant during the next century as long as

(1) World Ocean pollution, especially by oil products, does not exceed the level of 1990 by any more than 10%;
(2) agricultural land areas do not expand at the expense of forests;
(3) the rate of fossil fuel consumption does not exceed the level of 1990 by any more than 15%; and
(4) alternative energy sources (atomic, wind, etc.) are developed at a rate which does not hinder food production.

The role of soil–plant formation for the absorption of excess atmospheric carbon dioxide under the above scenario can be estimated by showing the data in a geographic grid of $4^\circ \times 5^\circ$ lat./long. (Table 6.23). The role of the World Ocean is considered by taking water temperature in the surface layer into account. It has been shown that atmospheric CO_2 concentration could reach a mixing level of 556.7 ppm during the 21st century. The dynamics of industrial CO_2 distribution between the atmosphere, oceans, and vegetation will fluctuate with an amplitude less than 25%. As industrial CO_2 emission between 1990 to 2090 increases, so the atmosphere's share will rise and the contribution of the oceans to its absorption will increase; whereas that of biota will stabilize after going through a small maximum. At the end of the 21st century and beginning of the 22nd century, when human economic activity has likely reached heights never seen before, the contribution of the oceans (especially the Arctic Basin) to industrial CO_2 absorption will be considerably higher than that of vegetation. This is due to the fact that, with an increase in CO_2 concentration in the

Table 6.23. A model estimate of surplus CO_2 absorption by vegetation in Russia. The anthropogenic emission of carbon is assumed to be 6.5 GtC/yr.

Soil–plant formation	*Carbon flow absorbed by vegetation* (10^6 tC/yr)
Arctic deserts and tundra, sub-Arctic grassland and marshes	3.2
Tundra, mountain-tundra, and forest-tundra	10.7
North taiga forests	11.8
Mid-taiga forests	33.2
South taiga forests	24.9

atmosphere, the ability of the upper ocean layers to absorb industrial CO_2 will be supported by the transformation of biogeochemical processes in deep ocean layers. The restoration of plant cover and elimination of ocean pollution are the main near-time problems (Watson *et al.*, 2000). For example, it was shown that if the natural/disturbed land relation changes from 2/3 in 1990 to 3/2 in 2050, then atmospheric CO_2 concentration would reach no more than 497.3 ppm during the 21st century. This illustrates that the role of the biospheric system in global change needs to be investigated more thoroughly.

Simulation results show that there is an overall exaggeration of the importance of global climate change caused by anthropogenic CO_2 emissions. Thus, the existing arguments for climate change are not reliable. It is necessary to develop the GSM by understanding and inserting currently missing correlations between the elements of the NSS and by taking biotic regulation processes into account, which hitherto has not been the case.

This study showed that the role of the Arctic Ocean in global CO_2 balance has been estimated imprecisely. Therefore, the Kyoto Protocol reflecting the problems of climate warming via emission of greenhouse gases suffers from a lack of objective reasons. In fact, current climate models are still not reliably reflecting the correlation of global temperature with anthropogenic emissions of greenhouse gases. These models fail to consider the role of biospheric processes on land and in the oceans (i.e., the biotic regulation of the environment and the functioning of the ocean chemical system). Relevant models and datasets are synthesized in the framework of the Millennium Ecosystems Assessment Program (MEAP) which was established to help provide the knowledge base to improve decisions and to build a capacity for analyzing and supplying existing information about the dynamics of the NSS (MEA, 2005). In this context, Secretary-General of the United Nations Kofi Annan said: "The Millennium Ecosystem Assessment is an unprecedented contribution to our global mission for development, sustainability and peace." The MEAP might well solve the problem of global model synthesis to obtain forecasts of the dynamics of the NSS.

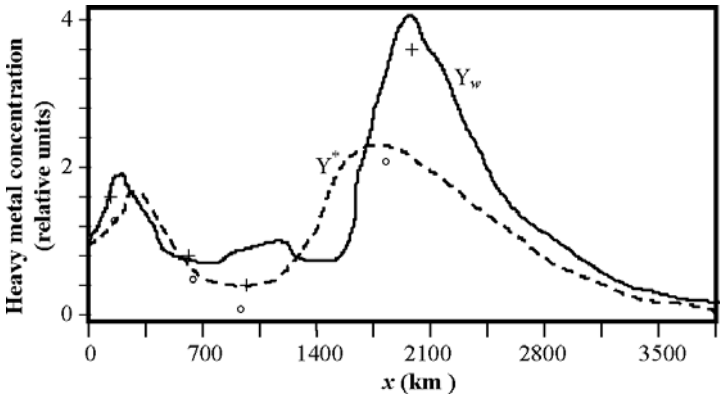

Figure 6.13. Distribution of heavy metal concentration in water (dashed line) and in sediments (solid line) as a function of distance x from Lake Baikal. The signs "○" and "+" correspond to the measured concentrations of metals in the water and sediment, respectively. The quantities $Y_w = [e_w(x) + \psi_w(x)]/[e_w(0) + \psi_w(0)]$ and $Y^* = [e^*(x) + \psi^*(x)]/[e^*(0) + \psi^*(0)]$.

A summary of existing simulations of the global carbon dioxide cycle shows the existence of long-term studies concerning this problem. The main conclusion is that the exchange of carbon between the atmosphere and biosphere has spotty spatial characteristics. This spottiness, taken into account in the models of the carbon dioxide cycle, produces large errors. Hence, the Kyoto Protocol's conclusions have been based on incomplete estimates. There are many carbon flows (natural and anthropogenic), mentioned in Figure 3.3, that have yet to be satisfactorily described parametrically. The principal key questions relating to the exchange of carbon between the atmosphere and the terrestrial pool of above-ground biomass, below-ground biomass, soils, and hydrospheric systems are discussed by Marchuk and Kondratyev (1992), Watson *et al.* (2000), Kondratyev (1999b, 2000a), and Gorshkov *et al.* (2000). The Arctic Basin is the most weakly studied part of the biosphere, but its role in CO_2 absorption processes is arguably the most important in the world. Figure 6.14 demonstrates high variability in the forecasting of carbon dioxide dynamics under different anthropogenic scenarios.

(1) The pessimistic scenario of Keeling and Bacastow (1977) describes a situation where the ocean's role in carbon exchange with the atmosphere is restricted to physical processes, disregarding all the other processes.
(2) The optimistic scenario of Bjorkstrom (1979) takes into account the ocean–carbonate system by parameterizing the H_2 and H_3 flows in Figure 3.3.
(3) The scenario of the IPCC, Intergovernmental Panel on Climate Change (Watson *et al.*, 2000), is based on specific activity requirements concerning land use strategy (e.g., planting vs. regeneration through silvicultural activities).
(4) The realistic scenario of Kondratyev (1999a, b) foresaw the current tendencies in the world's energy, demographic, and urbanization processes. This scenario is realized by the GSM (Krapivin, 1993; Kondratyev and Krapivin, 2001a, b).

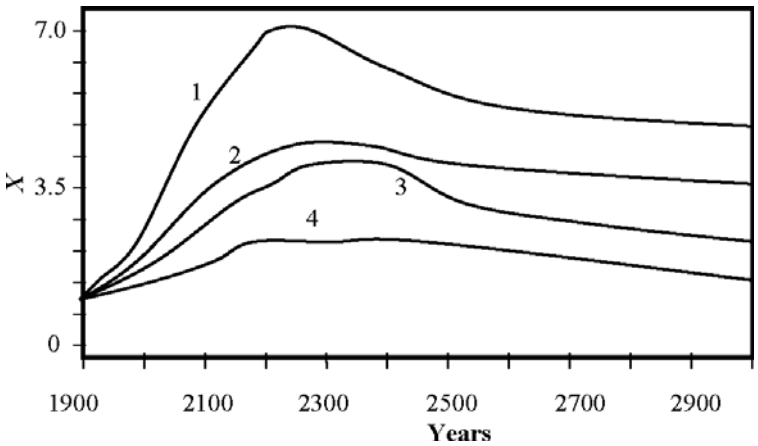

Figure 6.14. Forecasting the carbon dioxide content in the atmosphere obtained under different anthropogenic scenarios: 1 Keeling and Bacastow pessimistic scenario; 2 Bjorkstrom optimistic scenario; 3 IPCC scenario ; 4 Kondratyev realistic scenario. The ordinate $X = C_a(t)/C_a(1900)$.

In scenario (3) a greenhouse effect via CO_2 is clearly problematic. To estimate the dynamics of atmospheric temperature dependence on carbon dioxide it is necessary to use a correlation describing the greenhouse effect. There are various empirical functional representations of warming effects (Krapivin, 1999a, b). The following simple correlation approximates the existing empirical dependence of the atmospheric temperature deviation ΔT_{CO_2} on variations in the atmospheric carbon dioxide parameter $X = C_a(t)/C_a(1900)$:

$$\Delta T_{CO_2} = \begin{cases} 0.911 + 1.509 \ln X - 1.25 \exp\{-0.82(X-1)\}, & \text{when } X \geq 1; \\ 2.63X^2 + 6.27X + 1.509 \ln X - 3.988, & \text{when } X < 1. \end{cases}$$

Finally, according to GSM calculations, future emissions of CO_2 will make the Earth warm up by 0.2°C to 1.3°C by the year 2100. Such variations in ΔT_{CO_2} depend on assumptions about the intensity of urbanization and about land use strategy. The calculation results show that the dynamics of industrial CO_2 distribution between the atmosphere and oceans changes with the increasing preponderance of flows H_3 in northern water areas. At the end of the 21st century and beginning of the 22nd century, at the height of human economic activity, the contribution of the oceans to industrial CO_2 absorption will be considerably lower than that of vegetation. This is due to the fact that, with an increase in CO_2 concentration in the atmosphere, the partial pressure in the oceans rises and its ability to absorb industrial CO_2 decreases, whereas the productivity of vegetation does not fall. By the end of the 22nd century, with the projected decrease in human impact, the contribution of the oceans increases due to the growing role of its deep layers. Atmospheric CO_2 will decrease at the same rate as that of the oceans increases.

The entire area of the Arctic Ocean is only 3.8% of the world's total ocean surface, but its role in CO_2 absorption varies from 23% to 38% (16.7 GtC yr^{-1}–

28.9 GtC yr^{-1}). This role is greatly influenced by seasonal variations in the ice cover and in ecosystem productivity. This is the reason the results of this study have a preliminary character. It is necessary to fine-tune the parametrical descriptions of flows H_i^C from Figure 3.6. The authors of this book understand that policy-oriented computer tools aimed at supporting decision-making processes related to global change would need to be redesigned to support a new methodology in global modeling based on simulation models with detailed spatial descriptions of biosphere systems.

7

Nature–society system and climate, its interactive component

7.1 EARTH'S HEAT BALANCE, AND PROBLEMS FACING SOCIETY

Most of the environmental processes acting near the Earth's surface derive their energy from the Earth–atmosphere heat exchange. Much of this heat comes from radiant energy initially provided by solar radiation absorption. The absorbed energy is used to warm the atmosphere, to evaporate water, to warm the surface, along with a host of other processes including biogeochemical cycles and the many events taking place in human activity. The Earth's radiation balance (ERB) is the balance of incoming and outgoing components of radiation. These components are balanced over long time periods and over the Earth as a whole. Otherwise, the Earth would be continually cooling or warming. However, over a short period of time, radiant energy can be non-uniformly distributed over the Earth. It is due to this non-uniform distribution of energy fluxes that problems with evaluating global climate dynamics are encountered.

The discussions on global warming with predictions of global natural disasters held during recent decades are of little use, as a rule, because the conclusions made have been based on analysis of a limited observation series and application of inadequate climate models. Nevertheless, an ''orthodox'' concept of a coming global ecological catastrophe due to global warming is supported by many international documents. Understanding the real dynamics of the atmosphere–hydrosphere–lithosphere–cryosphere–biosphere (AHLCB) climate system is still far from being adequate, even more so when external (cosmic) impacts on the climate system have not been taken into account.

A full-scale complex study of the dynamics of the AHLCB system has not been started as yet. On the whole, there are isolated studies with details of partial processes taking place in this system. But, these studies by and large disregard glaciers and ice sheets which cover about 10% of the Earth's land area. Glaciers are masses of ice that accumulate from snowfall over long time periods and descend from higher to lower

ground. Seasonal snow cover, the largest component of the cryosphere, covers up to 33% of the Earth's total land surface. Sea ice forms, grows, and melts in the ocean depending on numerous parameters, most of them unknown. Satellite data indicate that during the last 30 years the Arctic sea ice extent has been decreasing at a rate of about 3% per decade, while the Northern Hemisphere snow cover has been decreasing by about the same amount during spring and summer. So, with this in mind, the dramatic conclusions of global-warming supporters is a sort of "global irony".

One of the underlying reasons for these contradictory opinions about global climate change is connected with the limited empirical diagnostics of climate mainly through analyzing comparatively short (about a century and a half) data series on surface air temperature (SAT). In contrast, though, it is apparent that what is fundamentally important for understanding the laws of spatiotemporal variability of climate are data on the climate system's energy: mainly, results of observations and numerical modeling of the ERB. Despite such studies having a comparatively long history, it is only during the last few decades that regular satellite observations of ERB components have been made, resulting in accumulation of a comparatively representative database of the global dynamics of the Earth's radiation field and its components: solar radiation absorbed by the Earth–atmosphere system and outgoing longwave radiation.

Only recently have attempts been made to calculate the global fields of the ERB and its components from numerical climate modeling using 3-D global models of the climate system's dynamics, rather than from the prescribed input characteristics of the fields of temperature, cloudiness, and atmospheric composition. A good example of successful modeling is the model developed at the Goddard Institute for Space Studies (GISS) in the U.S.A. which can be used to calculate the Earth's radiation field. The radiation balance has been calculated from changes in radiative forcing between 1880 and 2003 by means of the following climate-forming factors (Schmidt *et al.*, 2006):

- greenhouse gases including CO_2, CH_4, N_2O, CFC, and some other minor gas components;
- scattering (sulfate) and absorbing (black carbon) aerosols;
- extra-atmospheric solar radiation (solar constant);
- snow albedo;
- stratospheric aerosol;
- indirect climatic impact of tropospheric aerosol (through changes of processes in clouds); and
- processes on land surface (land use).

The data in Table 7.1 illustrate the outcome. The results of evaluating mean global ERB confirm just how confusing they are for conclusions about the spatiotemporal variability of ERB components. Note that in 2003 the radiative forcing due to indirect impacts of aerosol was estimated at $1.39\,W\,m^{-2}$, and the error reached 50%. According to Table 7.1, the total effective radiative forcing constitutes $+1.8\,W\,m^{-2}$, with the main contribution to both greenhouse gases and to uncertainty

Table 7.1. Efficient RF for the period 1880–2003 which takes GHGs, atmospheric aerosols, and other factors into account.

Forcing factor	*Radiative forcing* ($W \cdot m^{-2}$)
Greenhouse gases	
Well mixed	2.75
Ozone	0.24
Stratospheric H_2O (due to CH_4)	0.06
Total	3.05 ± 0.4
Extra-atmospheric solar radiation	$0.22(\times 2)$
Land use	$-0.09(\times 2)$
Snow albedo	$0.74(\times 2)$
Aerosols	
Volcanic	0.00
Black	0.43
Scattering tropospheric	−1.05
Indirect impacts of aerosols	−0.77
Total	-1.39 ± 0.7
Arithmetic sum of individual radiative forcings	1.93
Interactive consideration of all radiative forcings	1.80 ± 0.85

$\pm 0.85\,W\,m^{-2}$ resting with aerosols. Thus, aerosols are mainly responsible for uncertain estimates of global climate change, though there is no doubt that they are only part of the problem. More complicated problems appear in attempts to assess the leading role of non-linear processes in forming the Earth's climate (Kondratyev *et al.*, 2006a, b).

The main result of numerical modeling obtained at GISS consists in estimates of the mean global ERB imbalance (positive imbalance), which before 1960 constituted only several tenths of $W\,m^{-2}$, but then (with the exception of short periods of explosive volcanic eruptions) it constantly increased reaching its present level of $+0.85 \pm 0.15\,W\,m^{-2}$. This level reflects today's global climate warming. The observed accumulation of heat by the World Ocean, the main reservoir of excess energy, confirms the reality of this "imbalance". According to calculated data, an increase in the heat content in the upper 700 m layer of the ocean during the last decade constituted $6.0 \pm 0.6\,W\,m^{-2}$. The observed value of this warming of the ocean is $5.5\,W\,m^{-2}$. The calculated meridional section of SST for different versions of numerical modeling revealed considerable differences between model results and observations. This reflects the chaotic character of ocean weather. Nevertheless, the basic features of the mean zonal field of SST trends, on the whole, correspond to those

observed, revealing a deeper penetration of heat anomalies to oceanic depths in middle and high latitudes than in the tropics.

It should be emphasized that detection of the mean global energy imbalance is important conceptually, since this imbalance serves as an indicator of any breakdown in global ecological equilibrium. It is apparent that in the absence of anthropogenic impacts, the received (absorbed solar radiation) and spent (longwave outgoing radiation) energy should balance. Breaking the energy (heat) balance of the planet reflects the beginning of the dangerous process of ecological equilibrium breakdown on a global scale. Another indicator of this loss is the breaking of the closedness of global biogeochemical cycles.

The increase in mean global SAT observed between 1880 and 2003 constituted 0.6°C–0.7°C, which corresponds to a level of forcing of $\sim 1.0\,W\,m^{-2}$. The presence of excess heat means the existence of a heat reservoir ($0.85\,W\,m^{-2}$), which due to the strong inertia of the climate system should determine further global warming even keeping the greenhouse gas content in the atmosphere constant. Historical analogies show that such a level of forcing could not exist for long periods. In fact, if the imbalance value had remained throughout the Holocene (10,000 years) at a level of $\sim 1.0\,W\,m^{-2}$, it would have been enough for a 1 km ice layer to melt or for the SST in the layer above the thermocline to reach 100°C. Therefore, it is quite natural that on a geological timescale the imbalance could not exceed $1.0\,W\,m^{-2}$.

In estimating the reliability of calculated mean global ERB components, the role played by albedo is arguably the most complicated. Analysis of the data on the annual change in albedo obtained using climate models revealed the presence of considerable (beyond the range in variability of greenhouse radiative forcing) differences, both between various models and with observations results. Calculated albedo values and their empirical estimates have different annual variability. These differences testify to the unreliability of numerical modeling results determined by inadequate consideration of the impact of clouds and aerosols on albedo formation. With the present level of errors in satellite observations of albedo, reliably recognizing albedo changes is impossible in the context of an anthropogenically enhanced atmospheric greenhouse effect. The present situation is illustrated by the data in Table 7.2. It can be seen that the differences are dramatic (they even differ in sign). Hence, the notion of global warming that creates the illusion of global-scale uniform climate warming is incorrect. This means that further development of systems of ground and satellite observations aimed at accumulating a long series of reliable observation data is paramount in the present climatology. The complexity and importance of this problem follows from comparison of available satellite data according to which the mean global albedo of the Earth is ~0.29, and the extra-atmospheric total flux of solar radiation constitutes $341\,W\,m^{-2}$. This means that a change in Earth albedo by as little as 0.01 is equivalent to a change in radiation balance of $3.4\,W\,m^{-2}$, equivalent to CO_2 doubling in the atmosphere.

The contradiction between observed and modeled data on the radiation balance/albedo relationship has been confirmed by numerous publications on this subject (Heinrich and Hinzpeter, 1975). Some data reveal a decrease in outgoing longwave radiation by about $2.0\,W\,m^{-2}$ over the period March 2000–February 2004, which is

Table 7.2. Observed values of global mean RF and equivalent changes in the Earth's albedo ($\times 10^3$).

Forcings	*Albedo*
Enhancement of the atmospheric greenhouse effect during the industrial era ($2.4 \pm 0.2\,\mathrm{W \cdot m^{-2}}$)	-7 ± 6
Anthropogenic aerosol radiative forcing during the industrial era	$+4 \pm 4$
Estimates of albedo changes from data on the outgoing shortwave radiation reflected by the Moon (2000–2004)	$+16$
Changes in albedo from data of satellite observations (2000–2004)	-6
Changes in net radiation	
From satellite data for the period 1983–2001	-8
From data of ground observations for the period 1985–2000	-13
From data of ground observations for the period 1950–1990	$+20$

equivalent to a decrease in Earth's albedo by ~0.006. At the same time, there are estimates that testify to the considerable increase in outgoing shortwave radiation by $6\,\mathrm{W\,m^{-2}}$ and, respectively, an increase in albedo by 0.17.

The equation for shortwave radiation balance Q_s is as follows:

$$Q_s = G - R = D + H - R = G(1 - a),$$

where G is global radiation; D is direct radiation; H is diffuse radiation; R is reflected portion of global radiation (4%); and a is albedo.

The equation for longwave radiation balance is:

$$Q_l = AE = AO - AG,$$

where AE is effective radiation; AO is radiation from the Earth's surface; and AG is trapped radiation (radiative forcing, or greenhouse effect).

The total radiation balance is described by the following equation:

$$Q_t = Q_s - Q_l = G - R - AE.$$

These equations of the Earth's energy balance show that albedo is the main parameter regulating it. The climatic effect of albedo changes can be shown in different ways. Keeping variations in the properties of the land surface, aerosol, and snow and ice covers in mind, then with a decrease of albedo the Earth should warm, and with an increase of albedo it should cool. Put another way there should be a substantial decrease in mean global annual heat in the ocean. Analysis of observational data for the period 1992–2002 shows an increase of heat supplies in the World Ocean by $0.7 \pm 0.4\,\mathrm{W\,m^{-2}}$. If we only take albedo change into account, the decrease in outgoing longwave radiation should correspond to this value. On the whole, satellite observations have not detected any important role of cloud feedback in

the albedo increase, which testifies to the necessity of continuing cloud observations from space.

Processing observational data on total radiation for the period 1960–1990 shows the negative trend of total radiation on the land surface varying within $6\,W\,m^{-2}$–$9\,W\,m^{-2}$. This is equivalent to a decrease in total radiation of 4%–6% over 30 years. This effect has been called the Earth's "eclipse" by some authors. But from 1990 a general "brightening" of the Earth was observed, connected with decreasing aerosol pollution of the atmosphere due to reduced industrial ejections over the former U.S.S.R. This conclusion was confirmed by a number of actinometric observations at Tõravere (Tartumaa, Estonia). For example, Tooming (2002) obtained data at the Tartu–Tõravere Actinometric Station data from 1955 to 2000 that showed a decrease in global radiation by as much as 20% during the last 46 years can be explained primarily by the relatively high negative trend in snow cover duration and surface albedo. Data given by Baltensperger *et al.* (2005) for larger territories show that the spatiotemporal dynamics of optical aerosol depth is substantially inhomogeneous.

Within the framework of the International Satellite Cloud Climatology Project (ISCCP) numerical modeling of radiation balances was undertaken both for the land surface and the Earth as a whole, at a spatial resolution of 280 km and a time step of 3 hours over a 21-year period (1983–2004). Comparing the results with observational data showed that the improved method of calculation and specified input information allow errors in evaluating the radiation balances for the land surface to be reduced from 20–$25\,W\,m^{-2}$ to $10\,W\,m^{-2}$–$15\,W\,m^{-2}$, and on a global scale from $10\,W\,m^{-2}$–$15\,W\,m^{-2}$ to $5\,W\,m^{-2}$–$10\,W\,m^{-2}$. Moreover, an increasing trend of total radiation by 0.1% per year was observed (Zhang *et al.*, 2004). By improving climate models and, what is more, specifying the spatiotemporal distributions of the parameters of these models we can improve estimates of the ERB and assess the role of various factors in its dynamics.

Analysis of mean annual estimates of the radiation balance shows that the impact of clouds consists in shifting longwave radiative cooling toward the intra-tropical convergence zone, helping to stabilize the tropical atmosphere and enhance the forcing on atmospheric circulation by increasing the horizontal gradient at which it is heated. There is also a shifting of longwave cooling to higher altitudes in the storm zone at mid-latitudes which destabilizes barocline zones but reduces the horizontal gradient of heating in these zones.

In December 1999, NASA launched the Terra satellite which carried five scientific instruments for remote sensing of the climate system: ASTER, CERES, MISR, MODIS, and MOPITT. The multi-beam Multi-angle Imaging Spectroradiometer (MISR) provides measurements of outgoing shortwave radiation at wavelengths of 446 nm, 558 nm, 672 nm, and 866 nm with a spatial resolution of 275 m–1,100m in nine viewing directions within $\pm 70^{\circ}$ with respect to the satellite trajectory. Such multi-beam observations of outgoing short-wave radiation can be used to retrieve details about atmospheric aerosols, the surface, and cloud cover, important additions to results of satellite observations in fixed directions. The radiation balance calculated using MISR data and satellite observations of Oklahoma (U.S.A.) made on March 3,

2000, resulted in reducing error down to 4% by moving from a 2-D to a 3-D climate model (Marchand and Ackerman, 2004).

A new stage in the development of ERB satellite observations is the use of instruments to measure ERB components carried by the second generation of Meteosat satellites. Routine observations from these satellites made since December 2002 have produced data on total outgoing radiation at wavelengths 0.32 μm–100.0 μm and outgoing shortwave radiation at wavelengths 0.32 μm–4.0 μm every 15 minutes, with a spatial resolution of about 40 m and an error of no more than 10%. The scanning multi-channel radiometer Spinning Enhanced Visible and Infra Red Imager (SEVERI) carried by Meteosat-8 provides information about cloud-induced radiative forcing at a high spatiotemporal resolution, which opens up prospects for a more reliable analysis of factors affecting ERB formation (Harries *et al.*, 2005).

Thus, studies and estimates of the ecological equilibrium on a global scale are closely connected with the state of studies of ERB components and with dependences on all the parameters involved in the natural–anthropogenic environment. A still serious difficulty remains about the inadequacy of available methods and algorithms for processing and interpreting data on NSS dynamics observations. The reliability of observational data on the state of the ERB depends both on the equipment of environmental monitoring systems and how the data are processed. Technical means should resolve the problem of obtaining information about the climate system's components at the necessary spatiotemporal resolution, and processing methods need to be found to minimize errors in estimates of the radiation balance.

To assess the ERB, it is necessary to develop a co-ordinated network of global ground and satellite observations equipped with technical and algorithmic means to provide data of a single standard for use in studies. Unfortunately, there is no such network at present, and the data obtained are processed fragmentarily and in small volumes. Nevertheless, progress is expected in the near future due to the pressing necessity to resolve global energy problems. However, understanding the way in which climate change is determined by the complicated relationship between interactive components of the AHLCB climate system and obtaining reliable estimates of the parameters of this interaction remain as obstacles, mainly due to random systems of nature monitoring and the absence of an efficient international mechanism to oversee observational and numerical modeling data. Nevertheless, a retreat from unfounded "apocalyptic" estimates of climate and political statements has recently been observed, which instills hope for constructive resolutions of climate problems at the international level (IPCC, 2007).

The paradox in contradictory estimates of climate change is that in the course of climate discussions some fundamental and clearly apparent facts have been strangely disregarded, despite being studied in detail in many publications by Russian climatologists (Kondratyev and Krapivin, 2003a, b, 2006a–c). Unfortunately, it is a fact that many international organizations dealing with the planning and realization of programs of climate studies ignore these publications, even after they have been translated in English (Kondratyev 1999a; Kondratyev and Cracknell, 1998; Kondratyev *et al.*, 2003b). Russian scientists have come up with constructive ideas

on how best to overcome many of the difficulties facing climate studies, as mentioned in their reports at the World Climate Conference held in Moscow in 2003.

7.2 NATURAL ECODYNAMICS ASSESSED BY OBSERVATIONAL DATA

7.2.1 Reality, suggestions, and fictions

7.2.1.1 Uncertainty and interactivity of climatic processes

The unprecedented increase of interest in climate observed in recent decades has been responsible for both scientific and applied developments in climatology, resulting in considerable advances in understanding the causes of present climate change, paleoclimatic laws, and in substantiating scenarios of possible climate change in future. It is scenarios—not predictions—whose possibilities should be assessed as doubtful. Unfortunately, the many exaggerations and apocalyptic forecasts have played too serious a role in the growing attention to climate problems. For instance, complete melting of Arctic sea ice in the first half of this century is predicted, due to which climate change, formulated as a concept of anthropogenic global warming, has become the focus in geopolicy (Boehmer-Christiansen, 2000; Kondratyev, 1998b). It is paradoxical that the presidents and prime ministers of various countries discuss whether the Kyoto Protocol should be considered as a scientifically grounded document, as took place, for instance, in the U.S.A. Confusion can be blamed, in particular, on the lack of sufficiently clear and agreed terminology. Putting aside for a moment definition of the notion of climate, one should remember, for instance, that so far the notion of ''climate change'' has been defined as anthropogenically induced climate change, though one of the main unsolved problems consists in the absence of convincing quantitative estimates of the contribution of anthropogenic factors to the formation of global climate (there is no doubt however that anthropogenic impacts on climate do exist). International documents outlining present ideas about climate use the prevalent notion of consensus with respect to scientific conclusions, as if the development of science was determined not by a difference of views and respective discussions—but by a general agreement on some concrete problems. Apart from definitions, there exists the problem of conceptual uncertainty in different areas of climate science.

At the World Summit on Sustainable Development held in September 2002, in Johannesburg (South Africa) a further unclear notion, ''sustainable development'', appeared, which has still not been defined exactly. Discussions of climate change and sustainable development were continued at numerous sessions of the U.N. Commission on Sustainable Development where climate problems were the focus. At the G-8 meeting in Genoa (July, 2001) President Vladimir Putin proposed organizing in Moscow the World Climate Change Conference, which was held on September 29–October 3, 2003. It is appropriate here to recall the undoubted progress of the U.N. Conference on Environment and Development (UNCED) held in Rio de Janeiro, June 3–14, 1992 and the UN General Assembly meeting in special session held 5 years later (New York, June 23–27, 1997), which consisted only in attracting

the attention of governments and the world community to problems of global change and sustainable development. Unfortunately, both these forums were not adequately prepared. The most important negative result was the failed attempt to implement the ''Earth Charter'' intended to formulate and substantiate priorities. Instead, a most amorphous and declarative document, the ''Rio Declaration'', was approved (Kondratyev, 1999b).

The Rio Declaration is a set of 27 principles covering environmental protection and responsible development. These principles (not legally binding) define the development rights of people and their responsibilities to protect the common environment. The Declaration recognizes that the only way to achieve long-term social and economic success is to link it with environmental protection and to establish equitable global partnerships between governments and key figures from society and business.

Nowadays, the following three global ecological problems are the focus:

- climate change (''global warming'');
- the fate of the ozone layer in the stratosphere; and
- closedness of global biochemical cycles (the concept of biotic regulation of the environment).

The sad paradox is that, despite the primary importance of the latter problem convincingly substantiated in the scientific literature and the secondary role of the two former ones, UNCED documents have missed the primary importance of the following sequence of events: socio-economic development (stimulated by growing population size) → anthropogenic impact on the biosphere → consequences of these impacts for the environment (climate, ozone, etc.).

This lack of understanding resulted in unfoundedly bringing the problem of global warming to the forefront by adopting a document which is lame, confusing, and unjust to the developing world: the U.N. Framework Convention on Climate Change (UNFCCC). This focuses, regardless of scientific substantiations, on the anthropogenic origin of global climate warming and recommendations for developed countries to reduce greenhouse gases emissions to the atmosphere (mainly carbon dioxide emissions).

In December 1997 the third Conference of the Parties (COP) (over 160 countries) was held in Tokyo (Japan). It concentrated on long and hot discussions on the necessity to recommend a 5% CO_2 emission reduction by 2008–2012 (with respect to emissions at the level of 1990), despite the absurdity of such a discussion and the lack at the time of any visible success in reducing CO_2 emissions (global emissions continue and will grow not only in developing but also in many developed countries, including the U.S.A). Naturally, the top priority of developing countries is to increase living standards—not to curtail industry for the sake of CO_2 emission reduction. But, this is the condition to be paid for UNCED ratification by the U.S.A. and other countries of the ''golden billion''. The history of the UNFCCC is marked by illustrations of massive (mainly bureaucratic) activity that annually eats up hundreds of millions of dollars (instead of investing them in science). The U.N. Development

Program/Global Ecological Fund (UNDP/GEF) report, as of July 30, 1998, showed that the financing of 267 projects by the GEF cost $1.9 billion (GEF, 1998). What was the cost of getting 10,000 people to participate in the Conference in Kyoto? The recent Sixth Session of the UNFCCC Conference of the Parties (COP-6, November 13–24, 2000, The Netherlands) as well as the International Conference on Freshwater (December 3–7, 2001, Bonn) were also well populated, with representatives from 178 countries (and then they were mainly officials—not specialists).

Maybe this situation is the consequence of scientific bases of global change problems having been inadequately elaborated. Although this conclusion is partly valid, as far back as 1990 there were publications (Gorshkov, 1990; Kondratyev, 1990) devoted to key aspects of global ecology. Gorshkov (1990) and Gorshkov *et al.* (2000) proposed and substantiated the fundamental concept of biotic regulation of the environment, and Kondratyev (2002) demonstrated the groundlessness of the "greenhouse" hypothesis of global warming and emphasized the need to study the atmosphere–ocean–land–ice cover–biosphere climate system by taking into account the complexity of feedbacks between its interactive components. The problem of a global observing system was thoroughly analyzed, especially developments in the field of remote sensing and the use of respective observational data (Grigoryev and Kondratyev, 2001c; Kondratyev, 1990, 1992, 1998a, 1999b). Yet another work was the special problem of atmospheric ozone variability (Kondratyev and Varotsos, 2000).

Let us now make a few brief comments on global climate change that vividly reflect existing delusions. The most important are as follows:

- Observational data (still inadequate regarding comprehensiveness and reliability) do not confirm the anthropogenic origin of global warming (which is especially true for the data of ground observations in the U.S.A., in the Arctic, and for satellite microwave remote-sensing results).
- If the enhancement of the atmospheric greenhouse effect due to supposed doubling of CO_2 concentration in the atmosphere is about $4\,W\,m^{-2}$, then the uncertainties about the climate-forming role of atmospheric aerosols and clouds in numerical climate modeling reach tens or even hundreds of $W\,m^{-2}$.
- The numerical climate modeling results used to substantiate the "greenhouse global warming" hypothesis do not actually agree with observations and, what is worse, have been adjusted to agree with observational data.
- Recommendations concerning the levels of GHG emission reduction based on these results make no sense whatsoever, and their realization may have far-reaching negative socio-economic consequences. Numerical modeling data show that even if KP recommendations are fully achieved the decrease in mean global annual SAT will not exceed a few hundredths of a degree (Wigley, 1999; Wigley and Raper, 2001).

Recently, efforts have concentrated on analyzing numerical climate modeling uncertainties (inadequacy). Perhaps, the most serious source of uncertainties is inadequate consideration of interactive processes in the aerosol–clouds–radiation

system (Charlson *et al.*, 2001; Kondratyev and Galindo, 1997; Kondratyev, 1998b, 1999a; Kondratyev and Cracknell, 1998). There is no doubt that the most complicated aspect of numerical climate modeling is understanding the interactive dynamics of the biosphere, which can be illustrated by two concrete examples, which, of course, only to some degree reflect the complexity of the problem.

To explain the decrease in the diurnal trend of SAT (DTR) by ~3 K–5 K detected from observational data between 1951 and 1993 resulting from a rapid increase of minimum temperature, we consider the impact of various factors: changes in cloud amount, water vapor content, and tropospheric aerosol, in addition to turbidity and soil humidity. Positive trends in the first three factors could lead to a decrease of total radiation in daylight and to an increase in atmospheric counter-emission at night, whereas variations in heat and moisture exchange between the surface and the atmosphere, which should be much more substantial in daylight than at night, could result from the changing intensity of turbulent mixing and soil moisture.

The strongly manifested interactivity of climate-forming processes and the inadequacy of their parameterization in climate models seriously complicate the evaluation of contributions of various mechanisms of DTR decrease. In this connection Collatz *et al.* (2000) using the SiB2 approximated model of land biosphere, numerically modeled the response of the diurnal change in temperature of a vegetation-covered land surface to changes in external forcing and the biophysical state of the vegetation cover. Various scenarios were considered to discover the possible impact of interactive dynamics of the vegetation cover on DTR. Analysis of the numerical modeling results showed that an increase in longwave deficit (LWD) determines the increase in air temperature over the vegetation cover T_m at night, promoting a decrease in DTR. But under conditions of global warming, changes in T_m or an increase of T_m+ LWD favor an increase in both minimum and maximum temperature, which determines the negligible impact of these factors on DTR. This reaction is the consequence of diurnal change in aerodynamic stability and radiation balance.

Many numerical experiments on climate modeling are based on the use of atmospheric general circulation models (GCMs) together with land surface models (LSMs). The results of such numerical experiments depend to a great degree on specific features of the interaction between the GCM and LSM designed to retrieve the surface–atmosphere exchange between radiation, momentum, and energy. The desire to take into account the variety of land ecosystems has led to LSMs becoming much more complex due to including sub-models that take into account photosynthesis, vegetation cover dynamics, and biogeochemical cycles, which radically increases model reality.

Based on using the simple SiB model of the biosphere as an LSM version, Kim *et al.* (2001) undertook various numerical experiments whose results showed the importance not only of the sensitivity of SiB to a change in many morphological parameters of vegetation cover, but also the sensitivity of transpiration of high vegetation cover to parameters that characterize vegetation cover resistance. The improved SiB2 model enabled consideration of the biogeochemical processes that determine the surface–atmosphere exchange between water vapor, energy, and carbon dioxide. Using the Sib2 and Sib2-Paddy models, and the meso-meteorological model

GAME-Tropics the results from numerically modeling processes taking place on a test rice field in Thailand (17°03′N, 99°42′E) were compared with data from the monsoon experiment in Asia (GAME), part of the global field experiment GEWEX (September 1–6, 1999) which studies energy and water cycles during the rainy season. Good agreement was observed between the results of the two models and observational data on the diurnal change in radiation balance and latent heat flux, except for estimates calculated using the SiB2 model. There was also good agreement between observed and modeled fluxes of latent heat and heat in soil, as well as the rate of carbon assimilation by the SiB2-Paddy model, but once again the SiB2 model gave substantial systematic errors. By adjusting parameters the SiB2-Paddy model makes it possible to obtain reliable estimates of the temperature of soil, water, and vegetation cover. Calculations of the radiation balance, balances between energy and water, as well as latent heat and rate of CO_2 assimilation were adequate. Such results mean there is a good chance for adequate consideration of the biosphere (as an interactive component of the climate system).

De Rosnay *et al.* (2000) assessed the reliability of schemes that parameterize land surface processes to find the correspondence between calculated mean annual fluxes of energy and moisture depending on detailed consideration of the vertical structure of soil. These schemes are used in general circulation models of the atmosphere (GCMAs). The calculations testify to the strong dependence of fluxes on vertical resolution. The 11-layer scheme parameterizing heat and moisture transfer in the top 1 mm thick layer of soil was found to be adequate.

An important part of numerical climate modeling is unraveling a complicated set of problems concerning atmospheric chemistry. It is well known, for instance, that formation of the concentration field of a greenhouse gas such as tropospheric ozone (TO) under various conditions (city, regional, and global distributions) is greatly affected by various short-lived minor gas constituent (MGC) ozone precursors, including nitrogen oxides ($NO_x \equiv NO + NO_2$), methane (CH_4), many organic compounds, hydrogen, and carbon oxide (CO). Each of these MGCs is characterized by specific natural (biospheric) and anthropogenic sources.

Since TO is a greenhouse gas, emissions of it can indirectly affect the formation of atmospheric greenhouse effect by influencing the TO concentration field. Moreover, MGC/TO precursors change the hydroxyl concentration field and, hence, the oxidation power of the troposphere. In its turn, the distribution of hydroxyl concentration in the troposphere controls the lifetime and, thus, the level of concentration of methane at the global scale.

Such a complicated interactivity of processes can both directly and indirectly affect formation of the atmospheric greenhouse effect. Derwent *et al.* (2001) described a global 3-D Lagrangian chemistry transport model (STOCHEM) which reproduces chemical processes including MGC transport and can be used to reproduce interrelated fields of TO and methane concentration (Johnson *et al.*, 2002) under conditions of emission to the atmosphere of short-lived TO precursors such as CH_4, CO, NO_x, and hydrogen. At the same time, the radiative forcing (RF) of NO_x emissions depends on the location of emissions: near the surface or in the upper troposphere, in the Northern or Southern Hemisphere. For each short-lived MGC/

TO precursor, estimates of global warming potential (GWP) can be obtained from integration data of the response of methane and TO to RF over a 100-year period. For example, the combined impact of methane and TO gives a GWP of 23.3.

Calculation results show that the indirect RF caused by changes in methane and TO content is considerable for all MGC/TO precursors. Whereas RF due to changes in the content of methane is determined mainly by the effect of methane emissions, in the case of TO it is controlled by all MGC precursors, especially by nitrogen oxides. The indirect RF connected with TO can be so great that MGC/TO precursors should be considered like those of MGCs, which should be taken into account when evaluating possible climate change and measures needed for its prevention.

Despite the "anti-Kyoto" statements of President George W. Bush, the headlines of many American newspapers in January 2001 were quite dramatic. *The Washington Post* and *The International Herald Tribune* reported that scientists had published dreadful predictions of warming and forthcoming climate change foretelling a global disaster in this century. The Earth's warming was considered as a new danger sign for the world population. Discussions of the danger of global warming still continue. For instance, *CBS News* on January 20, 2005 broadcast:

> "An ancient version of global warming may have been to blame for the greatest mass extinction in Earth's history. In an event known as the 'Great Dying', some 250 million years ago, 90 percent of all marine life and nearly three-quarters of land-based plants and animals went extinct. Scientists have long debated the cause of this calamity—which occurred before the era of dinosaurs—with possibilities including such disasters as meteor impacts."

There are various explanations for planetary climate warming. For example, researcher-paleontologist Peter Ward (2002) from the University of Washington thinks global warming is caused by volcanic activity. Ward and Brownlee (2004) believe that

> "we live in a turbulent period of human history, a time of catastrophic wars, sweeping political movements, revolutionary social change, bewildering discovery, and religious and philosophic tumult."

We cannot disagree with Stanley (2005) and Stanley *et al.* (2005) that our planet is a system of integrated components driven by the Earth's internal heat and external energy from the Sun. It is evident that geospheric processes like plate tectonics, volcanism, and the rock cycle are linked to the hydrosphere, atmosphere, climate system, and biosphere, and their interactions form the global processes that we observe.

Different opinions concerning global warming are determined by new scenarios for climate change in the 21st century, which predict such changes to be more substantial than previously supposed. According to data from IPCC (2001), the increase in mean annual global SAT could reach 5.8°C by 2100. Five years earlier (IPCC, 1996) this estimate was only 3.5°C.

As Kerr (2001a, b) rightly pointed out, the latest report (IPCC, 2001) said the world could be as much as 5.8°C warmer in 2100 than it is today. Five years ago, the panel set the upper end of the range at 3.5°C. Climatologists, however, were more impressed by something that drew little public notice: the range of the IPCC's projections has actually widened over the past 5 years. To many climate modelers, this is not surprising. Moreover, numerical modeling is restricted by the very limited amounts of observational data: the SAT data series, for example, covers only about 100 years.

Though most specialists believe observed global warming is probably determined by the growth in GHG concentration, in many respects the range of estimates of possible climate change have not converged—but widened.

Basic uncertainties in the estimates of climate change relate to three aspects

- detection of global warming from observational data;
- ascription of global warming as anthropogenically induced; and
- forecast of future climate changes.

According to Kerr (2001a, b), new data from IPCC (2001) narrow the range of uncertainties in the case of the first two aspects of the problem, yet future climate forecasts have become still more uncertain. According to IPCC (2001), observed global warming constituted $0.6^{\circ} \pm 0.2^{\circ}$C (at the 95% level of statistic significance), with the greater part of warming observed during the last 50 years being (at a probability between 66% and 90%) determined by the growth in GHG concentrations. Since one of the main reasons for uncertainties in numerical climate modeling is still linked with inadequate consideration of the climate-forming role of atmospheric aerosols and clouds, it should be noted that the more we know about aerosols, the better we understand how little we know about them. This especially concerns estimates of the impact of aerosols on clouds and, respectively, on climate, which vary widely.

Unfortunately, the role of uncertainties in numerical climate modeling was not properly assessed in IPCC (2001). This prompted many specialists to seriously criticize the report (Kondratyev and Demirchian, 2001; Elsaesser, 2001; Schrope, 2001). IPCC (2007) has retained the basic shortcomings of the former IPCC reports, introducing the words "likely" or "confidence" as symbolic corrections. However, for the first time this report contains assessments that are impartial and does not explicitly state the anthropogenic origin of observed global warming.

It is clear that the observed increase in carbon dioxide, methane, and nitrous oxide in the atmosphere cannot be explained by anthropogenic causes only. We need to bear in mind that the changeability of GHG biogeochemical cycles is a complex function of numerous parameters controlled by the NSS. Unfortunately, there is no reliable information about the correlations between many of them. This fact is admitted by experts in IPCC (2007).

IPCC (2007) repeats the error of previous IPCC reports by considering the climate change problem separately from global ecodynamics. Ecological, geodynamic, geophysical, economic, and social processes that must be studied as a global

single system. This is the only way that RF components can be assessed reliably. Nevertheless, *Nature Magazine* (**445**(7128), February 8, 2007, p. 567) took the opposite view:

> ''The IPCC report has served a useful purpose in removing the last ground from under the sceptics's feet, leaving them looking marooned and ridiculous.''

This comment beggars belief. However, as a political or social statement maybe it is fair enough—but it is not a scientific statement. A few centuries ago what would have been the consensus on the heliocentric nature of the solar system? Or in the 19th century what would have been the consensus on Darwin's theory of evolution or on the age of the Earth and Hutton's unconformity? History has proven over and over again that truth is not a matter of counting votes, it lies in the field of ecoinformatics which provides the methodology for combining both data and knowledge about the environment.

As far as global change is concerned, estimation of present and possible future changes in global climate is, of course, paramount (Kondratyev, 2001), though in these estimates the concept of global warming is still preserved, as seen in IPCC (2001, 2007). We believe this is nothing more than inertia from earlier speculative ideas that are far from being scientific, as convincingly analyzed by Boehmer-Christiansen (1997, 2000, 2002). A vivid illustration of the contradictory character of climate estimates are the radically different statements on this subject by the two presidential candidates during the U.S. election campaign (From the Candidates, 2000). While Al Gore is a well-known protagonist for global warming and supports the Kyoto Protocol, George W. Bush protested against such a (ecological) policy like that of KP, which would lead to radical increases in prices of petrol, oil products for heating, natural gas, and electricity. Ratification of such an agreement would cause serious damage to the U.S. economy. The KP is ineffective, inadequate, and unjust with respect to America, since it excludes 80% of the world from participation in realizing KP recommendations, including such basic centers of population concentration as China and India. In George W. Bush's opinion, primary importance should be given to development of new ecologically pure technologies and the use of market mechanisms, including freedom from regulation of electricity and natural gas markets, taxation on emissions, and emissions trading. George W. Bush believes that natural gas and nuclear energy will play an important role in reducing America's dependence on foreign oil and in providing the country with energy resources in the 21st century. By agreeing with radical critics of KP, we should note that the opinion of George W. Bush about market mechanisms is specific to the U.S.A. and the concept of emissions trading is disputable.

Pravda on October 26, 2004 published articles headlined ''Russia has to ratify the Kyoto Protocol to become a WTO member,'' ''Russia needs to ratify the document to make it work, as Russia is the world's second largest source of greenhouse gases.'' The adherents of KP ratification in Russia have attempted to sway public opinion and could win despite the opinion of many experts. Nevertheless, discussions on this subject still continue.

A convincing illustration of the groundlessness of KP is the result of the Sixth Session of the UNFCCC Conference of the Parties (COP-6) of the representatives of the signatory countries held on November 13–24, 2000, in The Hague. There were 7,000 participants in this conference representing 182 governments, 323 intergovernmental and non-governmental organizations, and 443 from the mass media. Congressman Joe Barton (a Republican from Texas) announced that if George W. Bush won the election, then he would recommend him to reject the KP and start negotiations in order to free the economy from unsubstantiated ecological restrictions, since

> "what we see here (at COP-6) is rather a senseless exercise or, at least, an exercise in making things up, and therefore nothing discussed during this week should be supported by voting."

Formerly, at the U.S. representatives' press briefing (November 10, 1998; Buenos Aires, Argentina; 4th Conference of the Parties on the UNFCCC) he told them:

> "I must tell you, having been an official observer in Kyoto, and now at this conference, I do not see that much has changed. It appears to me that the Clinton administration intends to implement this treaty by osmosis, simply let it kind of filter in and everybody assumes that it is the thing to do. Well, I want to inform all our good friends and allies in Western Europe and Japan and Asia, Central and South America, that the United States democracy doesn't work that way."

Congressman Joe Knollenberg continued:

> "The Kyoto Protocol is, I believe, fatally flawed. It's too much, too soon, and there are too few developing nations that are considered in this whole scheme. I think what we have to do, because of the immature science involved here, I think we have to slow down. Let's not walk away from it, but let's slow down. Let's perfect the science. We haven't really had any kind of debate through Congress or otherwise on this whole issue of carbon dioxide and global warming."

Although the Executive Director of the U.N. Environment Program (UNEP) Klaus Töpfer rejected the proposition to consider nuclear energy as an important prospect for future energy, representatives from the U.S.A. and Japan announced in the Hague that they would be ready to support financing of projects on nuclear energy in developing countries as a means of reducing CO_2 emissions to the atmosphere.

Discussions in the Hague were characterized by the difference in opinion between the U.S.A. and countries of the European Union which rejected the proposition of the U.S.A. to balance carbon by using various mechanisms (including planting of forests as a sink of carbon) and demanded that the U.S.A. implement recommendations to reduce CO_2 emissions to the atmosphere.

Recommendations approved at the COP-6.2 (second part of COP-6) meeting in July 2001 in Bonn can only be described as absurd (U.N., 2002). The notion of certified emission reduction (CER) was introduced, which means substituting carbon sinks, like forests, for a real reduction in emissions (WI, 2006; Seiler-Hausmann *et al.*, 2004). According to this innovation, Japan, Russia, and Canada are permitted to accumulate CER due to forests in these countries. The absurdity of this recommendation is mainly determined by the fact that the global carbon cycle is still far from being understood, and therefore getting reliable estimates of the role of CER as a factor affecting the global climate is unreal. The subject matter that caused heated discussions consisted of the three ''flexibility mechanisms'' (i.e., joint accomplishment, emissions trading, development of pure technologies). This can only be assessed as purely rhetorical. Seiler-Hausmann *et al.* (2004) discussed the concepts of ''eco-efficiency'' and ''produce more with less''. That is to say, when goods and services satisfy human needs, when increases in the standard of living are at competitive prices, and when environmental impacts and resource intensity are decreased to such a degree that keeps them within the limits of Earth's expected carrying capacity. Eco-efficiency, a term first proposed by the World Business Council for Sustainable Development in 1992, is a management approach that allows businesses to carry out environmental protection measures from a market-oriented point of view, with the aim of illustrating that ecology and economy do not need to be contradictory. Indeed, eco-efficiency has been portrayed as a win–win situation for both business and the environment.

The main aspect of global climate change, despite general agreement about global climate warming in the 20th century (especially regarding the last quarter of the century), relates to identifying the causes of warming (and especially estimating quantitatively the contributions of various factors to global carbon change), which remains even today the subject of heated scientific discussions. This is true of climate forecasts that take anthropogenic impacts into account. It is a sign of hope that IPCC (2007) rejected the definition of the notion of ''climate change'' approved by the UNFCCC as determined by only anthropogenic factors, and agreed that an adequate definition should take on board both natural and anthropogenic causes of climate change. It should be added that the traditional definition of climate is ''an event characterized by the estimates of its parameters averaged over 30 years.'' Let us now briefly discuss observational data based mainly on IPCC (2001, 2007).

7.2.1.2 Observational data

The main cause of contradictions in studies of climate and current changes in it rests with the inadequacy of observational databases from the viewpoint of their completeness and quality. Of course, climate is made up of many parameters, such as

- air temperature and humidity near the Earth surface and in the free atmosphere;
- precipitation (liquid and solid);
- cloud amount, the height of their lower and upper boundaries;
- the microphysical and optical properties of clouds;

- radiation balance and its components;
- the microphysical and optical parameters of atmospheric aerosols; and
- chemical composition of the atmosphere, etc.

Meanwhile, empirical analysis of climate data is limited, as a rule, by SAT observations that are only available for a data series of 100–150 years. However, even these data series are heterogeneous, especially with regard to the global database, which is the main source of information for substantiation of the global warming concept. Also, the fact should be borne in mind that the globally averaged secular trend of SAT values is based, to a great extent, on the use of imperfect observed data on sea surface temperature (SST).

When using observational data to diagnose climate change, emphasis should be laid on analyzing climate variability in which the consideration of movements—not averages—is the important thing. Unfortunately, there have been no attempts to use this approach. The same refers to estimates of the internal correlation of observation series. But, analysis of the secular trend of SAT shows that by filtering out the contribution to temperature variations in recent decades at the expense of internal correlations (i.e., determined by the climate system's inertia), it turns out that temperature has practically not changed. The fact is paradoxical: the increase in global mean SAT during the last 20–30 years is the basis for conclusions concerning anthropogenic contribution to present-day climate change.

Air temperature. According to SAT observations (which began in 1860), annual and global averages of air temperature increased by $0.6° \pm 0.2°C$ according to IPCC (2001) and by 0.76 [0.57 to 0.95] °C according to IPCC (2007). This is approximately 0.15°C higher than the value given in the IPCC-1996 report (Kondratyev, 1999b), which was explained by the high SAT level between 1995 and 2000. Observational data revealed a strong spatiotemporal variability in annual mean SAT over the globe. This manifested itself, for instance, in climate warming in the 20th century taking place during two time periods: 1919–1945 and since 1976. Warming in the Northern Hemisphere in the 20th century was, apparently, the strongest for the last 1,000 years, the 1990s being the warmest decade, and 1998 the warmest year. An important feature of climate dynamics consisted in the average rate of increase of nocturnal (minimum) SAT values on land being almost twice as high as that of diurnal (maximum) SAT values since 1950 (0.2°C against 0.1°C/10 years). This favored longer frost-free periods in many regions of moderate and high latitudes.

IPCC (2001) does not mention the earlier supposed increase of climate warming in the NH high latitudes as a characteristic indicator of anthropogenic global warming. However, an analysis of direct SAT measurements at North Pole stations over 30 years (Adamenko and Kondratyev, 1999) and of dendroclimatic indirect data for the last 2–3 centuries shows that there had not been any homogeneous enhancement in warming. Climate changes during the last century and the last decade were characterized by their strong spatiotemporal heterogeneity: in the Arctic, there were regions that experienced both climate warming and climate cooling simultaneously (Sieg *et al.*, 1996; Soros, 2000). IPCC (2007) emphasizes the following facts:

- Mountain glaciers have receded and snow cover has decreased in both hemispheres, causing a rise in World Ocean level. The rate of this for 1961–2003 and 1993–2003 constituted 1.8 ± 0.5 mm/yr and 3.1 ± 0.7 mm/yr.
- The Arctic temperature varied widely over 10-year periods, with the warmest being between 1925 and 1945. From satellite observations, the annual mean ice cover in the Arctic since 1978 has decreased at the rate of 2.7% per decade, and in summer this reached 7.4%.
- Since 1980, the temperature of the permafrost upper layer increased by 3°C. Since 1900, the maximum area of seasonally freezing land in northern latitudes diminished by 7%.

From airborne observations (which began in the 1950s when the adequacy of such observations became satisfactory), the trends in global mean SAT and in lower troposphere temperature were almost the same (about 0.10°C/10 years) (Angell, 1999, 2000a, b). From satellite microwave remote sensing (which began in 1979), there was an increase in global mean temperature of the lower troposphere by about 0.06°C/10 years, much below the SAT increase (~0.15°C/10 years). This difference in warming manifests itself mainly in ocean areas in the tropics and sub-tropics, and it is not clear why this is so (Christy *et al.*, 1998).

Snow and ice cover extent. In the 20th century, since the end of the 1960s a 10% decrease in snow cover extent has been observed as has a two-week reduction in the annual duration of lake and river ice cover at NH middle and high latitudes, while in non-polar regions mountain glaciers retreated. The change in NH sea ice cover extent in spring and summer since the 1950s varied within 10%–15%. In recent decades (between late summer and early fall) the Arctic sea ice cover thickness has decreased by about 40%, but in winter the decrease was less substantial. From NASA estimates, the total area of Arctic sea ice constituted 6.0 million km^2 in 2002, 5.6 million km^2 in 2005, and 5.9 million km^2 in 2006. According to Chapman and Walsh (1993), since 1961 the Arctic sea ice cover extent has been decreasing by 3.6%/10 years. More pessimistic estimates were given by the Nansen Environmental and Remote Sensing Center in Norway. From its data, this rate constituted 4.6%, and for the period 1978–1994 it constituted 5.8% (Johannessen *et al.*, 1996).

Regular satellite observations (which began in the 1970s) have not revealed any marked trend in variations of Antarctic ice cover extent. The Antarctic contains more than 90% of the world's ice, and the loss of any significant part of it would cause a substantial sea level rise. According to IPCC (2007), melting of the Antarctic ice sheet was raising World Ocean level at a rate of $0.14 \pm 0.41\,mm\,yr^{-1}$ between 1961 and 2003 and $0.21 \pm 0.35\,mm\,yr^{-1}$ between 1993 and 2003. As can be seen from these values, the level of uncertainty in estimates of the state of the Antarctic ice sheet remains great.

Surface level and ocean upper-layer heat content. During the 20th century the World Ocean level rose by 0.1 m–0.2 m. Apparently, this was caused by the thermal

expansion of seawater and ice melting on land due to global warming. The rate of World Ocean level rise in the 20th century exceeded 10 times that observed during the last 3,000 years. Since the end of the 1950s (when SST changes became frequent), the heat content of the ocean upper layer has been increasing.

Levitus *et al.* (2001) analyzed data on the warming of some components of the climate system during the second half of the 20th century. These data were derived from the growth of the heat content of the atmosphere and ocean as well as from estimates of heat losses as a result of some components of the cryosphere melting. The results led to the conclusion that the heat content of the atmosphere and ocean is growing. The growth of the heat content in the 3 km ocean layer between 1950 and 1990 exceeded (at least, by an order of magnitude) the increase of the heat content in other components of the climate system. The ocean absorbs more than 80% of additional heat received by the climate system. While the observed increase in ocean heat content between 1955 and 1996 reached 18.2×10^{22} Joule, that for the atmosphere constituted only 6.6×10^{21} Joule. The values of latent heat due to water phase transformations were

- 8.1×10^{21} Joule (a decrease of the mass of glaciers on land);
- 3.2×10^{21} Joule (a decrease of the Antarctic sea ice cover extent);
- 1.1×10^{21} Joule (melting of mountain glaciers);
- 4.6×10^{19} Joule (a decrease of the NH snow cover extent); and
- 2.4×10^{19} Joule (melting of the Arctic permafrost).

Observational data were compared (Levitus *et al.*, 2001) with results of numerical modeling using the GFDL interactive model of the atmosphere–ocean system by considering

(1) radiative forcings determined by the observed growth in GHG concentrations, changes in the content of sulfate aerosol in the atmosphere, extra-atmospheric insolation, and volcanic aerosol; and
(2) only GHGs and sulfate aerosol.

The results led to the conclusion that changes observed in the ocean heat content can mainly be explained by the growth in GHG concentrations in the atmosphere, though we should bear in mind the substantial uncertainty in RF estimates due to sulfate aerosol and volcanic eruptions. The latter reduces the reliability of work (Levitus *et al.*, 2001) trying to ascertain anthropogenic warming. Pointing to the strong interannual variability in World Ocean heat content, Levitus *et al.* (2001) emphasized that the extreme heating of the World Ocean during the 1990s was partly connected with multi-decadal warming of the Atlantic and Indian Oceans as well as with two-year oscillations of the Pacific. The changes observed in World Ocean heat content can also be connected with hemispheric or global variability in the atmosphere from sea level up to the stratosphere. Understanding the nature of such

possible connections plays an important role in understanding the mechanisms that govern global climate. Some data on the climate system's heat balance are given in Table 7.3.

As mentioned above, recent attempts to identify the level of atmospheric climate change have been confined to analyses of comparatively long data series on SAT, though smaller volumes of data on changes in sea ice cover extent, vertical temperature profile (radiosonde data), and results of satellite microwave sensing have also been considered (Christy *et al.*, 1998). However, numerical modeling results show

Table 7.3. Comparison of the heat balance of the climate system. From Levitus *et al.* (2001).

Component of the climate system	*Time period of change*	*Observed or estimated change*	*Assumption made in calculation by means of GCM*	*Heat content increase or total heat of fusion*
World Ocean	1955–1996	Observed temperature increase		18.2×10^{22} J
Global atmosphere	1955–1996	Observed temperature increase		6.6×10^{21} J
Decrease in the mass of continental glaciers	1955–1996	—	Assumed 1.8 mm per year increase in sea level	8.1×10^{21} J
Decrease in Antarctic sea ice extent	1950s–1970s	Estimated 311 km reduction in sea ice edge	100% ice coverage of 2 m thickness	3.2×10^{21} J
Mountain glacier decrease	1961–1997	3.7×10^3 km^3 decrease in mountain glacier ice volume	—	1.1×10^{21} J
Decrease in Northern Hemisphere sea ice extent	1978–1996	Areal change based on satellite measurements	100% ice coverage of 2 m thickness	4.6×10^{19} J
Decrease in Arctic perennial sea ice volume	1950s–1990s	40% decrease in sea ice thickness	Thickness of the melted sea ice = 1.3 m	2.4×10^{19} J

Notation: ρ is the density of ice ($\rho = 9.17 \times 10^{11}$ kg $\cdot$ km^{-3}), and λ is latent heat ($\lambda = 3.34 \times 10^5$ J $\cdot$ kg^{-1}).

that data on the annual trend and on the diurnal trend of winter air temperature need to be more representative than SAT.

Since the World Ocean is the most inertial component of the global climate system, analyzing its variability is a top priority, especially as Levitus *et al.* (2001) detected annual increases in the heat content of the upper layer of all oceans over the last 45 years. With this in mind, Barnett *et al.* (2001) compared numerical modeling results of the heat content of the upper 3 km layer of various oceans with observational data. Calculations were made using the "parallel" climate model (PCM) for the atmosphere–ocean system without any flux adjustment. Calculations were made of five versions of the forecast growth in GHG concentration and sulfate aerosol content in the atmosphere.

This comparison showed that calculated anomalies in heat content do not differ from observational values (between 1950 and 1990) by more than 5%, with the exception (for global averaging) of data for the 1970s, when the model does not reproduce the heat content anomaly observed in this decade. On the whole, the probability that these anomalies in heat content are explained only by internal variability of the climate system does not exceed 5%, which implies the anthropogenic nature of climate change.

The nature of the warming of various oceans can be quite different. Intensive vertical mixing and rapid penetration of warming into deep layers are typical of the Atlantic Ocean (especially in its southern sector). In other oceans this process is much slower. An important conclusion from such results is the need for climate models to not only simulate SAT changes—but also those in ocean heat content. Numerical modeling has its weak points, as noted by Barnett *et al.* (2001), so estimating internally induced climate variability completely based on data from numerical modeling is fraught with problems.

The impact of enhanced greenhouse heating on SST in the tropical Pacific can considerably affect global-scale precipitation. Developments in this area based on using results from both observational data and numerical modeling have led to quite different conclusions. Climate warming in recent decades has a spatial structure similar to that of an El Niño–Southern Oscillation (ENSO) event. But since there are no data on such a structure for the whole century, the observed warming is assumed to be a manifestation of multi-decadal natural variability of climate—not the result of greenhouse forcing.

Initial numerical modeling results obtained using interactive models of the atmosphere–ocean system showed that the structure of warming characterized by the zonal SST gradient in the equatorial band should be similar to El Niño, but some theoretical developments suggest similarities between this structure and La Niña. To resolve this controversy, numerical climate modeling was performed (Platt and Austin, 2002) using the CSIRO Mark 2 interactive model developed at the Commonwealth Scientific and Industrial Research Organization of Australia. The results showed formation, first, of a spatial structure of warming similar to La Niña (the strongest warming being observed in extra-tropical latitudes and a weak La Niña-like structure in the tropics). Later on (after the 1960s) this warming is transformed into a structure similar to El Niño (CRC, 2005; Pittick, 2003). Such results

have been obtained using three versions of numerical modeling (apart from the control integration for the 1,000-year period) in which the growth in GHG concentrations in the atmosphere was prescribed from observational data (1880–1990) and according to the scenario IS92a (1990–2100). The climate-forming role of aerosol was not considered (Alcamo *et al.*, 1995; Leggett *et al.*, 1992).

Transformation of the spatial structure of climate warming is determined by warm extra-tropical waters, which move southward and through the sub-tropics reach the tropical belt where upwelling occurs. This is the cause of climate change. These results support the conclusion that the warming (with a spatial structure similar to El Niño) observed during recent decades can at least partially be explained by anthropogenic contributions to the atmospheric greenhouse effect. However, though the structure of observed and calculated warming is similar, observations made before 1950 are less reliable. Moreover, conditions similar to La Niña have recently been observed (in 1995–1996 and in 1998–2000).

La Niña, "sister" of El Niño, also refers to a set of anomalous climate conditions in the tropical Pacific, but with anomalously cool SSTs, strong east-to-west trade winds, exceptionally heavy rains in usually rainy areas near the western Pacific, and very dry weather in usually dry areas near the eastern Pacific. In many ways, the climate anomalies associated with La Niña are opposite to those that characterize El Niño. During La Niña episodes, equatorial SSTs are abnormally cold from the Date Line eastward to the west coast of South America, and tropical rains and convection tend to be focused over the western equatorial Pacific and Indonesia. Over the eastern equatorial Pacific the rains are typically weaker as SSTs remain well below 28°C in this region throughout the episode. This pattern represents an amplification of climatological mean conditions which are characterized by heavy rains across Indonesia and light rains over the eastern equatorial Pacific. This persistent pattern of tropical rainfall contributes to stronger-than-average monsoon systems over Australia/Southern Asia, South and Central America, and Africa. Historically, El Niño and La Niña events have usually alternated with a period of about 2–7 years. However, since the late 1970s, El Niño years have outnumbered La Niña years by a factor of about 2 to 1.

Other climatic parameters. Observational data testify to the following:

- During the 20th century, precipitation intensity increased by 0.5%–1%/10 years over most land regions in NH middle and high latitudes.
- Precipitation intensity decreased by about 0.3%/10 years over most land in sub-tropical latitudes, and quite recently it decreased.
- Changes in precipitation and evaporation over the oceans have led to water freshening in middle and high latitudes and to the growth in ocean salinity in low latitudes.
- Since the 1960s, mid-latitude westerlies have enhanced in both hemispheres.
- Since the 1970s, droughts have intensified over large regions in the tropics and sub-tropics.

- During the last 50 years events have frequently been observed with drastic temperature drops, frequent warm days and nights, and not-so-frequent cold days and nights.
- Since the 1970s, cyclonic activity in the tropics has intensified.

As for the World Ocean, the lack of adequate observational data means reliable trends of precipitation cannot be detected. In recent decades, though, it is likely that intensive and extreme precipitation in NH middle and high latitudes has become more frequent. Since the mid-1970s, ENSO events have been frequent, stable and intensive. This ENSO dynamics was reflected in specific regional variations of precipitation and SAT in most zones of the tropics and sub-tropics. Data on the intensity and frequency of occurrence of tropical and extra-tropical cyclones as well as local storms still remain fragmentary and inadequate and conclusions on any trends cannot be reached (Grigoryev and Kondratyev, 2001a, b).

Concentrations of greenhouse gases and anthropogenic aerosols in the atmosphere. Ever since 1750 the CO_2 concentration in the atmosphere has increased by about one-third reaching the highest level for the last 420,000 years (and, probably, for the last 20 million years), which can be seen from ice core data (IPCC, 2001). The growth of CO_2 concentration by about two-thirds during the last 20 years is explained by emissions to the atmosphere due to fossil fuel burning (deforestation and, to a lesser extent, the cement industry contribute one-third). It is of interest that by the end of 1999, CO_2 emissions in the U.S.A. exceeded the 1990 level by 12%, and if the current rate of increase continues by 2008 this value will likely raise by 10% (Victor, 2001). Meanwhile, according to the Kyoto Protocol, emissions should be reduced by 7% by the year 2008 with regard to the level of 1990, which requires a total reduction of about 25% (which, of course, is just not feasible).

According to available observational data, both the World Ocean and land are global sinks for CO_2. In the ocean, chemical and biological processes are responsible for it, whereas on land it is connected with enhanced so-called "fertilization" of vegetation due to increased concentrations of CO_2 and nitrogen, as well as with changes in land use. On the whole, our understanding of the global carbon cycle leaves much to be desired (Kondratyev and Demirchian, 2000).

There is no doubt that fossil fuel burning will remain the main constituent in CO_2 concentration growth in the 21st century. The role of the biosphere (both of the ocean and land) as a barrier to increased CO_2 will reduce in time. According to IPCC (2001), the probable interval of CO_2 concentration values by the end of the century will constitute 540 ppm–970 ppm (pre-industrial and present values are, respectively, 280 ppm and 367 ppm). Change in land use (Watson *et al.*, 2000; Aspinall and Justice, 2004; IPCC, 2000; Singh *et al.*, 2001) is an important factor of the global carbon cycle, but even if all carbon emitted to the atmosphere due to land use is assimilated by the land biosphere, this will only lead to a decrease in CO_2 concentration between 40 ppm and 70 ppm. As for prognostic estimates of other GHG concentrations by the year 2010, they vary widely. For instance, some estimates predict TO as a GHG might

equal the contribution of methane and be just as important a factor of air quality reduction over most of the Northern Hemisphere.

The concentration of methane in the atmosphere has increased by a factor of 2.5 compared with that observed in 1750, and goes on growing. The global atmospheric concentration of CH_4 has increased from a pre-industrial value of about 715 ppb to 1,732 ppb in the early 1990s, and to 1,774 ppb in 2005 (IPCC, 2007). The annual rate of CH_4 increase has reduced, however, and became more variable in the 1990s than in the 1980s. Ever since 1750, nitrous oxide concentration has increased by 16%. As a result of the Montreal Protocol and subsequent supplements to it, concentrations of several halocarbon compounds (which function like greenhouse and ozone-destroying gases) have either increased more slowly or started decreasing. On the other hand, concentrations of their substitutes and some other synthetic compounds have started growing rapidly (e.g., perfluorocarbons, PFCs, and sulfur hexafluoride, SF_6).

Estimation of RF change, characterized by an enhanced atmospheric greenhouse effect and determined by increases of MGCs well mixed in the atmosphere, gave a total value of $2.42\,W\,m^{-2}$, with the following contributions of various MGCs: CO_2 ($1.46\,W\,m^{-2}$), CH_4 ($0.48\,W\,m^{-2}$), halocarbon compounds ($0.33\,W\,m^{-2}$), N_2O ($0.15\,W\,m^{-2}$). The decrease in total ozone content observed in the last 20 years could lead to a negative RF constituting $-0.15\,W\,m^{-2}$, which may well reach zero in the current century if measures to protect the ozone layer are successful. The increase in tropospheric ozone content by about one-third observed since 1750 could lead to a positive RF reaching $0.33\,W\,m^{-2}$.

Since the IPCC-1996 report, substantial change has been observed in estimates of RF determined not solely by purely scattering sulfate aerosol as traditionally done before, but also by other types of aerosol, especially carbon (soot), an efficient solar radiation absorber, as well as by organic, sea salt, and mineral aerosol (Table 7.4). The strong spatiotemporal variability of aerosol content in the atmosphere and of its properties seriously complicates assessment of the climatic implications of aerosol (Kondratyev, 1999a; Kondratyev *et al.*, 2006a). New results of numerical climate modeling obtained by Hansen *et al.* (2000) radically changed our understanding of the role of various factors in RF formation. According to Hansen *et al.* (2000), climate warming due to the growth of CO_2 concentration and cooling due to anthropogenic emissions of methane (mainly due to changes in rice production) and carbon (absorbing) aerosol cancel each other out.

The change in extra-atmospheric solar radiation is a climate-forming factor that should be considered. The contribution of such a change to RF since 1750 might be as much as 20% compared with the contribution of CO_2. This is mainly explained by enhanced extra-atmospheric insolation in the second half of the 20th century (consideration of the 11-year cycle of insolation is vital here). However, the mechanisms that underly the impact of solar activity on climate are still far from being understood. Nonetheless, IPCC (2007) contains some conclusions and estimates.

- The atmospheric concentration of CO_2 in 2005 exceeded by far the natural range over the last 650,000 years (180 ppm to 300 ppm) as determined from ice cores.

Table 7.4. Global average RF estimates and ranges in 2005 by IPCC (2007).

Character of RF	*RF terms*	*RF values* ($W \cdot m^{-2}$)
Anthropogenic	Long-lived GHG	
	CO_2	1.66 [1.49 to 1.83]
	N_2O	0.16 [0.14 to 0.19]
	CH_4	0.48 [0.43 to 0.53]
	Halocarbons	0.34 [0.31 to 0.37]
	Ozone	
	Stratospheric	−0.05 [−0.15 to 0.05]
	Tropospheric	0.35 [0.25 to 0.65]
	Surface albedo	
	Land use	−0.2 [−0.4 to 0.0]
	Black carbon on snow	0.1 [0.0 to 0.2]
	Total aerosol	
	Direct effect	−0.5 [−0.9 to −0.1]
	Cloud albedo effect	−0.7 [−1.8 to −0.3]
	Linear contrails	0.01 [0.003 to 0.03]
Natural	Solar irradiance	0.12 [0.06 to 0.30]

The annual CO_2 concentration growth rate was 1.9 ppm per year between 1995 and 2005 with year-to-year variability.

- Annual fossil carbon dioxide emissions increased from an average of 6.4 [6.0 to 6.8] GtC per year in the 1990s to 7.2 [6.9 to 7.5] GtC per year in 2000–2005. CO_2 emissions associated with land use change were estimated at 1.6 [0.5 to 2.7] GtC per year over the 1990s.
- The atmospheric concentration of CH_4 in 2005 exceeded by far the natural range of the last 650,000 years (320 ppb to 790 ppb) as determined from ice cores.
- The global atmospheric nitrous oxide concentration increased from a pre-industrial value of about 270 ppb to 319 ppb in 2005. The growth rate has been approximately constant since 1980 and more than 30% of all nitrous oxide emissions are primarily due to agriculture.

7.2.1.3 Results of climate numerical modeling and their reliability

The problem of numerical climate modeling has been thoroughly analyzed in numerous publications (Kondratyev, 1998b, 1999b; Kondratyev and Demirchian, 2000; Soon *et al.*, 2000; Bengtsson, 1999; Houghton, 2001a, b; Schlesinger and Andronova, 2000; Schröder, 2000; McGuffie and Henderson-Sellers, 2001). So, we will confine ourselves to brief comments. Considerable progress has been achieved in developing

more adequate numerical climate models by taking the main components of the atmosphere–hydrosphere–lithosphere–cryosphere–biosphere climate system taken into account. The extreme complexity of climate models and empirical parameterization of the various (especially sub-grid) processes used in them hinders analyzing model adequacy, especially from the viewpoint of their application to predict future climate. As a result of this, attempts undertaken so far to compare the results of numerical climate modeling with observational data have been rather schematic, controversial, and unconvincing.

For instance, conclusions about the secular trend of annual mean global SAT for the last century and a half are unconvincing. If, as the IPCC-1996 Report indicates, there is a good agreement between observed and calculated trends of SAT (with the growth of CO_2 and sulfate aerosol taken into account) then, following Hansen *et al.* (2000), the consideration of methane and carbon aerosol should be more important. Unfortunately, in both cases the conclusions are based on arbitrary opinions, and the agreement with observations is, in fact, no more than an adjustment. Moreover, it is clear that, for a comparison of theory with observations to be thorough, consideration of regional climate changes (not only SAT) and not only averages of climatic parameters—but also their variability characterized by higher order moments.

According to Charlson *et al.* (2001), anthropogenic aerosols strongly affect cloud albedo. Here, estimates of global mean disturbing forcings of clouds are opposite in sign to RF as a result of greenhouse gases; they might be even greater in absolute value.

The parameterization of biospheric dynamics is the Achilles' heel of climate models. In attempts to bring this about, many numerical experiments have been undertaken to assess the effect of deforestation in the Amazon Basin, which have led to the conclusion that the consequence of complete deforestation of this region (tropical rainforest becoming grassland), will be increased evaporation from the Earth surface, decreased precipitation, but surface temperature will rise. The resulting increase of SAT will vary between 0.3°C and 3°C. Such changes are determined mainly by an increase in surface albedo and a decrease in soil moisture. The associated decrease in energy and water vapor fluxes to the atmosphere, reduction of moist convection, and release of latent heat will result in atmospheric heating being reduced, which will produce the following changes to atmospheric circulation:

- Changes in upward and downward air fluxes in the tropics and sub-tropics (known as Hadley circulation cells). The Hadley cell is a circulation pattern that dominates the tropical atmosphere, with air rising near the equator, flowing poleward at 10 km–15 km above the surface, descending in the sub-tropics, and flowing equatorward near the surface. This circulation is intimately related to trade winds, tropical rainbelts, subtropical deserts, and jet streams. Trade winds are a pattern of wind in bands around the Earth's equatorial region. Trade winds prevail in the tropics, blowing from the high-pressure area in the horse[1]

[1] Horse latitudes, or subtropical highs, are subtropic latitudes between 30° and 35°, both north and south.

latitudes toward the low-pressure area around the equator. Trade winds blow predominantly from the northeast in the Northern Hemisphere and from the southeast in the Southern Hemisphere. Jet streams are fast-flowing, relatively narrow air currents observed in the atmosphere at around 11 km (36,000 ft) above the surface of the Earth, just beneath the tropopause. They form at the boundaries of adjacent air masses that have significant differences in temperature, such as where polar air meets warmer air to the south.

- Variations in the conditions of generation of Rossby waves propagating from the tropics to mid-latitudes. Rossby waves, also known as planetary waves as they owe their origin to the shape and rotation of the Earth, are most intriguing natural phenomena. They are easily observed in the atmosphere (i.e., as large-scale meanders of the mid-latitude jet stream), but their existence in the oceans, first theorized by Carl-Gustav Rossby in the 1930s, was only indirectly confirmed before the advent of satellite oceanography.

For a more detailed analysis of the impact of deforestation on atmospheric circulation and climate, Gedney and Valdes (2001) performed numerical experiments to reproduce the present ("control") climate and conditions of complete deforestation of the Amazon Basin. For this purpose, a 19-level spectral model of atmospheric general circulation (MPI ECHAM3 T42 L19) was used (Busch *et al.*, 1998). The ECHAM numerical model was developed from the ECMWF (European Center for Medium Range Weather Forecast) model and contains several changes in order to adjust the model to climate simulations. These changes were carried out in Hamburg at the Max-Planck Institut für Meteorologie, Deutches Klimarechenzentrum, and Meteorologisches Institut der Universität Hamburg. Spherical harmonics with a reference resolution of T42 were used to formulate the model, which is vertically divided into 19 layers. Deforestation should result in the following changes to basic climate-forming parameters: albedo ($13.1\% \rightarrow 17.7\%$); roughness ($2.65\,\text{m} \rightarrow 0.2\,\text{m}$); share of vegetation cover ($0.95 \rightarrow 0.85$); leaf area index ($4.9 \rightarrow 1.9$); minimum resistance of vegetation cover ($150\,\text{s}\cdot\text{m}^{-1} \rightarrow 200\,\text{s}\cdot\text{m}^{-1}$); and root zone depth ($1.5\,\text{m} \rightarrow 1.0\,\text{m}$). All this should lead to a change in soil type. Studing the numerical modeling results reveals a deforestation-induced substantial change of precipitation in winter in the northeastern sector of the Atlantic Ocean, which propagates farther eastward, toward Western Europe. These variations are connected with changes in the large-scale atmospheric general circulation in middle and high latitudes. Application of a simple model to reproduce these variations confirmed their being caused by propagation of planetary waves, and testified to the fact that the results, which reveal a connection between processes in the region of deforestation as well as in the North Atlantic and Western Europe, are independent of the choice of a model, with the level of changes corresponding to estimates of anthropogenic climate change due to the growth of CO_2 and aerosol concentrations.

Zhang *et al.* (2001) undertook a much wider numerical modeling of the climatic consequences of deforestation in the tropics with greenhouse warming increasing as a result of CO_2 doubling, using the CCM1-Oz global climate model developed at the National Center for Atmospheric Research, NCAR (U.S.A.). Calculations demon-

strated a strong decrease in evapotranspiration ($\sim$80 mm yr^{-1}) and precipitation ($\sim$312 mm yr^{-1}) as well as a SAT increase of 3.0 K in the Amazon Basin. Similar but weaker changes are observed in southeastern Asia (precipitation decreases of 172 mm yr^{-1}, and warming increases of 2.1 K). Still weaker changes occur in Africa (precipitation increases of 25 mm yr^{-1}). Analysis of the results of energy balance estimates suggests climate warming takes place not only due to the enhanced greenhouse effect—but also due to decreasing evapotranspiration caused by deforestation. Statistically substantial climate change due to deforestation in the tropics also appear at mid-latitudes.

The IPCC-1996 Report (Khandekar *et al.*, 2005) reached a conclusion, which has caused heated discussion, that the balance of evidence suggests a discernible human influence on global climate, and made a statement that the "anthropogenic signal" stands out against a background of natural climate variability. According to IPCC (2001), detection and ascription studies consistently find evidence for the anthropogenic signal in the climate record of the last 35–50 years. Natural forcings may have contributed to the observed warming in the first half of the 20th century but most of the warming over the last 50 years cannot be explained. The report contains, however, the statement that reconstruction of climate for the last 1,000 years and model estimates of its natural changes testify to a small probability that the climate warming observed in the second half of the 20th century could have been totally natural in origin. But, then, the high uncertainty of the quantitative estimates obtained for anthropogenic warming was emphasized, especially from the viewpoint of contributions of various factors to the warming, especially atmospheric aerosols (IPCC, 2001). The contradictions in these statements and conclusions are so apparent that no comment is necessary. Moreover, IPCC (2007) fails to remove these contradictions, other than by attempts at mitigating them using such words as "likely" and "very likely".

Integral models describing the dynamics of the interaction between socio-economic development and nature should play the leading role in substantiating future climate predictions. However, the reliability of predictions made using such extremely complicated models with inadequate input information raises doubts. For the immediate future, integral models should only serve as a means of obtaining very conditional scenarios. More encouraging are ideas developed by Bartsev *et al.* (2003) and Degermendzhy and Bartsev (2003) where uncertainties in global modeling are overcome using low-sized models.

According to new data for various scenarios of the growth of concentration of GHGs and aerosols, the global mean SAT increase during the period 1990–2100 should be within 1.4°C–5.8°C (IPCC, 2001), whereas according to IPCC-1996, this interval is 1.5°C–3.5°C. The Fourth IPCC Report, which considered various scenarios, gives a broad spectrum of possible temperature changes within the range 1.1°C–2.9°C. Wigley and Raper (2001) believe, with a 90% probability, this SAT interval constitutes 1.7°C–4.9°C. The improvement of models and the increase of their number have not reduced—but expanded—the divergence of this process. It is important that differences in SAT values calculated from various models with similar scenarios of MGC emissions are approximately equal.

As for regional climate predictions, they are still statistically unreliable. Probably, the conclusion that warming in many land areas will be more rapid than global mean warming, especially in high latitudes during the cold half of the year, can be considered reliable. Particularly remarkable was the pre-calculated climate warming in the northern regions of North America, as well as in northern and central Asia, where it exceeds the global mean value by 40%. In contrast, in southern and southeastern Asia in summer and in the south of South America in winter the warming should be weaker than global mean warming. Numerical modeling reveals a future increase in atmospheric water content and intensified precipitation. In particular, an enhancement of precipitation is possible at middle and high latitudes of the Northern Hemisphere, as well as in the Antarctic in winter (this conclusion is of special interest in the context of glacier dynamics). At low latitudes there may be regions where both intensification and attenuation of precipitation will be observed (depending on the choice of MGC emission scenario).

In connection with the great interest in potential extreme events, IPCC (2001, 2007) contain respective prognostic estimates for comparison with present observations (Table 7.5). This was discussed in detail by Grigoryev and Kondratyev (2001c) and Kondratyev (1998b). Vagueness of the tabulated conclusions is explained by scarce observational data and unreliable numerical modeling results.

Calculations of anthropogenic (greenhouse) climate change show that thermohaline circulation (THC) in NH oceans may weaken in the future. However, even the models that show this weakening still demonstrate that greenhouse warming in Europe will persist. So far, no one knows whether irreversible collapse of THC is a possibility or which threshold conditions correspond to such a collapse. No existing model predicts total cessation of THC for the next 60 years.

Numerical modeling of the global warming process shows a further decrease in the snow and sea ice cover extent in the Northern Hemisphere. Glaciers are expected to retreat further (except the ice sheets in Greenland and in the Antarctic, including the western Antarctic) in the 21st century. The prescribed scenarios for the growth of GHG concentrations between 1990 and 2100 expect World Ocean level to rise between 0.14 m and 0.8 m (about 0.47 m on average), which exceeds the rate in the 20th century by a factor of 2–4.

Implications of the anthropogenic impact on global climate are expected to be long term. For example,

- Stabilization of the level of CO_2 in the atmosphere will require considerable reduction in CO_2 emissions to the atmosphere and an even greater reduction in emissions of other GHGs.
- The effect of CO_2 emissions on CO_2 concentrations in the atmosphere is not immediate—but gradual. Even several centuries after cessation of emissions, the share of CO_2 in the atmosphere may well reach 20%–30% with respect to overall emissions.
- The increase in global mean SAT and the rise in World Ocean level (due to thermally induced expansion) is likely to continue for hundreds of years after stabilization of the level of CO_2 because of the huge inertia of the ocean.

Table 7.5. Observed and predicted anomalous changes of weather and climate.

Phenomenon	*Observations (second half of the 19th century*	*Forecast (2050–2100)*
Anomalous maxima of temperature and the number of unusually hot days	Almost all land regions	Such anomalies are revealed by most models
Increased heat index	Many land regions	Such anomalies are revealed by most models
Abnormally intensive precipitation	Many regions in middle and high latitudes of the Northern Hemisphere	Such anomalies are revealed by most models
Abnormally high temperature minima and reduction in the number of cold days	Almost all land regions	Such anomalies are revealed by most models
Decrease in the number of days with frost	Almost all land regions	Possible if the increase in minimum temperatures is taken into account
Decrease in the amplitude of diurnal change of temperature	Many land regions	Almost all models
Summertime dehydration of continents	Some regions	Almost all models
Maximum wind intensification in tropical cyclones	Not observed, but studied cases are few	Some models
Intensification of average and maximum rains in tropical cyclones	Data are insufficient	Some models

- The response of ice sheets to previous climate changes can last for millennia after stabilization. According to model calculations, maintenance of local annual mean warming at the 3°C level for millennia could lead to complete melting of the Greenland ice sheet. At 5°C, the World Ocean level should rise (due to the melting of the Greenland ice sheet) by 3 m in 1,000 years. Present models of ice sheet dynamics in the western Antarctic show that, as in the case of the Greenland ice sheet, its complete melting would result in an increase in ocean level of no more than 3 m in 1,000 years. But, we should keep in mind the inadequacy of studies into possible long-term dynamics of the cryosphere of the western Antarctic.

Conclusions about observed and, even more so, potential climate change in the future are very uncertain. This applies both to the diagnostic data of present climate dynamics and to numerical modeling results. These issues have been studied in detail (Kondratyev, 1992, 1999b; Sun *et al.*, 2001; Watanabe, 2000). According to IPCC (2001, 2007), developments along the following lines should be given top priority:

- putting a halt to further degradation of the network set up to make routine meteorological observations;
- continuing studies in global climate diagnostics to obtain long-term series of observational data at a higher spatiotemporal resolution than has been the case;
- understanding better the interaction between ocean climate system components (including those at deep layers) and the atmosphere;
- understanding better the laws that control long-term variability of climate;
- broadening ensemble approaches to climate modeling, especially in the assessments of probabilities;
- developing a totality (hierarchy) of global and regional models with emphasis on the numerical modeling of regional impacts and extreme changes; and
- developing interactive physico-biological climate models and models of socio-economic development in order to analyze the relationship between the environment and society.

As a second priority the following should be added:

- Studies of the paleoclimate, especially of sudden short-term changes (Kukla, 2000), are important to understand the laws of the present climate and climate prediction.
- The intensive development of spaceborne remote sensing has not provided adequate global information about the climate system, since the functioning of the existing system of space-based and routine observations is far from optimal. Despite considerable efforts and progress in developing the Global Climate Observing System (GCOS), Global Ocean Observing System (GOOS), Global Terrestrial Observing System (GTOS), and (later) the Integrated Global Observing System (IGOS), the problem of optimizing the global observing system remains unsolved. The fact has not been grasped that, apart from accumulating long and homogeneous series of observational data in the interests of the climate system diagnostics, problem-oriented (focused) observation experiments are needed to solve problems such as the global carbon cycle, anthropogenic impacts on stratospheric and tropospheric ozone, dynamics of the processes in the aerosol–clouds–radiation system, biotic regulation of the environment, etc. (Kondratyev, 1992, 1998a; Gorshkov *et al.*, 2000).
- Estimates of the level of anthropogenic impact on global climate contained in IPCC documents are vague. As Reilly *et al.* (2001) justly noted, the reason for this is the absence of quantitative estimates of the uncertainty of the results obtained (e.g., the supposed increase of SAT within 1.5°C–4.5°C). What is worse, trying to make decisions fit with ecological policy (e.g., to the Kyoto Protocol)

is not scientific (Sun *et al.*, 2001). This raises into question the feasibility of forecasts up to 2100, when the impossibility of predicting prospects for global socio-economic development is considered. The answer is clear: only conditional scenarios are possible, it would be inexpedient and even dangerous to take them as the basis for making policy decisions. This is especially true of regional scenarios, which are of actual practical interest—but not of such global averages as the average temperature of a hospital. Though Allen *et al.* (2001) try to justify the absence of quantitative estimates of uncertainties, this logic cannot be accepted. Things came to a head in 1990 when the IPCC was severely pressed to make a statement ascribing observed climate change to anthropogenic forcings; otherwise it would be done by somebody else. The arguments of Wigley and Raper (2001) in support of the conclusions of IPCC (2001) are quite simply unconvincing.

- IPCC (2007), like its predecessors, failed to come up with any new prospects for understanding global climate change. Like the other IPCC reports, it warns—some would say intimidates—the world population about possible negative climate changes. For instance, *The Washington Post* (February 2, 2007) emphasized the following points from the Report:
  (1) "Global warming is 'very likely' caused by man, meaning more than 90 percent certain. That's the strongest expression of certainty to date from the panel."
  (2) "If nothing is done to change current emissions patterns of greenhouse gases, global temperature could increase as much as 22 degrees Fahrenheit by 2100."
  (3) "But if the world does get greenhouse gas emissions under control (something scientists say they hope can be done) the best estimate is about 3 degrees Fahrenheit."
  (4) "Sea levels are projected to rise 7 to 23 inches by the end of the century. Add another 4 to 8 inches if recent surprising melting of polar ice sheets continues."

These conclusions have been widely propagated among the world population who are not in a position to assess them critically. However, climate-warming skeptics, who have knowledge of climatology, have come up with many arguments questioning the anthropogenic character of the warming of land surface that has been observed. One of these arguments is the indisputable difference between this warming and the temperature decrease in the lower atmosphere recorded by satellites during recent decades (Hopkin, 2007).

7.2.1.4 Analysis of existing information

The shortage of reliable estimates of the contribution of anthropogenic factors to formation of today's climate highlights just how difficult it is to understand the dynamical laws of the climate system, let alone evaluation of possible climate changes in future. At the same time, nobody rejects anthropogenically induced enhancement

of the atmospheric greenhouse effect. So, the primitive understanding of global warming as being a general increase of temperature, growing with latitude, is fraught with danger. Analysis of observational data from high latitudes in the Northern Hemisphere (Adamenko and Kondratyev, 1999) showed that such judgments do not match the reality.

To assess the reality of climate predictions, it is critically important to test the adequacy of models by reproducing current observed changes and looking at the paleodynamics of climate from indirect data. When it comes to the question of how current observed data can be used, the situation becomes paradoxical: the experience gained from testing adequacy is confined to the use of average temperatures, while different information and moments of a higher order are what is needed. Goody *et al.* (1998) drew attention to the prospects of using space-derived observations of the spectral distribution of outgoing longwave radiation. Unfortunately, adequate planning of the climate observing system was not discussed. The present paradoxical situation is characterized by a huge number of poorly systematized satellite observations combined with degradation of the routine (*in situ*) observations mentioned above.

It is very difficult to test the adequacy of global climate models by comparing the results of numerical modeling with observational data. Most often, this problem is solved by comparing a long data series on annual mean global SAT. The main conclusion, despite substantial (sometimes radical) differences in the way climate-forming processes are considered, is almost always the same: on the whole, results of calculations agree with observational data. The contribution of anthropogenic factors and, especially, the greenhouse effect (without being able to substantiate it quantitatively) to formation of the climate characterizes—even dominates—such conclusions. Of course, such an approach to verification of the models should not be taken seriously since

(i) Climate models still fall short of what is required regarding interactive account of biospheric processes, aerosol–clouds–radiation interaction, and many other factors.
(ii) The only long-term (100–150 years) series of SAT observations is far from being adequate regarding calculations of annual mean global SAT values.

Recent developments by GCOS, GOOS, GTOS, IGOS are useful, but they still have not come up with the means of optimizing a global observing system. This problem was discussed in detail in Kondratyev (1998b), Kondratyev and Cracknell (1998), and Goody *et al.* (1998, 2001). The problem revolves around the imperfection of climate models, which should serve as the conceptual basis when planning observations and be specified as models are being improved. In this connection, it should be emphasized that what is needed is not illusory statements about global climate models being good enough—but an analysis of *differences* revealing weak points in the models. It is evident that a *totality* of climate parameters should be considered—not only SAT—with emphasis on the models' capability to simulate climate change (including, at the very least, moments of second order).

Paleodata reveal the strongest and sometimes very fast climate changes in the geological past. Alverson *et al.* (2000) noted, for instance, that changes in ocean level, both raised and lowered, had exceeded 100 m at a stable rate of more than 1 m per 1,000 years. Such changes are much greater than anthropogenic changes due to a doubling of CO_2 concentration in the atmosphere, which reflects the groundless misgivings broadcast about anthropogenic climate forcings. The real problem we face consists in analyzing the sensitivity of society and its infrastructures to potential climate changes than to provide detailed future climate predictions. It should be borne in mind that for many countries, including the U.S.A. and Russia, predicted warming is a benefit rather than a danger. In this connection, the value of paleodata as a climate predictor can be higher than that of conditional scenarios obtained on the basis of numerical modeling.

As for climate predictions and KP recommendations to reduce GHG emissions to the atmosphere, well it is clear that climate predictions cannot be interpreted other than as conditional scenarios, and KP recommendations, respectively, should be considered unrealistic. Thus, the sooner the IPCC rejects the ungrounded, unrealistic, and dangerous (for socio-economic development) recommendations contained in the Kyoto Protocol the better. The complete failure of the sixth Conference of the Parties (COP-6) by representatives of the signatory countries to the UNFCCC held in the Hague in November 2000 and of the subsequent meeting in Bonn testifies to the futility of these expensive conferences and to a need for serious scientific discussions on the problem of global climate change, free from domination of adherents of the global warming concept. The reality is that GHG emissions to the atmosphere are still growing (and this process will continue), while discussions on the importance of "flexible market mechanisms" (i.e., emissions trading, etc.) are totally rhetorical.

Not all assessments of the present state of climate theory are optimistic. An extensive discussion on the global warming paradigm was organized at the conference in London on January 27, 2005 at the Hadley Center where various points of view were considered. Some climate scientists insist, unlike others, that human activity and climate change are directly linked. Professor Fred Singer, former director of the U.S. Weather Satellite Service, told the BBC:

> "It's certainly not a cause of alarm. The greenhouse warming from increased gas emissions is, as far as we can tell, insignificant. The IPCC's predictions are based entirely on models, not observations. You must either improve the models or prove the observations are wrong."

In this connection it is appropriate to state that there is no point in contesting that anthropogenic factors impact the environment (we know they do), but estimates of the level of this impact remain still doubtful.

Kerr (2001a, b) believes that information contained in IPCC (2001) substantially diminishes any uncertainties in detecting the "anthropogenic signal" in climate, emphasizes the anthropogenic origin of global climate change, and does not narrow—but broadens—the interval of uncertainties of climate predictions. According to IPCC (2001), most of the warming observed during the last 50 years has been

determined (with a probability between 66% and 90%) by increasing concentrations of GHGs. Such vagueness in formulation, also characteristic of IPCC (2007), is an apparent reflection of the level of uncertainties of numerical climate-modeling results. For instance, as follows from model results obtained by Barnett *et al.* (2001), detection of an anthropogenic signal depends much on our knowledge about heat processes in the top 30 m layer of the World Ocean and on the reliability of prescribed scenarios of future climate change.

Soros (2000) pointed out that CO_2 emissions in the U.S.A. constitute about 16% compared with the 1990 level, 6% in the European Union, about 5% in Japan, and about 24% in Australia. Thus, the 1990s were not characterized by stabilization—but increase—of the level of CO_2 emissions to the atmosphere. Moreover, there are no indications that any serious efforts are being made to reduce emissions (the decrease in CO_2 emissions observed in Germany and the U.K. has nothing to do with KP recommendations). Soros (2000) further pointed out correctly the loss of confidence in KP and the apparent absence of prospects for its final ratification. Nevertheless, Australia has recently signed up to KP.

Tol (2000) justly noted,

> " . . . we should not be mistaken about the statement that the world without fossil fuels would be a paradise. Though renewable sources of energy look attractive on small scales, large-scale perspectives are not clear. For instance, now the limits of hydro-energy and limited possibilities of wind-energy are clear."

All this reflects the truth that it is necessary to find ways for civilization to develop and to substantiate an ecological policy that lives in harmony with the NSS. The solution of this problem will require unprecedented co-operative efforts between experts from the fields of environmental science and social science.

7.2.2 Natural ecodynamics and biogeochemical cycles

The present means of observing natural–anthropogenic processes from space and the use of various ground-based information systems throws up a great deal of information about the state of various NSS components. This information is used by national and international organizations to evaluate the current state of the environment when making decisions on realization of anthropogenic projects and predicting consequences for the environment. Unfortunately, so far, conditions for optimal decision-making have not been formed, since there is no scientifically substantiated co-ordination between environmental changes and the dynamics of anthropogenic processes. Nevertheless, all Earth-observing systems have the aim of getting data on global environmental changes, with emphasis on some subject-oriented problems:

- Evaluation of the distribution of atmospheric carbon sinks into biospheric reservoirs.

- The state of forests, processes of deforestation and afforestation.
- Desertification and changes in the structure of land covers.
- The state of water resources, distribution of freshwater supplies and the state of components of the global water balance.
- Intensity and spatiotemporal characteristics of dangerous natural events.
- SAT variations and climatic trends.
- Change in atmospheric gas composition.
- Interaction between the World Ocean, atmosphere, and land.

This enumeration of the paramount problems facing global ecodynamics in various environmental monitoring programs is interpreted, as a rule, from stereotypical positions regarding global change. However, there is general agreement that the atmosphere–hydrosphere–lithosphere–cryosphere–biosphere (AHLCB) global system is extremely complicated and characterized by numerous feedbacks between its components. Therefore, when collecting data on individual components, it is necessary to take into account their environment, which controls energy fluxes and forms the conditions under which each component of the environment, both natural and anthropogenic, functions.

In most cases, analysis of observational data is reduced to considering three categories of information:

(1) SAT variations during the last century and a half (and especially during the last 20–30 years, when the most significant increase of global mean annual SAT was observed).
(2) Changes in the Earth's cover structure.
(3) Paleoclimatic changes.

The latter attract attention because they can be compared with present climate trends and, to some extent, can be used as analog of possible climate change in the future. Such attempts are ongoing, though the incorrectness of paleo-analogs for prediction of future climate has been substantiated repeatedly and convincingly. Other characteristics of the environment are reduced (somehow or other) to characteristics of climate.

By definition, climate is characterized by estimates of meteorological parameters averaged over a time period of 30 years. For instance, climate anomalies for the 1990s are defined as the deviation from averages for the period 1961–1990. Nevertheless, analysis of the spatiotemporal climate variability for individual years is widely practiced. In particular, the World Meteorological Organization (WMO) publishes annual summaries of global climate (Yan and Torres, 2007).

The 1990s were, on the whole, the warmest decade since meteorological observations began (1860), and 1999 was fifth according to anomalies in global mean annual SAT (+0.33°C) over the period 1860–1999 (the average anomalies of SAT in the Northern and Southern Hemispheres were +0.45°C and +0.2°C, respectively). At the same time, the global mean SAT in October 1999 was 0.2°C below the average for the period 1979–1999. Trends in annual mean temperature anomalies for the globe show

relatively stable temperatures from the beginning of the record through about 1910, with a relatively rapid and steady warming in the early 1940s followed by another period of relatively stable temperatures through the mid-1970s. Then another rapid rise similar to that in the earlier part of the century is observed. The year 1998 was the warmest in the global mean temperature series to date (0.58°C above the 1961–1990 reference period mean) followed by 2005 (0.48°C above). Jones *et al.* (1999) report the 1961–1990 reference period means for the globe, Northern Hemisphere, and Southern Hemisphere as 14.0°C, 14.6°C, and 13.4°C, respectively. Nine of the ten warmest years in the series have now occurred in the 10-year period, 1995–2004. The only year in the last decade not among the warmest is 1996 (replaced in the "warmest list" by 1999). The ten warmest years, in descending order, are 1998, 2005, 2003 and 2002 (tie), 2004, 2001, 1997, 1995, 1999, and 1990. A linear regression model applied to annual anomalies indicates a warming trend of about 0.69°C since the record began in the mid-19th century.

In 1999 a band of maximum annual mean positive SAT anomalies stretched from the North American continent eastward across the Atlantic Ocean and the Eurasian continent toward the equatorial western sector of the Pacific Ocean. Minimum SAT anomalies were observed in a broad band of the central and northeastern region of the Pacific Ocean (including a decrease of SAT). Analysis of the observational data revealed the prevalence of positive temperature anomalies in many regions of the globe. The most vivid anomalous situations include both warming and cooling events (Scafetta *et al.*, 2004). Here are some aspects of temperature variations in 1999:

(1) A cold wave observed in January led to a SAT decrease in Norway, Sweden, and some regions of Russia down to levels not observed since the end of the 19th century.
(2) A temperature decrease in February in Western Europe was followed by particularly heavy snowfall in the Alps.
(3) SAT dropped to values below the norm in Western Australia, though the extreme warming observed in early January led to intensive bush fires.
(4) The March temperature in Iceland reached a minimum for the last 20 years.
(5) In April, heatwaves formed in the northern and central regions of India, and in July and August in the northeastern and mid-western regions of the U.S.A.
(6) Extremely hot and dry weather was observed in the western Pacific, and SAT anomalies in central and northwestern Europe exceeded 5°C.
(7) On the Australian continent the maximum average SAT in November–December was the lowest since 1950.
(8) The second half of the year in central and southern regions of Africa was colder than usual; the Sahel region was more cloudy, cold, and moist than in previous years.
(9) The warming in the U.S.A. through the last 50 years was weaker than over the rest of the globe, with a weak cooling in the eastern part of the U.S.A.

The decrease in land and ocean temperature in the tropics in 1999 was caused by a La Niña event (a cold version of an El Niño), which continued for the whole year.

This year was characterized by destructive meteorological disasters, especially floods. In Australia, the U.S.A., and Asia there were many tropical storms, in Europe heavy snowfall, avalanches, and storms, and again in the U.S.A. droughts and tornados.

Analysis of the observed SAT data suggests that since 1850 there has been an irregular but substantial trend in climate warming over the globe. This trend was very weak from the mid-19th century until 1910, and then it increased to 0.1°C/10 years. Two long-term episodes of cooling were separated by an interval of weak cooling, especially in the Northern Hemisphere. In the periods 1951–1960 until 1981–1990 the sign of the interhemispherical temperature difference changed: the Northern Hemisphere became colder than the Southern Hemisphere.

The present global warming is considered by some specialists to be connected with sudden changes in the Pacific Ocean in about 1976 or with a gradual warming in the tropical Pacific combined with other regional-scale events (Table 7.6). The presence of such patterns has been well established and mainly ascribed to instability in the atmosphere–ocean system in the tropical Pacific. Periodicities of about 4–6 years and 2–3 years have been detected connected with the ENSO event. It is difficult to detect any regularities in decadal and interdecadal variability because of the insufficiently long series of observations. Nevertheless, additional observations of SST variability in the Atlantic Ocean have made it possible to detect the following patterns:

- a gradual increase in SST in both hemispheres in 1910–1940, with its subsequent increase in the Northern Hemisphere until the mid-1950s, but a lower SST in the Southern Hemisphere;
- a cooling in the NH ocean in 1960–1970 with an SST increase in the Southern Hemisphere, which determined a change in sign of the interhemispherical SST contrast in the early 1970s; and
- finally, an SST increase in both hemispheres in the 1980s with a small weakening of this trend in recent years.

The insufficient length of the series of instrumental observations means we cannot interpret such global patterns as a manifestation of a more or less monotonic SST increase or as a part of long-term secular oscillations. Indirect data show oscillations with periods from 65 to 500 years. Possible external factors influencing variability include an increase in CO_2 concentration, change in extra-atmospheric insolation, and volcanic eruptions. A new and surprising result was detection of the fact that one event of large-scale warming and cooling was preceded by a similar SST variability near the southern end of Greenland and (soon after this) in the central Pacific in the Northern Hemisphere. This reflects the important role of high-latitude processes in the northern Atlantic and possible interaction (through the atmosphere) with the Pacific Ocean.

On variability timescales of 7–12 years (approximately decadal) no regular oscillations coherent globally have been detected. In the northern Atlantic, 13 to 15-year and 90-year oscillations have been manifested. Near Cape Hatteras, inter-decadal oscillations have propagated along the Gulf Stream to the northern Atlantic

Table 7.6. Regional temperature change, 1901–1996. From Karl (1998).

Region	*Area of Earth* (%)	*Mean temperature change* (°C)	*Region*	*Area of Earth* (%)	*Mean temperature change* (°C)
Spitzbergen	0.01	+4.06	Alaska/W. Yukon	0.33	−0.12
Canada minus W. Yukon	1.02	+0.96	North Atlantic	1.93	−0.11
Western Europe	1.84	+0.51	Southeast U.S.A.	0.35	−0.37
West Siberia/Russia	2.17	+1.19	Southwest China/Tibet	0.82	−0.44
East Siberia	1.50	+1.30	Nigeria	0.29	−0.43
North Pacific	1.42	+0.90	Bolivia	0.28	−0.46
Japan + environs	1.06	+1.12	Tananarive	0.06	−0.61
Sea Route, N. America–Auckland	1.90	+0.65	Arabian Sea/ Bay of Bengal	3.28	+0.53
Mexico	0.61	+0.72	Tasman Sea	0.52	+0.38
Caribbean	0.62	+0.48	Madagascar + environs	1.03	+0.64
India	0.82	+0.45	South Africa	0.55	+0.76
Middle East	0.80	+0.46	Chile/Argentina	0.87	+0.67
East China	0.50	+0.42	Peru/Ecuador/ Colombia	0.66	+0.69
Southeast Asia	2.03	+0.48	Northeast Atlantic	0.69	+0.64
Southwest Atlantic	1.38	+0.75	New Zealand	0.19	+0.71
Southeast Atlantic	1.23	+0.84	Timbuktu	0.06	+1.38
South Georgia	0.01	+1.91	Middle Atlantic	4.40	+0.44
East Australia	1.44	+0.64	Continental U.S.A.	1.67	+0.41
Capetown to Australia	2.34	+0.92			

where their phases changed (earlier similar results were rather contradictory). In the search for interdecadal ENSO oscillations the data considered did not reveal any substantial maximum of SST variability with periods of more than 10 years either in the Pacific Ocean or over the whole World Ocean, but in the Indian Ocean 20-year oscillations of SST were detected, which turned out to be particularly regular during the first half of the 20th century (similar oscillations were observed earlier).

Analysis of 7 to 8-year oscillations revealed a contrast in their phases in the subtropical and sub-polar cycles of the northern Atlantic. Three prevailing periods have been recorded for interannual variability (2–6 years): 24–30 months, 40 months, and 60–65 months. The first of these periodicities is the well-known quasi-2-year component of ENSO which manifests itself most strongly in the tropics of the western sector of the Pacific, with anomalies (of a constant sign) propagating along the western coast of North and South America (in other oceans this variability is negligibly small).

An important new result is the detection of two distinctly different low-frequency modes of oscillation having a general physical nature and characterized by a rather abrupt change of periodicity in the 1960s from about 5 years to almost 4 years. This totality of observational data suggests that the ENSO irregularity occurs due to the interaction with annual change of the internal instability of the atmosphere–ocean system in the tropics of the Pacific. Since the mode of quasi-2-year oscillations is also observed in other oceans, but does not correlate with the index of southern oscillations in the tropical Pacific, the conclusion suggests itself that the stronger quasi-4-year signal that forms here can have an effect beyond the Pacific, whereas the opposite process is practically impossible.

A weak oscillation with periods of about 28–30 months is observed in the SST field in the SH Atlantic Ocean and agrees with the previously detected "Erminito" event which is possibly an analog of El Niño. Analysis of the data of SST satellite observations since 1982 revealed warming over most of the tropics and in the NH mid-latitudes with a global mean trend of $\pm 0.005^{\circ}$C/yr. On the whole, during the last 50 years of the 20th century (1948–1998) there was substantial warming of the World Ocean. The upper 300 m layer was heated most (by 0.31°C, on average), whereas the increase in temperature of the 3 km layer constituted 0.06°C. This increase of the ocean's upper-layer temperature took place before the SAT increase started in 1970.

Data on the change of global mean temperature for the last five centuries has shown that global warming constituted about 1.0 K. It was only in the 20th century, which turned out to be the warmest, that the increase in continental surface temperature reached 0.5 K (about 80% of climate warming occurred in the 19th and 20th centuries). In the last five centuries warming was stronger in the Northern Hemisphere (1.1 K) than in the Southern Hemisphere (0.8 K). On the whole, the results agree with conclusions from data on tree rings, though the latter reveal a somewhat weaker secular trend of SAT, which can be explained by specific features of dendroclimatic methods. Paleo-information on SAT is mainly based on oxygen isotope data from Greenland and Antarctic ice cores and temperature measured in deep drill holes.

Satellite data on sea ice cover extent are important as an indicator of global climate dynamics. Numerous studies revealed a statistically substantial decrease in the global area of sea ice constituting $(-0.01 \pm 0.003) \times 10^6$ km^2/10 years. Satellite data on changes in the Greenland glacier mass balance can also serve as an indicator of climate dynamics. Results of laser altimetry for northern Greenland for the period 1994–1999 show that at altitudes above 2 km the ice sheet is, on the whole, in a state of balance, with local changes of different signs. A decrease in glacier thickness prevailed at low altitudes, exceeding 1 m yr^{-1}, enough to raise the level of the World Ocean by 0.13 mm yr^{-1} (this is equivalent to ~7% of the observed rise in ocean level).

The Arctic region as a whole plays a key role in observations of environmental change. The Arctic includes the Arctic Ocean (which overlies the North Pole) and parts of Canada, Greenland (a territory of Denmark), Russia, the United States (Alaska), Iceland, Norway, Sweden, and Finland. Several international programs have recently started to study the role played by the Arctic region in observed environmental changes in other regions of the globe. Among them is the SEARCH (Study of Environmental Arctic Change) project, which is an inter-agency effort to understand the nature, extent, and future development of system-scale change presently seen in the Arctic. Other programs include the

- International Arctic Polynya Program (IAPP), which was designed in 1990 to determine the physical, chemical, and biological role of polynyas in the Arctic. Three polynyas were selected for investigation and intercomparison: the North East Water (NEW) polynya (which lies northeast of Greenland), the North Water (NOW) polynya which forms at the north end of Baffin Bay, and the St. Lawrence Island Polynya (SLIP) in the northeastern Pacific.
- Canadian Arctic Shelf Ecosystem Study (CASES), which is an international effort under Canadian leadership to understand the biogeochemical and ecological consequences of sea ice variability and change on the Mackenzie Shelf in the Beaufort Sea (Arctic Ocean).
- International Arctic Ozone Study, which runs campaigns in winter every year. NASA researchers and many scientists from the U.S.A., the E.U., Canada, Iceland, Japan, Norway, Poland, Russia, and Switzerland work together in winter to measure ozone and other atmospheric gases. The scientists use aircraft, large and small balloons, ground-based instruments, and satellites.
- International Study of Arctic Change (ISAC), which is designed as a long-term international, interdisciplinary, pan-Arctic program to document changes in the Arctic. The objectives of ISAC are to take a system approach to facilitate expansion and to extend our knowledge of the Arctic system as well as to document changes in the Arctic with respect to spatiotemporal patterns.
- International Arctic Buoy Program (IABP), which is aimed at maintaining a network of drifting buoys in the Arctic Ocean to provide meteorological and oceanographic data for real-time operational requirements and research purposes including support to the World Climate Research Program (WCRP) and the World Weather Watch (WWW) program.

The main goals of these programs are resolution of two problems.

(i) Assessment and synthesis of knowledge about how climate and UV radiation have changed in the Arctic, their prediction for the future, as well as probable impacts of these changes on ecodynamics in other latitudes; human health; and social, cultural, and economic systems.
(ii) Provision of useful information and recommendations for governments, organizations, and Joe Public in order to assist decision-making in response to the consequences of climate change.

The present warming in the Arctic and concomitant increased temperatures results in ice melting, decrease in its thickness and extent, permafrost melting, and sea level rise. In the last 30 years there has been a 10% decrease in sea ice extent in the Arctic, and the rate of this decrease in the last 20 years was 20% higher than for the entire 30 years. The amount of Arctic land ice is 3.1 million km^2, which is equivalent to an 8 m rise in sea level (were it to melt). The rate at which Greenland ice has melted in the last 20 years is 0.7%/year, and for the period 1979–2004 it is estimated at 15.9%. The ice of the Arctic and Antarctic is a powerful stabilizing factor, since with all ice supplies taken into account ($\sim 28 \times 10^6$ km^2), serious climate change can only occur on a timescale of centuries. For instance, even with a rise in Arctic temperature of 3°C the whole ice sheet of Greenland would take 1,000 years to melt. On the whole, ice supplies on the planet and climate are interactive components of global ecodynamics.

Recently close attention has been given to assessment of climate in Siberia and the Far East as regions adjacent to the Arctic. Here a 0.5°–0.9°C increase of temperature in the last decade was observed, the trends of average temperatures increasing from north to south. Precipitation was redistributed, with an increase in winter and a negligible decrease in some regions in summer. For instance, in the Amur River basin over the last 30 years precipitation in the cold period of the year increased by 35%, and annual precipitation increased by 12.3%.

Water is a key component of ecosystems. Observations of moisture cycle parameters have shown a considerable increase in precipitation rate since 1950. In the last 30 years there was a considerable increase of the number of days with intensive precipitation. The present state of global water resources is characterized by the following factors:

- The global volume of water constitutes ~1.4 billion km^3.
- The volume of freshwater resources is ~35 million km^3, or 2.5% of total water volume.
- Of these freshwater resources about 24 million km^3 or 68.9% are in the form of ice or persistent snow cover in mountains, the Antarctic, and the Arctic.
- About 8 million km^3 or 30.8% are under ground in the form of ground water (in shallow and deep basins at depths of 2,000 m), soil moisture, marsh water, and permafrost.

- Freshwater lakes and rivers contain ~105,000 km^3 or 0.3% of global freshwater supplies.
- The total volume of freshwater supplies used by ecosystems and people constitutes ~200,000 km^3 (i.e., less than 1% of total freshwater supplies).
- The annual draw-off of ground water is estimated at 600 km^3–700 km^3 or about 20% of global water draw-off. About 1.5 billion people use ground water as drinking water.
- According to estimates for 2000, agriculture takes up 70% of the global expenditure of freshwater.
- Per capita use of water in developed countries is about 10 times greater than in developing countries. In developed countries this estimate varies between 500 L/da and 800 L/da, and in developing countries from 60 L/da to 150 L/da.
- Industry uses about 20% of global freshwater draw-off. From 57% to 69% of global water draw-off is used in power generation at hydroelectric power stations and nuclear stations, 30%–40% in industrial processes, and 0.5%–3% in thermal energy.

These along with other data about various parameters of the environment cannot be considered sufficiently complete to resolve the many problems of global ecodynamics studies, since they were not gathered with solution of these problems in mind. The natural anomalies observed in the last decade characterized by fewer cold periods, intensified wind speed in tropical cyclones, and other abrupt deviations from average trends of temperature and precipitation, cannot be formally explained. The reason is that available data are either superfluous regionally or inadequate globally.

A good example of the lack of co-ordination of information at both regional and global levels manifests itself in the evaluation of vegetation cover dynamics. Indeed, one of the principal aspects of global ecodynamics consists in assessing the response of vegetation communities to climate change. Unfortunately, we do not know whether reversibility between climate change and vegetation exists stably, though in fact it is observed in some regions. For instance, the northeast of Brazil is characterized by a semi-desert climate. The dry season lasts for 8 months and prevents moist tropical forests from developing (they cannot survive without rain for longer than 4 months). This threshold is, in a sense, the controlling factor of relationships between climate and vegetation in a given region. On the whole, primary production is known to react to climate changes. For instance, coniferous forests in the southeast of the U.S.A. are characterized by a 5-day variability in primary production of 0.55 $gC\,m^{-2}\,da^{-1}$. This variability for conifers decreases in northern latitudes. In contrast, for broad-leaved forests, their sensitivity to climate change grows from south to north.

International programs on environmental studies pay special attention to tropical forests, which are found in more than 70 countries. These forests support 50% to 90% of all species of animals and plants. They are directly linked with the

livelihoods of more than half a billion people. Tropical forests are prime candidates for intensive transformation into other types of Earth cover. For instance, in Cameroon between 1991 and 2001 tropical forests were being transformed into palm oil plantations at a rate of 342.8 ha/yr. Of special concern are the Amazon and Russia's forests, the rate of deforestation of the latter being practically unknown. At the International Conference on Land-Cover and Land-Use Change Processes in the North-East Asia Region (NEAR, February 2–5, 2005, held in Harbin) it was noted that in the Far East (about 36% of which is Russian) the state of forestry with respect to 1990 has improved (Qi and Gutman, 2005). The forest area increased as a result of abrupt reduction of cultivated territories. However, on the whole, forest preservation throughout Russia remains inadequately studied.

With the evaluation of global ecodynamics by means of observations in mind, interest has recently increased in studies of global processes in the atmosphere and the World Ocean. One effective indicator of their state is the level of pollution. Atmospheric transparency determines the direction and intensity of heat fluxes, and the ocean's surface purity regulates the exchange of gas and heat with the atmosphere. Suffice it to say that the albedo of the atmosphere–ocean system can change sign several times depending on pollution of this media. In nature, the processes involved in degassing the planet are known to regulate this albedo variability. Human interference leads to destabilization of the natural equilibrium, though huge reserves of energy and biomass in the World Ocean (directly or through feedbacks) guarantee a high level of stability, and up to the present the processes of self-purification have resisted all anthropogenic impacts. Unfortunately, we do not know the limits of the World Ocean to self-purification.

The interdependency of environmental processes is diverse and has been experimentally studied spatiotemporally, though only a small fraction of processes have been studied. Analysis of satellite data shows that in recent years natural processes have changed substantially due to urbanization. Indeed, cities are one of the most important and vivid phenomena of civilization. From 1970 to 2004, the size of world urban population increased from 35% to 50.1%. The contribution of developing countries to this increase was about 90%. On the whole, the level of urbanization in the early 21st century was: North America 77.2%, Latin America 75.3%, Europe 74.8%, Oceania and Australia 70.2%, Africa 37.9%, and Asia 36.7%. In 2004, 3.3 billion people lived in cities.

In urban areas the pattern of distribution of aerosol forcing on climate changes drastically, and due to the high concentration of aerosol the process of cloud formation changes, which breaks natural levels in the atmosphere–surface system's albedo.

Thus, the wealth of knowledge about the dynamics of the environment suggests the conclusion that the observed trend should be a cause of anxiety for people. Present global changes differ from similar changes in the past by the presence of anthropogenic noise, whose impact manifests itself mainly with negative consequences for nature. It was with this in mind that in 2003 preparation of the 10-year Strategic Plan of the U.S. Climate Change Science Program was completed.

The program has five major goals:

(1) Using current knowledge of the present and past climate and environment, including natural variability, to improve our understanding of the causes of observed climate change.
(2) Obtaining more reliable quantitative estimates of the factors that determine changes in the Earth's climate and the systems concerned.
(3) Reducing the level of uncertainty of prognostic estimates of future changes in climate and the systems concerned.
(4) Getting a better understanding of the sensitivity and malleability of natural and regulated ecosystems as well as anthropogenic systems to climate and global change in general.
(5) Analyzing the possibilities of using and recognizing the limits of improving knowledge on risk control in the context of the problem of climate change.

Realization of these goals will require revision of the environmental monitoring strategy and creation of new systems to observe natural and anthropogenic processes. The present science in the field of the global ecodynamics still lacks the necessary technologies to reach the goals mentioned above. A promising first step of the international community in this direction is the signing by 60 countries of the agreement on combining national Earth-observing systems into a single global information network (GEO, 2005).

7.3 GLOBAL CLIMATE CHANGE STUDIES

7.3.1 Regional climate and its prediction

As mentioned above, the dominating anthropogenic concept of global climate change is based on information about the secular change in annual mean global SAT calculated from the ground-based network of meteorological stations and ship observations of water temperature in the upper layer of the World Ocean as well as numerical modeling of SAT variations during the last century and a half. Meanwhile, there is little doubt that global mean SAT needs further analysis, as SAT values calculated from observational data are not only riddled with errors that cannot be estimated reliably, they are also just not representative enough. On the other hand, it is apparent that forming a reliable idea of the pattern of climate variability can only be obtained by considering 3-D fields of air temperature and other climatic parameters (i.e., by analyzing regional-scale variability of climate).

Information on regional climate change is both diverse and voluminous. We will confine ourselves to a few of the most typical illustrations based mainly on the report prepared by National Climatic Data Center (NCDC) (Levinson and Waple, 2004), which characterizes specific features of climate in various regions of the globe in 2003 against a background of long-term climatic variability.

One of the important features of climate formation not only at the regional but also at the global scale consists in its considerable variability caused by the internal dynamics of the climate system. One of the most substantial factors of internal dynamics is the ENSO event. Warming as a result of ENSO began in October–November 2002 and ended in March–April 2003. However, despite ENSO ending in the boreal spring, ENSO-induced warming brought about regional anomalies of precipitation over a vast region of the Pacific, including formation of a zone of abnormal moistening along the western coast of South America and a moisture deficit zone in the eastern part of Australia and in the southwestern sector of the Pacific Ocean. The global mean SAT in 2003 turned out to be close to the three maximum values observed since 1880, but below the record SAT level in 1998.

The global mean SAT in 2003 exceeded the average for 1961–1990 by 0.46°C. According to data from satellite thermal sensing, the global mean temperature of the middle troposphere in 2003 was one-third that of average warming for 1979–1998.

The hurricane season in 2003 was extremely active in the basin of the Atlantic Ocean with sixteen tropical storms, seven hurricanes, and three super-hurricanes. Five of these tropical cyclones led to landslides in the northeast of Mexico. In 2003, destructive hurricanes devastated New Scotland and Bermuda. The formation of five tropical storms in the Gulf of Mexico turned out to be a specific feature of a region in the Atlantic Ocean. Three tropical storms formed outside the usual time interval (June–November), one formed in April, and two in December. In the eastern sector of the Pacific Ocean in the Northern Hemisphere, the activity of storm formation was below usual (there were no large-scale storms here at all).

The summer of 2003 witnessed in some regions of Western Europe one of the warmest summer seasons with heatwaves affecting mainly central and Western Europe. Two anomalous heatwaves in June and July–August (particularly the second one) were especially powerful. The accompanying droughts led to forest fires, which covered considerable areas in the south of France and in Portugal in July and August. The 2003 summer in Western Europe was, apparently, the hottest since 1840. The heatwave in France killed more than 11,000 people (Pirard *et al.*, 2005). In Germany the summer of 2003 was the hottest in the 20th century and (except for some regions of northern and northwestern Germany) the warmest since instrumental observations began).

The most anomalous situations occurring in March 2003 include

- Record-breaking intensive precipitation in the middle Atlantic, and in the southeast and along the eastern coast of the U.S.A.
- Record-breaking low SAT and unusual snowfall over the European territory of Russia.
- An unprecedented 546 tornados in May in the U.S.A.
- A long-term drought in the west of the U.S.A., where in some regions it was the fourth or fifth year experiencing a lack of precipitation.
- Heavy bush fires in the eastern part of Australia in January and powerful forest fires in the south of California in October.
- Abnormally intensive precipitation in western Africa and in the Sahel.

- A return to the normal level of precipitation in India in the summer monsoon.
- Close to a record-breaking extent of the ozone hole in the Antarctic, reaching a maximum (28.2 million km^2) in September 2003.

The world is warming, but that does not mean it will get hotter everywhere. As a result of climate change, some places are expected to get colder, others wetter or drier. Warmer-than-average conditions occurred throughout most land areas of the world in 2005. The largest anomalies were widespread throughout high-latitude regions of the Northern Hemisphere, which include much of Russia, Scandinavia, Canada, and Alaska. Temperatures in these regions were 3°C–5°C (5.4°F–9.0°F) above the 1961–1990 average. There were no vast areas of negative anomalies. Notable temperature extremes in 2005 include a severe heatwave that enveloped the southwestern U.S.A in early to mid-July. Maximum temperatures above 40°C (104°F) affected parts of Nevada, California, Arizona, and southern Utah. Numerous temperature records were set around the region. Las Vegas, NV, tied their all-time record-breaking high temperature of 47.2°C (117°F) on the 19th, equalling the old record set on July 24, 1942. Death Valley witnessed seven consecutive days (July 14–20) with temperatures equal to or above 51.7°C (125°F). Across Australia, exceptionally warm and dry weather prevailed during March–May 2005. The Australian mean temperature during March–May was 1.62°C (2.92°F) above the long-term average, which is the warmest on record.

Recent years have been marked by growing interest in the study of climate change in NH and SH high latitudes, which was determined, to a considerable extent, by the decision to designate 2007–2008 the Third International Polar Year. Basic conclusions regarding the diagnostics of the Arctic climate stem from analysis of the spatiotemporal variability of polar climate. Of great interest here are new results from paleoclimatic analysis of an ice core from the Vostok Station (Kondratyev, 2004a), which demonstrated the presence of a negative correlation between changes in CO_2 concentration in the atmosphere and air temperature. Paleoclimatic developments are increasingly being used to understand the laws of climate dynamics.

The data on the Antarctic discussed in Levinson and Waple (2004) showed that the last decade in this region was abnormally cold. From the end of the 1970s to mid-winter of 1990 the sea ice cover extent around the Antarctic continent was growing.

For an informative analysis of the regional features of climate we can recommend Filatov (2004), dedicated to studies of the climate of Karelia. An important contribution to studies of regional climate changes has been made by observations of the climate of cities and by analysis of individual long series of meteorological observations. A new important step in understanding the data of empirical diagnostics of climate involves both development and application of interactive models of the climate system as well as an ensemble approach to numerical climate modeling.

7.3.2 Global water balance and sustainable development

Of course, the water cycle is critically important not only in the context of climate change studies but also (to a greater extent) as the principal means of life support on

Earth. Owing to respective feedbacks the water cycle functions as an integrator of the various processes taking place in the nature–society system. The following questions spring to mind:

- What mechanisms and processes are responsible for the formation and variability of water cycles and to what extent are they affected anthropogenically?
- In what way is the control of interactions between the global water cycle and other cycles (carbon, energy, etc.) accomplished by feedback processes and how do these processes change over time?
- What are the uncertainties in predicting annual change and interannual variability as well as in making long-term projections of various parameters (components) of the water cycle and what are the possibilities of reducing the levels of these uncertainties?
- What are the consequences of water cycle variability on various spatiotemporal scales for human activity and ecosystems, how can this variability influence the Earth's system, thus affecting the transport of deposits and biogenes and affecting biogeochemical cycles?
- What are the possibilities of using information about the global carbon cycle in decision-making in the field of ecological policy with regard to water resources?

Improvements in methods of calculating shortwave (SW) and longwave (LW) radiation fluxes have favored the much more reliable calculation of radiation fluxes and RF. However, the problem of the influence of cloud cover dynamics is far from being resolved. An important development in 1990 led to the discovery of systematic underestimation in earlier calculated values of cloud-absorbed solar radiation by about 40%, which naturally told on the reliability of numerical climate modeling results in the context of cloud feedback functioning. Reliability can be raised using the results of numerical modeling of climatic implications of clouds with processes of different scales taken into account, including direct reproduction of cloud cover dynamics, especially the powerful convective cloudiness in the tropics. Use of modern MMF models has given promising results and provided a sufficiently adequate reproduction of the diurnal trend of precipitation. Considerable progress has been achieved resulting in a decrease in uncertainty level from 25% and more to less than 3%, especially by using such remote-sensing means as microwave radiometers (Chukhlantsev, 2006).

In January 2003, ICESat was launched to obtain information about ice cover, clouds, and land surface topography (Zwally *et al.*, 2005). ICESat carries the Geoscience Laser Altimeter System to measure changes in the thickness of ice sheets in Antarctica and Greenland, which cover 10% of the Earth's land area and contain 77% of the Earth's freshwater. ICESat measures the elevations of clouds and land while traveling at 17,000 mph from pole to pole and circling the Earth once every 100 minutes. ICESat also gauges the vertical structure of clouds and aerosols in the atmosphere, maps the topography of land surfaces, and measures the roughness, reflectivity, vegetation heights, snow cover, and sea ice surface characteristics. The data from this satellite, covering both polar regions, provide information about land surface topography and vegetation cover, ice sheet dynamics, and characteristics of

the water cycle, aerosol, and clouds. Together with data from Terra and Aqua, much more comprehensive information will be obtained about the Greenland ice sheet and interannual variations of the sea ice cover in the Arctic. The data from Aqua give a higher spatial resolution and more diverse multi-spectral information than have been obtained earlier. Satellite data supplement the results of aircraft observations.

GRACE was successfully launched in March 2002 to monitor climate and the Earth's gravity field and has opened up possibilities to obtain global-scale information about the spatiotemporal variability of gravity determined by non-uniform distribution of masses in the Earth's crust. These data make it possible, in particular, to study the gravity field variability caused by factors like variations of both surface and deep sea currents, river run-off, and ground water, as well as water exchange between ice sheets, glaciers, and oceans. Analysis of GRACE data will enable us to monitor variations of the extent and volume of water contained in inland water basins (large water reservoirs, lakes, and ground water) as well as changes in the drifting of warm water zones in the Pacific Ocean (El Niño) and in the dynamics of tectonic plates. Reproduction of GRACE data by numerical modeling of temporal variations of the Mississippi River basin water balance was successful. The remote sensing of water supplies open up prospects for monitoring the dynamics of regional water balances and, respectively, obtaining (on national and international scales) ideas on how best to regulate water resources.

Studies demonstrating the presence of close bonds between the water and carbon cycles and climate have become especially urgent. For instance, it has been shown that about 60% of carbon land supplies in North America might be connected with precipitation intensification over the North American continent, though it was supposed earlier that the main role was played by the joint impact of SAT increase and "fertilization" due to the growth of CO_2 concentration in the atmosphere. New studies of chemical airing (see below for definition) by considering such factors as precipitation, river run-off, and water alkalinity have led to the conclusion that the loss (export) of carbon (from alkalinity data) increases with growing river run-off and precipitation in the basin of Mississippi River. Chemical airing is the process that transforms CO_2 into dissolved bicarbonate and carbonate, which are then transported by river run-off into the ocean. River-induced transport of alkaline waters from land to the ocean turns out to be the main source of seawater alkalinity and thus a mechanism for regulation of the level of carbonate concentration in the oceans. It can be of great importance in formation of the global carbon cycle and functioning of the World Ocean as a zone of carbon sink.

Interesting results have been obtained from studies of the spate of forest fires occurring in 1997–1998 due to a drought caused by El Niño. According to observational data and numerical modeling results, carbon emissions to the atmosphere due to forest fires have increased by 2.1 ± 0.8 PgC, which constitutes $66 \pm 24\%$ with respect to the observed anomalous increase of CO_2 concentration. On the whole, these results have demonstrated that the interannual temporal variability and intensity of water and energy cycles is one of the most important factors in carbon cycle formation. For instance, persistent forest fires in a region that has been a sink for a long time can suddenly make that region a source of carbon.

The study of energy and water cycles carried out within the GEWEX program with regard to the carbon cycle was an important step forward. For example, analysis of data for the Mississippi River basin into the closedness of cycles has shown that cycles can be balanced within the error $\sim+15\%$. Meteorological studies into the causes of precipitation in warm seasons in the southwest of the U.S.A. have shown that monsoons play a substantial role.

The most important developments in the field of water resource study are

- Accumulation of an integral hydrological database.
- Substantiation of an integral strategy for the global observing system with emphasis on the water cycle. Accordingly, the field observation experiment CEOP was set up to carry out frequent observations.
- Preparation and application of new spaceborne remote-sensing equipment to measure the water content in the troposphere and lower stratosphere. For example, the Microwave Limb Sounder (MLS) carried by the Aura satellite launched in 2004.
- The retrospective analysis of all available observational data (especially from satellites) on the known parameters of water and energy cycles (with priority given to long-term global data on precipitation).
- Re-analysis of regional data on climate dynamics for the period 1979–2003.
- Launchings of satellites CloudSat (Stephens *et al.*, 2002) and CALIPSO (Vaughan *et al.*, 2004) to obtain data on aerosol and cloud cover characteristics. CloudSat was a joint initiative between the U.S.A. and Canada, and CALIPSO between the U.S.A. and France.
- Global monitoring of precipitation using the GPM satellite with a complex of instruments to substitute those carried by TRMM and SSM/I.
- Cloud climatic feedback (with emphasis on convective clouds in the tropics).
- The impact of changes in temperature and hydrological characteristics on concentrations of pollutants and pathogens in the atmosphere near the Earth surface and in ground waters. The principal motivation here was the urgency of checking drinking water quality.
- The monitoring of soil moisture as part of a study into drought.
- Prediction of climate in the interests of solving problems about water resource control.

CALIPSO combines an active lidar instrument with passive infrared and visible imagers to probe the vertical structure and properties of thin clouds and aerosols over the globe. CALIPSO was launched on April 28, 2006 with the cloud-profiling radar system on the CloudSat satellite. The CALIPSO-CloudSat Validation Experiment (CC-Vex) was conducted over the southeastern U.S.A. and adjacent waters from July 26 to August 14, 2006. Two aircraft, based at Robins AFB in the middle of Georgia, were involved in the experiment: the NASA ER-2 carrying a cloud radar (CRS), lidar (CPL), and MODIS airborne simulator (MAS), and the Weather Modification Inc. (WMI) Learjet carrying various cloud probes for *in situ* sampling. A third aircraft, the NASA King Air B200, carrying a high-spectral-resolution lidar (HSRL) was

based at NASA Langley Research Center in Virginia. A total of 12 flights were conducted during CloudSat/CALIPSO satellite overpasses, including 4 night flights, observing a variety of thin and thick cirrus, mid-level clouds, precipitating clouds, and aerosols.

GPM is an international co-operative constellation of precipitation-measuring satellites designed to measure the global 4-D variability of rainfall, latent heating, and the microphysics of variability. This information will be used to improve the prediction of climate change, weather, freshwater resources, and severe storms.

GPM will answer the following questions posed by NASA's Earth Science Enterprise major category of "How Does Precipitation Impact Our Changing Earth?":

- How are global precipitation, evaporation, and cycling of water changing?
- What are the effects of clouds and surface hydrological processes on Earth's climate?
- How are variations in local weather, precipitation, and water resources related to global climate variation?
- How can weather forecast duration and reliability be improved by new space-based observations, data assimilation, and modeling?
- How well can transient climate variations be understood and predicted?
- How well can long-term climatic trends be assessed or predicted?

7.3.3 Globalization of land use strategies

Since land surface processes are one of the main yet inadequately studied climate-forming factors, the following strategic questions have been posed (CCSP, 2004):

- What means and methods are needed to find more reliable characteristics of both past and present changes in land surface?
- What are the main factors of the dynamics of land use and processes on land surface?
- What will land use and land covers be in 5–50 years?
- In what way does climate variability affect land use and the characteristics of land surface and what are the feedbacks between land surface processes and climate processes?
- What are the possible consequences of the impact of land surface changes on the environment, socio-economic development, and human health?

Key developments are along the following lines:

(i) *Projections for land use and land surface changes*. These projections take into account, in particular, changes due to deforestation as a result of growing population size. According to available estimates, more than 70 million acres of forested territories and agricultural soils in the U.S.A. will be transformed (mainly into urban regions) in the period to 2025. On the other hand, there is the possibility of transforming agricultural and other soils into forested territories. This illustrates the complexity of carbon budget dynamics and the difficulty of

creating a new NLCD database to characterize the present state of land surface (mainly from satellite data).

(ii) *Land use in the Amazon*. Special attention to the ecodynamics of this region has been determined by location here of swaths of felled tropical forest. A U.N. program is planned to evaluate global tropical forest dynamics using space-derived information.

Developments in the near future will be along the following lines:

- assessment of agricultural soils on a global scale;
- preparation of a new (more detailed) map of forest biomass resources for the whole territory of Russia from Landsat data (at a spectral resolution of 500 m) and Terra data (250 m) combined with the results of a land inventory, which will make it possible to reliably assess the role of Russian forests as a carbon reservoir;
- accumulation of a database on changes in Alaska's land surface in 1950–2001 (averaged over the year using satellite data at a resolution of 1 km) to characterize its succession;
- projection of land use changes and their effect on forests;
- complex studies of regional climate with emphasis on the land surface processes connected with changes in hydrological conditions in the southeast of the U.S.A. and subsequent evolution of such developments under tropical conditions;
- impacts of urbanization on ecosystem dynamics in semi-arid regions of the U.S.A., bearing in mind the need to find a solution to the problems of water resources and carbon budget.

A climate-induced increase in land ecosystem productivity can be observed. Analysis of data on climate for the period 1982–1999 and results of the satellite remote sensing of net primary production (NPP) during the same period revealed a global mean increase in primary production on land of 6.3% (or by 3.4 PgC) with a considerable spatial non-uniformity manifested as a considerable increase of NPP over 25% of the territory and a substantial decrease in productive land of 7%. The contribution to NPP growth of 80% is due to ecosystems in tropical regions and in high latitudes of the Northern Hemisphere. Apparently, an increase of NPP in the tropics is connected with a decrease of cloud amount, which intensifies incoming solar radiation, and in other regions with the complex impact of SAT changes, precipitation, and solar radiation.

Analysis of data on the carbon budget within the WCRP studies of GHG removal from the atmosphere in national parks in 13 states of the U.S.A. yielded interesting results (Kondratyev and Krapivin, 2005). According to these data, in these parks the amount of carbon accumulated in the top 20 cm layer of soil constituted $\sim$910 kg ha^{-1} yr^{-1}. Hence, over the whole territory of the program (5.6 million ha) the atmosphere was loosing annually 5.1 million tC.

7.3.4 Global carbon cycle as an indicator of climate change

Considering the detailed discussion of these problems in Kondratyev *et al.* (2003b, 2004a) and Kondratyev and Krapivin (2004a, b), we will confine ourselves to enumerating the key questions to be addressed within the CCSP (CCSP, 2004):

- Can we identify the specific features involved in spatiotemporal variability of sources and sinks of carbon over North America on timescales from seasonal to secular, and what are the processes that affect carbon cycle dynamics the most?
- Can we identify the respective features of variability and the factors determining them as regards ocean components (sources and sinks) of carbon cycle?
- What is the impact of land surface processes (land use included) at local, regional, and global scales on the formation of carbon sources and sinks in the present? What was it in the past and what is it likely to be in the future?
- What is the variability of carbon sources and sinks on land, in the ocean, and in the atmosphere on timescales from seasonal to secular and in what way can the respective information be used to get a better understanding of the laws of global carbon cycle formation?
- What are the likely future changes in concentrations of carbon dioxide, methane, and other carbon-containing GHGs in the atmosphere as well as changes in the sources and sinks of carbon on land and in the ocean?
- What will the response of the Earth's system and its components be to various strategies proposed to regulate the carbon content in the environment? Do we know enough to answer this question?

The key problems facing studies are given in the following sections.

7.3.4.1 Present trends of GHG content in the atmosphere

Analysis of the data of observations at 50 stations of the global network since the late 1970s revealed a continuous increase in the atmosphere of CO_2, CH_4, N_2O, and other GHGs with the relative increase of CO_2 and N_2O being almost the same, whereas the increase of CH_4 substantially slowed down and almost ceased. As for contributions to the formation of RF, in the case of CO_2 it exceeded 60%, and for CH_4 it was below 20%. The rate of CO_2 increase averaged over the past few decades constituted about 1.5 ppm/yr with a strong interannual variability. Consideration of NEE observation results (i.e., CO_2 exchange between land and atmosphere ecosystems) over the U.S.A. within the AmeriFlux program (Hargrove *et al.*, 2003) showed in this case an assimilation of carbon by ecosystems that function as CO_2 sinks from the atmosphere. From the data for time intervals within 3–10 years, the annual assimilation of carbon varied within 2 t ha^{-1}–4 t ha^{-1} for forests and about 1 t ha^{-1} or less in the case of crops and grass cover. Also, the AmeriFlux program made it possible to obtain regular data on micrometeorological and biological observations important for understanding the processes of carbon cycle formation and its determining biological factors.

7.3.4.2 Inventory of anthropogenic carbon content in the ocean

Field observational programs, such as the experiment to study circulation in the ocean and in the atmosphere (WOCE), the joint experiment to study the carbon cycle in the ocean (JGOFS), the study of ocean–atmosphere carbon exchange (OACES), have created the basis for obtaining new and more reliable estimates of the income of anthropogenic CO_2 to the World Ocean and CO_2 transport in the ocean. Results for 1991–1998 show that the income of anthropogenic carbon totaled about 117 ± 19 PgC but there was strong spatiotemporal variability. Especially strong contrasts were recorded between the northern Atlantic where the presence of anthropogenic CO_2 was traced to the ocean bottom, and the Pacific tropics where CO_2 was absent at depths below 600 m. Though CO_2 emissions to the atmosphere due to fossil fuel combustion take place mainly in the Northern Hemisphere, about 60% of anthropogenic CO_2 is concentrated in SH oceans, which is determined by transport due to the subtropical convergence zone.

7.3.4.3 Specification of carbon budget estimates

There is now the possibility of estimating the carbon budget by using data of satellite observations of ocean color made with SeaWiFS and MODIS instruments calibrated by comparing them with observations by the Marine Optical Buoy (MOBY) (Lavender *et al.*, 1998, 2005; Pinkerton *et al.*, 2003). Calibration ensures that errors in the retrieval of chlorophyll concentration in seawater do not exceed 6%, which makes it possible to substantially raise the reliability of estimates of primary production and, hence, of the carbon budget.

To promptly estimate the carbon supply in forests of the U.S.A., a computer algorithm, called Cole's parallel merge sort algorithm, was developed and used to specify all available data on the carbon budget inventory (Cole, 1988).

New estimates of carbon dynamics from data of direct (fluctuating) measurements of the atmosphere–ocean CO_2 exchange at two sites of virgin Amazon forest led to the conclusion that the annual trend of this exchange is opposite to that obtained earlier. For 7 months of the wet season the forest releases carbon, and for the 5 months of the dry season the forest serves as a carbon sink. The short duration of the dry season strongly limits respiration processes (as a result of the detritus surface drying up) but only weakly affects the process of photosynthesis due to the presence of sufficient moisture in deep layers of the soil. After precipitation resumes (beginning of the wet season) a large amount of wood debris decays and, respectively, CO_2 enters the atmosphere.

The main goals of studies within the North American Carbon Program (NACP) and Carbon Cycle and Climate of the Ocean Program include

- regular observations within the NACP at theAmeriFlux and AgriFlux networks, as well as from masts 500 m high and from oceanic platforms together with satellite remote sensing;

- expansion of the network of observations from aircraft and high masts (the number of masts will reach 15) as well as specialized measurements of the atmosphere–ocean CO_2 exchange in the North Atlantic and in the Pacific Ocean (Northern Hemisphere and equatorial band) to provide new developments in the field of numerical modeling with the necessary input information;
- analysis of new satellite data from the EOS system;
- specialized observations of various landscapes, and ship observations of pCO_2 in the NH Atlantic and Pacific Oceans;
- study of relationships between climate, phytoplankton, carbon, and iron content in the Antarctic Ocean;
- processing of satellite information on the annual trend and interannual variability of ocean primary production;
- numerical modeling of the global carbon cycle;
- analysis of the impact of forest ecodynamics on GHG emissions to the atmosphere;
- continuation of development of the Orbiting Carbon Observatory (OCO), which after launch in 2008 will collect precise global measurements of carbon dioxide in the Earth's atmosphere.

7.3.4.4 Control of natural resources to restrain GHG emissions

Regulating land ecosystem dynamics to hold back GHG emissions to the atmosphere as well as adapting to climate change are feasible using various approaches. For instance, in the case of forests it is possible to stimulate forests to accumulate carbon through intensified growth of vegetation by adding fertilizer to the soil. Results of the 8-year field observational experiment at a site of broad-leaved forest in the state of Tennessee (U.S.A.) demonstrated the impact of precipitation on nutrient cycles and survivability of young trees, but did not reveal such an impact for big trees, growth of root systems, or litter decay. On the whole, forests resist precipitation changes, but changes in hydrological processes can lead to a long-term impact on the species composition of trees. Another field experiment carried out in Wisconsin showed the supposed stimulation of growth of an aspen forest as a result of increased CO_2 canceled out by the opposite impact of simultaneous growth of tropospheric ozone.

The stimulating impact of increased CO_2 in the atmosphere on the growth of crops is well known. However, recent studies have revealed a negative effect of this trend on harvest. An artificial doubling of CO_2 concentration over the grass prairies in the northeast of Colorado (i.e., laboratory experiments) showed that forage obtained under such conditions is less digestible than that produced with a natural CO_2 concentration. In another experiment, increased CO_2 stimulated the growth of five prevalent weed species much more than other plants. Hence, the danger arises of weed growth with increasing CO_2. According to the data from yet another field experiment, with a doubling of CO_2 about 90% of the leaves of white clover are eaten by pests. Thus, the impact of CO_2 increase on crops is contradictory.

7.3.5 Ecosystem dynamics and change of living conditions

Without repeating ourselves (Kondratyev, 2004a, b; Kondratyev *et al.*, 2004a, b) we will now pose the key questions:

(i) What are the most important feedbacks (and their quantitative relationship) between ecosystem dynamics and global changes (mainly, climate)?
(ii) What are the possible consequences of the impact of global changes on ecosystems?
(iii) What are the possibilities of providing sustainable development of ecosystems and the respective needs of society in the light of supposed global changes?

To answer these questions, the results of the developments (outlined in the following sections) supported by the CCSP are of primary importance.

7.3.5.1 The decrease in ocean primary production since the early 1980s

As mentioned above, according to satellite remote sensing since the 1980s, net primary production has decreased by more than 6%, with ~70% of this decrease falling on high latitudes. During this period the SST in the NH Atlantic and Pacific Oceans increased, respectively, by 0.7°C and 0.4°C. However, the decrease of primary production in the Antarctic Ocean was not connected with climate warming. This decrease in primary production reflected a drop in the carbon sink due to photosynthesis weakening in high-latitude oceans. It is still unclear whether these changes are part of a long-term trend or a response to climate variations on a decadal scale, like the PDV or the North Atlantic Oscillation (NAO), which is the dominant mode of winter climate variability in the North Atlantic region ranging from central North America to Europe and farther into northern Asia. The NAO is a large-scale see-saw in atmospheric mass between the subtropical high and the polar low, similar to the SO, which exhibits a tendency to remain in one phase for intervals lasting several years (Hurrell *et al.*, 2003; Hurrell and Dickson, 2004; Hurrell, 2005; Stenseth *et al.*, 2004).

7.3.5.2 Impact of changes in climate regime on marine ecosystems

Climate changes on multi-decadal scales affect both marine and continental ecosystems, which necessitates the monitoring of such changes to provide measures set up to regulate ecosystem dynamics with the necessary information. What is important here is an understanding of the consequences of climate change in the NH Pacific region, where in 1998 a warm-to-cold phase shift of PDV took place, followed by an immediate intensification in the amount of plankton and change in its species composition as well as a considerable increase in populations of salmon and other valuable species in the northwestern region of the Pacific Ocean. In the northern Atlantic, NAO-associated changes in the amount of zooplankton and fish were observed, especially in the Gulf of Haine. Considering relevant new data, indicators

of ecological changes were developed to ensure a more adequate ecological policy to regulate ecosystem dynamics.

Data from a large number of species of plants and animals corresponding to a wide range of natural ecosystems enabled have facilitated detection of changes in natural habitat and in habitation features (migration, blossoming, egg laying, etc.) of many species depending of climatic conditions. However, determination of concrete cause-and-effect relations is seriously hindered by the multi-factor character of biological changes. One study that gathered data on more than 1,700 species demonstrated a considerable poleward shift in the natural habitat averaging 6.1 km/10 years in intervals from 16 to 132 years. For example, spatiotemporal variability determined by climatic trends in the 20th century was demonstrated for 279 species. Analysis of data for 143 species (from mollusks to mammals and from grass to trees) revealed persistent shifting connected with temperature changes. On the whole, the results reflect the impacts of global climate warming on populations of animals and plants.

7.3.5.3 Interdepartmental comparisons of ecosystem models with observational data

Comparison of 13 models simulating forest ecosystems (with built-in schemes parameterizing the processes involved and with different spatiotemporal resolutions) with data of field observations in the eastern part of Tennessee showed that no model prevails across the board. Good "inter-model" agreement is observed in the case of the water cycle, but considerable difference is typical of the carbon cycle. Data averaged over results for all models agree best with observations. Models that disregard the key components of forest ecosystems or important processes (like root zone dynamics or soil moisture) were unable to reproduce the response of ecosystems to a transient drought. The best agreement with observations can be seen in models that realistically parameterize the key processes determining forest ecosystem dynamics with a high temporal resolution (of the order of one or several hours). The prognostic potential of models decreases under drought conditions.

Key developments determined by the CCSP will be along the following lines:

- assessment of the impact of climate in the Arctic (ACIA program) on the environment, human health (i.e., the shortage of UV solar radiation), economic infrastructures, etc.;
- analysis of data from field observational experiments to evaluate the impact of increased atmospheric CO_2 on agricultural ecosystems;
- forecast of localization and ecological impact of weeds using both ground and space-based observational means;
- prediction of forest fires, assessment of ecological consequences of application of chemically dangerous agents in forests (this primarily refers to the western U.S.A.), and carbon accumulation by ecosystems. Here, top priority rests with the development and application of the MAPSS program, which maps the atmosphere–vegetation cover–soil system;
- quantitative description of the impact of climate warming on boreal forests on the basis of observational data and numerical modeling;

- development of the LTEP for long-term monitoring of coastal water ecosystem dynamics;
- quantitative evaluation of the impact of varying temperature and precipitation on the development of soil bacteria communities and microfauna in the biologically active soil layer;
- analysis of possible impacts of climate change on land use and watersheds;
- quantitative estimation of the impact of grazing by domestic animals on the cycles of carbon and nitrogen from observational data at various meadows;
- developments of forest ecosystem models to analyze the forest dynamics under conditions of changing climate; and
- quantitative estimation of the impact of climate change on ecosystem production.

7.3.6 Socio-economic aspects of ecosystem dynamics

The key questions to be answered within the CCSP are

- What are the level, interactions, and significance of the human dimension (i.e., socio-economic factors) in the development of society and its role in global environmental changes?
- What are the present and possible future impacts of global environment variability on economic development?
- What factors determine the capability of society to react to occurring changes?
- What possibilities are there to achieve sustainable development and reduce human sensitivity to forcings?
- What possible methods are there for decision-making in the interests of sustainable development under conditions of NSS complexity and high-level uncertainty regarding global environment variability?
- What are the possible impacts of global environmental change on human health?
- What information about ecodynamics and socio-economic factors is needed to evaluate the respective cumulative risks for human health?

Developments as a consequence of these questions are likely to be along the following lines:

(1) *Regional problems of ecodynamics*. What is important here are studies into the power supply, reconstruction of ecosystems, recovery of human health, and special phenomena such as droughts and forest fires at both local and regional levels. We need to integrate physics, chemistry, and biology (with respective socio-economic aspects taken into account) to make adequate decisions in ecological policy. Studies of the dependence of forest fires on climatic conditions can serve as an illustration of possible approaches to the solution of such problems (a principal goal is prediction of anthropogenic forest fires).
(2) *Analysis of economic efficiency*. Quantitative assessment of the economic efficiency of one or another ecological policy can only be determined by taking

as many priorities as possible into account. What is important here is the use of simulation models of ecodynamics, especially models simulating changes in land supplies of carbon to assess the response of carbon supplies in vegetation and the soil to specific features of land use and changes in land surface characteristics, to variations in atmospheric CO_2 content, and to climate. Solution of such problems will mean more reliable prediction of global trajectories of CO_2 emissions to the atmosphere.

(3) *Possible consequences of global climate change for forestry and agriculture over the U.S.A.* Analysis of such changes under various scenarios of possible changes in global climate suggests that the impact on forestry and agriculture in the U.S.A. is likely to be economically favorable. This has partly to do with the growth in forest productivity (as a result of increased CO_2) and the capability of forests to adapt to climate change. As for agriculture, according to available prognostic estimates for the period to 2060, the positive impact of global warming on agriculture in the U.S.A. will be less economically favorable than previously thought.

(4) *Impact of UV solar radiation on human health*. Intensive developments along these lines are being carried out to study the impact of a lowering level of biologically active UV solar radiation due to the decreasing total ozone content in the atmosphere on the development of skin cancer and cataracts.

Planned developments will be along the following lines:

- creation of centers responsible for decision-making under conditions of uncertainties (DMUU) which should remain operational until 2008;
- energy consumption housekeeping (with the U.S.A., China, and Indonesia taken as exemplars) and its prospects in light of present demographic trends;
- analysis of the efficiency of seasonal weather forecasts and prospects for predicting interannual climatic variability;
- substantiation of possibilities to adapt economic activity to climate change;
- prediction of possible rises in sea level and substantiation of respective measures;
- assessment of global change consequences regarding risk and the multitude of stress factors; and
- climate variability and human health (i.e., shortage of UV solar radiation).

Despite the impressive information content of the U.S. program of climate studies (CCSP, 2004), it should be mentioned that this program

- Still lacks the systematic character necessary for such a program (principally, the program lacks a sequential approach to solution of climate problems as an integral part of global change problems).
- Fails to substantiate a single approach to creating a global observing system. The ESSP (i.e., the partnership set up for complex study of the Earth's system) does not resolve such a problem.
- Pays insufficient attention to paleoclimatic problems.

These three general considerations should be the basis for further program developments.

7.4 PRESENT STATE AND PROSPECTS FOR WORLD ECONOMIC DEVELOPMENT

7.4.1 Biogeochemical cycles and energy

As human activities intensify (as a result of continuing growth in population size) the need arises for further development of energy. Energy production is still based on using hydrocarbon raw materials, which lead to serious ecological consequences. It is no mere chance that on the agenda of the G-8 meeting held on July 7–8, 2005 in Scotland, from two key problems the problem of global climate warming was chosen, and the next session of the G-8 (St. Petersburg, December 2006, Russia) concentrated on discussions of energy problems. An important socio-economic aspect of recent changes is the massive rise in oil and natural gas prices, as well as growing uncertainties in relationships between Russia and the consumers of its energy resources (Kondratyev and Krapivin, 2006b, c). Energy supply has become key to further intensification of human activities. The urgency of the situation can be illustrated by considering a large developing country such as Brazil.

A serious crisis broke out in Brazil in 2001, which resulted in energy consumption limits being introduced to avoid catastrophic energy blackouts. The main causes of the crisis were

- Prolonged droughts continuing (in different regions) for 6 years (1996–2001), resulting in a reduction of hydropower production.
- Growing energy consumption.
- Delays in commissioning power stations.

The contribution of hydropower stations to energy production in Brazil in 2002 constituted 85%. Planning a hydropower system foresaw an event of three successive drought years. However, in April 2001 the volume of water in reservoirs of hydropower stations constituted only 20%–30% compared with the maximum. It is this that forced the Brazilian government to seriously limit energy consumption.

In late 2006 the problem of energy supply to Europe suddenly appeared as a result of the conflict between Russia, on the one hand, and Ukraine and Byelorussia, on the other, concerning payments for consumed energy and its transport to other countries across their territories. Lengthy discussions followed on this problem. For instance, Taro Aso, Head of the Ministry of Foreign Affairs of Japan, called on European countries to diversify the sources of energy to reduce their dependence on Russia. In the course of the meeting with his Hungarian counterpart Kinga Göncz

he said that while he understood the dependence of many European countries on Russian oil, it might be worthwhile to think about diversifying delivery as much as possible. Minister Aso called the position of Russia "the policy of natural resources", stating that Moscow "uses energy as a weapon". The Spanish newspaper *ABC* noted in its editorial of January 10, 2007 that suspension of energy supply to the European Union by Russia could become a problem every winter, and while a year ago it was gas transported across Ukraine, today it is oil transported across Byelorussia. Europe every now and then demonstrates its growing vulnerability and dependence on external energy sources and, at the same time, its isolation when it comes to solving energy problems.

Naturally, for energy to become "eco-dependent" will mean diversifying the means of production. A complex analysis is needed of the present state and prospects for future development of energy on a global scale, bearing in mind diversifying the means of production, instilling the need to be economical in the use of energy, raising the efficiency of energy production, and minimizing negative ecological consequences (e.g., by transiting from hydrocarbon to pure energy). It is a question of reaching both nationally and internationally a level of energy production that is ecologically safe, stable, and meets the growing needs of business. For instance, the U.S.A. is currently spending about $0.5 billion every day on oil import mainly from the Near East.

The main problem consists in the inability of market mechanisms to regulate energy when it comes to its stability and ecological safety, which results in governments and international organizations getting involved. The discussion of energy problems is usually limited to analyzing the dynamics of consumer prices of energy and the crises that arise as a result of shortages of energy resources. For instance, the price of natural gas varied weakly around $2 per MBTU (million of British thermal units) during the 1980s, but passed the $4 mark in January 2003. The price of gas in 2007 in various countries ranged from $0.14 in Venezuela to $5.64 in England. The cost of crude oil went up from $20 per barrel to $40 (July 2004) reaching the current level (2008) of $94. Note that the Energy Information Administration of the U.S. Department of Energy forecast the oil price reaching $20 per barrel by 2020. Crude oil prices behave in the same way as any other commodity with wide price swings at times of shortage or oversupply. The crude oil price cycle responds to changes in demand as well as OPEC and non-OPEC supply.

Table 7.7 illustrates the rapid increase of global fossil fuel consumption from the data of the World Resources Institute for 1950–2003. We shall now consider more detailed statistical data for different kinds of fossil fuel and energy resources in general, with emphasis on extremely non-uniform distributions of energy consumption for different countries (Table 7.8).

Of course, the fact that the average American spends 10 times more energy resources than the average Chinese and 20 times more than the average Indian is well known.

Table 7.7. Global consumption of fossil fuels (million tons of oil equivalent) 1950 through 2006.

Year	*Coal*	*Oil*	*Natural gas*
1950	1,074.3	470.8	171.9
1960	1,544.2	951.4	416.3
1970	1,553.9	2,254.5	924.7
1980	1,814.1	2,972.7	1,304.8
1990	2,270.5	3,136.1	1,774.2
2000	2,364.3	3,556.2	2,193.2
2001	2,384.8	3,572.6	2,214.1
2002	2,432.2	3,606.6	2,286.3
2003	2,632.8	3,675.3	2,341.8
2004	2,805.5	3,813.7	2,435.3
2005	2,957.0	3,861.3	2,512.2
2006	3,090.1	3,889.8	2,574.9

Table 7.8. The annual energy consumption and CO_2 emissions in different countries.

Country	*Commercial energy (per capita consumption in oil equivalent)*	*Oil (barrels per day per thousand people)*	*Electric power (kW per hour per capita)*	*Per capita emissions of carbon dioxide* (t)
U.S.A.	8.1	70.2	12,331	19.7
Japan	4.1	42.0	7,628	9.1
Germany	4.1	32.5	5,963	9.7
Poland	2.4	10.9	2,511	8.1
Brazil	1.1	10.5	1,878	1.8
China	0.9	4.2	827	2.3
India	0.5	2.0	355	1.1
Ethiopia	0.3	0.3	22	0.1

Table 7.9. Current coal consumption (million tons oil equivalent) and future trends.

Region	*2006*	*2010*	*2020*	*2030*
North America	611.6	639.7	681.3	634.3
South and Central America	21.8	35.4	70.3	54.7
Europe and Eurasia	552.9	510.4	412.8	379.1
Middle East	8.9	8.4	6.6	5.1
Africa	102.8	132.2	121.9	98.5
Asia Pacific	1,792.1	1,998.6	2,097.4	1,856.3
Total world	*3,090.1*	*3,324.7*	*3,390.3*	*3,028.0*
European Union 25	305.0	298.4	265.9	243.7
OECD	1,171.5	1,183.1	1,156.5	1,099.6
Former Soviet Union	183.9	207.8	213.6	197.5
Other EMEs*	1,734.7	1,797.4	1,857.2	1,788.8

* EME stands for European and Middle East countries.

7.4.2 Coal and its role in the future of global energy

Despite misgivings about the ecological consequences, coal remains a dominating source of energy with a level of global consumption of almost 5 Mt in 2001 and future growth up to 7.6 Mt in 2030. Over 4,970 Mt of hard coal is currently produced, a 78% increase over the past 25 years. Coal production has grown fastest in Asia, while Europe has actually seen a decline in production. Table 7.9 illustrates the present and presumed levels of coal consumption in different countries. As can be seen, the growth in coal consumption is concentrated in three countries: China, India, and the U.S.A., all of which have large coal supplies. A decline in coal consumption in Western Europe and in some other regions is mainly connected with the growing role of natural gas as a source of energy. The same situation can also be observed in the U.S.A., though high rates of coal consumption continue. This has led, in particular, to natural gas prices more than doubling since 1999. The prospects for replacing coal (or natural gas) by renewable energy sources remain still distant. The development and use of pure technologies (IGCC technologies included) are more likely. IGCC is a clean coal technology that turns coal into gas, and then removes impurities from the coal gas before it is burnt. This results in lower emissions of sulfur dioxide, particulates, and mercury. It also results in improved efficiency compared with conventional

pulverized coal. IGCC technology offers a number of important environmental benefits:

- IGCC has the best emission characteristics of all coal-based technologies.
- IGCC provides for efficient removal of sulfur compounds, particulates and mercury before the gas is burned, instead of removing the compounds from the exhaust gases following combustion.
- Nitrogen oxide (NO_x) emissions are on a par with emissions from a conventional coal-fired plant equipped with state-of-the-art emission controls.
- Emissions of carbon dioxide are comparable with emissions from a conventional coal plant. However, should future environmental regulations require the removal of CO_2, an IGCC plant can separate and sequester CO_2 from the process at a significantly lower cost than conventional technologies.
- The IGCC process requires about one-third less water than a pulverized coal plant.
- The IGCC process generates less solid waste than a conventional coal plant.
- IGCC plants enjoy greater fuel flexibility than conventional coal plants.
- IGCC plants can use various coal types, biomass, and other refinery byproducts.

7.4.3 Oil and its role in sustainable development

Alhough the transition from hydrocarbon energy to other means of energy production is becoming increasingly attractive to governments and business, the fact is that coal, oil, and natural gas still dominate, and there is little doubt that pressure on the oil market in coming decades will grow. Just looking at a single statistic illustrates this inevitability: in China there are currently 8 cars per 1,000 people, whereas in the U.S.A. there are 780 cars per 1,000 people. Of course, the rapid economic development of countries such as China and India with a joint population of about 2.5 billion people will inevitably increase the need for energy resources. The same refers to the U.S.A. as well, where the present oil consumption exceeds 20 million barrels per day. With oil extraction in the U.S.A. proper decreasing as existing deposits run out, dependence of this country on oil import (mainly from the Middle East) intensifies. As a consequence, the U.S.A. is considering introduction of a special oil tax, initially at a level of $5 per barrel, to stimulate measures for economic use of oil resources. Plans are also underway to intensify the use of Alaskan oil resources, where it is possible to raise daily oil extraction up to 1–1.3 million barrels (at present, oil extraction from Alaska is limited by an ecological ban).

7.4.4 Natural gas and economic growth

Compared with oil (and especially coal), natural gas as an energy carrier and raw material has several important advantages: reduced environmental pollution in industry, households, and energy production, where coal has been extensively replaced by gas. There are also wide possibilities for gas to be used in chemistry. In the U.S.A. and many other countries, natural gas has become the prevalent energy

carrier, though petrol plays the leading role in transport. As in the case of petrol, in recent years there have been sudden leaps in natural gas prices, from \$2.5/MBTU in the winter of 2002 to more than \$9/MBTU in October 2004, which affected particularly badly the competitive ability of some branches of chemistry.

The following data give the percentage use of various energy carriers in the U.S.A. according to estimates for 2005: petrol (40), natural gas (23), coal (23), nuclear energy (8), renewable energy resources (6). Natural gas use in the U.S.A. can be further broken down by economic sector (%): industry (32), social sector (23), power production (23), commercial use (14), and other spheres (8). The global distribution of the use of gas in different regions is illustrated by the following figures (%): the Near East (36), Eastern Europe and the former U.S.S.R. (33), Asia and Oceania (8), Africa (6), North America (4), Central and South America (4), and Western Europe (9).

According to estimates by the U.S. Energy Information Administration, known global resources of natural gas exceed 70 times annual global consumption, with established resources increasing annually since 1970 as a result of exploration. The comparatively small contribution of natural gas as an energy carrier in the U.S.A. means energy development here will focus on more intensive use of resources from Alaska (this will require construction of a long and expensive gas pipe) and with further increase of the import of liquefied gas. The main problem here is the building of ports and the related infrastructure for gas distribution.

7.4.5 Nuclear energy: yes or no

Now that the world has recovered from the Chernobyl shock, conditions are ripe for relatively objective assessment of the present state of and prospects for nuclear energy, especially in light of its recent successful development. For example, in France nuclear power stations (NPSs) provide more than 70% of power production, and two NPSs in Scotland contribute 55% to total U.K. power production. As an aside, wind energy production in the U.K. constitutes a mere 0.3% of total production. Nuclear energy is successfully developing in China, Iran, and other countries as well. There has also been a gradual increase in the U.S.A., where there have been discussions about the need to build a new NPS. More than 100 NPSs are in operation throughout the globe, which provide about 20% of world energy consumption. Oil ($>$50%) and natural gas ($\sim$17%) still lead the field in energy production. In developing countries, nuclear energy constitutes about 25% of energy production.

The advantages of nuclear energy include its ecological purity (in particular, no GHG emissions to the atmosphere), abundant supplies of raw materials, and low running costs, all of which determines lower electricity charges. In the U.S.A., nuclear power costs 1.5 cents per kilowatt-hour, whereas in the case of thermal power stations operating on coal and gas it is 2 and 3.5 cents per kilowatt-hour, respectively. Factors holding back nuclear energy development include the high cost of NPS construction. For instance, the cost of constructing (which takes 5 years) an NPS with 1,000 MW capacity can reach \$2 billion. This reduces to \$1.4 billion if new technologies of coal transformation to natural gas are used, with the added benefit of lowering the level of

emissions. Considering the costs of NPS construction, exploitation, and its presumed 40-year lifetime at 85% capacity, electricity charges will rise to 6.7 cents per kilowatt-hour (coal) and 4–5.6 cents per kilowatt-hour (gas turbines). However, reactor safety and storage/disposal of used fuel remain as unsolved problems.

7.4.6 Prospects and possibility of using hydrogen energy

First predictions of the possibilities of using hydrogen fuel by 2000 were made in 1970. These predictions were never realized, but in his address to the nation in 2003 President George W. Bush unveiled the "Hydrogen Fuel Initiative" which foresaw investments of $1.2 billion over 5 years to develop the necessary technologies for hydrogen energy production by 2020 and putting in place the infrastructure needed for cars to run on hydrogen. In his speech on February 6, 2003 in the National Building Museum (Washington, D.C., see *www.nei.org/newsandevents/speechesandtestimony/2003/buildingmuseumprebushextended*), he said: "We saw cars engineered to run on hydrogen ... And there are a lot of advantages that I want to explain to the American people about why this initiative makes sense. First, the hydrogen can be produced from domestic sources, initially, natural gas; eventually, biomass, ethanol, clean coal, or nuclear energy. That's important. If you can produce something yourself, it means you're less dependent upon somebody else to produce it." Still more ambitious plans were voiced by Arnold Schwarzenegger (Governor of California) according to which by the year 2010 a network of 150–200 hydrogen filling stations will operate in this state. However, there is no doubt that before hydrogen energy becomes a reality, serious work must be carried out concerning a wide range of problems, from hydrogen production to means of its storage and distribution, right through to finding a way of getting it into and storing it in fuel tanks.

At present the annual production of hydrogen in the U.S.A. constitutes 9 million tons, one-third of which is used for ammonia production and two-thirds at oil refineries. From the most optimistic assessments, the mass application of hydrogen fuel cannot become a reality before 2050, and this will require annual production of 111 million tH/yr. The initial components for hydrogen production are carbon and oxygen, and one possible technology is water electrolysis which gives off hydrogen as an accompanying emission of water vapor and heat. This technology is very simple and ecologically safe—but expensive (especially with present power prices). Producing hydrogen by means of renewable energy sources (wind, solar energy, biomass burning) is also expensive.

The technology used for hydrogen production is based on fossil fuels containing carbon and hydrogen (natural gas is the most appropriate). This technology is much more economical than electrolysis, but still exceeds 2–4 times the cost of petrol production per unit of applied energy. Moreover, the limited nature of natural gas resources may cause a rise in its price, which needs to be kept in mind. Another technological difficulty in the use of natural gas is the emission of CO_2 (and the concomitant negative ecological consequences). From the viewpoint of simplicity, coal is much more promising, but in this case ecological consequences are even more serious. Another possibility is to use nuclear energy to produce hydrogen (by means

of electrolysis or high-temperature thermochemical technology). Yet another is photochemical transformation of marine algae, the feasibility (and economy) of which requires thorough analysis.

Of course, there are serious difficulties of distribution and storage (in cars, in particular) of hydrogen fuel because of its low density and inflammability. As for production and distribution, well this will involve the production of hydrogen at large plants with its subsequent distribution through gas pipes. There is also the possibility of transporting hydrogen in its liquid form. This will entail serious technical and economic analysis, with the problem of hydrogen storage in cars being especially difficult. Finally, the technical aspects of hydrogen fuel application with regard to fuel cells and improved internal combustion engines remain unclear.

Thus, there are a number of technical obstacles along the path to mass application of hydrogen fuel. To surmount them will involve serious investment and effort which will arguably take several decades.

7.4.7 Economic development and renewable resources

If we exclude the power industry, the overall contribution of renewable sources of energy to power generation remains small. This can be illustrated by comparative data for the U.S.A. (Table 7.10). Naturally, hydroenergy prevails among renewable energy sources, but there are a number of reasons that prospects for its further development are limited. Second best (with a large gap between) is wind energy with a high rate of growth (11% since 1990). Energy production from geothermal sources remains at a low level. For example, in the U.S.A. since 1995 the use of geothermal energy has dropped by 20%. In other countries, such as Japan, the Philippines, and Costa Rica, the use of geothermal energy in this period increased by 32.1%, 55.6%, and 158.2%, respectively. But, on the whole, power generated from geothermal sources constitutes only 0.25% of total world production.

Table 7.10. Energy production and levels of generation from data for the U.S.A. for 2003.

Type of fuel	*Power*		*Generation*	
	1,000 MW	%	10^9 kW/h	%
Fossil/Nuclear	823	89.4	3,493	90.7
All renewable sources	98	10.6	359	9.3
Hydroenergy	79	8.6	275	7.1
Other types	19	2.0	84	2.2
Wind	7	0.7	11	0.3
Geothermal sources	2	0.2	13	0.3
Solar energy	0.5	0.1	1	0.0
Wood/Municipal solid waste	9.0	1.0	59	1.5
Total	*920*	*100*	*3,852*	*100*

Alhough, ecologically, the use of renewable sources of energy is to be welcomed, they cannot be the panacea for all our energy needs, because of their comparatively high cost. For instance, in the case of photoelectric converters of solar energy, total expense on generating such energy (evaluated in kWh) is 3–4 times higher than in the case the new technology IGCC. The role of renewable energy sources in the future will depend on how competitive they are with non-renewable sources. Overcoming this will require serious financial support.

Nevertheless, renewable sources of energy will be the focus of future energy technologies.

- Solar energy has been used in many traditional technologies for centuries and has come widespread where other power supplies are absent, such as in remote locations and in space. Solar energy is currently used in a number of applications such as heat production, electricity generation, desalination of seawater, and lighting.
- Wind power is a source of cheap energy and is generated by wind turbines. In 2005, the global capacity of wind-powered generators was 58,982 megawatts (less than 1% of worldwide electricity use). For example, since the late 1970s the U.S.A. cost goals for wind power have continued to be about $0.04 per kilowatt-hour. Future wind plants are expected to play a significant role in global energy production.
- Hydropower takes the energy of moving water and converts it into electricity. The energy of moving water has been exploited for centuries. But the spatial distribution of rivers imposes restrictions on countries in the generation of hydropower energy. Global hydrological networks need to be set up to overcome this.
- Hydrogen holds great promise as a clean and affordable source of energy. Hydrogen can be obtained from fossil sources (such as methane). It can also be used to replace dwindling supplies of petroleum in future.

Table 7.11 considers the pros and cons of various energy carriers. The main conclusion is that both now and in the near future, non-renewable energy sources (fossil fuel and nuclear energy) will still prevail; with global energy developing in this way studies into ecological safety become paramount. It is also necessary to consider natural disasters, such as Hurricane Katrina, which in late October 2005 wreaked havoc with U.S. energy, destroying the energy infrastructure in the Gulf of Mexico. There was a transient rise in oil and gas prices by 10%–20%, and during the winter of 2005–2006 they (as expected) grew only by 5%–10%. Hurricane Katrina led to decreased gas and oil extraction in the Gulf of Mexico by 1.34% and 24.6%, respectively, at that time. The prospects for global energy can only be assessed by adopting a systematic approach that takes both anthropogenic and natural factors into account.

Table 7.11. Pros and cons of using different energy carriers.

Energy carrier Problem	*Coal*	*Oil*	*Natural gas*	*Nuclear energy*	*Renewable sources*	*Hydrogen energy*
Are there problems of fuel delivery?	*No.* Explored resources are enormous	*Yes and no.* Known resources are enough for decades (at present prices)	*No.* The level of known resources grows annually, exceeding 70 times global consumption	*No.* There are enough resources of uranium, plutonium, thorium and possibility to use the reprocessing of nuclear fuel	*Yes and no.* Resources are great but not infinite, there are difficulties with territory allocation	*Yes and no.* There are different possibilities of production of hydrogen as a source of energy
Are there problems of cost?	*No.* The cheapest energy carrier, whose price is lowering	*Yes.* Wide price fluctuations strongly affect the economics of its use	*Yes.* Though large resources do exist, they are often located far from the consumer	*Yes.* Ecological efficiency of nuclear stations can be raised only by reducing the construction cost of NPSs	*Yes.* Costs are decreasing (especially in the case of wind energy)	*Yes.* The major problem: heavy cost of production
Are there negative ecological consequences?	*Yes.* Serious ecological consequences do exist	*Yes.* Oil spills, greenhouse gas emissions	*To some extent.* As in the case of coal and oil, but to a lesser extent	*Yes and no.* No emissions problem, but there are difficulties with waste storage	*No.* Only limited ecological consequences are possible	*Yes and no.* Some negative ecological consequences are connected aith hydrogen production

Dependence on unreliable delivery?	*No* The most significant consumers have rich reserves of coal	*Yes.* Possible instability of deliveries from the Near East and from Russia in connection with development of terrorism	*To some extent.* As in the case of oil	*No.* There are sufficient supplies of uranium	*No.* Serve as a substitute for non-renewable resources	*Maybe.* Dependence on hydrogen production from natural gas
Serious technical difficulties?	*Yes.* Technologies to reduce harmful gas emissions as well as CO_2 capture and assimilation are still inadequately developed	*Yes and no.* Development of possible new sources of oil and improved engines are necessary	*No.* Use of present technologies can be continued	*No.* There are only problems of reduction of the construction cost and development of methods for waste storage	*Yes.* Further improvement of photo-transformers and other technical means	*Yes.* Many technical problems for hydrogen energy remain unsolved

7.5 MODERN SOCIETY AND ECOLOGICAL RESTRICTIONS

7.5.1 Global instability

The present ecological situation worldwide can be exemplified by growing instability, a civilization crisis, the global scale of which is expressed through deterioration of human and animal habitats. The dominant features in global ecodynamics in the late 20th–early 21st century include the rapid growth in population (mainly in developing countries), urban population growth at the expense of rural population (the growing number of cities), broadening scales of such dangerous diseases as HIV/AIDS, hepatitis, tuberculosis, etc. U.N. data predict global population in 2050 to reach 8.9 billion people. This means that the decrease in per capita consumption (expected as a result of the growing efficiency of technologies) will be canceled out by the impact of population growth. For instance, if meat consumption by the average American increases by 20% by 2050 (compared with 2000), then due to the growth of population size in the U.S.A. the total mean consumption will increase by 5 million tons. An important general fact is that despite the prevailing growth of population size in developing countries, their contribution to the impact on the environment will not necessarily exceed that reached in developed countries. For instance, U.S. population size will annually increase by about 3 million people and in India by 16 million people, but the impact of the U.S.A. on the environment (due to its higher per capita consumption) will be more substantial. This is illustrated, in particular, by estimates of growing CO_2 emissions to the atmosphere: 15.7 million tC in the U.S.A., and 4.9 million tC in India.

7.5.2 Correlation between production and consumption

Key to ensuring NSS sustainable development is the production/consumption ratio stated at the World Summit on Sustainable Development in Johannesburg in 2002. China is a good example of the consumption dynamics observed in recent decades. Until quite recently China was a country of cyclists. However, a traveler in the 1980s visiting such cities as Beijing and Shanghai will see quite another picture today. In 2002 there were about 2 million cars in China, in 2003 the number increased daily by 11,000, and today the number has exceeded 4 million. In 2007, car sales increased by more than 77%, and by 2015 the expectation is 150 million cars.

A considerable part of global population (more than 1.7 billion people) can now be classed as consumers, half of whom live in developing countries. In recent decades there has been a continuous increase in consumption in developed countries, a "revolution in consumption". The total per capita consumption due to goods and services reached $26 trillion dollars in 2006 (in dollars of 2005), exceeding the level of 1960 by $10.9 trillion, but there are vast differences between the situations in different countries. For instance, 60% of per capita consumption falls on 16% of the world population in the U.S.A. and Western Europe, whereas the share of consumption by one-third of the global population in South Asia and sub-Saharan Africa constitutes a mere 3.2% (Table 7.12).

Table 7.12. Share of global consumption and population in different regions.

Region	*Consumption* (%)	*Population* (%)
U.S.A. and Canada	31.5	5.2
Western Europe	28.7	6.4
Eastern Asia and Oceania	21.4	32.9
Latin America and the Caribbean	6.7	8.5
Eastern Europe and Central Asia	3.3	7.9
Southern Asia	2.0	22.4
Australia and New Zealand	1.5	0.4
Near East and Northern Africa	1.4	4.1
Sub-Saharan Africa	1.2	10.9

In 2007 about 2.66 billion people lived at or just above the breadline ($2 per day) and about 0.92 billion people in extreme poverty (<$1 per day). The number of consumers with an annual income greater than $10,294 (this level is considered the poverty threshold in Western Europe) constituted 1.76 billion people in 2006.

As can be seen from Table 7.13, almost half of consumers live in developing countries, China and India constituting more than 20%, although of course the average Chinese or Indian consumes much less than the average West European.

In addition to Sub-Saharan Africa being a disaster-prone region, the level of consumption there in 2001 was 20% lower than in any year of the two previous decades. According to available estimates, the number of consumers will at least double by 2015. Table 7.14 illustrates the number of consumers in ten representative countries in 2002, and Table 7.15 family expenditure on food in different countries in 1998.

The overwhelming—some would say criminal—feature of domestic consumption is that it is not aimed at satisfying basic levels of comfort or survival, but has to do with expense on luxury items (sports cars, jewelry, vacations, cruises, etc.). Such expense has reached huge levels (tens of billions of dollars). Satisfying such basic things as the need for food, drinking water, education, and healthcare for the world's poorest is possible with a mere fraction of these expenses.

The necessity to satisfy the growth in consumption leads to an increase in the use of natural resources. Between 1960 and 1995 the global use of mineral raw materials increased by a factor of 2.5: metals 2.1, wood 2.3, and synthetic materials 5.6. This increase considerably exceeded the growth in population size, despite its extreme non-uniformity. For instance, the U.S.A. whose population constitutes about 5% of the world's consumes about one-fourth of the global resources of fossil fuel. The U.S.A.,

Table 7.13. Global distribution of consumers.

Region	*Number of consumers* (millions)	*Share of consumers* (%)	*Share with respect to global consumers* (%)
U.S.A. and Canada	271.4	85	16
Western Europe	348.9	89	20
Eastern Asia and Pacific Ocean region	494.0	27	29
Latin America and Caribbean region	167.8	32	10
Eastern Europe and Central Asia	173.2	36	10
Southern Asia	140.7	10	8
Australia and New Zealand	19.8	84	1
Near East and Northern Africa	78.0	25	4
Sub-Saharan Africa	34.2	5	2
Developed countries	912	80	53
Developing countries	816	17	47
Global	*1,728*	*28*	*100*

Canada, Australia, Japan, and Western Europe whose population constitutes about 15% of the world's annually use 61% of produced aluminum, 60% of lead, 59% of copper, and 49% of steel. Annual utilization of aluminum by the average American constitutes 22 kg, for the average Indian it is only 2 kg, and for the average African it is less than 1 kg.

The general conclusion is that with an abundance of food and other goods, conditions become ripe for unhealthy levels of consumption. Cheap energy and improved transport favor the growth of consumption. The introduction of new technology and its take-up by consumers is now faster than ever. For example, in the U.S.A. it took 38 years for the number of radio listeners to reach the 50 million level, for TV viewers it was 13 years, and for Internet surfers it was 4 years. The necessity to sell produced goods has stimulated a rapid increase in global expenditure on advertizing, reaching in 2002 a massive $446 billion (in dollars of 1991), which constituted almost a nine-fold increase compared with 1950. At present, each credit card owner in the U.S.A. pays interest of about $1,900, which is equivalent to the average per capita income in the 39 poorest countries.

Table 7.14. Number of consumers.

Country	*Number of consumers* (millions)	*Percentage share of country population total* (%)
U.S.A.	242.5	84
China	239.8	19
India	121.9	12
Japan	120.7	95
Germany	76.3	92
Russia	61.3	43
Brazil	57.8	33
France	53.1	89
Italy	52.8	91
U.K.	50.4	86

Table 7.15. Family expenditure on food.

Country	*Per capita expenditure on self* (U.S.$)	*Share spent on food* (%)
Tanzania	375	67
Madagascar	608	61
Tajikistan	660	48
Lebanon	6,135	31
Hong Kong	12,468	10
Japan	13,568	12
Denmark	16,385	16
U.S.A.	21,515	13

This unhealthy level of consumption results in enhanced impacts on the environment and natural resources. Almost all ecosystems in the world have been impacted. An indicator of the impact on global ecosystems called the "ecological imprint" has been introduced. This characterizes the size of productive land area needed to ensure

the production of needed resources and assimilation of emissions. Estimates have shown that the global mean size of such a biologically productive land area should be 1.9 ha, and from the viewpoint of emission assimilation 2.3 ha. Of course, these averages mask the real inequality in the sizes of ecological imprints, which vary from 9 ha for the average American to 0.47 ha for the average Mozambican. These figures mean that total global consumption exceeded the ecological capacity of the planet as long ago as the late 1970s–early 1980s. It goes without saying that life is only possible with adequate reserves of natural resources.

Excess consumption (from the viewpoint of the load on ecosystems) in many countries correlates with the lowering of health indicators resulting in diseases related to such excess consumption. For instance, smoking increases annual global mortality by 5 million people. Data for 1999 reveal smoking-induced expenditure on medical services and economy losses in the U.S.A. reached \$150 billion, exceeding ~15 times the incomes of the five largest tobacco manufacturers. Also important are the consequences of excess weight due to improper diet (respective medical expenses in 1999 reached \$117 billion).

Against a background of material prosperity (on average), the social health of U.S. society in the last 30 years has got much worse, which manifests itself through growing poverty, suicides among young people, lack of an adequate medical service, and a great disparity in incomes (the rich get richer, and the poor get poorer).

The continuing growth of consumption in developed countries, on the one hand, and the respective serious negative aspects, on the other hand, throw up a few questions.

- Are higher living standards as a result of increasing consumption typical of global consumers?
- Is it possible to balance consumption and environmental protection?
- Can the ways of the consumption society be changed to ensure sustainable development?
- Is society prepared to give top priority to satisfying the needs of all its members?

The concept of consumption society economics based on unlimited consumption clearly cannot work because of the unavoidable environmental consequences. Realization of such a concept would break economical, ecological, and social limitations (thresholds). The main conclusion is that there is no hope for the consumption society.

7.5.3 Systems that are vital for life

7.5.3.1 Freshwater

Let us now analyze the state of some of the most important systems of life support, such as freshwater and energy supplies. Freshwater attracts a lot of attention since, on the one hand, water is a key component of ecosystems and, on the other hand, about one-third of the global population will experience a deficit of water at some

time or other. This and other facts determined the announcement by the U.N. of the Fresh Water Decade (2005–2015).

The sufficient supply of pure water is of fundamental importance for achieving the goals of socio-economic development and environmental protection. Enhancing anthropogenic impacts on the environment are of concern here. For instance, the area of freshwater wetlands, which play an important role in natural water purification and in formation of the water cycle, have almost halved in the last 20 years. At the same time, economic assessment puts a value on their losses equivalent to \$20,000/ha/yr. About 2% of 10,000 species of freshwater fish are either on the brink of extermination or are extinct. The number of large dams in the world increased from 5,000 in 1950 to more than 45,000 today, the negative ecological consequences of which need no comment.

The geographical distribution of freshwater resources is extremely non-uniform: six countries (Brazil, Russia, Canada, Indonesia, China, Colombia) have about half of global resources. Non-uniformity is also typical of individual countries. For instance, although China has 7% of world freshwater resources (but a 21% share of world population), most of the country is arid. Naturally, countries that lack water are forced to use ground water, which leads to a lowering of the water table.

Moreover, these data illustrate existing socio-economic contrasts. About every fifth person in the developing world (1.1 billion people) daily runs the risk of falling ill for lack of good-quality drinking water. However, the main problem is not the absence of water at all, but unfavorable socio-economic conditions.

Agriculture is the basic consumer of the freshwater of rivers, lakes, and ground water (about 70% on a global scale and up to 90% in many developing countries). Since the growing use of irrigation will have to face up to the scantiness of freshwater resources in the near future, the efficiency of freshwater use gains in importance, and fortunately there are many ways to raise this efficiency. One of which is the use of micro-irrigation (drip irrigation included) the scale of which remains rather limited.

There is a much room for economy in the use of water in food production. For instance, to produce 10 g of protein in the form of beef requires five times as much water than for 10 g of rice, and for 500 Calories this difference is 20-fold. With a lavish meat diet, the average American requires 5.4 L/day, whereas for a vegetarian this amount is halved.

The water supply in cities and realization of measures on water economy are further problems. Industrial usage of freshwater, which constitutes 22% of used (on a global scale) freshwater resources (59% of this in developed and 10% in developing countries) is the most urgent problem.

7.5.3.2 Energy

During the period 1850–1970, global population size more than tripled, and energy production increased 12 times. Today (2007) population size has increased by 93%, and fossil fuel consumption by 87%. There appears to be no rigid connection between energy production and economic growth. Measures on energy economy taken between 1970 and 1997 fulfilled economic growth with a 28% decrease in the "energy

intensity" of production. Global fossil fuel consumption in 2002 increased by 1.3% (up to 8,034 million tons of oil equivalent) compared with 0.3% in 2001. Compared with 1950, the level of fossil fuel consumption increased by a factor of 4.7. Now fossil fuels fulfill 80% of global energy consumption. World use of oil as the dominant fossil fuel surged by 3.4% in 2004, to 82.4 million barrels per day. This represents the fastest rate of increase in 16 years, according to *Vital Signs* (2005). Fossil fuel burning continued to rise despite soaring energy prices in recent years: in 2004, coal use jumped 6.3% and natural gas consumption rose 3.3%; in 2005, oil use increased 1.3%.

Respective trends for the consumption of various kinds of fossil fuel are rather non-uniform. While the global mean increase of oil consumption in 2002 constituted only 0.5%, in China it reached 5.7%, the Near East 2.5%, and the former U.S.S.R. countries 1.9%, mainly due to export growth. In the U.S.A. (which consumes 26% of global oil) the level of consumption increased negligibly. In some countries (Japan, South Korea, Australia, New Zealand) this indicator lowered (on average) by 0.6%, and in the countries of Latin America by 2.6%. In 2006 global oil consumption growth was weaker by 1.2 Mbbl/day (1.4%) than that in 2005. The change of global gas production between 2006 and 2005 was 2.3% (WI, 2007).

After a transient but significant decrease of coal consumption in the late 1990s, in 2002 global consumption increased (compared with 2001) by 1.9% (2,298 million tons of oil equivalent). In the U.S.A. (which consumes 25% of global coal) a 0.5% decrease was observed, and in China (which consumes 23% of global coal) a 4.9% increase (despite a ban in the use of coal in some regions, where frequent smog and acid rains are observed). Worldwide, global coal consumption increased by 4.5% reaching 3,090.1 million tons oil equivalent in 2006. Distribution of coal consumption by different regions is: North America −0.7%, Southern and Central America 5.3%, Europe and Eurasia 3.1%, the Middle East −1.1%, Africa 2.4%, and Asia Pacific 7.0%.

Global mean growth of natural gas consumption constituted 2% in 2000 (2,428.0 billion cubic meters) and 2.5% in 2006 (2,850.8 billion cubic meters), but in the U.S.A. (which consumes 22%–27% of global natural gas) there was a 1.7%–3.7% decrease (in the previous five years), which was determined mainly by several mild winters (BP, 2007). A decrease in natural gas consumption was also observed in some other developed countries, reaching a maximum in Japan (10.4%), but in Norway the increase was much greater (up to 81%). On the whole, natural gas witnessed the most rapid growth of consumption (compared with other fossil fuels) fulfilling currently almost 24% of global energy needs (compared with 22.5% a decade ago). Various factors determine such an increase including the availability of natural gas in many countries and its weaker (compared with other fossil fuels) negative impact on the environment.

The levels of energy consumption differ strongly between various countries. The population of the richest countries consumes (per capita) on average 25 times more energy than the population of the poorest countries. For 2.5 billion people in the world (living mainly in Asia and Africa), the main source of energy remains wood (or other kinds of biomass). Let us take a look at both ends of the spectrum: the U.S.A.

and Ethiopia. In the U.S.A., the per capita commercial energy consumption constitutes (in weight units of oil equivalent) 8.1 t/yr, but in Ethiopia this is only 0.3 t/yr. The respective extreme global levels of oil consumption are 70.2 bbl da^{-1} and 0.3 bbl da^{-1} per thousand people, and of electric power 12,331 kW and 22 kW per thousand people. Hence, the level of per capita CO_2 emission to the atmosphere reaches 19.7 t in the U.S.A. and only 0.1 t in Ethiopia.

According to estimates of the International Energy Agency, in the period 2000–2003 the annual global mean production of primary energy should be 1.7%, reaching the level 15,300 million tons of oil equivalent in 2030. The growing need for energy (mainly in developing countries) should be 90% satisfied by fossil fuels. However, even by 2030, about 18% of global population will be deprived of such modern sources of energy as electricity. Of course, these predictions should be considered conditional.

There has been substantial progress in the use of alternative sources of energy, such as nuclear and wind energy. The attitude to nuclear energy in different countries remains ambiguous. The number of nuclear reactors in the world (in NPSs) has increased to 437 due to the commissioning in 2007 of new reactors in China (4), South Korea (2), and the Czech Republic (1). In 2002, construction was started of six new reactors in India, and 26 others worldwide were in the process of construction (their combined power will be 20,959 MW). In the U.K. NPSs are considered uncompetitive, and Belgium plans to ban them by 2025.

As for the use of wind energy, well at the end of 2002 the total power production due to wind generators constituted 27% (in Western Europe 31%). Compared with 1998, wind energy production has tripled, making it the most rapidly developing source of energy. Western Europe's contribution to global wind energy constitutes 73%, with the most coming from Germany, Spain, and Denmark.

The increased use of fossil fuels and related growth of CO_2 emissions to the atmosphere have aroused concern regarding possible anthropogenic global climate change. Without a detailed discussion of the cause-and-effect bonds between temperature and CO_2 concentration. Note that, despite the adoption of international documents about the necessity to reduce GHGs emissions to the atmosphere (CO_2 included), global mean CO_2 concentration continues to grow. This trend will likely remain in the near future. In 2002, 6.44 billion tC were emitted to the atmosphere (a 1% increase compared with 2001), and CO_2 concentration reached 372.9 ppm, increasing by 18% between 1960 and 2002, and since the beginning of the industrial revolution (1750) by 31%. About 24% of global CO_2 emissions are down to the U.S.A., with per capita CO_2 emissions exceeding 17 times those observed in India. Similar trends in the growth of anthropogenic emissions are observed for other GHGs, which considerably complicates nature–society relationships.

All of this means that the present state of human society (including socio-economic and ecological conditions) cannot be considered stable from all points of view. The growing database shows that the present structure of consumption results in worsening living standards for many people, manifested through health problems, water quality, destroyed ecosystems, etc. Despite the continuing improvement of technologies and measures on energy supply, under conditions of the

growing global population size and growing level of per capita consumption (especially in developed countries), the prospects for global sustainable development in the 21st century are far from clear.

The possibility to achieve the same average level of energy consumption as in developed countries (and this level is much lower than in the U.S.A.) is out of the question. It would necessitate an eight-fold (maybe more) increase of energy production during the period 2007–2050. It is clear that this increase is impossible using fossil fuels. Even if such an increase were feasible, it would be followed by negative ecological consequences. Nevertheless, the prospects for sufficiently intensive development of alternative energy sources in the 21st century remain unclear.

Nevertheless, humankind should search for ways to achieve sustainable development. The developed countries should take the lead in solving this problem, by supporting policies aimed at ecologically pure production and creation of efficient methods of energy supply. In other words, the paradigm for socio-economic development should be changed from the consumption society to priorities of social and spiritual values. Concrete analysis of ways of bringing about this development will require the efforts of specialists in the field of social sciences. Some related ideas were mentioned by Corcoran (2005) in the context of Earth Charter problems. In principle, supplies of some kinds of energy on Earth are unlimited, but their use requires considerable progress in many spheres of knowledge as well as the indicated change in priorities of global ecodynamics.

7.5.4 Future analysis of human life

The UNEP-conceived International Human Dimensions Program on Global Environmental Change (IHDP) outlines priorities pertinent to the environment and the development goals for a millennium. The fundamental objective in this program is the need to consider correlations between key problems of ecodynamics determined by numerous feedbacks and the non-linearity of the NSS, due to which "threshold effects" can occur as can synergy between technologies and ecological policy. Numerous illustrations of the urgency of taking into account various correlations are contained in global climate change problems.

Adequate analysis of the role of feedbacks and the non-linearity of the NSS is seriously complicated by the fragmentary character of available information. It is a pity here that the concept of biotic regulation of the environment developed by Russian scientists has still not been accepted, for it might serve as the conceptual basis for solution of the problems of global ecodynamics. It is important that biospheric mechanisms also serve as the basis for the system of life support in manned space vehicles. Unfortunately, the concept of biotic regulation remains "unnoticed" in the West, which can be illustrated, in particular, by a discussion of the Gaia conception which contains rhetorical statements about the Earth as an "autotrophic self-regulated super-organism". Of course, maintenance of environmental stability is one of the basic goals of all living organisms. Therefore, an important task of present-day science is to point out the priorities for global ecodynamics and to search for real ways to achieve sustainable development.

7.6 ECOLOGICAL CRISES AND DISASTERS

7.6.1 Essence of the problem

As civilization develops, the forecasting of future environment changes and relevant changes in the living conditions of people have become most important. The first problem of interest is the origin and propagation of dangerous natural phenomena (i.e., natural disasters) which lead to loss of life and cause serious economic damage. At present, natural disasters include floods, droughts, hurricanes, storms, tornados, tsunami, volcanic eruptions, landslides, landslips, mud flows, snow avalanches, earthquakes, forest fires, dust storms, heavy frosts, heatwaves, epidemics, locust plagues, and many other natural events. Their occurrence is mostly of anthropogenic origin.

Natural anomalies of different spatiotemporal scales are known to have played an important role in the evolution of nature as mechanisms for natural system regulation. With the development of industry and growth of population size, these mechanisms have suffered substantial changes and reached a level that threatens life. This is mainly related with the growth and propagation of anthropogenic forcings in the environment. Many relevant studies have been conducted. They show that the frequency of natural disasters and their scale have grown, increasing the risk of loss of life, economic losses, and damage to social infrastructure (Figure 7.1, Tables 7.16–7.18). For instance, in 2001 some 650 natural disasters occurred in the world costing the lives of more than 25,000 people and causing damage estimated at more than $35

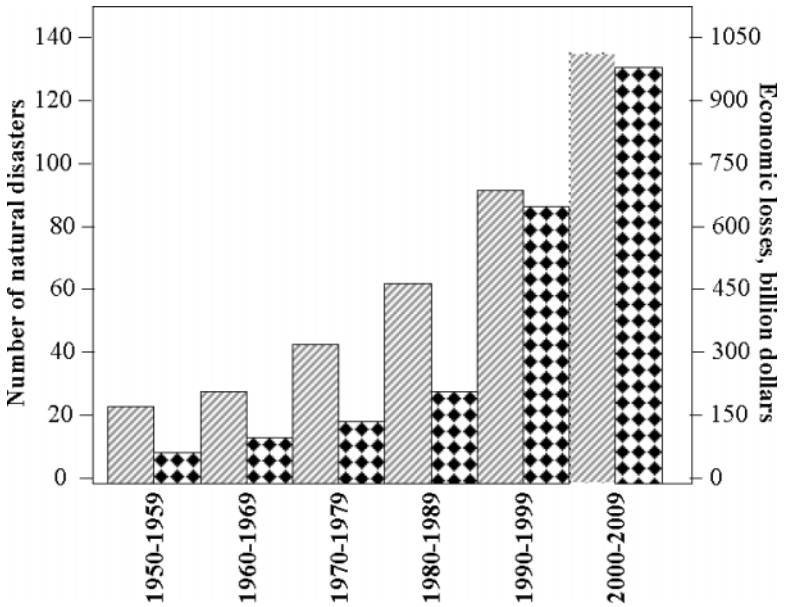

Figure 7.1. Dynamics of the number of largest natural disasters. From Munich Re (2004). Notation: diagonal hatching = natural disasters, checkerboard pattern = economic losses.

Table 7.16. Continental distribution of natural disasters and the resulting damage (Ruck, 2002; Phelan, 2004; Munich Re, 2005a, b).

Region	*Number of natural disasters*			*Number of fatalities*			*Economic losses, millions of U.S.$. Insurance payments are given in brackets*		
	2002	*2003*	*2004*	*2002*	*2003*	*2004*	*2002*	*2003*	*2004*
Africa	51	57	36	661	2,778	1,322	308 (158)	5,158 (0)	444 (0)
America	181	206	185	825	946	4830	13,933 (6,259)	21,969 (13,247)	68,183 (34,585)
Asia	261	245	245	8,570	53,921	170,254	13,965 (385)	18,230 (600)	72,706 (7887)
Australia and Oceania	69	65	52	61	47	67	2192 (11)	628 (246)	343 (124)
Europe	136	126	124	459	20194	371	2,4246 (5,897)	18,619 (1,690)	3,765 (1,218)
Globe	*698*	*699*	*642*	*10,576*	*77,886*	*176,844*	*54,644 (12,750)*	*64,604 (15,810)*	*145,441 (355,080)*

Table 7.17. Statistics on the most powerful natural disasters (Ruck, 2002; Munich Re, 2005a, b; Enz, 2006).

Years	*1950–59*	*1960–69*	*1970–79*	*1980–89*	*1990-99*	*1992–02*	*2003–05*
Number of natural disasters	20	27	47	63	91	70	38
Economic losses, billions of dollars	42.1	75.5	138.4	213.9	659.9	550.9	767.8

billion. In 2002, the death toll dropped to 11,000, but economic damage reached $55 billion. In 2003, there the death toll reached 50,000 and economic losses reached $60 billion. In Russia alone the number of natural disasters in the last decade increased from 60 to 280. In 2004, in the U.S.A. there were a record number of tornados (562), beating the record held by 1992 which witnessed 399 tornados. The beginning of 2004 saw an increase in extreme situations mainly of weather origin, and the year ended with a global disaster on December 26, with huge losses for countries

Table 7.18. Most powerful earthquakes in the history of humankind (Grigoryev and Kondratyev, 2001a, b; Hanson, 2005).

Year	*Region*	*Fatalities* (thousands)
365	The East Mediterranean region (excluding Syria)	50
844	Syria (Damascus)	50
893	Armenia	100
893	India	180
1138	Syria	100
1268	Turkey (Semjiya)	60
1290	China (Djili)	100
1456	Italy (Naples)	60
1556	China (Shengshi)	830
1626	Italy (Naples)	70
1667	Azerbaijan (Shemakha)	80
1668	China (Shandung)	50
1693	Italy (Sicily)	60
1727	Iran (Tebriz)	77
1730	Japan (Hokkaido)	137
1737	India (Bengaluru, Calcutta)	300
1739	China (Ninaya)	50
1755	Portugal (Lisbon)	60
1783	Italy (Calabria)	50
1868	Ecuador (Ibarra)	70
1908	Italy (Messina)	82.5
1920	China (Hanshu)	180
1920	China (Ningsha)	200
1923	Japan (Canto)	140

(*continued*)

Table 7.18 (*cont.*)

Year	*Region*	*Fatalities* (thousands)
1923	Japan (Tokyo)	99.3
1932	China (Hanshu)	70
1935	Pakistan (Kuetta)	60
1948	Turkmenistan (Ashkhabad)	110
1957	Gobi-Altai (Mongolia, Buriatiya, Irkutsk and Chita Region)	0
1970	Peru (Chimbote)	66
1970	Iran	50
1972	Nicaragua	5
1972	Iran	5
1974	Pakistan	5.3
1974	Guatemala	22.084
1976	Indonesia	5
1976	Turkey (Van)	4
1976	China (Tien Shan)	255
1976	Guatemala	22.085
1976	Philippines	3.739
1978	Iran	25
1985	Mexico	9.5
1988	Armenia	25
1988	Turkey	25
1990	Iran (western part)	40
1993	India	9.475
1994	U.S.A. (California)	0.061
1995	Japan, Kobe	6.43
1998	Afghanistan (Takhar)	4

Year	*Region*	*Fatalities* (thousands)
1999	Turkey	19.118
1999	Russia, earthquake in Neftegorsk	2
2001	India, Pakistan	15
2002	Alaska, U.S.A.	0
2002	Afghanistan	1
2003	Iran (southeast)	26.271
2004	Southeastern Asia (Sumatra, Thailand, India, Sri Lanka)	283
2004	Niigata Prefecture, Japan	0.04
2005	Indonesia, Malaysia	2
2005	Nias Island, Indonesia, Northern Sumatra	2.5
2006	Indonesia	5.749
2007	China (Yunnan)	0.3

in the Indian Ocean basin, and hundreds of thousands of victims. In Sri Lanka alone the damage was estimated at $3.5 billion. This tragedy recurred on March 28, 2005, when a magnitude 8.7 earthquake with its epicenter only 200 km southeast of the December 26 epicenter cost the lives of hundreds of people and devastated large areas in Indonesia and Malaysia. On the whole, 19 earthquakes of magnitude 5 were recorded in 2004.

Indices of losses caused by natural disasters depend much on the preparedness of the regional population to reduce the risk of losses. The heaviest losses are caused by floods and hurricanes. The spatial distribution of natural disasters is also non-uniform (Table 7.16). For example, the percentage distribution of natural disasters by type and continent is as follows: tropical storms 32%, floods 32%, earthquakes 12%, droughts 10%, other disasters 14%; Asia 38%, America 26%, Africa 14%, Europe 14%, and Oceania 8%.

Natural disasters have always been regulators of evolution. However, the human)element in natural disaster occurrence highlights the need to maintain the stabilizing role of such regulators in the future. Therefore, the principal goal for humankind is to find a means of reducing the level of anthropogenic change in the biosphere.

7.6.2 How natural disasters affect human life

Natural disasters can be geographic, spatial, temporal, ecological, economic, and socio-political in scale. The generally accepted definition of natural disasters subdivides them into categories. For example, large-scale disasters lead to the loss of many thousands of lives and substantial damage to housing, businesses, and the infrastructure of a given region. Hence, the scale of natural disasters depends on how developed the region is economically and socio-politically and what degree of protection has been put in place against natural disasters (i.e., sea walls, levees, readiness of emergency services, etc.). Therefore, studies of the causes of natural disasters should include analysis of population density and the level of poverty of a given region. Studies over the last 25 years show the dependence of losses from natural disasters in developing countries is much stronger than in developed countries. In the last decade there was an approximate five-fold increase in the number and scale of natural disasters and a nine-fold increase in the danger they posed. Using this information enables us to indicate the likely dangers in the near future that pose threats for the population of these countries. Prediction and warning of imminent natural disasters in the world, on the whole, should be the number one priority for all countries, irrespective of their economic development.

The development and scale of natural disasters depend on natural background conditions which can either hinder or favor the propagation of the phenomenon and, hence, weaken or intensify its impact on the environment. The number of victims among the population depends on the level of social development, which is manifested through the level of sophistication of systems at predicting, warning, and preventing possible natural disasters. In fact, a multitude of factors can be considered as natural and social forerunners to a natural disaster. Assessment of the scale of a natural disaster depends on the human response to it. For instance, the danger posed by a tropical cyclone is determined by the combined impact of all its components: wind, rain, and storm surges. Wind speed in a tropical cyclone can exceed 250 km/hr and cover a band 40 km–800 km wide. Such a wind speed destroys buildings, knocks out communications, devastates vegetation, and inevitably results in people losing their lives and property being severely damaged. During the lifetime of a tropical cyclone, rains can deposit 2,500 mm of water, which inevitably leads to floods. One of the deadly elements of a tropical cyclone is the storm surge, when seawater rises above the normal by as much as 7 m (although higher levels have been reported). This leads to rapid flooding of coastal lowlands. Finally, when winds and storm surges combine this leads to propagation of huge waves that destroy all before them: beaches, agricultural land, all manner of constructions, and homes in the coastal zone. The cyclone body usually moves at a speed of 24 km/hr increasing up to 80 km/hr as the cyclone moves away from the place of origin. The destructive power of the accompanying waves is irresistible.

Calculating the scale of natural disasters presumes, first, predicting their ecological consequences. They manifest themselves, gradually over time, as reduced productivity of ecosystems, changes in the structure of the water balance over the territory, and violation of vital environmental parameters. In other words, when

developing technology to estimate the scale of natural disasters, it is necessary to take into account criteria from a wide range of fields: medico-biological, economic, social, botanical, soil, zoological, and geodynamical. One component of this technology is the classification of natural disasters and use of knowledge from different sciences, especially those sciences leading to perspective technologies for future use. For example, there is an urgent need to understand the role of climate change in the processes of genetic modification, or the discovery of correlations between environmental changes and technical, economic, and political responses to these changes.

7.6.3 Natural disasters as an ecodynamics component

For almost 4 billion years, living beings have been changing the planetary chemistry and climate and, possibly, determining the habitability of the planet. Put another way, the reason the present world is inhabited is because today's organisms evolved in the past in harmony with changing geological and biological conditions. Among the many processes regulating the environment, natural disasters occuped a niche of their own and played their part in biospheric evolution. However, we are currently witnessing an increasing trend of anthropogenically induced natural disasters, such as floods, forest and peat fires, deforestation, desertification, and epidemics, which are changing the character of natural feedbacks and, hence, changing the role of natural disasters.

The regulatory role of natural disasters can be seen in different ways. For instance, tropical hurricanes form upwelling zones in the World Ocean, which promote the productivity of respective water basins, but, on land, they destroy forested areas that remove carbon from the cycle, thus reducing the removal of CO_2 from the atmosphere and enhancing the greenhouse effect. Forest fires, both anthropogenic and natural, are another example. Lightning prevails among the natural causes of fires. On average, the frequency of strikes in tropical forests and moderate-zone forests is, respectively, 50 and 5 strikes per square kilometer. The probability of catching fire depends much on the moisture content of the territory. From available estimates, lightning strikes annually cause more than 20,000 forest fires. Their geography is determined by climate, and their propagation and scale are functions of numerous factors of the environment (soil moisture, temperature, density and type of trees, relief, etc.).

The beginning of the 21st century witnessed vast forest fires in Russia, Europe, America, Australia, and South-East Asia. For example, in the summer of 2004, 197 forest fires were recorded across Russia. They flared up in the Krasnoyarskiy Krai, Komi, and Saha Republics, in the Arkhangelskaya, Vladimirskaya, Irkutskaya, Kirovskaya, Sverdlovskaya, and Tchitinskaya Regions, as well as in the Far East. The scale of these forest fires can be judged by their number: Arkhangelskaya 12, Yakut 22, and Komi 20. The most numerous forest fires in Russia were in the Far East (47). Since Russian forests play a significant role in CO_2 absorption from the atmosphere, their state is the focus of attention of the scientific world, if not of the population as a whole. There are many international nature protection programs

studying the state of forests across Russia (Goldammer and Furyaev, 1996; Kovalev, 2003).

This NOAA AVHRR satellite image composite shows fire activities in the Russian Federation (Yurganov *et al.*, 2006). According to satellite-derived analysis undertaken by the Sukachev Institute for Forests (Krasnoyarsk), the total areas burned by August 25, 2003 and by June 5, 2006 in the Russian Federation were 23,470,000 ha and 10,079,945 ha, respectively. These data confirm the growing concern about forest fires in Russia, especially in light of the importance of Russian forests to the global climate system. The role Russian forests play in the functioning of the global biogeochemical system should be further studied and assessed in detail.

7.6.4 Outlook for the future of global ecodynamics

The present trend of the interaction between human society and the environment confirms intensive deforestation and desertification as the most characteristic and widespread processes (especially in the latter decades of the 20th century). The ecological consequences of these processes include degradation of conditions under which people live and violation of the stabilizing role of vegetation in the energy exchange between the planet and space. There is a general decrease in the diversity of living creatures. Therefore, when considering the prospects for life on Earth, we should first assess the level of environmental degradation, since with the passage of time local and regional changes in the environment develop into global ones. The amplitudes of these changes are determined by mechanisms in the functioning of the NSS that ensure optimal changes in its components. Humankind increasingly deviates from this optimality in how it interacts with the inert, abiotic, and biotic components of the natural environment. However, at the same time, humankind is striving to comprehend the character of large-scale interactions with nature as manifested by the joint efforts of the many sciences studying the cause-and-effect relations in this system. In particular, finding an indicator to assess the appearance of the planet as a result of changes in forested areas is now very urgent. Biocomplexity is a good candidate. It is defined as the sum of all energy connections between various types of biospheric ecosystems, and is a sufficiently informative indicator of this change. It shows that further felling of wild forests will drastically reduce biodiversity and change the albedo over a large territory, leading inexorably to considerable change in global climate. With a 10% decrease in wild forest area by 2050, biodiversity will decrease by 18%, and by 2100 the concentration of CO_2 will grow by 44%. However, if there is a 10% increase of this area, biodiversity will rise by 32% and CO_2 concentration will drop by 15%.

An important component of life on our planet is volcanic activity. Throughout geological history, continents have repeatedly merged and separated. Apparently, about 2.5 billion years ago there were 20 continents, and 2 billion years later in the early Proterozoic they numbered only 13. In 1.5 billion years time Australia, America, Africa, and Eurasia will combine with the Antarctic to form a supercontinent. Of course, the volcanic boundaries of continents will also change. These seemingly slow processes must not be neglected in studies and assessments of present

trends in changes in the ecological situation on Earth. Intensive degassing deep in the Earth and global disasters are synchronous. Such events as El Niño and the formation of ozone holes depend much on the intensity of the hydrogen flow from the depths of the Earth to the atmosphere, and methane emissions in degassing zones affect variations of CO_2 concentration in the atmosphere.

Future events can be forecast from current trends in ecological situations. Let us take the Aral Sea as an example. Much has been written on this subject and a large number of scenarios have been worked out. But, the sad conclusion is that if the influence on the hydrological regime of this zone continues in the near future there will be desertification and salinity over huge areas of Middle Asia. To estimate the scale of such a disaster, it is necessary to bear in mind variations in the distribution of precipitation over vast areas from the steppes of Stavropolye and Kalmykia to the Pamir and Tien Shan mountains. These variations are predetermined by large-scale spatiotemporal changes in fluxes of atmospheric moisture from the Caspian and Aral Seas, Gulf of Kara Bogaz Gol (KBG), large reservoirs and sewage works, saline lands, and other typical evaporators of surface and ground waters throughout Middle Asia.

The 1950s to 1960s were representative of the optimal balance between ecology and people living beside the Caspian Sea and the prospects for many-sided development of the near Caspian and Middle Asian regions were good. For example, the Caspian Sea level varied between -28 m and -28.5 m with respect to the World Ocean level, and its area varied between 370 km^2/yr and 375 km^2/yr. However, from available estimates, the surface area of the Caspian Sea reached 420 km^2 in 1994 showing an increasing trend and the volume of evaporated water exceeded that of 1960 by $\sim$50 km^3/yr. More than half this amount could be attributed to the northern shallow part of the sea. It is expected that with the rising level of the Caspian Sea (3 m from 1978), upwellings will occur with waves propagating for tens of kilometers inland from the coastline, contaminating ground water, destroying levees, leaching from the sea harmful wastes and poisonous products of extraction (such as sulfur), and processing hydrocarbon-containing materials.

By applying a model approach to analysis of the water balance of the Aral Sea region, we can consider various hypothetical situations of the impact on the water balance to see if it can be transformed from the present unfavorable state to one that functions stably from the viewpoint of economy and hydrometeorology. One way out of this critical situation is to reduce the amount of water taken for irrigation. Of course, removing the Kara Kum Canal is not an option, since many agricultural areas depend on it. Nevertheless, the governments of Kazakhstan and Uzbekistan are considering the possibility of partially reducing the area given over to cotton plantations in order to return any unnecessary water to the Aral Sea. A search for other ways of preventing an ecological catastrophe in Middle Asia resulted in various scenarios, including the transfer of some Siberian river water (rejected by many scientists). A more realistic scenario consists in artificial irrigation, taking water from the Caspian Sea, saline lands, and hollows on the eastern coast of the Caspian Sea. This is feasible because these areas are at a lower level (-25.7 m) than the Caspian Sea. Such areas include the lifeless Kultuk (-27 m), Kaidok (-31 m), KBG Gulf

(−32 m), Kaundy (−57 m), Karin Arik (−31 m), and Charala Sor (−30 m). As a result of evaporation, water builds up here at the rate of 0.2 km^3/day, and is transported with a little help from the wind to the Turan lowland and farther on to the sources of the Syr Darya and Amu Darya Rivers. The contribution of excess atmospheric water from the Caspian Sea to the growth of river run-off to the Caspian Sea could be as much as ~40 km^3/yr. By maintaining constant wind direction between the Caspian and Aral Seas, there is the possibility of the Aral Sea returning to its 1960 state in 12–15 years.

After the December 26, 2004 earthquake (which registered magnitude 9 on the Richter scale) at the northwestern end of Sumatra, the prediction of extreme natural events has become urgent. It is clear that, at the moment, geophysics can only make suggestions as to the causes of earthquakes and put forward different hypotheses for their occurrence (e.g., shifts in the Earth's crust). The most difficult problem facing science today is earthquake prediction. Despite the presence of centers specifically set up to record minute oscillations in the Earth's crust, the progress of the scientific community in understanding the laws that control the development of the Earth as a planet is slow. Nevertheless, some progress has been achieved in predicting other types of natural disasters due to development of the theory of climate and global ecodynamics. However, no estimates or predictions can be made without making certain climate scenarios or likely strategies of humankind development available. Therefore, it is important that these scenarios are set up by giving a prominent place to the pre-history of NSS development.

One possible approach to predicting earthquakes and volcanic eruptions is by using statistics of these natural disasters as input information for the recently developed technology of evolution modeling. Prediction of random number series using evolution modeling makes it possible to determine with some accuracy the time of occurrence of the next event. For example, this approach came up with the following estimates. In the next 20 years, we should expect annually, on average, 2–3 earthquakes of magnitude >7 and 4–5 earthquakes of magnitude 5–7. We should also expect five large-scale volcanic eruptions by 2020.

Assessment of variability in global water balance components would also be of interest. Based on the scenario that foresees population size increasing to 11 billion people by 2100, we should see the precipitation rate in northwestern Europe increasing by 2020, causing a 400 km^3/day decrease in atmospheric moisture fluxes from the European continent to America. In other regions, changes in moisture cycle should vary within ±7% with a gradual growth in amplitude by 2100. As a result, by the end of the century the rate of precipitation should increase in the regions of the Pacific coast of America, northeast India, and southwest China, and the zone of heavy rains in Europe should broaden northward. Hence, floods in these regions should be more frequent. At the same time, the rain rate on the eastern coast of North America, in the countries of Middle Asia and the Near East should decrease, and the regime of contrasts in rainy/dry season alternation should change in southeastern Asia. For the European continent, a negative factor is likely to be a marked decrease in rainfall in Greece, Italy, and in the Caucasus. In central Europe the rain regime should not change by more than 3%.

7.7 NUMERICAL MODELING OF THE DYNAMICS OF THE NATURE–SOCIETY SYSTEM

The problem of the combined evolution of humans and nature can be traced back to the beginning of the industrial period, when the impact of population on natural processes became noticeable. The rate of this impact has been rapidly increasing over time, and now life itself is at stake.

Anthropogenic processes in the biosphere have become comparable with natural processes. The appearance of the land surface is rapidly changing, forests are decreasing, and cultivated land is growing. Anthropogenically introduced forest fires in different regions vary from 10% to 75%. For example, the tropics, which cover 30% of the Earth's surface (4.6 billion ha), contain 42% of the Earth's forests, the area of which decreases by 12 million ha per year. This is caused by population growth in tropical countries (by 24% per year on average), which leads to an annual increase in ploughed lands of 100 million ha. Similar trends can also be observed in other regions of the globe. On the whole, the global loss of forests by 2000 constituted $\sim$0.5 million ha.

Similar negative trends in other natural formations can be observed all over the globe. The extent to which global biogeochemical processes are being impacted by humans introducing chemical elements to the biosphere and violating natural cycles in which these elements transform is of concern to scientists. The normally positive balance of organic matter in the geological cover of the Earth has now become negative, as a result of human activity, leading inexorably to the growth of GHGs. The quantitative characteristics of these processes are well known.

To assess the trends in biosphere dynamics and understand the level of danger facing the environment from human activity, many investigators, using databases on environmental parameters and their understanding of the unique character of natural systems, are trying to create global models and, from their own experience of the unique character of natural systems, have created models to predict the possible consequences of anthropogenic activity.

The biosphere on a global scale, unlike its local components, can be studied experimentally. Therefore, all we can do here is to carry out global experiments using numerical models of the biosphere on computers. These models require a formalization of climatic, biotic, geochemical, economic, and social processes. As mentioned in the works of many Russian and other specialists on modeling global processes, the level of adequacy of these studies is determined by the extent to which real processes are simplified in the models (Krapivin and Kondratyev, 2002; Kondratyev *et al.*, 2004a; Krapivin and Varotsos, 2007; Degermendzhy, 2008).

Pachauri (2004) convincingly confirmed the thesis of Kondratyev *et al.* (2002a, b) that effective and safe study of correlations between natural and anthropogenic processes is only possible using a global model that reflects the diversity of the phase space of the NSS. Furthermore, Pachauri (2004) posed three questions:

(i) In what way has man's activity affected the climate system of our planet?

(ii) What are the consequences of climate change and what types and levels of the impacts are caused by human activity?
(iii) What can humankind undertake to soften climate change and to adapt themselves to a level of climate change, which seems to be unavoidable now and probably tomorrow?

Clearly, the GMNSS can answer these questions. But, its use presumes the availability of comprehensive databases and knowledge from different scientific branches. By using a modeled biosphere instead of the biosphere itself we can get answers about the consequences of changes to natural systems as a result of human projects.

With the combination of available databases and numerical modeling of global processes, it is possible to achieve acceptable similarity between the observed behavior of the biosphere and model predictions. There has been remarkable progress at the Institute of Biophysics, Siberian Branch of Russian Academy of Sciences (Krasnoyarsk) in assessing biospheric stability thresholds using basic theoretical and experimental models, the results of which agree with the global monitoring data.

Figure 7.2 shows the conceptual diagram of the global model of NSS functioning. This diagram was achieved by many authors under different modifications (Krapivin, 1993; Degermendzhy, 2008; Kondratyev and Krapivin, 2004a; Krapivin, Svirezhev, and Tarko, 1982; Krapivin *et al*., 1996a; Kondratyev *et al*., 2004a). The last improvement of this diagram was described by Krapivin and Varotsos (2007).

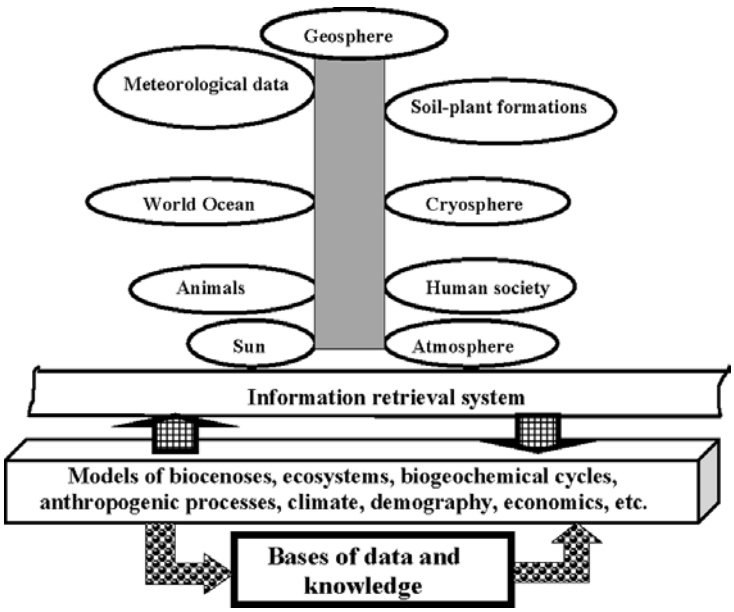

Figure 7.2. Organization of the global model of NSS functioning.

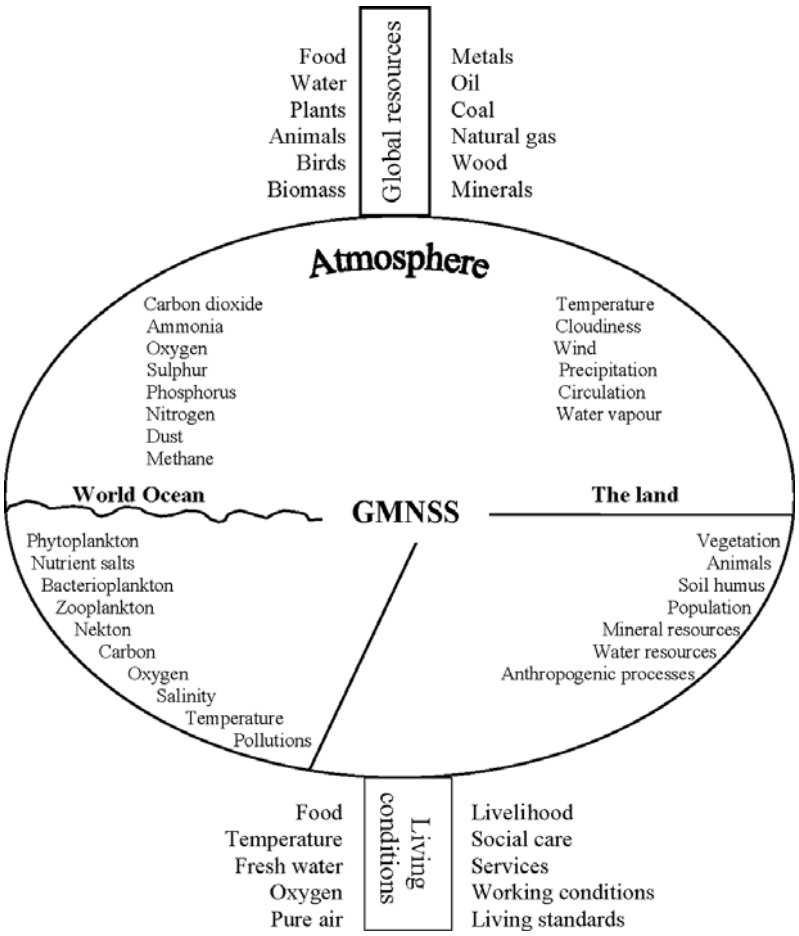

Figure 7.3. Key elements of the nature–society system and energy components that need to be considered for global ecodynamics forecast in the framework of global model use.

Figure 7.3 shows the basic components taken into account in this realization of the GMNSS. A block-scheme of the GMNSS is based on the hierarchy of the units that parametrize interactions between key elements of the NSS. The model structure has the units that realize the controlling functions and are responsible for modeling the biogeochemical and biogeocoenotic processes. The GMNSS database is formed as two structures:

(1) Data of the first type for the global model units are stored as geographical maps and as tables of model equation coefficients.
(2) Data of the second type are represented as fragments of record (possibly irregularly) in time and space (i.e., CO_2 concentration, temperature, precipitation, pressure, population density, availability of resources, etc.).

Figure 7.2 is realized by introducing the geographical grid $\{\varphi_I, \lambda_j\}$ with steps of sampling of land surface and the World Ocean of $\Delta\varphi_i$ and $\Delta\lambda_j$ in latitude φ and longitude λ, respectively, so that within a pixel $\{(\varphi_i, \lambda_j)$: $\varphi_i \le \varphi < \varphi_i + \Delta\varphi_i$, $\lambda_j \le \lambda < \lambda_j + \Delta\lambda_j\}$ all processes and elements of the NSS are considered as homogeneous and parametrized by point models. The choice of the size of pixels is determined by several conditions governed by the spatial resolution of satellite measurements and the available global database. It is clear that the precision of the global model depends on the quality of the knowledge base and database renewal.

A management procedure for global model precision was proposed by Kondratyev, Krapivin, and Pshenin (2000). The main idea behind this procedure consists in the use of evolutionary modeling for the synthesis of a combined model whose structure is subject to adaptation against the background of the history of a system of the biosphere and climate components. The form of such a synthesis depends on the spatiotemporal completeness of the global database.

Figure 7.4 explains the technology for the synthesis of the global system of environmental control using standard means of telecommunication. The basic component of this technology is the GMNSS, which plays the role of consumer of data delivered by the global environment observation systems. Kelley *et al.* (1992) called this technology GIMS (GeoInformation Monitoring System) technology. This technology proposes the criteria that allow the selection of the informational structure of the geoinformation-monitoring system representing the hierarchical

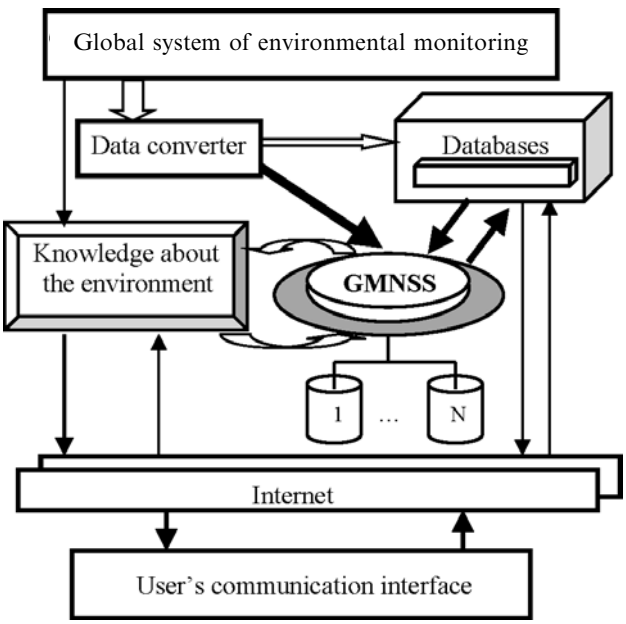

Figure 7.4. The principal scheme from GIMS technology to synthesize the global system of control of the environment using standardized means of telecommunications and GMNSS.

subordination of the models at various levels. Application of GIMS technology can help to solve the following principal problems:

- What kinds of instruments are going to be used for conducting the so-called ground-truth and remote-sensing measurements?
- What is the cost to be paid for on-site and remote-sensing information?
- What kind of balance is going to be taken into consideration between the information content of on-site and remote sensing and the cost of these types of observations?
- What kinds of mathematical models must be used for both the interpolation of data and their extrapolation in terms of time and space with the goals to reduce the frequency and thus the cost of the observations and to increase the reliability of forecasting the environmental behavior of the observed items?

These and other problems can be solved by using a monitoring system based on combining the functions of environmental data acquisition, control of the data archives, data analysis, and forecasting the characteristics of the most important processes in the environment. In other words, this unification is the new information technology that combines the model of the functioning of typical geoecosystems, the computer cartography system, the means of artificial intelligence, and global environment observation systems. The latter results in creation of the geoinformation-monitoring system, which is capable of solving the problem of NSS sustainable development.

References

Aagard K. (ed.) (1998). *Proceedings of the ACSYS Conference on Polar Processes and Global Climate (Rosario, Orcas Island, WA, November 3–6, 1997)*. WCRP-106 (WMO/TD No. 908), Geneva. 307 pp.

Aagard K.; and Carmack E.C. (1994). The Arctic Ocean and climate: A perspective. *Geophysical Monograph 85, AGU, Washington, D.C.*, 5–20.

Abrahamson D.E. (1989). *Challenge of Global Warming*. Island Press, Washington, D.C., 376 pp.

ACIA (2000). *Arctic Climate Impact Assessment. Implementation Plan*. The Assessment Steering Committee, Alaska, Fairbanks, 35 pp.

ACIA (2001). *Report from the Arctic Climate Impact Assessment Modeling and Scenarios Workshop (Stockholm, Sweden, January 29–31, 2001)*. The ACIA Secretariat, Fairbanks, 28 pp.

ACSYS (1994). *Initial Implementation Plan*. WCRP-85 (WMO/TD No. 627), Geneva, Switzerland, 66 pp.

Adamenko V.N.; and Kondratyev K.Ya. (1999). Global climate changes and their empirical diagnostics. In: Yu.A. Izrael, G.V. Kalabin, and V.V. Nikonov (eds.), *Anthropogenic Impact on the Nature of the North and its Ecological Implications*. Kola Scientific Center, Russian Academy of Sciences, Apatity, pp. 17–34 [in Russian].

Agirre-Basurko E.; Ibarra-Berastegi, G.; and Madariaga I. (2006). Regression and multilayer perception-based models to forecast hourly O_3 and NO_2 levels in the Bilbao area. *Environmental Modelling & Software*, **21**(4), 430–446.

Aibulatov N.A. (2000). *Cold War Echo in the Russian Arctic Seas*. Geos, Moscow, 307 pp. [in Russian].

Alcamo J.; Bouwman A.; Edmonds J.; Grübler A.; Morita T.; and Sugandhy A. (1995). An Evaluation of the IPCC IS92 Emission Scenarios. In: J.T. Houghton, L.G. Meira Filho, J. Bruce, Hoesung Lee, B.A. Callander, E. Haites, N. Harris, and K. Maskell (eds.), *Climate Change 1994, Radiative Forcing of Climate Change and an Evaluation of the IPCC IS92 Emission Scenarios*. Cambridge University Press, Cambridge, U.K., pp. 233–304.

Alcano J.; Leemans R.; and Kreileman E. (eds.) (2001). *Global Change Scenarios of the 21st Century*. Elsevier, Amsterdam, 232 pp.

Alekseev G.V. (1998). Arctic climate dynamics in the global environment. *World Clim. Res. Progr./World Meteorol. Org., Geneva*, **908**, 11–14.

Alekseev V.V.; Kryshev I.I.; and Sazhykina T.G. (1992). *Physical and Mathematical Modeling of the Ecosystem*. Hydrometeoizdat, Sankt-Petersburg, 367 pp. [in Russian].

Alessio S.; Longhetto A.; and Richiardone R. (2004). Evolutionary spectral analysis of European climatic series. *Il Nuovo Cimento C.*, **27**(1), 73–98.

Alexandrov G.A.; Yamagata Y.; Saigusa N.; and Oikawa T. (2005). Long-term carbon exchange at aTakayama, Japan forest: Re-calibration of TsuBiMo with eddy-covariance measurements at Takayama. *Agricultural and Forest Meteorology*, **134**(1–4), 135–142.

Allen M. (2002). Climate of the twentieth century: Detection of change and attribution of causes. *Weather*, **57**(8), 296–303.

Allen M.R.; Stott P.A.; Mitchell J.F.B.; Schnur R.; and Delworth T.L. (1999). Uncertainty in Forecasts of Anthropogenic Climate Change. RAL Techn. Rept., No. RAL-TR-084, 10 pp.

Allen M.; Raper S.; and Mitchell J. (2001). Uncertainty in the IPCC's Third Assessment Report. *Science*, **293**(5529), 430–433.

Alley R.B.; Marotzke J.; Nordhaus W.D.; Overpeck J.T.; Peteet D.M.; Pielke Jr. R.A.; Pierrehumbert R.T.; Rhines P.B.; Stocker T.F.; Talley L.D.; and Wallace J.M. (2002). Abrupt climate change. *Science*, **299**(5615), 2005–2010.

Allison I.; Barry R.G.; and Goodison B.E. (eds.) (2001). *Climate and Cryosphere (CliC) Project Science and Co-Ordination Plan, Version 1*. WCRP-114 (WMO/TD No. 1053), Geneva, 73 pp.

Aloyan A.E. (2004). Numerical Modelling of Minor Gas Constituents and aerosols in the atmosphere. *Ecological Modelling*, **179**, 163–175.

Alverson K.D.; Oldfield F.; and Bradley R.S. (eds.) (2000). *Past Global Changes and Their Significance for the Future*. Pergamon Press, London, 479 pp.

Anderson T.L.; Charlson R.J.; Schwartz S.E.; Knutti R.; Boucher O.; Rodhe H.; and Heintzenberg J. (2003). Climate forcing by aerosols: A hazy picture. *Science*, **300**, 102–104.

Anderson P.; Petrino R.; Halpern P.; and Tintinalli J. (2006). The globalization of emergency medicine and its importance for public health. *Bulletin of the World Health Organization*, **84**(10), 835–839.

Ando K.; Matsumoto T.; Nagahama T.; Ueki I.; Takatsuki Y.; and Kuroda Y. (2005). Drift characteristics of a moored conductivity–temperature sensor and correction of salinity data. *J. Atmos. Oceanic Technol.*, **22**, 282–291.

Andrews M. (2004). Get healthy, get wealthy. *Money*, **33**(12), 57–58.

Angell J.K. (1999). Comparison of surface and tropospheric temperature trends estimated from a 63-station radiosonde network, 1958–1968. *Geophys. Res. Lett.*, **26**(17), 2761–2764.

Angell J.K. (2000a). Difference in radiosonde temperature trends for the period 1979–1998 of MSU data and the period 1959–1998 twice as long. *Geophys. Res. Lett.*, **27**(15), 2177–2180.

Angell J.K. (2000b). Tropospheric temperature variations adjusted for El Niño, 1958–1998. *J. Geophys. Res.*, **105**(D9), 11841–11849.

Angione R.J.; Medeiros E.J.;and Roosen R.G. (1976). Stratospheric ozone as viewed from the Chappuis band. *Nature*, **261**, 289–290.

Aota M.; Shirasawa K.; Krapivin V.F; and Mkrtchyan F.A. (1992). Simulation model of the Okhotsk Sea geoecosystem. *Proceedings of the 7th Int. Symp. on Okhotsk Sea & Sea Ice*

(February 2–5, 1992, Mombetsu, Japan). Okhotsk Sea & Cold Ocean Res. Assoc., Mombetsu, pp. 311–313.

Aota M.; Shirasawa K.; Krapivin V.F.; and Mkrtchyan F.A. (1993). A project of the Okhotsk Sea GIMS. *Proc. of the 8th Int. Sympos. on Okhotsk Sea & Sea Ice and ISY/Polar Ice Extent Workshop (February 1–5, 1993, Mombetsu, Japan)*. Okhotsk Sea & Cold Ocean Res. Assoc., Mombetsu, pp. 498–500.

APR (2006). *Global Environment Facility Annual Performance Report 2006*. Global Environment Facility, Washington, D.C., 89 pp.

ARCUS (1998a). *Toward an Arctic System Synthesis: Results and Recommendations*. Arctic Research Consortium of the United States, Fairbanks, Alaska, 165 pp.

ARCUS (1998b). *Toward Prediction of the Arctic System: Predicting Future States of the Arctic System on Seasonal-to-Century Time Scales by Interacting Observations, Process Research, Modeling, and Assessment*. Arctic Research Consortium of the United States, Fairbanks, Alaska, 54 pp.

Arneth A.; Kurbatova J.; Kolle O.; Shibistova O.B.; Lloyd J.; Vygodskaya N.; and Schulze E.-D. (2002). Comparative ecosystem–atmosphere exchange of energy and mass in a European Russian and a central Siberian bog, II. Interseasonal and interannual veriability of CO_2 fluxes. *Tellus*, **54B**(5), 514–530.

Arrhenius S. (1896). On the influence of carbonic acid in the air upon the temperature of the ground. *The London, Edinburgh and Dublin Philosophical Magazine and Journal of Sciences*, **41**, 237–276.

Arruda W.Z.; Lentini C.A.D.; and Campos E.J.D. (2005). The use of satellite derived upper ocean heat content to the study of climate variability in the South Atlantic. *Revista Brasileira de Cartografia*, **57**(2), 87–92.

Arutiunian V.O.; Aloyan A.E.; Chi J.; and Kuznetsov Yu.A. (2004). Numerical modeling of regional transport of gas components taking into consideration photochemical transformation. *Proceedings of RAS: Physics of the Atmosphere and Ocean*, **49**(4), 501–513 [in Russian].

Ashby W.R. (1956). *An Introduction to Cybernetics*. Chapman & Hall, London, 325 pp.

Aspinall R.; and Justice C. (2004). *A Land Use and Land Cover Change Science Strategy*. Summary of a Workshop held at the Smithsonian Institution, November 19–21, 2003. LUIWG, Washington, D.C., 20 pp.

Austin A.T.; Yahdjian L.; Stark J.M.; Belnap J.; Porporato A.; Norton U.; Ravetta D.A.; and Schaeffer S.M. (2004). Water pulses and biogeochemical cycles in arid and semiarid ecosystems. *Oecologia*, **141**, 221–235.

Avery G.B.; Kieber R.J.; Willey J.D.; Shank G.C.; and Whitehead R.F. (2004). Impact of hurricanes on the flux of rainwater and Cape Fear River water dissolved organic carbon to Long Bay, southeastern United States. *Global Biogeochemical Cycles*, **18**(GB3085), doi:10.1029/2004GB002229.

Babu S.S.; Moorthy K.K.; and Satheesh S.K. (2004). Aerosol black carbon over Arabian Sea during intermonsoon and summer monsoon seasons. *Geophys. Res. Lett.*, **31**(6), LOG104/1–LOG104/5.

Bacastow R. (1981). Numerical evaluation of the evasion factor. In: Bolin B. (ed.), *Carbon Cycle Modelling*, SCOPE-16. Wiley, New York, pp. 95–101.

Baker D.F.; Law R.M.; Gurney K.R.; Rayner P.; Peylin P.; Denning A.S.; Bousquet P.; Bruhwiler L.; Chen Y.-H.; Ciais P.; Fung I.Y.;Heimann M.; John J.; Maki T.; Maksyutov S.; Masarie K.; Prather M.; Pak B.; Taguchi S.; and Zhu Z. (2006). TransCom 3 inversion intercomparison: Impact of transport model errors on the interannual variability of

regional CO_2 fluxes, 1988–2003. *Global Biogeochemical Cycles*, **20**(GB1002), doi: 10.1029/2004GB002439.

Baltensperger U.; Barrie L.; and Wehrli C. (eds.) (2005). *WMO/GAW Experts Workshop on a Global Surface-Based Network for Long Term Observations of Column Aerosol Optical Properties (Davos, Switzerland, March 8–10, 2004)*. WMO Publ., Davos, Switzerland, 148 pp.

Bampfylde C.J.; Brown N.D.; Gavaghan D.J.; and Maini P.K. (2005). Modelling rain forest diversity: The role of competition. *Ecological Modelling*, **188**(2–4), 253–278.

Barbieri A.F.; and Carr D.L. (2005). Gender-specific out-migration, deforestation and urbanization in the Ecuadorian Amazon. *Global and Planetary Change*, **47**(2–4), 99–110.

Bard S. (1999) Global transport of anthropogenic contaminants and the consequences for the Arctic marine ecosystems. *Marine Pollution Bulletin*, **38**(5), 356–379.

Barenbaum A.A. (2000). Selforganizing mechanisms in global geochemical cycle of the substance on the Earth. *Synergetics*, **3**, 275–295 [in Russian].

Barenbaum A.A. (2002). *Galaxy, Solar System, Earth*. Geos, Moscow, 392 pp. [in Russian].

Barenbaum A.A. (2004). Mechanism for the formation of oil and gas accumulations. *Proceedings of Russian Academy of Sciences*, **399**(6), 802–805 [in Russian].

Barnett T.P.; Pierce D.W.; and Schnur R. (2001). Detection of anthropogenic climate change in the World's Oceans. *Science*, **292**(5515), 270–274.

Barnett V. (2003). *Environmental Statistics: Methods and Applications*. Wiley, London, 320 pp.

Baron P.A.; and Willeke K. (2001). *Aerosol Measurement: Principles, Techniques, and Applications*. Wiley, Washington, D.C., 226 pp.

Barr J.G.; Fuentes J.D.; and Bottenheim J.W. (2003). Radiative forcing of phytogenic aerosols. *J. Geophys. Res.*, **108**(D15), ACH15/1–ACH15/3.

Bartsev S.I.; Degermendzhy A.G.; and Erokhin D.V. (2003). Global generalized models of carbon dioxide dynamics. *Problems of the Environment and Natural Resources*, **12**, 11–28 [in Russian].

Baskent E.Z.; and Keles S. (2005). Spatial forest planning: A review. *Ecological Modelling*, **188**(2–4), 145–173.

Bazhin N.M. (2000). Methane emission from a residual layer. *Proceedings of the Second Int. Methane Mitigation Conference (June 18–23, 2000, Novosibirsk)*. Novosibirsk State University Publ., Novosibirsk, pp. 231–236.

Bazilevich N.I.; and Rodin L.E. (1967). The map-schemes of productivity and of the biological cycle of the most significant types of land vegetation. *Bulletin of the All-Union Geographical Society*, **99**(3), 190–194 [in Russian].

Bazzaz F.A. (1986). Global CO_2 levels and the response of plants at the population and community levels. In: C. Rozenzweig and R. Dickinson (eds), *Climate–Vegetation Interactions*. UCAR, Maryland, pp. 31–35.

Beever D.; Brentrup F.; Eveilard P.; Fixen P.; Heffer P.; Herz B.; Larson R.; and Pallière C. (2007). *Sustainable Management of the Nitrogen Cycle in Agriculture and Mitigation of Reactive Nitrogen Side Effects*. IFA, Paris, 32 pp.

Bekoryukov V.I.; and Fedorov V.V. (1987). Empirical model of total ozone content above the Southern Hemisphere. *Meteorology and Hydrology (Moscow)*, **3**, 47–53 [in Russian].

Bellman R.; and Dreyfus S. (1962). *Applied Dynamic Programming*. Princeton University Press, Princeton, NJ, 457 pp.

Bellman R.E.; and Roth R.S. (1966). A technique for the analysis of a broad class of biological systems. In: H.C. Oestreicher and D.R. Moore (eds.), *Cybernetic Problems in Bionics*. Gordon & Breach, New York, pp. 725–737.

Bengtsson L. (1999). Climate modelling and prediction: Achievements and challenges. *WCRP/WMO Publ.*, **954**, 59–73.

Berger U.; and Dameris M. (1993). Cooling of the upper atmosphere due to CO_2 increases: A model study. *Ann. Geophys.*, **11**(9), 809–819.

Beyer A.; and Matthies M. (2001). Long-range transport potential of semivolatile organic chemicals in coupled air–water systems. *Environ. Sci. & Pollut. Res.*, **8**(3), 173–179.

Bhatti J.; Lal R.; Apps M.; and Price M. (2006). *Climate Change and Managed Ecosystems*. Taylor & Francis/CRC, Boca Raton, 446 pp.

Bichele I.; Moldau H.; and Ross Yu. (1980). *Sub-model for the Assimilation, Distribution, and Vegetation Growth under Condition of Water Deficit*. Tartu Astrophysical Observatory, Report A-5, Tartu, 22 pp. [in Russian].

Bjorkstrom A. (1979). A model of CO_2 interaction between atmosphere, ocean and land biota. In: *Global Carbon Cycle*, SCOPE-13. Wiley, New York, pp. 403–458.

Blanchard F.; and Boucher J. (2002). Présence d'espèces tropicales de poissons dans l'Atlantique Nord et réchauffement climatique. *French IGBP-WCRP-News Lett.*, **12**, 3536.

Boden T.A.; Kaiser D.P.; Speranski R.J.; and Stoss F.W. (1994). *TREND's 93: A compendium of data on global change*. Carbon Dioxide Informational Analysis Center, Oak Ridge Nat. Lab., Oak Ridge, 176 pp.

Bodenbender J.; Wassmann R.; Papen H.; and Rennenberg H. (1999). Temporal and spatial variation of sulfur–gas transfer between coastal marine sediments and the atmosphere. *Atmospheric Environment*, **33**(21), 3487–3502.

Bodri L.; and Čermák V. (1999). Climate change of last millenium inferred from borehole temperatures: Regional patterns of climate changes in the Czech Republic. Part III. *Global and Planet. Change*, **21**(4), 225–235.

Boehmer-Christiansen S.A. (1997). Who is driving climate change policy? *IEA Stud. Educ.*, **10**, 53–72.

Boehmer-Christiansen S.A. (2000). Who determines the policy concerning climate changes and how is it done? *Bulletin of the Russian Geographical Society*, **132**(3), 6–22 [in Russian].

Boehmer-Christiansen S.A. (2002). Keywords investing against climate change: Why failure remains possible. *Environmental Politics*, **11**(3), 1–30.

Boehmer-Christiansen S.A.; and Kellow A. (2002). *International Environmental Policy: Interests and the Failure of the Kyoto Protocol*. Edward Elgar, Cheltenham, U.K., 214 pp.

Bolin B. (1999). Global environmental change and the need for international research programmes. *WCRP/WMO, WMO/TD*, **954**, 11–14.

Bolin B. (2004). Climate and science knowledge and understanding necessary to act in uncertain conditions (with the accent on reasonable and uncontradictory results). *Proceedings of the All-World Conference on Climate Change (September 29–October 3, 2003, Moscow)*. Gidrometeoizdat, Moscow, pp. 40–46 [in Russian].

Bolin R.; and Sukumar R. (2000). Global perspective. In: R. Watson, I.R. Noble, B. Bolin, N.H. Ravindranath, D.J. Verardo, and D.J. Dokken (eds.), *Land Use, Land-Use Change, and Forestry*. Cambridge Univ. Press, Cambridge, pp. 23–51.

Borisenkov E.P. (2003). The greenhouse effect. Problems, myths, reality. *Astrakhan Herald of Ecological Education*, **1(5)**, 5–12 [in Russian].

Borodin L.F.; and Gordina L.I. (1983). An algorithm of randomized line-broken approximation. In: N.A. Armand (ed.), *Statistical Methods for the Data Processing of Environmental Remote Sensing*. IREE Publ., Moscow, pp. 100–104 [in Russian].

Borodin L.F.; and Krapivin V.F. (1998). Remote measurements of the Earth's surface characteristics. *Problems of the Environment and Natural Resources*, **7**, 38–54 [in Russian].

Borodin L.F.; Valendik E.N.; and Mironov A.S. (1978). SHF-radiophysical methods and the problems of forest and peat fires. *Radiotechnics and Electronics*, **10**, 1121–1129 [in Russian].

Borodin L.F.; Krapivin V.F.; and Bui T.L. (1996). Application of GIMS-technology to monitor the Aral–Caspian aquageosystem. *Problems of the Environment and Natural Resources*, **10**, 46–61 [in Russian].

Bowen D.Q. (2000). Tracing climate evolution. *Earth Heritage*, Issue Mill., 8–9

Boysen M. (ed.) (2000). *Biennial Report 1998 & 1999*. Potsdam Institute for Climate Impact Research, Potsdam, 130 pp.

BP (2005). *Putting Energy in the Spotlight*. BP Statistical Review of World Energy, London, 44 pp.

BP (2007). *BP Statistical Review of World Energy June 2007*. British Petroleum, London, 48 pp.

Bras R.L. (1990). *Hydrology*. Addison-Wesley, New York, 643 pp.

Brasseur G.P. (2005). *Aeronomy of the Middle Atmosphere: Chemistry and Physics of the Stratosphere and Mesosphere*. Springer-Verlag, Berlin, 644 pp.

Bratcher A.J.; and Giese B.S. (2002). Tropical Pacific decadal variability and global warming. *Geophysical Research Letters*, **29(19)**, 1918–1924.

Brenguier J.-L. (2003). Introduction to special section: An experimental study of the aerosol indirect effect for validation of climate model parameterizations. *J. Geophys. Res.*, **108**(D15), CMP1/1–CMP1/3.

Brenguier J.-L.; Pawlowska H.; and Schüller L. (2003). Cloud microphysical and radiative properties for parameterization and satellite monitoring of the indirect effect of aerosol on climate. *J. Geophys. Res.*, **108**(D15), CMP6/1–CMP6/14.

Bréon F.M.; and Doutriaux-Boucher M. (2005). A comparison of cloud droplet radii measured from space. *IEEE Trans. Geosci. Remote Sensing*, **43**, 1796–1805

Bricker S.B.; Clement C.G.; Pirhalla D.E.; Orlando S.P.; and Farrow D.R.G. (1999). *National Estuarine Eutrophication Assessment: Effects of Nutrient Enrichment in the Nation's Estuaries*. NOAA, National Ocean Service, Special Projects Office and the National Centers for Coastal Ocean Science, Silver Spring, MD, 71 pp.

Broecker W.S. (2003). Does the trigger for abrupt climate change reside in the ocean or in the atmosphere? *Science*, **300**(5625), 1519–1522.

Brooks S.D.; Garland R.M.; Wise M.E.; Prenni A.J.; Cushing M.; Hewitt E.; and Tolbert M.A. (2003). Phase changes in internally mixed maleic acid/ammonium sulphate. *J. Geophys. Res.*, **108**(D15), ACH23/1–ACH23/10.

Bruntland G. (ed.) (1987). *Our Common Future: The World Commission on Environment and Development*. Oxford University Press, Oxford, U.K., 318 pp.

Buesseler K.O.; Steinberg D.K.; Michaels A.F.; Johnson R.J.; Andrews J.E.; Valdes J.R.; and Price J.F. (2000). A comparison of the quantity and composition of material caught in a neutrally buoyant versus surface-tethered sediment trap. *Deep-Sea Res. I*, **47**, 277–294.

Bui K.N. (2001). Simulation system for mesoscale hydrophysical experiments. *Actual Problems of Present Science*, **3**, 132–141 [in Russian].

Bui K.N.; and Ambrosimov A.K. (2001). Model of anthropogenic impacts on the ecosystem of Vietnam's lagoons. *Problems of Present Science*, **3**, 119–128 [in Russian].

Bukatova I.L.; Michasev Yu.I.; and Sharov A.M. (1991). *Evoinformatics: Theory and Experience of Evolutionary Modeling*. Science Publ., Moscow, 205 pp. [in Russian].

Bunyard P. (1999). Eradicating the Amazon rainforest will wreak havoc on climate. *Ecologist*, **29(2)**, 81–84.

Burgheimer J.; Wilske B.; Maseyk K.; Karnieli A.; Zaady E.; Yakir D.; and Kesselmeier J. (2006). Ground and space spectral measurements for assessing the semi-arid ecosystem

phenology related to CO_2 fluxes of biological soil crusts. *Remote Sensing of Environment*, **101**(1), 1–12.

Busch U.; Beckmann B.-R.; and Roth R. (1998). Study of storm weather situations in observation and ECHAM3/T42 model simulation. *Tellus A*, **50**(4), 411–423.

Byakola T. (2000). Technological options and policy measures for methane mitigation in Uganda: Possibilities and limitations. *Proceedings of the Second International Methane Mitigation Conference (June 18–23, 2000, Novosibirsk)*. Novosibirsk State University, Novosibirsk, pp. 95–100.

Cai W.; and Whetton P. H. (2002). Evidence for a time-varying pattern of greenhouse warming in the Pacific Ocean. *Geophys. Res. Lett.*, **27**(16), 2577–2580.

Canadel I.G.; Dickinson R.; Hibbard K.; Raupach M.; and Young O. (eds.) (2003). *Global Carbon Project: The Science Framework and Implementation*, Report No. 1. Earth System Science Partnership, Canberra, 69 pp.

CCSP (2004). *Our Changing Planet: The U. S. Climate Change Science Program for Fiscal Years 2004 and 2005*. A Report by the Climate Change Science Program and the Subcommitee on Global Change Program, Washington, D.C., 159 pp.

Cech T.V. (2004). *Principles of Water Resources: History, Development, Management, and Policy*. Wiley, Amsterdam, 480 pp.

Chahine M.T. (1992). The hydrological cycle and its influence on climate. *Nature (U.K.)*, **359**(6394), 373–380.

Chamberlain J.W.; and Hunten D.M. (1986). *Theory of Planetary Atmospheres: An Introduction to Their Physics and Chemistry*, International Geophysics Series. Academic Press, San Diego, 481 pp.

Chance K. (2005). Ultraviolet and visible spectroscopy and spaceborne remote sensing of the Earth's atmosphere. *Comptes Rendus Physique*, **6**, 836–847.

Chang C.-P.; Zhang Y.; and Li T. (2000). Interannual and interdecadal variations of the East Asian summer monsoon and tropical Pacific SSTs. Part 1: Roles of the subtropical ridge. *J. Climate*, **13**, 4310–4325.

Chapin III S.F.; Matson P.A.; and Mooney H.A. (2002). *Principles of Terrestrial Ecosystem Ecology*. Springer-Verlag, New York, 464 pp.

Chapman W.L.; and Walsh J.E. (1993). Recent variations of sea ice and air temperatures in high latitudes. *Bulletin of the American Meteorological Society*, **74**, 33–47.

Charlock T.P.; Rose F.G.; Rutan D.A.; Alberta T.L.; Kratz D.P.; Coleman L.H.; Smith G.L.; Manalo-Smith N.; and Bess T.D. (1997). *Compute Surface and Atmospheric Fluxes (System 5.0)*. CERES Algorithm Theoretical Basis Document, CERES Publ., Hampton, VA, 84 pp.

Charlson R.J.; Seinfeld S.H.; Nenes A.; Külmälä M.; Laaksonen A.; and Facchini M.C. (2001). Reshaping the theory of cloud formation. *Science*, **292**(5524), 2025–2026.

Chédin A.; Hollingsworth A.; Scott N.A.; Serrar S.; Crevoisier C.; and Armante R. (2002). Annual and seasonal variations of atmospheric CO_2, N_2O and CO concentrations retrieved from NOAA/TOVS satellite observations. *Geophys. Res. Letters*, **29**, 110–114.

Chen W.; Chen J.; and Cihlar J. (2000). An integrated terrestrial ecosystem carbon-budget model based on changes in disturbance, climate, and atmospheric chemistry. *Ecological Modelling*, **135**(1), 55–79.

Chen Z.; Ivanov P.C.; Hu K.; and Stanley H.E. (2002). Effect of nonstationarities on detrended fluctuation analysis. *Physical Review*, **E65**(4), art. no. 041107.

Chen J.M.; Liu J.; Leblanc S.G.; Lacaze R.; and Roujean J.-L. (2003). Multi-angular optical remote sensing for assessing vegetation structure and carbon absorption. *Remote Sensing of Environment*, **84**(4), 516–525.

Chen Z.; Hu K.; Carpena P.; Bernaola-Galvan P.; Stanley H.E.; and Ivanov P. (2005). Effect of nonlinearities on detrended fluctuation analysis. *Physical Review*, **E71**, art. no. 011104.

Chiesi M.; Maselli F.; Bindi M.; Fibbi L.; Cherubini P.; Arlotta E.; Tirone G.; Matteucci G.; and Seufert G. (2005). Modelling carbon budget of Mediterranean forests using ground and remote measurements. *Agricultural and Forest Meteorology*, **135**(1–4), 22–34.

Chin M.; Ginoux P.; Kinne S.; Holben B.N.; Duncan B.N.; Martin R.V.; Logan J.A.; Higurashi A.; and Nakajima T. (2002). Tropospheric aerosol optical thickness from the GOCART model and comparisons with satellite and sunphotometer measurements. *J. Atmos. Sci.*, **59**, 461–483.

Chinlon L. (ed.) (1989). *Optoelectronic Technology and Lightwave Communications Systems*. Van Nostrand Reinhold, New York, 766 pp.

Chock D.P.; and Winkler S.L. (2000). A trajectory–grid approach for solving the condensation and evaporation equations of aerosols. *Atmospheric Environment*, **34**(18), 2957–2973.

Choi S.-D.; and Chang Y.-S. (2006). Carbon monoxide monitoring in Northeast Asia using MOPITT: Effects of biomass burning and regional pollution in April 2000. *Atmospheric Environment*, **40**(4), 686–697.

Choi Y.; Wang Y.; Zeng T.; Martin R.V.; Kurosu T.P.; and Chance K. (2005). Evidence of lightning Nox and convective transport of pollutants in satellite observations over North America. *Geophys. Res. Lett.*, **32**(L02805), 1–5, doi:10.1029/2004GL021436.

Chou M.-D.; Chan P.K.; and Wang M. (2002). Aerosol radiative forcing derived from SeaWiFS-retrieved aerosol optical properties. *J. Atmos. Sci.*, **59**(3), 748–757.

Christensen J.H. (1997). The Danish Eulerian hemispheric model: A three-dimensional air pollution model used for the Arctic. *Atmospheric Environment*, **31**(24), 4169–4191.

Christy J.R. and Spencer R.W. (2003). Reliability of satellite data sets. *Science*, **301**(5636), 1046–1047.

Christy J.R.; Spencer R.W.; and Lobl E.S. (1998). Analysis of the merging procedure for the MSU daily temperature time series. *J. Climate*, **11**, 2016–2041.

Chuang Y.-L.; Oren R.; Bertozzi A.L.; Phillips N.; and Katul G.G. (2006). The porous media model for the hydraulic system of a conifer tree: Linking sap flux data to transpiration rate. *Ecological Modelling*, **191**(3–4), 447–468.

Chukhlantsev A.A. (2006). *Microwave Radiometry of Vegetation Canopies*. Springer-Verlag, Berlin, 287 pp.

Chýlek P.; Henderson B.; and Mushchenko M. (2003). Aerosol radiative forcing and the accuracy of satellite aerosol optical depth retrieval. *J. Geophys. Res.*, **108**(D24), AAC4/1–AAC4/8.

Coconea G. (2000). Methane gas emissions from the Romanian natural gas transport system. *Proceedings of the Second International Methane Mitigation Conference (June 18–23, 2000, Novosibirsk)*. Novosibirsk State University Publ., Novosibirsk, pp. 297–302.

Cole R. (1988). Parallel merge sort. *SIAM Journal on Computing*, **17**(4), 770–785.

Collatz G.J.; Berry J.A.; Farquhar J.A.; and Pierce J. (1990). The relationship between the rubisco reaction mechanism and models of leaf photosynthesis. *Plant Cell Environment*, **13**, 219–225.

Collatz G.J.; Ball G.J.; Grivet J.T.; and Berry J.A. (1991). Physiological and environmental regulation of stomatal conductance, photosynthesis and transpiration: A model that includes a laminar boundary layer. *Agricultural and Forest Meteorology*, **54**, 107–136.

Collatz G.J.; Ribas-Carbo M.; and Berry J.A. (1992). Coupled photosynthesis stomatal conductance model for leaves of C_4 plants. *Aust. J. Plant Physiol.*, **19**, 519–538.

Collatz G.J.; Bounoua L.; Los S.O.; Rondell D.A.; Fung I.F.; and Sellers P.J. (2000). A mechanism for the influence of vegetation on the response of the diurnal temperature range to changing climate. *Geophys. Res. Lett.*, **27**(20), 3381–3384.

Collins M.; and Senior C. A. (2002). Projections of future climate change. *Weather*, **57**(8), 283–287.

Cooper L.; and Romanovsky V. (2001). RAISE Plan focuses on ship-based research in Russia. *Witness the Arctic*, **9**(1), 7–8.

Corcoran P.B. (ed.) (2005). *Toward a Sustainable World: The Earth Charter in Action*. Royal Tropical Institute Publ., The Netherlands, 192 pp.

Cordova A.M.; Longo K.; Freitas S.; Gatti L.V.; Artaxo P.;Procópio A.; Silva Dias M.A.F.; and Freitas E.D. (2004). Nitrogen oxides measurements in an Amazon site and enhancements associated with a cold front. *Atmos. Chem. Phys. Discuss.*, **4**, 2301–2331.

Corstanje R.; and Reddy K.R. (2004). Response of Biogeochemical Indicators to a Drawdown and Subsequent Reflood. *J. Environ. Qual.*, **33**, 2357–2366.

Cosca C.E.; Feely R.A.; Boutin J.; Ercheto J.; McPhaden M.J.; Chavez F.P.; and Strutton P.J. (2003). Seasonal and interannual CO_2 fluxes for the central and eastern equatorial Pacific Ocean as determined from fCO_2–SST relationships. *J. Geophysical Research*, **108**, doi:10.1029/2000JC000677.

Cox G.W. (1985). *Measurement of Species Diversity*. Laboratory of General Ecology, IA/W.C. Brown Publisher, Dubuque, pp. 163–167.

Cozzi L. (2003). *World Energy Outlook Insights: Global Energy Investment Outlook*. IEA, Paris, 20 pp.

CRC (2005). *Cooperative Centre for Catchment Hydrology, Annual Report 2004–2005*. CRC Press, Clayton Campus, Australia, 124 pp.

Crowley T.J. (2000). Causes of climate change over the past 1000 years. *Science*, **289**(5477), 270–277.

Crowley T.J.; and Kim K. (1994). Milankovitch forcing of the last interglacial sea level. *Science*, **265**, 1565–1568.

Cuffney T.F.; Meador M.R.; Porter S.D.; and Gurtz M.E. (2000). Responses of Physical, Chemical, and Biological Indicators of Water Quality to a Gradient of Agricultural Land Use in the Yakima River Basin, Washington. *Environmental Monitoring and Assessment*, **64**(1), 259–270.

Dameris M.; Grewe V.; Ponater M.; Deckert R.; Eyring V.; Mager F.; Matthes S.; Schnadt C.; Stenke A.; Steil B.; Bruhl C.; and Giorgetta M. A. (2005). Long-term changes and variability in a transient simulation with a chemistry–climate model employing realistic forcing. *Atmospheric Chemistry and Physics*, **5**, 2121–2145.

Dan L.; Ji J.; and Li Y. (2005). Climatic and biological simulations in a two-way coupled atmosphere–biosphere model (CABM). *Global and Planetary Change*, **47**(2–4), 153–169.

Dansgaard W.; Johnsen S.J.; Clausen H.B.; Dahl-Jensen D.; Gundestrup N.S.; Hammer C.U.; Hvidberg C.S.; Steffensen J.P.; Sveinbjörnsdottir A.E.; Jouzel J.; and Bond G. (1993). Evidence for general instability of past climate from a 250-kyr ice-core record. *Nature*, **364**, 218–220.

Darcy H. (1856). *Les fontaines publiques de la Ville de Dijon*. Dalmont, Paris, 647 pp.

Davi H.; Dufrêne E.; Granier A.; Le Dantec V.; Barbaroux C.; François C.; Bréda N.; and Montpied P. (2005). Modelling carbon and water cycles in a beach forest. Part II: Validation of the main processes from organ to stand scale. *Ecological Modelling*, **185**(2–4), 387–405.

Dearden P.; and Mitchel B. (2005). *Environmental Change and Challenge: A Canadian Perspective*, Second Edition. Oxford University Press, London, 512 pp.

Degermendzhy A.G. (1987). Objective laws of mixed culture formations under aquatic ecosystem modelling (taking the example of Krasnoyarsk Reservoir). PhD dissertation thesis, Krasnoyarsk University, 511 pp. [in Russian].

Degermendzhy A.G. (2008). New directions in biophysical ecology. In: A.P. Cracknell, V.F. Krapivin, and C.A. Varotsos (eds.), *Problems of Global Climatology and Ecodynamics*. Springer/Praxis, Chichester, U.K., pp. 198–214.

Degermendzhy A.G.; and Bartsev S.I. (2003). Global small-scale models of dynamics and stability of the biosphere. *Problems of the Environment and Natural Resources*, **7**, 32–49.

Delvich K. (1972). Nitrogen cycle. In: M.S. Gilyarov (ed.), *Biosphere*. Mir Publ., Moscow, pp. 105–119 [in Russian].

Delworth T.L.; and Knutson T.R. (2000). Simulation of early 20th century global warming. *Science*, **287**(5461), 2246–2250.

Dementjeva T.V. (2000). Emission of gases from peat-bog ecosystems. *Proceedings of the Second International Methane Mitigation Conference (June 18–23, 2000, Novosibirsk)*. Novosibirsk State University Publ., Novosibirsk, pp. 223–226.

Demirchian K.S.; and Kondratyev K.Ya. (1999). Scientific basis for predictions on the influence of energy on climate. *Proceedings of Russian Academy of Sciences, Energy*, **6**, 3–46 [in Russian].

Demirchian K.S.; Demirchian K.K.; Danilevich Ya.B.; and Kondratyev K.Ya. (2002). Global climate warming, energetics and geopolicy. *Annals of RAS, Energy*, **3**, 221–235 [in Russian].

Denzer R.; Riparbelli C.; Villa M.; and Güttler R. (2005). Environmental knowledge and Information Systems GIMMI: Geographic information and mathematical models inter-operability. *Environmental Modelling & Software*, **20**(12), 1478–1485.

De Rosnay P.; Bruen M.; and Polcher J. (2000). Sensitivity of surface fluxes to the number of layers in the soil model used in GCMs. *Geophys. Res. Lett.*, **27**(20), 3329–3332.

Derwent R.G.; Collins W.J.; Johnson C.E.; and Stevenson D.S. (2001). Transient behaviour of tropospheric ozone precursors in a global 3-D CTM and their indirect greenhouse effects. *Clim. Change*, **49**(4), 463–487.

Dessler E.A.; and Parson E.A. (2005). *The Science and Politics of Climate Change: A Guide to the Debate*. Cambridge University Press, Cambridge, U.K., 324 pp.

Dickson R. (1999). All change in the Arctic. *Nature*, **397**, 389–391.

Dimitroulopoulou C.; and Marsh A.R.W. (1997). Modelling studies of NO_3 night-time chemistry and its effects on subsequent ozone formation. *Atmospheric Environment*, **31**(18), 3041–3057.

Dong L.B. (2004). *The Behrens–Fisher Problem: An Empirical Likelihood Approach*. Econometrics Working Paper EWP0404, University of Victoria, Victoria, Canada, 30 pp.

Dufrêne E.; Davi H.; François C.; le Maire G.; Le Dantec V.; and Granier A. (2005). Modelling carbon and water cycles in a beach forest. Part I: Model description and uncertainty analysis on modelled NEE. *Ecological Modelling*, **185**(2–4), 407–436.

Dulnev G.N.; and Ushakovskaya E.D. (1988). Analysis of the influence exerted by physicogeometric parameters on the temperature field of an object. *J. of Engineering Physics and Thermophysics*, **57**(6), 1487–1492.

Dunn C.F. (2007). *Biogeochemistry in Mineral Exploration*. Elsevier Science, Berlin, 464 pp.

Ebel A. (2001). Evaluation and reliability of meso-scale air pollution simulations. *Lect. Notes Comput. Sc.*, **2179**, 255–263.

Egan W.G.; Hogan A.W.; and Zhu H. (1991). Physical variation of water vapor, and the relation with carbon dioxide. *Geophys. Res. Lett.*, **18**(12), 2245–2248.

EIA (2005). *International Energy Outlook 2005*. DOE/EIA-0484, Washington, D.C., 194 pp.

El-Askary M.; Sarkar S.; Kafatos M.; and El-Ghazawi T. (2003). A multisensor approach to dust storm monitoring over the Nile Delta. *IEEE Transaction on Geoscience and Remote Sensing*, **41**(10), 2386–2391.

Elsaesser H.W. (2001). *The Current Status of Global Warming*. Marshall Institute Publ., Washington, D.C., 5 pp.

Enz R. (ed.) (2006). Natural catastrophes and man-made disasters: High earthquake casualties, new dimension in windstorm losses. *Sigma*, **2**, 1–40.

EPA (2001). *Non-CO_2 Greenhouse Gas Emissions from Developed Countries: 1990–2010*, EPA-430-R-01-007. U.S. Environmental Protection Agency, Washington, D.C., 132 pp.

EPA (2005). *Proceedings of EPA Science Forum 2005: Collaborative Science for Environmental Solutions (May 16–18, 2005, Washington)*. EPA, Washington, D.C., 162 pp.

EPA (2006). *Inventory of U.S. Greenhouse Gas Emissions and Sinks: 1990–2004*, Report No. EPA 430-R-06-002. U.S. Environmental Protection Agency, Washington, D.C., 459 pp.

Eriksson E. (1963). The yearly circulation of sulfur in nature. *J. of Geophys. Res.*, **68**, 4001–4007.

ESI (2005). *2005 Environmental Sustainability Index*. Yale Center for Environmental Law and Policy, New Haven, USA, 414 pp.

Essex C.; and McKitrick R. (2002). *Taken by Storm: The Troubled Science, Policy and Politics of Global Warming*. Key Porter Books, Toronto, 320 pp.

Everett J.T.; and Fitzharris B.B. (eds.) (2001). *The Regional Impacts of Climate Change. Chapter 3: The Arctic and Antarctic*. IPCC-2001 (*http://www.grida.no/climate/ipcc/regional/042.htm*).

Everett J.T.; Okemwa E.; Regier H.A.; Troadec J.P.; Krovnin A.; and Lluch-Belda D. (1995). Fisheries. In: Watson R.T., Zinyowera M.C., and Moss R.H. (eds.), *The IPCC Second Assessment Report. Volume 2: Scientific-technical Analyses of Impacts, Adaptations, and Mitigation of Climate Change*. Cambridge University Press, Cambridge, pp. 1–31.

Eyring V.; Harris N.R.P.; Rex M.; Shepherd T.G.; Fahey D.W.; Amanatidis G.T.; Austin J.; Chipperfield M.P.; Dameris M.; Forster P.M.F.; Gettelman A.; Graf H.F.; Nagashima T.; Newman P.A.; Pawson S.; Prather M.J.; Pyle J.A.; Salawitch R.J.; Santer B.D.; and Waugh D.W. (2005). A strategy for process-oriented validation of coupled chemistry–climate models. *Bulletin of the American Meteorological Society*, **86**(8), 1117.

Falkowski P.G. (1997). Evolution of nitrogen cycle and its influence on the biological sequestration of CO_2 in the ocean. *Nature*, **387**, 272–275.

Fang J.; Chen A.; Peng C.; Zhao S.; and Ci L. (2001). Changes in forest biomass carbon storage in China between 1949 and 1998. *Science*, **292**, 2320–2322.

Fankhauser S. and Tol R.S.J. (1997). The social costs of climate change: The IPCC second assessment report and beyond. *Mitigation and Adaptation Strategies for Global Change*, **1**(4), 385–403.

FAO (2006). *State of Food and Agriculture 2006: Food Aid for Food security?* FAO Agriculture Series No. 37, Rome, 180 pp.

Fasham M.J.R. (ed.) (2003). *Ocean Biogeochemistry*. Springer-Verlag, Berlin, 283 pp.

Feczkó T.; Molnár Á.; Mészáros E.; and Major G. (2002). Regional climate forcing of aerosol estimated by a box model for a rural site in Central Europe during summer. *Atmospheric Environment*, **36**, 4125–4131.

Feingold G. (2003). Modeling of the first indirect effect: Analysis of measurement requirements. *Geophys. Res. Lett.*, **30**(19), ASC7/1–ASC7/4.

Feingold G.; Eberhard W.L.; Veron D.E.; and Previdi M. (2003). First measurements of the Twomey indirect effect using ground-based remote sensors. *Geophys. Res. Lett.*, **30**(6), 20/1–20/4.

Felzer B.; Kicklighter D.W.; Melillo J.M.; Wang C.; Zhuang Q.; and Prinn R. (2004). Effects of Ozone on Net Primary Production and Carbon Sequestration in the Conterminous United States using a Biogeochemistry Model. *Tellus*, **56B**, 230–248.

Fenoglio S.; Badino G.; and Bona F. (2002). Benthic macroinvertebrate communities as indicators of river environment quality. *Revista de Biología Tropical*, **50**(3–4), 1125–1131.

Fiebig M.; Petzold A.; Wandlinger U.; Wendisch M.; Kiemle C.; Stifter A.; Ebert M.; Rother T.; and Leiterer U. (2002). Optical closure for an aerosol column: Method, accuracy, and inferable properties applied to a biomass-burning aerosol and its radiative forcing. *J. Geophys. Res.*, **107**(D21), LAC11/1–LAC11/13.

Field C.B.; and Raupach M.R. (eds.) (2004). *Global Carbon Cycle: Integrating Humans, Climate, and the Natural World*. Island Press, Washington, D.C., 584 pp.

Field J.G.; Hempel G.; and Summerhayer C.P. (eds.) (2002). *Oceans 2020: Science Trends and the Challenge of Sustainability*. Island Press, Washington, D.C., 296 pp.

Fierer N.; Allen A.S.; Schimel J.P.; and Holden P.A. (2003). Controls on microbial CO_2 production in surface and subsurface soil horizons. *Global Change Biology*, **9**, 1322–1332.

Filatov N.N. (2004). *Climate of Karelia: Changeability and Influence on Water Objects and Reservoirs*. Karelian Scientific Center of RAS, Petrozavodsk, 224 pp. [in Russian].

Fitzwater S.E.; Johnson K.S.; Elrod V.A.; Ryan J.P.; Colletti L.J.; Tanner S.J.; Gordon R.M.; and Chavez F.P. (2003). Iron, nutrient and phytoplankton biomass relationships in upwelling waters of the California coasts system. *Continental Shelf Research*, **23**, 1523–1544.

Folland C.; Frich P.; Basnett T.; Rayner N.; Parker D.; and Horton B. (2000). Uncertainties in climate datasets: A challenge for WMO. *WMO Bull.*, **49**(1), 59–68.

Folland C.K.; Karl T.R.; and Salinger M.J. (2002). Observed climate variability and change. *Weather*, **57**(3), 269–278.

Follows M.J.; Ito T.; and Dutkiewicz S. (2006). On the solution of the carbonate chemistry system in ocean biogeochemistry models. *Ocean Modelling*, **12**(3–4), 290–301.

Fortmann M. (2004). Zum Einfluss troposphärischer Aerosole auf das Klima der Arktis. *Ber. Polar- und Meeresforsch.*, **486**(I–II), 1–142.

Fourie G.; Djolov G.; Syrakov D.; Pienaar K.; and Prodanova M. (2004). Modelling long-range transport and chemical transformation of pollutants in the Southern Africa region. *Proceedings of Ninth International Conference on Harmonisation within Atmospheric Dispersion Modelling for Regulatory Purposes (June 1–4, 2004, Garmisch-Partenkirchen, Germany)*, pp. 320–324.

Fox J. (2001). *Chomsky and Globalization*. Icon Books, London, 80 pp.

Franzen L.G.; Mattson J.O.; Martensson U.; Nihlén T.; and Rapp A. (1994). Yellow snow over the Alps and Subarctic from dust storm in Africa, March 1991. *Ambio*, **23**(3), 233–235.

Frederick K.D. (1994). Integrated assessment of the impacts of climate change on natural resources: An Introductory essay. *Clim. Change*, **28**(102), 1–14.

Freitas S.R.; Longo K.M.; Silva Dias M.A.F.; Silva Dias P.L.; Chatfield R.; Prins E.; Artaxo P.; Grell G.A.; and Recuero F.S. (2005). Monitoring the transport of biomass burning emissions in South America. *Environmental Fluid Mechanics*, **5**(1–2), 135–167.

Friedrich R. (ed.) (2001). *Generation and Evaluation of Emission Data*. GENEMIS Annual Report 2001, Stuttgart, Germany, 87 pp.

From the Candidates (2000). Gore and Bush address key environmental issues. *Resources*, Fall, Issue 141, Washington, D.C., pp. 5–8.

Fung I.; John J.; Lerner J.; Matthews E.; Prather M.; Steele L.P.; and Fraser P.J. (1991). Three-dimensional model synthesis of the global methane cycle. *J. Geophys. Res.*, **96**, 13033–13065.

Galbraith D.; Smith P.; Mortimer N.; Stewart R.; Hobson M.; McPherson G.; Matthews R.; Mitchell P.; Nijnik M.; Norris J.; Skiba U.; Smith J.;and Towers W. (2006). *Review of Greenhouse Gas Life Cycle Emissions, Air Pollution Impacts and Economics of Biomass Production and Consumption in Scotland*. Environmental Research Report 2006/02, Scottish Executive Environment and Rural Affairs Department, Edindurgh, 267 pp.

Gale J.; and Freund P. (2000). Reducing methane emissions to combat global climate change: The role Russia can play. *Proceedings of the Second International Methane Mitigation Conference (June 18–23, 2000, Novosibirsk)*. Novosibirsk State University Publ., Novosibirsk, pp. 73–80.

Galeano E. (1997). *Open Veins of Latin America: Five Centuries of the Pillage of a Continent*. Monthly Review Press, New York, 360 pp.

Garcia S.M.; and Grainger R.J.R. (2005). Gloom and doom? The future of marine capture fisheries. *Philosophical Transactions Royal Society London B Biological Science*, **360**(1453), 21–46.

Garcia-Barrón L.; and Pita M. F. (2004). Stochastic analysis of time series of temperatures in the south-west of the Iberian Peninsula. *Atmósfera*, **17**(4), 225–244.

Gedney N.; and Valdes P. J. (2000). The effect of Amazonian deforestation on the northern hemisphere circulation and climate. *Geophys. Res. Lett.*, **27**(19), 3053–3056.

GEF (1998). *Caspian Ecological Programme*. UNDP Publ., Baku, Azerbaijan, 74 pp.

Gelchu A.; and Pauly D. (2007). Growth and distribution of port-based global fishing effort within countries' EEZs from 1970 to 1995. *Fisheries Center Research Reports, University of British Columbia, Vancouver, Canada*, **15**(4), 1–105.

GEO (2005). *Work Plan for 2006, Version 2*. Group on Earth Observations, Cover Memorandum, November 28, 2005, Geneva, 38 pp.

Gillett N.P.; Allen M.R.; McDonald R.E.; Senior G.A.; Shindell D.T.; and Schmidt G.A. (2002). How linear is the Arctic Oscillation response to greenhouse gases? *J. Geophys. Res.*, **107**(D3), ACL1/1–ACL1/7.

Ginoux P.; Prospero J.; and Torres O. (2002). Long-term simulation of dust distribution with the GOCART model: Correlation with the North Atlantic Oscillation. In: J.A. Lee and T.M. Zobeck (eds.), *Proceedings of ICAR5/GCTE-SEN Joint Conference*. International Center for Arid and Semiarid Lands Studies, Texas Tech. University, Lubbock, Texas, pp. 241–245.

Giorgi F.; Bi X.; and Qian Y. (2003). Indirect and direct effects of anthropogenic sulfate on the climate of East Asia as simulated with a regional coupled climate-chemistry/aerosol model. *Climatic Change*, **58**, 345–376.

Girnis P.R.; Orphan V.J.; Hallam S.J.; and DeLong E.F. (2003). Growth and methane oxidation rates of anaerobic methanotrophic archaea in a continuous-flow bioreactor. *Applied and Environmental Microbiology*, **69**, 5472–5482.

Gloersen P.; Parkinson C.L.; Cavalieri D.J.; Comiso J.C.; and Zwally H.J. (1999). Spatial distribution of trends and seasonality in the hemispheric ice covers: 1978–1996. *J. Geophys. Res.*, **104**(C9), 20827–20835.

Goldammer J.G.; and Furyaev V.V. (1996). *Fire in Ecosystems of Boreal Eurasia*. Kluwer Academic Publishers, Dordrecht, 390 pp.

Goldman H.V. (ed.) (1999). Proceedings of the International Symposium on Polar Aspects of Global Change (Trømso, Norway, August 24–28, 1998). *Polar Research*, **18**(2), 1–404.

Gong S.L.; and Barrie L.A. (2003). Simulating the impact of sea salt on global nss sulphate aerosol. *J. Geophys. Res.*, **108**(D16), AAC4/1–AAC4/18.

Goodhand J. (1999). From wars to complex political emergencies: Understanding conflict and peace-building in the new world disorder. *Third World Quarterly*, **20**(1), 13–26.

Goody R.; Anderson J.; and North G. (1998). Testing climate models: An approach. *Bull. Am. Meteorol. Soc.*, **79**, 2541–2549.

Goody R.; Anderson J.; Karl T.; Miller R.; North G.; Simpson J.; Stephens C.; and Washington W. (2001). Why monitor the climate? *Bull. Amer. Meteorol. Soc.*, **83**(6), 873–878.

GOOS (2002). *Joint GCOS–GOOS–WCRP Ocean Observations Panel for Climate (OOPC) (Sixth Session, May 2–5, 2001, Melbourne, Australia)*. IOC, Paris, 61 pp.

Gordeev V.V.; Gulidov A.V.; Holms P.; and Peterson B. (2000). River outflow of nutrients to Russian Arctic: Achievements and Problems. *Proceedings of the Second Conference: Ecology of Siberian River Basins and the Arctic' (November 24–26, 2000, Tomsk)*, pp. 108–113 [in Russian].

Gorshkov V.G. (1990). *Biosphere Energetics and Environment Stability*. ARISTI Publ., Moscow, 238 pp. [in Russian].

Gorshkov V.G.; Gorshkov V.V.; and Makarieva A.M. (2000). *Biotic Regulation of the Environment: Key Issues of Global Change*. Springer/Praxis, Chichester, U.K., 367 pp.

Goudrian J.; van Keulen H.; and van Laar H.H. (eds.) (1990). *The Greenhouse Effect and Primary Productivity in European Agro-ecosystems*. Pudoc, Wageningen, 90 pp.

Govindan R.B.; Vyushin D.; Bunde A.; Brenner S.; Havlin S.; and Schellnhuber H.J. (2002). Global climate models violate scaling of the observed atmospheric variability. *Physical Review Letters*, **89**(2), art. no. 028501.

Grankov A.G.; Krapivin V.F.; and Soldatov V.Yu. (2006). Diagnostics of the tropical hurricane beginning in the ocean basing on the monitoring data and mathematical model. *Proceedings of the International Symposium on Ecoinformatics Problems (Moscow, December 5–7, 2006)*. IREE Publ., Moscow, pp. 5–14 [in Russian].

Grant R.F.; Arain A.; Arora V.; Barr A.; Black T.A.; Chen J.; Wang S.; Yuan F.; and Zhang Y. (2005). Intercomparison of techniques to model high temperature effects on CO_2 and energy exchange in temperate and boreal coniferous forests. *Ecological Modelling*, **188**(2–4), 217–252.

Grassl H. (2000). Status and improvements of coupled general circulation models. *Science*, **288**, 1991–1997.

Grebmeier J.M.; Whitledge T.E.; Aagaard K.; Bergmann M.; Carmack E.C.; Codispoti L.A.; Darby D.; Dunton K.H.; Melnikov I.A.; Moore S.; Takizawa T.; Walsh J.J.; Wassman P.; and Wheeler P. (eds.) (2001). *Arctic System Science Ocean–Atmosphere–Ice Interactions: Western Arctic Shelf–Basin Interactions (SBI)*. Phase II Field Implementation Plan, SBI Project Office, The University of Tennessee, Knoxville, Tennessee, 30 pp.

Grebmeier J.M.; DiTullio G.R.; Barray J.P.; and Cooper L.W. (2003). Benthic carbon cycling in the Ross Sea polynya, Antarctica: Benthic community metabolism and sediment tracers. *Antarctic Research Series*, **78**, 301–326.

Griffin D.W.; Kellogg C.A.; and Shinn E.A. (2001). Dust in the wind: Long range transport of dust in the atmosphere and its implications for global public and ecosystem health. *Global Change and Human Health*, **2**(1), 20–33.

Griggs D.J.; and Noguer M. (2002). Climate Change 2001: The Scientific Basis. Contribution of Working Group 1 to the Third Assessment Report of the Intergovernmental Panel on Climate Change. *Weather*, **57**(8), 267–269.

Grigoryev Al.A.; and Kondratyev K.Ya. (2001a). *Ecological Disasters*. St. Petersburg State University Publ., St. Petersburg, 691 pp. [in Russian].

Grigoryev Al.A.; and Kondratyev K.Ya. (2001b). *Ecological Catastrophes*. St. Petersburg State University Publ., St. Petersburg, 206 pp. [in Russian].

Grigoryev Al.A.; and Kondratyev K.Ya. (2001c). *Ecodynamics and Geopolitics: Ecological Catastrophes*, Vol. 2. St. Petersburg State University Publ., St. Petersburg, 688 pp. [in Russian].

Grytsai A.; Grytsai Z.; Evtushevsky A.; and Milinevsky G. (2005). Interannual variability of planetary waves in the ozone layer at 65 degrees S. *Int. J Remote Sens.*, **26**(16), 3377–3387.

Guerschman J.P.; and Paruelo J.M. (2005). Agricultural impacts on ecosystem functioning in temperate areas of North and South America. *Global and Planetary Change*, **47**(2–4), 170–180.

Gulyaev Yu.V.; Krapivin V.F.; and Bukatova I.L. (1987). On the way to evolutionary informatics. *Herald of Soviet Academy of Sciences*, **11**, 53–61 [in Russian].

Gulyaev Yu.V.; Bukatova I.L.; and Krapivin V.F. (1989a). Evolutionary computer technology. In: E.P. Novitchikhin (ed.), *Methods of Informatics in Radiophysical Investigations of the Environment*. Science Publ., Moscow, pp. 25–43 [in Russian].

Gulyaev Yu.V.; Bukatova I.L.; Golubeva L.N.; and Krapivin V.F. (1989b). Evolutionary informatics and "intellectual" special processors. *Institute of Radioengineering and Electronics, Russian Academy of Sciences, Report No*. **6**(507), Moscow, 39 pp. [in Russian].

Gulyaev Yu.V.; Rogalsky V.I.; Krapivin V.F.; Novitchikhin E.P.; and Yushkov V.P. (1991). Mathematical Modeling of Natural Objects in Global Space System of Ecological Control. *Institute of Radioengineering and Electronics, Russian Academy of Sciences, Report No*. **2**(553), Moscow, 33 pp. [in Russian].

Gyalistras D. (2002). How uncertain are regional climate change scenarios? Examples for Europe and the Alps. *PIK Report No*. **75**, Potsdam, pp. 85–100.

Haigh J.D. (2001). Climate variability and the influence of the Sun. *Science*, **294**(5549), 2109–2111.

Han Z.; Ueda H.; and Sakurai T. (2006). Model study on acidifying wet deposition in East Asia during wintertime. *Atmospheric Environment*, **40**(13), 2360–2373.

Hansen J.; Sato M.; Lacis A.; Ruedy R.; Tegen L.; and Matthews E. (1998). Climate forcing in the Industrial era. *Proc. U.S. National Acad. Sci.*, **95**(22), 12753–12758.

Hansen J.; Ruedy R.; Glascoe J.; and Sato M. (1999). GISS analysis of surface temperature change. *J. Geophys. Res.*, **104**(D24), 30997–31022.

Hansen J.; Sato M.; Ruedy R.; Lacis A.; and Oinas V. (2000). Global warming in the twenty-first century: An alternative scenario. *Proc. U.S. National Acad. Sci.*, **97**(18), 9875–9880.

Hansen J.; Sato M.; Nazarenko L.; Ruedy R.; Laws A.; Koch D.; Tegen I.; Hall T.; Shindell D.; Santer B.; Stone P.; Novakov T.; Thomason L.; Wang R.; Wang Y.; Jacob D.; Hollandsworth S.; Bishop L.; Logan J.; Thompson A.; Stolarski R.; Lean J.; Willson R.;Levitus S.; Antonov J.; Rayner R.; Parker D.; and Christy J. (2002). Climate forcings in Goddard Institute for Space Studies S1 2000 simulations. *J. Geophys. Res.*, **107**(D18), ACL2/1–ACL2/37.

Hanshaw M.N.; Lozier M.S.; and Palter J.B. (2006). The Integrated Impact of Tropical Cyclones on Sea Surface Chlorophyll in the North Atlantic. *American Geophysical Union, Fall Meeting 2006*, abstract #A13A–0878, Washington, 2006AGUFM.A13A0878H.

Hanson B. (2005). Learning from natural disasters. *Science*, **308**, 1125.

Hardy J.T. (2003). *Climate Change*. Wiley, Washington, D.C., 260 pp.

Hargrove W.W.; Hoffman F.M.; and Law B.E. (2003). New Analysis Reveals Representativeness of AmeriFlux Network. *Earth Observing System Transactions, American Geophysical Union*, **84**(48), 529–535.

Harries J.E.; Russel J.E.; Hanafin J.A.; Brindley H.; Futyan J.; Rufus J.; Kellock S.; Matthews G.; Wrigley R.; Last A.; Mueller J.; Mossavati R.; Ashmall J.; Sawyer E., Parker D.; Caldwell M.; Allan P.M.; Smith A.; Bates M.J.; Coan B.; Stewart B.C.; Lepine D.R.; Cornwall L.A.; Corney D.R.; Ricketts M.J.; Drummond D.; Smart D.; Cutler R.; Dewitte S.; Clerbaux N.; Gonzalez L.; Ipe A., Bertrand C.; Joukoff A.; Crommelynck D.; Nelms N.; Llewellyn-Jones D.T.; Butcher G.; Smith G.L.; Szewczyk Z.P.; Mlynczak P.E.; Slingo A.; Allan R.P.; and Ringer M.A. (2005). The Geostationary Earth Radiation Budget Project. *Bull. Amer. Meteorol. Soc.*, **86**(7), 945–960.

Harrison J.A.; Matson P.A.; and Fendorf S. (2005). Effects of a diel oxygen cycle on nitrogen transformations and greenhouse gas emission in a eutrophied, subtropical stream. *Aquatic Sciences*, **67**, 308–315.

Haszpra L.; Barcza Z.; Davis K.J.; and Tarczay K. (2005). Long–term tall tower carbon dioxide flux monitoring over an area of mixed vegetation. *Agricultural and Forest Meteorology*, **132**(1–2), 58–77.

Hattas D.; Stock W.D.; Mabusela W.T.; and Green I.R. (2005). Phytochemical changes in leaves of subtropical grasses and fynbos shrubs at elevated atmospheric CO_2 concentrations. *Global and Planetary Change*, **47**(2–4), 181–192.

Hays M.D., Fine P.M., Geron C.D., Kleeman M.J., and Gullett B.K. (2005). Open burning of agricultural biomass: Physical and chemical properties of particle-phase emissions. *Atmospheric Environment*, **39**(36), 6747–6764.

Heffer P.; and Prud'homme M. (2006). *Medium-term Outlook for Global Fertilizer Demand, Supply and Trade, 2006–2010*, Summary Report. International Fertilizer Industry Association, Paris, 9 pp.

Hein R.; Dameris M.; Schnadt C.; Land C.; Grewe V.; Kohler I.; Ponater M.; Sausen R.; Steil B.; Landgraf J.; and Bruhl C. (2001). Results of an interactively coupled atmospheric chemistry–general circulation model: Comparison with observations. *Ann. Geophysicae*, **19**(4), 435–457.

Heinrich H. (1988). Origin and consequences of cyclic ice rafting in the northeast Atlantic Ocean during the past 130,000 years. *Quat. Res.*, **29**, 142–152.

Heinrich M.; and Hinzpeter H. (1975). Radiation balance and albedo in the tropical Atlantic during ATEX 1969. *Meteorologie und Aeronomie*, **8**, 56–64.

Hellebrandt H.J.; Kern J.; and Scholz V. (2003). Long-term studies on greenhouse gas fluxes during cultivation of energy crops on sandy soils. *Atmospheric Environment*, **37**(12), 1635–1644.

Henderson B.; and Chýlek P. (2005). The effect of spatial resolution on satellite aerosol optical depth retrieval. *IEEE Transactions on Geoscience and Remote Sensing*, **43**(9), 1984–1990.

Holland D.M. (2001). Explaining the Weddell Polynya: A large ocean eddy shed at Maud Rise. *Science*, **292**, 1697–1700.

Holland G.; and Nowlin W. (eds.) (2001). *Principles of the Global Ocean Observing System (GOOS) Capacity Building*, GOOS Report No. 69. UNESCO, IOC, Paris, 23 pp.

Holloway G.; and Sou T. (2001). Is Arctic sea ice rapidly thinning? *Ice and Climate News*, **1**, 2–5.

Hopkin M. (2007). Climate change 2007: Climate sceptics switch focus to economics. *Nature*, **445**, 582–583.

Horton K.E. (1937). Determination of infiltration capacity for larger drainage basins. *Transactions American Geophysical Union*, **18**, 371–385.

Hoskins B.J. (2003). Climate change at cruising altitude? *Science*, **301**, 469–470.
Houghton J.T. (2001a). Global climate and human activities. *EOLSS Article*, **1–2**, 1–13.
Houghton J.T. (2001b). The IPCC Report 2001. *Proceedings of the First Solar and Space Weather Euroconference: The Solar Cycle and Terrectrial Climate (Santa Cruz de Tenerife, September 25–29, 2000)*. ESA SP, Noordwijk, **463**, pp. 255–259.
Houghton J.T. (2003). Global warming is now a weapon of mass destruction. *The Guardian*, Monday July 28.
Houghton J.T.; Jenkins G.J.; and Ephraums J.J. (eds.) (1990). *Scientific Assessment of Climate change: Report of Working Group I*. Cambridge University Press, Cambridge, U.K., 365 pp.
Houghton J.T.; Ding Y.; Griggs D.J.; and Noguer M. (2001). *Climate Change 2001: The Scientific Basis*, contribution of Working Group I to the Third Assessment Report of the Intergovernmental Panel Group on Climate Change. Cambridge Univ. Press, Cambridge, U.K. 892 pp.
Howarth R.W.; Stewart J.W.B.; and Ivanov M.V. (eds.). (1992). *Sulphur Cycling on the Continents: Wetlands, Terrestrial Ecosystems, and Associated Water Bodies*. Wiley, Chichester, U.K., 372 pp.
Hu K.; Ivanov P.C.; Chen Z.; Carpena P.; and Stanley H.E. (2001). Effect of trends on detrended fluctuation analysis. *Physical Review*, **E64**(1), art. no. 011114.
Huang S.; Pollack H.N.; and Shen P.-Y. (2000). Temperature trends over the past five centuries reconstructed from borehole temperatures. *Nature*, **403**, 756–758.
Hubbard K.G.; and Lin X. (2002). Realtime data filtering models for air temperature measurements. *Geophys. Res. Lett.*, **29**(10), 67/1–67/4.
Hughes T.P.; Baird A.H.; Bellwood D.R.; Card M.; Connoly S.R.; Folke C.; Grosberg R.; Hoegh-Gulberg O.; Jackson J.B.C.; Kleypas J.; Lough J.M.; Marshall P.; Myström M.; Palumbi S.R.; Pandolfi J.M.; and Rosen B.J. (2003). Climate change, human impacts, and the resilience of coral reefs. *Science*, **301**, 529–533.
Hulme M.; Barrow E.M.; Arnell N.W.; Harrison P.A.; Johns T.C.; and Downing T.E. (1999). Relative impacts of human-induced climate change and climate variability. *Nature*, **397**, 689–691.
Hurrell J.W. (2005). The North Atlantic Oscillation: Encyclopedia of World Climatology. In: J.E. Oliver (ed.), *Encyclopedia of Earth Sciences*, Springer-Verlag, Berlin, pp. 536–539.
Hurrell J.W.; and Dickson R.R. (2004). Climate variability over the North Atlantic. In: N.C. Stenseth, G. Ottersen, J.W. Hurrell, A. Belgrano, and B. Planque (eds.), *Ecological Effects of Climatic Variations in the North Atlantic Ocean*. Oxford University Press, Oxford, pp. 254–261.
Hurrell J.W.; Kushnir Y.; Visbeck M.; and Ottersen G. (2003). The North Atlantic Oscillation: Climate significance and environmental impacts. In: J.W. Hurrell, Y. Kushnir, G. Ottersen, and M. Visbeck (eds.), *An Overview of the North Atlantic Oscillation*, Geophysical Monograph Series. American Geophysical Union, Washington, **134**, 1–35.
IASC (2001). *The International Arctic Science Committee Project Catalogue*. IASC, Oslo, 57 pp.
Ichikawa A. (2004). *Global Warming: The Research Challenges*, a report of Japan's Global Warming Initiative. Springer-Verlag, Berlin, 161 pp.
Ichii K.; Hashimoto H.; Nemani R.; and White M. (2005). Modeling the interannual variability and trends in gross and net primary productivity of tropical forests from 1982 to 1999. *Global and Planetary Change*, **48**(4), 274–286.
IEA (2002). *Energy Policies of IEA Countries*. OECD/IEA, Paris, 137 pp.
IEA (2005a). *Energy Policies of IEA Countries*. IEA Books, Paris, 588 pp.
IEA (2005b). *Key World Energy Statistics*. IEA Books, Paris, 82 pp.

IEA (2005c). *World Energy Outlook: Middle East and North Africa Insights*. IEA Books, Paris, 600 pp.

IEA (2006). *Energy Technology Perspectives: Scenarios and Strategies to 2050*. IEA Books, Paris, 484 pp.

IEA (2007a). *Energy Balances on Non-OECD Countries, 2004–2005*. IEA Books, Paris, 482 pp.

IEA (2007b). *Key World Energy Statistics*. IEA Books, Paris, 82 pp.

IGOS (2001). *An Ocean Theme for the IGOS Partnership*, Final Report from the Ocean Theme Team. NASA, Washington, D.C., 40 pp.

IGOS (2004). *Report of the IGOS International Workshop: Towards the Implementation of the Integrated Global Observing Strategy (IGOS) (February 4–6, 2004, Tokyo)*. JAXA, Tokyo, 18 pp.

Inomata Y.; Iwasaka Y.; Osada K.; Hayashi M.; Mori I.; Kido M.; Hara K.; and Sakai T. (2006). Vertical distributions of particles and sulphur gases (volatile sulfur compounds and SO_2) over East Asia: Comparison with two aircraft-borne measurements under the Asian continental outflow in spring and winter. *Atmospheric Environment*, **40**(3), 430–444.

Inoue M.; and Isozaki H. (2003). *People and Forest: Policy and Local Reality in Southern Asia, the Russian Far East, and Japan*. Springer-Verlag, Berlin, 376 pp.

IPCC (1996). *Climate Change 1995: Science of Climate Change*. Contribution of Working Group I to the Second Assessment Report of the Intergovernmental Panel on Climate Change. Cambridge University Press, Cambridge, MA, 879 pp.

IPCC (2000). *Land Use, Land-Use Change, and Forestry: Summary for Policymakers*. IPCC Special Report, Montreal, Canada, 30 pp.

IPCC (2001). *Climate Change 2001: Impacts, Adaptation, and Vulnerability*. Cambridge University Press, Cambridge, U.K., 881 pp.

IPCC (2003). *Report on Expert Workshop on Mitigation and Adaptation*. IPCC, Geneva, 11 pp.

IPCC (2005). *Special Report on Carbon Dioxide Capture and Storage*, Final Draft. IPCC, London, 571 pp.

IPCC (2007). *Climate Change 2007: The Physical Science Basis*. 10th Session of Working Group 1 of the IPCC, Paris, 18 pp.

Ito A.; and Oikawa T. (2002). A simulation model of the carbon cycle in land ecosystems (Sim-CYCLE): A description based on dry-matter production theory and plot scale validation. *Ecological Modelling*, **151**, 143–176.

Ito A.; Saigusa N.; Murayama S.; and Yamamoto S. (2005). Long-term carbon exchange at a Takayama, Japan forest. Modeling of gross and net carbon dioxide exchange over a cool-temperate deciduous broad-leaved forest in Japan: Analysis of seasonal and interannual change. *Agricultural and Forest Meteorology*, **134**(1–4), 122–134.

Ivachnenko A.G.; Krotov G.I.; and Cheberkus V.I. (1980). Multi-row algorithm of long-term prediction of self-organization. *Automatics (Kiev)*, **4**, 28–47 [in Ukrainian].

Ivachnenko A.G.; Peka P.Yu.; and Vostrov N.N. (1984). *Combined Method for Water and Oil Field Modeling*. Naukova Dumka, Kiev, Ukraine, 150 pp. [in Russian].

Ivanov A. (1978). *An Introduction to Oceanography*. Mir, Moscow, 392 pp. [in Russian].

Izrael Yu.A.; Gruza G.V.; Semenov S.M.; Nazarov I.M.; and Kvasnikova E.V. (eds.) (2004). *All-World Conference on Climate Change (September 29–October 3, 2003, Moscow)*. Gidrometeoizdat, Moscow, 620 pp. [in Russian].

Jackson P. (1999). *Introduction to Expert Systems*. Addison-Wesley, London, 560 pp.

Jacobson M.Z. (2002a). *Atmospheric Pollution*. Cambridge University Press, Cambridge, U.K., 412 pp.

Jacobson M.Z. (2002b). Control of fossil-fuel particulate black carbon and organic matter, possibly the most effective method of slowing global warming. *J. Geophys. Res.*, **107**(D19), 4410, doi:10.1029/2001JD002044.

Jaeglé L.; Martin R.V.; Chance K.; Steinberger L.; Kurosu T.P.; Jacob D.J.; Modi A.I.; Yoboue V.; Sigha-Nkamdjou L.; and Galy-Lacaux C. (2004). Satellite mapping of rain-induced nitric oxide emissions from soils. *J. Geophys. Res.*, **109**(D21310), 1–10, doi:10.1029/2004JD004787.

Jaeglé L.; Steinberger L.; Martin R.V.; and Chance K. (2005). Global partitioning of NO_x sources using satellite observations: Relative roles of fossil fuel combustion, biomass burning and soil emissions. *Faraday Discuss.*, **130**, 407–423, doi:10.1039/b502128f.

Jagovkina S.V.; Karol I.L.; Zubov V.A.; Lagun V.E.; Reshemikov A.I.; and Rosanov E.V. (2000). An estimation of the gas deposits leakage input into the total methane flux from the West Siberian region. *Proceedings of the Second International Methane Mitigation Conference (June 18–23, 2000, Novosibirsk)*. Novosibirsk State University Publ., Novosibirsk, pp. 263–267.

Jassal R.; Black A.; Novak M.; Morgenstern K.; Nesic Z.; and Gaumont-Guay D. (2005). Relationship between soil CO_2 concentrations and forest-floor CO_2 effluxes. *Agricultural and Forest Meteorology*, **130**(3–4), 176–192.

Jaworowski Z. (1999). The global warming folly. *21st Century Science and Technology*, **12**(4), 64–75.

Jiang C.; Cronin M.F.; Kelly K.A.; and Thompson L. (2005). Evaluation of a hybrid satellite- and NWP-based turbulent heat flux product using Tropical Atmosphere–Ocean (TAO) buoys. *J. Geophys. Res.*, **110**(C9), C09007, doi:10.1029/2004JC002824.

Johannessen O.M.; Bjorgo E.; and Miles M.W. (1996). Global Warming and the Arctic (Letter). *Science*, **271**, 129.

Johnson D.E.; and Ulyatt M.I. (2000). Variations in the proportion of methane of total greenhouse gas emissions from US and NZ dairy production systems. *Proceedings of the Second International Methane Mitigation Conference (June 18–23, 2000, Novosibirsk)*. Novosibirsk State University Publ., Novosibirsk, pp. 249–254.

Johnson C.E.; Stevenson D.S.; Collins W.J.; and Derwent R.G. (2002). Interannual variability in methane growth rate simulated with a coupled Ocean–Atmosphere–Chemistry model. *Geophysical Research Letters*, **29**(19), 1–4.

Johnson B.T.; Shine K.P.; and Forster P.M. (2004). The semi-direct aerosol effect: Impact of absorbing aerosols on marine stratocumulus. *Quart. J. Roy. Meteorol. Soc.*, **130**, Part B, No. 599, 1407–1422.

Jones P.D.; New M.; Parker D.E.; Martin S.; and Rigor I.G. (1999). Surface air temperature and its changes over the past 150 years. *Reviews of Geophysics*, **37**, 173–199.

Jones S.K.; Rees R.M.; Skiba U.M.; and Ball B.C. (2005). Greenhouse gas emissions from a managed grassland. *Global and Planetary Change*, **47**(2–4), 201–211.

Kaiser J. (2000). Global warming, insects take the stage at snowbird. *Science*, **289**(5487), 2031–2032.

Kalabin G.V. (2000). *Ecodynamics of the Anthropogenic Environment: Province of the North*. Kola Sci. Center, Russian Acad. Sci., Apatity, 294 pp. [in Russian].

Kalb D.; Pansters W.; and Siebers H. (2004). *Globaliszation and Development: Themes and Concepts in Current Research*. Springer-Verlag, Berlin, 203 pp.

Kantelhardt J.W.; Zschiegner S.A.; Koscielny-Bunde E.; Havlin S.; Bunde A.; and Stanley H.E. (2002). Multifractal detrended fluctuation analysis of nonstationary time series. *Physica*, **A316**(14), 87–114.

Karibaeva K.N.; Esekin B.K.; Kurochkina L.Ya.; Losev K.S.; Makarieva A.M.; Gorshkov V.G.; and Shukurov E.D. (2004). Scientific basis of strategic directions in nature-defense politics. *Ecology and Education*, **1**–**2**, 2–9 [in Russian].

Karimov G.U.; and Chukanin K.I. (1988). Scheme for pollution transport to the Arctic troposphere. In: K.Ya. Kondratyev (ed.), *Monitoring the Arctic Climate*. Hydrometeoizdat, St. Petersburg, pp. 168–180 [in Russian].

Karl T.R. (1998). Regional Trends and Variations of Temperature and Precipitation. In: R.T. Watson, M.C. Zinyowera, and R.H. Moss (eds.), *The Regional Impacts of Climate Change*. Cambridge University Press, Cambridge, U.K., pp. 87–119.

Karl T.; and Gleckler P. J. (2001). Tracking changes in AMIP model performance. *Abstracts of Eighth Sci. Assembly of IAMAS (Innsbruck, July 10–18, 2001)*, pp. 8–9.

Karley M.J.; Beven K.J.; and Oliver H.R. (1993). A method for predicting spatial distribution of evaporation using simple meteorological data. *Proceedings of Int. Symposium: Ech. Proc. Land Surf. Range Space and Time Scales (Yokohama, July 13–16, 1993)*. IAHS Publ., **212**, 619–626.

Karol′ I. L. (2000). Impact of the flights of world transport aircraft on the ozonosphere and climate. *Meteorology and Hydrology*, **7**, 17–32 [in Russian].

Kazansky A.V.; and Filatov S.V. (1987). *Investigation of Two Ways for the Determination of Surface Ocean Temperature by Means of Distribution of Satellite Measurements in the IR Range*. Institute of Automatics and Management Processes, Far East Branch of Russian Academy of Sciences, Vladivostok, 22 pp. [in Russian].

Keeling C.D.; and Bacastow R.B. (1977). Impact of industrial gases on climate. In: R.R. Revelle (ed.), *Energy and Climate*. National Academy of Sciences, Washington, D.C., 72–95.

Keeling C.D.; and Whorf T.P. (2005). Atmospheric CO_2 records from sites in the SIO air sampling network. In: D.P. Boden, R.J. Kaiser, and F.W. Stoss (eds.), *Trends: A Compendium of Data on Global Change*. Carbon Dioxide Information Analysis Center, Oak Ridge National Laboratory, U.S. Department of Energy, Oak Ridge, Tenn. (*http://cdiac.esd.ornl.gov/trends/co2/sio-mlo.htm*).

Keeling R.F.; and Visbeck M. (2001). Antarctic stratification and glacial CO_2. *Nature*, **412**(6847), 605–606.

Kelley J.J. (1987). Carbon dioxide in the Arctic environment. *Journal of Earth Sci.*, **35**(2), 341–354.

Kelley J.J.; and Gosink T. (1992). *The Arctic Environment: Air/Sea/Land Exchange of Trace Gases*. Univ. of Alaska Fairbanks, Fairbanks, Report No. CP 92-7, Dec. 1992, 29 pp.

Kelley J.J.; Rochon G.L.; Novoselova O.A.; Krapivin V.F.; and Mkrtchyan F.A. (1992). Toward the global geo-eco-information monitoring. *Proceedings of the First International Symposium: Ecoinformatics Problems (December 14–18, 1992, Moscow)*. IREE Publ., Moscow, pp. 3–7.

Kelley J.J.; Krapivin V.F.; and Popovich P.R. (1999). The problems in Arctic environment monitoring. *Problems of the Environment and Natural Resources*, **6**, 32–40 [in Russian].

Kemball-Cook S., Wang B.; and Fu X. (2002). Simulation of the intraseasonal oscillation in the ECHAM-4 model: The impact of coupling with an ocean model. *Journal of the Atmospheric Sciences*, **59**(9), 1433–1453.

Keppler F.; Hamilton J.T.G.; Bra M.; and Röckmann T. (2006). Methane emissions from terrestrial plants under aerobic conditions. *Nature*, **439**, 187–191.

Kerr R.A. (2001a). Rising global temperature, rising uncertainty. *Science*, **292**(5515), 192–194.

Kerr R.A. (2001b). World starts taming the greenhouse. *Science*, **293**(5530), 583.

Khalil M.A.K.; Rasmussen R.A.; Ren L.; Wang M.X.; Shearer M.J.; Dalluge R.W.; and Duan C.-L. (2000). Methane emissions from rice fields. *Proceedings of the Second International Methane Mitigation Conference (June 18–23, 2000, Novosibirsk)*. Novosibirsk State University Publ., Novosibirsk, pp. 13–30.

Khandekar M.L.; Murty T.S.; and Chittibabu P. (2005). The Global Warming Debate: A Review of the State of Science. *Pure and Applied Geophysics*, **162**(8–9), 1557–1586.

Kim W.; Arai T.; Kanae S.; Oki T.; and Musiake K. (2001). Application of the Simple Biosphere Model (SiB2) to a paddy field for a period of growing season in GAME-Tropics. *J. Meteorol. Soc. Jap.*, **79**(18), 387–400.

Kiseleva S.V. (1990). Investigation of CO_2 transfer processes under different states of the water–air boundary. PhD thesis, Moscow State University, 171 pp. [in Russian].

Kitao M.; Lei T.T.; Koike T.; Kayama M.; Tobita H.; and Maruyama Y. (2007). Interaction of drought and elevated CO_2 on photosynthetic down-regulation and susceptibility to photoinhibition in Japanese white birch (*Betula platyphylla* var. *japonica*) seedlings grown under limited N availability. *Tree Physiology*, **27**, 727–735.

Knutson T.R.; Delwoorth T.U.; Dixon. K.W.; and Stouffer R.J. (1999). Model assessment of regional temperature trends (1949–1997). *J. Geophys. Res.*, **104**(D24), 30981–30996.

Kohler M.A. (1954). Lake and pan evaporation. *U.S. Geological Survey, Professional Papers*, **269**, 127–148.

Kohler M.A.; and Richards M.A. (1962). Multicapacity basin accounting for predicting runoff from storm precipitation. *J. Geophys. Res.*, **67**(13), 5187–5197.

Kondratyev K.Ya. (1986). *Natural and Anthropogenic Changes of Climate*. Science Publ., Leningrad, 52 pp. [in Russian].

Kondratyev K.Ya. (1990). *Key Problems in Global Ecology*. ARISTI Publ., Moscow, 454 pp. [in Russian].

Kondratyev K.Ya. (1992). *Global Climate*. Science Publ., St. Petersburg, 359 pp. [in Russian].

Kondratyev, K.Ya. (1996). Global changes and demographic dynamics. *Proceedings of the Russian Geographical Society*, **128**(3), 1–12 [in Russian].

Kondratyev K.Ya. (1998a). Environmental risk: Real and hypothetical. *Proc. of the Russian Geographical Soc.*, **130**(3), 13–24 [in Russian].

Kondratyev K.Ya. (1998b). *Multidimensional Global Change*. Wiley/Praxis, Chichester, U.K., 761 pp.

Kondratyev K.Ya. (1999a). *Climatic Effects of Aerosols and Clouds*. Springer/Praxis, Chichester, U.K., 264 pp.

Kondratyev K.Ya. (1999b). *Ecodynamics and Geopolicy. Vol. 1. Global Problems*. St. Petersburg Branch of RAS Publ., 1036 pp. [in Russian].

Kondratyev K.Ya. (2000a). Earth researches from space: Scientific plane of the EOS system. *Earth Research from Space (Moscow)*, **3**, 82–91 [in Russian].

Kondratyev K.Ya. (2000b). Global changes on the boundary of two centuries. *Herald of RAS*, **70**(9), 788–796.

Kondratyev K.Ya. (2001). Key issues of global change at the end of the second millenium. In: R.R. Ernst (ed.), *Our Fragile World: Challenges and Opportunities for Sustainable Development*. EOLSS Vorrunner volumes 1–2, Eolss Publishers, Oxford, U.K., pp. 100–106.

Kondratyev K.Ya. (2002). Global climate change: Reality, hypotheses, and fiction. *Research of the Earth from Space*, **1**, 3–23 [in Russian].

Kondratyev K.Ya. (2003). Radiative forcing due to aerosol. *Optics of the Atmosphere and Ocean*, **16**(1), 5–18 [in Russian].

Kondratyev K.Ya. (2004a). Global climate change: Observational data and numerical modelling results. *Research of the Earth from Space*, **2**, 3–25 [in Russian].

Kondratyev K.Ya. (2004b). Global climate change: Unsolved problems. *Meteorology and Hydrology*, **4**, 93–102 [in Russian].

Kondratyev K.Ya. (2004c). Priorities of global climatology. *Proceedings of the Russian Geographical Society*, **136**(2), 3–25 [in Russian].

Kondratyev K.Ya. (2005). Sustainable development in the context of the consumption society problems. In: V.N. Troyan and I.A. Dementyev (eds.), *Sustainable Development and Ecological Management*. St. Petersburg State Univ. Publ., St. Petersburg, pp. 29–62 [in Russian].

Kondratyev K.Ya. and Cracknell A.P. (1998). *Observing Global Climate Change*. Taylor & Francis, London, 761 pp.

Kondratyev K.Ya.; and Demirchian K.S. (2000). Global climate changes and carbon cycle. *Proc. Russ. Geogr. Soc.*, **132**(4), 1–20 [in Russian].

Kondratyev K.Ya.; and Demirchian K. S. (2001). Global climate and Kyoto Protocol. *Herald of RAS*, **71**(11), 100–107 [in Russian].

Kondratyev K.Ya. and Galindo I. (1997). Volcanic Activity and Climate. A. Deepak Publ., Hampton, VA., 382 pp.

Kondratyev K.Ya.; and Isidorov V.A. (2001). Global carbon cycle. *Atmosphere and Ocean Optics*, **14**(1), 1–10 [in Russian].

Kondratyev K.Ya.; and Johannessen O.M. (1993). *Arctic and Climate*. St. Petersburg State University Publ., St. Petersburg, 140 pp. [in Russian].

Kondratyev K.Ya.; and Krapivin V.F. (2001a). Biocomplexity and global geoinformation monitoring. *Earth Research from Space (Moscow)*, **1**, 3–10 [in Russian].

Kondratyev K.Ya.; and Krapivin V.F. (2001b). Expert system for greenhouse effect control. *Problems of Environment and Natural Resources*, **6**, 23–40 [in Russian].

Kondratyev K.Ya.; and Krapivin V.F. (2003a). Global carbon cycle and climate. *Research of the Earth from Space*, **1**, 3–15 [in Russian].

Kondratyev K.Ya.; and Krapivin V.F. (2003b). Global changes: Real and potential in future. *Research of the Earth from Space*, **4**, 1–10 [in Russian].

Kondratyev K.Ya. and Krapivin V.F. (2004a). *Global Carbon Cycle Modelling*. Science Publ., Moscow, 335 pp. [in Russian].

Kondratyev K.Ya.; and Krapivin V.F. (2004b). Monitoring and prediction of natural disasters. *Il Nuovo Cimento*, **27C**(6), 657–672.

Kondratyev K.Ya.; and Krapivin V.F. (2005). Global climate dynamics: Future elaboration. 2. Investigative strategy of the U.S.A. *Proceedings of Russian Geographical Society*, **4**, 1–14 [in Russian].

Kondratyev K.Ya.; and Krapivin V.F. (2006a). Earth's radiation budget as an indicator of global ecological equilibrium. *Earth Research from Space (Moscow)*, **6**, 3–9 [in Russian].

Kondratyev K.Ya.; and Krapivin V.F. (2006b). Present state and perspectives of global energetics development. *Energy: Economics, Engineering, Ecology*, **2**, 17–23 [in Russian].

Kondratyev K.Ya.; and Krapivin V.F. (2006c). Present state and future for global energy development in the context of global ecodynamics. *Proceedings of Russian Geographical Society*, **138**(3), 14–30 [in Russian].

Kondratyev K.Ya.; and Varotsos C. (1995). Atmospheric greenhouse-effect in the context of global climate-change. *Nuovo Cimento della Società Italiana di Fisica C: Geophysics and Space Physics*, **18**(2), 123–151.

Kondratyev K.Ya.; and Varotsos C.A., (2000), *Atmospheric Ozone Variability: Implications for Climate Change, Human Health and Ecosystems*. Springer/Praxis, Chichester, U.K.

Kondratyev K.Ya.; Johannessen O.M.; and Melentyev V.V. (1996). *High-Latitude Climate and Remote Sensing*. Wiley/Praxis, Chichester, U.K., 200 pp.

Kondratyev K.Ya.; Krapivin V.F.; and Pshenin E.S. (2000). Concept behind regional geoinformation monitoring. *Earth Research from Space (Moscow)*, **6**, 3–10 [in Russian].

Kondratyev K.Ya.; Grigoryev Al.A.; and Varotsos C.A. (2002a). *Environmental Disasters: Anthropogenic and Natural*. Springer/Praxis, Chichester, U.K., 400 pp.

Kondratyev K.Ya.; Krapivin V.F.; and Phillips G.W. (2002b). *Global Environmental Change: Modelling and Monitoring*. Springer-Verlag, Heidelberg, 319 pp.

Kondratyev K. Ya.; Krapivin V. F.; and Savinykh V. P. (2003a). *Prospects for Civilization Development: Multi-Dimensional Analysis*. Logos Publ., Moscow, 575 pp. [in Russian].

Kondratyev K.Ya.; Krapivin V.F.; and Varotsos C.A. (2003b). *Global Carbon Cycle and Climate Change*. Springer/Praxis, Chichester, U.K., 343 pp.

Kondratyev K.Ya.; Losev K.S.; Ananicheva M.D.; and Chesnokova I.V. (2003c). *Natural–Scientific Foundations for Life Stability*. CAGL Publ., Moscow, 240 pp. [in Russian].

Kondratyev K.Ya.; Losev K.S.; Ananicheva M.D.; and Chesnokova I.V. (2003d). Costs of running ecological services in Russia. *Herald of RAS*, **73**(1), 3–10 [in Russian].

Kondratyev K.Ya.; Krapivin V.F.; Varotsos C.A.; and Savinikh V.P. (2004a). *Global Ecodynamics: A Multidimensional Analysis*. Springer/Praxis, Chichester, U.K., 649 pp.

Kondratyev K.Ya.; Losev K.S.; Ananicheva M.D.; and Chesnokova I.V. (2004b). *Stability of Life on Earth*. Springer/Praxis, Chichester, U.K., 152 pp.

Kondratyev K.Ya.; Krapivin V.F.;Lakasa H.; and Savinikh V.P. (2005). *Globalization and Sustainable Development: Ecological Aspects. Introduction*. Science Publ., St. Petersburg, 240 pp. [in Russian].

Kondratyev K.Ya.; Ivlev L.S.; Krapivin V.F.; and Varotsos C.A. (2006a). *Atmospheric Aerosol Properties: Formation, Processes and Impacts*. Springer/Praxis, Chichester, U.K., 572 pp.

Kondratyev K.Ya.; Krapivin V.F.; and Varotsos C.A. (2006b). *Natural Disasters as Interactive Components of Global Ecodynamics*. Springer/Praxis, Chichester, U.K., 620 pp.

Korstenshtein V.N. (1984). *Dissolved Gases of the Subsurface Hydrosphere of the Earth*. Nedra, Moscow, 289 pp. [in Russian].

Koscielny-Bunde E.; Bunde A.; Havlin S.; Roman H.E.; Goldreich Y.; and Schellnhuber H.J. (1998). Indication of a universal persistence law governing atmospheric variability. *Physical Review Letters*, **81**(3), 729732.

Kovalev N.A. (2003). The wildland fire season 2002 in Russian Federation. *International Forest Fire News*, **28**, 1–34.

Kraabol A.G.; and Stordal F. (2000). Modelling chemistry in aircraft plumes 2: The chemical conservation of NO_x to reservoir species under different conditions. *Atmospheric Environment*, **34**(23), 3951–3962.

Kraabol A.G.; Konopka P.; Stordal F.; and Schlager H. (2000). Modelling chemistry in aircraft plumes 1: Comparison with observations and evaluation of a layered approach. *Atmospheric Environment*, **34**(23), 3939–3950.

Krahmann G.; and Visbeck M. (2003). Arctic sea ice response to Northern Annual Mode wind forcing. *Geophysical Research Abstracts*, **5**, 13830.

Kram P. (1999). Application of the forest–soil–water model. *Ecological Modelling*, **120**(1), 9–30.

Krapivin V.F. (1978). *On the Theory of Complex System Survivability*. Soviet Radio Publ., Moscow, 248 pp. [in Russian].

Krapivin V.F. (1993). Mathematical model for global ecological investigations. *Ecological Modelling*, **67**(2–4), 103–127.

Krapivin, V.F. (1995) Simulation model for the investigation of pollution dynamics in the Arctic basin. *Oceanology (Moscow)*, **35**, 366–75 [in Russian].

Krapivin V.F. (1996). The estimation of the Peruvian current ecosystem by a mathematical model of biosphere. *Ecological Modelling*, **91(1)**, 1–14.

Krapivin, V.F. (1999a) Greenhouse effect and global biogeochemical carbon dioxide cycle. *Problems of Environment and Natural Resources*, **12**, 2–16 [in Russian].

Krapivin V.F. (1999b). Informational support of ecological investigations in the Arctic Basin. *Problems of Environment and Natural Resources*, **1**, 11–20 [in Russian].

Krapivin V.F. (2000a). Biospheric oxygen balance and its modeling. *Problems of Environment and Natural Resources*, **10**, 15–25 [in Russian].

Krapivin V.F. (2000b). Global nitrogen cycle modeling. *Problems of Environment and Natural Resources*, **10**, 2–15 [in Russian].

Krapivin V.F. (2000c). Greenhouse effect and global carbon dioxide cycle. *Problems of Environment and Natural Resources*, **2**, 2–18 [in Russian].

Krapivin V.F. (2000d). Simulation model of biogeochemical cycle of phosphorus in the biosphere. *Problems of Environment and Natural Resources*, **10**, 26–30 [in Russian].

Krapivin V.F.; and Klimov V.V. (1995). Valuation of convergence of "physical mixture" strategies in matrix games. *Theory and Control Systems*, **6**, 209–217 [in Russian].

Krapivin V.F.; and Klimov V.V. (1997). Stable strategies in games with gain functions $M(x-y)$. *Methods of Cybernetics and Informational Technologies (Saratov)*, **2**, 36–45 [in Russian].

Krapivin V.F.; and Kondratyev K.Ya. (2002). *Global Environmental Change: Ecoinformatics*. St. Petersburg State University Publ., St. Petersburg, 724 pp. [in Russian].

Krapivin V.F.; and Phillips G.W. (2001a). A remote sensing-based expert system to study the Aral–Caspian aquageosystem water regime. *Remote Sensing of Environment*, **75**, 201–215.

Krapivin V.F. and Phillips G.W. (2001b). Application of a global model to the study of Arctic basin pollution: Radionuclides, heavy metals and oil carbohydrates. *Environmental Modelling and Software*, **16**, 1–17.

Krapivin V.F.; and Potapov I.I. (2002). *Methods of Ecoinformatics*. ARISTI Publ., Moscow, 496 pp. [in Russian].

Krapivin V.F.; and Potapov I.I. (2006). Monitoring of the chemical cycles in the environment. *Ecological Systems and Devices*, **12**, 3–11 [in Russian].

Krapivin V.F.; and Potapov I.I. (2007). What is happening to the biosphere? *Problems of Environment and Natural Resources*, **5**, 3–15 [in Russian].

Krapivin V.F.; and Varotsos C.A. (2007). *Globalization and Sustainable Development: Environmental Agendas*. Springer/Praxis, Chichester, U.K., 304 pp.

Krapivin V.F.; and Vilkova L.P. (1990). Model estimation of excess CO_2 distribution in biosphere structure. *Ecological Modelling*, **50**, 57–78.

Krapivin V.F., Svirezhev Yu.M., and Tarko A.M. (1982). *Mathematical Modeling of Global Biosphere Processes*. Science Publ. House, Moscow, 272 pp. [in Russian].

Krapivin V.F.; Bui T.L.; Rochon G.L.; and Hicks D.R. (1996a). A global simulation model as a method for estimating the role of regional areas in global change. *Proc. of the Second HoChiMinh City Conference on Mechanics (September 24–25, 1996)*. Inst. of Applied Mechanics, HoChiMinh, pp. 68–69.

Krapivin V.F.; Vilkova L.P.; Rochon G.L.; and Hicks D.R. (1996b). Model estimation of the role of urban areas in global CO_2 dynamics. *Proc. of Eco-Informa '96 (November 4–7, 1996, Florida)*, pp. 17–22.

Krapivin V.F.; Cherepenin V.A.; Nazaryan N.A.; Phillips G.W.; and Tsang F.Y. (1997). Simulation model of radionuclide transport in the Angara–Yenisey river system. *Problems of the Environment and Natural Resources*, **2**, 41–58 [in Russian].

Krapivin V.F.; Cherepenin V.A.; Phillips G.W.; August R.A.; Pautkin A.Yu.; Harper M.J.; and Tsang F.Y. (1998). An application of modelling technology to the study of radionuclear pollutants and heavy metals dynamics in the Angara–Yenisey river system. *Ecological Modelling*, **111**(1), 121–134.

Krapivin V.F.; Mkrtchyan F.A.; Son N.C.; and Potapov I.I. (2004). Device for the measurement of geophysical parameters. *Ecological Systems and Devices*, **2**, 11–15 [in Russian].

Krapivin V.F.; Shutko A.M.; Chukhlantsev A.A.; Golovachev S.P.; and Phillips G.W. (2006). GIMS-based method vegetation microwave monitoring. *Environmental Modelling and Software*, **21**(3), 330–345.

Kravtsov Yu.V. (2002). Investigation of the ecologo-geochemical state of underground and surface waters of the Urengoy Oil–Gas–Condensate Deposit. Thesis of PhD dissertation, Tyumen State University, Tyumen, 200 pp.

Kuck L.R.; Balsley B.B.; Helmig D.; Conway T.J.; Tans P.P.; Davis K.; Jensen M.L.; Bognar J.A.; Arrieta R.V.; Rodriquez R.; and Birks J.W. (2000). Measurements of landscape-scale fluxes of carbon dioxide in the Peruvian Amazon by vertical profiling through the atmospheric boundary layer. *Journal of Geophysical Research*, **105**(D17), 22137–22146.

Kukla G. (2000). The last interglacial. *Science*, **287**, 987–988.

Kuzmin P.O. (1957). Hydrological investigations of land waters. *Int. Assoc. Sci. Hydrol.*, **3**, 468–478.

Labonte R. (2001). Liberalization, health and World Trade Organization. *J. Epidemiol. Community Health*, **55**(9), 620–621.

Labonte R.; and Sanger M. (2006a). Glossary of the World Trade Organisation and public health: Part 1. *J. Epidemiol. Community Health*, **60**(8), 655–661.

Labonte R.; and Sanger M. (2006b). Glossary of the World Trade Organisation and public health: Part 2. *J. Epidemiol. Community Health*, **60**(9), 738–744.

Lal R.; and Stewart B.A. (eds.) (1994). *Soil Process and Water Quality*. Taylor & Francis/CRC Press, London, 285 pp.

Lamptey B.L.; Barron E.J.; and Pollard D. (2005). Impacts of agriculture and urbanization on the climate of the Northeastern United States. *Global and Planetary Change*, **49**(3–4), 203–221.

Lane N. (2003). *Oxygen: The Molecule that Made the World*. Oxford University Press, Oxford, NJ, 384 pp.

Langmann B. (2000). Numerical modelling of regional scale transport and photochemistry directly together with meteorological processes. *Atmospheric Environment*, **34**(21), 3585–3598.

Lau W.K.; and Waliser D. (2005). *Intraseasonal Variability in the Atmosphere–Ocean Climate System*. Springer-Verlag, Berlin, 436 pp.

Lavender S.J.; Pinkerton M.P.; Moore G.F.; and Aiken J. (1998). A comparison of MOS and SeaWiFS satellite imagery in the Western English Channel. *Proceedings of the Second International Workshop on MOS–IRS and Ocean Color (June 10–15, 1998, Berlin)*. Institute of Space Sensor Technology, Berlin, Germany, pp. 111–115.

Lavender S.J.; Pinkerton M.H.; Moore G.F.; Aiken J.; and Blondeau-Patissier D. (2005). Modification to the Atmospheric Correction of SeaWiFS Ocean Colour Images over Turbid Waters. *Continental Shelf Research*, **25**, 539–555.

Ledley T.S.; Sundquist E.T.; Schwartz S.E.; Hall D.K.; Fellows J.D.; and Killeen T.L. (1999). Climate Change and Greenhouse Gases. *EOS*, **80**(39), 453–458.

Lee K. (2001). The global dimensions of cholera. *Global Change and Human Health*, **2**(1), 6–17.

Lee K.; McMichael T.; Butler C.; Ahern M.; and Bradley D. (2002). Global Change and Health: The Good, The Bad and The Evidence. *Global Change and Human Health*, **3**(1), 16–19.

Lee M.; Nakane K.; Nakatsubo T.; and Koizumi H. (2005). Long-term carbon exchanges at a Takayama, Japan forest: The importance of root respiration in annual soil carbon fluxes in a cool-temperate deciduous forest. *Agricultural and Forest Meteorology*, **134**(1–4), 95–101.

Legendre L.; and Krapivin V.F. (1992). Model for vertical structure of phytoplankton community in Arctic regions. *Proc. of 7th Int. Symp. on Okhotsk Sea & Sea Ice (February 2–5, 1992, Mombetsu, Japan)*. Okhotsk Sea & Cold Ocean Res. Assoc., Mombetsu, pp. 314–316.

Legendre P.; and Legendre L. (1998). *Numerical Ecology*. Elsevier, Amsterdam, 853 pp.

Leggett J.; Pepper W.J.; and Swart R.J. (1992). Emissions Scenarios for IPCC: An Update. In: J.T. Houghton, B.A. Callander, and S.K. Varney (eds.), *Climate Change 1992: The Supplementary Report to the IPCC Scientific Assessment*. Cambridge University Press, Cambridge, U.K., pp. 69–95.

Lemke P. (2001). Open windows to the polar oceans. *Science*, **292**, 1670–1671.

Leonova G.A. (2004). Biogeochemical Indicators of Aquatic Ecosystem Pollution by Heavy Metals. *Water Resources*, **31**(2), 195–202.

Leveque C.; and Mounolou J.-C. (2003). *Biodiversity*. Wiley, Paris, 256 pp.

Levinson D.H.; and Waple A.M. (eds.) (2004). State of the Climate in 2003. *Bull. Amer. Meteorol. Soc.*, **85**(6), 1–72.

Levis S.; Wiedinmyer C.; Bonan G. B.; and Guenther A. (2003). Simulating biogenic volatile organic compounds emissions in the Community Climate System Model. *J. Geophys. Res.*, **108**(D21), ACH2/1–ACH2/9.

Levitus S.; Antonov J.I.; Boyer T.P.; and Stephens C. (2000). Warming of the World Ocean. *Science*, **287**, 2225–2229.

Levitus S.; Antonov J.I.; Wang J.; Delworth T.L.; Dixon K.W.; and Broccoli A.J. (2001). Anthropogenic warming of Earth's climate system. *Science*, **292**(5515), 267–270.

Licki J.; Korotkov A.V.; Prius C.F.L.; Karjalainen T.; Victor D.G.; and Kauppi P.E. (2003). Increased carbon sink in temperate and boreal forests. *Climate Change*, **61**, 89–99.

Liikanen A.; and Martikainen P.J. (2003). Effect of ammonium and oxygen on methane and nitrous oxide fluxes across sediment–water interface in a eutrophic lake. *Chemosphere*, **52**(8), 1287–1293.

Lin D.-L.; Sakoda A.; Shibasaki R.; Goto N.; and Suzuki M. (2000). Modelling a global biogeochemical nitrogen cycle in terrestrial ecosystems. *Ecological Modelling*, **135**(1), 89–110.

Lin C.-Y.; Liu S.C.; Chou C.-K.; Huang S.-J.; Liu C.-M.; Kuo C.-H.;and Young C.-Y. (2005). Long-range transport of aerosols and their impact on the air quality of Taiwan. *Atmospheric Environment*, **39**(33), 6066–6076.

Lindsey R.; and Simmon R. (2003). Escape from the Amazon. *The Earth Observer*, **15**(2), 8–13.

Liping G.; Erda L.; and Zhongpei L. (2000). Methane emission flux and mitigation options and its relationship with N_2O emission from paddy soils. *Proceedings of the Second International Methane Mitigation Conference (June 18–23, 2000, Novosibirsk)*. Novosibirsk State University Publ., Novosibirsk, pp. 217–222.

Liu X.; Chance K.; Sioris C.E.; Kurosu T.P.; Spurr R.J.D.; Martin R.V.; Fu T.-M.; Logan J.A.; Jacob D.J.; Palmer P.I.; Newchurch M.J.; Megretskaia I.A.; and Chatfield R.B. (2006). First directly-retrieved global distribution of tropospheric column ozone from

GOME: Comparison with the GEOS–CHEM model. *J. Geophys. Res.*, **111**(D02308), doi:10.1029/2005JD006564, 1–17.

Lloyd A.H.; and Fastie C.L. (2002). Spatial and temporal variability in the growth and climate response of treeline trees in Alaska. *Clim. Change*, **52**, 481–509.

Loginov V.F.; and Mikutski V.S. (2000). Assessment of the anthropogenic signal in the climate of cities. *Proc. Russ. Geogr. Soc.*, **132**(1), 23–31 [in Russian].

Logofet D.O. (1993). *Matrices and Graphs: Stability Problems in Mathematical Ecology*. Taylor & Francis/CRC Press, Boca Raton, 308 pp.

Logofet D.O. (2002). Matrix population models: Construction, analysis and interpretation. *Ecological Modelling*, **148**(3), 307–310.

Ma J.; Richter A.; Burrows J.P.; Nüß H.; and van Aardenne A. (2006). Comparison of model-simulated tropospheric NO_2 over China with GOME-satellite data. *Atmospheric Environment*, **40**(4), 593–604.

MacDonald G.; Edwards M.; and Retelle M. (2001). PARCS develops two updated research goals. *Witness the Arctic*, **9**(1), 8–9.

Maddox G.H. (1999). Africa and Environmental History. *Environmental History*, **4**, 162–167.

Mahlman J.D. (1998). Science and nonscience concerning human-caused climate warming. *Ann. Rev. Energy and Environ., Palo Alto (CA)*, **23**, 83–105.

Mahoney J.R. (2003). *The U.S. Climate Change Science Program: Vision for the Program and Highlights of the Science Strategic Plan*. A report by the Climate Change Science Program and the Subcommittee on Global Change Research, Washington, D.C., 41 pp.

Majorovicz H.; Safanda J.; and Skinner W. (2002). East to west retardation in the onset of the recent warming across Canada inferred from inversions of temperature logs. *J. Geophys. Res.*, **107**(B10), ETG6/11–ETG6/12.

Makarov I.M. (2000). *Risk Management: Risk, Sustainable Development, Synergy*. Science Publ., Moscow, 432 pp. [in Russian].

Malinetskii G.G. (2007). Planning the future and technological challenges for Russia. *Integral*, **8**(32), 22–24 [in Russian].

Manwell J.F.; McGowan J.G.; and Rogers A.L. (2002). *Wind Energy Explained: Theory, Design and Application*. Wiley, New York, 590 pp.

Marchand R.; and Ackerman T. (2004). Evaluation of radiometric measurements from the NASA Multiangle Imaging Spectroradiometer (MISR): Two- and three-dimensional radiative transfer modeling of an inhomogeneous stratocumulus cloud deck. *J. Geophys. Res.*, **109**, D18208, doi:10.1029/2004JD004710.

Marchuk G.I.; and Kondratyev K.Ya. (1992). *Priorities of Global Ecology*. Science Publ., Moscow, 264 pp. [in Russian].

Maria S.F.; Russel L.M.; Gilles M.K.; and Myneni S.C.B. (2004). Organic aerosol growth mechanisms and their climate-forcing implications. *Science*, **306**(5703), 1921–1924.

Markowicz K.M.; Flatau P.J.; Vogelmann A.M.; Quinn P.K.; and Welton E.J. (2003). Clear-sky infrared aerosol radiative forcing at the surface and the top of the atmosphere. Quart. J. Roy. Meteorol. Soc., **129**(594), 2927–2947.

Marti J.; and Ernst G.G.J. (eds.) (2005). *Volcanoes and the Environment*. Cambridge Univ. Press., Cambridge, 488 pp.

Marzano F.S.; Vulpiani G.; and Rose W.I. (2006). Microphysical characterization of microwave radar reflectivity due to volcanic ash clouds. *IEEE Transactions on Geoscience and Remote Sensing*, **44**(2), 313–327.

Matishov G.G. (1998). Strategy of Arctic studies. *Herald of the Russian Acad. Sci.*, **68**(6), 515–520 [in Russian].

Matishov G.G. (2000). Contemporary problems of oceanology and geography of the World Ocean. *Herald of the Russian Acad. Sci.*, **70**(8), 682–687 [in Russian].

Matishov D.G.; and Matishov G.G. (2001). *Radiational Ecological Oceanology*. Kola Science Center, Russian Acad. Sci., Apatity, 419 pp. [in Russian].

Matson P.A.; McDowell H.; Townsend A.R.; and Vitousek P.M. (1999). The globalization of N deposition: Ecosystem consequences in tropical environments. *Biogeochemistry*, **46**, 67–83.

Matson P.A.; Lohse K.A.; and Yall S.J. (2002). The globalization of nitrogen deposition: Consequences for terrestrial ecosystems. *Ambio*, **31**(2), 113–119.

Matthies M.; and Scheringer M. (eds.) (2001). Long-range transport in the environment. *Environ. Sci. & Pollut. Res.*, **8**(3), 149–150.

Mayers J.C. (2004). London's wettest summer and wettest year: 1903. *Weather*, **59**(10), 274–278.

McCauley L.L.; and Meier M.F. (eds.) (1991). *Arctic System Science: Land/Atmosphere/Ice Interactions*. ARCUS, Fairbanks, AL, 48 pp.

McGuffie K.; and Henderson-Sellers A. (2001). Forty years of numerical climate modelling. *International Journal of Climatology*, **21**, 1067–1109.

Mcintyre A.D. (1999). The environment and the oil companies. *Marine Pollution Bulletin*, **38**(3), 155–156.

McKitrick R. (2002). Trends in data on air temperature obtained with internal correlations taken into account. *Proc. Russ. Geogr. Soc.*, **134**(3), 16–24 [in Russian].

McKitrick R. (ed.) (2007). *Independent Summary for Policy-Makers: IPCC Fourth Assessment Report*. Fraser Institute, Vancouver, D.C., 64 pp.

McMichael A.J.; Bolin B.; Costanza R.; Daily G.C.; Folke C.; Lindahl-Kiessling K.; Lindgren E.; and Niklasson B. (1999). Globalization and the Sustainability of Human Health. *BioScience*, **49**(3), 205–210.

McNulty S.G. (2002). Hurricane impacts on US forest carbon sequestration. *Environmental Pollution*, **116**, 817–824.

McPhaden M.J.; and Hayes S.P. (1991). On the Variability of Winds, Sea Surface Temperature, and Surface Layer Heat Content in the Western Equatorial Pacific. *Journal of Geophysical Research*, **96**, 3331–3342.

McVean G. (2003). *Demographic Models*. Oxford Univ. Press, Oxford, 29 pp.

MEA (2005). *Ecosystems and Human Well-being: Current State and Trends*. Island Press, Washington, D.C., 948 pp.

Meadows M. (2000). United Kingdom methane emissions: Trends, projections and mitigation options. *Proceedings of the Second International Methane Mitigation Conference (June 18–23, 2000, Novosibirsk)*. Novosibirsk State University Publ., Novosibirsk, pp. 37–44.

Mearns L.O.; Bogardi I.; Giorgi F.; Matyasovsky I.; and Palecki M. (1999). Comparison of climate change scenarios generated from regional climate model experiments and statistical downscaling. *J. Geophys. Res.*, **104**(D6), 6603–6621.

Medlyn B.E.; Berbigier P.; Clement R.; Grelle A.; Loustau D.; Linder S.; Wingate L.; Jarvis P.G.; Sigurdsson B.D.; and McMurtrie R.E. (2005). Carbon balance of coniferous forests growing in contrasting climates: Model-based analysis. *Agricultural and Forest Meteorology*, **131**(1–2), 97–124.

Meijer E.W.; and Velthoven P. (1997). The effect of the conversion of nitrogen oxides in aircraft exhaust plumes in global models. *Geophys. Res. Lett.*, **24**(23), 3013–3016.

Melillo J.; Field C.B.; and Moldan B. (eds.) (2003). *Interactions of the Main Biogeochemical Cycles: Global Change and Human Impacts*, SCOPE Series Vol. 61. Island Press, Washington, D.C., 320 pp.

Melnikova I.N.; and Vasilyev A.V. (2004). *Short-Wave Solar Radiation in the Earth's Atmosphere*. Springer-Verlag, Berlin, 303 pp.

Mendelsohn R.; and Rosenberg N. J. (1994). Framework for integrated assessment of global warming impacts. *Clim. Change*, **28**(1–2), 15–44.

Menon S.; Brenguier J.-L.; Boucher O.; Davison P.; del Genio A.D.; Feichter J.; Ghan S.; Guibert S.; Liu X.; Lohman U.; Pawlowska H.; Penner J.E.; Quaas J.; Roberts D.L.; Schüller L.; and Snider J. (2003). Evaluating aerosol/cloud/radiation process parameterizations with single-column models and Second Aerosol Characterization Experiment (ACE-2) cloudy column observations. *J. Geophys. Res.*, **108**(D24), AAC2/1–AAC2/19.

Milesi C.; Hashimoto H.; Running S.W.; and Nemani R.R. (2005). Climate variability, vegetation productivity and people at risk. *Global and Planetary Change*, **47**(2–4), 221–231.

Milliman J.D. (2001). Delivery and fate of fluvial water and sediment to the sea: A marine geologist's view of European rivers. *Scientia Marina*, **65(2)**, 121–132.

Milliman J.D.; and Kao J.S. (2005). Hyperpycnal discharge of fluvial sediment to the ocean: Impact of Super-Typhoon Herb (1996) on Taiwanese rivers. *Journal of Geology*, **113**, 503–516.

Milne A. (2004). *Doomsday: The Science of Catastrophic Events*. Praeger, Westport, CT, 194 pp.

Mintzer I.M. (1987). *A Matter of Degrees: The Potential for Controlling the Greenhouse Effect*. World Resources Institute Res. Rep. No. 15, New York, 70 pp.

Mironov B. (2005). *A Sentence for the Russia Murders*. Orthodoxy Initiative Inc., Minsk, 575 pp. [in Russian].

Mitra A.P. (2004). Indian Ocean Experiment (INDOEX): An overview. *Indian J. Mar. Sci.*, **33**(1), 30–39.

Mitsch W.J. (ed.) (2005). *Wetland Creation, Restoration, and Conservation*. Elsevier, Amsterdam, 182 pp.

Mkrtchyan F.A. (1982). *Optimal Signal Distinguishing and Monitoring Problems*. Science Publ., Moscow, 184 pp. [in Russian].

Mohr T. and Bridge J. (2003). The evolution of the integrated global Earth observing system. *Studying the Earth from Space*, **1**, 64–73.

Möhler O.; and Arnold F. (1992). Gaseous sulfuric acid and sulfur dioxide measurements in the Arctic troposphere and lower stratosphere: Implications for hydroxyl radical abundances. *Ber. Bunsenges. Phys. Chem.*, **96**, 280–283.

Moiseev N.N. (1979). *Mathematics Used in Experiments*. Science Publ., Moscow, 224 pp [in Russian].

Moiseev N.N. (1988). *Human Ecology from the View of a Mathematician*. Young Guard Publ., Moscow, 254 pp. [in Russian].

Moiseev N.N. (1990). *Man and Noosphere*. Young Guard Publ., Moscow, 352 pp. [in Russian].

Moiseev N.N. (1993). *The Ascent of Reason*. Science Publ., Moscow, 175 pp. [in Russian]

Moiseev N.N. (2001). *Meditation about Rational Society*. Sustainable World Publ., Moscow, 212 pp. [in Russian].

Moiseev N.N.; Alexandrov V.V.; and Tarko A.M. (1985). *Man and Biosphere*. Science Publ., Moscow, 272 pp. [in Russian].

Mon J.; Flury M.; and Harsh J.B. (2006). A quantitative structure–activity relationship (QSAR) analysis of triarylmethane dye tracers. *Journal of Hydrology*, **316**(1–4), 84–97.

Monin A.S.; and Krasnitsky V.P. (1985). *Phenomena on the Ocean Surface*. Hydrometeoizdat, Leningrad, 375 pp. [in Russian].

Monin A.S.; and Shishkov Yu.A. (1990). *Global Ecological Problems*. Knowledge Publ., Moscow, 43 pp. [in Russian].

Monson R. (2004). *Ecological Aspects of Biogeochemical Cycles*, report from a NEON Science Workshop. AIBS Publ., Boulder, CO, 25 pp.

Moody-Stuart M. (2006). *People, Planet and Profits*. IISD Commentary, New York, 9 pp.

Morgan J.; and Codispoti L. (eds.) (1995). *Department of Defense Arctic Nuclear Waste Assessment Program: FY's 1993–1994*. Office of Naval Research, ONR 322-95-5, Arlington, VA, pp.15–30.

Morison J. (2001). SEARCH research opportunities emerging (Winter 2000/2001). *Witness the Arctic*, **8**(2), 8–9.

Morison J.; and Calder J. (2001). SEARCH develops implementation framework. *Witness the Arctic*, **9(1)**, 3–4.

Moritz R.E.; Bitz C.M.; and Steig E.J. (2002). Dynamics of recent climate change in the Arctic. *Science*, **297**(5586), 1497–1502.

Moron V.; Vautard R.; and Ghil M. (1998). Trends, interdecadal and interannual oscillations in global sea-surface temperatures. *Climate Dynamics*, **7–8**, 545–469.

Morris J. (1997). Introduction: Climate change: Prevention or adaptation? *IEA Stud. Educ.*, **10**, 13–37.

Mosier A.R.; Syers J.K.; and Freney J.R. (eds.) (2004). *Agriculture and Nitrogen Cycle: Assessing the Impacts of Fertilizer Use on Food Production and the Environment*. Island Press, Washington, D.C., 344 pp.

Muller, R.; and Peter, T. (1992). The numerical modeling of the sedimentation of polar stratospheric cloud particles. *Ber. Bunsenges Phys. Chem.*, **96**, 353–61.

Munich Re (2004). *Annual Report 2003: More than Words*. Münchener Rückversicherungs-Gesellschaft, Munich, Germany, 234 pp.

Munich Re (2005a). *Annual Report 2004: Advancing Innovation*. Münchener Rückversicherungs-Gesellshaft, Munich, Germany, 220 pp.

Munich Re (2005b). *Topic Geo. Annual Review: Natural Catastrophes 2004*. Münchener Rückversicherungs-Gesellshaft, Munich, Germany, 60 pp.

Munich Re (2007). *Topic Geo. Natural Catastrophes 2006: Analyses, Assessments, Positions*. Münchener Rückversicherungs-Gesellshaft, Munich, Germany, 54 pp.

Munoz-Alpizar R., Blanchet J.-P., and Quintanar A.I. (2003). Application of the NARCM model to high-resolution aerosol simulations: Case study of Mexico City basin during the *Investigación Sobre Materia Particulada y Deterioro Atmosférico* [Investigation into particulate matter and atmospheric deterioration] aerosol and visibility research measurements campaign. *J. Geophys. Res.*, **108**(D15), AAC7/1–AAC7/14.

Munzi S.; Rovera S.; and Caneva G. (2007). Epiphytic lichens as indicators of environmental quality in Rome. *Environmental Pollution*, **146**(2), 350–358.

Murata A.; and Takizawa T. (2002). Impact of a coccolithophorid bloom on the CO_2 system in surface waters of the eastern Bering Sea shelf. *Geophysical Research Letters*, **29**(11), 1547, doi:10.1029/2001GL013906.

Murayama S.; Yamamoto S.; Saigusa N.; Kondo H.; and Takamura C. (2005). Long-term carbon exchange at a Takayama, Japan forest: Statistical analyses of inter-annual variations in the vertical profile of atmospheric CO_2 mixing ratio and carbon budget in a cool-temperate deciduous forest in Japan. *Agricultural and Forest Meteorology*, **134**(1–4), 17–26.

Myeong S.; Nowak D.J.; and Duggin M.J. (2006). A temporal analysis of urban forest carbon storage using remote sensing. *Remote Sensing of Environment*, **101**(2), 277–282.

Myhre G.; Stordal F.; Johmsrud M.; Ignatov A.; Mischenko M.I.; Geogdzhaev I.V.; Tanré D.; Denzé J.-L.; Goloub P.; Nakajima T.; Higurashi A.; Torres O.; and Holben B. (2004). Intercomparison of satellite retrieved aerosol optical depth over the ocean. *J. Atmos. Sci.*, **61**, 499–513.

Myhre G.; Stordal F.; Johnsrud M.; Diner D.J.; Geogdzhayev I.V.; Haywood J.M.; Holben B.N.; Holzer-Popp T.; Ignatov A.; Kahn R.A.; Kaufman Y.J.; Loeb N.; Martonchik J.V.; Mishchenko M.I.; Nalli N.R.; Remer L.A.; Schroedter-Homscheidt M.; Tanré D., Torres O.; and Wang M. (2005). Intercomparison of satellite retrieved aerosol optical depth over ocean during the period September 1997 to December 2000. *Atmos. Chem. Phys.*, **5**, 1697–1719.

Nadelhoffer K.L.; Emmet B.A.; Gundersen P.; Kjonaas O.J.; Koopmans C.J.; Schleppi P.; Tietem A.; and Wright R.F. (1999). Nitrogen deposition makes a minor contribution to carbon sequestration in temperate forests. *Nature*, **398**(6723), 145–148.

Nagurny, A.P.; and Maistrova, V.V. (2002). Long-term temperature trends for the free atmosphere in the Arctic. *Proceedings of RAS*, **389**(3), 295–301 [in Russian].

Nalder I.A.; and Wein R. (2006). A model for the investigation of long-term carbon dynamics in boreal forests of western Canada. *Ecological Modelling*, **192**(1–2), 37–66.

Nechaev A.A. (1997). Methodology for predicting economic structure by means of interbranch comparisons. In: Yu.V. Yakovets (ed.), *Forecast Theory and Future of Russia*. N.D. Kondratyev's International Fund, Moscow, pp. 58–67 [in Russian].

Nefedova E.I. (1994). Mathematical modeling of global carbon cycle in the atmosphere–ocean system. PhD thesis, Computer Center of RAS, Moscow, 112 pp. [in Russian].

Nefedova E.I.; and Tarko A.M. (1993). Investigation of the global carbon cycle within the framework of a zonal model in the atmosphere–ocean system. *Proceedings of RAS*, **333**(5), 645–647 [in Russian].

Nicolis C.; and Nicolis G. (1995). From short-scale atmospheric variability to global climate dynamics: Toward a systematic theory of averaging. *J. of Atm. Sci.*, **52**(11), 1903–1913.

Nielsen T.T. (1999). Characterization of fire regimes in the Experiment for Regional Sources and Sinks of Oxidants (EXPRESSO) study area. *J. Geophys. Res.*, **104**(D23), 30713–30723.

Nishida K.; Nemani R.R.; Glassy J.M.; and Running S.W. (2003). Development of an evapotranspiration index from Aqua/MODIS for monitoring surface moisture status. *IEEE Trans. on Geosci. and Remote Sensing*, **41**(2), 493–501.

Nitu C.; Krapivin V.F.; and Bruno A. (2000a). *Intelligent Techniques in Ecology*. Printech, Bucharest, 150 pp.

Nitu C.; Krapivin V.F.; and Bruno A. (2000b). *System Modelling in Ecology*. Printech, Bucharest, 260 pp.

Nitu C.; Krapivin V.F.; and Pruteanu E. (2004). *Ecoinformatics: Intelligent Systems in Ecology*. Magic Print, Onesti, Bucharest, 411 pp.

Noji E.K. (2001). Bioterrorism: A "new" global environmental health threat. *Global Change and Human Health*, **2**(1), 46–53.

Norton R.G. (2003). *Agricultural Development Policy: Concepts and Experiences*. Wiley, Amsterdam, 512 pp.

Oechel W.C.; Vourlitis G.L.; Hastings S.J.; Zulneta R.C.; Hinzman L.; and Kane D. (2000). Acclimation of ecosystem CO_2 exchange in the Alaskan Arctic in response to climate warming. *Nature*, **406**(6799), 978–981.

Oganesian V.V. (2004). Climate change in Moscow from 1879 to 2002: Values of extremes in temperature and precipitation. *Meteorology and Hydrology*, **9**, 31–37 [in Russian].

Oostenrijk R.; Heyens C.; Klimont Z.; Elzen M.J.E.D.; and Amann M. (2006). Exploring the ancillary benefits of the Kyoto Protocol for air pollution in Europe. *Energy Policy*, **34**, 444–460.

Orheim O. (ed.) (2000). The Recent Arctic Ocean Warming. *Proceedings Joint Science Day: Marine Climate of the Arctic (Tromso, April 25–29, 2000)*. Norsk Polarinstitutt Internrapport No. 3, 32 pp.

Osborne S.R.; Haywood J.M.; Francis P.N.; and Dubovik O. (2004). Short-wave radiative effects of biomass burning aerosol during SAFARI 2000. *Quart. J. Roy. Meteorol. Soc.*, **130**, Part B, No. 599, 1423–1447.

OSPAR (2003). *Annual Report 2002–2003*, Vol. 2. OSPAR Commission, London, 111 pp.

Osterkamp T.E. (2005). The recent warming of permafrost in Alaska. *Global and Planetary Change*, **49**(3–4), 187–202.

Otero L.A.; Ristori P.R.; Holben B.; and Quel E.J. (2004). Detection of biomass burning aerosol in Córdoba, Argentina, using the AERONET/NASA data base. *Óptica Pura y Aplicada*, **37**(3), 3359–3363.

Overland J.E.; and Adams J.M. (2001). On the temporal character and regionality of the Arctic Oscillation. *Geophys. Res. Lett.*, **28**(14), 2811–2814.

Pachauri R.K. (2004). Climate and Humanity. *Proceedings of the All-World Conference on Climate Change (September 29–October 3, 2003, Moscow)*. Gidrometeoizdat, Moscow, pp. 62–67 [in Russian].

Pagurova V.I. (1968). *Criteria for the Comparison of Average Values by Two Normal Measurements*. Computer Center of RAS, Moscow, 57 pp.

Palmer T.N.; Alessandri A.; Anderson U.; Cantelaube P.; Davey M.; Délécluse P.; Déqué M.; Diez E.; Doblas-Reyes F.J.; Feddersen H.; Graham R.; Gualdi S.; Guérémy J.-F.; Hagedorn R.; Hoshen M.; Keenlyside N.; Latif M.; Lazar A.; Maisornave E.; Marletto V.; Morse A.P.;Orfila B.; Rogel P.; Terres J.-M.; and Thomson M.C. (2004). Development of a European Multimodel Ensemble System for Seasonal-to-Interannual Prediction. *Bull. Amer. Meteorol. Soc.*, **85**(6), 853–872.

Palutikof J.P.; and Holt T. (2004). Climate change and the occurrence of extremes: Some implications for the Mediterranean Basin. In: A. Marquina (ed.), *Environmental Challenges in the Mediterranean 2000–2050*. Kluwer Academic, Dordrecht, The Netherlands, pp. 61–73.

Palutikof J.P.; Goodess C.M.; Watkins S.J.; and Burgess P.E. (1999). Long-term climate change. *Progr. Environ. Sci.*, **1**(1), 89–96.

Pan H. (2005). The cost efficiency of Kyoto flexible mechanisms: A top-down study with the GEM-E3 world model. *Environmental Modelling & Software*, **20**(11), 1401–1411.

Pan Y.; McGuire A.D.; Melillo J.M.; Kicklighter D.W.; Sitch S.; and Prentice I.C. (2002). A biogeochemistry-based dynamic vegetation model and its application along a moisture gradient in the continental United States. *Journal of Vegetation Science*, **13**, 369–382.

Panikov N.S.; and Dedysh S.N. (2000). Cold season CH_4 and CO_2 emission from boreal peat bogs (West Siberia): Winter fluxes and thaw activation dynamics. *Global Biogeochemical Cycles*, **14**(4), 1071–1080.

Parchomenko V.P.; and Tarko A.M. (2002). *Analysis of Present Problems in the World and Russia*. Computer Center of RAS, Moscow, 54 pp. [in Russian].

Park K.-H.; Thompson A.G.; Marinier M.; Clark K.; and Wagner-Riddle C. (2006). Greenhouse gas emissions from stored liquid swine manure in a cold climate. *Atmospheric Environment*, **40**(4), 618–627.

Parkinson C.L. (2003). Aqua: An Earth-observing satellite mission to examine water and other climate variables. *IEEE Trans. on Geosci. and Remote Sensing*, **41**(2), 173–183.

Parson E.A.; and Fisher-Vanden K. (1997). Integrated assessment models of global climate change. *Annual Review of Energy and the Environment*, **22**, 589–628.

Parson E.A. and Fisher-Vanden K. (1999). Joint implementation of greenhouse gas abatement under the Kyoto Protocol's "Clean Development Mechanism": Its Scope and Limits. *Policy Sciences*, **32**(3), 207–224.

Pasini A.; Loré M.; and Ameli F. (2006). Neural network modelling for the analysis of forcings/temperatures relationships at different scales in the climate system. *Ecological Modelling*, **191**(1), 58–67.

Pauly D.; and Maclean J. (2003). *In a Perfect Ocean: The State of Fisheries and Ecosystems in the North Atlantic Ocean*. Island Press, Washington, D.C., 175 pp.

Pauly D.; Watson R.; and Alden J. (2005). Global trends in world fisheries: Impact on marine ecosystems and food security. *Philos. Trans. R. Soc. B*, **360**, 5–12.

Pavolonis M.J.; and Key J.R. (2003). Antarctic cloud radiative forcing at the surface estimated from the AVHRR Polar Pathfinder and ISCCP D1 data sets, 1985–93. *J. Appl. Meteorol.*, **42**, 827–840.

Payne J.R.; McNabb G.D.; and Clayton J.R. (1991) Oil-weathering behavior in Arctic environments. *Polar Res.*, **10**(2), 631–662.

Peng C.K.; Buldyrev S.V.; Havlin S.; Simons M.; Stanley H.E.; and Goldberger A.L. (1994). Mosaic organization of DNA nucleotides. *Physical Review*, **E49**(2), 1685–1689.

Peng Y.; and Lohmann U. (2003). Sensitivity study of the spectral dispersion of the cloud droplet size distribution on the indirect aerosol effect. *Geophys. Res. Lett.*, **30**(10), 14/1–14/4.

Penman H.L. (1948). Natural evaporation from open water, bare soil and grass. *Proc. R. Soc. (London)*, **193**, 120–145.

Penner J.E.; Zhang S.Y.; and Chuang C.C. (2003). Soot and smoke aerosol may not warm climate. *J. Geophys. Res.*, **108**(D21), AAC1/1–AAC1/9.

Pentius F. (2003). *Drinking Water Regulation and Health*. Wiley, New York, 1029 pp.

Perry I. (2001). Marine ecosystem and climate interactions in the Past, Present, and Future: Report of a workshop between GLOBEC, PAGES and CLIVAR. *Newsletter*, **7**(1), 6–8.

Pervaniuk V.S. (2001). A spatial numerical model of the global biogeochemical cycles of carbon and nitrogen in the atmosphere–ocean system. Ph.D. thesis, Computing Center of RAS, 118 pp. [in Russsian].

Pervaniuk, V.S.; and Tarko, A.M. (2001). Modelling the global carbon cycle in the atmosphere–ocean system. *Numerical Modelling*, **13**(11), 13–22 [in Russian].

Phelan, J.P. (2004). *Topics: Annual Review of North American Natural Catastrophes 2003*. American Re, Princeton, NJ, 48 pp.

Philbrick C.R. (2002). Overview of Raman lidar techniques for air pollution measurements in lidar remote sensing for industry and environmental monitoring. *SPIE Proceedings*, **4484**, 136–150.

Phillips G.W.; August R.A.; Cherepenin V.A.; Harper M.J.; King S.E.; Krapivin V.F.; Pautkin A.Yu; and Tsang F.Y. (1997). Radionuclear pollutants in the Angara and Yenisey rivers of Siberia. *Radioprotection-Colloques*, **32**, 299–304.

Pinkerton M.H.; Lavender S.J.; and Aiken J. (2003). Validation of SeaWiFS ocean color satellite data using a moored databuoy. *J. Geophys. Res.*, **108**(C5), 10.1029/2002JC001337.

Pirard P.; Vandentorren S.; Pascal M.; Laaidii K.; Le Tertre A.; Cassadou S.; and Ledrans M. (2005). Summary of the mortality impact assessment of the 2003 heat wave in France. *Euro Surveillance*, **10**(7), 153–156.

Pittick B. (2003). *Climate Change: An Australian Guide to the Science and Potential Impacts*. Australian Greenhouse Office Publ., Canberra, 250 pp.

Platt C.M.R.; and Austin R.T. (2002). Remotely controlled, continuous observations of infrared radiance with the CSIRO/ARM Mark II radiometer of the SGP CART site. *Proceedings of the 12th Atmospheric Radiation Measurement (ARM) Science Team Meeting (St. Petersburg, Florida, April 8–12, 2002)*, pp. 1–10.

Plotnikov V.V. (1996).Long-term prognosis of Okhotsk Sea ice conditions by considering large-scale atmospheric processes. *Meteorology and Hydrology (Moscow)*, **12**, 93–100 [in Russian].

Plus M.; Chapelle A.; Ménesguen A.; Deslous–Paoli J.-M.; and Auby I. (2003). Modelling seasonal dynamics of biomasses and nitrogen contents in a seagrass meadow (*Zostera noltii* Hornem.): Application to the Thau lagoon (French Mediterranean coast). *Ecological Modelling*, **161**, 213–238.

Podgorny I.A. and Ramanathan V. (2001). A modeling study of the direct effect of aerosols over the tropical Indian Ocean. J. Geophys. Res., 104(20), 24097–24104.

Polischuk Yu.M. (1992). *Simulation–Linguistic Modeling of the System with Natural Components*. Science Publ., Novosibirsk, 228 pp. [in Russian].

Popovicheva O.B.; Starik A.M.; and Favorsky O.N. (2000). Impacts of aviation on the gas and aerosol composition of the atmosphere. *Bull. of Russian Ac. Sc.: FAO*, **2**, 163–176 [in Russian].

Potapov I.I.; Krapivin V.F.; and Soldatov V.Yu. (2006). Risk assessment in the geoinformation monitoring regime. *Ecological Systems and Devices*, **8**, 11–18 [in Russian].

Potter C.; Klooster S.; and Genovese V. (2003). Satellite data help predict terrestrial carbon sinks. *EOS*, **84**(46), 502–508.

Potter C.; Klooster S.; Tan P.; Steinbach M.; Kumar V.; and Genovese V. (2005). Variability in terrestrial carbon sinks over two decades: Part 2—Eurasia. *Global and Planetary Change*, **49**(3–4), 177–186.

Preller R.H.; and Cheng A.B.E. (1999). Modeling the transport of radiactive contaminants in the Arctic. *Marine Pollution Bulletin*, **38**(2), 71–91.

Prentice I.C. (2001). The carbon cycle and atmospheric carbon dioxide. In: *Climate Change 2001: Impacts, Adaptation, and Vulnerability*, a report of Working Group II of IPCC. Cambridge University Press, Cambridge, UK, pp. 183–237.

Prescott-Allen R. (2001). *Wellbeing of Nations: A Country-by-Country Index of Quality of Life and the Environment*. Island Press, Washington, D.C., 350 pp.

Priestley C.H.B.; and Taylor R.J. (1972). On the assessment of surface heat flux and evapotranspiration using large scale parameters. *Monthly Weather Rev.*, **100**, 81–92.

Qi J.; and Gutman G. (2005).*International Conference on Land Cover and Land Use Change Processes in North East Asia Region*, Summary Report. Michigan University Press, East Lansing, MI, 14 pp.

Rakipova L.R.; and Vishniakova O.N. (1973). The influence of carbon dioxide variations on the atmosphere thermodynamic regime. *Meteorology and Hydrology*, **5**, 23–31 [in Russian].

Ramad F. (1981). *Principles of Applied Ecology*. Hydrometeoizdat, Leningrad, 544 pp. [in Russian].

Ramanathan V.; and Coakley J.A. (1978). Climate modelling through radiative–convective models. *Revs. Geophys. Space Phys.*, **16**, 465–489.

Randel W.J.; Wu F.; and Rios W.R. (2003). Thermal variability of the tropical tropopause region derived from GPS/MET observations. *J. Geophys. Res.*, **108**(D1), 7/1–7/12.

Rayward-Smith V.J.; Osman I.H.; Reeves R.; and Smith G.D. (eds.) (1996). *Modern Heuristic Search Methods*. Wiley, Washington, D.C., 314 pp.

Reilly J.; Stone P.H.; Forest C.E.; Webster M.D.; Jacoby H.D.; and Prinn R.G. (2001). Uncertainty and climate change assessments. *Science*, **293**(5529), 430–433.

Renner M. (2002). Overview: Making the Connections. In: L. Starke (ed.), *Vital-Signs 2002–2003: The Trends that Are Shaping Our Future*. Earthscan, London, pp.15–170.

Rhee T.S.; Brenninkmeijer C.A.M.; and Röckmann T. (2005). The overwhelming role of soils in the global atmospheric hydrogen cycle. *Atmos. Cham. Phys. Discuss.*, **5**, 11215–11248.

Riccio A.; Barone G.; Chianese E.; and Giunta G. (2006). A hierarchical Bayesian approach to the spatio-temporal modeling of air quality data. *Atmospheric Environment*, **40**(3), 554–566.

Riedlinger S.H.; and Preller R.H. (1991). The development of a coupled ice–ocean model for forecasting ice conditions in the Arctic. *J. of Geophys. Res.*, **96**, 16955–16977.

Riedo M.; Gyalistras D.; and Fuhrer J. (2000). Net primary production and carbon stocks in differently managed grasslands: Simulation of site-specific sensitivity to climate change. *Ecological Modelling*, **134**(2–3), 207–227.

Roeckner E.; Arpe K.; Bengtsson L.; Christoph M.; Claussen M.; Dümenil L.; Esch M.; Giorgetta M.;Schlese U.; and Schulzweida U. (1996). *The Atmospheric General Circulation Model ECHAM-4: Model Description and Simulation of Present-Day Climate*. Max-Planck-Institut für Meteorologie Report No. 218, Hamburg, Germany, 90 pp.

Rogers A.N.; Bromwich D.H.; Sinclair E.N.; and Cullather R.I. (2001). The atmospheric hydrologic cycle over the Arctic Basin from reanalyses. Part 2. Interannual variability. *Journal of Climate*, **14**(11), 2414–2429.

Roll G.U. (1968). *Physics of Atmospheric Processes above the Sea.* Hydrometeoizdat, Leningrad, 400 pp. [in Russian].

Rosenberg J. (2001). *The Follies of Globalization Theory*. Verso Publ., London, 224 pp.

Rosengrant M.W.; Cai X.; and Cline S.A. (2002). *Global Water Outlook to 2025: Averting an Impending Crisis*. IWMI Publ., Colombo, Sri Lanka, 36 pp.

Rossby C.-G. (1939). Relation between variations in the intensity of the zonal circulation of the atmosphere and the displacements of the semi-permanent centers of action. *J. Marine Research*, **2**, 38–55.

Rossow W.B. (2003). Workshop on climate system feedbacks. *GEWEX News.*, **13**(1), 12–14.

Roth R.S. (1981). Technique in the identification of deterministic systems. *IEEE Transactions on Automatic Control*, **AC-26(5)**, 1169–1176.

Rovinsky F.Ya.; Chernogaeva G.M.; and Paramonov S.G. (1995). A role of river flow and atmospheric transport in the pollution of Russian northern seas. *Meteorology and Hydrology (Moscow)*, **9**, 22–29 [in Russian].

Rubincam D. P. (2004). Black body temperature, orbital elements, the Milankovitch precession index, and the Seversmith psychroterms. *Theoretical and Applied Climatology*, **79**(1–2), 111–131.

Ruck, M. (2002). *Natural Catastrophes 2002: Annual Review*. Munich Re Topics, Dresden, Germany, 50 pp.

Rudels B.; Larsson A.-M.; and Sehistendt P.-I. (1991). Stratification and water mass formation in the Arctic Ocean. *Polar Res.*, **10**(1), 19–31.

Rundgren M.; Björck S.; and Hammarlund D. (2005). Last interglacial atmospheric CO_2 changes from stomatal index data and their relation to climate variations. *Global and Planetary Change*, **49**(1–2), 47–62.

Russo G.; Eva C.; Palau C.; Caneva A.; and Saechini A. (2000). The recent abrupt increase in the precipitation rate, as seen in an ultra-centennial series of precipiation. *Il Nuovo Cimento*, **23C**(1), 39–51.

Saigusa N.; Yamamoto S.; Murayama S.; and Kondo H. (2005). Long-term carbon exchange at a Takayama, Japan forest: Interiannual variability of carbon budget components in an AsiaFlux forest site estimated by long-term flux measurements. *Agricultural and Forest Meteorology*, **134**(1–4), 4–16.

Saito M.; Miyata A.; Nagai H.; and Yamada T. (2005). Seasonal variation of carbon dioxide in rice paddy field in Japan. *Agricultural and Forest Meteorology*, **135**(1–4), 93–109.

Saleska S.R.; Miller S.D.; Matross D.M.; Goulden M.L.; Wofsy S.C.; da Rocha H.R.; de Camargo P.B.; Crill P.; Daube B.C.; de Freitas H.C.; Hutyra L.; Keller M.; Kirchhoff V.; Menton M.; Munger J.W.; Pyle E.H.; Rice A.H.; and Silva H. (2003). Carbon in Amazon forests: Unexpected seasonal fluxes and disturbance-induced losses. *Science*, **302**, 1554–1557.

Sanets E.V.; and Chuduk V.N. (2005). Sulphur atmospheric deposition in areas with different anthropogenic loads in Belarus. *Atmospheric Research*, **77**(1–4), 88–99.

Santer B.D.; Wigley T.M.L.; Boyle J.S.; Gaffen D.J.; Hnilo J.J.; Nychka D.; Parker D.E.; and Taylor K.E. (2000). Statistical significance of trends and trend differences in layer average atmospheric temperature time series. *J. Geophys. Res.*, **105**(D6), 7337–7356.

Santer B.D.; Sausen R.; Wigley T.M.L.; Boyle J.S.; Achuta Rao K.; Doutriaux C.; Hansen J.E.; Meehl G.A.; Roeckner E.; Ruedy R.; Schmidt G.; and Taylor K.E. (2003). Behavior of tropopause height and atmospheric temperature in models, re-analysis, and observations: Decadal changes. *J. Geophys. Res.*, **108**(D1), 1/1–1/22.

Scafetta N.; Grigolini P.; Imholt T.; Roberts J.; and West B.J. (2004). Solar turbulence in earth's global and regional anomalies. *Physical Review*, **E69**(026303), 1–13.

Schlesinger M.E.; and Andronova N. (2000). Temperature changes during the 19th and 20th Centuries. *Geophys. Res. Lett.*, **27**, 2137–2140.

Schlesinger M.E.; Ramankutty N.; and Andronova N. (2000). Temperature oscillations in the North Atlantic. *Science*, **289**(5479), 547.

Schlesinger W.H. (2005). *Biogeochemistry: Treatise on Geochemistry*, Vol. 8. Elsevier Science, Berlin, 720 pp.

Schmidt G.A.; Ruedy R.; Hansen J.E.; Aleinov I.; Bell N.; Bauer M.; Bauer S.; Cairns B.; Canuto V.; Cheng Y.; Del Genio A.; Faluvegi G.; Friend A.D.; Hall T.M.; Hu Y.; Kelley M.; Kiang N.Y.; Koch D.; Lacis A.A.; Lerner J.; Lo K.K.; Miller R.L.; Nazarenko L.; Oinas V., Perlwitz Ja., Perlwitz Ju., Rind D., Romanou A., Russell G.L., Sato Mki., Shindell D.T.; Stone P.H.; Sun S.; Tausnev N.; Thresher D.; and Yao M.-S. (2006). Present day atmospheric simulations using GISS Model E: Comparison to in-situ, satellite and reanalysis data. *J. Climate*, **19**, 153–192.

Schofield N.; Burt A.; and Connell D. (2003). *Environmental Water Qllocation: Principles, Policies and Practices*. Land & Water Australia, Canberra, 39 pp.

Schröder W. (ed.) (2000). *Long and Short Term Variability in Sun's History and Global Change*. Science Edition, D-28777, Bremen-Roennebeck, 63 pp.

Schrope M. (2001). Consensus science, or consensus politics? *Nature*, **412**(6843), 112–114.

Schulze E.-D. (ed.) (2000). *Global Biogeochemical Cycles in the Climate System*. Academic Press, New York, 416 pp.

Schwarzenbach R.P. (2002). *Environmental Organic Chemistry*. Wiley, New York, 1314 pp.

Seidov D.G. (1987). Mathematical models of oceanic circulation. *Earth and World*, **5**, 28–34 [in Russian].

Seiler-Hausmann J.-D.; Liedtke C.; and von Weizsäcker E.U. (eds.) (2004). *Eco-efficiency and Beyond: Towards the Sustainable Enterprise*. Greenleaf Publishing, Sheffield, U.K., 248 pp.

Sellers P.; Meeson B.W.; Hall F.G.; Asrar G.; Murphy R.E.; Schiffer R.A.; Bretherton F.P.; Dickinson R.E.; Ellingson R.G.; Field C.B.; Huemmrich K.F.; Justice C.O.; Melack J.M.;

Roulet N.T.; Schimel D.S.; and Try P.D. (1995). Remote sensing of the land surface for studies of global change: Models–algorithms–experiments. *Remote Sensing of Environment*, **51**(1), 3–26.

Sellers P.J.; Randall D.A.; Collatz G.J.; Randall D.A.; Dazlich D.A.; Zhang C.; Berry J.A.; Field C.B.; Collelo G.D.; and Bounoua L. (1996). A revised land surface parametrization (SiB2) for atmospheric GCMs. Part 1: Model formulation. *Journal of Climate*, **9**(4), 676–705.

Shamir N.J.; and Veizer J. (2003). Celestial driver of Phanerozoic climate? *GSA Today*, **13**(7), 4–10.

Shugalei L.S.; Petrukhina A.N.; and Shapchenkova O.A. (2005). Biogeochemical cycles of heavy metals in birch stands of the zone of technogenic influence of the Berezovo hydroelectric power station KAFEC. *Siberian Ecological Journal*, **1**, 13–21 [in Russian].

Shutko A.M. (1987). *Microwave Radiometry of Water Surface and Soils*. Science Publ., Moscow, 190 pp. [in Russian].

Sieg C.H.; Meko D.; DeGaetano A.T.; and Ni W. (1996). Dendroclimate potential in the northern great plains. In: S. Dean, D.M. Meko, and T.W. Swetnam (eds.), *The International Conference on Tree-Rings, Environment and Humanity: Processes and Relationships between Tree Rings, Environment, and Humanity (Tucson, Arizona, May 17–21, 1994)*, pp. 295–302.

Siegenthaler U.; and Sarmiento J.L. (1993). Atmospheric carbon dioxide and the ocean. *Nature*, **365**, 119–125.

Sims D.A.; Rahman A.F.; Cordova V.D.; Baldocchi D.D.; Flanagan L.B.; Goldstein A.H.; Hollinger D.Y.; Misson L.; Monson R.K.; Schmid H.P.; Wofsy S.C.; and Xu L. (2005). Midday values of gross CO_2 flux and light use efficiency during satellite overpasses can be used to directly estimate eight-day mean flux. *Agricultural and Forest Meteorology*, **131**(1–2), 1–12.

Singh H.B.; and Jacob D.J. (2000). Future directions: Satellite observations of tropospheric chemistry. *Atmospheric Environment*, **34**, 4399–4401.

Singh R.B.; Fox J.; and Himiyama Y. (eds.) (2001). *Land Use and Cover Change*. Science Publishers, New York, 312 pp.

Skinner B.J. (1979). Earth Resources. *Proceedings of the National Academy of Sciences, U.S.A.*, **76**(9), 4212–4217.

Smeets E.; and Weterings R. (1999). *Environmental Indicators: Typology and Overview*. EEA Technical Report No. 25, Copenhagen, The Netherlands, 19 pp.

Smil V. (1997). Global population and the nitrogen cycle. *Scientific American*, **6**, 77–81.

Smith K.A.; Thomson P.E.; Clayton H.; McTaggart I.P.; and Conen F. (1998). Effects of temperature, water content and nitrogen fertilisation on emissions of nitrous oxide by soils. *Atmospheric Environment*, **32**(19), 3301–3309.

Smith S.V., Swaney D.P.; McManus L.T.; Bartley J.D.; Sandhei P.T.; McLaughlin C.J.; Dupra V.C.; Crossland C.J.; Buddemeier R.W.; Maxwell B.A.; and Wulff F. (2003). Humans, Hydrology, and the Distribution of Inorganic Nutrient Loading to the Ocean. *BioScience*, **53**(3), 235–245.

Smitha A.; Rao K.H.; and Sengupta D. (2006). Effect of May 2003 tropical cyclone on physical and biological processes in the Bay of Bengal. *International Journal of Remote Sensing*, **27**(23), 5301–5314.

Sokolov V.A. (1971). *Geochemistry of Natural Gases*. Nedra, Moscow, 336 pp.

Soldatov V.Yu. (2007). Diagnosing the ocean–atmosphere system using the percolation model. *Problems of Environment and Natural Resources*, **5**, 52–63 [in Russian].

Somes N.L.G. (1999). Numerical simulation of wet land hydrodynamics. *Environment International*, **25**(6–7), 773–779.

Soon W.; Postmentier E.; and Baliunas S. (2000). Climate hypersensitivity to solar forcing? *Ann. Geophysicae*, **18**, 583–588.

Soon W.; Baliunas S.; Idso C.; Idso S.; and Legates D. R. (2003). Reconstructing climatic and environmental changes of the past 1000 years: A re-appraisal. *Energy and Environment*, **14**(2–3), 233–296.

Sorochtin O.G. (2001). Greenhouse effect: Myth and reality. *Herald of RANS*, **1**(1), 8–21 [in Russian].

Soros M.S. (2000). Preserving the atmosphere as a global commons. *Environment Change and Security Project Report*. The Woodrow Wilson Center, Washington, D.C., **6**, 149–155.

Spoor M. (ed.) (2004). *Globalization, Poverty and Conflict*. Springer-Verlag, Berlin, 339 pp.

Sportisse B. (2000). Box models versus Eulerian models in air pollution modelling. *Atmospheric Environment*, **35**(1), 173–178.

SRES (2000). *Mission Scenarios: Summary for Policymakers*. IPCC Special Report of Working Group III, WMO/UNEP, Washington, D.C., 20 pp.

Stanley E. (1999). Scaling, universality, and renormalization: Three pillars of modern critical phenomena. *Reviews of Modern Physics*, **71**(2), S358–S366.

Stanley S.M. (2005). *Earth System History*. W.H. Freeman & Co., New York, 567 pp.

Stanley S.M.; Ward P.D.; and Brownlee D. (2005). *Earth System History and the Life and Death of Planet Earth*. W.H. Freeman & Co., New York, 209 pp.

Starke L. (ed.) (2002). *Vital-Signs 2002–2003: The Trends that Are Shaping Our Future*. Earthscan, London, 216 pp.

Starke L. (ed.) (2004). *State of the World-2004: Progress towards a Sustainable Society*. Earthscan, London, 246 pp.

Steffen W.; Sanderson A.; Tyson P.; Jäger J.; Matson P.; Moore III B.; Oldfield F.; Richardson K.; Schellnhuber H.; Turner II B.; and Wasson R. (2005). *Global Change and the Earth System*. Springer-Verlag, Berlin, 336 pp.

Stein A.F.; and Lamb D. (2000). The sensitivity of sulphur wet deposition to atmospheric oxidants. *Atmospheric Environment*, **34**(11), 1681–1690.

Stenseth N.C.; Ottersen G.; Hurrell J.W.; and Belgrano A. (eds.) (2004). *Marine Ecosystems and Climate Variation. The North Atlantic: A Comparative Perspective*. Oxford University Press, Oxford, U.K., 272 pp.

Stephens G.L.; Vane D.G.; Boain R.J.; Mace G.G.; Sassen K.; Wang Z.; Illingworth A.J.; O'Connor E.J.; Rossow W.B.; Durden S.L.; Miller S.D.; Austin R.T.; Benedetti A.; and Mitrescu C. (2002). The CloudSat mission and the a-train: A new dimension of space-based observations of clouds and precipitation. *Bulletin of the American Meteorological Society*, **83**(12), 1769–1790.

Stevens C.; and Verne R. (2004). *Renewable Bioresources: Scope and Modification for Non-Food Applications*. Wiley, Brussels, 320 pp.

Stevenson, D.S.; Johnson, C.E.; Collins, W.J.; Derwent, R.G.; and Edwards, J.M. (2000). Future estimates of tropospheric ozone radiative forcing and methane turnover: The impact of climate change. *Geophys. Res. Lett.*, **27**(14), 2073–2076.

Stevenson F.J.; and Cole M.A. (1999). *Cycles of Soils: Carbon, Nitrogen, Phosphorus, Sulphur, Micronutrients*. Wiley, New York, 448 pp.

Stockwell D.Z.; Giannakopoulos C.; Plantevin P.H.; Carver G.D.; Chipperfield M.P.; Law K.S.; Pyle J.A.; Shallcross D.E.; and Wang K.Y. (1999). Modelling NO_x from lightning and its impact on global chemical fields. *Atmospheric Environment*, **33**(27), 4477–4493.

Stoll-Kleemann S.; and O'Riordan T. (2004). The possible role of public private partnerships. *IHDP Update*, **3**, 6–8.

Stone R.S. (1998). Monitoring aerosol optical depth at Barrow, Alaska and South Pole: Historical overview, recent results, and future goals. *J. Geophys. Res.*, **103**, 16565–16579.

Stone R.S.; Dutton E.G.; Harris S.M.; and Longenecker D. (2002). Earlier spring snowmelt in northern Alaska as an indicator of climate change. *J. Geophys. Res.*, **107**(D10), ACL10/1–ACL10/15.

Straub C.P. (ed.) (1989). *Practical Handbook of Environmental Control*. CRC Press, Boca Raton, Florida, 537 pp.

Strong A.E.; Kearns E.J.; and Gjovig K.K. (2000). Sea surface temperature signals from satellites update. *Geophys. Res. Lett.*, **27**(11), 1667–1670.

Sun V.; Baliunas S.; Demirchian K.S.; Kondratyev K.Ya.; Idso S.B.; and Postmentier E.S. (2001). Influence of CO_2 anthropogenic flows on the climate: Unsolving problems. *Proceedings of Russian Geographical Society*, **133**(2), 1–19 [in Russian].

Suzuki A. (1992). Results of the collection of fishes, and tropical to temperate migrant fishes coming to the Okhotsk Sea coast during 1989 to 1991 in Northern Hokkaido, Japan. *Proceedings of the Seventh International Symposium on Okhotsk Sea and Sea Ice, February 2–5, 1992, Mombetsu, Hokkaido, Japan*. Okhotsk Sea & Cold Ocean Research Association Publ., Sapporo, Japan, pp. 225–231.

Syvitski J.P.M.; Peckham S.D.; Hilberman R.; and Mulder T. (2003). Predicting the terrestrial flux of sediment to the global ocean: A planetary perspective. *Sedimentary Geology*, **162**, 5–24.

Syvorotkin V.L. (2002). *Abyssal Decontamination of the Earth and Global Catastrophes*. Geoinformcenter, Moscow, 250 pp. [in Russian].

Talkner P.; and Weber R.O. (2000). Power spectrum and detrended fluctuation analysis: Application to daily temperatures. *Physical Review*, Part A, **E62**(1), 150–160.

Tarko A.M. (2001). Investigation of global biosphere processes with the aid of a global spatial carbon dioxide cycle model. *Proceedings of the Sixth International Carbon Dioxide Conference, Extended Abstracts (October 1–2, 2001, Tohoku University, Sendai, Japan)*, Vol. 2, pp. 899–902.

Tarko A.M. (2003). *Analysis of Global and Regional Changes in Biogeochemical Carbon Cycle: A Spatially Distributed Model*, Interim Report IR-03-041. IIASA, Laxenburg, Austria, 28 pp.

Tarko A.M. (2005). *Mathematical Modeling of Anthropogenic Changes in Global Biospheric Processes*. Physics–Mathematics Publ., Moscow, 278 pp. [in Russian].

Terborgh J. (1992). *Diversity and the Tropical Rain Forest*. Scientific American Library, Washington, D.C., 242 pp.

Terziev F.S. (ed.) (1992). *Hydrometeorology and Hydrochemistry of USSR Seas. Vol. 1: Barents Sea*. Gidrometeoizdat, St. Petersburg, 182 pp. [in Russian].

Terziev F.S.; Zatuchnoy B.M.; and Gershanovitch D.E. (1993). *Okhotsk Sea*. Gidrometeopress, St. Petersburg, 167 pp. [in Russian].

Tett S.F.B.; Stott P.A.; Allen M.R.; Ingram W.J.; and Mitchell J.F.B. (1999). Causes of twentieth-century temperature change near the Earth's surface. *Nature*, **399**, 569–572.

Thomas W.; Hegels E.; Slijkhuis S.; Spurr R.; and Chance K. (1998a). Detection of biomass burning combustion products in South East Asia from backscatter data taken by the GOME spectrometer. *Geophysical Research Letters*, **25**, 1317–1320

Thomas W.; Hegels E.; Slijkhuis S.; Spurr R.; and Chance K. (1998b). Detection of trace species in the troposphere using back-scatter spectra, obtained by the GOME spectrometer. *Geophys. Res. Lett.*, **25**, 1317–1320.

Tol R.S.J. (2000). International climate policy: An assessment. *IHDP Update*, **3**, 11–12.

Tooming H. (2002). Dependence of global radiation on cloudiness and surface albedo in Tartu, Estonia. *Theoretical and Applied Climatology*, **72**(3–4), 165–172.

Trites A.W.; Livingston P.A.; Mackinson S.; Vasconcellos M.C.; Springer A.M.; and Pauly D. (1999). *Ecosystem Change and the Decline of Marine Mammals in the Eastern Bering Sea*. Fisheries Center Res. Rep., Fairbanks, AL, 100 pp.

Troyan V.N.; and Dementiev I.A. (eds.) (2005). *Sustainable Development and Economical Management*. St. Petersburg University Publ., St. Petersburg, 479 pp.

Twomey S. (1974). Pollution and the planetary albedo. *Atmospheric Environment*, **8**, 1251–1256.

U.N. (2002). *Activities of Intergovernmental and Non-Governmental Organizations of UNFCCC: Article 6 (Education, Training and Public Awareness)*. UNFCCC Publ., New York, 203 pp.

Usbeck R. (1999). *Modeling of Marine Biogeochemical Cycles with an Emphasis on Vertical Particulate Fluxes*. Alfred-Wegener-Institut für Polar- und Meeresforschung, Bremenhaven, Germany, 112 pp.

Vakulenko N.V.; Kotlyakov V.M.; Monin A.S.; and Sonechkin D.M. (2006). Symmetry of glacier cycles of the late Pleistocene from Vostok and Kupol C station data in the Antarctic. *Proceedings of RAS*, **407**(1), 111–115 [in Russian].

Valera F.; Thompson E.; and Rosch E. (1991). *The Embodied Mind: Cognitive Science and Human Experience*. Cambridge University Press, Cambridge, MA, 292 pp.

Valette-Silver N.J., Hameedi M.J., Efurd D.W., and Robertson A. (1999). Status of the contamination in sediments and biota from the western Beaufort Sea (Alaska). *Marine Pollution Bulletin*, **38**(8), 702–722.

Van der Leeuw S.E.; and Aschan-Leygonie C. (2000). A long-term perspective on resilience in socio-natural systems. *Proceedings of the Workshop on "System Shocks–System Resilience" (Abisko, Sweden, May 22–26, 2000)*, pp. 1–32.

Vanin P. (2002). *Economic Growth and Social Development*. Anno Accademico, Milan, Italy, 116 pp.

Varotsos C. (2004). Power-law correlations in column ozone over Antarctica. *International Journal of Remote Sensing*, **26**, 3333–3342.

Varotsos C. (2002). Climate change problems and carbon dioxide emissions: Expecting "Rio + 10". *Environ. Sci & Pollut Res.*, **9**(2), 97–98.

Varotsos C. (2005). Power-law correlations in column ozone over Antarctica. *International Journal of Remote Sensing*, **26**(16), 3333–3342.

Varotsos C.; and Kirk-Davidoff D. (2006). Long-memory processes in ozone and temperature variations at the region 60 degrees S–60 degrees N. *Atmos. Chem. Phys.*, **6**, 4093–4100.

Varotsos C.A.; and Kondratyev K.Ya. (1998). Total ozone dynamics in mid-latitudes of the Northern Hemisphere. *Proc. of RAS*, **359**(6), 821–822 [in Russian].

Varotsos C.; Alexandris D.; Chronopoulos G.; and Tzanis C. (2001). Aircraft observations of the solar ultraviolet irradiance throughout the troposphere. *Journal of Geophysical Research-Atmospheres*, **106**(D14), 14843–14854.

Varotsos C.; Ondov J.; and Efstathiou M. (2005). Scaling properties of air pollution in Athens, Greece and Baltimore, Maryland. *Atmospheric Environment*, **39**, 4041–4047.

Varotsos C.; Assimakopoulos M.N.; and Efstathiou M. (2007). Technical Note: Long-term memory effect in the atmospheric CO_2 concentration at Mauna Loa. *Atmospheric Chemistry and Physics*, **7**, 629–634.

Varotsos P.A.; Sarlis N.V.; and Skordas E.S. (2003a). Long-range correlations in the electric signals that precede rupture: Further investigations. *Physical Review*, **E67**, 21109–21121.

Varotsos P.A.; Sarlis N.V.; and Skordas E.S. (2003b). Attempt to distinguish electric signals of a dichotomous nature. *Physical Review*, **E68**(3), art. no. 031106.

Vasilyev A.V.; and Melnikova I.N. (2002). *Short-Wave Solar Radiation in the Earth's Atmosphere: Calculations, Measurements, Interpretation*. St. Petersburg Sci. Center of RAS, St. Petersburg, 388 pp. [in Russian].

Vaughan M.; Young S.; Winker D.; Powell K.; Omar A.; Liu Z.; Hu Y.; and Hostetler C. (2004). Fully automated analysis of space-based lidar data: An overview of the CALIPSO retrieval algorithms and data products. *Proc. SPIE*, **5575**, 16–30.

Vay S.A.; Anderson B.E.; Conway T.J.; Sachse G.W.; Collins J.E.; Blake D.R.; and Westberg D.J. (1999). Airborne observation of the tropospheric CO_2 distribution and its controlling factors over the South Pacific Basin. *J. Geophys. Res.*, **104**(D5), 5663–5676.

Verma S.B.; Dobermann A.; Cassman K.G.; Walters D.T.; Knops J.M.; Arkebauer T.J.; Suyker A.E.; Burba G.G.; Amos B.; Yang H.; Ginting D.; Hubbard K.G.; Gitelson A.A.; and Walter-Shea E.A. (2005). Annual carbon dioxide exchange in irrigated and rainfed maize-based agroecosystems. *Agricultural and Forest Meteorology*, **131**(1–2), 77–96.

Vernadsky V.I. (1944). A few words about the noosphere. *Progress in Present Biology*, **18**(2), 49–93 [in Russian].

Vernadsky V.I. (1977). *Natural World Meditation: Scientific Thought as a Planetary Phenomenon*. Science Publ., Moscow, 239 pp. [in Russian].

Vetrov A.A.; and Romankevich E.A. (2004). *Carbon Cycle in the Russian Arctic Seas*. Springer-Verlag, Berlin, 332 pp.

Victor D.G. (2001). *The Collapse of the Kyoto Protocol and the Struggle to Slow Global Warming*. Princeton University Press, Princeton, NJ, 192 pp.

Vinogradov B.V. (1983). Quantitative expression for the function of soil moisture remote identification. *Proceedings of Soviet Academy of Sciences*, **272**(1), 247–250 [in Russian].

Vital Signs (2005). Worldwatch Institute, Washington, D.C., 139 pp.

Vitousek P.M. (2004). *Nutrient Cycling and Limitation: Hawai'i as a Model System*. Princeton University Press, Princeton, NJ, 232 pp.

Vogelmann A.M.; Flatau P.J.; Szcordrak M.; Markowicz K.M.; and Minnett P.J. (2003). Observations of large aerosol infrared forcing at the surface. *Geophys. Res. Lett.*, **30**(12), 1655, doi:10.1029/20022002GL016829.

Vogelsang T.J.; and Franses P.H. (2005). Are winters getting warmer? *Environmental Modelling & Software*, **20**(11), 1449–1455.

Voitov G.I. (1986). Chemistry and scale of present-day flux of natural gases in different geostructural Earth zones. *Journal of All-Union Chemical Society*, **31**(5), 533–539 [in Russian].

Voitov G.I. (1999). On cold methane degassing in the Earth's troposphere. *Proceedings of Geological Institute of RAS: Theoretical and Regional Problems*. Science Publ., Moscow, **515**, 242–251 [in Russian].

Vörösmarty C.J.; Hinzman L.D.; Peterson B.J.; Bromwich D.H.; Hamilton L.C.; Morison J.; Romanovsky V.E.; Sturm M.; and Webb R.S. (2001). *The Hydrological Cycle and Its Role in Arctic and Global Environmental Change: A Rationale and Strategy for Synthesis Study*. Arctic Research Consortium of the U.S., Fairbanks, AL, 84 pp.

Wainwright J.; and Mulligan M. (eds.) (2003). *Environmental Modelling: Finding Simplicity in Complexity*. Wiley, Amsterdam, 352 pp.

Walker D.A.; Bockheim J.G.; Chapin F.S.; Eugster W.; King J.Y.; McFadden J.; Michaelson G.J.; Nelson F.E.; Oechel W.C.; Ping C.L.; Reeburgh W.S.; Regli S.; Shiklomanov N.I.;

and Vourlitis G.L. (1998). Energy and trace-gas fluxes across a soil–pH boundary in the Arctic. *Nature*, **394**, 469–472.

Walker G. (2003). *Snowball Earth: The Story of the Great Global Catastrophe that Spawned Life as We Know It*. Crown Publishers, Washington, D.C., 269 pp.

Wallace J.M. (1998). Observed climatic variability: Spatial structure. In: D.L.T. Anderson and J. Willebrand (eds.), *Decadal Climate Variability: Dynamics and Predictability*. Springer-Verlag, Berlin, pp. 31–81.

Wallace J.M. and Thompson D.W.J. (2002). Annual modes and climate prediction. *Phys. Today*, **55**(2), 28–33.

Walsh J.E.; and Chapman W.L. (2001). Twentieth-century sea ice variations from observational data. *Ann. Glaciology*, **33**, 444–448.

Wania R.; Prentice C.; Harrison S.; Hornibrook E.; Gedney N.; Christensen T.; and Clymo R. (2004). The role of natural wetlands in the global methane cycle. *EOS*, **85**, 466.

Wang P.-H.; Minnis P.; Wielicki B.A.; Wong T.; Cess R.D.; Zhang M.; Vann L.B.; and Kent G.S. (2003). Characteristics of the 1997/1998 El Niño cloud distributions from SAGE-II observations. *J. Geophys. Res.*, **108**(D1), 5/1–5/11.

Wang Q.; Watanabe M.; and Ouyang Z. (2005a). Simulation of water and carbon fkuxes using BIOME-BGC model over crops in China. *Agricultural and Forest Meteorology*, **131**(3–4), 209–224.

Wang W.; Davis K.J.; Cook B.D.; Bakwin P.S.; Yi C.; Butler M.P.; and Ricciuto D.M. (2005b). Surface layer CO_2 budget and advective contributions to measurements of net ecosystem–atmosphere exchange of CO_2. *Agricultural and Forest Meteorology*, **135**(1–4), 202–214.

Wange G.; and Archer D.J. (2003). Evaporation of groundwater from arid playas measured by C-band SAR. *IEEE Trans. on Geosci. and Remote Sensing*, **41**(7), 1641–1650.

Wania F.; Hoff J.T.; Jai C.Q.; and Mackay D. (1998). The effects of snow and ice on the environmental behavior of hydrophobic organic chemicals. *Environmental Pollution*, **102**(1), 25–41.

Waple A.M.; and Lawrimore J.H. (eds.) (2003). State of the climate in 2002. *Bull. Amer. Meteorol. Soc.*, **84**(6), S1–S68.

Ward P. (2002). *Future Evolution*. W.H. Freeman & Co., New York, 210 pp.

Ward P. and Brownlee D. (2004). *The Life and Death of Planet Earth: How the New Science of Astrobiology Charts the Ultimate Fate of Our World*. W.H. Freeman & Co., New York, 210 pp.

Watanabe M. (2000). *Mechanisms of the Decadal Climate Variability in the Midlatitude Atmosphere–Ocean System*. Center for Climate System Research, University of Tokyo, **12**, 157 pp.

Watson R.T.; Zinyowera M.C.; and Moss R.H. (eds) (1996). *Climate Change 1995: Impacts, Adaptations and Mitigation of Climate Change: Scientific–Technical Analyses*. Cambridge University Press, Cambridge, U.K., 878 pp.

Watson R.T.; Noble I.R.; Bolin B.; Ravindranath N.H.; Verardo D.J.; and Dokken D.J. (eds.) (2000). *Land Use, Land-use Change, and Forestry*. Cambridge University Press, Cambridge, U.K., 377 pp.

Wauben W.M.F.; Van Velthoven P.F.J.; and Kelder H. (1997). 3d chemistry transport model study of changes in atmospheric ozone due to aircraft-NO emissions. *Atmospheric Environment*, **31**(12), 1819–1836.

Weaver C.P. (2003). Efficiency of storm tracks an important climate parameter? The role of cloud radiative forcing in poleward heat transport. *J. Geophys. Res.*, **108**(D1), 5/1–5/6.

Weber G.R. (1992). *Global Warming: The Rest of the Story*. Dr. Boettiger Verlag, Wiesbaden, Germany, 188 pp.

Weeks S.J.; Pitcher G.C.; and Bernard S. (2004). Satellite monitoring of the evolution of a coccolithophorid bloom in the Southern Benguela upwelling system. *Oceanography*, **17**(1), 83–89.

Weis R.F.; Jahnke R.A.; and Keeling C.D. (1982). Seasonal effects of temperature and salinity of the partial pressure of CO_2 in seawater. *Nature*, **300**, 511–513.

Weisenstein D.K.; Ko M.K.W.; Dyominov I.G.; Pitarui G.; Riccardully L.; Visconti G.; and Bekki S. (1998). The effect of sulfur emissions from HSCT aircraft: A 2D model intercomparison. *J. Geophys. Res.*, **103**(ND1), 1527–1547.

WEO (2002). *World Energy Outlook*. OECD/IEA, Paris, 533 pp.

WEO (2004). *World Energy Outlook*. OECD/IEA, Paris, 550 pp.

WEO (2005). *Middle East and North Africa Insights*. IEA, London, 600 pp.

Weller G.; and Lange M. (eds.) (1999). *Impacts of Global Climate Change in the Arctic Region*. Intern. Arctic Science Com., Fairbanks, AL, 59 pp.

WHO (2000). *WHO Report on Global Surveillance of Epidemic-prone Infections, Diseases. Chapter 4: Cholera*. World Health Organization, Geneva, Switzerland, 18 pp.

WHO (2006). Cholera 2005. *Weekly Epidemiological Record*, **81**(31), 297–308.

WI (2006). *Wuppertal Institute for Climate Environment and Energy*. Annual Report 2005/2006, Wuppertal, Germany, 57 pp.

WI (2007). *Vital Signs: The Trends that Are Shaping Our Future*. Worldwatch Institute, Washington, D.C., 160 pp.

Widmann M.; Jones J.M.; and von Storch H. (2004). Reconstruction of large-scale atmospheric circulation and data assimilation in paleoclimatology. *PAGES News*, **12**(2), 12–13.

Wielgolaski F.E. (ed.) (1997). *Polar and Alpine Tundra*. Elsevier, New York. 930 pp.

Wigley T.M.L. (1999). *The Science of Climate Change: Global and U.S. Perspectives*. Pew Center on Global Climate Change, Arlington, VA, 48 pp.

Wigley T.M.L.; and Raper S.C.B. (2001). Interpretation of high projections for global-mean warming. *Science*, **293**(5529), 451–455.

William A.J. (2004). *Soil Physics*. Wiley, Amsterdam, 384 pp.

Williams G.R. (2005). The coupling of biogeochemical cycles of nutrients. *Biogeochemistry*, **4**(1), 61–75.

Wilson E.O. (2002). *The Future of Life*. Vintage Books, Hopkinton, MA, 256 pp.

Witness the Arctic (1994), **2**(1), 1–15.

Wojick D.E. (2001). *The UN IPCC Artful Bias, Glaring Omissions, False Confidence and Misleading Statistics in the Summary for Policymakers*. Available at *www.john-daly.com/quests/un_ipcc.htm*

Wood S.I.; Henao J.; and Rosengrant M.W. (2004). The role of nitrogen in sustaining food production and estimating future nitrogen fertilizer needs to meet food demand. In: A.R. Mosier, J.K. Syers, and J.R. Freney (eds.), *Agriculture and Nitrogen Cycle: Assessing the Impacts of Fertilizer Use on Food Production and the Environment*. Island Press, Washington, D.C., pp. 145–176.

Woodcock A. (1999a). Global warming: A natural event? *Weather*, **54**(5), 162–163.

Woodcock A. (1999b). Global warming: The debate heats up. *Weather*, **55**(4), 143–144.

WSSD (2003). *Science and Technology for Sustainable Development, A G8 Action Plan (June 1–3, 2003, Évian-les-Bains, France)*, 4 pp.

Xu Y.; and Carmichael G.R. (1999). An assessment of sulfur deposition pathways in Asia. *Atmospheric Environment*, **33**(21), 3473–3486.

Yabe T.; Höller R.; Tohno S.; and Kadahara M. (2003). An aerosol climatology at Kyoto: Observed local radiative forcing and columnar optical properties. *J. Appl. Meteorol.*, **42**, 841–850.

Yakovets Yu.V. (ed.) (1997). *Forecasting Theory and Future of Russia*. International N.D. Kondratyev's Fund, Moscow, 487 pp.

Yamagata T.; Behera S.K.; Luo J.J.; Masson S.; Jury M.R.; and Rao S.A. (2004). Coupled Ocean–Atmosphere variability in the tropical Indian Ocean. In: C. Wang, X.-P. Xie, and J.A. Carton (eds), *Earth Climate: The Ocean–Atmosphere Interactions*. Springer-Verlag, Berlin, pp. 189–212.

Yan H.; and Torres J.C.C. (eds.) (2007). Socio-economic benefits: Meteorological and hydrological services. *WMO Bulletin*, **56**(1), 76 pp.

Yohe G.; Malone E.; Brenkert A.; Schlesinger M.; Meij H.; Xing X.; and Lee G. (2006). *A Synthetic Assessment of the Global Distribution of Vulnerability to Climate Change from the IPCC Perspective that Reflects Exposure and Adaptive Capacity*. CIESIN, New York, 17 pp.

Yu R.; Zhang M.; and Cess R.D. (1999). Analysis of the atmosphere energy budget: A consistency study of available data sets. *J. Geophys. Res.*, **104**(D8), 9655–9661.

Yue T.X.; Fan Z.M.; and Liu J.Y. (2005). Changes of major terrestrial ecosystems in China since 1960. *Global and Planetary Change*, **48**(4), 287–302.

Yurganov L.; McMillan W.; Dzhola A.; and Grechko E. (2006). *2006 Boreal Forest Fires: Tropospheric CO Perturbations Detected from Ground and Space*. American Geophysical Union, Fall Meeting 2006, Washington, pp. 200–205.

Zaitsev S.I. (1988). Laboratory modeling of the C_2 exchange processes between the atmosphere and ocean. PhD thesis, Moscow State University, 170 pp. [in Russian].

Zavarzin G.A. (2003). The setting of biogeochemical cycles. *Paleontology J.*, **6**, 16–24 [in Russian].

Zender C.S., Bian H., and Newman D. (2003). Mineral dust entrainment and deposition (DEAD) model: Description and 1990s dust climatology. *J. Geophys. Res.*, **108**(D14), AAC8/1–AAC8/19.

Zhang H.; Henderson-Sellers A.; and McGuffie K. (2001). The compounding effects of tropical deforestation and greenhouse warming on climate. *Climatic Change*, **49**(3), 309–338.

Zhang Y-C.; Rossow W.B.; Lacis A.A.; Oinas V.; and Mishchenko M.I. (2004). Calculation of radiative fluxes from the surface to top of atmosphere based on ISCCP and other global data sets: Refinements of the radiative transfer model and the input data. *J. Geophys. Res.*, **109**, 1–27.

Zhu C.; and Anderson G. (2002). *Environmental Applications of Geochemical Modeling*. Cambrodge Univ. Press., Cambridge, U.K., 298 pp.

Zhu J.; and Liu Z. (2003). Long-range persistence of acid deposition. *Atmospheric Environment*, **37**, 2605–2613.

Zonneveld C. (1998). A cell-based model for the chlorophyll a to carbon ratio in phytoplankton. *Ecological Modelling*, **113**(1–3), 55–70.

Zuev V.V. (2000). Destruction of the ozone layer: An ecological catastrophe or the greatest mystery of the century? *Proceedings of the Second Symposium on the Ecology of Siberian Rivers and the Arctic (Tomsk, November 24–26, 2000)*, pp. 36–40 [in Russian].

Zwally H.J.; Giovinetto M.B.; Li J.; Cornejo H.G.; Beckley M.A.; Brenner A.C.; Saba J.L.; and Yi D. (2005). Mass changes of the Greenland and Antarctic ice sheets and shelves and contributions to sea-level rise: 1992–2002. *Journal of Climatology*, **51**(175), 509–527.

Index

Printing: Mercedes-Druck, Berlin
Binding: Stein+Lehmann, Berlin